

Dedicated to building research infrastructure and the promotion of Science, Technology, Engineering and Math (STEM) education in West Virginia

2013 – 2014 STUDENT RESEARCH REPORTS

Summer Internships

Undergraduate Research Fellowship Program

Graduate Research Fellowship Program

NASA West Virginia Space Grant Consortium
West Virginia University
PO Box 6070
Morgantown, WV 26506-6070
(304) 293-4099

www.nasa.wvu.edu

Published July 2014



PREFACE

The National Space Grant College and Fellowship Program (also known as Space Grant) was first established under Title II of the National Aeronautics and Space Administration (NASA) Authorization Act of 1988 (P.L. 100-147). Space Grant is a unique national state-based network in 50 states, Puerto Rico and the District of Columbia. The program is a component of NASA's Education Directorate portfolio charged with carrying out effective education, research, and public outreach activities in science, technology, engineering and mathematics (STEM), particularly in fields most relevant to NASA's future workforce.

Currently, Space Grant is comprised of 52 consortia that engage over 1,000 affiliates nationally, including more than 600 colleges/universities, and state, industry, non-profit and federal partners, including NASA Centers. They work collectively to meet the nation's needs for developing and training a high-tech workforce to sustain a robust U.S. space science and space exploration program.

As one of the 52 university-based Space Grant consortia, the West Virginia Space Grant Consortium (WVSGC or Consortium) was established in August 1991. The Consortium is housed in the Benjamin M. Statler College of Engineering and Mineral Resources on the Evansdale Campus of West Virginia University in Morgantown, West Virginia. It is comprised of 12 West Virginia academic institutions and 8 corporate and scientific partners (a list of affiliates is listed on page 2). It is dedicated to building research infrastructure and promoting STEM education in West Virginia. The Consortium's programs focus on research, collaborations with high technology industries, student fellowships as well as K-12, and public outreach programs. This is consistent with the strategic vision for the state's participation in the nation's current and future endeavors in science and technology.

This publication is a compilation of student reports from summer internships, the NASA Undergraduate Research Fellowship Program and the NASA Graduate Research Fellowship Program for the 2013-2014 fiscal year.

On behalf of the Board of Directors of NASA WVSGC, we would like to take this opportunity to express our appreciation to students who applied for these programs, the mentoring offered to West Virginia students by their faculty advisors in their research projects as well as the different internship locations that provided these opportunities. Without them, our internships and fellowship programs would not be where they are today: a crucial step in the workforce development pipeline for NASA and the high technology sector in the United States.

For additional information on our programs, please contact our office or visit www.nasa.wvu.edu.

CONSORTIUM AFFILIATES

West Virginia University (Lead)

Bethany College

Bluefield State College

Fairmont State University

Glenville State College

Marshall University

NASA Independent Verification & Validation Facility

National Radio Astronomy Observatory

Polyhedron Learning Media, Inc.

Shepherd University

TechConnect WV

The Clay Center for the Arts and Sciences of West Virginia

TMC Technologies, Inc.

West Liberty University

WV High Technology Consortium Foundation

West Virginia State University

WVU Institute of Technology

West Virginia Wesleyan College

Wheeling Jesuit University

TABLE OF CONTENTS

LIST OF PROGRAMS.....	1
I. SUMMER INTERNSHIPS.....	6
Brown, Robert. West Virginia University. TMC Technologies. <i>Acronyms: Technical Document Analysis Software</i>	I-1
Didion, Alan Michael. West Virginia University. Ames Academy. <i>Anechoic Chamber Wind Tunnel Nozzle Modification Design & Implementation</i>	I-5
Forrester, Conor. West Virginia Wesleyan College. West Virginia Wesleyan College. <i>A Study of High Technology Applied to the Wood Industry in West Virginia</i>	I-21
Haynes, Danielle. Bluefield State College. Bluefield State College. <i>Decreased Mortality Rate of Mice through Serial in Vitro Passage of Starved Cells of Pseudomonas aeruginosa in Water</i>	I-32
Heywood, Stephen. West Virginia State University. West Virginia State University. <i>ID2 Over-Expression Effects on Other Genes that are Dysregulated in Meningiomas</i>	I-39
Hobbs, Jaclyn. West Virginia University. NASA IV&V Facility. <i>Robotics Virtual Interactive Evaluation and Understanding</i>	I-46
Inskeep, Jacob. West Virginia University. NASA LARSS. <i>CFD Modeling Interactions of Shockwaves and Exhaust Nozzle Plumes in the Glenn Research Center 1' x 1' Supersonic Wind Tunnel</i>	I-55
Isme, Mardochee. Bluefield State College. Bluefield State College. <i>Mechanistic Studies of Norepinephrine in Growth and Gene Expression of Pseudomonas Isolates</i>	I-64
Kaufman, Ashley. West Virginia University. NASA LARSS. <i>Re-Formatting NASA's Airborne Study Data to Support CCMI Activities</i>	I-69
McKenzie, Ozias. West Virginia University. West Virginia University. <i>Summer 2013 Research Experience with the Flight Control Systems Laboratory</i>	I-76
Mills, Sarah. West Virginia University. NASA LARSS. <i>Airborne Wind Energy Dual Use Feasibility Investigation</i>	I-83
Price, Robert. Bluefield State College. Bluefield State College. <i>Determination of Mice Infected with Long-Term Starved Pseudomonas aeruginosa</i>	I-90
Richmond, Sasha. Bluefield State College. Bluefield State College. <i>Increased Infiltration of Leukocytes in the Regions of Genital Tract of Stressed During Chlamydia Trachomatis Infection</i>	I-95
Spada, Vincent. West Virginia University. NASA LARSS. <i>Computational Fluid Dynamics Modeling of Temperature Gradients at the National Transonic Facility</i>	I-101
Spicer, Matthew. West Virginia Wesleyan College. West Virginia Wesleyan College. <i>A Study of High Technology Applied to the Wood Industry</i>	I-111

Webb, Ashley. Fairmont State University. NASA Wallops Flight Facility. <i>Summer 2013 Wallops Information System Data Management Internship at Wallops Flight Facility</i>	I-123
--	-------

II. NASA UNDERGRADUATE RESEARCH FELLOWSHIP PROGRAM.....9

Bowman, Brandon. West Virginia University. Dr. Antarpreet Jutla. <i>Satellite Based Diagnostic Approach to Monitor Hydroclimatic Conditions for Emergence of West Nile Virus</i>	II-1
--	------

Carden, Dillon. West Virginia University. Dr. Kostas Sierros. <i>Piezoelectric, PDMS-Based Devices</i>	II-11
--	-------

Carte, Adam. West Virginia University. Dr. Ashok Bidwai. <i>Computational Analysis of CK2 Targets in Drosophila Genetic Studies</i>	II-18
---	-------

Cavender, Hannah, West Virginia State University. Dr. Genia Sklute. <i>Complexation of Aluminum by Nitrogen-Containing Ligands</i>	II-28
--	-------

Cordonier, Guy. West Virginia University. Dr. Kostas Sierros. <i>Biodegradable P-N Junction</i>	II-31
---	-------

Dennison, Zane. Fairmont State University. Dr. Mark Flood. <i>Using Aquatic Organisms to Assess the Effectiveness of Acid Mine Drainage Remediation in the Three Fork Creek Watershed</i>	II-37
---	-------

Greza, Lucas. West Virginia Wesleyan College. Dr. Joseph E. Wiest. <i>Vibrations in Aircraft at Supersonic Speeds</i>	II-43
---	-------

Hajiran, Cyrus. West Virginia University. Dr. Letha J. Sooter. <i>Identification of Antibody Fragments Specific for High-Grade Prostatic Intraepithelial Neoplasia Cells via SELEX</i>	II-49
--	-------

Hunter, Zachary. Marshall University. Dr. Scott Day. <i>Probe Density and Capture Efficiency Dependence on Dendrimer Size</i>	II-57
---	-------

Massie, Melissa. Marshall University. Dr. Nalini Santanam. <i>Effect of Omega 3 Fat Diet on Obesity in Antioxidant Mice</i>	II-69
---	-------

Mayfield, Brianna. Marshall University. Dr. Elizabeth Murray. <i>Cell Culture Bioassay Development for Prynnesium parvum Toxins</i>	II-74
---	-------

Spencer, Dustin. Fairmont State University. Dr. Mark Flood. <i>Does Local Marcellus Well Drilling Impact Water Quality in Streams?</i>	II-83
--	-------

Vance, Jenna. Marshall University. Dr. Maria Serrat. <i>Unilateral Heating: A Novel Model to Induce Differential Extremity Growth in Mice</i>	II-91
---	-------

III. NASA GRADUATE RESEARCH FELLOWSHIP PROGRAM	6
Komar, Colin. West Virginia University. Dr. Paul Cassak. <i>A Comparative Analysis of Dayside Magnetic Reconnection Models</i>	<i>II-1</i>
Majot, Adam. West Virginia University. Dr. Ashok P. Bidwai. <i>Enhancer Analysis of the Gene Rough</i>	<i>II-16</i>
Nande, Rounak. Marshall University. Dr. Pier Paolo Claudio. <i>Ultrasound Mediated Gene Delivery in Immune-Competent Mice</i>	<i>II-23</i>
Owen, Benjamin. Marshall University. Dr. Lawrence M. Grover. <i>Role of Kv7 Channels in Controlling Neuronal Excitability</i>	<i>II-32</i>
Rankin, Lyndsay. Marshall University. Dr. Anne Axel. <i>Measuring Forest Quality in Grazed Tropical Dry Forests of Southern Madagascar</i>	<i>II-45</i>
Wolf, May. Marshall University. Dr. Pier Paolo Claudio. <i>Investigation of Benzyl isothiocyanates Regulation of Metastatic Processes in HNSCC Cell Lines.....</i>	<i>II-61</i>

LIST OF PROGRAMS

I. SUMMER INTERNSHIPS

For the 2013-2014 fiscal year, we have sixteen undergraduate and graduate students who successfully received internship opportunities. Below is a list of their names, the university they attend, the internship facility as well as their research topic. A copy of their research reports is included under Section I.

Brown, Robert

University: West Virginia University
Location: TMC Technologies in Fairmont, West Virginia
Research: *Acronyms: Technical Document Analysis Software*

Didion, Alan Michael

University: West Virginia University
Location: Ames Academy in Moffett Field, California
Research: *Anechoic Chamber Wind Tunnel Nozzle Modification Design & Implementation*

Forrester, Conor

University: West Virginia Wesleyan College
Location: West Virginia Wesleyan College in Buckhannon, West Virginia
Research: *A Study of High Technology Applied to the Wood Industry in West Virginia*

Haynes, Danielle

University: Bluefield State College
Location: Bluefield State College in Bluefield, West Virginia
Research: *Decreased Mortality Rate of Mice through Serial in Vitro Passage of Starved Cells of Pseudomonas aeruginosa in Water*

Heywood, Stephen

University: West Virginia State University
Location: West Virginia State University in Dunbar, West Virginia
Research: *ID2 Over-Expression Effects on Other Genes that are Dysregulated in Meningiomas*

Hobbs, Jaclyn

University: West Virginia University
Location: NASA IV&V Facility in Fairmont, West Virginia
Research: *Robotics Virtual Interactive Evaluation and Understanding*

Inskeep, Jacob

University: West Virginia University
Location: NASA Langley Aerospace Research Summer Scholars Project (LARSS) in Hampton, VA

Research: *CFD Modeling Interactions of Shockwaves and Exhaust Nozzle Plumes in the Glenn Research Center 1' x 1' Supersonic Wind Tunnel*

Isme, Mardochee

University: Bluefield State College

Location: Bluefield State College in Bluefield, West Virginia

Research: *Mechanistic Studies of Norepinephrine in Growth and Gene Expression of Pseudomonas Isolates*

Kaufman, Ashley

University: West Virginia University

Location: NASA LARSS in Hampton, Virginia

Research: *Re-Formatting NASA's Airborne Study Data to Support CCMI Activities*

McKenzie, Ozias

University: West Virginia University

Location: West Virginia University in Morgantown, West Virginia

Research: *Summer 2013 Research Experience with the Flight Control Systems Laboratory (FCSL)*

Mills, Sarah

University: West Virginia University

Location: NASA LARSS in Hampton, Virginia

Research: *Airborne Wind Energy Dual Use Feasibility Investigation*

Price, Robert

University: Bluefield State College

Location: Bluefield State College in Bluefield, West Virginia

Research: *Determination of Mice Infected with Long-Term Starved Pseudomonas aeruginosa*

Richmond, Sasha

University: Bluefield State College

Location: Bluefield State College in Bluefield, West Virginia

Research: *Increased Infiltration of Leukocytes in the Regions of Genital Tract of Stressed During Chlamydia Trachomatis Infection*

Spada, Vincent

University: West Virginia University

Location: NASA LARSS in Hampton, Virginia

Research: *Computational Fluid Dynamics Modeling of Temperature Gradients at the National Transonic Facility*

Spicer, Matthew

University: West Virginia Wesleyan College

Location: West Virginia Wesleyan College in Buckhannon, West Virginia

Research: *A Study of High Technology Applied to the Wood Industry*

Webb, Ashley

University: Fairmont State University

Location: NASA Wallops Flight Facility in Wallops Island, Virginia

Research: *Summer 2013 Wallops Information System Data Management Internship at Wallops Flight Facility*

II. NASA UNDERGRADUATE RESEARCH FELLOWSHIP PROGRAM

The NASA WVSGC Undergraduate Research Fellowship Program provides support for undergraduate students under the supervision of their academic advisor. For the 2013-2014 fiscal year, we have thirteen undergraduate students who were awarded research fellowships. Below is a list of their names, the university they attend, their mentor as well as their research topic. A copy of their research reports is included under Section II.

Bowman, Brandon

University: West Virginia University

Mentor: Dr. Antarpreet Jutla

Research: *Satellite Based Diagnostic Approach to Monitor Hydroclimatic Conditions for Emergence of West Nile Virus*

Carden, Dillon

University: West Virginia University

Mentor: Dr. Kostas Sierros

Research: *Piezoelectric, PDMS-Based Devices*

Carte, Adam

University: West Virginia University

Mentor: Dr. Ashok Bidwai

Research: *Computational Analysis of CK2 Targets in Drosophila Genetic Studies*

Cavender, Hannah

University: West Virginia State University

Mentor: Dr. Genia Sklute

Research: *Complexation of Aluminum by Nitrogen-Containing Ligands*

Cordonier, Guy

University: West Virginia University

Mentor: Dr. Kostas Sierros

Research: *Biodegradable P-N Junction*

Dennison, Zane

University: Fairmont State University

Mentor: Dr. Mark Flood

Research: *Using Aquatic Organisms to Assess the Effectiveness of Acid Mine Drainage Remediation in the Three Fork Creek Watershed*

Greza, Lucas

University: West Virginia Wesleyan College
Mentor: Dr. Joseph E. Wiest
Research: *Vibrations in Aircraft at Supersonic Speeds*

Hajiran, Cyrus

University: West Virginia University
Mentor: Dr. Letha J. Sooter
Research: *Identification of Antibody Fragments Specific for High-Grade Prostatic Intraepithelial Neoplasia Cells via SELEX*

Hunter, Zachary

University: Marshall University
Mentor: Dr. Scott Day
Research: *Probe Density and Capture Efficiency Dependence on Dendrimer Size*

Massie, Melissa

University: Marshall University
Mentor: Dr. Nalini Santanam
Research: *Effect of Omega 3 Fat Diet on Obesity in Antioxidant Mice*

Mayfield, Brianna

University: Marshall University
Mentor: Dr. Elizabeth Murray
Research: *Cell Culture Bioassay Development for *Prymnesium parvum* Toxins*

Spencer, Dustin

University: Fairmont State University
Mentor: Dr. Mark Flood
Research: *Does Local Marcellus Well Drilling Impact Water Quality in Streams?*

Vance, Jenna

University: Marshall University
Mentor: Dr. Maria Serrat
Research: *Unilateral Heating: A Novel Model to Induce Differential Extremity Growth in Mice*

III. NASA GRADUATE RESEARCH FELLOWSHIP PROGRAM

The NASA WVSGC Graduate Research Fellowship Program provides funding for graduate students working on a thesis or dissertation with faculty from member institutions. For the 2013-2014 fiscal year, we have six graduate students who were awarded research fellowships. Below is a list of their names, the university they attend, their mentor as well as their research topic. A copy of their research reports is included under Section III.

Komar, Colin

University: West Virginia University
Mentor: Dr. Paul Cassak
Research: *A Comparative Analysis of Dayside Magnetic Reconnection Models*

Majot, Adam

University: West Virginia University
Mentor: Dr. Ashok P. Bidwai
Research: *Enhancer Analysis of the Gene Rough*

Nande, Rounak

University: Marshall University
Mentor: Dr. Pier Paolo Claudio
Research: *Ultrasound Mediated Gene Delivery in Immune-Competent Mice*

Owen, Benjamin

University: Marshall University
Mentor: Dr. Lawrence M. Grover
Research: *Role of Kv7 Channels in Controlling Neuronal Excitability*

Rankin, Lyndsay

University: Marshall University
Mentor: Dr. Anne Axel
Research: *Measuring Forest Quality in Grazed Tropical Dry Forests of Southern Madagascar*

Wolf, May

University: Marshall University
Mentor: Dr. Pier Paolo Claudio
Research: *Investigation of Benzyl isothiocyanates Regulation of Metastatic Processes in HNSCC Cell Lines*

I. Summer Internships Reports

ACRONYMS: TECHNICAL DOCUMENT ANALYSIS SOFTWARE

Robert J. Brown
Computer Science – LCSEE
West Virginia University
Morgantown, WV 26505

ABSTRACT

Through the course of this research, a new tool for analyzing acronyms within technical documents has been developed. The Acronym Quality Assurance tool (AcroQAt), greatly reduces the amount of time needed to review acronym usage within documentation. Through AcroQAt's automation of reviewing acronym standards, human error is minimized, and greater efficiency is gained.

INTRODUCTION

Technology is advancing by leaps and bounds every day, and with such advances, technical documentation also becomes increasingly complex and lengthy. Part of the complexity of such documents is the use of acronyms. In formal documentation, even acronyms must follow a set of standards. Each acronym must always, on first use, be defined at length and then followed with parenthetical abbreviation – an example would be that of the Federal Bureau of Investigation (FBI). After the first correct use of an acronym, the abbreviation may be used freely throughout the document. The free use of the acronym can cause confusion to document reviewers. To aid in this confusion, a list of every acronym and definition pair is kept in a table at the end of documentation for reference – this is also a standard that must be met when using acronyms in formal documentation. Because these formal documents are typically prepared in parts by several employees each defining their own acronyms, and then combined for review by Quality Assurance (QA) managers, these standards are not always completely upheld. This piecing together of documentation makes the proof-reading task of the QA team extremely tedious, time consuming, and error prone – especially when the documents can sometimes reach thousands of pages. Current advances in technology can be utilized to automate the task of ensuring that each acronym in the final acronym list is used within the document, and that each acronym is defined only once within the body of the paper. This automation greatly reduces the number of overall grade-crushing document error ‘dings’ that a company may receive from a customer’s reviewing QA team.

BACKGROUND

TMC Technologies of Fairmont, West Virginia, is an Information Technology (IT) services company. Of the company’s many areas of expertise, this project particularly involved their advanced knowledge in Quality Assurance and Testing, Software Design Development and Maintenance, as well as Software Test and Evaluation. In these areas, one of the tasks of TMC is producing formal documents that sometimes contain hundreds of acronyms amongst thousands of pages of technical jargon. Companies such as TMC must follow strict guidelines when submitting documents to their contracted customers. The customer’s QA team reviews these documents, and ‘dings’ errors that they may find. These dings reduce the overall document score that the company receives. These customers typically keep track of, and make readily available these company

scores, and use them through the decision making process of hiring, or re-hiring a company's services. So, as may be thought, obtaining the highest score possible is the overall goal of these companies.

A Vice President of TMC, Carlos Martinez, set forth to minimize dings that the company might receive due to acronyms, and agreed to embark upon the task of intern mentorship, provided the intern would use their knowledge to help develop a software tool that could automate the repetitive tasks used to verify acronym usages and lists within documents.

METHODS

Initial Design

The first attempt at creating a program that would automate finding each acronym within a document, and compare it to a set of guidelines, involved the use of Microsoft Word 2007 Professional Edition's built in Macro features. Macros in Word are written using Visual Basic, and can automate tasks within Word using a few keystrokes, or button clicks. The looping structures needed within the program to check numerous rules, however, proved to be very slow compared to other languages like C or Python – sometimes taking several minutes to produce the desired outputs. The ability to integrate the tool with Microsoft Word was a highly desired trait, as it is the word processing program of choice within the company. However, a larger goal was to reduce the overall amount of time spent analyzing the document for acronym errors. Mr. Martinez also made it a personal goal to ensure that the intern was given experience in the software development process, and continually changed and added to the functionality of the program. Because of these factors, a different approach was taken.

Current Design

Because integration within word was still highly desired, but document processing needed to be accomplished much more quickly, a second language was used. A C program was developed to perform the parsing of the document through the use of a regular expression, and several other algorithms for checking the standard acronym rules. The program was able to be integrated into the macro function with a few shell commands. The resulting program was able to analyze documents much more quickly than the original design.

Design Additions

Having worked out several bugs involving spaces in file names, and crashes due to missing acronym list tables, the tool, AcroQAt, was working well, however it now needed an easy way to be passed around the company. As the tool was originally developed as a Word macro for one machine, once again a few changes needed to be made. The tool was transferred to a template document that could be placed in a Word specific application folder through the use of a batch file. This allowed the program to be treated like a Word Add-in, and allowed it to be installed across multiple computers – provided they were using the same operating system, and version of Word. The program was verified to work on previous versions of Windows – Windows XP, and Windows Vista (both using Microsoft Word 2007 Professional Edition) – however, the program was designed for use on Windows 7.

RESULTS

The final resulting tool was tested on additional office computers through the use of the batch installer. Though the tool was very much operational and useable, it was still very much in the beginning stages of development. Due to this fact, it was decided that including an installation manual and user's guide would be a wise decision. Upon creation of this documentation, and distribution to the self-proclaimed least technologically savvy member of the building, the user was able to install the program to their version of Word, and use the tool against one of their documents. The installation and analysis took only a few minutes, with the installation process being the lengthiest portion.

The tool is able to produce an alphabetized list of all the acronyms contained within the document, as well as a document containing the text around each usage of the acronym – which makes finding problem areas much easier and less error prone. If a table containing the list of acronyms exists at the end of the document, the tool produces a document comparing the list of acronyms found by the tool against the table at the end of the document. The resulting document shows the discrepancies between the two lists using Word's built in file comparison tools. Finally, the tool analyzes the produced documents, and creates analysis documentation. This final document shows which acronyms have been incorrectly defined within the document, acronyms that are missing definitions, acronyms that are defined multiple times, and even acronyms that are only used once within the document. Each issue is accompanied with the text around the acronym, so that the user can easily reference the error. This document allows the user to address problem acronyms directly, rather than manually reading through each page of the document.

Use of the tool's created documents allowed acronym lists to be created from scratch in a matter of minutes versus the hours it could take previously. The documents also allowed for error checking to be done far more quickly than the manual methods that Mr. Martinez currently had to use.

FUTURE PLANS

Though some uses of tables can still cause issues for the AcroQAt program, one example being that a table exists within the document, but there are no tables containing an acronym list, the tool was believed to be a great help to the TMC Company. Due to the method used to find acronyms within documents, sometimes false acronyms, like headings in all caps, are labeled as acronyms. A black-list feature has already been created to help relieve some of these false positives.

Through some research, there were other tools available on the market that accomplished similar tasks of creating acronym lists, but many of them accomplished simply that task. Other programs would create the list, and then guess at the definition based on a library of acronyms. None were found, though, that were capable of analyzing the acronyms found for documentation standards errors. Because the tool was so helpful in this aspect, and because Mr. Martinez wanted to really facilitate experience in the lifecycle of software, the decision was made to make the tool freely available to anyone that would care to have access, and would like to provide feedback. The site <http://www.acroqat.com> is currently being created so that anyone that would desire to use the tool may download the installation program and manual, as well as provide feedback, or contact the developers. The site will also be used to track the number of times the program is downloaded.

Provided there are substantial downloads and enough feedback, plans to further develop the program with additional features, and a little more flair, have already been made.

CONCLUSION

The creation of the AcroQAt program met the original terms set forth by Mr. Carlos Martinez of TMC Technologies. AcroQAt is capable of quickly analyzing documents, and producing outputs to quickly fix problem areas, leaving much more time to be applied elsewhere; as was desired by Mr. Martinez. Mr. Martinez has also provided the resources needed to continue the educational experience of software development, as well as his expertise and continuing mentorship. The overall experience associated with developing the program was an incredible success on both party's efforts. In AcroQAt's current stage, it is an extremely effective and helpful tool, and will hopefully only continue to provide educational opportunities and become even more helpful reviewing documents in the future.

ACKNOWLEDGEMENTS

The author would like to thank NASA, TMC Technologies, and the West Virginia Space Grant Consortium for providing students with the opportunity to gain hands on experiences with companies in their related field of study. Without the funding provided, there would have been no possible way for the author to embark upon this experience. A special thank you would also like to be extended to Mr. Carlos Martinez of TMC Technologies of Fairmont, West Virginia, for his guidance, career advice, and field expertise throughout the entire project experience. Another thank you should be extended to Candy Cordwell, and Dr. Majid Jaridi of West Virginia University for their aid throughout the process of the internship as well. Without their networking abilities and guidance, this opportunity would never have occurred. Also, the author would like to extend thanks to Mr. Cody Costa for his assistance in creating graphics for use in the manuals, as well as the AcroQAt web page.

ANECHOIC CHAMBER WIND TUNNEL NOZZLE MODIFICATION DESIGN, FABRICATION, & IMPLEMENTATION: A SUMMARY

NASA AMES AERONAUTICS ACADEMY, SUMMER 2013

Alan M. Didion
Mechanical & Aerospace Engineering, Physics
West Virginia University Morgantown, WV 26505

ABSTRACT

The NASA Ames Research Center anechoic chamber wind tunnel facility is in need of new nozzle equipment to complete its recent refurbishment and restore full testing capabilities. Rather than fabricating an entirely new nozzle, an ineffective eight by ten inch rectangular nozzle was modified such that it can achieve a desired exit Mach of 0.3 with fully developed boundary layer flow. To address this issue, an extension to the existing nozzle was designed, fabricated and tested to achieve the desired conditions while preventing the motor stall conditions previously experienced. The new extension is to be fastened securely and withstand the drag and loads at full capacity with a factor of safety four or more while being capable of supporting an interchangeable instrument plate system for boundary layer microphone arrays and instruments. The design incorporates findings of a computational fluid dynamics (CFD) analysis and finite element analysis (FEA). Upon completion of the fabrication process, test readiness analyses were conducted and performance data was generated to revise the facility's standard operating procedure (SOP). At the conclusion, the new equipment is expected to be used for many aeroacoustic tests over several years.

Note: This report is a summary for the West Virginia Space Grant Consortium of the experiences of the author during the summer of 2013 and is abridged to comply with the related restrictions. For a more detailed report of experimental setup and results and project work conducted by the other team members, see the additional attached papers as they were submitted to the NASA Ames Academy management.

INTRODUCTION

Problem Statement

The anechoic chamber wind tunnel facility at NASA Ames Research Center is undergoing moderate renovations. For upcoming tests, the facility must be able to measure acoustic vibrations from within the boundary layer of flow with Mach number of approximately 0.3. The current eight by ten inch rectangular exit fiberglass nozzle can only reach half of the desired speed due to limitations of the tunnel motor. It was proposed that the nozzle be modified from its current non-functional state to achieve the necessary speed. This modification would be faster and cheaper than a complete redesign and fabrication.



Figure 1: The existing rectangular exit nozzle

The nozzle as it exists does not provide the necessary back-pressure to load the tunnel blower motor. Because of this, the motor reaches its current limit far before the nozzle exit reaches the desired Mach number of 0.3. The proposed modification was to attach an extension with half of the exit area, which should provide additional back pressure and double the speed attainable. The extension must be capable of supporting a flat, tangential instrument plate and five to ten pounds of instruments, all while withstanding drag. In order to avoid excessive safety instrumentation, the modification is to be designed to a factor of safety of four or more, per Ames safety requirements.

Project Motivation

The NASA strategic plan, strategic goal 5, objective 5.2 is to “Ensure vital assets are ready, available, and appropriately sized to conduct NASA’s missions.” This implies that the wind tunnel facilities (vital assets) at Ames are to be continually maintained and adjusted to support the needs of the agency. From this outcome, the author and his team generated a top- down need hierarchy to justify the project.

- Need:** Bring the NASA Ames Research Center anechoic chamber wind tunnel facility back into full operation and restore full testing capabilities.
- Goal:** Obtain a nozzle with which to run acoustic tests in the anechoic chamber wind tunnel.
- Objective:** Design a modification for the existing 8” x 10” rectangular fiberglass nozzle.
- Constraints:** - Attempt to keep the fabrication costs below three thousand dollars.
- Complete the design, fabrication and calibration before the end of the summer.

NASA Academy History

NASA Academy was founded in 1993 at Goddard Space Flight Center and is a selective summer program focused on honing leadership and professional skills as well as technical prowess. The Academy advertises an experience of “extreme professionalism” and expects its students to live and operate as a tight-knit team, working on individual projects during the day and a group project in the evenings. At the end of the ten week “boot camp-like” experience, the students are inducted into the NASA Academy Alumni Association, a tight professional network of past Academy graduates. The NASA Ames Academy recently split into the Academy for Space Exploration, which is heavily science based, and the Aeronautics Academy, which is heavily engineering based.

FACILITIES

NASA Ames Research Center

NASA Ames Research Center started as a National Advisory Council for Aeronautics (NACA) center in 1939. It is one of the primary NASA assets responsible for aeronautics research and testing. Ames is also the center most active in the field of astrobiology and boasts the world’s largest (80’ by 120’) and second largest (40’ by 80’) wind tunnels. It also has ties with the military, sitting immediately adjacent to Moffett federal airfield. Positioned in the heart of California’s “silicon valley”, the center enjoys big-name neighbors like Google and Microsoft in addition to the nearly year-round clear weather. Many of the facilities are entirely unique and thus Ames enjoys a constant schedule of government and private research and development contracts.

Experimental Aero-physics Branch

The experimental aero-physics branch at Ames is housed almost entirely within the fluid mechanics laboratory (FML) building, N260. Its organizational code is directorate A (aeronautics), division O (wind tunnel operations), branch X (experimental), or AOX. Code AOX is tasked with widely varying projects from planetary entry parachute testing to evaluating the aerodynamics of semi-trucks. AOX specializes in the fields of aeroacoustics, flow visualization, and instrument development.

The FML is one of the most dangerous places at Ames due to its combination of high- power facilities, usage of various chemicals, usage of laser equipment, and usage of tools. Because of this, it has one of the most stringent safety policies in the center; interns undergo almost an entire week of safety training before being allowed to leave the office and use any of the laboratory’s facilities. Measures in place to reduce injuries include sleep hour requirements, personal protective equipment (PPE) requirements, operator certifications and more.

The facilities housed at the FML supply testing capabilities for a wide range of applications. The building holds a total of six mid-sized wind tunnels of various shapes and configurations, with the maximum speed being approximately Mach 0.6, or about 460 miles per hour. In addition, the facility houses a water channel that is often used for simple flow visualization. The FML facilities are powerful while still being accessible and affordable, and are thus some of the favorites for small companies and television programs such as Mythbusters. The building operates its own modest machine shop as well as an instrument development laboratory for invention of new, novel measurement techniques.

The anechoic chamber wind tunnel facility is located in the national full-scale aerodynamics complex (NFAC), building N221, and is operated primarily by code AOX for acoustic and aeroacoustic testing. The facility consists of a sealed test section chamber with fiberglass spikes and pillows coating every surface. Through the test section, a wind tunnel nozzle blows air into a collector which exhausts into the rest of the building. The chamber is capable of negating acoustic reflections between 250 Hz and 30 kHz, maintaining a background noise level of less than 20 dBA. The centrifugal blower is powered by a 100 hp electric motor and is capable of producing a flow of up to Mach 0.5 (about 375 mph) under the right conditions.

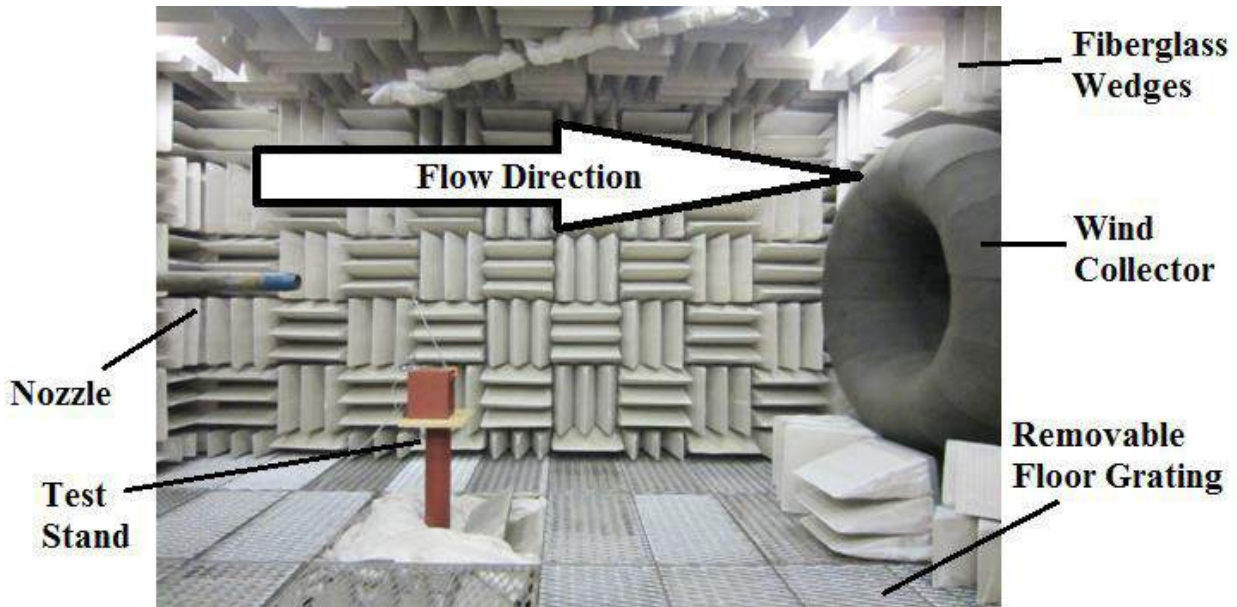


Figure 2: The anechoic chamber wind tunnel facility [1].

Prior to the author's arrival at the facility, the chamber was only being used for static acoustic measurements; the wind tunnel component had not been consistently used for nearly a year. With the additional capabilities provided by the new nozzle assembly, the tunnel will be used for upcoming tests involving measure acoustic levels within the boundary layer of Mach 0.3 flow. The new nozzle will be used in nearly every acoustic test for years to come. These tests will involve using a stand-off microphone array to measure the acoustic vibrations emitted by a model in the flow. Models may vary from scaled launch vehicles to aircraft components to car parts.

BACKGROUND

The driving concept behind wind tunnel testing is that accelerating flow over a stationary body is often easier than accelerating the body itself and allows a stationary observer to examine the effects on the body. Therefore, wind tunnels have been utilized for every manner of aerodynamics testing since the mid-1800's. Wind tunnels come in all shapes, sizes and configurations. They range from makeshift desktop rigs to miniscule hypersonic test sections fed by immense pressure differentials to full-scale facilities such as Ames' 80' x 120' test section, capable of testing a fully assembled Boeing 737.

Anechoic chamber are often seen in recording studios and television stations. They serve to cancel sound reflections and thus reduce echo and produce higher quality sound. The characteristic background noise and sound cancelling capabilities of each chamber vary based on their geometry, materials, intended purpose and quality of construction. The anechoic chamber at Ames is one of the few in the world that doubles as a wind tunnel test section and was built with the primary purpose of developing aeroacoustic instruments for use in the Ames 40' x 80' test section and thus can achieve approximately the same flow regime.

Aeroacoustics is the field of study which examines the acoustic or sound properties of a body immersed in a flow. The field is still heavily experimental as computational aeroacoustics methods are still quite immature and inaccurate, thus aeroacoustics-capable facilities are highly valued. By

studying aeroacoustics, engineers can determine, for example, what parts of an aircraft produce harmful noise or vibrations and redesign the vehicle to minimize the issue. Combined with military stealth interests, one can see that the government would be very interested in such studies.

MODIFICATION DESIGN

Characterization of Existing System

The first step in the design process was to characterize the existing 8-inch by 10-inch nozzle and model it on the computer using the computer-aided drafting (CAD) software, SolidWorks, as can be seen Figure 3. Approximate dimensions were documented, however they needed to be exact given that it was to be modified and fitted with an extension that needed a tight fit and clean edge interface. If a nozzle extension was created too small, then it would not fit onto the existing nozzle; however, if the extension was too large, there would be gaps that cannot exist due to the need for smooth flow along the boundary layer.

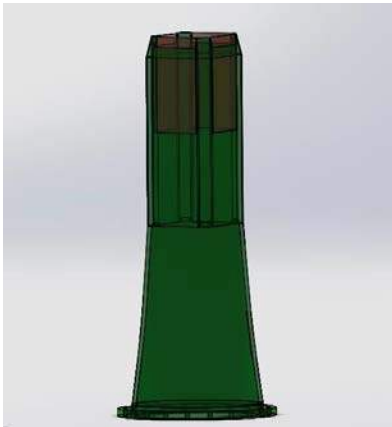


Figure 3: SolidWorks CAD model of existing nozzle.

Table 1: Dimensions of the existing nozzle.

Nozzle		
Len	47.7	[in]
Wall thickness	0.5	[in]
Flange		
Inner radius	16.	[in]
Outer radius	2	[in]
Nozzle		
Height, width	8,	[in]
Corner radius	1.2	[in]
Chamfer length	2.5	[in]
Chamfer angle	1	[deg]
Steel plate inserts		
Len	1	[in]
Thickness	0.2	[in]

The existing nozzle is made primarily of fiberglass. It has four steel plates within the top walls of the rectangular nozzle exit. It is presumed that the metal plates were installed for support and rigidity of the thin tips as a chamfer slims the 0.5 inch fiberglass to a pointed edge. This nozzle attaches to the wall at its base which is a circular flange which acts as the inlet for the wind tunnel's air flow. All nozzles that are compatible with the wind tunnel located in the anechoic chamber have the same attachment system to the wall with twenty bolt holes. The circular flange is contracted with a loft to form the rectangular shape that leads to the exit. The corners of the rectangular portion of the nozzle are rounded so as to smooth the geometry and to reduce boundary layer interactions at sharp corners. Some of the important nozzle dimensions are recorded in Figure 3 and were used to create the SolidWorks model that was referenced for the design of the nozzle extension and attachment system.

Nozzle Extension Design

To produce the flow speed and characteristics desired for upcoming tests, the outlet dimensions of the new rectangular extension were set to 4" in height by 10" in width. In addition, it was decided that the extension must have a place on which to attach an approximately 25 pound instrument mounting plate. Working from a preliminary design provided, a set of

requirements for the extension was drafted and agreed upon by the team and the principal investigator, Clif Horne [2].

These requirements in Table 2 would serve as the team’s guide to completing the project to the specifications, and helped to organize the progress and evaluate the success of the project. Also determined were a set of recommendations; these were either non-critical preferences of the principal investigator or simply points of advice to help in the design process.

Table 2: Project design requirements and recommendations.

Project Requirements:
1. The modified nozzle shall be extended 16” from current length.
2. The modified nozzle shall have a rectangular exit of 4” by 10”
3. The modified nozzle shall be capable of supporting a 20” long by 16” wide flat plate tangent to the air flow at the nozzle exit.
4. The flat plate shall be modifiable for the various test configurations.
5. The design of the assembly shall incorporate a factor of safety of four or more.
Recommendations:
1. Complete the project with a budget of less than three thousand dollars.
2. Modify the nozzle with a removable extension.
3. Fabricate the extension from acrylic.
4. Use a cubic transition curve to design the contraction as to minimize boundary layer growth.
5. Maintain a rounded internal corner geometry.
6. Shrink the rounded corner radius to 0.5”.
7. The existing nozzle tip may be trimmed accordingly to accommodate the new extension.
8. Consider equipment loading in addition to the weights of the components themselves.
a. Extension: add ~20 lbf
b. Plate: add ~5 lbf

The nozzle extension was designed such that the large end would fit relatively tightly onto the outlet of the existing nozzle, with room for insulation to seal the flow. With the outlet geometry mostly set by the requirements, the contraction section of the extension was the primary focus of the design. The contraction was to be designed such that the “height” dimension would shrink from 8” to 4” in less than 16” and while leaving the “width” dimension at 10”. After some research, it was determined that a fifth order polynomial curve was the most efficient profile after which to model the contraction [3]. The boundary conditions of such a higher order curve exceed the recommendations of a third order polynomial in that the boundaries of the curve begin and end perfectly tangential to the axial direction with two inflection points within the contraction. The equation is as follows:

Equation 1: Fifth order contraction equation [3].

$$y(x) = H_i - (H_i - H_e) \left[6 \left(\frac{x}{L} \right)^5 - 15 \left(\frac{x}{L} \right)^4 + 10 \left(\frac{x}{L} \right)^3 \right]$$

Table 3: Contraction equation symbols.

Parameter	Symbol	Value	Unit
Vertical position	y	variable	[in]
Horizontal position	x	variable	[in]
Inlet height	H_i	8	[in]
Exit height	H_e	4	[in]
Contraction length	L	8	[in]

It was also determined that the optimal contraction shall feature a contraction length equal to the inlet height, thus the curve was designed to fully contract in a distance of only 8". Incorporating the inlet and outlet chamfer sections, a SolidWorks model was generated with optimal contraction and a constant wall thickness of 0.5". Knowing that the future plans of the extension include fitting it with a removable instrument plate, a bracket with pre-made holes was incorporated into the outside of the model for mounting such a fixture.

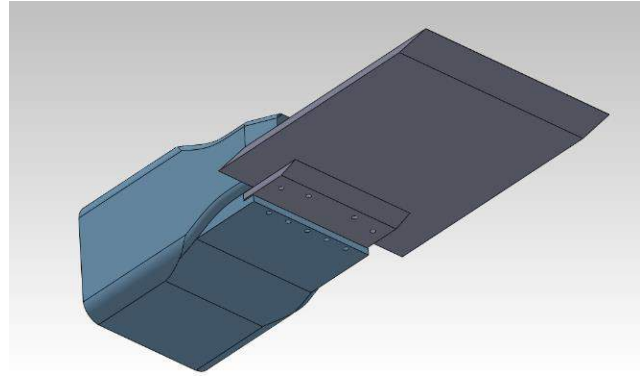
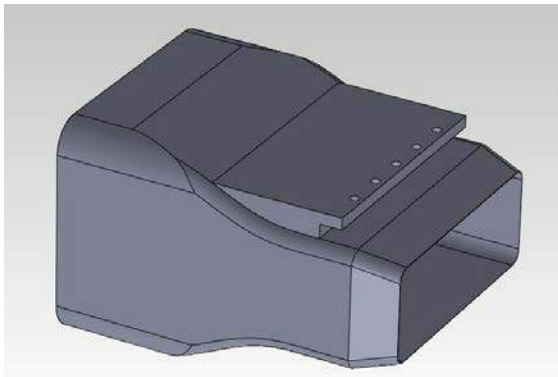


Figure 4: Solid model of the nozzle extension. Figure 5: The model fitted with a blank instrument plate.

Several options were examined to manufacture the nozzle extension, including cast acrylic, machined aluminum and various methods of three-dimensional printing. In order to provide the highest degree of accuracy for the fifth order contraction, and to avoid the prohibitive expense of computer-numerically-controlled (CNC) machining (~ \$10k), three-dimensional printing was chosen. Several companies were polled for production quotes; most returning invalid results due to their printers being unable to fit the bounding-box of the model, others returning prices in excess of five to six thousand dollars for a part manufactured by Stereolithography (SLA). Finally, a company with a large enough selective laser sintering (SLS) machine was found. Shapeways could manufacture the part for just over three thousand dollars and have it delivered in less than two weeks. The length of the part between the inlet and contraction was trimmed modestly, bringing the price within budget to \$2905.81. The part was manufactured and arrived at the laboratory in just under one week.

SLS manufacturing consists of fusing powdered plastic, ceramic or metal via laser pulse. A powder bed is traced with a high-powered laser in the desired pattern. Once the layer is complete, a new layer of powder is brushed over the top and the process repeats. Once every layer is fused to specification, the loose un-fused powder is removed and the solid part is cleaned. Modern SLS technique can precisely and efficiently construct intricate models and pieces of hardware from a

computer model in a matter of hours. The material used by Shapeways to manufacture the nozzle extension is called “fine polyamide PA 2200”. It is a strong, non-toxic plastic similar to nylon. The mechanical properties of the material were suitable for the purposes of this project and are detailed in the table below.

Table 4: PA 2200 plastic material properties [4].

Property	Value	Unit
Bulk density	0.45	[g/cm ³]
Tensile modulus	247	[ksi]
Tensile strength	6962	[psi]
Elongation at break	24	[%]
Melting point	172-180	[deg C]

Computational Flow Analysis

To verify the expected performance of the nozzle extension, a full system CAD model was assembled in SolidWorks and a flow simulation was performed. The existing nozzle model was fastened to an inlet in a simplified analog to the anechoic chamber. The extension was attached to its end and flow was blown through the nozzle into the collector, as represented by an atmospheric pressure sink. A simple sphere was also added to the jet flow simply to verify the model’s handling of flow redirection. Below, Figure 6 and Figure 7 show the flow simulation setup and preliminary results.

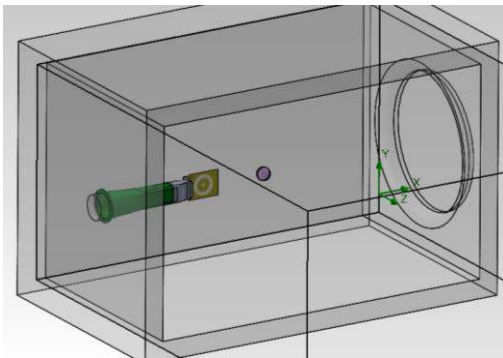


Figure 6: Flow simulation model setup.

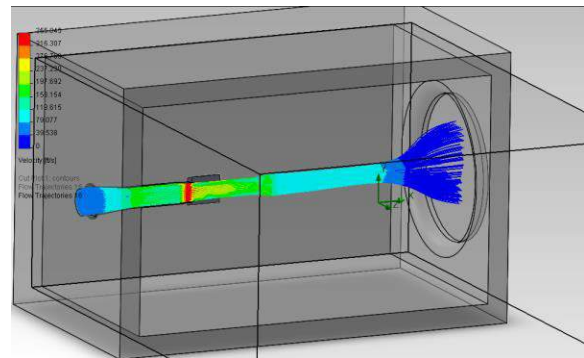


Figure 7: Preliminary flow simulation data.

In Figure 8, note the higher velocity (warmer colors) at the nozzle contraction and very low velocities at the collector. This preliminary simulation served to verify that the model is functional, the chamber and nozzle behave at least roughly as expected, and that the nozzle is capable of achieving the proper Mach number when fed the proper air mass flow rate. The preliminary visualization however includes only air that has passed through the inlet, and provides no insight on the entrained flow around the potential core.

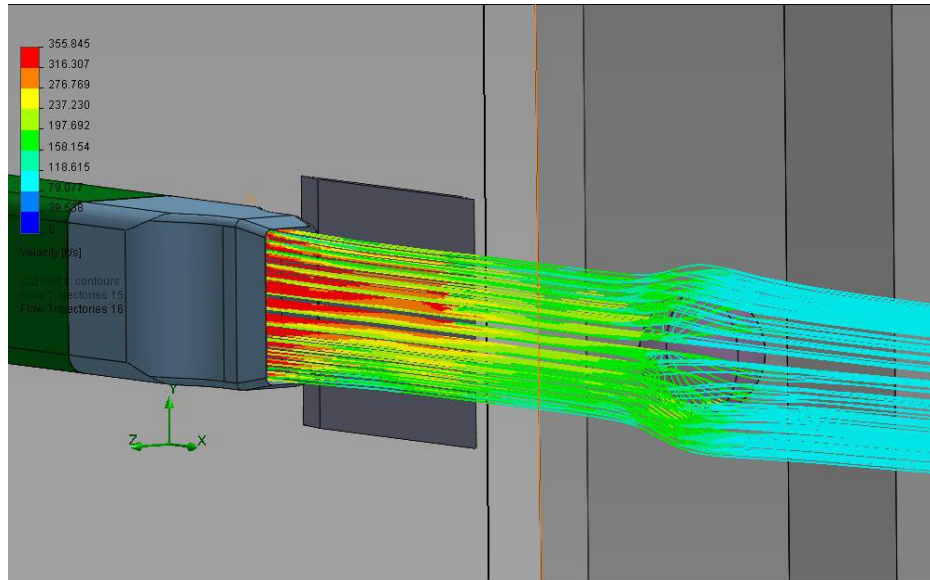


Figure 8: Preliminary flow visualization of the potential core flow over a generic sphere.

To further characterize the expected flow patterns, higher resolution flow simulations were performed, this time generating velocity cut plots along each of the two axes of symmetry of the nozzle exit. These plots detail the velocity of the air flow as it passes through the nozzle, out the extension, and over the instrument plate to dissipate in the chamber. From these images, experimentalists can know what to expect in terms of the size of the flow boundary layer and potential core; it is very important to know the capabilities of wind tunnel equipment when planning experimental tests. Figure 9 shows the velocity of the flow in the top-view midplane of the nozzle exit. Warmer colors indicate higher velocities while cold colors indicate slower velocities. From this image, the experimentalist can know what sort of boundary layer to expect from the instrument plate attachment.

Warmer colors indicate higher velocities while cold colors indicate slower velocities. From this image, the experimentalist can know what sort of boundary layer to expect from the instrument plate attachment.

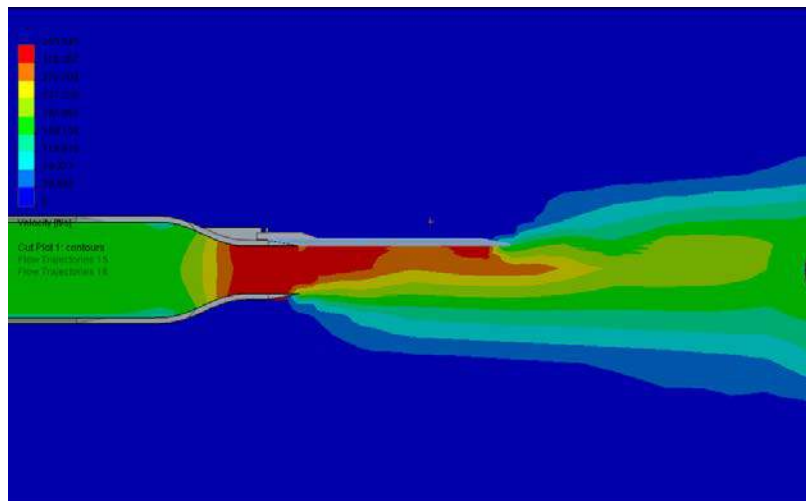


Figure 9: Cut plot across the minor axis of the nozzle.

From a side perspective, Figure 10 shows the decay of the potential core of the flow. In this image it is important to note how the core decays from a parabolic velocity distribution quickly after passing over the instrument plate (the blue highlighted square). The core then shrinks toward the center as the outer entrained air spreads to dissipate in the chamber and pass through the collector.

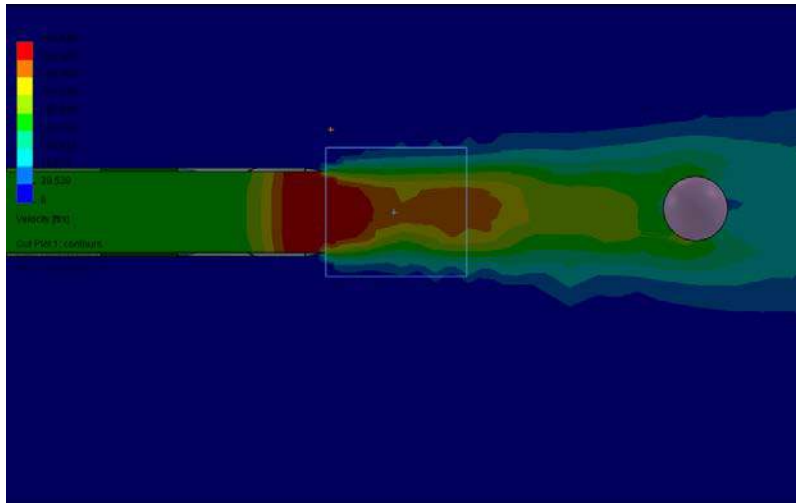


Figure 10: Cut plot across the major axis of the nozzle.

In addition to providing detailed fluid dynamics maps and images for experimental reference, this analysis served to provide the expected drag force that would be experienced by the nozzle extension. By integrating the pressure distribution over the internal surface of the extension and adding in a minor component of skin friction drag, the total axial force on the extension was calculated.

Table 5: SolidWorks drag data.

Goal Name	Unit	Value	Averaged Value
SG Normal Force 1	[lbf]	22.14755188	21.94017185
SG X - Component of Normal Force 1	[lbf]	22.12074724	21.91319018
SG Y - Component of Normal Force 1	[lbf]	-1.087854893	-1.086201424
SG Z - Component of Normal Force 1	[lbf]	-0.056278476	-0.057202415
SG Force 2	[lbf]	23.39311404	23.18608098
SG X - Component of Force 1	[lbf]	23.36782619	23.16063508
SG Y - Component of Force 1	[lbf]	-1.085936043	-1.084373937
SG Z - Component of Force 1	[lbf]	-0.056800659	-0.05778232
SG Shear Force 1	[lbf]	1.247080536	1.247446377
SG X - Component of Shear Force 1	[lbf]	1.24707895	1.247444899
SG Y - Component of Shear Force 1	[lbf]	0.00191885	0.001827487
SG Z - Component of Shear Force 1	[lbf]	-0.000522184	-0.000579905

By examining the data in Table 5, one can see that pressure drag (normal force) comprises approximately 20 pounds of axial drag while internal skin friction (shear force) accounts for about one pound. Together, the part experiences approximately 23 pounds of axial drag while operating at an approximate Mach number of 0.3.

Please see the attached full-length report for details regarding the subsequent high-resolution CFD analysis, attachment design and implementation and testing results.

AERONAUTICS ACADEMY GROUP PROJECT (RAPTOR)

As part of the NASA Academy program, students are required to participate in a group project in addition to their “day job” individual project. The 2013 Ames Aeronautics Academy was tasked with building and testing a set of quadcopters while studying their feasibility for a scaled-up passenger transportation system to supplement the existing system in the San Francisco Bay Area. The project was comprised of two major efforts: one to examine the theoretical feasibility of such a system and design the large-scale rotorcraft, and the other to build quadcopters and rovers to simulate the route logistics and air traffic operations on a small scale. The author was tasked primarily with heading hardware integration and testing, piloting, as well as serving as technical liaison to the software group.

Details on this project can be found in the attached full-length report.

ADDITIONAL PROJECTS

The FML is a unique place even within NASA Ames. Its eclectic assortment of facilities and the broad expertise of its employees, along with the large intern force they take on each summer, make it a magnet for projects seeking skillful resolution. The main lobby proudly displays artifacts from numerous projects, big and small, that have been involved with the FML in some way; there are models of ships, planes, spacecraft, tennis balls and trucks. This reflects directly on the interns; there is rarely a student who is responsible only for their individual project. As such, below are detailed a few side projects that the author participated in throughout the course of the main project.

Instrument Panel Redesign & Fabrication

To support stationary acoustic tests taking place in the anechoic chamber, the author’s team was asked to redesign instrument panels to fit a new array of sensor equipment. The team was given the CAD drawing of the previous instrument panel and asked to modify it for the new instrument layout; the team then had the new plates cut from aluminum with a precision water jet machine and assembled the new boxes for installation in the laboratory.

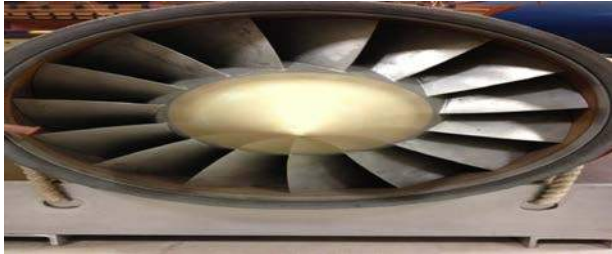


Figure 11: The newly machined faceplate

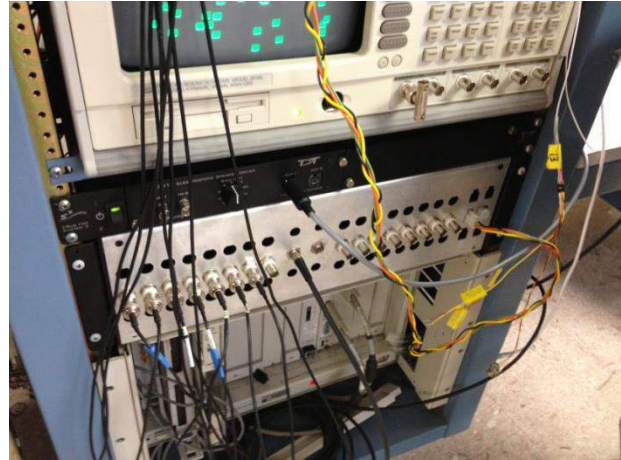


Figure 12: The new assembly in use

Jet Engine Reverse Engineering

Slated to be disposed of from storage at another lab at Ames, a small jet engine was acquired by the FML during the summer of 2013. The engine was missing most of its plumbing and a soft grinding could be heard from the turbine when the shaft was spun. Due to the damage, it was decided that the engine was not worth refurbishing to running conditions and would be better put toward educational usage, possibly by cross-sectioning the entire assembly.

Mostly unmarked and lacking any documentation, its model and manufacturer were entirely unknown and a reverse engineering process had to be set into motion. The exercise was a lesson in deductive reasoning and analytical research; every bit of information had to be drawn from the case of the engine and researched tirelessly.



Figure 13: The engine as it sits in the FML high bay

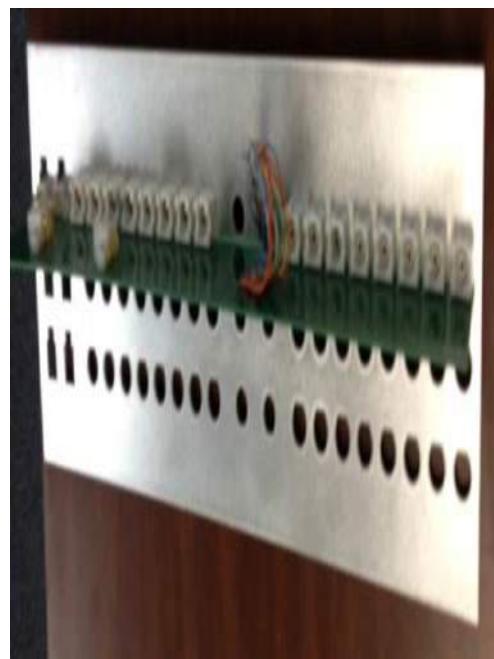


Figure 14: The inlet of the engine

Upon close inspection, it could be noted that the engine was a low bypass ratio turbofan, the fasteners used were metric and it was mostly unmarked. It is relatively lightweight but the construction is not impeccable, it could be surmised that the engine was of “disposable” nature, such as those used on unmanned aerial vehicles (UAV’s), air breathing launch vehicles and cruise missiles. The metric fasteners suggested, but did not mandate, a non-United States country of origin. Armed with this knowledge, several engine manufacturers were picked as possible candidates. Teledyne, Microturbo and Williams International all had engines of comparable size and use.

It was finally determined that the engine was a model P8300-15 turbofan engine, manufactured by Williams International. It was used as the main propulsion for the German TAURUS KEPD 350 air-launched cruise missile, which are still in use but are no longer manufactured [6]. This explanation accounts for the disposable design, metric fasteners and lack of marking characteristics. This model of engine is not listed on Williams International’s list of discontinued or currently in production engines, most probably due to its use as propulsion on a German cruise missile. After further investigation, it was found that NASA had approximately 15 of these engines and was using them to simulate larger engines in Ames’s wind tunnels.

Education & Public Outreach

The FML is one of the most popular tour destinations at Ames, primarily for its wide array of facilities and testing history, as well as for its laid-back nature and willingness to run equipment right before the eyes of the visitors. Being a busy branch, the FML expects its summer interns to conduct tours for the nearly one thousand yearly visitors. This helps the interns gain public relations skills and gain experience running the FML’s facilities.

Upon their return to their home universities, many Academy students already have plans to give informational outreach presentations on behalf of their state Space Grant Consortia. It is the hope of the authors that these presentations serve to increase application and enrollment in NASA and other aerospace and STEM programs, and to inspire the next generation of explorers, as only NASA can.

On August 22, 2013 the Aeronautics Academy group project was presented to the entire Ames Research Center in a centerwide press release. It is the hope of the authors that this presentation served to strengthen the reputation of the Academy program within the ranks of the agency and secure support for its continuation through the coming years.

Each week throughout the course of the summer, one Academy student was responsible for operating the NASA Ames Academy Twitter account. There, posts were dispersed to the public detailing the experiences of the Academy students, hopefully raising the reputation and visibility of the Academy program within the ranks of college and university students.

CONCLUSION

At the conclusion of the summer, many changes had been made to the anechoic chamber wind tunnel facility. These changes range from minor corrections to previously existing documentation to generation of pages of calibration data and reactivation of the tunnel. These major results are listed below.

- The 4” by 10” nozzle is now operational, making the anechoic chamber wind tunnel once again desirable for active blowing aeroacoustic testing.
- The 4” by 10” nozzle has been calibrated.
- The 7” circular nozzle has been calibrated.
- The tunnel’s LabVIEW remote operation program has been calibrated.
- The anechoic chamber wind tunnel SOP has been revised and experimental calibration data for both the 7” circular and the 4” by 10” rectangular nozzles has been added, as well as LabVIEW calibration data.
- Code AOX is now in possession of detailed CAD representations of the 4” by 10” nozzle as well as its associated CFD generated flow patterns for experimental reference.

At the completion of the project, it can be noted that nearly all initial requirements have been met. One of the exceptions being requirement 1, which was relaxed at the permission of the principal investigator; the nozzle extension was shortened in order to reduce its manufacturing cost and because the requirement was arbitrary. In addition, recommendation 3 was relaxed, and the extension was manufactured by means of SLS rather than acrylic for concerns of cost. Finally, recommendation 4 was upgraded from a third to fifth order polynomial contraction curve.

Unfortunately, while many additional goals were completed that were not initially foreseen, some of the initial goals of the project were not met. The next step, which is already being pursued by PI: Clif Horne, is to finalize the design of the microphone array and instrument plate to be attached to the extension, fabricate the piece and put it into operation, taking acoustic measurements from the boundary layer of the nozzle exit flow.

In addition, Clif and others in the aeroacoustics team are planning testing involving aiming phased microphone arrays at models placed in the flow of the nozzle. These phased arrays will be capable of comparing the timing of vibrations to localize the source of the noise. These tests will serve to optimize aircraft, automobile and rocket components to minimize noise, harmful vibrations and energy losses.

ACKNOWLEDGEMENTS

The author would like to sincerely thank and acknowledge the following for their support throughout and beyond this project:

- Project teammates Karly McLaughlin (MIT) and Christina Middleton (Cornell)
- Principal investigator: Clifton Horne
- Experimental aerophysics branch chief, Rabi Mehta
- Fluid mechanics laboratory intern manager, Kurtis Long
- The 2013 NASA Ames Aeronautics Academy staff and administration
- Lockheed Martin
- NASA Ames Research Center
- The NASA West Virginia Space Grant Consortium

REFERENCES

- [1] Ames Fluid Mechanics Laboratory, Anechoic Chamber Wind Tunnel Safe Operating Procedures, 2013.
- [2] Clifton Horne, Preliminary Nozzle Extension Design, 2013.
- [3] Kurtis Long & Christina Ngo, Presentation: Wind Tunnel Components, 2012.
- [4] EOS Manufacturing, PA 2200 Material Data Sheet, 2008.
- [5] R. D. Mehta, "Sports Ball Aerodynamics," 1985.
- [6] RPDefense, 2013. [Online]. Available: <http://rpdefense.over-blog.com/tag/South%20Korea/>.
- [7] *Air Properties*. [Online]. Available: <http://www.engineeringtoolbox.com/air-properties-d_156.html>.
- [8] "AISI Steel Mechanical Characteristics - Yield, Tensile, Elongation, Hardness, Izod - Engineers Edge." *AISI Steel Mechanical Characteristics - Yield, Tensile, Elongation*,
- [9] "EFunda: Properties of Carbon Steels Details." *Properties of Carbon Steels Details*. EFunda, n.d. Web. 10 July 2013.
- [10] R.E. Kaunda. *Cardiovascular Physiology Concepts*. N.p.: n.p., n.d. Print.
- [11] S. Silverman. (2011, July 26). *The Average Pitching Velocity*. Available: <<http://www.livestrong.com/article/501890-the-average-pitching-velocity/>>.
- [12] *SOFTBALL 2012 & 2013 Rules & Interpretations*. [Online]. Available: <<http://www.naia.org/fls/27900/1NAIA/resources/sid/Rules%20Books/SBR.pdf>>.
- [13] *Spin Rate Data*. [Online]. Available: <revfire.com/coaching_data.htm>.
- [14] *Symscape: Computational Fluid Dynamics Software for All*. [Online]. Available: <<http://www.symscape.com>>.
- [15] *What's the Average Pitch Speed?*. [Online]. Available: <http://www.mizfastpitchdiamonds.com/news_article/show/9307?referrer_id=312>.

A STUDY OF HIGH TECHNOLOGY APPLIED TO THE WOOD INDUSTRY IN WEST VIRGINIA

Conor Forrester
Department of Physics and Engineering
West Virginia Wesleyan College
Buckhannon, WV 26201

ABSTRACT

For the second consecutive summer, the Physics/Engineering Department at West Virginia Wesleyan College has presented me with a research opportunity. This summer, the focus was to work with Jim Hinkle and his staff at the West Virginia Split Wail company in Buckhannon, West Virginia. My main area of study was to become familiar with the various steps and processes of the workplace. This would provide me with great hands-on experience with an industry of which I don't have prior knowledge. By becoming familiar with the history of wood products and this industry I could then begin to focus on the proposed area of study, which is to offer new product possibilities or suggestions to the company.

INTRODUCTION

The use for wood has been around from the beginnings of human adaptation. Through its use in war, farming, construction, and agriculture, humans began to quickly understand wood's capabilities and necessities to everyday life. Its physical properties and strengths were immediately noticeable, eventually leading to the research of its chemical and biological complexions. Today, wood has evolved into a grand material in industrial engineering aspects. The ability for wood to be readily available in these industries speaks volumes of its value and importance.

BACKGROUND

The uses of wood involved the consideration of quality, cost, and availability. Techniques with copper tools that began thousands of years ago have lead to the extensive tools and modern construction industry that we experience today. Through today's process of krafting and pulping, boards can be precisely fitted and matched, along with reaping the benefits of wood's most natural materials. Wood also transformed the idea of transportation, starting with the magnificent invention of the wheel. Breakthroughs in the United States emerged as wood became a large factor for the railroad industry in energy sources, bridges, and railroad cars ("History, Nature, and Products of Wood." pg. 1). Wood was first used in the housing with the formation of log cabins from large, straight trees. As this industry progressed, wood was used for foundations for concrete as well as truss and roof supports.

Plywood and veneer have long been known for their influence on international trade and supply due to their decorative value. Highly-decorated arts have been used with veneer products dating back to the ancient Greeks, Romans, and Egyptians. The development of softwood plywood was not seen until the 1900's in the United States. Thin layers of softwood were glued together at

certain angles along grain lines to form this type of wood. Thus also emerged the creation of weather-resistant adhesives, particularly in demand during World War II.

Another important wood development in the late 19th century was wet process fiberboard. Manufactured from natural and recycled fibers, they are ideal for green building components. There are no timber or tropical forestry products used in this process, making fiberboard very helpful to the environment and cost efficient as well. The sawmill industry plays an important role by providing recyclable content such as sawdust, wood chips, demolition wood, and post-consumer kraft paper. Producing wet process fiberboard utilizes the use of closed-loop water systems, which allows massive amounts of water to be recycled (“What About Fiberboard for Green Building?” pg.1). Again, this makes fiberboard very efficient to the environment and the economy.

There are currently over 340 wood processors and 15,000 employees in the West Virginia wood industry. The quality of wood is getting very high marks among national competitors. Oak and hickory are the dominant forest groups. Although, yellow poplar, black locust, sweet gum, and red maple are important woods to the West Virginia Region as well. West Virginia is the third most forest-covered state in the nation (“Wood Products.” pg.1). Spanning 12 million acres and harvesting 75 billion feet of timber boards, West Virginia is home to a very thriving wood industry.

There are many areas of profitability for this industry including occupations such as team assemblers, cabinetmakers, bench makers, carpenters, woodworking machine operators, material movers, and saw machine operators. Each wood company in West Virginia can be expected to make a profit of 2 million dollars a year solely from labor costs (“Wood Products.” pg.1). This is due to the low cost of living in West Virginia, which in turn make labor costs lower. There is also the price of utilities to consider. West Virginia companies may save up to one-hundred thousand dollars annually compared to companies in neighboring states. This is largely because of the low electric rates throughout West Virginia.

The system of highways throughout West Virginia proves to be very effective for transporting products across the state. The highways are also use for intermodal transportation if products need to be shipped by trucking, air, water, or rail. Therefore, products from West Virginia have very reliable shipping sources to the Northeast, South, Midwest, and even internationally.

Soon after transportation advancements propelled the wood industry, scientists began to discover the benefits from lignin and its biodegradation processes. Lignin is an important emerging material in the efforts to find useful biodegradable resources. However, lignin is an undesirable product at the end of the process of turning wood into paper because of color, poor mechanical properties, and it is too porous. Lignin must be removed during the digestion of wood without causing damage to the cellulose fibers through the process of krafting. Lignin is an amorphous three-dimensional substance. Its molecular weight is a task to determine because of the polydisperse molecular structure (Buchberger, Javor, Tanzcos. Pg.1). White-rot fungi organisms are known to have the most effective natural processes of degrading lignin within wood. Through this, they are also a major agent for recycling carbon tissue from lignin (Hatakka pg.1). They are a group of taxonomically heterogeneous higher fungi because of their ability to depolymerize lignin with a specific set of enzymes. They are also other effective fungi capable of depolymerizing lignin, as well as compost and bacteria in soil.

Because carbon comes largely from lignin, or the processes that break down lignin, this places lignin at the center of natural recycling. Because of its rather recent discovery, lignin degradation has not yet been fully determined chemically. The enzymes are certainly valuable as they have provided methods of effective environmental protection within the wood industry. Proper treatments of many xenobiotic compounds, stains, and dyes are good examples of the enzyme capabilities.

Some common products are produced from the contribution of the biodegradation process including calcium, sugars, sulfur, and water. Specific sugar products such as calcium lignosulfonates can be provided to customers with carbon-based sugar needs. Lignosulfonates are great reducers in concrete mixers because of their excellent water-insolubility (“Lignin Products and Uses.” Pg.1). Other uses include mineral pelleting and granulating production aid, oil drilling additives, animal feed additives, road dust controllers, Torula yeast production, and dispersants in the construction and wood industries. Because of its natural carbon-based chemical complexion, lignosulfonates are also approved to be used in organic products.

The chemical composition of cellulose, lignin, and other extractives also gave a greater understanding about wood and how it could be used in the industry. There is a specific chemical composition for wood that includes cellulose, hemicelluloses, lignin, and extractives. The product properties depend on the contributions to the fiber properties from the chemical compositions of the wood.

Cellulose is the major component of the fiber walls and makes up about 40-45 percent of the dry weight of wood. The chemical composition of cellulose consists of linear chains of D-glucose linked by β -1,4-glycosidic bonds. The molecular structure allows cellulose to contain properties such as hydrophylicity, chirality, degradability, and broad chemical variability initiated by the high donor reactivity of the hydroxyl groups. Cellulose also tends to make strong bonds with hydrogen from the hydroxyl groups, giving cellulose a sturdy crystalline structure. The purest form of cellulose has been found to contain two very complex crystal phases: $I\alpha$ and $I\beta$. $I\alpha$ -rich specimens are usually found in cell walls of algae as well as bacterial cellulose. $I\beta$ -rich specimens are usually found in the fibers of cotton, wood, and ramie. The solid structure of cellulose, with pockets of chemical instability, and the size of the fibers all contribute to the rigidity and flexibility of the wood. Chemically treated woods have an even greater limit to accessibility to water and other chemicals (“Chemical Composition of Wood.” Pg.1).

Hemicelluloses have a much lower degree of polymerization than that of cellulose; cellulose ranges from 1,000 to 10,000 while hemicelluloses range from 30-500. The main hemicelluloses of softwood are galactoglucomannans and arabinoglucuronoxylan while hardwood contains glucuronoxylan.

There are also two important chemical processes to consider with cellulose and hemicelluloses: kraft pulping and kraft cooking. Kraft pulping is the process of turning wood into wood pulp. The wood is first wetted and preheated with steam. After being placed in a pressurized vessel and treated with sodium sulfide, it is time for the cooking process. The goal of this process is to eliminate lignin, which connects the fibers together in the wood. This leaves only the pure fibers of cellulose. Following this is the aggressive bleaching of the pulp with oxidizing agents as well as caustic soda. The recovery process finally allows for the delamination of the cell wall and

collapse of lumen. There are many functions from these processes; most of them being paper related. This includes corrugated boxes, office papers, liquid cartons, high-grade folding boxboard, labels, bags, and cups. Magazine pages also contain some pulp to give them resistance to folding and extra strength. One of the desired strategies for use of kraft processes is refining. If refining is done correctly, bonding strength conditions will be met. Refining is most commonly done by controlling the amount of flow to a refiner or controlling the amount of energy expended per dry mass of pulp (“Kraft Pulp.” Pg.1).

Extractives account for about one to five percent of the composition of wood. They are relatively small molecules and are not located within the cell wall. There are lipid extractive components, phenolic extractive components, alkanes, proteins, and monosaccharides among the usual extractives in wood. They can be extracted through wood or bark with solvents such as ether, acetone, ethanol, or water. Resin acids and fatty acids help give characteristics to hardwoods and softwoods because it is water-insoluble (Cole pg.1). Resin acids in softwoods count for forty to forty-five percent of extractives with forty to sixty percent being fatty acids. Hardwoods contain no resin acids and have a higher concentration of sixty to ninety percent of fatty acids among the extractives.

DISCUSSION

After conducting a good amount of background research on the history of the wood industry, both worldwide and in West Virginia, I could begin to focus on specific areas of interest at the West Virginia Split Rail company. Two types of common trees they use, including yellow poplar and yellow pine trees soon became topics to focus on as well. Structural laminated-glued (glulam) timber is a very efficient source of timber in the engineering aspect of the wood industry. Bridges of the stress-laminated and deck-and-stringer designs along with long-span roofs can all incorporate the practical use of Yellow Poplar. These trees are very strong and flexible, thus making their abundance in West Virginia very advantageous to the surrounding region (Davalos, Hernandez, Russell, Sonti pg. 1).

Yellow pine does not refer to one specific tree, but rather a group of different species of pine trees that resemble a yellowish color of wood. These include the Loblolly, Longleaf, Shortleaf, and Slash Pines. It is found naturally within the forests of the Northeastern United States (Whittemore pg.1). As the tree matures, most of the lower branches die, leaving a large portion of the tree bare. Because of this, it is very valuable within the timber industry.

Dr. Wiest, Dr. Popson, and I met with Dane Moore to discuss my how I could begin to gain knowledge about the sawmill industry. Dane is the inventory manager of the West Virginia Split Rail company. Working alongside fellow managers Keith Barbo and Mark Waldo, they collaborate well in their areas of expertise to make a smooth running for the company. My task under Dane was to look for new ways to improve the methods and steps within the sawmill and also to suggest overall new procedures or products from my observations and analysis.

OBSERVATIONS

I received a tour from Larry Riley, one of the mills supervisors. I first observed the logs being brought from the trucks by the forklift. They were placed in the debarker where they were then stripped of bark, knots, and other outer imperfections. The logs would then be allowed to roll

slowly down next to the head saw that would place the logs in a position to be properly cut to the appropriate thickness. The clamps held the logs very steady as the saw rapidly cut through and retreated to its original position. The operator could then re-adjust the log by gradually nudging a lever to twist the log so that it could be cut along a different path. This allowed for the most production that was possible to be achieved from each log. The boards then traveled along a conveyor belt where they were specifically shaped into ideal fence posts by the rail pointer. Some of these fence posts would be manually carried to a router machine where the board would be manually lined up with routers to make precise holes in the posts. Both sets of posts were then bundled together to be sent off for shipping in trucks. All of the bi-products from these processes in the form of chips, sawdust, and bark were salvaged and sent up to the Kingsford factory in Parsons, West Virginia. Dane explained to me the importance of establishing a market for a mill's bi-products or else the mill could not sustain itself as a business.

I took a bit of time to observe and research how each part of the mill works. The entire mill is fairly a low technology system but it does work fast and efficiently from what I quickly saw. The debarker was the easiest machine for me to fully observe because I could stand directly beside the operator's side without blocking his workspace and it was in a clear view for me.

The debarking process at WVSR involves the use of a Rosser head debarker. These debarkers are most common throughout hardwood sawmills. Debarkers are very useful for removing damages within the bark and other material such as gravel and mud from the sawmill yard. At WVSR, the logs are placed on a small pile held by several metal prongs. The operator then has control of releasing the logs one at a time onto a conveyor belt that leads the logs toward the debarker. The logs are fed into the debarker from a separate infeed conveyor. The log is fed into a cradle that is spun by rollers. At the same time, a rolling cutter passes along the log as its length is slowly passed through the system. The teeth in the roller cut to about a depth of one inch into the wood (Froome pg.1). The system motor is powered by hydraulics technology. While a log is being debarked, a second log can be simultaneously lined up in front of the debarker on the separate conveyor belt. The operator can then pass the first debarked log onto the outfeed conveyor and immediately enter the next log into the debarker. At times, the operator may need to use a chainsaw to remove large knots before it enters the debarker. The operator can also reverse logs after going through the debarker, should they need to be touched up once more. While observing, I concluded that the operator must be alert and dedicated to the process as there are many levers for different parts of the operation.

The head saw also ran off of hydraulics technology as it swung rapidly back and forth to precise locations to make flawless cuts again and again. Dane had recently upgraded the saw system by adding clamps, which held the log in place to avoid any miscuts. The rail pointer is the most complicated machine in the mill because it runs off a series of computer programs to properly shape each rail. It was difficult thus far to see how I could suggest new ways of improvement considering Dane and his staff had just made upgrades to the mill and were not particularly looking for change.

Dane showed a large set of data that he had taken since September 26, 2006 on the efficiency of the mill. The key factors in the set of data focused on the number of miscuts as well as the number of junk boards. The miscuts occurred from either the head sawyer not lining up the machine correctly or if the machine's grip slipped slightly. Both scenarios ended causing a cut that resulted

in wasting the board. Each miscut totaled four dollars to account for the loss of production. Dane had kept track of the number of over 38,000 total miscuts since the beginning of his spreadsheet, which totaled to nearly 155,000 dollars in costs of loss of production. The junk boards are simply boards that contain too much rot, knots, or other imperfections that will not satisfy as proper fence posts or fence lines. Dane explained the junk boards he was okay with because how can someone detect that there will be a defect too great to use in the industry? It is an unfortunate natural occurrence. The company had been searching for a way to limit the number of junk boards as they had been reaching anywhere from 15 to 35 miscuts per day for the past several years. As I mentioned earlier, they had introduced a new system where they installed clamps to hold the log in place so the head sawyer and the machine would not make as many mistakes. Within the first day, the number of miscuts was cut in half from twenty three to twelve. Within the following five days, the installation has proved to be a great investment with the number of miscuts dwindling to five over the course of five days.

Dane shared with me some insight on his business with the lumber mill in Keyser, West Virginia. West Virginia Split Rail receives truck loads of logs from the Keyser mill and pays the mill a certain rate per ton. Dane also does business with the Petersburg mill in West Virginia. West Virginia Split Rail incorporates the valuable use of Macola software to maintain inventory communication between inventory and sales. There is constantly production to be done within the mill operations in order to meet allocated needs of customers. The inventory builds heavily throughout the winter months of well over 200,000 rails. During the seasonal months of April and May, the mill has sold their entire inventory and has been well under way with a successful supply and demand system.

Macola, an Exact software, is designed to improve organization and profitability in the workplace (“Exact Macola Review.” Pg.1). Sales, marketing and inventory are the focus points of software users. It is ideal for West Virginia Split Rail because it is a small size business looking to communicate its business and products. As inventory manager, Dane can use Macola to quickly match his confirm and organize his production orders. A key factor in using Macola is to keep the spreadsheets well organized. For example, if incorrect information is scheduled within the spreadsheet and it is not readily available in the mill, a trucker from a customer company may travel a great distance only to be disappointed with no raw material of which to take back. This is costly because now the trucker must be paid for his travels but no product has been sold. Therefore, communication must be a top priority between the industrial, inventory, and sales managers.

The drying kiln is a very important part of the sawmill system. Immediately after the manufactured products are cut, they are placed in the drying kiln. West Virginia Split Rail operates the kiln based on a piece count of rails rather than a total amount of board feet simply because it works better for the company. The average yellow pine post is cut to about 3x6x6 feet. Considering the dimensions of the kiln, there can be up to about 60,000 board feet in the kiln at one time. This is equivalent to four tractor trailer loads.

The kiln uses natural gas as its source of heated energy. The gas is used on contract and therefore is much cheaper than the average price of gas. A 2,000,000 BTU burner is used to power the kiln. It works by heating a winding pipe to high temperatures, hot enough so that the pipe gives off an orange tint. Then, air is circulated by a series of three fans throughout the kiln. By sweeping through and extracting the heat from the pipe, the air can then circulate through the bundles of

wood to begin the drying process. The air is also circulated on and off in both directions to ensure maximum dryness in the five day process to dry the posts. It is also important to vent the kiln at certain times. Otherwise, the air will become saturated with too much water vapor and stall the drying process. The venting method is used during the day at WVSR because there is a higher ambient temperature during the day than at night. This will help save energy simply because the burner will not have to use as much fuel to convert the ambient air to the desirable temperature within the kiln. The installation of panels in the vents prevents the expelled saturated air from re-entering into the kiln, which gives a much more effective circulation of air. The pressure within the kiln remains ambient as it is not tight enough to contain various air pressures.

Before the posts are dried within the kiln, they are immediately treated with mildewcide. This form of surface treatment serves as a temporary solution to keeping mold and mildew from growing on the posts. Essentially, the mildewcide kills the sap on the surface of the posts that would otherwise serve as a food source for mold and mildew. Besides having a food source, mold and mildew also need water and heat to survive. After having the sap taken away during the surface treatment of mildewcide, the drying within the kiln takes away the existence of water. Therefore, mold and mildew are no longer issues after these two processes.

Only dry posts are dried within the kiln rather than rails. Because rails are not in direct contact with the ground, they do not need to be dried. The yellow pine posts dry fairly quickly and are left in the kiln from Monday morning until Friday afternoon. The moisture content of wood is surprisingly heavy as it nearly matches the weight of the wood. For example, ten pounds of a twenty pound post would consist of water. The free water of the post is the water that the log will give up freely and naturally over the course of a few days. This accounts for seventy percent of the water in each post. The remaining thirty percent of the water in each post is known as bound water, in which this water is extracted by means of the kiln. This water is difficult to extract because the cellulose chemistry holds the hydrogen bonds closely together. By heating the kiln to a high temperature, it will get the hydrogen molecules moving and ultimately breaking free of the oxygen molecules. However, it is impossible to extract all water from the posts, especially in the course of five days. Therefore, a goal of twenty percent bound water remaining in the posts has become the desired amount at WVSR.

ANALYSIS

The idea of partial vacuum kilns got me thinking that this would be a good method to suggest towards the West Virginia Split Rail company. There are many positive effects by using a partial vacuum drying kiln versus a standard kiln. First, the wood can be dried much faster in a partial vacuum kiln, which in turn will allow the company to deliver its products faster and begin new production. The ratio of water molecule sizes compared to wood cell sizes can be thought of as large caves being the cell walls with large holes in them connecting other cell wells big enough for water molecules to move through (“Basic Concepts Regarding Sawing and Drying Lumber.” Pg. 19.) Below boiling point, water has a strong tendency to attract itself to these cell walls. This makes it more difficult for a standard kiln to remove the water because it cannot lower the boiling point. Vacuum kilns, on the other hand, can lower the boiling point of the water down near one-hundred degrees Fahrenheit. This would save on costs for gas because the temperature would not have to be extremely high. This would also prevent any cracks forming in the pores of the wood due to excess heat. I believe a partial vacuum drying kiln would be a great investment for West Virginia Split Rail.

The old methods of calculating board feet are another issue that I believe would be useful for WVSR to consider. These methods usually fall along the lines of the inventory manager or a two-man crew pacing the log piles and taking measurements. A great solution would include a simple, acceptable method that would take only one person to determine board footage. John Calkins discovered this solution with a device with Laser Technology Inc. called the Trupulse 360 laser rangefinder. It is a very simple solution to the old methods. One can simply stand in a location at a reasonable distance from the log pile and use the rangefinder to determine all measurements of the log pile. The most important solution is arguably improved safety so workers do not have to stand on top of and near log piles to determine these measurements. Another great improvement is accuracy. Inventory managers can now have exact calculations rather than going by educated guesses (Cox pg. 2). Again, this is another great product that I would suggest to WVSR.

There are many other innovative products offered to the wood industry to improve applications, processes, and conservation of power.

Photoelectric proximity sensors can be used for non-contact detection of the position of wood in industrial applications. The control of production and quality of product is one of the most important uses of these sensors. They also prevent major accidents within machinery as well as protect employees should possible harmful malfunctions within machinery occur. There is also the useful calibrated application of height, shape, and volume detection. Luminescence sensors are ideal for fluorescent markings from chalk, ink, or labels on nearly any type of wood (“Innovative Solutions for the Wood Industry.” pg.6).

Log sorting can be done through the use of laser measuring systems and automation light grids. The height of an arm detector can determine the log’s diameter, which can lead to the calculation of rotational time. These hold-down arms are very sturdy and shock-absorbent, which ensures accurate results. Three dimensional cameras are also an innovative method of sorting logs (“Innovative Solutions for the Wood Industry.” Pg.9). Full three dimensional profiles of logs can be created, allowing for detection of irregularities within the log and cross sectional sorting.

Wood industry companies certainly value the quality of production and disposal management. Cameras are also useful in determining whether or not left over wood chips will make further value. Without impeding progress, these cameras can simultaneously project three dimensional profiling of the wood chips with lighting analysis. Volume of these wood chips can also be determined, which can make them useful for other processes such as wood pulping. Cameras can measure the distance of logs to the edge of the deflecting walls to make certain that the log is efficiently cut. Quality specifications also include spaces in wood that should or should not be filled. By recognizing these differences, camera systems can help determine where insulation flakes should be kept from building up as well as signal to robots where certain holes should be filled with the correct material (“3-D Measurement of Wood Components.” Pg.1).

Engineering measurements can be made with the use of cameras when determining cant measurement. The positions of knots are detected with the use of scattered laser pointers and the curvature of the log (“Innovative Solutions for the Wood Industry.” Pg.16). Therefore, the blade can be positioned to avoid these knots and possible damage to equipment and wasting the log entirely.

Hazardous conditions and possible severe injury have long been problems in the wood industry. Finding the perfect balance to protect employees and maintain profit and productivity is a tough challenge to engineers. The installment of intelligent multi-scanning curtains is a great innovative way to provide both of these features within a wood industry (“Innovative Solutions for the Wood Industry.” Pg.19). The laser alignment in the system allows for boards to flow constantly. It also allows workers to reach in the flow without turning off the system, thus ensuring safety and keeps productivity running smoothly.

Cross cutting calculations are very important as well. With a combination of luminescence and proximity sensors, machines can make cuts within a millimeter of the precise measurements labeled with ink, chalk, or other markings on any type of wood (“Innovative Solutions for the Wood Industry.” Pg.22). Again, because these sensors contain non-contact technology, the safety of employees is assured.

These examples examine the efficiency state-of-the-art cameras as well as sensors used in the wood industry. Engineering and modern science takes a great step forward with these superior products and systems within the wood industry. The advancements in technology allow the manual aspects of the industry to become much more productive and safer. However, I would not necessarily suggest that WVSR adopt these practices because they are a smaller company compared to other wood industries.

FUTURE PLANS

On rare occasions, some posts within the heart of the bundle can give off a bright pink color. Dane has mentioned this to me and shown me pictures of some of their bundles containing this color on some pieces of wood. However, the pinkish glow goes away within two or three days. Dane and the other managers are not sure of what causes this phenomenon. A possible cause of this could be from lithium present in the mildewcide treatment. When lithium combines with water, it gives off hydrogen gas. The source of water could come from humidity within the bundle of wood. If the excess water is evaporated, the chemical compound lithium hydroxide is left remaining. If the compound phenolphthalein is present, it will turn pink from the combination with lithium hydroxide (“Alkali Metals.” Pg.1). The catch is that phenolphthalein turns pink in basic conditions while it remains colorless in acidic conditions (“Phenolphthalein.” Pg.1). Because trees are acidic in nature, this may be a significant reason why this occurrence is rare. Another important factor may be the amount of humidity within the bundle for this reaction to occur.

The chemical formula for phenolphthalein is composed of 20 carbon molecules, 14 hydrogen molecules and 4 oxygen molecules (Baum pg.1). It is commonly used in laboratories as a primary pH indicator. It turns pink in alkaline solutions in a pH range of 8.2 to 10. Again, because the compound is naturally mildly acidic, it would contribute to the reason of this rare occurrence in nature. From my research, I am intrigued by this phenomenon, but I am unsure if my hypothesis on this matter is heading in the right direction at all. Regardless, I am determined to conduct experiments on this in the near future of the Fall 2013.

CONCLUSION

My research throughout the past ten weeks has taught me a great deal about the history of the wood industry and its importance in West Virginia. West Virginia Split Rail continues to serve its

purpose as a great provider and contributor to the region's wood business. At first, I was unsure of how to adapt to a new work environment and be able to determine useful suggestions for an industry of which I was not familiar. However, I soon became self-driven and was able to complete my task with the help of Dr. Wiest and Dr. Popson as well. My research on recent matters concerning the pink wood phenomenon will likely provide me with a great source of fall research in the coming months.

ACKNOWLEDGEMENTS

The author would like to thank NASA and the WV Space Grant Consortium for bringing great opportunities to the region for undergraduate students to become involved in advancing research fields. Thanks to Dr. G. Albert Popson, who gave time to help collaborate the organization of the project. A special thanks to Dr. Joseph E. Wiest for overseeing the development of the project and providing essential guidance.

REFERENCES

“History, Nature, and Products of Wood.”

Retrieved From <http://www.eolss.net/Sample-Chapters/C10/E5-03-03-01.pdf>

“What About Fiberboard for Green Building?”

Retrieved From <http://www.templeinland.com/pdf/fiberboard/afagreenbuilding.pdf>

(2013). “Wood Products.”

Retrieved From

<http://www.wvcommerce.org/business/industries/woodproducts/default.aspx>

T. Javor, W. Buchberger, I. Tanzcos. “Determination of Lignin Degradation Compounds in Different Wood Digestion Solutions by Capillary Electrophoresis.”

Retrieved From

http://www.lenzing.com/fileadmin/template/pdf/konzern/lenzinger_berichte/ausgabe_79_2000/LB_2000_Javor_10_ev.pdf

Hatakka, Annele. “Biodegradation of Lignin.”

Retrieved From http://www.wiley-vch.de/books/biopoly/pdf/v01_kap05.pdf

“Lignin Products and Uses.”

Retrieved From <http://flambeauriverpapers.com/lignin/lignin-products/>

“Chemical Composition of Wood.”

Retrieved From

http://ipst.gatech.edu/faculty/ragauskas_art/technical_reviews/Chemical%20Overview%20of%20Wood.pdf

Cole, Barbara. “Extractive Components of Wood.”

Retrieved From <http://chemistry.umeche.maine.edu/Green/Afternoon/Cole.pdf>

“Kraft Pulp.” Retrieved From <http://www4.ncsu.edu/~hubbe/KRFT.htm>

Moody, Russell C., Hernandez, Roland., Davalos, Julio F., Sonti, Somnath Sharma. (1993).

“Yellow Poplar Glulam Timber Beam Performance.”

Retrieved From <http://www.woodcenter.org/docs/fplrp520.pdf>

Whittemore, Frank. “Yellow Pine Tree Facts.”

Retrieved From <http://www.gardenguides.com/92255-yellow-pine-tree.html>

Froome, Alan. (1 March 2004). "Sawmill Process Begins with Bucking, Debarking." Industrial Reporting Inc.
Retrieved From <http://www.timberlinemag.com/articledatabase/view.asp?articleID=1215>

(2009). "Exact Macola Review."
Retrieved From <http://www.accountingsoftwareworld.com/software-reviews/exact-macola>

(2002, March). "Basic Concepts Regarding Sawing and Drying Lumber."
Retrieved From <https://www.woodmizer.com/us/portals/1/pdf/lumber101.pdf>

Cox, Tim. (2012, April). "Laser Technology Inc. Rangefinder, Software Improves LoInventory Control." Retrieved From <http://www.lasertech.com/fsms/Timberline-2012e.pdf>

(2008). "Innovative Solutions for the Wood Industry."
Retrieved From <http://www.sick-automation.ru/images/File/pdf/Industry/wood.pdf>

(2013, February). "3-D Measurement of Wood Components."
Retrieved From <http://www.scs.ch/blog/en/2013/02/3d-measurement-of-wood-components/>

"Alkali Metals."
Retrieved From <http://chemed.chem.wisc.edu/chempaths/GenChem-Textbook/Group-IA-Alkali-Metals-544.html>

(2013, June). "Phenolphthalein." Retrieved From <http://en.wikipedia.org/wiki/Phenolphthalein>

Baum, Josh. (2013). "Why Does Phenolphthalein Change Color?"
Retrieved From http://www.ehow.com/how-does_5271431_phenolphthalein-change-color.html

DECREASED MORTALITY RATE OF MICE THROUGH SERIAL *IN VITRO* PASSAGE OF STARVED CELLS OF *PSEUDOMONAS AERUGINOSA* IN WATER.

Danielle Haynes
Graduate
B.S. Applied Sciences (Pre-Pharmacy)
Bluefield State College
Bluefield, WV 24701

ABSTRACT

Pseudomonas aeruginosa is often detected in the water system of space shuttle but its behavior and existence mechanism is not well defined. To promote our understanding of the mechanisms of *P.aeruginosa* colonizing the water supply of a space craft, the survival kinetics in sterile water and the pathogenicity of starved cells *P.aeruginosa* in a mouse model is underway in our laboratory. Infection experiments showed that starved *P.aeruginosa* resulted in reduced death rate of mice compared to stock culture of the parental strain, ATCC 12055. To determine whether *in vitro* passage would result in further weakening of virulence in mice, long-term starved *P.aeruginosa* in water were passaged for a week *in vitro* and Swiss Webster were inoculated intraperitoneally with lethal doses. Ninety percent of mice inoculated with the passaged starved cells survived the infection, compared to 30 % of mice receiving the stock culture of the parental strain, ATCC 12055. Furthermore, formalin-killed *P. aeruginosa* starved cells resulted in 90% protection in mice challenged with a lethal dose of the strain compared to 0% protection compared to the control. These results suggest that starved cells of *P.aeruginosa* through serial *in vitro* passage have potential for vaccine development, although further investigation is needed.

INTRODUCTION

Pseudomonas aeruginosa is a gram-negative pathogen that causes infections in humans especially individual with an immune comprised system, burn victims and cystic fibrosis patients. This bacterium is important to NASA due to its existence in water systems in the space crafts and because it causes infection to the crew members during spaceflight. The ability of the *P. aeruginosa* to live in sterile water for prolonged periods of time is not well understood. In our lab we have investigated long term starvation in sterile water of different strains of *P. aeruginosa*. Our data has shown that they have the ability to survive for 1485 days in water, morphological changes appear during starvation and total protein profiles are also altered during the prolonged period of starvation in sterile water. The purpose of this study was to (i) to determine the kinetics of the starved bacteria within the organs of mice infected with starved cells; (ii) to test the infection ability of serially *in vitro* passed starved cells; (iii) to test the potential use of starved cells as a potential vaccine. Our hypothesis is the infection ability of serially *in vitro* passed starved cells would be higher than non-starved cells and starved cells and the serially *in vitro* passed starved cells would show potential for a vaccine.

METHODS AND MATERIALS

Bacterial strain

Pseudomonas aeruginosa strain 12055 was donated by Dr. Hongwei Yu's laboratory at Marshall University was used in this study. Luria Bertani (LB) broth or *Pseudomonas* isolation agar (PIA) was used for stock culturing and bacterial inoculums preparation.

Animals

Six to seven weeks old female Swiss Webster mice from the Hilltop laboratory were used in this study

Bacterial growth kinetics and starvation in sterile water

For the long-term starvation kinetics 1×10^8 CFU/mL of *P. aeruginosa* were inoculated in sterile distilled water and placed at room temperature. Viable plate counts were done at time intervals to determine the amount of the bacteria in each culture over the period of starvation.

Serial in vitro Passage of Starved Cells

Starved cells were grown overnight in LB broth at 37°C with shaking. Cells were harvested from broth and resuspended in LB broth each time for 4 rounds of serial in vitro passage. Serially in vitro Passed Starved Cells Starved and non-starved Cells were grown overnight in LB broth at 37°C with slow shaking. Cells were harvested by washing with PBS. The pellet was then resuspended in 10mL of sterile Phosphate Buffer Saline (PBS). A ten-fold serial dilution was made to the desired concentration of 10^7 for mice inoculation. Five mice for each dilution of the passage and non-starved cells were injected with 100µL of the passage or non-starved cells at each dilution intraperitoneally (IP). Mice were observed every 4 hours post-infection. Mice infected with non-starved cells were dissected at time of death. At 24 hours post-infection mice infected with starved passage cells were sacrificed using CO₂ inhalation. The heart, lungs, liver, kidneys, and the spleen were harvested and homogenized in sterile PBS using a Tissue Ruptor from Qiagen (Valencia CA). Different doses, 10^{-1} to 10^{-4} were plated into PIA and incubated for 24 hours at 37°C for CFU/ml determination.

Preparation of Formalin Killed Whole Cells

After undergoing passage starved bacteria cells were obtained and added to PBS and Formalin (1:1) then left overnight at room temperature. At 24 hours starved cells were harvested, washed of formalin, and resuspended in PBS. A viable plate count was performed and zero cell growth was shown.

Protection Studies

Formalin killed whole cells of ATCC 12055 were intraperitoneally given to 15 mice as a vaccination in the amount of 200µL. Stock ATCC 12055 was grown overnight in LB broth at 37°C with shaking was harvested and then diluted to a lethal dose of 10^8 CFU/ml. At 6hrs after injection of formalin killed whole cells, 5 non-immunized mice were infected with 100µL of stock 12055. Immunized mice were also challenged in groups of 5 with the stock bacteria at 6, 24, and 48 hrs. Mice were monitored every 4 hours for observations and death rate analysis.

RESULTS

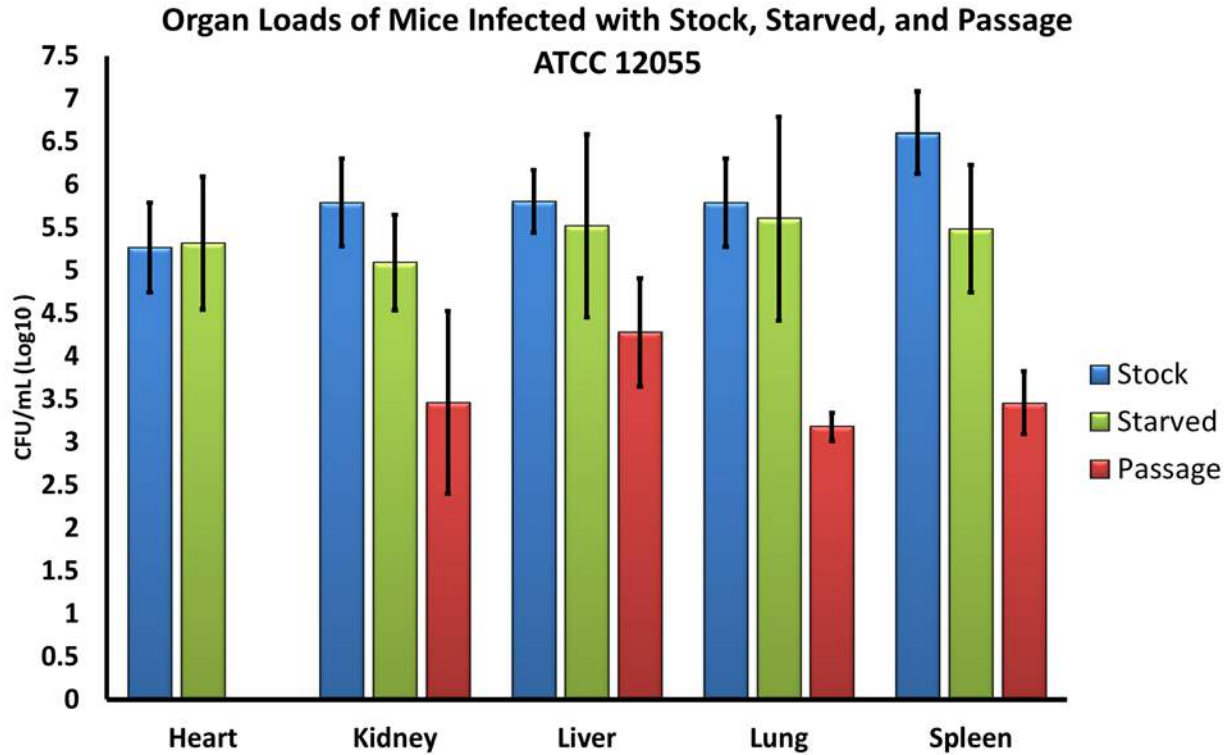


Figure 1: Organ load of Surviving Mice of Infection with Stock Starved and Passage ATCC 12055.

Organs isolated from infected mice were homogenized in sterile PBS, plated on PIA, and incubated for 24 hours at 37°C. Colonies were counted after 24 hours of incubation.

	Number of dead mice	Number of survivors	Accumulated numbers			Percentage of death
			Dead	Survivors	Total mice	Dead/total × 100
Stock	8	2	8	2	10	8/10=80.0%
Passage	1	9	1	9	10	1/10=10.0%

Table 1: Decrease Mortality Rate of Mice Infected with Serially in vitro Passed Cells of ATCC 12055.

	Number of dead mice	Number of survivors	Accumulated numbers			Percentage of death
			Dead	Survivors	Total mice	Dead/Total x 100
Non-Immunized	5	0	5	0	5	5/5=100.0%
6 Hours	1	4	1	4	5	1/5=20.0%
24 Hours	5	5	0	5	5	0/5=0.0%
48 Hours	5	5	0	5	5	0/5=0.0%

Table 2: Protection of Mice Immunized with Formalin Killed Whole Cells of Starved *Pseudomonas aeruginosa*

SUMMARY AND CONCLUSIONS

P.aeruginosa starved in distilled water showed to maintain a constant growth compared to that of the tap water which had a 2 log difference at 140 days for starvation. The LD50 of the Non-Starved cells (5.149×10^7) was lower to that of the Starved cells (1.298×10^8). The non-starved cells with a lower LD50 show to be more pathogenic than that of the starved cells. Changes of colony pigmentation of cells were observed through long-term starvation and the changes in colony pigmentation may have biological relevance to play a key role in the long-term survival and the degree of pathogenicity. The non-starved colonies showed two variants when plated, one being medium sized and mucoid with a slight light green pigmentation while the other colonies were medium sized and dome shaped with only a khaki pigment. The starved *P.aeruginosa* colonies were larger than those of the non-starved bacteria. These colonies were also showed three variants. The first of these variants was very large with a light yellow-green pigment and were raised into a dome shape. The second of these variants were dome shaped but khaki colored and mucoid. The last of the three variants grew very close together and have a medium to dark green pigment. The third variant's colonies were also quite misshapen and very flat. Organ load determination of the tissues revealed early invasion of the bacterium in spleen, liver, kidneys and lungs. During starvation in sterile water *P. aeruginosa* strain 12055 seems to lose some of its natural pathogenic factors. Lethality was higher in mice inoculated with non-starved cells compared to mice infected with starved cells. Further research showed that the organ load determination of the tissues revealed early invasion of the bacterium in spleen, liver, kidneys and lungs. The overall results obtained from these experiments suggest that infection that leads to death of mice was decreased with *P.aeruginosa* that are under starvation conditions. During the study exploring whether or not the starved, passed, and formalin killed whole cells of the bacteria would have any potential for a possible immunization we found that ninety percent of mice inoculated with the passaged starved

cells survived the infection with wild type of *Pseudomonas aeruginosa*. Formalin-killed *P.aeruginosa* starved cells resulted in 90% protection in mice challenged with a lethal dose of the strain compared to 0% protection compared to the control. These results suggest that starved cells of *P.aeruginosa* through serial *in vitro* passage have potential for vaccine development.

RESEARCH TRAINING

As a student who began my research before taking microbiology, then only received my microbiology lab online, my time in the research lab at Bluefield State College has given me one of the only opportunities to learn hands-on lab techniques, procedures, and skills that I will need in the future. During my first year of research I learned safety regulations when dealing with a bacterium such as *Pseudomonas aeruginosa* but I also learned how to subculture a bacteria and perform serial dilutions to be plated allowing us to observe changing morphology of the bacteria colonies. In the lab I also had my first experiences and training in working with animals (Swiss-Webster mice). I learned the proper way to handle mice, maintain their cages and diets, stress the mice, sacrifice mice, and inject them interperitoneally. I have also now learned proper sterilization techniques via autoclaves within the lab and how to perform multiple dissections and organ loads with mice. During my research this summer I got to have a much more hands and partnership approach concerning the direction of my research project and the methods of how to go about achieving the decided objectives. More than anything research experience has really taught me how to think logically and in a long term manner. I am no longer a student simply shadowing a professor or PI as they work in the lab, but with the help and instruction of Dr. Belay I have become a science graduate that can go so far to ask great scientific questions that not even he has considered yet. The realization of becoming a scientific thinker and effective and productive work is a very fulfilling one. I have also had the opportunity to learn how to independently create, organize, and present a poster and full research paper for conference, presentation, or publication formats.

UNDERGRADUATE RESEARCH DAY AT THE CAPITAL

I, as well as two other students, Michael Bowling and Brandon Kirby, received the chance to go to the capital building in Charleston, WV to share my researcher with other undergraduate researchers from colleges and universities in West Virginia. At this conference we also had the great opportunity to meet and share our research projects and experiences with the officials of our states and counties. Not only was it a great experience as my very first time at the capital buildings but it was amazing to be able to meet and speak with or states politicians and officials and see their interest in the sciences and research occurring in the areas that they serve.

WV-INBRE SUMMER RESEARCH SYMPOSIUM

The research I have performed this year gave me the opportunity to present for the second time at WV-INBRE Summer Research Symposium in Huntington, WV at Marshall University. This was my first time at Marshall University. Attending this symposium gave me another look at what some of the research at our neighboring universities is exploring. Not only did I get the chance to communicate my findings to other participants but I also got a chance to see what other students in my field were working on during their summer research programs, some of which was very similar or even complementary to my own. This gave way to meaningful, scientific conversation on research matters and sparked ideals and questions for all of us about our own research. It was a great chance to make new friends and contacts that are on similar paths as me that I will surely work with again in the future. I also got to meet professors and mentors from the other colleges

who attended the symposium, some of which also presented research they have been conducting. I especially enjoyed my time speaking with a professor from Marshall who works very closely with Dr. Belay on the same topic. It was great that he had an opportunity to see our current findings. The symposium was a success and great preparation for future opportunities.

ANNUAL BIOMEDICAL RESEARCH CONFERENCE FOR MINORITY STUDENTS

I have been fortunate enough to be asked to attend and present my lab research at the Annual Biomedical Research Conference for Minority Students (ABRCMS) for a second year in a row. This conference will be taking place November 13-16, 2013 in Nashville, Tennessee I will present this research as well as the work I currently have in progress that will continue. The 13th annual ABRCMS is:

“...the largest, professional conference for biomedical and behavioral students, including mathematics, attracting approximately 3,300 individuals, including 1,700 undergraduate students, 400 graduate students and postdoctoral scientists and 1200 faculty, program directors and administrators. Students come from over 350 U.S. colleges and universities. All are pursuing advanced training in the biomedical and behavioral sciences, including mathematics, and many have conducted independent research. The conference is designed to encourage underrepresented minority students to pursue advanced training in the biomedical and behavioral sciences, including mathematics and provide faculty mentors and advisors with resources for facilitating students’ success. More than 500 representatives from graduate programs at US colleges and universities as well as scientists from government agencies, foundations, and professional scientific societies join ABRCMS in the exhibitors program to share information about graduate school and summer internship opportunities. These representatives present research opportunities, funding sources, and professional networks.”

Attending the conference will give me the chance to present my research on a national level once again. I will meet and communicate with thousands of minority students like myself within my field, as well as network with professors, researchers, and recruiters from graduate programs around the nation. As a first year pharmacy school student, continuing research and attending this conference will build a lasting relationship with my previous advisor that will be beneficial for my future as both a pharmacist and a researcher. My attendance to the ABRCMS will reinforce the experience that I have had performing, organizing, and communicating my research in the past two years.

FUTURE RESEARCH

Further studies are needed to understand the loss of some of the pathogenic factors and to further characterize this bacterium during starvation in water. We will repeat the mouse model to confirm and validate the results and data we have already collected. We will also continue researching specific aspects of *Pseudomonas aeruginosa* more in depth. The immunization experiments will be performed again to confirm the data collected and will also be expanded with different conditions to find the best strategy for immunization.

ACKNOWLEDGEMENTS

This project was supported by NIH Grant 5P20RR016477 to the West Virginia IDeA Network for Biomedical Research Excellence and NASA West Virginia Space Grant Consortium/NASA WV EPSCoR and mentor Dr. Tesfaye Belaye.

ID2 OVER-EXPRESSION EFFECTS ON OTHER GENES THAT ARE DYSREGULATED IN MENINGIOMAS

Stephen Heywood
Chemistry
West Virginia State University
Institute, West Virginia 25112

ABSTRACT

Although meningiomas are common primary central nervous system tumors their pathobiology is poorly understood. Intracranial meningiomas are twice as frequent in women as men and spinal meningiomas ten times as frequent in women, therefore, the female sex steroid hormones progesterone and β -estradiol are suspected factors in meningioma tumorigenesis. Gene expression within meningioma cells may play a key role in the diagnosis, prognostics and treatment of these tumors. In earlier studies, we observed that with the treatment of TSA and sodium butyrate, the Inhibitor of DNA Binding 2 (ID2) gene is up-regulated, while Transmembrane 4 L six family member 1 (TM4SF1) was down-regulated. TM4SF1, also known as tumor associated antigen L6, is highly expressed in some carcinomas. We hypothesized that the up-regulation of ID2 gene expression could be responsible for the down-regulation of TM4SF1 while also affecting the expression of other genes. ID2 was over-expressed in CH157MN meningioma cells and effects of the ID2 over-expression on expression of TM4SF1 and several other genes were examined. No significant effect on TM4SF1 was observed. Results of these studies to date do not support our initial hypothesis although the ID2 over-expression did affect moderate up-regulation of fibroblast growth factor 2.

INTRODUCTION

Intracranial meningiomas are twice as frequent in women as men and spinal meningiomas ten times as frequent in women, therefore, the female sex steroid hormones progesterone and β -estradiol are suspected factors in meningioma tumorigenesis. However, no mechanisms have been demonstrated for female sex hormones in meningioma formation or progression. Microarray data from the mentor's lab (Hankins *et al.* 2008) indicate that a number of steroid responsive genes are differentially expressed between meningiomas and normal meninges. These include the negative transcriptional regulator, ID2, and the tetraspanin, TM4SF1.

Inhibitor of DNA binding 2 (ID2) is a member of the helix-loop-helix (HLH) transcription family. The ID proteins lack a basic domain for DNA binding but form heterodimers with other HLH transcription factors and act as dominant inhibitors. ID2 protein can also bind retinoblastoma protein, releasing E2F from transcriptionally inactive RB-E2F complexes (Lasorella *et al.* 2000). ID proteins are thought to play a role in the balance between cell growth and differentiation and ID2 has been implicated as both an oncogene and a tumor suppressor. Over-expression of the ID2 gene can account for the increased cell growth of cancer cells. ID2 expression is associated with diagnosis and prognosis of different types of carcinoma, as well as a potential prognostic factor for neuroblastoma, and cervical cancer (Lasorella *et al.* 2001). It has been found that an increased

expression level of ID2 is associated with tumor size, lymph node metastasis, and clinical stage in nasopharyngeal carcinomas (Liu *et al.* 2012).

TM4SF1 is a tetraspanin. Tetraspanins mediate signal transduction events and play roles in cell growth, development, and motility. TM4SF1 is estrogen regulated in breast cancer cells and is down-regulated in some meningiomas expressing progesterone receptor as compared to those without (Santen *et al.* 2005, Claus *et al.* 2008).

In work I conducted as part of a Summer Undergraduate Research Experience (SURE) in 2012 with generous support from the NASA West Virginia Space Grant Consortium I evaluated the expression of ID2, TM4SF1 and a second tetraspanin, epithelial membrane protein 2 (EMP2) after treatment of CH157-MN meningioma cells with progesterone, 17 β -estradiol or their antagonists (RU486 and ZK164015, respectively) and, separately with inhibitors of DNA methyltransferase, 5-aza-2'-deoxycytidine (dACT), and histone deacetylase inhibitors trichostatin A (TSA) and sodium butyrate (NaB). Most notable was an eight-fold up-regulation of ID2 expression by both HDACi's while there was a mirror image down-regulation of TM4SF1 (Figure 1). While up-regulation of genes often occurs when histone deacetylases are inhibited, the down-regulation of TM4SF1 was an unexpected result. A similar pattern was later seen for CDKN1B (p27Kip1) as for TM4SF1 (results not shown). These results led us to hypothesize that ID2 up-regulation could be responsible for the down-regulation of TM4SF1 and CDKN1B.

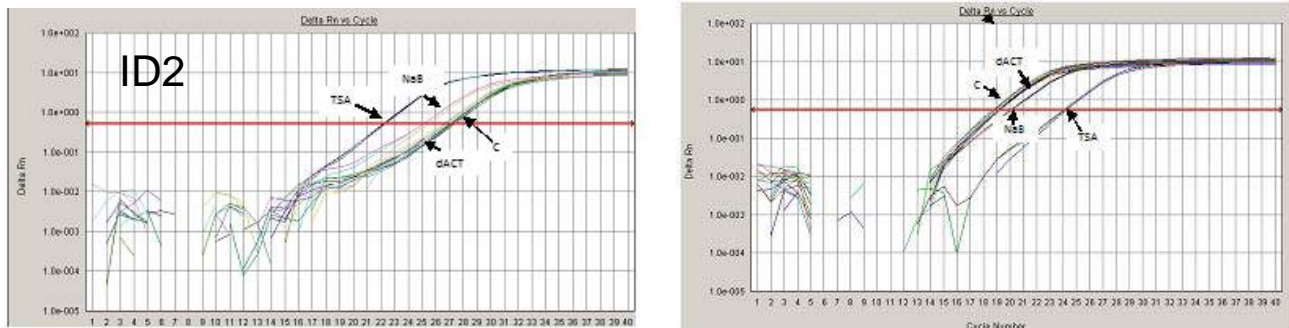


Figure 1. Up-regulation of ID2 expression and down-regulation of TM4SF1 expression by inhibitors of histone deacetylases.

Real-time RT-PCR amplification traces showing up-regulation of ID2 (left) and mirror image down-regulation of TM4SF1 (right) after treatment with the histone deacetylase inhibitors trichostatin A (TSA) or sodium butyrate (NaB). The DNA methyltransferase inhibitor dACT, did not affect RNA levels for either gene.

Our objective in the current study was to evaluate the response of several genes, including TM4SF1 and CDKN1B to transient transfection with an ID2 expression vector in meningioma cells *in vitro*. Additionally, FGF2, SLC20A2, NF2, CCND1, JUN, MTUS, and Chmp1A were examined relative to the up-regulation of ID2. There is some evidence for dys-regulation of the expression of each of these in meningiomas and the biological functions of these genes have all been affiliated with cellular cycle, transport of molecular molecules and tumor suppression.

MATERIALS AND METHODS

A full-length human cDNA clone in the pCMV6-XL5 expression vector (Origene) was transfected into *E. coli* DH5 α and amplified. The amplified plasmid was subsequently isolated from the bacterial cells and purified using a QIAGEN EndoFree Plasmid Maxi kit to give endotoxin-free vector for transfection of the meningioma cells. CH157-MN meningioma cells were transiently transfected with the ID2 expression vector using TurboFectin (Origene). At time periods ranging from 24 to 48 hours post-transfection (severe toxicity occurred at longer periods) mRNA was isolated from the meningioma cells using RNeasy (QIAGEN). Separately, cells were treated with the DNA methyltransferase inhibitor 5-aza 2'-deoxycytidine (dACT), and the histone methyltransferase inhibitors UNC0638 and chaetocin and mRNA isolated using RNeasy. The mRNA was reversed transcribed using the Improm II RT kit (Promega). Gene expression was evaluated by real-time PCR on an ABI Prism 7000 using iTaq Sybr Green (Biorad). GAPDH message levels were evaluated as a loading control. Fold changes in message levels were evaluated using the $2^{-\Delta\Delta C_t}$ method (Livak & Schmittgen 2001). To examine ID2 protein expression, protein was collected using RIPA buffer and quantified using BCA assays before performing dot ELISA and western blotting with 10C3 monoclonal antibody (Abcam).

RESULTS

Transfection of CH157MN cells with the ID2 expression vector resulted in an over 100,000 fold up-regulation of ID2 message after 1 to 2 days post-transfection (Figure 2). Beyond 2 days post-transfection, wide-spread cell death was observed, with most cells rounded-up and detached from the cell culture plates.

There was no change in TM4SF1 expression after transfection with the ID2 expression vector (Figure 3); CDKN1B, SLC20A2, CCND1, JUN, MTUS, and Chmp1A had similar results to TM4SF1. ID2 over-expression significantly up-regulated FGF2 expression (Figure 4). NF2 was slightly down-regulated (Figure 5); these results warrant replication, particularly since meningiomas are one of the hallmarks of neurofibromatosis and since over 50% of spontaneous meningiomas show either mutations in NF2 or down-regulation of NF2.

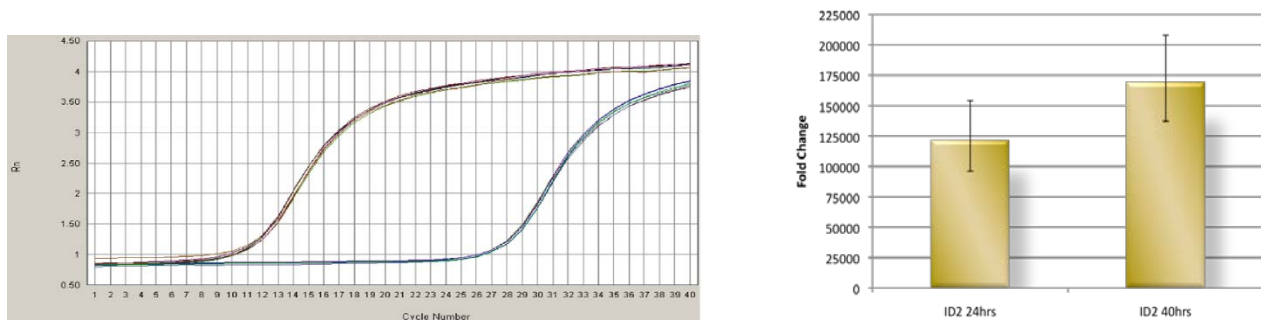


Figure 2. Over-expression of ID2 in CH157MN cells after transfection with ID2 expression vector.

Left: Real-time RT-PCR amplification traces showing up-regulation of ID2 hours after transfection with a full-length human cDNA clone in the pCMV6-XL5. Right: A bar graph showing the fold change in ID2 message levels after adjusting for levels of the GAPDH message.

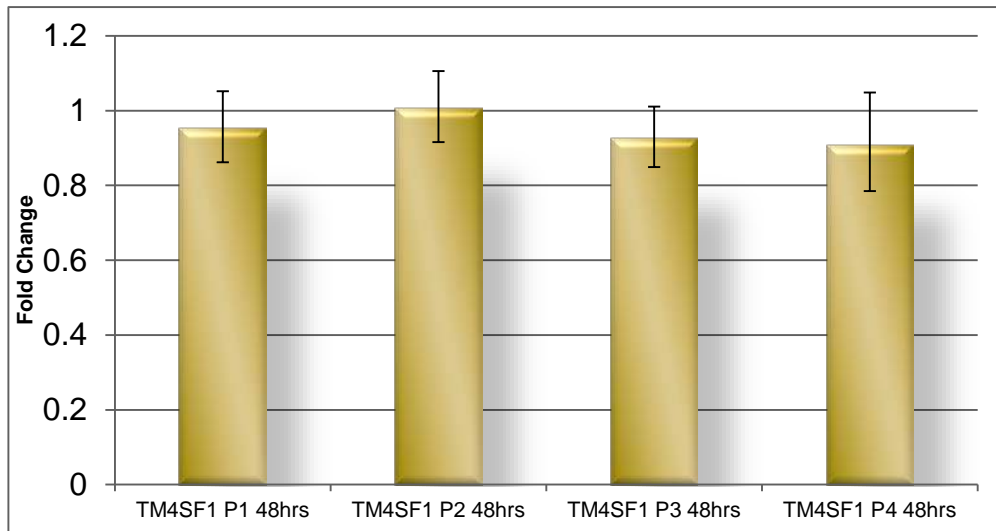


Figure 3. Over-expression of ID2 in CH157MN cells did not effect significant changes in the levels of TM4SF1 message.

Results of four separate replicate experiments are shown 48 hours post-transfection. Error bars represent standard errors of the means. Similar results were also observed seen for CDKN1B, SLC20A2, CCND1, JUN, MTUS, and CHIMP1A message levels when ID2 was over-expressed.

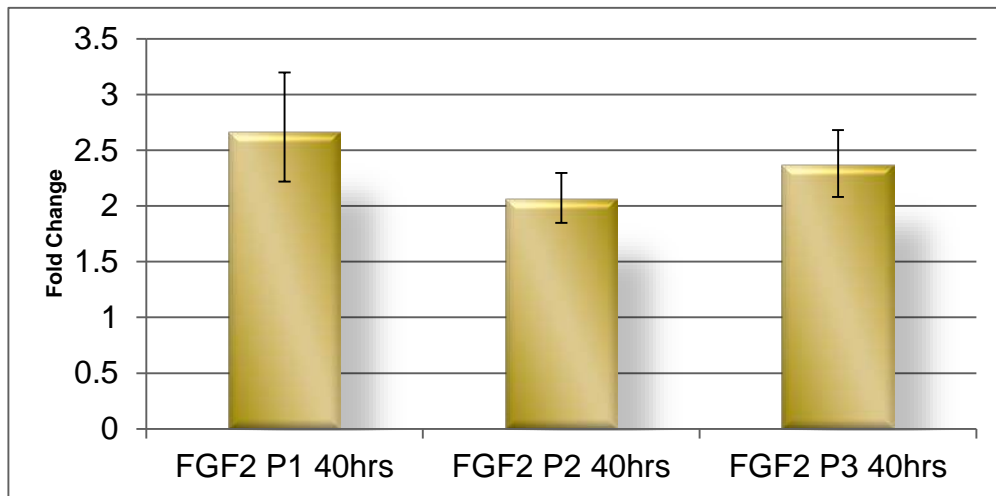


Figure 4. Over-expression of ID2 resulted in significant up-regulation of FGF2 message levels.

Results of three replicate experiments are show for 40 hours post-transfection. Error bars represent standard errors of the means.

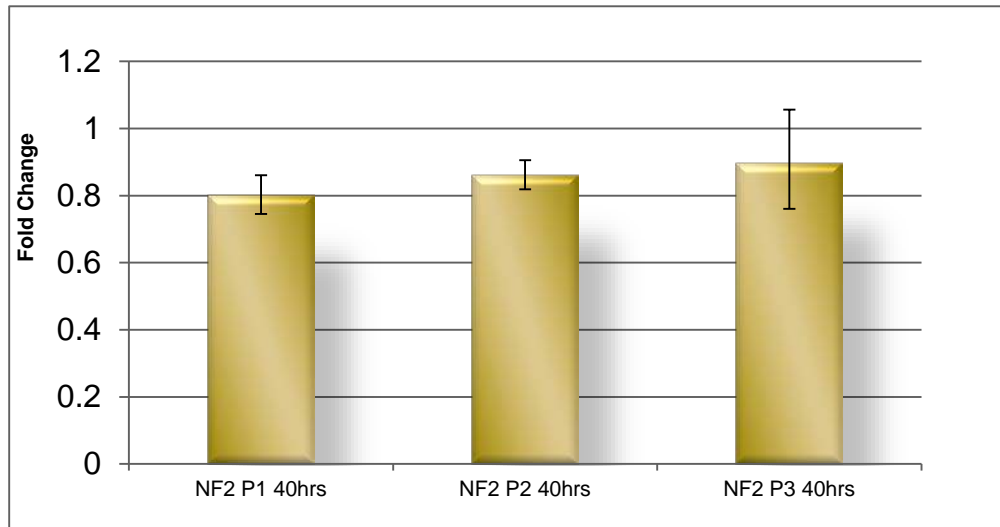


Figure 5. Over-expression of ID2 led to a slight down-regulation of NF2 message levels.

Error bars represent standard errors of the means.

DISCUSSION

The general lack of response of the genes tested for expression variations under ID2 over-expression conditions were contrary to our expectations, particularly in the case of TM4SF1 and CDKN1B where the results do not support our initial hypotheses. However, the evaluation of only one, very rapidly growing, meningioma cell line was completed. It remains to be seen whether the response to over-expression of ID2 will differ in other, more typical meningioma cell lines. Also, the massive over-expression that we observed using the vector and time points in this study may have resulted in effects that overwhelmed those that might be seen with a more modest over-expression. In the future, we will repeat the transfection experiments using shorter times between transfection and RNA collection. The vector that we used has the ID2 cDNA under control of a very strong viral promoter; substitution of a weaker promoter may also be used to achieve more modest over-expression of ID2. Another approach would be to further reduce the level of ID2 message in the meningioma cells using ID2 siRNA.

The effects of ID2 over-expression on the expression of FGF2 and NF2 could indicate a significant role of ID2 in meningioma tumorigenesis, however. The most common genetic abnormality which has been identified in sporadic low-grade meningiomas is loss or silencing of the neurofibromatosis type 2 (*NF2*) gene and neurofibromatosis type 2 patients invariably develop the tumors (Kimura *et al.* 1998, Lomas *et al.* 2005, Simon *et al.* 2007). It is possible that even a modest reduction in levels of the NF2 encoded protein, merlin, could contribute to meningioma tumorigenesis. Fibroblast growth factors (FGFs) are known to play significant roles in signaling pathways of embryonic development, cell proliferation, angiogenesis, wound healing, cell migration and morphogenesis and these growth factors have been implicated as factors in meningioma tumorigenesis. Todo *et al.* (1998) demonstrated that administration of exogenous FGF2 and FGF9, independently stimulated cell proliferation in human meningioma cells in vitro. Ueba *et al.* (1994) identified FGF2 in 90% of human glioma and meningioma specimens and latter also reported that expression levels of FGF2 correlated with the expression levels of FGFR1 and with degree of malignancy, indicating possible autocrine signaling involvement. Work in the

faculty mentor's lab recently demonstrated that inhibitors of FGF receptors, PD166866 and PD166285, significantly reduce cellular proliferation in multiple meningioma cell lines and that PD166285 significantly reduces phosphorylation of ERK1 and ERK2 (Bright 2012). The ERK pathway is thought to be the main pathway for mitogenic FGF signaling. Bright's work also demonstrated that super-physiological concentrations of 17 β -estradiol significantly up-regulates FGFR1 mRNA expression in one meningioma cell line *in vitro*. Together with the earlier studies, these findings suggest that FGFs are involved in autocrine signaling in meningioma cells and that their effects are at least in part conveyed through the ERK1/2 pathway. The work reported in this study indicates that ID2 expression, could contribute to FGF autocrine signaling in meningiomas.

We are currently testing the effects of the histone methyltransferase inhibitors chaetocin, UNC0638, and the DNA methyltransferase inhibitor dACT on ID2 and TM4SF1 expression.

Results of the western blot and dot ELISA analysis are not available at present time.

ACKNOWLEDGEMENTS

Supported by the NASA West Virginia Space Grant Consortium and by NIH Grants 5P20RR016477 and P20GM103434 to the West Virginia IDeA Network for Biomedical Research Funding. Also thanks to Dr. Gerald Hankins for being my research mentor.

VALUABLE ASPECTS OF THE PROGRAM

My time spent performing research under Dr. Hankins thanks to the NASA West Virginia Space Grant Consortium has been very valuable to me in many ways. Not only have I had the chance to experience real, current research first-hand, but also I have been immersed in a research environment and learned a great deal about the overall process. I learned a variety of procedures in my time spent in the lab such as RNA extraction and cDNA synthesis as well as a good deal about how to use and understand scientific literature better, how to write in the accepted way for scientific papers, and how to present findings in a variety of forms including PowerPoints and posters. Also, in my time spent in Dr. Hankins' research lab, I have been granted the privilege to interact with researchers on a daily basis for a couple of months, and not only met a number of very friendly people I intend to stay in contact with but also learned a great deal from each about all aspects of the research process ranging from tips on understanding scientific articles to tricks on how to remove one's gloves in an efficient way. I am very grateful for the opportunity that was given to me, and I hope to be fortunate enough to take part in this research again in the future.

REFERENCES

- Bright SH: Fibroblast growth factors as steroid-responsive autocrine signals in meningiomas. M.S. Thesis, West Virginia State University, May 2012.
- Claus EB, Park PJ, Carroll R, Chan J, Black PM: Specific genes expressed in association with progesterone receptors in meningioma. **Cancer Res** 68:314-322, 2008.
- Hankins GR, Sasaki T, Lieu AS, Saulle D, Karimi K, Li JZ, Helm GA: The identification of deleted in liver cancer-1 (DLC1) as a candidate meningioma tumor suppressor. **Neurosurgery** 63:771-781, 2008.
- Kimura Y, Koga H, Araki N, Mugita N, Fujita N, Takeshima H, Nishi T, Yamashima T, Moritake K, Saya H, Nakao M: The involvement of calpain-dependent proteolysis of the tumor suppressor NF2 (merlin) in schwannomas and meningiomas. **Nat Med** 4:915-922, 1998.
- Lasorella A, Nosedà M, Beyna M, Iavorne A: Id2 is a retinoblastoma protein target and mediates signaling by Myc oncoproteins. **Nature** 407:592-598, 2000.
- Lasorella A, Uo T, Iavorne A: Id proteins at the cross-roads of development and cancer. **Oncogene** 20:8326-8333, 2001.
- Liu Z, Chen J, Luo W, Yang H, Wu A, Zhen Y, Yu X, Wang H, Yao K, Li X, Fang W: Overexpressed DNA-binding protein inhibitor 2 as an unfavorable prognosis factor promotes cell proliferation in nasopharyngeal carcinoma. **Acta Biochem Biophys Sin** 44:503-512, 2012.
- Livak KJ, Schmittgen TD: Analysis of relative gene expression data using real-time quantitative PCR and the $2^{-\Delta\Delta C_t}$ method. **Methods** 25:402-408, 2001.
- Lomas J, Bello MJ, Arjona D, Alonso ME, Martinez-Glez V, Lopez-Marin I, Aminosò C, de Campos JM, Isla A, Vaquero J, Rey JA: Genetic and epigenetic alteration of the NF2 gene in sporadic meningiomas. **Genes Chromosomes Cancer** 42:314-319, 2005.
- Santen RJ, Lobenhofer EK, Afshari CA, Bao Y, Song RX: Adaptation of estrogen-regulated genes in long-term estradiol deprived MCF-7 breast cancer cells. **Breast Cancer Res Treat** 94:213-223, 2005.
- Todo T, Kondo T, Kirino T, Asai A, Adams EF, Nakamura S, Ikeda K, Kurokawa T: Expression and growth stimulatory effect of fibroblast growth factor 9 in human brain tumors. **Neurosurgery** 43: 337-346, 1998.
- Ueba T, Takahashi JA, Fukumoto M, Ohta M, Ito N, Oda Y, Kikuchi H, Hatanaka M: Expression of fibroblast growth factor receptor-1 in human glioma and meningioma Tissues. **Neurosurgery** 34: 221-226, 1994.

ROBOTICS VIRTUAL INTERACTIVE EVALUATION AND UNDERSTANDING

Jaclyn Hobbs
Department of Mechanical and Aerospace Engineering
West Virginia University
Morgantown, West Virginia 26505

ABSTRACT

The Robotics Capabilities IV&V project for summer 2013 is Robotics Virtual Interactive Evaluation and Understanding (VIEU). This project consists of creating a 3D computer aided design (CAD) model of the OSIRIS-REx spacecraft and generating a simulation of the mission's robotic capabilities using a software package called Blender. The overall goal of this project is to determine if a software tool like the Robotics VIEU simulation would be a useful aid to IV&V analysis and testing, and to manage the development of the simulation by generating requirements and objectives. These requirements and objectives are then passed on to the NASA Engineering Apprenticeship Program (NEAP) high school interns on the Robotics Capabilities IV&V project as tasks to complete in developing the simulation. Summer College Intern Program (SCIP) interns are responsible for defining the Robotics VIEU architecture and for overseeing the integration of development products.

The simulation needs to consist of an approximate 3D CAD model of the Touch and Go Sample Acquisition Mechanism (TAGSAM) on the OSIRIS-REx spacecraft whose movements can be controlled through simulated flight software written using the Python scripting interface in Blender.

The simulation should mimic the architecture of the mission, which includes a ground control user interface (UI) system and the on-board flight processing software. Creating the simulation also requires creating additional software to simulate the mechanical action of the TAGSAM. The software should be modularized so that the simulated flight software and the mechanical simulation are separated to an extent so that this simulation tool could be applied to any other project with very few modifications.

Additionally, during the development process, assumptions about the structure and requirements for the flight software should be documented so that they can be compared to the mission requirements for OSIRIS-REx. This can support requirements validation work done at the IV&V Facility.

Finally, this simulation tool should be evaluated to determine its applicability to current and future IV&V projects. This involves learning about past efforts of IV&V on robotic systems and determining how a simulation tool like this could assist in these efforts. From this, requirements for a production version of this simulation should be developed.

INTRODUCTION

The Robotics Capabilities IV&V project for the summer of 2013 is Robotics Virtual Interactive Evaluation and Understanding (R-VIEU). This project consists of creating a 3D computer aided design (CAD) model of the OSIRIS-REx spacecraft and generating a simulation of the mission's robotic capabilities using a software package called Blender. The overall goal of this project is to determine if a software tool like the R-VIEU simulation would be a useful aid to IV&V analysis and testing, and to manage the development of the simulation by generating requirements and objectives.

The OSIRIS-REx spacecraft will travel to a near-Earth carbonaceous asteroid (101955) Bennu return and analyze a sample (at least 60 grams), create maps of the asteroid, document the sample site, measure the orbit deviations, and compare to telescope-based observations. This sample will help scientists investigate planet formation and the origin of life, and the data will increase understanding of asteroids that have the chance to impact Earth.

For Blender, an investigation was needed to determine whether or not it was applicable to the project to create the software tool. Once that was determined, a 3D model of the OSIRIS-REx Touch and Go Sample Acquisition Mechanism (TAGSAM) needed to be developed and controlled through simulated flight software written using Python scripting in the Blender interface. Once the TAGSAM was constructed in Blender, off-nominal conditions had to be identified using different scenarios and modeled if possible. Continuing on the development of the TAGSAM, a user interface needed to be created to control the arm as well as to display the feedback telemetry. If the arm kinematics model was completed and robust, then the arm could be attached to a model of the spacecraft with 3 degrees of freedom in order to simulate spacecraft attitude. This enabled analysis of exclusion zones related to exposure and shadowing of the sampler head which would follow the mission requirements.

The simulation should mimic the architecture of the mission, which includes a ground control user interface (UI) system and the on-board flight processing software. Creating the simulation also requires creating additional software to simulate the mechanical actions of the TAGSAM. The software should be modularized so that the simulated flight software and the mechanical simulation are separated to an extent so that this simulation tool could be applied to any other project with very few modifications. This process for completing the tool and the requirements supports validation work at the IV&V facility, which can hopefully be applicable to current and future IV&V projects.

METHODS

Modeling

In order to create the visual aspect of the OSIRIS-Rex simulation, different pieces of the environment and the virtual world had to be modeled both in Blender and by importing files from Autodesk Inventor into Blender.

Table 1: List of OSIRIS-REx Instruments Designed

Developed in Blender	Developed in 3D Design Program
<ul style="list-style-type: none"> • GN&C LIDARs • MapCam • REXIS • OLA • OTES • PolyCam • SamCam • StowCam • SRC Capsule (Sample Return Capsule) • High Gain Antenna • Solar Panels • Solar Panel Accessories • Thruster • TAGSAM Sampler Head Storage Compartment 	<ul style="list-style-type: none"> • Body of OSIRIS-REx • TAGSAM (Touch and Go Sampler Acquisition Mechanism)

The table above states what modeling software was used for each instrument. The reason that these instruments and objects were chosen to be included into the simulation was the importance of seeing how the spacecraft is modeled and acts when going through the TAG (Touch and Go) process. These assumptions on how the spacecraft and TAGSAM were developed and designed are based on online resources. Access to the actual specific design requirements was not granted for this project.

Environment

Primarily for aesthetics, the environment for the simulation needed to include a background and an asteroid. The asteroid gives the software simulation tool a goal by showing the TAGSAM Sampler Head collect a sample from the asteroid. Simulation of the forces on the spacecraft when touching down could not be shown because the physics engine in Blender game engine did not prove to be reliable for rigid body arm physics. Consequently, this kept the R-VIEU team from being able to simulate the touch down beyond simply moving the models on the screen with no interaction between the two.

Cameras

The cameras on the spacecraft and in space were actually available through the camera function in Blender. These cameras allow the viewer to see the spacecraft from angles in space and include cameras on the spacecraft that actually simulate real cameras. Blender has an integrated camera function which allows the user to change the view of the screen and the angle. To use the cameras in Blender, add the camera function (which can be accessed under the Add tab) and place the camera in the scene. The cameras in Blender allow the user to view the scene and can provide still images if the user would like.

Materials

Blender has a vast array of tools that can help create virtually any type of physical material. A material in Blender sets the basic attributes of an object. Materials in Blender can actually be rendered in the Blender Game Engine; however, textures cannot be rendered. This is why materials were used in the OSIRIS-Rex simulation and should be used for any other simulation created in Blender.

Importing CAD Files

CAD files that had previously been assembled for the 3D printing were used for construction of the TAGSAM model. The CAD files that were imported into Blender were the TAGSAM's sampler head, the female joint, the male joint, the wrist joint and the shoulder joint. The R-VIEU team concluded that the prismatic joint of the TAGSAM would not be implemented into the model for time concerns.

The initial step was to import each CAD file into Blender. This is done by going to File in the default Blender window, selecting Import, selecting the file type to be imported from the available list, and then browsing to the desired file. Blender is only able to import certain types of file formats and retain the feature of the imported part. The full-size scale CAD files were imported in a .stl format which is a format that Blender recognizes, but errors can still occur when importing. One of the errors that occurred was the original files lost their scaling and had to be resized. The other error that occurred was that the Blender Game Engine can only render so many surfaces and vertices at a time before performance begins to suffer substantially. Importing all the CAD files with such detail made the Blender software extremely slow and testing could not continue. The sampler head for the TAGSAM contained many vertices because of its delicate detail and consequently, was the contributing the most to the performance issues. To fix this problem, the half-scale model of the TAGSAM's sampler head had to be imported into the program. This version did not contain as many details as the full-scale version. Once these errors were resolved each file was assembled and grouped using a certain function that is implemented in Blender called "parenting."

Python Scripting

Blender contains a full suite of Python modules that can be used to access and change properties about almost every aspect of Blender and objects in its 3D environment. Since the Blender Game Engine (BGE) is the focus of a simulation like R-VIEU, the BGE functions will be the most extensively used for this kind of simulation.

Software Architecture and Design

When creating simulations, one of the biggest challenges is modularizing the simulation software so that the "behind the scenes" operation of the simulation is entirely hidden from the operation of the real flight software (FSW) being tested through the simulation. Ideally, a simulation tool would provide the capability for the real FSW to be ran in a virtual environment where the FSW believes it is running on a real flight system. Simulated inputs to the virtual system could then be created to test how the FSW responds to different conditions. This level of sophistication was not achieved with the R-VIEU Blender simulation, but the concepts of architecting a simulation, mentioned above, were applied to R-VIEU as much as possible to ensure that the simulation, or at least its concepts, could be extended in the future through further development of the simulation tool itself or another tool like it.

The R-VIEU software consists of three major components, the ground station / user interface (UI), the flight software (FSW), and the mechanical/environment simulation. The FSW was written to emulate the behavior and interfaces of the real OSIRIS-REx flight software, drawn from mission and system requirements. The UI was created to give the user a way to input commands into the simulation and also read out the telemetry being sent back by the spacecraft. The mechanical simulation is the interface between the FSW and the Blender Game Engine. It takes the outputs for actuating the spacecraft from the FSW and translates them so that they can actuate the simulation. It converts position and orientation data about objects in the simulation into simulated sensor data that is then read back by the FSW.

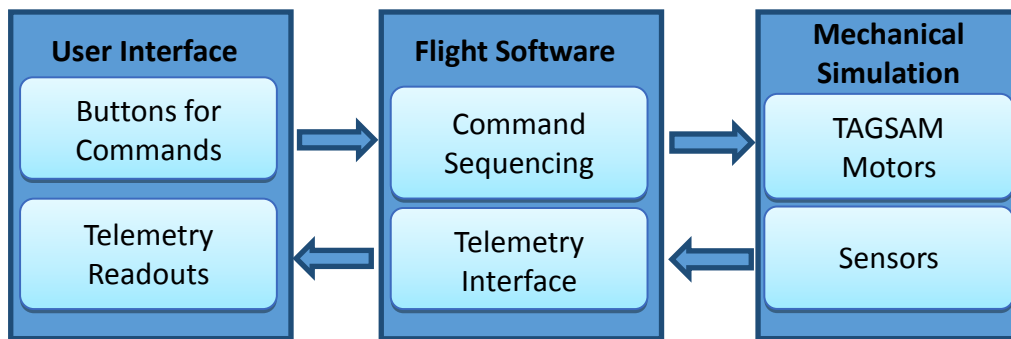


Figure 1: Software Architecture of OSIRIS-REx Simulation

The interfaces between each of these major software components are handled by a special type of global variable. Each interface is contained in a separate code file and variables are defined in each code file for each piece of data being transferred through that interface. For example, the UI to FSW interface contains the ID of the setpoint the UI is commanding TAGSAM to go to. The only inputs and outputs for the FSW are through these global variable interfaces, so the FSW is essentially isolated from the mechanical simulation and UI elements of the simulation software.

The mechanical simulation receives outputs from the FSW for commanding the different spacecraft actuators. These outputs are translated in different ways depending on what type of action they are supposed to be controlling. As per the OSIRIS-REx requirements, the shoulder and elbow motors are commanded to an angular position and the sampler head is commanded to drive in a specified direction for a specified duration of time. To actuate these joints in Blender, a “Joint” class was created so that each of the joints could be instantiated as objects and reusable methods could be used for rotating them based on the outputs from FSW.

A method called `set_Setpoint` in the Joint class accepts an angle setpoint and the current angle of the joint as input parameters. From these parameters, it rotates the joint in the direction that will drive the joint toward the setpoint. Once it is within a specified tolerance of the setpoint, the joint is then stopped. Another method in the Joint class, `get_Angle`, is used to read the current angular position of the joint for the purposes of feedback control and telemetry readouts.

A question about the operation of the shoulder and elbow joints was raised here since there was no requirement available that specifically defined this function. The question was: is the feedback control algorithm for driving the shoulder and elbow joints to their setpoints contained by the FSW,

or is it contained in a separate motor controller and all the FSW does is output an angle to that controller?

For the purposes of the R-VIEU project, an assumption was made to answer this question. The assumption was: there is a separate motor controller that handles the feedback control. The FSW simply outputs an angle setpoint for the shoulder and elbow joints. Since the flight software is the objective of the testing for R-VIEU, the feedback control was just built into the mechanical simulation component of the software.

Since the sampler head is driven differently than the shoulder and elbow joints, a different method, `sampler_Rotate`, was created in the `Joint` class specifically intended for controlling the sampler head. This method accepts a direction specified by a number, either 1, 0, or -1, and a duration in seconds. If the sampler is not moving, and it receives a duration input that is not zero seconds, it then starts a timer, and rotates in the indicated direction until the timer reaches the specified duration input. If it is moving, it will not accept a new duration input. The sampler head must finish its current movement before it can begin another.

Another question that heavily impacted the design of the R-VIEU simulation was raised due to no available requirement to answer it. How does the ground station interact with the FSW? Does the ground station send numeric setpoints that directly control the position of the arm or does the ground station simply send a setpoint ID which the FSW interprets and then decides what setpoints to drive the arm to? The assumption that was made to fill this gap was that the ground station simply sends a sequence ID and the FSW figures out where to drive the different joints to based on where it is currently versus where it is going.

Another question about the operation of the TAGSAM was then raised. Does the TAGSAM only move one joint at a time when transitioning between setpoints, or do multiple joints move at the same time? This question was critical to the development of the FSW setpoint sequencing control because the sequences would have to be defined very differently depending on which way the TAGSAM was intended to operate. Since no available requirements defined this behavior, the assumption was made that only one joint can move at a time. While it does make the operation of the TAGSAM slower and more drawn out, obeying keep-out zones is easier if only one joint is moving at a time because the motion of the arm is more predictable and the software controlling it is easier to debug. Also, this methodology was simpler to program and it was also confirmed by NASA IV&V analysts as being a realistic method of control on the real spacecraft.

Once the FSW receives a setpoint command from the UI, it then begins executing a predefined sequence to move the arm to the specified setpoint. Certain transitions are marked as invalid, because they would violate defined keep-out zones and potentially damage the TAGSAM or the spacecraft. The sequencing engine operates by stepping through a set of predefined sequences for moving the TAGSAM to each position. Certain transitions will execute special sequences upon knowing which setpoint the TAGSAM is currently at compared to which setpoint it is trying to go to. These special transitions are necessary to avoid violating keep-out zones. Each actuator that needs to be controlled in this manner must have a value in every step of each sequence, even for the steps where that particular actuator does not move. This is because an output must be written to each actuator every loop cycle and since each sequence is defined by Python “list” (comparable to an array in other high level programming languages) there must be some data written into each

element in the list. The actuators controlled directly by this sequencing are: the TAGSAM shoulder, the TAGSAM elbow, the TAGSAM sampler head, the SRC lid, the spacecraft thruster speed and direction, and the transfer of the sampler head to the SRC.

For sequencing, the UI sends FSW a command. The FSW will either then send the motor controller new setpoints to actuate the motors, or reject the command (if another command is executing or if the new command would cause an invalid transition).

The Python script `Cmd_Handling` controls sending commands to Flight Software from the UI. When a command is sent from here, it is sent for only one loop cycle using a leading edge latch function. This is important because otherwise, the flight software would detect errors resulting from holding down the send command button (the enter key on the keyboard) for more than one loop cycle.

The Flight Software has the setpoints and sequence definitions stored on it and sends current setpoints to Mechanical Outputs. `Sequencing2` is the Python file with the sequencing engine stored on it. (It is called `Sequencing2` because `Sequencing` was an older version with partial functionality and radically different architecture. It was kept as a backup during development of `Sequencing2`.)

`Sequencing2` contains four modules: `Get_Cmd`, `Get_Sequence`, `Sequence_Handling`, and `Seq_Exec`.

`Get_Cmd` takes the command sent in from `Cmd_Handling` and latches it until the sequence is complete, at which point it clears the current command. It will reject commands received while a sequence is executing.

`Get_Sequence` consists of two modules. The first one checks the incoming and most recent sequence. If it is defined as an invalid transition in the `Invalid_Trans` file, it will reject the transition and send `Get_Cmd` the signal to clear the current command. The second module takes the string that identifies the command and pulls a sequence from `Sequences`. It also defines the completion conditions for each step in the sequence.

`Sequence_Handling` advances the step number when a step is finished, and determines whether a sequence is complete. It sends `Get_Cmd` a signal when a sequence is finished.

`Seq_Exec` sends the values from the current step of the sequence to Mechanical Outputs. Each sequence is defined as a list of lists, with each step of the sequence being a member of the outer list.

The sequences are defined the same way regardless of the spacecraft's past setpoint, with some exceptions for important transitions. To ensure that only one joint moves at a time, the `None` data type can be sent to shoulder and elbow to hold it still.

CONCLUSION

A 3D interactive simulation like R-VIEU has many potential applications for IV&V and it enables testing and evaluation of many different aspects of flight software. It is primarily applicable to

systems with movable, robotic components that require controlled movements driven by flight software control.

The primary source of potential IV&V results came from identifying gaps in the mission and system requirements during construction of the simulation. Only a small number of requirements were available to the R-VIEU development team, so it is likely that many, if not all, requirements gaps discovered are actually covered in the full set of requirements. As mentioned in the Methodology Section above, many questions about the operation of the system arose during development of the R-VIEU software.

For OSIRIS-REx in R-VIEU, development the emulated flight software to control the TAGSAM generated a lot of questions about how the software should control the TAGSAM's actions. Going through this process requires the IV&V analyst to think through the same types of questions that the developers should have thought about when designing the system. This provides an excellent way to do requirements validation since the IV&V analyst has to think of answers to the same questions that the developers would have had to answer.

In addition, creation of the mechanical simulation aspect of R-VIEU generated questions about the design of the hardware-software interfaces. A tool like R-VIEU would provide different way to analyze hardware-software interfaces in addition to analyzing Interface Control Documents. It would provide the benefit of being able to actually test the software end of the hardware-software interfaces. Validation of the requirements for these interfaces could then be drawn from the results of these tests.

R-VIEU could also be used in another way to test flight software. Rather than creating emulated flight software based on requirements, real flight software could be run in a simulation environment and then interfaced with the mechanical simulation aspects of R-VIEU. This would provide a different perspective on IV&V analysis. Rather than validating requirements by creating an interpretation of the flight software, the functionality real flight software could be tested and verified by dropping it into a simulation environment that can interact with the 3D model in R-VIEU.

R-VIEU does not currently support a way to interface with a flight software simulator, but it could be a potential addition in the future. R-VIEU's functionality could be greatly improved by having the ability to run both emulated flight software written by the IV&V analyst based on requirements and a simulation environment where the real flight software could be run and interface with the mechanical simulation of R-VIEU. Comparing the results of these two approaches could provide a unique perspective on not only identifying software bugs, but also identifying issues with requirements.

Construction of the 3D CAD model also generated some questions about the mechanical design of the spacecraft as well. While not something typically identified by IV&V, a tool like R-VIEU could help identify issues in the mechanical layout of components, especially when they are in motion. This is something that would be of great benefit during the early design phases of the spacecraft, before most of the components have been constructed. Perhaps a modified version of the tool could be provided to the engineers designing the mechanical components of the mission in question. This version of the tool would enable them to import 3D CAD parts and assemblies

from their designs into the simulation and then provide a simple, manual control interface so that the assemblies can be actuated. The engineers could then visually inspect the operation of the components in order to identify any design issues.

Most of this visual evaluation can be accomplished with the base functions in most 3D CAD packages. A simple, real-time user interface for actuating the parts is typically not available directly through these packages, however, so the ability to control complex operations, such as the motion of multi-jointed robotic arms, would be greatly enhanced by this aspect of a tool like R-VIEU.

One important aspect that R-VIEU lacks, however, is the ability to simulate spacecraft physics. The true dynamics of spacecraft in orbit and in deep space are difficult to replicate on Earth, so having a virtual model of an operational spacecraft running real flight software would be able to provide a lot of insight into how the spacecraft would really operate the outer space environment. R-VIEU is currently not capable of providing this kind of physics simulation, however. While the Blender Game engine does have a physics engine, it did not provide reliable results for the multi-jointed TAGSAM. A more sophisticated software package than Blender would be required to provide a capable physics simulation.

The next step for R-VIEU would be to redevelop it with different simulation software that would support interfacing with a flight software simulator and would also support more reliable physics. These capabilities would greatly enhance the R-VIEU simulation and make it more useful as an IV&V tool.

ACKNOWLEDGEMENTS

This author would like to acknowledge the NASA IV&V Facility and the NASA West Virginia Space Grant Consortium for providing the resources which permits students a unique opportunity to participate and apply their education. This author would like to say a special thanks to Ricky Forquer, Donald Ohi, Jesse White, Nicholas Ohi, Matthew Gramlich, Jonathan Lister, and the faculty at NASA IV&V facility for their time, guidance, and assistance throughout the internship. More particularly, this author compliments the above individuals for their graciousness and patience. A special thanks to Candy Cordwell for affording this author a once in a lifetime opportunity to work with such a brilliant staff. Last, but not least, this author pledges to Ricky Forquer and Donald Ohi their efforts will not go unappreciated.

CFD MODELING INTERACTIONS OF SHOCKWAVES AND EXHAUST NOZZLE PLUMES IN THE GLENN RESEARCH CENTER 1' X 1' SUPERSONIC WIND TUNNEL

Jacob P. Inskeep
Department of Mechanical and Aerospace Engineering
West Virginia University
Morgantown, WV 26506

ABSTRACT

In order to facilitate sonic boom reduction, it is necessary to have a quantitative understanding of the interactions between tail and wing shockwaves and engine exhaust plumes. These shockwave and exhaust plume interactions can result in the shape changes for both the shockwave and exhaust plume as well as changes to the overall sonic boom signature of the vehicle. The goal of this study is to better understand these interactions so that they can be taken into account in the design of low boom aircraft.

The plume and shock interactions for this study are evaluated using Computational Fluid Dynamics for two different wedge shock generator configurations. Tetrahedral grids for flow calculation are generated using the GridTool and VGRID components of the Tetrahedral Unstructured Software System. Flow solutions are obtained using USM3D on the K supercomputing cluster. The first case features a simple wedge shock generator positioned in the flow field below the jet plume. The second case features a wedge shock generator affixed to the top wall of the test section. A third case uses identical geometry to the first case but is run using inviscid Euler calculations. All cases are run with a free stream Mach number of $M=1.96$ and a jet nozzle pressure ratio of $NPR=8.0$ in a model of the 1' x 1' supersonic wind tunnel at Glenn Research Center.

The produced flow solution for the first case shows the exhaust plume distorting to the shape and angle of the shock generator after encountering the leading edge shock as expected. The flow solution for the second case shows the exhaust plume distorting to the shape of the shock generator after encountering the leading edge shock in a similar manner to the first case. The third, inviscid case shows similar trends to the first case but higher Mach numbers are present throughout the flow. The shockwaves created by the shock generator pass through the exhaust plume in all cases. Also for all cases, the pressure signature of the leading and trailing edge shockwaves are reduced after passing through the exhaust plume though by a somewhat lesser amount in the inviscid case.

These results illustrate that interactions between wing and tail shocks and engine exhaust plumes can cause changes to an aircraft's sonic boom signature. Full understanding of this phenomenon will aid in the design of low boom aircraft to make the goal of overland supersonic flight possible.

INTRODUCTION

Reductions to the sonic boom signatures of supersonic aircraft could make supersonic flight over land a possibility. Currently, the FAA prohibits supersonic flight by civil aviators over land in the

United States due the substantial impact of sonic booms on the ground. The typical pressure signature of a supersonic aircraft at ground level is an N-wave. It is characterized by a steep spike in positive pressure followed by an expansion to negative pressure then a return to the original atmospheric conditions. While every surface on an aircraft creates its own shockwave, the individual waves tend to converge into the N-wave form by the time they reach ground level. Investigating the interactions between shockwaves generated by the tail or wing of an aircraft and the exhaust plume created by its engines may result in ways to reduce the boom signature of the aircraft. A previous study, “Exhaust Nozzle Plume and Shockwave Interaction”, showed that these interactions can cause changes to the shape of both the exhaust plume and the shockwave as well as a change in the resulting pressure signature of the shockwave (Ref. 1). The goal of this study is to provide insight into these interactions by use of a simple wedge shock generator and an exhaust nozzle plume. The geometries used for this computational flow study are a model of an upcoming physical test in the 1’ x 1’ supersonic wind tunnel at NASA Glenn Research Center.

METHODOLOGY

Two different configurations were tested in this study. Both configurations were a model of the test section of the 1’ x 1’ supersonic wind tunnel at Glenn Research Center and utilized a jet exhaust nozzle centered in the middle of the flow field attached to the bottom wall by a support structure. The first configuration used a wedge suspended in the flow field below the exhaust nozzle by a support structure. The second configuration tested in this study used a wedge affixed to the top wall of the flow field. The conditions for the tests were at standard atmospheric conditions for 50,000 ft. A free stream Mach number of $M=1.96$ and a nozzle pressure ratio of $NPR=8.0$ were used for both cases. The ratio of specific heats was kept at a constant 1.4 for all tests.

To facilitate flow simulation, a volumetric grid must be created from the CAD model. The GridTool component of the Tetrahedral Unstructured Software System (TetrUSS) was used to create surface patches from the CAD model and establish the flow boundary conditions associated with each surface. All solid surfaces were defined with the viscous surface setting, the inlet for the test section was set to the supersonic inflow setting, the jet nozzle used the exhaust core setting, and the outflow for the test section used the extrapolation setting (the recommended setting for supersonic flows). Next, the TetrUSS component VGRID was used to generate an unstructured tetrahedral grid for the flow simulation. The first configuration was created with a grid size of approximately 66 million cells. The second configuration’s grid size was approximately 62 million cells. A third grid was generated from the first configuration with a size of approximately 27 million cells for the purpose of running an inviscid flow simulation. Following generation, the grids were partitioned into 240 sections to prepare for parallel processing.

The flow field for each case was solved utilizing the USM3D code designed for unstructured tetrahedral grids. All cases were run on the K supercomputing cluster on 240 cores. The Spalart-Allmaras turbulence model was used for the flow calculations of the first 2 cases. The third case was run using the Inviscid Euler setting. To ensure satisfactory convergence of solutions, the cases were run for a minimum of 25000 iterations.

RESULTS & DISCUSSION

Wedge Below Nozzle Configuration

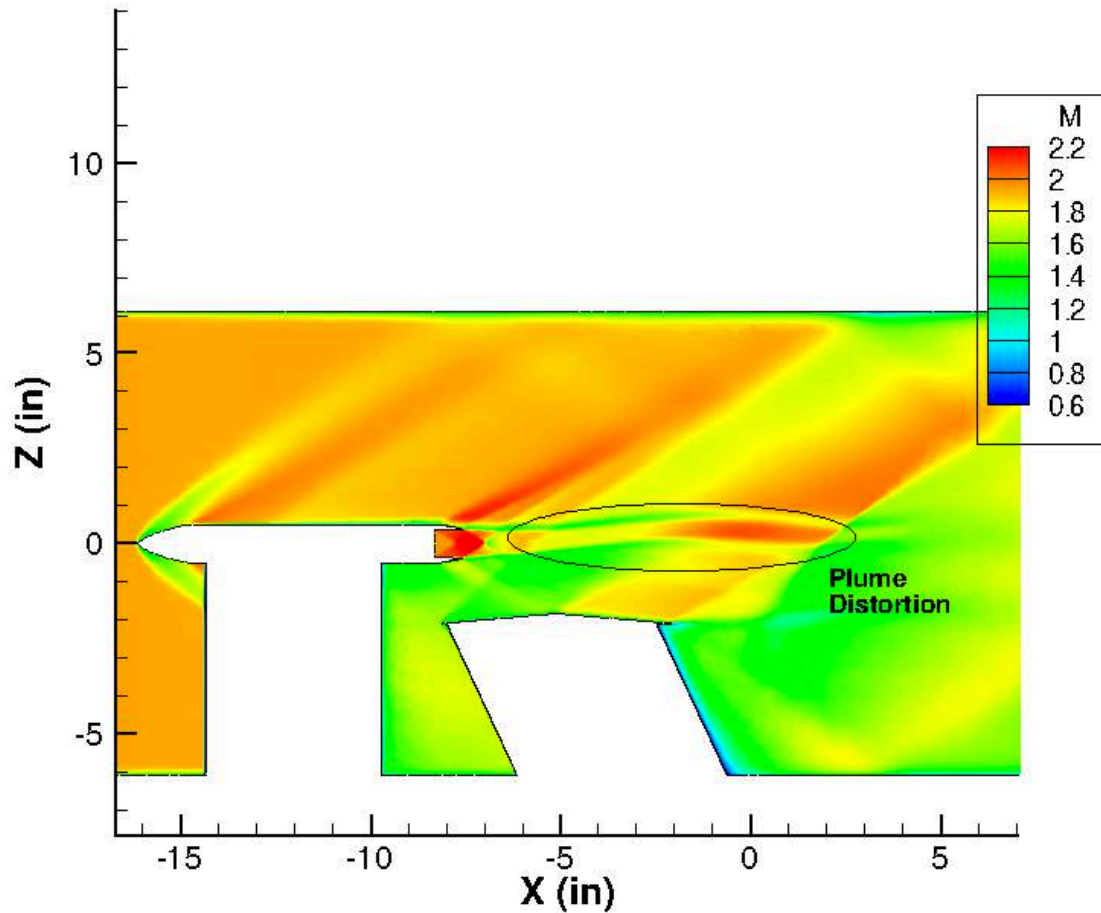


Figure 1: Flow Field for the Wedge Below Nozzle Configuration

The flow results for the first case (Figure 1) show that the exhaust plume distorts to match the shape and angle of the shock generator after encountering the produced shockwave. The exhaust plume returns to the original shape and direction after passing through the trailing shock. The flow results also show the leading edge shock from the wedge deflecting slightly down stream and the trailing edge shock deflecting slightly upstream.

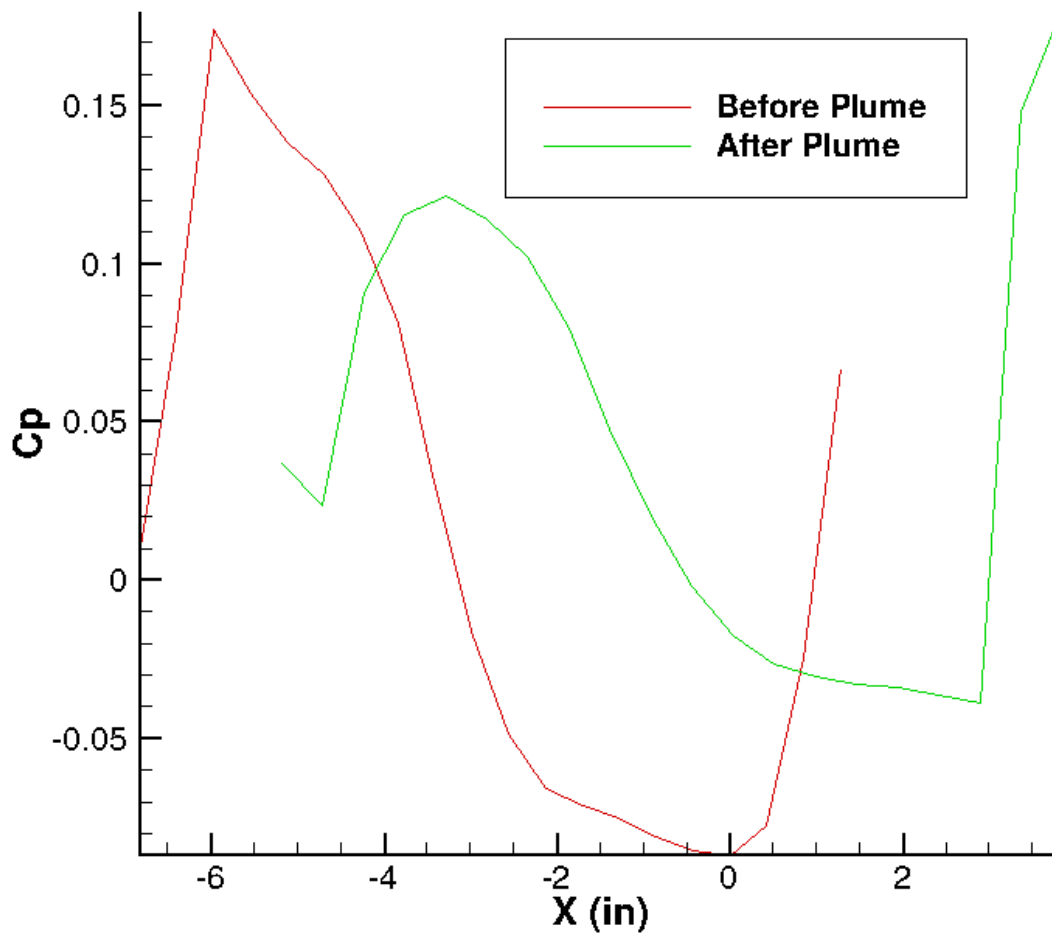


Figure 2: Pressure Signatures for Wedge Shock in Wedge Below Nozzle Configuration. The shifted profiles are a result of the oblique nature of the shockwaves.

Pressure measurements are taken from slices immediately above and below the exhaust nozzle plume to obtain a before and after profile of the shockwave created by the wedge (Figure 2). After passing through the exhaust plume, the peak maximum pressure coefficient, C_p , of the leading edge shock decreases from 0.17 to 0.12. The peak minimum C_p value for the trailing edge shock decreases from -0.086 to -0.039. This is an overall decrease of 36.5% peak to peak.

Top Wall Wedge Configuration

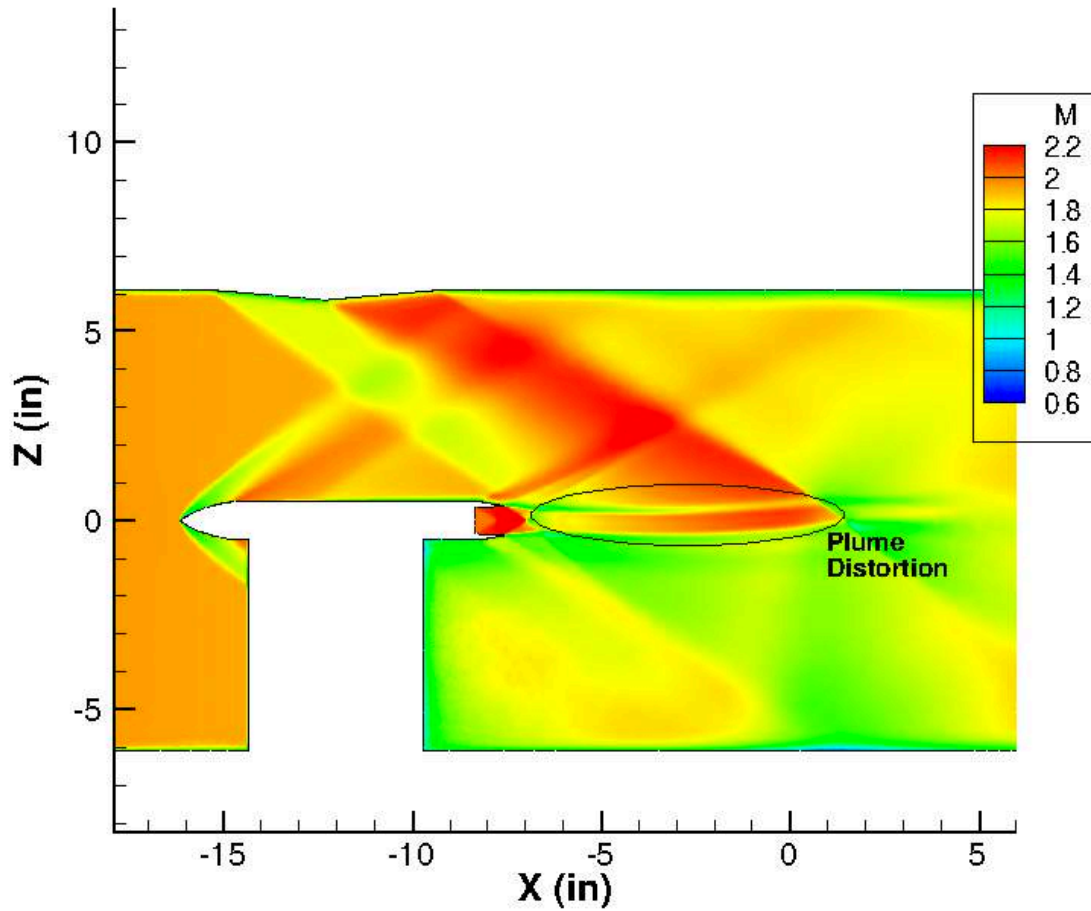


Figure 3: Flow Field for the Top Wall Wedge Configuration

The flow results for the second case (Figure 3) also show the exhaust plume distorting once encountering the wedge's leading edge shock and then returning to the original path after encountering the trailing edge shock. It should be noted that the distortion in this case is less pronounced than in the first case. The shock produced by the trailing edge of the wedge shifts slightly upstream after passing through the exhaust plume.

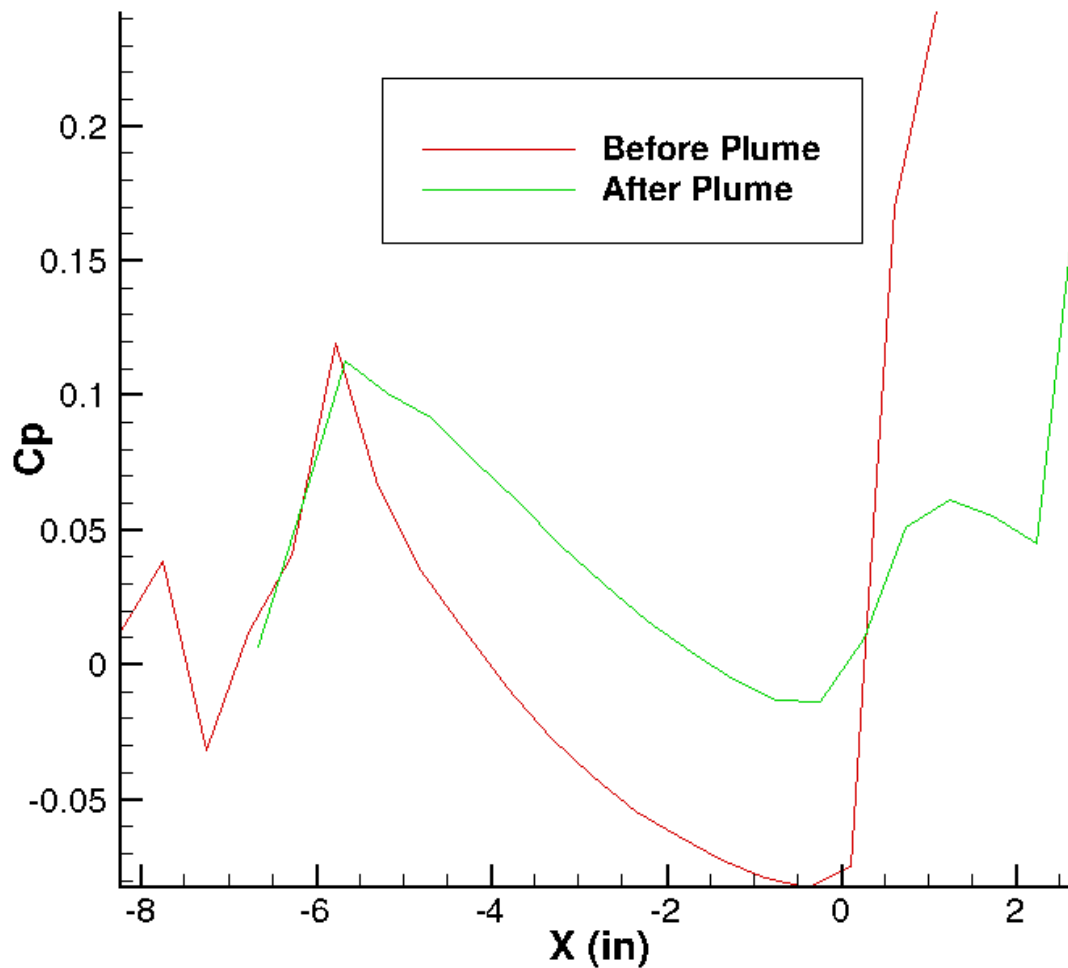


Figure 4: Pressure Signature for Wedge Shock in the Top Wall Wedge Configuration. The shifted profiles are a result of the oblique nature of the shockwaves.

Once again, pressure measurements are taken immediately above and below the exhaust plume (Figure 4). After passing through the exhaust plume, the peak maximum C_p of the leading edge shock decreases from 0.114 to 0.112. The peak minimum C_p value for the trailing edge shock decreases in total value from -0.082 to -0.013. This is an overall decrease of 36.2% peak to peak. It should be noted here that the data in this case is influenced significantly by the presence of shockwaves from other surfaces in the flow field. It is expected that the maximum peak of the pre-plume pressure curve would be higher without the presence of the expansion wave from the upper lip of the exhaust nozzle. It is also expected that the peak minimum value of the post-plume pressure curve would be lower without the presence of a shock reflected off the bottom wall of the test section.

Inviscid Wedge Below Plume Configuration

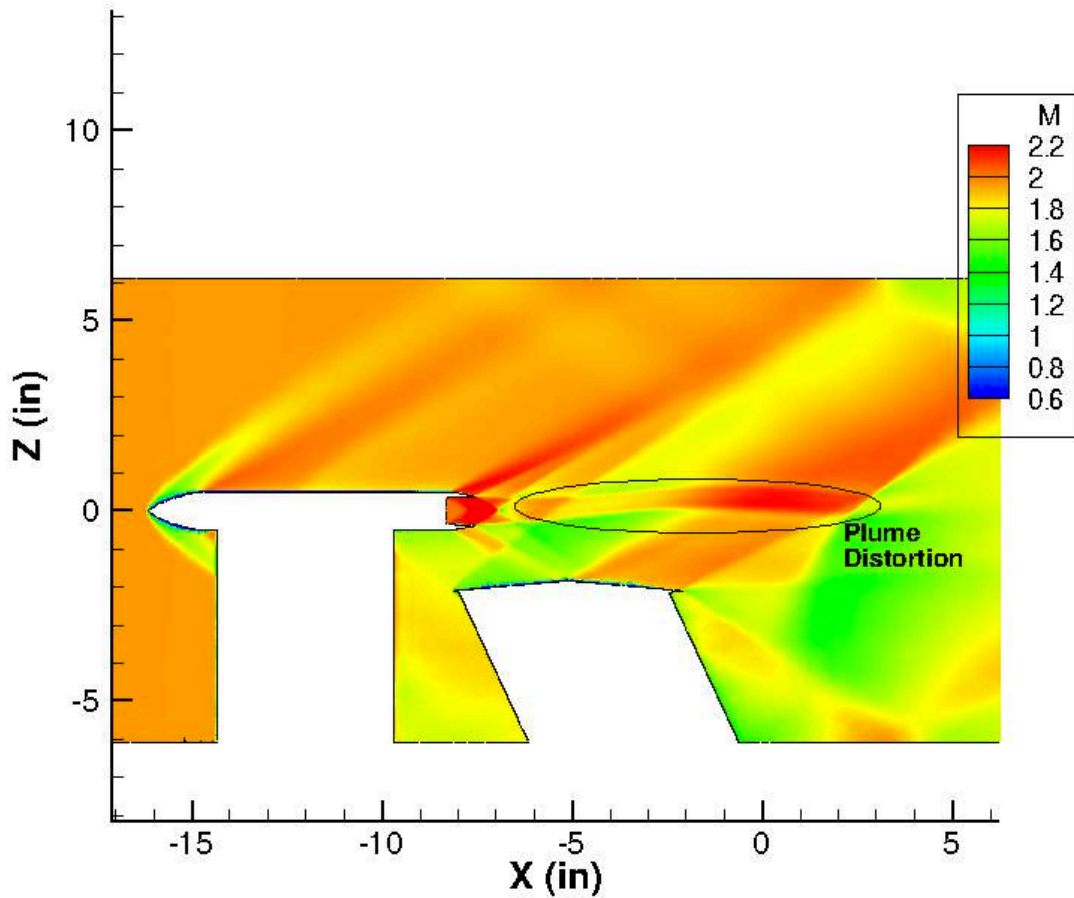


Figure 5: Flow Field for the Inviscid Wedge Below Nozzle Configuration

The flow results of the inviscid case (Figure 5) show that the exhaust plume distorts when encountering the wedges leading edge shock and returns to the original shape and direction after passing through the trailing edge shock. The wedge's leading and trailing edge shocks also distort in a similar manner to the first case. While the flow trends of the first case are preserved, the solution shows consistently higher Mach numbers throughout the flow field.

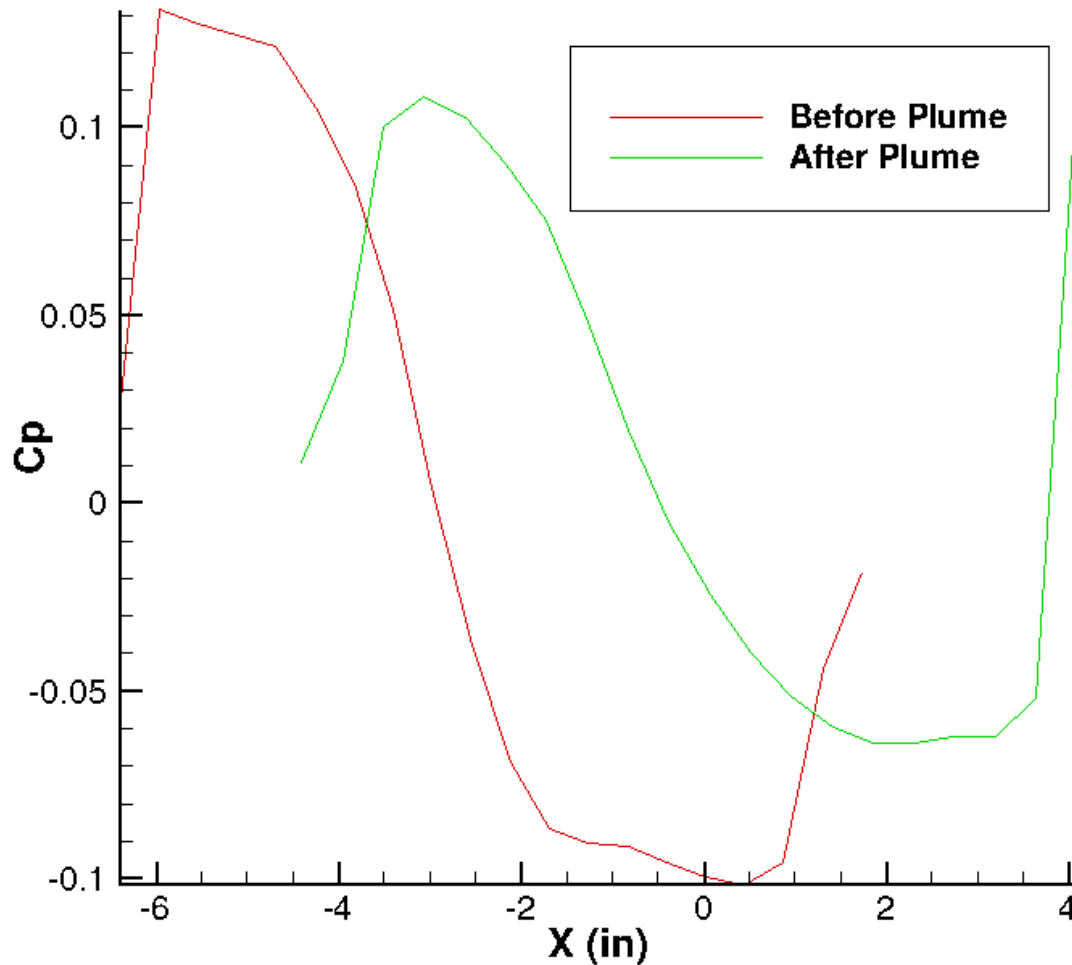


Figure 7: Pressure Signature for Wedge Shock in Inviscid Wedge Below Nozzle Configuration. The shifted profiles are a result of the oblique nature of the shockwaves.

Pressure measurements are taken immediately above and below the exhaust plume as in the viscous case (Figure 6). After passing through the exhaust plume, the peak maximum C_p of the leading edge shock decreases from 0.125 to 0.108. The peak minimum C_p value for the trailing edge shock decreases from -0.101 to -0.063. This is an overall decrease of 24.3% peak to peak. The thinner boundary on the exhaust plume and the higher Mach numbers in the flow field may account for some of the discrepancy between the viscous and inviscid tests.

CONCLUSIONS

This study shows that the interactions of exhaust plumes and shockwaves are real and significant. Shockwaves generated by the wedges do distort the shape of the exhaust plume as expected and the exhaust plume does distort the shape of generated shockwaves. The two viscous cases showed a significant reduction of more than 36% in their pressure signature amplitude after passing through the exhaust plume. While some of this reduction is due to natural dissipation, the result is substantial enough to warrant consideration in the design of low boom aircraft. As for the inviscid

case, the disparity between it and the viscous results suggest that it can be used for identifying trends but viscous calculations should be used to find more exact values.

More research is into this topic is required to fully understand how different geometries and flow conditions factor into these interactions. In order to get a better picture of the interactions taking place, tests should be run with additional configurations. Any upcoming tests should also be run at a variety of Mach numbers to investigate how the trends change under different conditions. There is currently an upcoming physical test of this experiment planned to take place in the 1' x 1' supersonic wind tunnel at NASA Glenn Research Center.

ACKNOWLEDGEMENTS

The author would like to thank NASA and the West Virginia Space Grant Consortium for providing the opportunity to engage in this research. The author would also like to thank Melissa Carter for providing mentorship and guidance throughout the process as well as all of the members of Configuration Aerodynamics Branch who were so helpful along the way.

REFERENCES

1. Castner, R., Elmiligi, A., and Cliff, S., "Exhaust Nozzle Plume and Shock Wave Interaction" *NASA Scientific and Technical Information Program*. Accessed on 07/16/2013 from http://ntrs.nasa.gov/archive/nasa/casi.ntrs.nasa.gov/20130010181_2013009767.pdf

MECHANISTIC STUDIES OF NOREPINEPHRINE IN GROWTH AND GENE EXPRESSION OF PSEUDOMONAS ISOLATES

Mardochee Isme
Senior, Applied Science
Bluefield State College
Dr. Tesfaye Belay

ABSTRACT

The stress hormone, norepinephrine supplementation to poor media enhances bacterial growth including that *Pseudomonas aeruginosa* and expression of virulence factors but the mechanism(s) is not well defined. It is speculated that norepinephrine assists bacterial growth by harvesting iron from the host. The purposes of this study were to determine the effect of norepinephrine on i) growth kinetics of different strains of *Pseudomonas aeruginosa*, ii) the gene expression of exotoxin A and siderophore genes such as pvdS, regA in *Pseudomonas aeruginosa* by growth kinetics and gene expression analysis. Eight isolates of *Pseudomonas aeruginosa* were grown in the presence or absence of norepinephrine in SAPI medium with bovine serum. Bacterial turbidity was measured by reading absorbance at 600 nm at four hours interval for 24 h. Supplementation of norepinephrine resulted in increased growth of *Pseudomonas aeruginosa* isolates. Treatment with 0.0001 M of norepinephrine yielded a two to three fold increase in absorbance readings of bacterial cultures during 6 to 12 h growth confirming previous findings that norepinephrine enhances bacterial growth. The magnitude of growth increase in the presence of norepinephrine was differential between isolates. Gene expression of iron-acquisition enhancing genes and exotoxin A production in isolates of *Pseudomonas aeruginosa* is underway.

INTRODUCTION

Pseudomonas aeruginosa is a gram-negative opportunistic pathogen that causes infections in cystic fibrosis patients, humans with an immune compromised system, and burn victims. This ubiquitous bacterium is medically important in the community. There's prime interest in NASA due its existence in water systems on space shuttles. *Pseudomonas aeruginosa* is an opportunistic bacterial pathogen with high levels of inherent antibiotic resistance. A bacterial pathogen's ability to obtain essential nutrients, i.e. iron, in its environment is necessary for successful infection. But iron, which exists in complex compounds within human hosts, is hard to obtain. Transferrin and lactoferrin are primarily found in serum and mucosal secretions. Norepinephrine aids in obtaining iron from these complex molecules. The purpose of this study was to examine the effects of Norepinephrine on the growth of *Pseudomonas aeruginosa* isolates. Our hypothesis was that the presence of Norepinephrine would show differential increased growth in between *Pseudomonas* strains.

MATERIALS AND METHODS

Eight isolates of *P. aeruginosa* were purchased from the American Type Culture Collection and two treatments of *Pseudomonas* were used in this study. The stock cultures of the bacterium were maintained in Luria broth (LB) plus 50% sterile glycerol and stored at -86°C until needed. 0.0319g

of Norepinephrine was dissolved into ten (10) mL of distilled water to prepare a 0.0001 M concentration. A 100 μ L volume was added to the poor medium, SAPI, with serum. Standard American Petroleum Institute (SAPI) Serum was prepared by combining a volume of 69% of SAPI medium, 30% of adult bovine serum (ABS), and 1% of HEPES buffer. It was then used for the treatment of the *Pseudomonas* strains. To prepare an inoculum, stock culture of an isolate was cultured in LB overnight at 37°C on a shaker-incubator. Bacterial cells were washed by centrifuging at 2,000xg for 10 minutes. Cell pellets were then re-suspended in ten (10) mL of phosphate buffered saline (PBS). A volume of one hundred (100) μ L of the original re-suspended cell pellets of each bacterial were mixed into twenty (20) mL of SAPI serum. Cultures receiving Norepinephrine treatments were given 100 μ L of 0.0001M Norepinephrine. A 0 hour spectrometer absorbance reading at 600 nm was conducted directly after, and then, the cultures were incubated for 4 hours at 37°C with gentle shaking. Absorbance readings were then conducted every 4 hours until 12 hours had elapsed. The final reading was done at 24 hours.

RESULTS

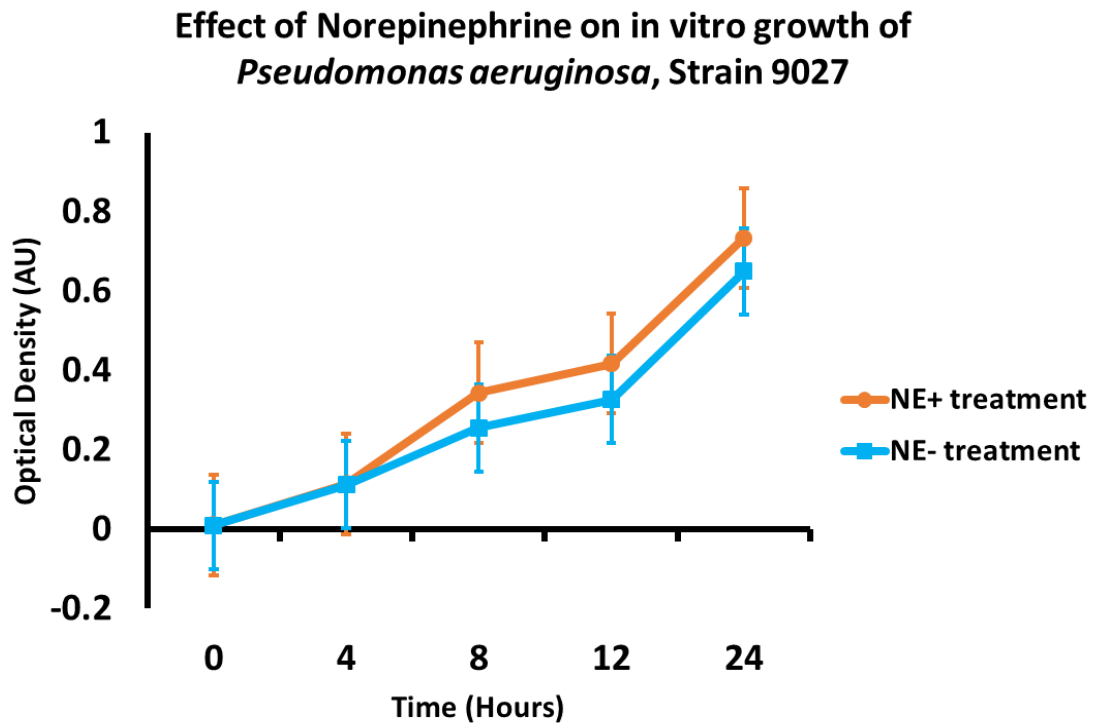


Figure 7: Effect of Norepinephrine on in vitro growth of *Pseudomonas* strain 9027. Exposure to the treatment shows slight, but insignificant change in growth between the two conditions.

Effect of Norepinephrine on in vitro growth of *Pseudomonas aeruginosa*, Strain 13525

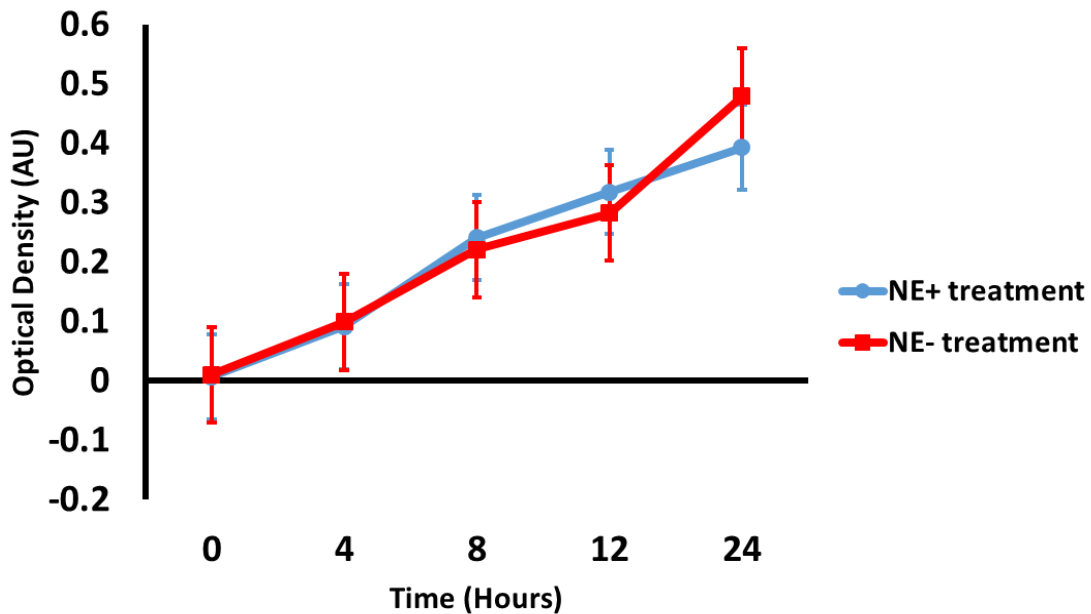


Figure 8: Effect of Norepinephrine on in vitro growth of *Pseudomonas* strain 13525. Exposure to the treatment shows little change in growth.

Effect of Norepinephrine on in vitro growth of *Pseudomonas aeruginosa*, Strain 15442

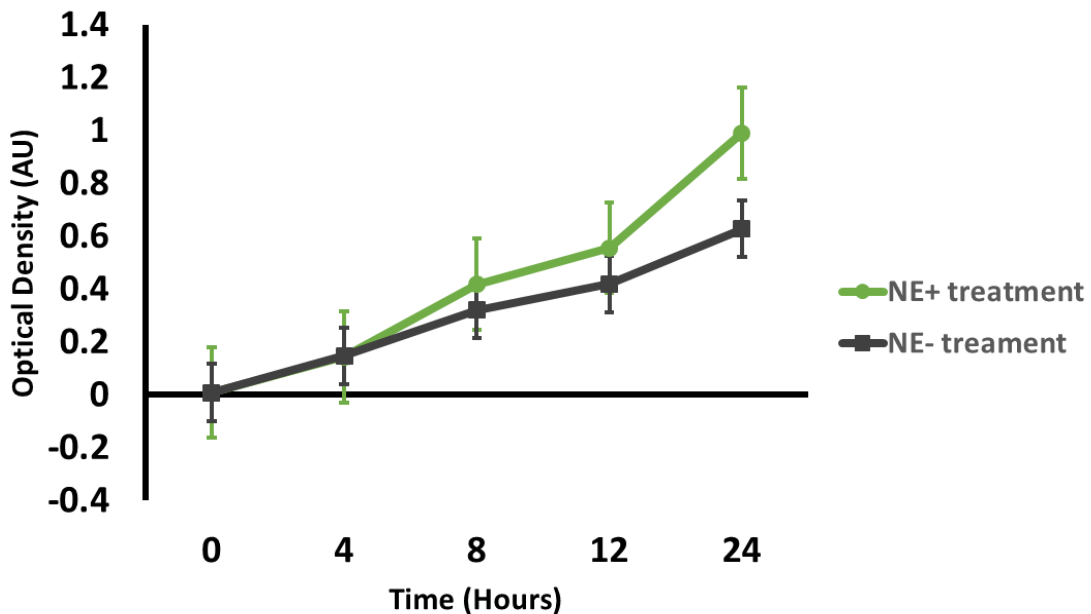


Figure 9: Effect of Norepinephrine on in vitro growth of *Pseudomonas* strain 15442. Exposure to the treatment shows significant increase in growth in the presence of the treatment.

**Effect of Norepinephrine on in vitro growth of
Pseudomonas aeruginosa, Strain 27853**

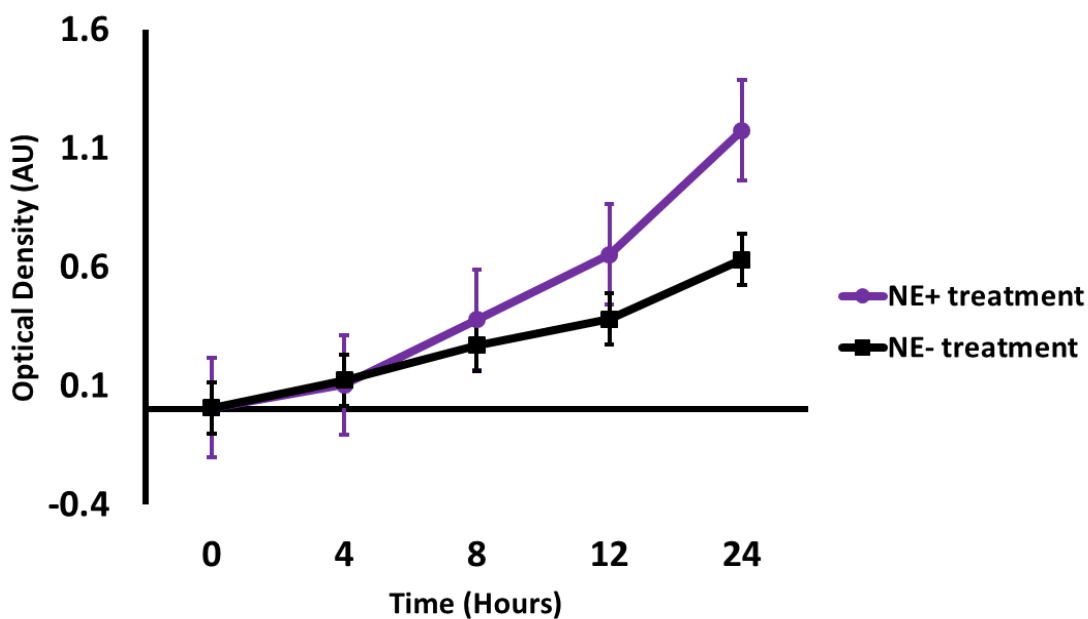


Figure 10: Effect of Norepinephrine on in vitro growth of *Pseudomonas* strain 15442. Exposure to the treatment shows significant increase in growth in the presence of the treatment.

	PAO1		383	
	12 hour	24 hour	12 hour	24 hour
NE+	0.141 ± 0.003	0.627 ± 0.014	0.193 ± 0.008	0.859 ± 0.007
NE-	0.110 ± 0.005	0.359 ± 0.008	0.147 ± 0.001	0.558 ± 0.023
	2192		ATCC	
	12 hour	24 hour	12 hour	24 hour
NE+	0.343 ± 0.011	0.859 ± 0.015	0.225 ± 0.006	0.753 ± 0.006
NE-	0.289 ± 0.009	0.768 ± 0.014	0.150 ± 0.003	0.515 ± 0.007

Table 2: Effect of Norepinephrine on clinical isolates of *Pseudomonas aeruginosa* strains: PAO1, 383, 2192, and ATCC. Exposure to treatment resulted in amplification of growth in all strains.

CONCLUSION

The use of a Norepinephrine treatment showed an increase growth in pathogenic *Pseudomonas aeruginosa* isolates. The non-pathogenic strain, 13525, showed no significant difference in growth in the presence of Norepinephrine. The strain 9027, although considered pathogenic, showed no significant difference in growth in the presence of Norepinephrine. This may indicate a lower level of pathogenicity compared to the other pathogenic strains. There were significant differences between the treated and non-treated conditions seen at both the 12 hour and 24 hour readings of strains PAO1, ATCC, 383, and 2192. Future studies will be conducted to continue this experiment and determine the effect of Norepinephrine on the gene expression of iron-acquiring genes in these strains.

ACKNOWLEDGEMENTS

NIH Grant 5P20RR016477 to the West Virginia IDeA Network for Biomedical Research Excellence, Dr. Tesfaye Belay, Chih-lung Fu, Bluefield State College and the NASA WV Space Grant Consortium for making this possible.

WORKS CITED

There are no sources in the current document.

RE-FORMATTING NASA'S AIRBORNE STUDY DATA TO SUPPORT CCMI ACTIVITIES

Ashley Kaufman
Dr. Gao Chen, Michael Shook
Science Directorate, Chemistry and Dynamics Branch
Hal Maring Atmospheric Composition Focus Area Science Mission Directorate

ACKNOWLEDGEMENTS

The success and final outcome of this NASA LARSS internship project required a lot of guidance and assistance from many people, and I am very fortunate to have received such outstanding support throughout the completion of my project work. All of my accomplishments would not have been possible without the help of some great people, and I would never forget to thank them.

First and foremost, this opportunity would have never presented itself if it weren't for the West Virginia Space Grant Consortium. They provided me with the financial support to be able to accept the internship offer and guided me through all the details and paperwork associated with the program. I am particularly grateful for their contribution, for without them I would not have even had the chance to participate in this program.

I would like to acknowledge my mentors, Dr. Gao Chen and Mr. Michael Shook, for being so patient and understanding as I became familiar and comfortable with my project tasks. I am very fortunate to have had such positive and caring role models helping me along the way. This internship would not have been as enjoyable without them. Mr. Ali Aknan also deserves recognition for providing me with the necessary data to complete my project.

I would also like to thank the LARSS coordinators, Debbie Murray and Sarah Pauls, for putting together such a fantastic and organized program. Because of all their hard work, this summer was bursting with fun activities and engaging presentations that challenged our interpersonal skills and creative ideas, provided us with valuable information on how to prepare for the future, and gave us insight on how to acquire and maintain future jobs.

The love and support from my family and friends helped me successfully complete this 10-week internship. I feel extremely privileged to have had this opportunity, and I am happy I got to share my summer with people who share similar passions, dreams, and life goals as myself. I greatly anticipate where this internship will eventually lead me in my future endeavors.

ABSTRACT

The composition and chemistry of the atmosphere is of importance primarily because of the interactions between the atmosphere and living organisms. The chemistry and dynamics of the troposphere, the lowest region of the atmosphere, and the stratosphere, the layer of earth's atmosphere above the troposphere, are progressively being studied and modeled as a distinct component in global models [7]. In addition, tropospheric and stratospheric global chemistry-climate models are continuously being challenged by new observations and process analyses.

Recent observations stressed insufficiencies in understanding and modeling of long-term composition trends and constituent lifetimes. This emphasizes that there is a need to better organize activities and evaluate scientific questions in the context of more comprehensive stratosphere-troposphere resolving models with chemistry. To address these issues, the Chemistry-Climate Model Initiative (CCMI) was established to manage chemistry-climate model evaluation and associated modeling activities [5]. Part of CCMI activity uses aircraft data for better understanding the gap.

Aircraft data are of great scientific value because they represent the most comprehensive set of simultaneous measurements with high spatial resolution [4]. There are now a variety of aircraft datasets that evaluate processes and trace gas distributions within models. Each of these datasets has its own strengths and limitations and often provides complementary information to other datasets. These datasets directly support the CCMI described above. Over the years, aircraft data has been presented in different formats, evolving to ICARTT 2010 from the original GTE and ICARTT 2004 formats. CCMI implements the ICARTT 2010 format, as it has become the NASA standard for aircraft data. The ICARTT file format criteria were developed to fulfill the data management needs for the International Consortium for Atmospheric Research on Transport and Transformation (ICARTT) campaign in 2004. Because of the ICARTT field campaign and its successes, the ICARTT data file format was exposed to a broad range of airborne research and naturally led to even wider acceptance of the ICARTT file format in later airborne studies [2]. The growing acceptance and extensive use has propelled the ICARTT data file format to be recognized as one of the standards for the airborne study community.

This LARSS internship project directly supports CCMI activity by taking data archives from NASA's Tropospheric Chemistry aircraft field studies such as TRACE-P, INTEX-NA, INTEX-B, and ARCTAS, and converting them to the newest ICARTT 2010 format. This will foster NASA's goal to promote a better understanding of air quality and climate change issues by archiving, managing, and sharing tropospheric composition data from their airborne field studies.

An atmospheric field campaign is an observational study planned for a specific location and a defined time period during which measurements are conducted from airborne platforms and/or ground sites to study physical and chemical processes in the atmosphere [5]. Airborne observations are the most effective way to obtain detailed atmospheric surveys and are critical for comprehensive investigations of atmospheric processes. These aircraft observations are widely used for model assessment and satellite data validation. The Chemistry-Climate Model Initiative (CCMI) was established to manage chemistry-climate model evaluation and associated modeling activities, which NASA's contribution to Tropospheric Chemistry directly supports. Beginning in 1987, the initial Global Tropospheric Experiment field (GTE) expeditions were designed, starting with the Atmospheric Boundary Layer Experiment (ABLE) projects. For the next fourteen years, the GTEs became a major component of the NASA Tropospheric Chemistry Program, ending with the Transport and Chemical Evolution over the Pacific (TRACE-P) in 2001. In 2004, the Intercontinental Chemical Transport Experiment (INTEX)-North America Phase A was conducted. This experiment was followed by Phase B two years later. Both of these missions looked at the inflow and outflow of pollution over North America. The Arctic Research of the Composition of the Troposphere from Aircraft and Satellites (ARCTAS) mission trailed the two-phase INTEX missions in 2008, followed by the ongoing Deriving Information on Surface Conditions from Column and Vertically Resolved Observations Relevant to Air Quality

(DISCOVER-AQ) mission, which began in 2011 [1]. An overlook of all fourteen missions' flight patterns and locations is shown in Figure 1 below.

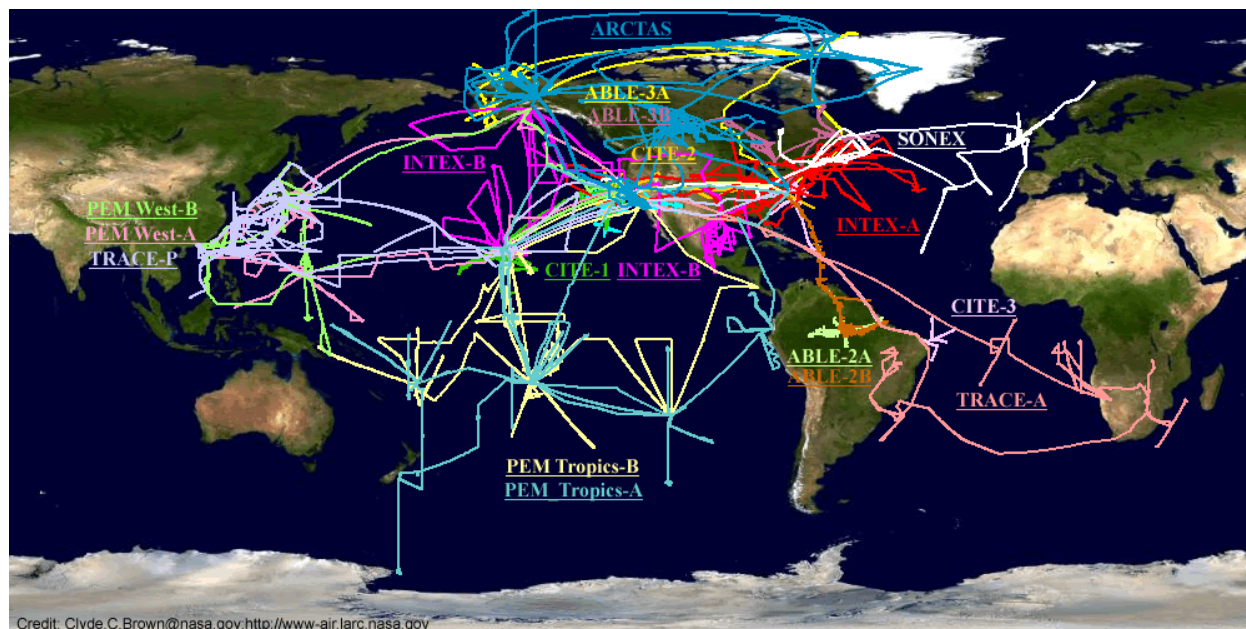


Figure 1: Locations and flight patterns for NASA's Tropospheric Chemistry Campaigns [6]

With a current total of fourteen complete missions, the NASA Tropospheric Chemistry Program has been accumulating large amounts of data in its archives. In order to distribute the datasets to the public, they must be presented in a format that is universally understood to allow for scientific collaboration. To properly manage the datasets from these aircraft field study campaigns, a format was needed that could handle airborne in-situ measurement data. The ICARTT file format was first established in 2004 primarily to facilitate data exchange and to promote collaborations among science teams. ICARTT (International Consortium for Atmospheric Research on Transport and Transformation) is a text-based, self-describing, and fairly simple-to-use file structure [2]. It is comprised of two main sections: a header section and a data section. The header section has the instructions for extracting data from the file and the critical information describing the data so that a user would have adequate information to either make direct use of the data or contact the measurement Principal Investigator (PI) to get further explanation on certain issues. The growing acceptance and extensive use has propelled the ICARTT data file format to be adopted as a NASA standard for airborne measurement data in 2010. Hereafter, we distinguish the ICARTT format between 2004 and 2010.

My LARSS summer intern project is to standardize the aircraft observational data to the ICARTT 2010 format for CCMi use. The datasets involved are TRACE-P, GTE Format; INTEX-NA, INTEX-B, and ARCTAS; ICARTT 2004 Format. To accomplish this task, I designed an algorithm and implemented it through a Perl program that easily reads the input from the file and extracts the header and data lines to transfer to the new output file. The header lines that get extracted are either statically defined within the ICARTT format standards (by line number) or dynamically defined by previous header line information. Once all the input lines are stored, the next step is to edit the appropriate input lines from the original file. To determine which input lines get modified, the ICARTT format standards are considered along with any changes made to the number of

variables, number of comment lines, and number of header lines defined in specific instances in the header information section. Lastly, the program prints the newly formatted data and edited header lines to a separate output file. As a side effect of dealing with file input and output, the formatted lines were output in a separate file to preserve the original data file. The formatting program evolved over the course of the project to get the output file to the ICARTT 2010 specifications and to minimize the amount of editing that would need to be done by hand. Perl was used as the programming language since it is efficient, easy to use, and good at handling text, regular expressions, and file input/output. Figure 2 shows an overview of the schematic of the algorithm to convert old file formats to the ICARTT 2010 format. The following pseudo-code goes through the steps to take in order to reproduce the formatting program:

Input filename

Attempt to open input file; if attempt fails, print error message and stop execution

Define necessary variables

While (a new line in the file exists)

- Read the file line
- If (on a header line):
 - If (line contains data that needs to be extracted)
 - Acquire the necessary information and store it in a variable
 - Else, store the header line as-is in the input array
- Else, if on a data line, format it if necessary and the line to the input array

Close input file

- If (input line needs modification)
 - Construct line according to ICARTT format from data acquired in input header lines
- Else, assign input array line directly to output array

Attempt to create and open output file; if attempt fails, print error message and stop execution

- For each (line in output array)
 - Print output line to output file

Close output file

End program

Based on this algorithm, I created two programs: one for converting from GTE format and the other for converting from ICARTT 2004. For ICARTT 2004 files, the primary task was to convert whitespace delimiters to comma delimiters, with some minor modifications to the file header. Converting GTE files was more complicated, as it required parsing the file header to extract metadata for creating the ICARTT 2010 file header. In addition, GTE files used a combination of space and comma delimiters, which needed to be converted to strictly comma delimiters. In some cases, the data columns in GTE format also had to be reordered to comply with ICARTT 2010 standards. Once the file conversions for both original formats were complete, the output filenames were adjusted to meet the naming convention outlined by the ICARTT 2010 standards. Table 1 provides a summary of all the files that were converted. During this internship project, a grand total of 962 files have been converted to ICARTT 2010, including merge files for constant time intervals as well as merges to time series provided by instruments within the merge.

Table 1: Summary of the merge file conversion

Mission Name	File type	# of files converted
ARCTAS	ICARTT 2004	352
INTEX-B	ICARTT 2004	159
INTEX-NA	ICARTT 2004	179
TRACE-P	GTE	272

After the files had been formatted, it was extremely important to check for errors. While tedious, each file was individually checked to make sure all lines were accounted for and all lines were accurately transferred over in their proper form. For files that were converted from the old ICARTT 2004 format to the new 2010 format, a comparison was conducted using Igor Pro, a scientific data analysis and programming tool, to make sure none of the data was altered from the format transformations. A program was created with Igor Pro to take in two files and scan the layout to make sure the data numbers did not differ from one file to the other. Using the Igor Pro program to confirm that there were no differences between the data in the old and new files ensured that the data was preserved during the reformatting process. Due to the complexity of the transformation from GTE format to ICARTT 2010 format, files converted from GTE format were checked manually to ensure no errors were made during the reformatting process.

The goal of converting these old datasets to the new ICARTT 2010 format was successful because of these formatting programs. My project contributed to CCMI efforts by providing airborne data from four NASA Tropospheric Chemistry missions in a standard format that allows for model-data inter-comparison studies. In addition, by making these changes to the file formats, the datasets will now be easier to interpret and will allow NASA to distribute the data to the public with anticipation of greater scientific collaboration.

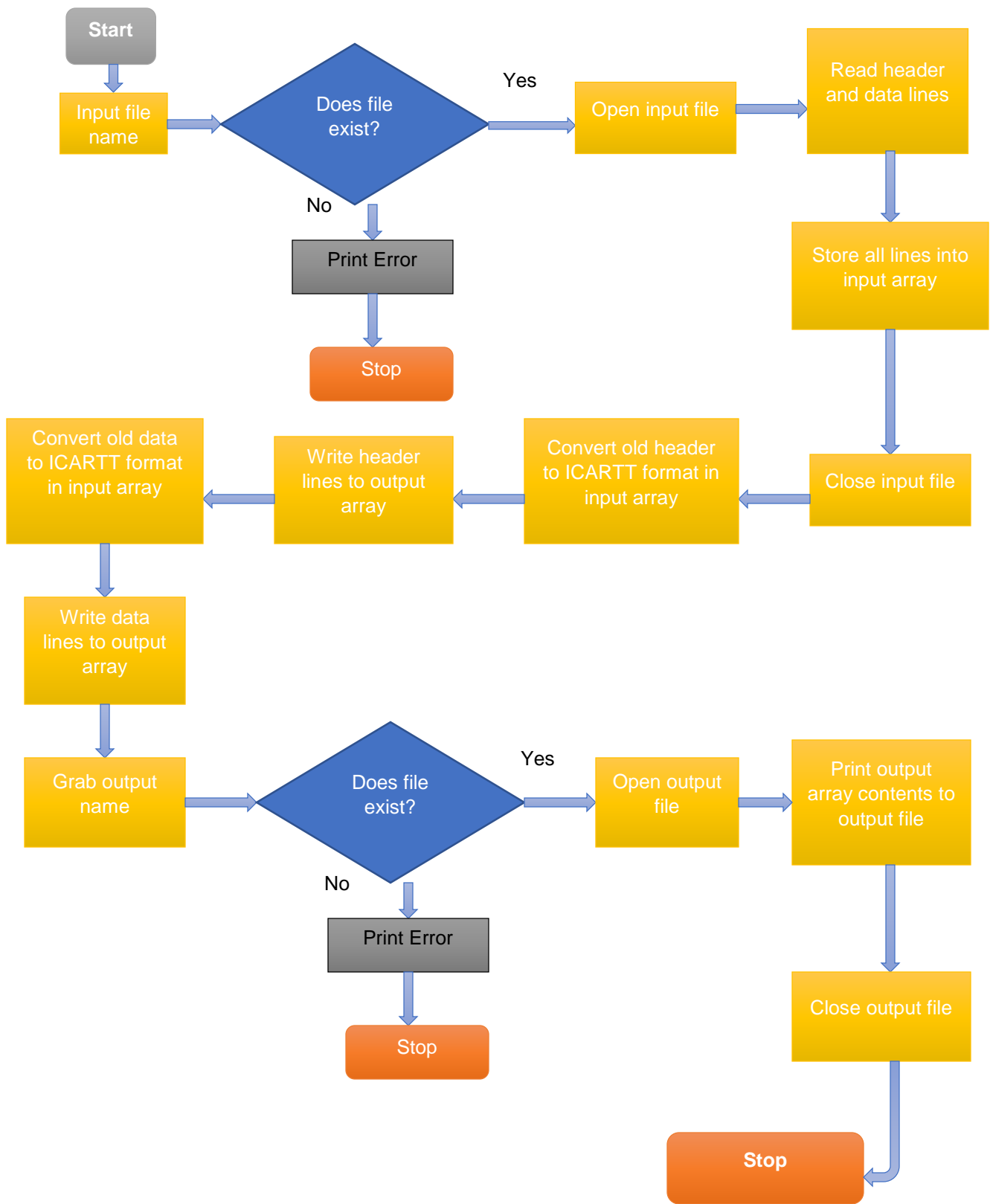


Figure 2: Flowchart of the formatting program-Shows the steps the program takes to convert the old data to the new ICARTT 2010 format

REFERENCES

- [1] Aknan, A., Chen, G. (2013, February 15). *Airborne Science Data for Atmospheric Composition*. Retrieved from <http://www-air.larc.nasa.gov/missions/merges/>
- [2] Aknan, A., Crawford, J., Chen, G., Williams, E. (2013 March). *ICARTT File Format Standards VI.1* Retrieved from <http://www-air.larc.nasa.gov/missions/etc/IcarttDataFormat.htm>
- [3] Angeli, E., Wagner, J., Lawrick, E., Moore, K., Anderson, M., Soderlund, L., & Brizee, A. (2010, May 5). *General format*. Retrieved from <http://owl.english.purdue.edu/owl/resource/560/01/>
- [4] Eyring, V. (2013, March 7). *Observations for model evaluation (comparability and process studies)*. Retrieved from http://www.pa.op.dlr.de/CCMI/CCMI_Obs4CCMI.html
- [5] Kusterer, J. (2013, June 30). *Field Campaigns* Retrieved from <https://eosweb.larc.nasa.gov/field-campaigns>
- [6] NASA (2013). [Map representing the flight patterns and locations of aircraft field studies] *NASA Tropospheric Chemistry*. Retrieved from http://www-air.larc.nasa.gov/trop_map.htm
- [7] NOAA (2010). *Why do we care about atmospheric ozone?* Retrieved from <http://www.esrl.noaa.gov/csd/assessments/ozone/2010/twentyquestions/Q3.pdf>

SUMMER 2013 RESEARCH EXPERIENCE WITH THE FLIGHT CONTROL SYSTEMS LABORATORY (FCSL)

Ozias McKenzie

Undergraduate Student, Department of Mechanical and Aerospace Engineering
West Virginia University
Morgantown, West Virginia 26506

ABSTRACT

This summer's research activities consisted of working with a quadcopter system, employing a Matlab/Simulink software simulation package, participating in laboratory experiments, and involvement in field testing activities. Initial work consisted of developing a SolidWorks model to determine geometric characteristics of the quadcopter vehicle. These properties were then applied in a Matlab/Simulink simulation to determine the vehicle's thrust characteristics and navigate through various simulated flight paths. Hands on work consisted of experimental testing of the quadcopter propulsion systems, specifically to determine the max thrust produced by the aircraft. The quadcopter was found to produce a thrust of approximately 1.7 kg, however after additional modifications to power packs it was capable of 2.75 kg. The quadcopter's maximum thrust was defined, allowing for constructive quadcopter simulations. This has been an informative experience; working with graduate students I learned various programming techniques and improved my team skills. After tasting research work, I am inspired to excel in my classes and my career as an engineer.

INTRODUCTION

The purpose of this fellowship was to obtain experience in a research team environment and develop skills related to hardware testing, simulation work, and practical application. Specifically, I assisted Mr. James Reil, a graduate student working with the quadcopter development and Dr. Seanor, from the MAE Department. My duties during this fellowship included defining the quadcopter physical parameters, creating flight paths for the simulation environment, and examining issues related to safe propulsion testing. The quadcopter required enough thrust to be able to transport a reasonable amount of load such as: a camera, GPS, or any other equipment that would be attached to the quadcopter. There had to be a clear definition of what the quadcopter capabilities are and any modifications must be carefully noted.

QUADCOPTER ANALYSIS

Due to my inexperience with computer programming, several programming exercises were required. Tutorials were taken in SolidWorks, Matlab, Simulink, Linux, and C++ to achieve a basic level of understanding. These programs gave me the ability to create virtual models, design flight paths, and simulate programs/run quadcopter from the CPU. In addition to learning new software programs, hardware tools were introduced as well. Devices such as an oscilloscope, solder iron, Spektrum DX6i Transmitter, and some power tools were utilized. Learning these

different tools while working on the quadcopter has improved my hardware and programming skills.

After receiving a Droidworx AD-4 quadcopter from the NASA Fairmont facility, the quadcopter was disassembled piece by piece. These pieces were then constructed into a SolidWorks CAD model of the vehicle, as shown in Figure 1.



Figure 1. SolidWorks Quadcopter Model

SolidWorks was then used to determine the moments of inertia and different dimensions of the quadcopter, which could be inputted to Matlab. The starting point for the simulation model was acquired through Peter Corke’s website [1], and the software has been modified to correlate with our quadcopter’s characteristics. All the quadcopter characteristics, seen in Table 1, were recorded in Matlab to simulate the quadcopter. Unfortunately, SolidWorks was unable to give a precise measurement on the propellers angles because the software package didn’t have the same dimensions as the actual quadcopter’s propellers. The EPP1045 propellers required physical examination to calculate the blade tip and blade root angles.

Table 1. Quadcopter Thrust Variables

Parameter	Value	Units	Parameter	Value	Units
A	0.0507	m^2	M	1.67	kg
C_t	0.0068	-	r	0.127	-
g	9.81	m/s^2	ω	800	rad/s^2
ρ	1.154	kg/m^3			

If the thrust capability remained lower than its weight than it will be unable to have lift. Enough thrust was required for the quadcopter to accelerate, transport cargo, or any other application required by the aircraft. Initially the quadcopter in the simulation would climb up in altitude extremely fast in the air because the thrust was miscalculated for the quadcopter. To maintain a steady flight condition, a flight control simulation was operated in Simulink that figured out the right thrust coefficient (C_t). According to Table 1, our quadcopter mass (M) is 1.67 kg. To maintain steady, level flight, the thrust (T) should equal $\frac{T}{4}g = 4.096 \text{ N}$. 1.67 kg. The thrust per rotor:

After inputting the variables from Table 1 in Equation 1, indicated our coefficient of thrust was 0.0068, which will be necessary in order to have stable flight during our simulation.[1]

$$C_t = \frac{T}{\rho A r^2 \omega^2}$$

Equation 1

Any miscalculation of the quadcopter properties would make the quadcopter unstable and unable to maintain flight.

SIMULATION WORK

Simulation work was accomplished within Matlab/Simulink environment. Some Matlab script files and the Simulink model were acquired through Peter Corke’s website [1] that provided a basic understanding of how the quadcopter would fly. Computer testing was necessary to ensure the quadcopter had stable flight conditions and provided an equivalent mathematical representation of the actual model. In Simulink (Figure 2), the model was constructed so the flight simulation program could be executed while the quadcopter trajectory was plotted.

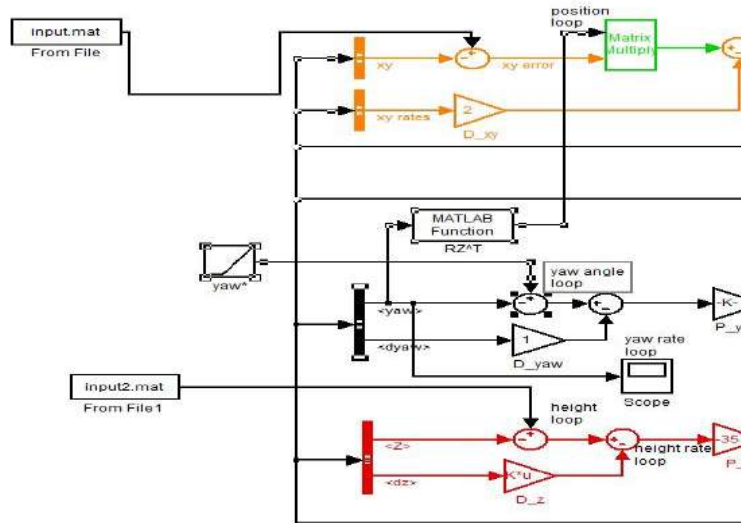


Figure 2. Simulink Model

In Figure 2 above, a function was sent from Matlab to a source block (top left) that controls the xy-direction of the quadcopter and another source block (bottom left) that controls the z-direction. After all the quadcopter properties have been accounted for it is now ready to be simulated, but there was still instability of the aircraft in flight. The thrust gains, shown in Figure 3, were then modified so that the aircraft was stable, which enabled it to follow its chosen flight trajectory.

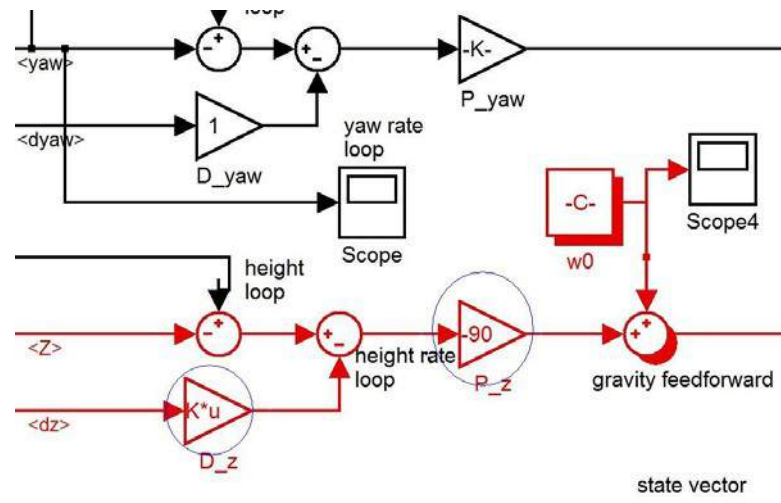


Figure 3. Gains in Simulink

The quadcopter could fly in a variety of predetermined paths such as a figure eight, triangular, circular, or star-shaped. Figure 4 illustrates where the quadcopter would execute its designated trajectory.

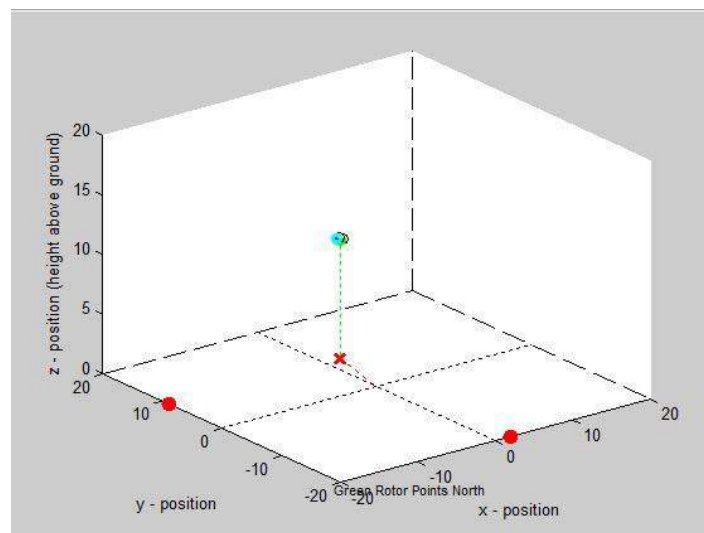


Figure 4. Simulation of the Quadcopter via Simulink [1]

The path could be selected by running a graphical user interface (GUI) as shown in Figure 5. The GUI is a Matlab tool that allows the programmer to determine what functions to execute. In this case it would be used to select what flight path the quadcopter should fly. In Figure 5, the programmer could choose a trajectory between the mentioned shapes, or create their own flight path. After the path was selected, the quadcopter would then fly this simulation as shown in Figure 4.

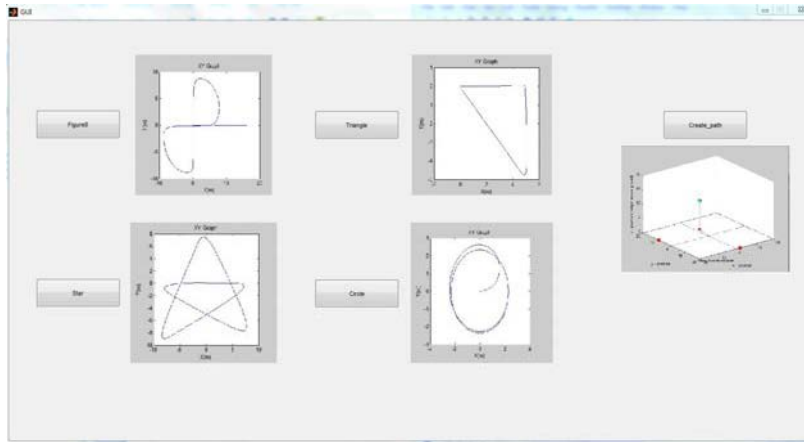


Figure 5. Matlab GUI

A quadcopter has six controllable degrees of freedom: up/down, left/right, backward/forward, roll, pitch, and yaw. Matlab code was written to record the data of the quadcopter and plot its flight path (x, y, and z, positions), thrust levels, pitch, yaw, and roll in respect to time, as shown in Figure 6. These graphs explained how the aircraft flew, if it was an unsuccessful flight it would help determine where it was malfunctioning.

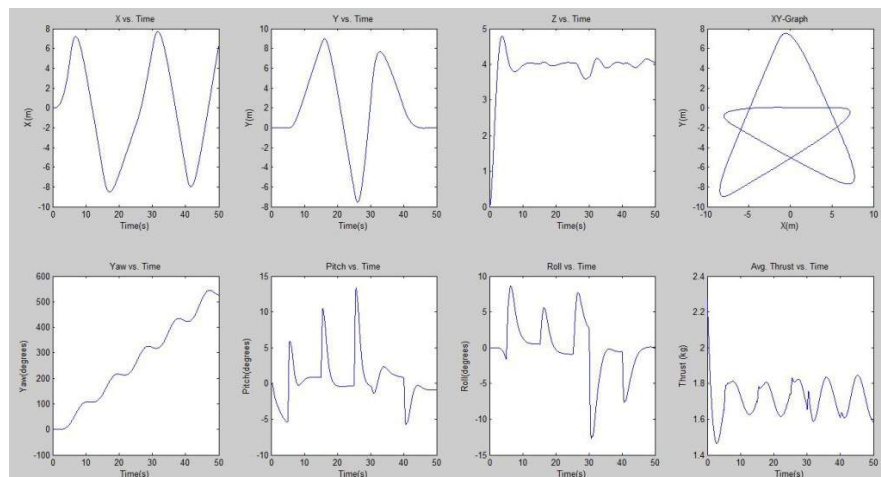


Figure 6. Data Gathered During Simulation

HARDWARE TESTING

After programming was completed, it was now time to begin hardware testing. The power and signal wires were connected from the CPU/transmitter to the electronic speed controllers (ESCs), which operated the quadcopter motors. It was mandatory for wires to be examined cautiously to prevent short circuits that could lead to over-heating, damage wires, or damage parts. Before testing could commence, there was always a strong focus on safety. In initial tests,

only one propeller was able to operate from the transmitter. The Spektrum transmitter programming was modified that ensured all four ESC's received signals simultaneously.

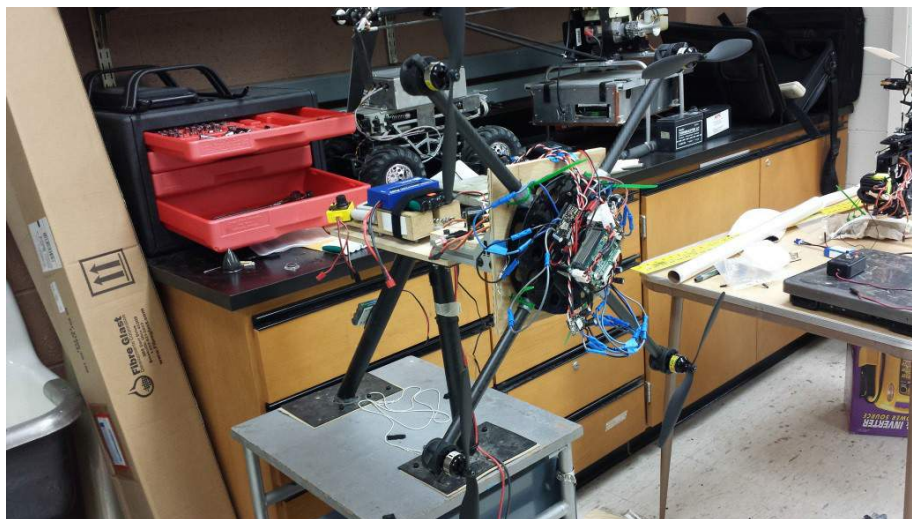


Figure 7. Quadcopter Thrust Testing

As shown in Figure 7, the quadcopter was attached to a wooden platform which was connected to a Medusa Power Analyzer Pro and Rapala Digital Scale (thrust indicator) to test the thrust, and measure amps and voltage. Several tests were conducted with the quadcopter to determine the maximum thrust. According to an average sum of some thrust calculators, each rotor should produce about 0.7 kg of thrust and therefore all four should produce around 2.79 kg of thrust. The quadcopter was first ran on a Zippy-K Flightmax 2500 mAh 3S1P 20C Lipo that produced a max thrust of 1.7 kg. This battery was only allowing a draw of 22.6 amps. This equated to a 40% error of maximum thrust output. The current was too low so there required to be a switch in batteries for a higher current draw. The Zippy Compact 3300 mAh 4s 35C Lipo Pack was attached to the quadcopter. This test drew 35.6 amps and resulted in about 2.75 kg of thrust which calculated out to be about 1.4% error. The second battery produced more thrust but it also weighed 0.17 kg more than the first battery. But because the amount of thrust was much greater (1.05 kg), the additional mass could be considered acceptable.

CONCLUSION

At the start of this summer fellowship the quadcopter weighed 1.5 kg and produced a maximum thrust level of about 1.7 kg. With the modifications of the quadcopter and the reconfiguring of the propulsion wiring, it now has a heavier mass of 1.67 kg (due to a higher capacity battery) and a 1.05 kg increase in thrust. Initially from simulation, it was found the quadcopter would have had difficulty in the take-off phase (according to initial calculations) but now has the ability to carry objects or attach new devices as payload.

PERSONAL EXPERIENCE AND FUTURE PLANS

Being a new experience to work with an unmanned aircraft system (UAS), I read several papers and performed multiple tutorials for various software programs. The Matlab programming was simple at first, but then came to be challenging because of the several errors that came about

with the first few programming attempts. Determining both the physical and dynamic variables of the quadcopter itself was difficult because with one small miscalculation the quadcopter simulation would malfunction and begin to fly out of control. Eventually these errors were solved and the quadcopter managed to achieve successful simulation tests with the generated flight paths, as noted earlier.

My communication skills were also increased by participating in bi-weekly meetings and presenting PowerPoint presentations about my research progress on various tasks with Mr. Reil and Dr. Seanor during this fellowship. Other than quadcopter laboratory tests and simulation conducted, I got an opportunity to assist with the Flight Control Systems Laboratory (FCSL) field testing team. I experienced flight testing activities with various UAV systems during the summer semester. Overall this was a rewarding educational experience that aids in my future coursework and provided a basis for a hands-on engineering experience.

ACKNOWLEDGEMENTS

Special thanks to the NASA West Virginia Space Grant Consortium for providing this summer research opportunity and experience. Thank you to everyone involved with helping me this summer:

Dr. Majid Jaridi	Director, Professor	NASA WV Space Grant
Ms. Candy Cordwell	Program Manager	NASA WV Space Grant
Dr. Brad Seanor	Research Assistant Professor	MAE Dept., Research Faculty
Mr. James Reil	Graduate Research Assistant	MAE Dept., MS Aero Engineering

REFERENCES

- [1] P. Corke, "Matlab Toolbox Software," [Online]. Available: <http://petercorke.com/Home/Home.html>. [Accessed 29 June 2013].

AIRBORNE WIND ENERGY DUAL USE FEASIBILITY INVESTIGATION

Sarah E. Mills
Aerospace Engineering
West Virginia University
Morgantown, WV 26506

ABSTRACT

The purpose of this project was to investigate potential dual uses for Airborne Wind Energy (AWE) and determine public opinion on AWE. By increasing the potential benefit to society with dual uses, the desire was to encourage NASA to become more involved with AWE research. Interviews and a public survey were conducted in order to gather information and opinions. The main dual uses for AWE that came up were surveillance, communication, and weather forecast. In general, the public viewed AWE favorably and was most interested in seeing AWE located offshore. The major concern that came up was safety.

INTRODUCTION

With the United States government setting goals to increase the use of renewable energy and the increasing popularity in the use of renewable energy, the timing is perfect to introduce airborne wind energy (AWE) to society. Initially, it might seem that research on AWE should be performed by the U.S. Department of Energy because it is a new concept for obtaining electricity. While this may be true, the Department of Energy has little experience with airborne vehicles and wind at higher altitudes. Unlike the Department of Energy, NASA has extensive experience in these areas. This makes NASA a better choice for continued research on AWE. The purpose of this project is to encourage NASA to direct more resources into research on AWE.

In order to encourage NASA, this project looks at potential dual uses for AWE and public response to AWE. With dual uses, AWE is capable of benefitting more people than if it only produces electricity. If the public views AWE favorably, then AWE will be able to have a much greater impact on society than it would without public support.

BACKGROUND

AWE is an approach to harnessing renewable wind energy. Instead of using a rigid structure to reach altitudes high enough to harness energy, AWE configurations fly at altitudes up to 2000ft while tethered to the ground. Traditional wind turbines generally operate at altitudes of approximately 240ft above the ground.

Wind speeds are faster at higher altitudes. Because the power generated by wind energy is dependent on the velocity of the wind cubed, more power can be generated at higher altitudes. By operating at higher altitudes than traditional wind turbines, AWE configurations are able to take advantage of the faster wind speeds.

There are two types of AWE. One type generates electricity on the ground using tension on the tether. The other generates electricity in the air using generators mounted to the device, and

transmits the electric energy to the ground through the tether. Within these types, there are multiple designs. A kite-pulled tether and a glider plane-pulled tether are designs in the ground generation of electricity category. A wing with turbines, a stationary rotating turbine, and an inflatable shell with an encased turbine are designs in the air generation of electricity category (Moore, 2010).

PROJECT

This project investigated dual-use functionality for AWE that would increase the benefit of AWE to society. Instead of depending solely on engineers to predict dual uses for AWE, experts in different areas in society were interviewed to determine dual uses from their perspective. This project also gathered public opinion on AWE and potential dual uses through a survey. The desired outcome was to establish multiple dual-uses for AWE technology with societal benefits that would provide compelling reasons to take advantage of AWE.

METHODS

In order to accomplish the goals for the project, an outline was created. This outline contained a detailed description of each task necessary to complete the project. Once the outline was created, a schedule was produced to confirm there was time to complete each task. Some of the tasks were divided between the people working on the project to accomplish them more efficiently.

Background research on AWE was the first main task for the project. It was necessary to gain knowledge on the topic while also looking at the various configurations different companies are working on. After the background research, a list of ideal characteristics for harvesting wind energy was created. Using that list, a Technique for Order Preference by Similarity to Ideal Solution (TOPSIS) Report was developed to compare four conventional land based wind turbines and five major AWE concepts. The designs were rated for how they met each criterion and then the average rating was calculated. This was to determine the best design for harnessing wind energy. Then ideas for dual uses and potential areas for implementation were compiled in a brainstorming session. A societal adoption path for AWE was drawn up at this point as well.

Contact information was obtained for organizations and professions identified in the brainstorming session on dual uses for AWE. These organizations or individuals in the organizations were contacted via email and/or phone. After the initial contact, face-to-face meetings were scheduled when possible. The purpose of meeting in person was to more clearly communicate the concept of AWE to someone who may have no prior knowledge of it.

In addition to identifying specific categories of people to contact, a survey was created to generate responses from the general public. The survey was passed out via Facebook and email. The objective of the survey was to identify public opinion on AWE. The survey also provided the opportunity for people to come up with their own ideas for dual uses and areas where this technology could be implemented.

The responses from the interviews and surveys were documented and analyzed as they arrived.

RESOURCES

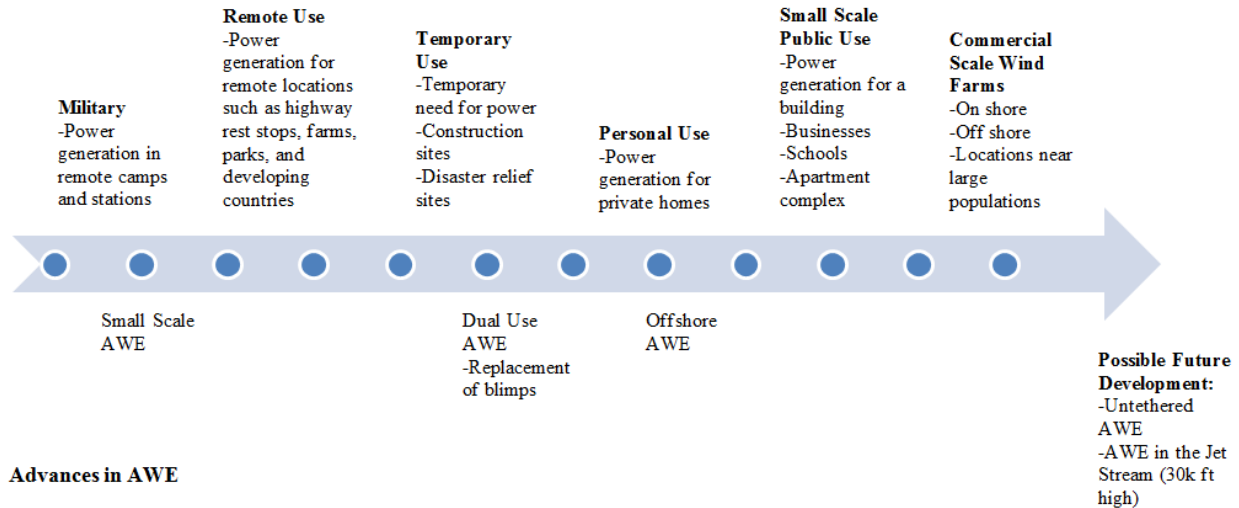
Resources available at the Langley Research Center were used to accomplish the project. An important resource to this project was employees at the center. Mark Moore, Dave North, Bill

Fredericks, and Kevin Antcliff all provided their expertise on AWE and advice for the project. Another resource was prior NASA presentations dealing with AWE, wind speed data, and examples for creating a TOPSIS report.

RESULTS

AWE Adoption Path

Introduction into Society



Advances in AWE

TOPSIS Report

Importance Ranking:	0.06383	0.10638	0.10638	0.06383	0.06383	0.06383	0.06383	0.06383	0.10638	0.02127	0.10638	0.02127	0.06383	0.06383	0.02127			
	Noise Level	Cost (at a typical on shore site)	Maintenance	Capacity Factor	Broad Wind Speed Operability	Ground Area Required	Environmental Impact	Visibility	Autonomou s	Durable in a range of weather	Safety	Lifespan	Max Altitude	Geographic Accessibility	Ease of Transport	Separation Value to Best Solution	Separation Value to Worst Solution	Relative Closeness to Ideal Solution
Windlift	0.0333	0.0370	0.0231	0.0041	0.0259	0.0132	0.0472	0.0292	0.0057	0.0034	0.0572	0.0014	0.0196	0.0228	0.0105	0.0831	0.0914	0.5237
Ampyx	0.0333	0.0555	0.0462	0.0123	0.0259	0.0132	0.0315	0.0292	0.0057	0.0034	0.0381	0.0082	0.0295	0.0228	0.0105	0.0701	0.0946	0.5746
Makani	0.0222	0.0555	0.0077	0.0368	0.0389	0.0132	0.0157	0.0292	0.0172	0.0069	0.0064	0.0041	0.0295	0.0228	0.0070	0.0980	0.0846	0.4633
Altaeros	0.0222	0.0370	0.0462	0.0245	0.0130	0.0397	0.0157	0.0194	0.0172	0.0011	0.0191	0.0014	0.0295	0.0342	0.0105	0.0758	0.0829	0.5224
Sky Wind Power	0.0222	0.0370	0.0693	0.0123	0.0259	0.0397	0.0157	0.0292	0.0057	0.0034	0.0191	0.0041	0.0295	0.0342	0.0070	0.0769	0.0973	0.5587
1.5MW General Electric	0.0111	0.0185	0.0231	0.0123	0.0043	0.0132	0.0052	0.0097	0.0515	0.0103	0.0381	0.0082	0.0033	0.0038	0.0035	0.1033	0.0623	0.3761
V82-1.65MW Vestas	0.0111	0.0185	0.0231	0.0123	0.0043	0.0132	0.0052	0.0097	0.0515	0.0103	0.0381	0.0082	0.0033	0.0038	0.0012	0.1035	0.0622	0.3755
126-3.3MW Vestas	0.0111	0.0185	0.0231	0.0123	0.0130	0.0044	0.0052	0.0097	0.0515	0.0103	0.0381	0.0082	0.0098	0.0114	0.0012	0.1001	0.0630	0.3862
V164-8.0 Vestas	0.0037	0.0062	0.0077	0.0368	0.0130	0.0044	0.0052	0.0032	0.0515	0.0069	0.0381	0.0122	0.0098	0.0038	0.0035	0.1148	0.0667	0.3675
Best Solution:	0.0333	0.0555	0.0693	0.0368	0.0389	0.0397	0.0472	0.0292	0.0515	0.0103	0.0572	0.0122	0.0295	0.0342	0.0105			
Worst Solution:	0.0037	0.0062	0.0077	0.0041	0.0043	0.0044	0.0052	0.0032	0.0057	0.0011	0.0064	0.0014	0.0033	0.0038	0.0012			

For this report a rating of one would be an ideal solution. The first five names on the left are AWE designs and the next four are traditional wind turbines. Based off the results from the TOPSIS report, the AWE designs all met the criteria better than the traditional wind turbines.

Weather Station Interview

Jeff Lawson, Chief Meteorologist at WVEC, was interviewed to obtain a professional opinion on dual uses for AWE that could aid in forecasting the weather. He said that currently aerostats with weather sensors are sent up although not many are used. Virginia only has one or two weather

aerostats for the whole state. By attaching lightweight weather sensors to AWE configurations, it would provide additional points to retrieve data. There is also inadequate data for offshore regions. According to Mr. Lawson, they work with satellite images and have to estimate the altitude of the top of clouds in order to predict weather conditions in those areas. The ability to attach sensors to AWE configurations offshore would improve accuracy for their work. Depending on the durability of the design, there is the potential to have additional data points ahead of and possibly during storms. AWE configurations could be used by airports to determine wind shear as well (J. Lawson, personal communication, July 25, 2013).

Fire Management Interview

Captain Anthony Chittum, Station Commander at the Langley Research Center Fire Station, was interviewed to obtain a professional opinion on dual uses for AWE that could assist the fire department. According to Capt. Chittum, improving communication capabilities is the most probable application the fire department would use. There is also the possibility of determining the location of a cell phone call more easily. Capt. Chittum said the fire department might also be able to use AWE for surveillance. It would act like a watch tower, especially in remote areas. He said it could provide real time aerial views for emergency locations and be a first line of sight for an emergency as well (A. Chittum, personal communication, July 26, 2013).

Police Department Interview

Assistant Chiefs Trent Sturgis and Joseph Moore, from the Newport News Police Department, were interviewed to obtain a professional opinion on dual uses for AWE that could benefit the police department. They said that surveillance would be the most probable application for the police department. The police department has used aerostats tethered at an altitude of 500ft for surveillance a few times in the past and found the use beneficial to their work. Surveillance capabilities would help them with observation and security for large events. It would also help along the waterfront for port security. Traffic control would benefit as well, with the ability to monitor accidents and direct traffic. According to Chiefs Sturgis and Moore, the capability of using both traditional and infrared cameras attached to an AWE configuration would be beneficial. The police department currently faces restrictions on other new airborne surveillance technologies. UAVs are capable of surveillance, but they are not allowed to operate within five miles of an airport. This restriction is particularly difficult for places like Newport News which have very little airspace left after accounting for multiple airports and military bases in the vicinity. If AWE configurations were allowed to operate within five miles of an airport, it would provide more options for surveillance. The use of UAVs by law enforcement agencies is currently restricted to emergency situations in VA as well. Because they are tethered to the ground, AWE configurations could bypass this law and provide surveillance for law enforcement agencies. In addition to surveillance, Chiefs Sturgis and Moore thought AWE could support communication technology. One possibility they mentioned was temporarily replacing phone towers during failures or natural disasters (T. Sturgis & J. Moore, personal communication, July 29, 2013).

Military Interview

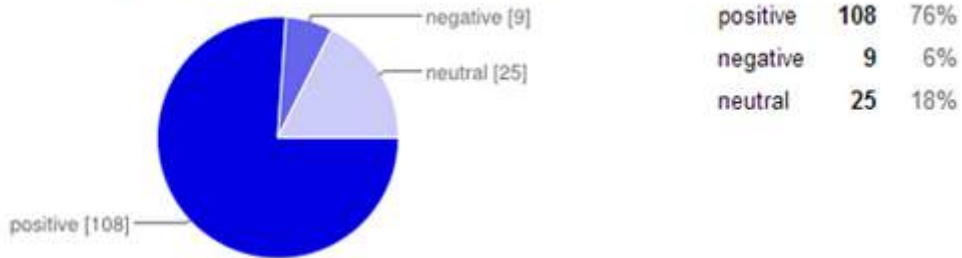
A meeting was held with Bill Fredericks, an employee at NASA Langley Research Center, to gain his advice on the project. Because Bill is a marine, he was also able to provide insight into dual uses for AWE pertaining to the military. Bill said that military camps currently use tethered aerostats for surveillance, but these aerostats must be lowered during high winds. This provides the enemy time to work without being watched. Because AWE is capable of operating at higher

winds, it would be able to provide more consistent surveillance which would improve security for the military. The military could also use AWE for a communication platform (W. Fredericks, personal communication, July 29, 2013).

Survey Results

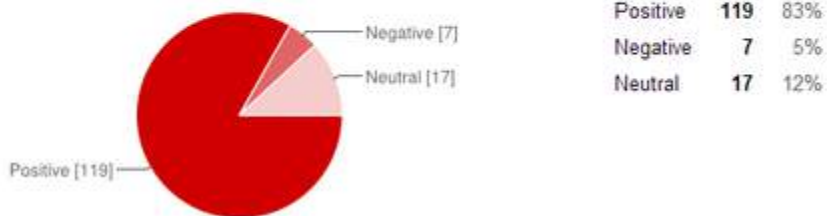
The survey contained a brief description of AWE and provided pictures of three designs. There were 143 respondents. The following charts show the responses to a few questions.

What is your initial opinion of Airborne Wind Energy?

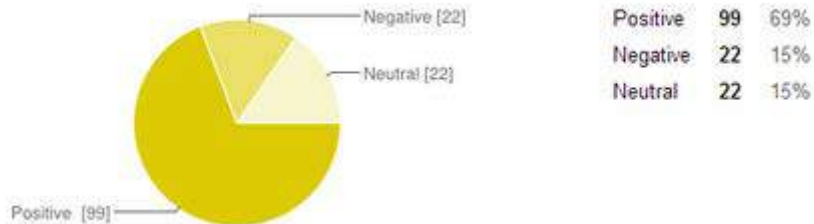


Locations for Operating AWE Configurations

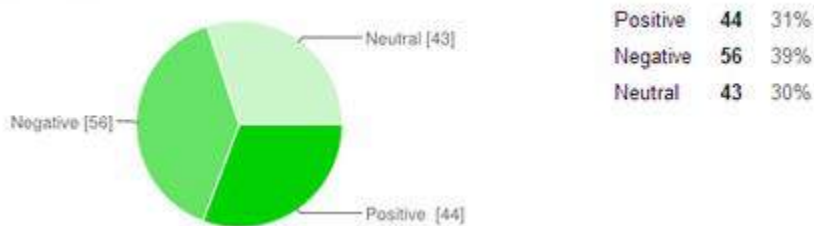
Off Shore



Rural Area



Urban Areas



76% of respondents viewed AWE favorably. 83% of respondents were receptive to the idea of AWE configurations operating offshore. 69% had a positive response to AWE operating in rural areas while only 31% had a positive response to it operating in urban areas.

The survey also provided the opportunity for respondents to voice their concerns about AWE. The concerns voiced dealt with safety, environmental impact, visual appeal, cost/benefit, and practicality of AWE configurations.

FUTURE STEPS

As research continues on AWE, there are a few steps that can be taken with the results from this project. In future research on AWE designs dual uses should be taken into account. This will allow for dual uses to be implemented into society at the same time as AWE is implemented. As safety is a major public concern for AWE configurations, the safety of designs needs to be proven before a widespread introduction to the public. A list of responses to public concerns should be created to distribute when presenting AWE to the public. By addressing concerns ahead of time, the public will be more receptive to AWE.

MOST VALUABLE ASPECTS OF LARSS PROGRAM

A valuable aspect of the LARSS program is program's desire to work on social and behavioral skills with interns in addition to the technical skills used on projects. The interns attended an etiquette luncheon and a career enhancement seminar during the program. Both of these events taught useful skills that young adults are not always aware of when entering the work field.

Another valuable aspect was gaining experience in a working environment. My mentor invited the other intern I worked with and me to attend weekly update meetings for another project he was involved with. Having worked on a similar, smaller scale project at school, it was interesting to see how the team went about accomplishing goals, dealing with problems, and working together. It also showed me the importance of weekly meetings for projects with multiple sub-teams.

SIGNIFICANT EXPERIENCES DURING PROJECT

The opportunity to travel to NASA's center located on Wallops Island was the most significant experience I had during my time in the LARSS program. A team in my directorate invited the interns in the directorate to join them when they went to Wallops to determine the capabilities of the facilities there. I was able to see two Orbital Antares rockets being assembled as well as the launch sites at Wallops. I also saw the testing facilities.

CONCLUSION

After completing the project, it was determined that expectations were met. Information gained from the weather station, police department, fire department, and military provided a list of dual uses for AWE that would benefit them. These uses include weather forecast, surveillance, and communication. A 76% positive response to the survey question asking opinions on AWE demonstrated a positive reception of AWE with the public.

There were a few areas of the project that could have been better. One area is the interviews. The initial plan was to have more interviews in other areas including the Red Cross, farmers, and lifesaving services operating on a beach. With the limited time, no contacts were found in these areas willing to discuss the project. Another area is the survey. The survey had no place to indicate age or geographic location of the respondents. This would have assisted in analyzing the responses. The survey also lacked a statement of the altitude at which traditional wind turbines generally

operate. This would have provided the respondents with a comparison for the altitudes at which AWE configurations operate and eliminated some confusion concerning AWE.

The results of this project can assist with future AWE developments. Dual uses should play a role in future design improvements and public concerns should be addressed when presenting AWE. NASA would be a great asset to AWE research and would benefit the public if it became more involved with AWE.

ACKNOWLEDGEMENTS

The author would like to thank NASA and the WV Space Grant Consortium for the opportunity to participate in the NASA LARSS Program. The author would also like to thank Mark Moore for his mentorship on the project. Thanks to Kinsey Rieth as well for her partnership on the project.

REFERENCES

Moore, M. D. (2010, January). NASA Airborne Wind Energy Introduction Summary.

DETERMINATION OF MICE INFECTED WITH LONG-TERM STARVED PSEUDOMONAS AERUGINOSA

Robert Price
Applied Science/Pre-Med
Bluefield State College
Bluefield, WV 24701

ABSTRACT

National Aeronautics and Space Administration (NASA) is interested in studying *Pseudomonas aeruginosa* because it causes opportunistic infection in astronauts. This bacterium is known to live in the water system of space shuttle but its existence mechanism is not known. Experimental infection of mice with starved *P. aeruginosa* has resulted in reduced health rate of mice compared to stock culture of the parental strain, ATCC 12055. The purpose of this study was to determine the organ load of starved cells of *P. aeruginosa* in a mouse model. Two groups of mice were intraperitoneally infected with fresh inoculums and sacrificed to detect bacteria in the different organs in 8 hours. No bacteria were detected in mice infected with starved or non-starved cells in mice sacrificed in less than 6 hours after infection. *P. aeruginosa* cells were present in the liver, kidney, heart, lung and spleen after 6 hrs of infection. The lung, heart, and liver had more bacteria present than the kidney and spleen. This study suggests that characteristics of starved *P. aeruginosa* has changed due to the loss of some of its natural virulence features but further investigation is needed to understand its starvation adaptation and pathogenesis.

INTRODUCTION

Pseudomonas aeruginosa is an opportunistic pathogen which causes various infections in individuals with an immune compromised system, patients living with a human immunodeficiency virus (HIV) infections and chronic pneumonia in cystic fibrosis patients. The biofilms has protected colonies by polysaccharide which plays a vital role for *Pseudomonas aeruginosa* resistance to antibiotic.

Pseudomonas aeruginosa is important to NASA due to one of the crew members of Apollo 13 developed an urinary tract infection and its existence in water for prolonged periods of times is not well understood. In the research lab at Bluefield State College a group of researchers have been investigating the long term starvation of the bacterium which has the ability to survive for 1485 days in water, morphological changes appear during starvation.

Pseudomonas aeruginosa is a rod-shaped, gram-negative, flagellated and ubiquitous organism that has the capability to survive in various parts of the environment, such as fresh surface water, food and moist surfaces. It has adaptive abilities which come from its flexibility to form biofilms, control the permeability of its outer membrane, its genetic regularity networks, and produce extensive capsules. *Pseudomonas aeruginosa* requires simply dietary requirements and often observed to be the most significant bacteria able to multiply in distilled water.

The ability of the *P. aeruginosa* to live in water for prolonged periods of time is not well understood. The national Aeronautics and Space Administration (NASA) is concerned about this bacterium because its long-term survival in space water pipes, it was isolated from water system in the space shuttle for several times. *P. aeruginosa* has caused urinary tract infection (UTI) in one of the Apollo 13 astronauts. At Bluefield State College a group of researchers has been

Investigating the long-term survival of different strains of *P. aeruginosa* in sterile water samples for over three years. The Prediction was as previous literature reviews have shown stresses bacteria have developed various mechanisms of survival to survive under harsh conditions; the starved cells of *Pseudomonas aeruginosa* may have a higher pathogenicity than the non-starved cells. The purpose of this study was to determine the organ load of starved cells of *P. aeruginosa* in a mouse model. The hypothesis was starved cells will spread to organs of mice in a small range of time.

MATERIALS AND METHODS

Bacterial Strain

Pseudomonas aeruginosa strain #12055 purchased from ATCC (Manassas VA) was used in this study. Stock cultures of the bacterium were maintained in trypticase soy broth medium (TSB) mixed with 50% glycerol and stored at -80°C until use. Stock culture was grown overnight at 37°C in Luria Bertani (LB).

Pseudomonas isolation agar (PIA) was used for stock culturing and bacterial inoculum preparation.

Animals

Six to seven weeks old female Swiss Webster mice from the Hilltop Lab Animals INC (Scottsdale, PA) were used in this study.

Bacterial growth kinetics and starvation in sterile water

Stock culture or batches of sterile double-distilled or tap water inoculated with *P. aeruginosa* stored at room temperature were used throughout the study. To compare the growth kinetics of starved and non-starved cells, samples of each bacterial culture were inoculated in broth and grown at 37°C at 165 rpm for 12 hours. Viable plate counts were done by plating serially diluted samples on PIA every two hours. For the long-term starvation kinetics 1×10^8 CFU/mL of *P. aeruginosa* were inoculated in sterile tap or distilled water and placed at room temperature. Viable plate counts were done every two weeks to determine the amount of the bacteria in each culture over the period of starvation.

Infection Protocol

Starved and Non-starved Cells were grown overnight in LB broth at 37°C with slow shaking. Cells were harvested by washing with PBS and the bacterial density was adjusted to the desired concentrations.

The pellet was then resuspended in 10ml of sterile Phosphate Buffer Saline (PBS). A ten-fold serial dilution was made to the desired concentrations of 10^7 , for mice inoculation. Seven mice for each dilution of the starved and non-starved cells were injected with 100 μ l of the starved or non-starved cells at each dilution intraperitoneally (IP). Mice were observed every 3 hours post-infection. Every three 2 mice were sacrificed post-infection using CO_2 inhalation. The heart, lungs, liver,

kidneys, and the spleen were harvested and homogenized in sterile PBS using Tissue Ruptor from Qiagen (Valencia CA). Different doses were plated into PIA and incubated for 24 hours at 37°C for CFU/ml determination.

RESULTS

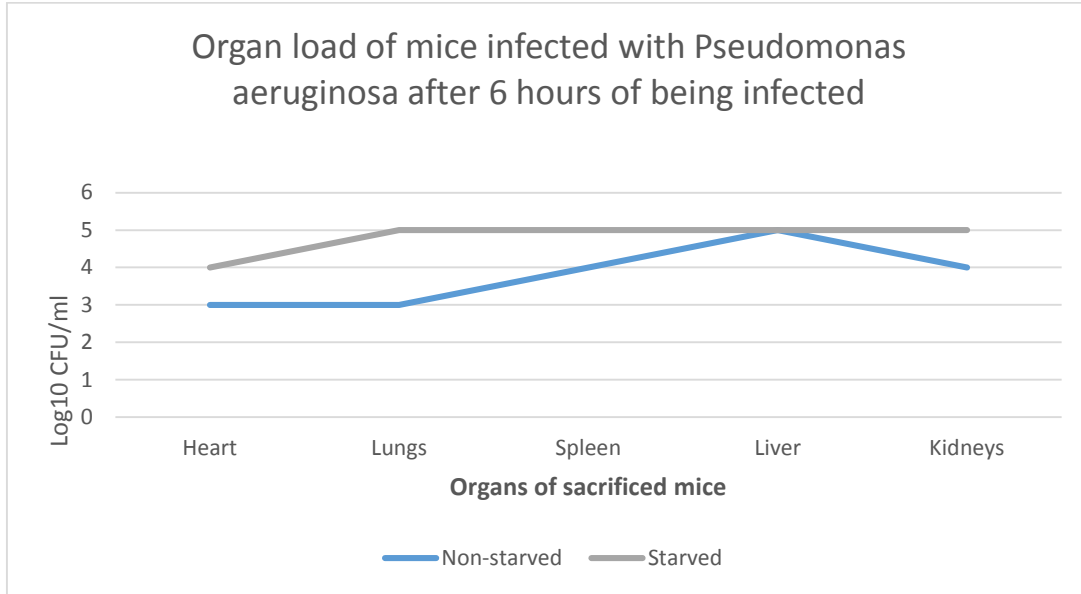


Chart 1: Organ load of mice infected with *Pseudomonas aeruginosa* showed after 6 hours more of starved cell of the bacterium were found in the heart, lungs, liver and kidneys

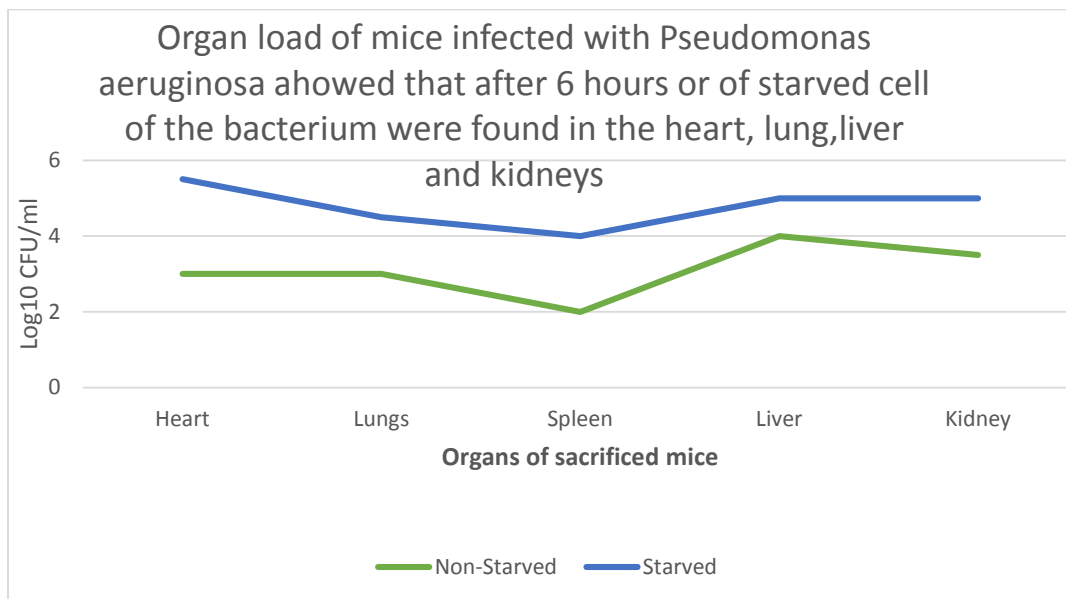
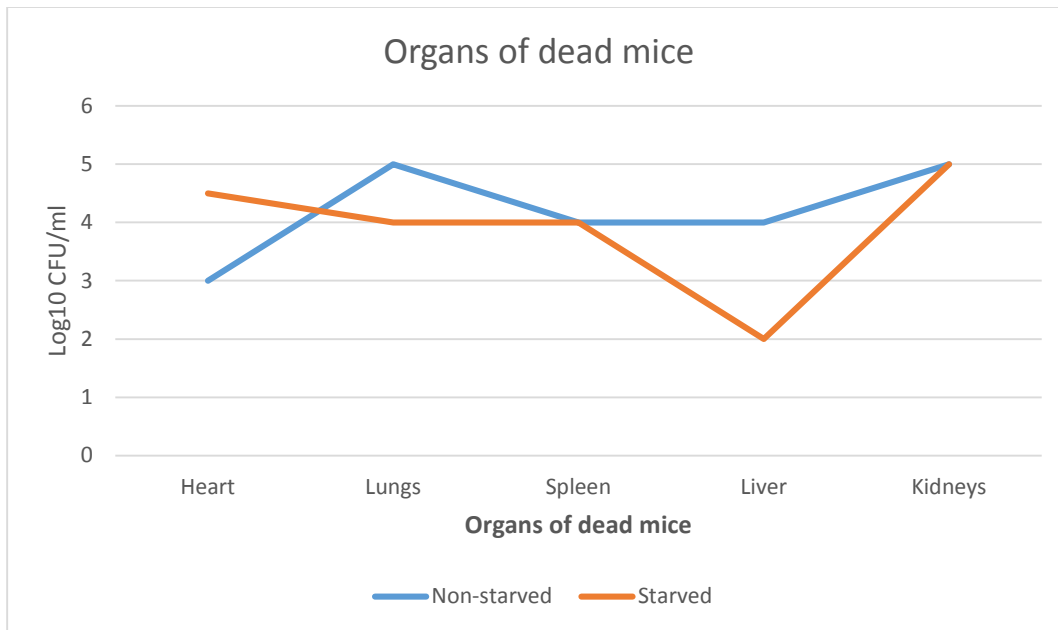


Chart 2: Organ load of mice infected with *Pseudomonas aeruginosa* showed that after 9 hours more of the non-starved cells of the bacterium were found in the lungs, heart, liver and kidneys. An increase was found in the starved cells, the spleen compare to the non-starved.



SUMMARY AND CONCLUSION

- 1) *Pseudomonas aeruginosa* showed up in the organs after 6 hours of infection using the Organ load of a mice infected with starved cells of *Pseudomonas aeruginosa*.
- 2) The heart, lungs, liver, spleen and kidneys showed signs of starved cells in *Pseudomonas aeruginosa*.
- 3) The results indicate that loss of mutations and pigmentation cause the loss on the infectivity.
- 4) The overall data that was determined during this experiment tells us that the death of mice require a higher dose of starved cells compared to non-starved cells. In order to understand how stained survival in water has an impact on the pathogenicity of *P. aeruginosa* is major for spaceflight missions and requires more studies at the bottom level.

ACKNOWLEDGEMENTS

The NASA West Virginia Space Grant Consortium and my research mentor Dr. Tesfaye Belay.

REFERENCES

- Kramer, M. (2013). "Bacteria in space grows in strange ways". Retrieved August 8, 2013 from <http://www.space.com>
- Woodeong, K. (2013). "Spaceflight Promotes Biofilm Formation by *Pseudomonas aeruginosa*." Retrieved August 8, 2013 from <http://www.plosone.org/article/>
- Howell, E. (2013). "So you wanna go to space can you put up with the Superpower Bacteria." Retrieved August 8, 2013 from <http://www.popsci.com/science/article/2013-06/so-you-wanna-go-space-can-you-put-superpower-bacteria>

- Kaplan, D.G. M. (2011). "Space Shuttle experiments test effects of microgravity on bacteria." Retrieved August 8, 2013 from <http://www.smartplanet.com/blog/pure-genius/space-shuttle-experiments-test-effect-of-microgravity-on-bacteria/6702>
- Todar, K. (2008-2012). *Todar's Online textbook of Bacteriology*. Retrieved on August 8, 2013 from <http://textbookofbacteriology.net/pseudomonas.html>

INCREASED INFILTRATION OF LEUKOCYTES IN THE REGIONS OF GENITAL TRACT OF STRESSED DURING *CHLAMYDIA TRACHOMATIS* INFECTION.

Sasha Richmond
Applied Science
Bluefield State College
Bluefield, WV 24701

ABSTRACT

Chlamydia genital infection, a sexually transmitted disease caused by *Chlamydia trachomatis*, has high prevalence in populations of low socioeconomic status. The factors associated with the high prevalence are not well known, but stress is speculated to play a big role in enhancing infection. Research in our lab has shown that application of cold-induced stress results in decreased resistance to *Chlamydia* infection in the mouse model. The purpose of study was to examine whether increased susceptibility to infection was associated with high degree of pathology in the model. Hematoxylin-eosin stained histological sections of the genital tract was evaluated. During primary and secondary infections, acute inflammatory cells (neutrophils) in the cervix or uterus areas in stressed mice infected with chlamydia was more than two to three-fold increase compared to non-stressed mice. Infiltration of neutrophils in the oviduct of stressed and infected group was more than 100-fold increase in stress mice. These results suggest that the large number of infiltrating leukocytes is a sign of acute inflammation that may be enhanced by exposure to stress. Vaginal swabs from stressed different mice strains also showed inclusion bodies in large numbers compared to non-stressed mice confirming that stress exposure increases intensity of chlamydia genital infection.

INTRODUCTION

Genital tract is a common sexually-transmitted infection, with an average of 2.8 million cases reported annually in the United States. The infection is often asymptomatic which presents a serious problem in women. If left untreated, the infection can cause fibrotic scarring of the genital tract which may ultimately lead to chronic abdominal pain, pelvic inflammatory disease, ectopic pregnancy, and infertility. Human and animal model studies suggest that stress is a risk factor for various infections because it may suppress immune system function, but the effect of stress on *Chlamydia* genital infection has not been well-defined. The major targets of chlamydial infection are mucosal epithelial cells. The purposes of this study were (i) to determine if the application of stress would result in an alteration of the pathology of the genital tract; (ii) to test if stress results in differential susceptibility of mouse strains. The data obtained from this study may provide further insight into how stress affects the host response to infection by *C. trachomatis*.

MATERIALS AND METHODS

Animals

Six- to seven-week-old female mice purchased from Hilltop Lab Animals, Inc.(Scottsdale, PA) or Jackson laboratories (Bar Harbor, ME) were housed in Bluefield State College Basic Science

Building room B206 laboratory vivarium. All animal protocols were approved by the Institutional Animal Care and Use Committee of BSC.

Cold water stress protocol

The cold water stress protocol used was established for inducing physical or psychological stress in mice. Mice were placed in a shallow container filled with 4 cm of cold water ($1\pm 0.5^{\circ}\text{C}$) for 5 minutes each day for 10 days or 24 days. Control mice were not subjected to cold water stress.

Chlamydia inoculation procedure

Mice were infected with *Chlamydia trachomatis mouse pneumonitis* (MoPn), purchased from the American ATCC. Seven to ten days prior to infection, mice were injected subcutaneously with 2.5 mg/ mouse of progesterone in 100 μL of phosphate-buffered saline (PBS) to regulate and sync the mice's menstrual cycles. Both the stressed and non-stressed mice were put under ketamine/xylazine anesthesia and inoculated intra-vaginally with 10^7 IFU of chlamydia per mouse in 30 μl of phosphate buffered saline (PBS).

Determination of Chlamydia Shedding in stressed mice

McCoy mouse fibroblasts were seeded into 96-well plates and incubated at 37°C with 5% CO_2 supply until monolayers were 90-95% confluent. Cervicovaginal swabs were collected at 3 days interval after infection and processed for chlamydia isolation by staining with fluorescence tagged anti-chlamydia anti-bodies.

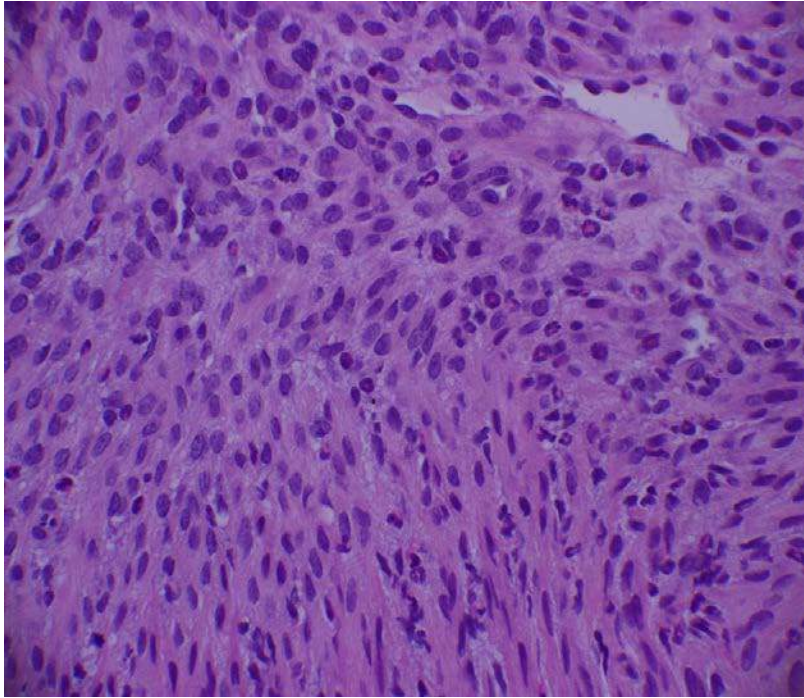
Harvesting of tissues for pathology

Mice were euthanized by CO_2 inhalation. Genital tracts were aseptically harvested the genital tract regions: cervix and uterus and oviduct were excised and placed in buffered formalin. The sections were stained with hematoxylin and eosin (H&E) at Marshall University pathology lab services.

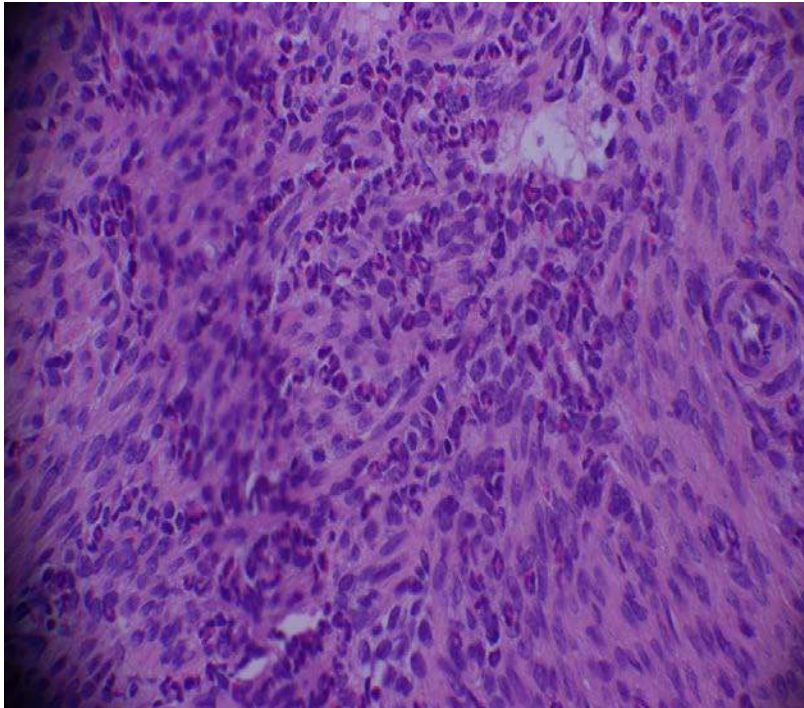
RESULTS

Table 1: Average Neutrophil Cell Counts in Stressed tissues of Genital tract of Stressed Mice Infected with *Chlamydia trachomatis*

Infection	Treatments			
	Region	Non Stressed Non Infected	Non Stressed Infected	Stressed Infected
Primary	Cervix	130 \pm 42	198.5 \pm 20	154 \pm 32
	Uterus	88.5 \pm 57	65 \pm 22	133.5 \pm 7
	Oviduct	1 \pm 0	1 \pm 0	124 \pm 17
Secondary	Cervix	20	130 \pm 92	149.5 \pm 21
	Uterus	2	53 \pm 17	65 \pm 42
	Oviduct	2	14 \pm 11	71.5 \pm 67



Fewer numbers of neutrophils in the cervix of non-stressed infected mice



A large number of neutrophils in the cervix of Stressed and *Chlamydia* Infected Mice

Table 2: Average inclusion forming units per/ml IFU/mL Counts in Stressed Mice Infected with *Chlamydia trachomatis*

Infection	Mice Strains			
	Ax10	MP14	MP15	Ax12
Day 3 after infection	$2.4 \times 10^4 \pm 19$	$1.2 \times 10^4 \pm 10$	$6.3 \times 10^3 \pm 5$	$1.2 \times 10^4 \pm 5$
Day 9 after infection	$6.4 \times 10^3 \pm 5$	$3.7 \times 10^3 \pm 3$	$4.7 \times 10^3 \pm 4$	$1.2 \times 10^3 \pm 2$

Table 3: Average inclusion forming units per/ml IFU/mL Counts in Different Stressed and Non-stressed Different Mice Infected with *Chlamydia trachomatis*

Infection	Mouse Strains			
	Ax10	MP14	MP15	Ax12
Day 3 after infection	$1.1 \times 10^5 \pm 9$	$7.4 \times 10^4 \pm 6$	$6.6 \times 10^3 \pm 5$	$4.5 \times 10^3 \pm 4$
Day 9 after infection	$3.3 \times 10^3 \pm 3$	$3.1 \times 10^3 \pm 3$	$8.4 \times 10^3 \pm 7$	$1.0 \times 10^3 \pm 1$

Table 4: IFU/mL Counts in Stressed and Non-stressed BALB/C Mice Infected with *Chlamydia trachomatis*

Infection	Treatments	
	Stressed	Non-stressed
Day 3	5.1x10 ³ ± 25	5.0x10 ³ ± 21
Day 6	5.6x10 ³ ± 28	4.6x10 ³ ± 22
Day 9	2.4 x10 ³ ± 12	4.0x10 ³ ± 20
Day 12	3.9x10 ³ ± 20	3.9x10 ³ ± 20
Day 15	4.1x10 ³ ± 20	3.9x10 ³ ± 20
Day 18	4.2x10 ³ ± 21	2.1x10 ³ ± 11
Day 21	2.5x10 ³ ± 12	3.1x10 ³ ± 15
Day 24	3.1x10 ³ ± 15	2.6x10 ³ ± 13

DISCUSSIONS

After working in Dr. Belay’s Lab for the summer the research that was done was then presented at the symposium at Marshall University and there will be further research done on this experiment. This was a very valuable experience because it helped us to broaden our horizons in our networking system and helped us to gain more knowledge about a certain bacteria along with insight of the aspect of doing hands-on researching.

CONCLUSIONS

- The pathology data show the presence of a large number of neutrophils in the regions of stressed mice compared to non-stressed mice suggesting acute inflammation.
- High IFU/ml counts were detected in swabs of stressed and non-stressed at day 3 and 6 after *Chlamydia* genital inoculation.
- IFU counts were significantly higher (2 log) in stressed BALB/c mice than non-stressed mice.
- Norepinephrine receptor knockout BALB-C mice are more susceptible to the genital *Chlamydia* infection compared to wild type.
- According to this course of infection in various strains, we were unable to determine the most susceptible strain to chlamydia infection.

- These results indicate that stress and the Norepinephrine hormone play an important role in genital *Chlamydia infection*.

ACKNOWLEDGEMENTS

This project was supported by NIH Grant 5P20RR016477 to the West Virginia IDeA Network for Biomedical Research Excellence.

A special thanks to the NASA WV Space Grant Consortium for sponsoring and Dr. Belay for allowing me to work in his lab.

COMPUTATIONAL FLUID DYNAMICS MODELING OF TEMPERATURE GRADIENTS AT THE NATIONAL TRANSONIC FACILITY

Vincent P. Spada Jr.
West Virginia University
Dr. Eric Walker
Research Directorate – Configuration Aerodynamics Branch
Aeronautics Research Mission Directorate
August 7, 2013

ABSTRACT

The National Transonic Facility (NTF) is a continuous-flow wind tunnel that uses cryogenic temperatures and increased pressure to match flight Reynolds numbers to determine aerodynamic properties of scaled models at transonic speeds. During a recent flow survey of the NTF test section, a small temperature gradient was detected under certain conditions. Since the NTF is primarily an aerodynamic performance facility, it is critical to determine if there is a potential bias in the flow conditions. The objective of this project is to assess the potential impact of the temperature gradient on test article aerodynamics. To accomplish this objective, a computational fluid dynamic analysis was performed on a supercritical airfoil in transonic flow with and without the presence of a free stream temperature gradient.

Numerical simulations of the airfoil in transonic flow were performed using Tetrahedral Unstructured Software System (TetrUSS), which is a computational fluid dynamics software suite designed to calculate and generate a flow representing different fluid properties. TetrUSS solves the Navier-Stokes equations to predict the viscous flow around a given geometry. For this work, the Spalart-Allmaras turbulence model was used to predict the turbulence in the flow field to create a more realistic simulation. The free-stream flow field and boundary conditions were set up to try to best mimic the conditions in the wind tunnel such as Mach number and temperature gradient. This study looked at different angles of attack, Mach numbers and temperature gradients. These cases were chosen to measure how much the temperature gradient affects aerodynamic properties such as pressure, drag and lift.

Results have shown that there are variations in the coefficient of drag, pressure and shock locations. The shock locations have moved forward with a gradient present at certain Mach numbers. This will affect other properties such as pressure distribution, which will have an effect with the drag on the airfoil. There is inconsistency with the drag and lift at each Mach number when a temperature gradient is present. A gradient over 25% creates unpredictable results.

INTRODUCTION/BACKGROUND

The National Transonic Facility (NTF) studies the aerodynamic effects of scaled models at high pressures and cryogenic temperatures. NTF is one of NASA's most famous wind tunnels. In the 1970s the U.S. Air force wanted a cryogenic tunnel while NASA wanted transonic capabilities. Around this time a cryogenic tunnel was a new concept in testing aeronautical vehicles. Recent

successes of the 0.3-meter cryogenic tunnel at Langley convinced the U.S. to build a cryogenic tunnel. In 1980 the U.S. government broke ground to build one tunnel with both cryogenic and transonic capabilities. NTF serves the needs of the commercial, military and scientific community; while establishing its reputation for testing well-known vehicles such as the Boeing 777, B-2 Bomber, F-18 Hornet and the Space Shuttle with its solid rocket boosters. (Gainer, 2013)

NTF's most famous capability is its ability to increase its Reynolds number to those seen in flight. Temperatures are cooled to cryogenic levels at around -250° Fahrenheit to achieve this. As the temperature decreases the pressure and density increases while the dynamic viscosity decreases. Nitrogen gas is used for this process which NTF supplies with its own liquid nitrogen plant. Since the tunnel is a transonic facility, it has the ability to prevent choking in the test section with its 12 slots and 14 reentry flaps. The interior in the tunnel is also thermally insulated to prevent heat transfer. (Gainer, 2013)

Recently a rotary rake test, which is a measurement tool used to measure the temperature in a cross-sectional area, was conducted and the results concluded that a temperature gradient does exist for certain conditions. The resistance temperature detection (RTD) probe detected a gradient that ranges from 5% to 10%; relative to the reference temperature of about -247° Fahrenheit. This will change the properties of the flow on the model; the concern is whether these changes are significant.

Tetrahedral Unstructured Software System (TetrUSS), which is a computational fluid dynamics software suite that involves grid generation and flow simulation, was used to compute multiple flow models around a super critical-3 airfoil to help detect any differences in properties. This CFD program was created at Langley's Research Center in the 1980s and evolved over time into a program with many unique capabilities. (Frink, 1992; Frink, 1994; Frink, 1996) It is also the recipient for the NASA software of the year award in 1996 and 2004. (Frink, 2006)

Methodology

TetrUSS was used to generate a grid with the airfoil and to compute the flow around the model with Unstructured Mesh 3 Dimensional (USM3D). The first part in creating a grid, which is the finite volume that holds the tetrahedral cells, is to create the geometry in Gridtools. The basic geometry was already created with the super-critical airfoil 3 in the middle. The geometry was then formatted to meet certain conditions. The in flow region was split up into different sections or patches that would be used to regulate the temperature gradient. Two of these patches would hold the engine boundary conditions that are used to create a flow that can control the Mach numbers and temperatures. These engines are the main tools used to model the temperature gradient. The airfoil in the middle of the geometry had a viscous

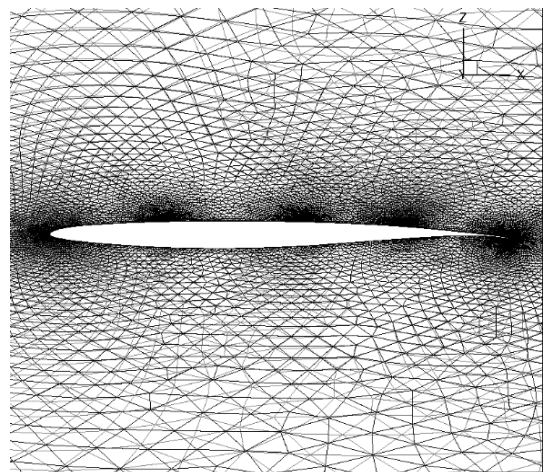


Figure 1. Unstructured tetrahedral cells around the airfoil in the completed grid.

boundary condition with a sub-layer of $y^+=1$. Sources, which influence cell size, were placed on top of the airfoil and in front of it. The source in the front is extended from the leading edge of the airfoil to the inflow region. Then sources were placed on top for shock locations. This would create a more precise flow in these areas of interest. After Gridtools, the geometry moved to Vgrid, where the tetrahedral cells were generated. The grid then moved on to Postgrid where the negative volume cells were removed and any remaining pockets were filled. (Frink, 2006)

The input file was then established to control the conditions in the flow solver. This file controls the flow conditions and solver parameters. The 10% and 5% gradients were created along with 25%, 35% and 50% gradients to exaggerate any changes in flow properties that may occur. Cases with no gradients were also created to act as a baseline. The Mach numbers chosen were 0.75, 0.83, and 0.90 and the angles of attack were 0° , 3° and 5° . These angles of attack were chosen because they are the standard cruising angles of attack for this type of airfoil. The 0.75 and 0.9 Mach numbers match conditions from the rake test in the tunnel and 0.83 was chosen to help establish a trend in the data.

After all the test cases were computed, the data was then transferred to a program called Tecplot, which is a visualization software. The data was plotted on x/y graphs and contour maps. This is where the flow was analyzed for any differences in properties.

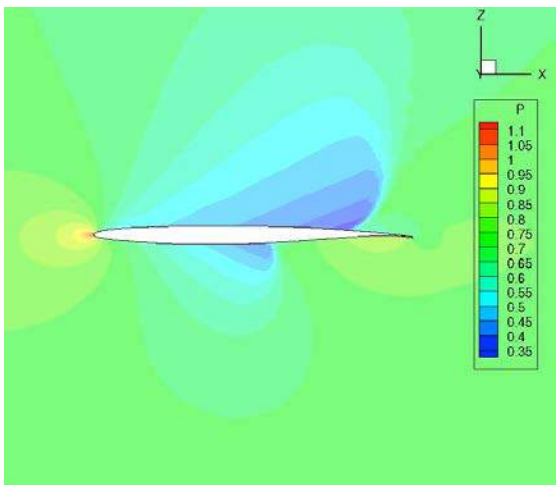


Figure 2. Pressure distribution along the airfoil at Mach 0.83 and angle of attack of 0 with a 10% gradient.

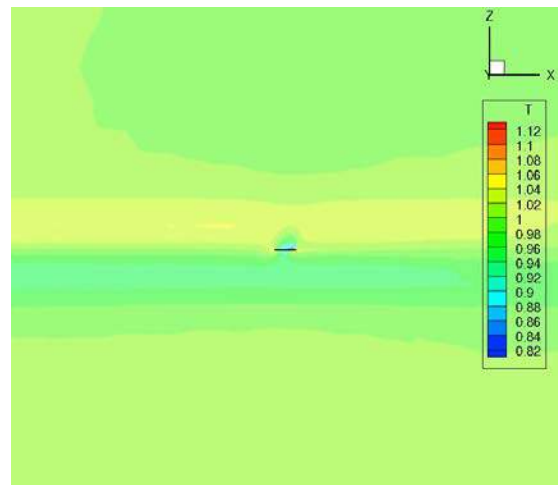


Figure 3. Temperature gradient generated at Mach 0.83 and angle of attack of 0 with a 10% gradient.

RESULTS

Refer to appendix for figures.

After analyzing the results, an overall trend in the coefficient of lift (C_l) has not appeared. In Figure 4, the lift has decreased at Mach 0.75 with a temperature gradient; but as the angle of attack went to 3, the lift was increased with a gradient. The inconsistency can also be seen in Figure 5, at Mach 0.75 the lift decreases with a gradient at an angle of attack of 0 and it increases at an angle of attack

of 3. As Mach increases to 0.83 the differences in lift is decreased as angle of attack increases and at Mach 0.9 the change in lift increases as angle of attack increases, as seen in Figure 6 and Figure 7. The inconsistency in the lift as alpha and Mach increases is a concern. The change in C_l along with the coefficient of drag (C_d) can be seen at Mach 0.9 at angle of attack of 0 in Figure 8.

C_d is measured to the 0.0001, which is equal to one count. The smallest difference of 1 drag count from the baseline occurred at Mach 0.75 at an angle of attack of 5 with a 5% gradient. As the Mach decreased though, the difference increased at Mach 0.83 then decreased at Mach 0.90. A different trend occurs at the different angles of attack. For an angle of attack of 3, as the Mach decreases the drag differences decreases and at angle of attack 5, as Mach decreases the difference increases. This is inconsistent relative to the change in Mach. The difference for these also ranges from approximately 2 to 50 drag counts, which is significant.

The gradient also creates variations in the pressure distribution along the top and bottom of the airfoil. This is likely caused by the velocity gradient that goes along with the temperature change. The effects from the 5% and 10% temperature change seem to be relatively small, as seen in Figures 9, 10 and 11; but as the gradient increases so does the differences in pressure. The separation is increased at the shock locations in which the coefficient of pressure (C_p) increases dramatically. This indicates that the shock locations move at different levels of gradients. At Mach 0.9, the location of the shocks move further upstream on the airfoil then the shock location without a change in temperature, as seen in Figure 11. At Mach 0.75 a different phenomenon happens. The shock also moves further upstream, but only at angle of attack 0 and 5. At 3 degrees angle of attack the shock moves downstream, as seen in Figure 9. As the shock moves further upstream with a gradient, this causes boundary layer separation sooner than normal, which can lead to a increase in drag. At Mach 0.83 an even greater anomaly occurs at every angle of attack. The shock location travels downstream with the low gradients, as the gradient increases the shock location travels back upstream to the baseline shock and passes it and continues as the gradient keeps increasing, as seen in Figure 10.

The coefficient of friction (C_f) also shows variations at each gradient. The friction on the surface of the airfoil increases as the temperature change increases. This happens at every Mach number and angle of attack. However, the difference in friction decreases as the angle of attack decreases, as seen in Figure 12 and Figure 13.

CONCLUSIONS

There are ways to continue this research to search further for acceptable trends in different properties. A greater number of cases can be ran with Mach numbers between 0.75 to 0.83 and 0.83 to 0.9. Modifications can also be made in Gridtools. Extra sources upstream from the airfoil can be created; two can be placed above and below the existing source that stretches from the leading edge to the inflow. A couple extra sources can be placed behind the airfoil. This could help create a finer flow to the airfoil and behind it. The small patch between the two engines can also be expanded. The amount of engines can also be doubled to four to create a more gradual gradient throughout the entire grid.

The gradient has a significant impact on the fluid properties on the airfoil. This impact has been proven hard to predict at different conditions. There are no clear trends for the differences in drag and lift with respect to the Mach or angle of attack. This would make it hard for the NTF engineers

to know what to expect to happen with a temperature gradient at different test conditions. There is a similar trend with the pressure distribution along the airfoil at the shock. The shock locations change with different gradients, which are expected; but for different speeds, the shock ranges from further upstream to further downstream from the baseline shock. As the temperature gradient increases, the effects on the properties also become very unpredictable. For gradients similar to those observed in the NTF, -5% and -10%, the results show significant impact on aerodynamic forces indicating that the gradients should be removed or minimized where possible.

ACKNOWLEDGEMENTS

The author would like to acknowledge the West Virginia Space Grant Consortium for funding this research and for the opportunity to enhance the engineering ability and providing a solid foundation for the author's engineering career. There is also a special thank you for Dr. Neil Frink, Dick Campbell, Dr. Steve Krist, Steve X.S. Bauer, and T.J. Wignall for their extraordinary assistance in the guidance through the CFD program TetrUSS. Special thanks for Dr. Eric Walker for the guidance through the entire research project.

REFERENCES

- Gainer, M. (2013). *History*. Retrieved from http://crgis.ndc.nasa.gov/historic/National_Transonic_Facility.
- Frink, N. (1996). *Assessment of an unstructured-grid method for predicting 3-d turbulent viscous flows*. Washington D.C.: American Institute of Aeronautics and Astronautics.
- Frink, N. (1994). *Recent progress toward a three-dimensional unstructured navier-stokes flow solver*. Washington D.C.: American Institute of Aeronautics and Astronautics.
- Frink, N. (1998). *Tetrahedral unstructured navier-stokes method for turbulent flows*. (Vol. 36). Washington D.C.: American Institute of Aeronautics and Astronautics.
- Frink, N. (1992). *Upwind scheme for solving the euler equations on unstructured tetrahedral meshes*. (Vol. 1). Washington D.C.: American Institute of Aeronautics and Astronautics.
- Frink, N. (2006, August 28). *Usm3d users manual* . Retrieved from <http://tetruss.larc.nasa.gov/usm3d/>.

APPENDIX

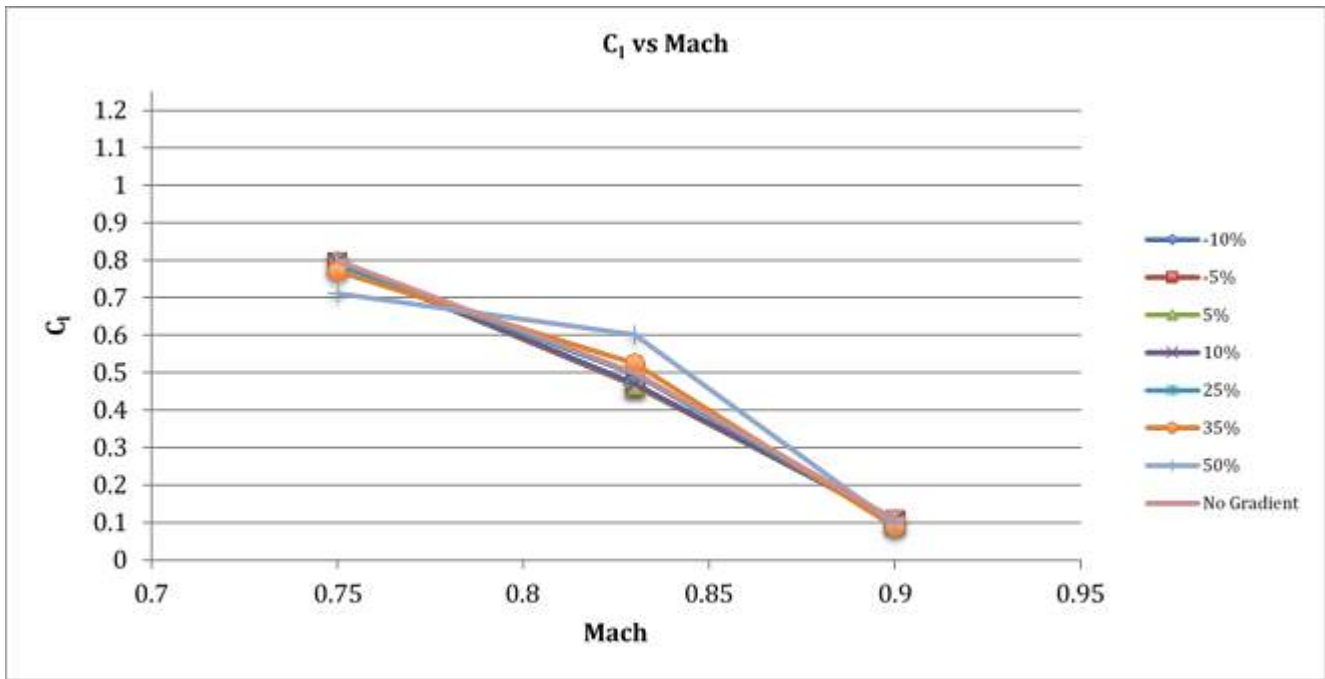


Figure 4. Coefficient of lift vs. Mach at angle of attack of 0.

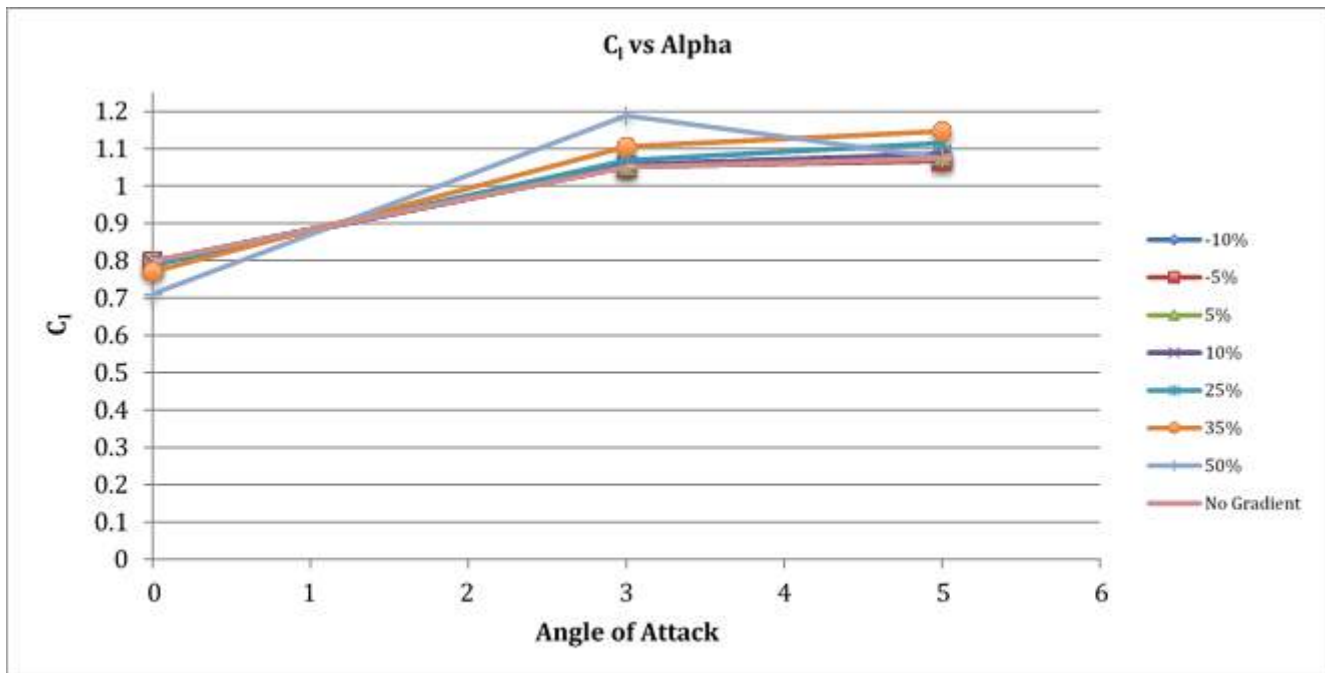


Figure 5. Coefficient of lift vs. angle of attack at Mach 0.75.

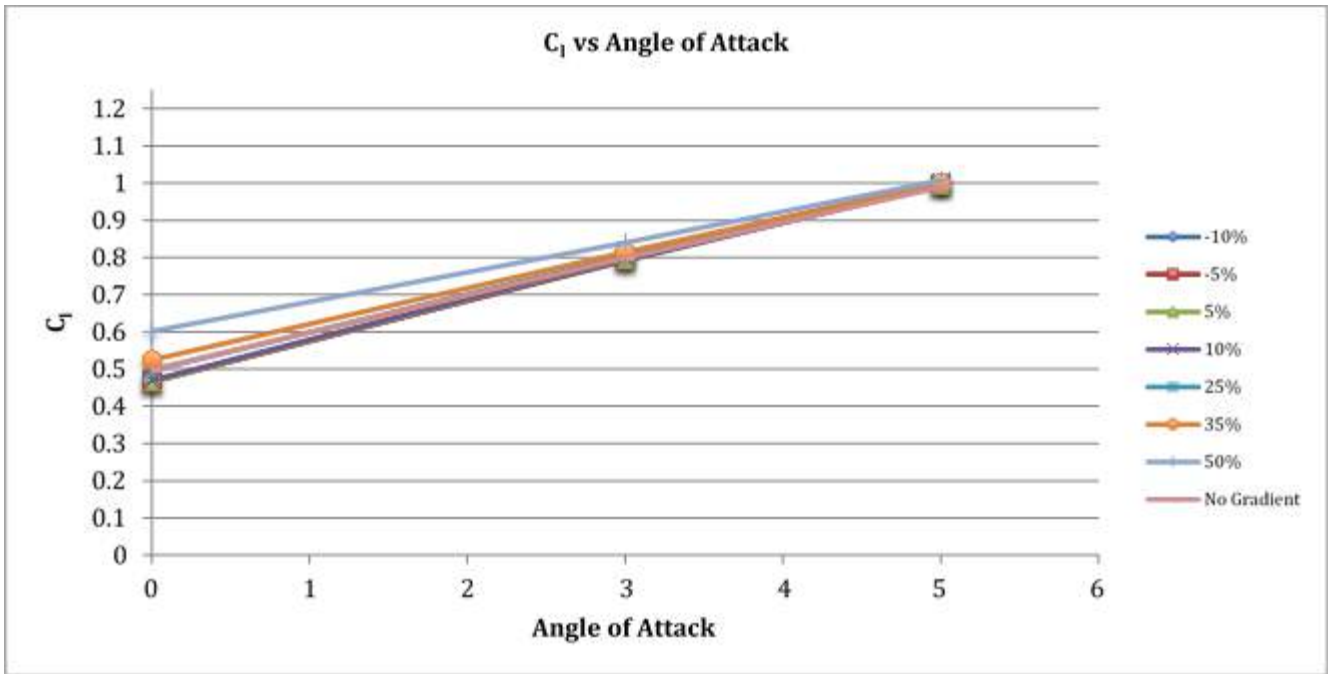


Figure 6. Coefficient of lift vs. angle of attack at Mach 0.83.

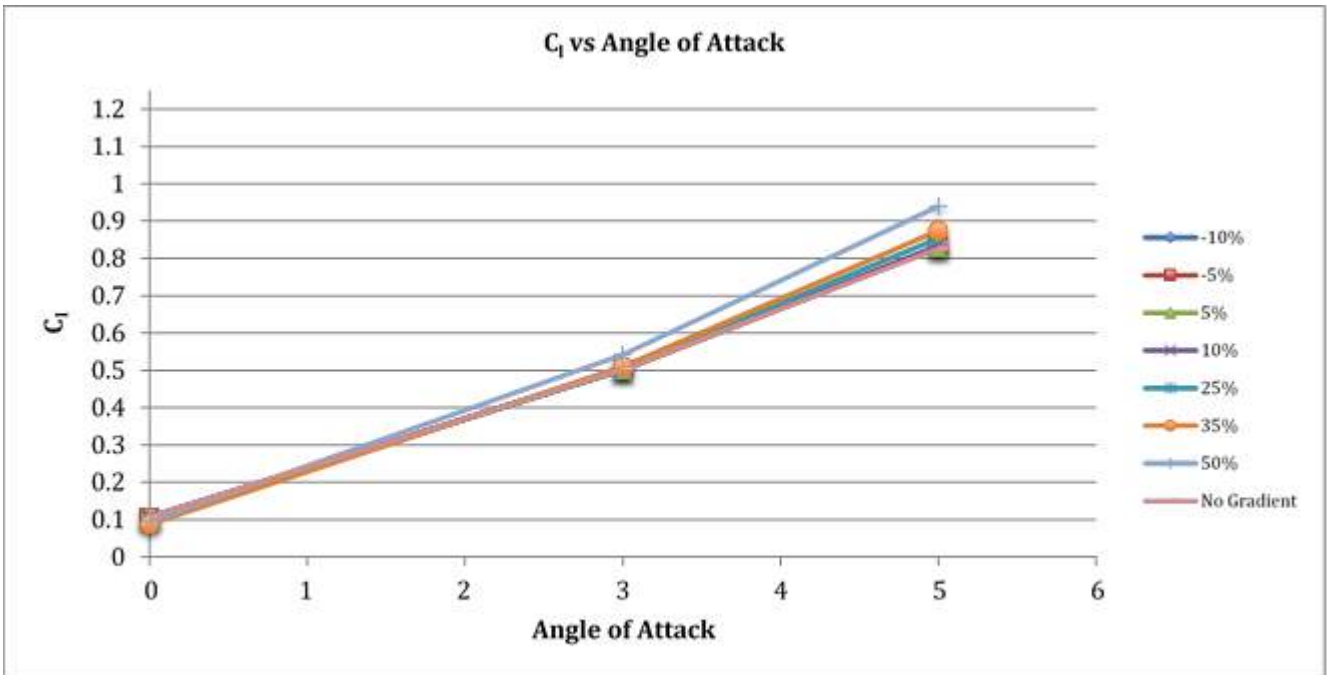


Figure 7. Coefficient of lift vs. angle of attack at Mach 0.90.

	(Dif) in CL	(Dif) in CD	(Dif) Cl/Cd
-10%	0.0027	0.00128	2.089
-5%	0.0020	0.00083	2.434
5%	0.0017	0.00089	1.900
10%	0.0026	0.00134	1.677
25%	0.0104	0.00562	1.845
35%	0.0208	0.01097	1.896
50%	0.0131	0.02539	0.517

Figure 8. Differences in Coefficient of Lift and Coefficient of Drag at Mach 0.9 and angle of attack of 0.

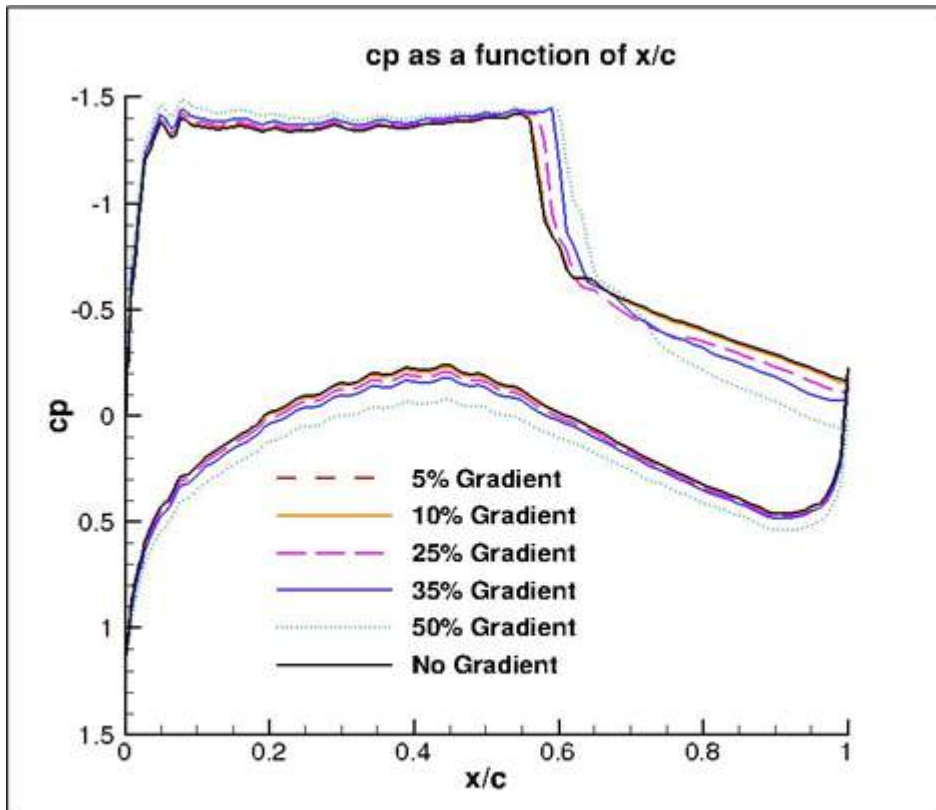


Figure 9. Coefficient of pressure vs. x/c at Mach 0.75 and angle of attack of 3. - 10% and -5% omitted due to similar results to 10% and 5%.

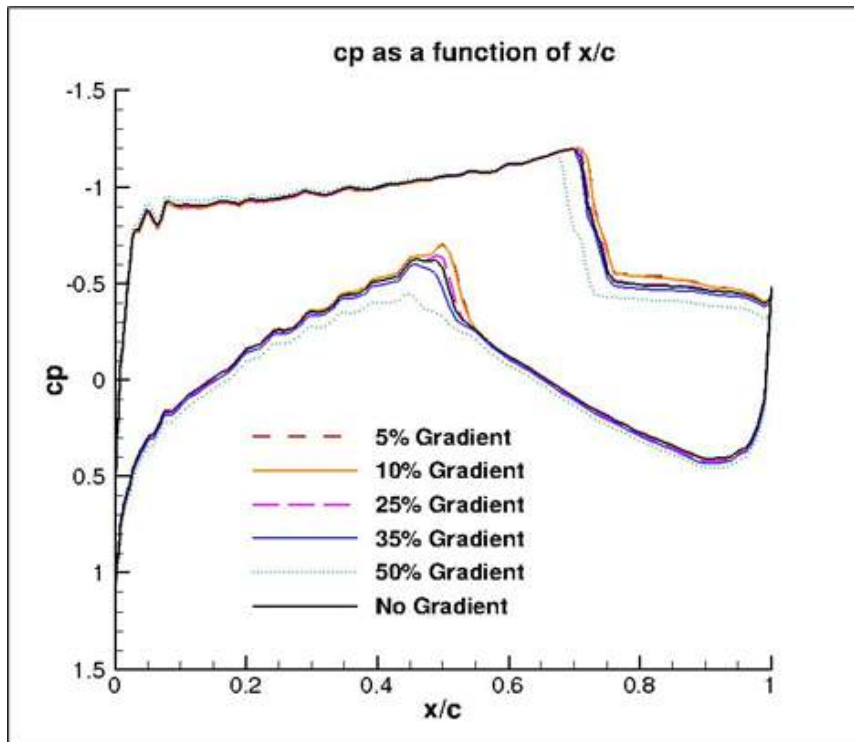


Figure 10. Coefficient of pressure vs. x/c at Mach 0.83 and angle of attack of 3. - 10% and -5% omitted due to similar results to 10% and 5%.

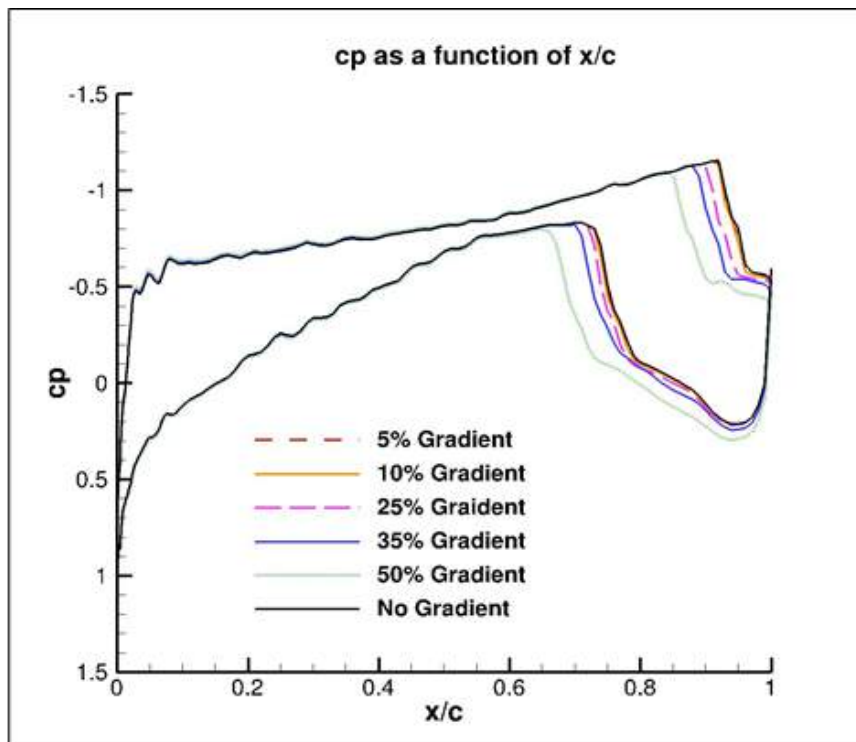


Figure 11. Coefficient of pressure vs. x/c at Mach 0.9 and angle of attack of 3. - 10% and -5% omitted due to similar results to 10% and 5%.

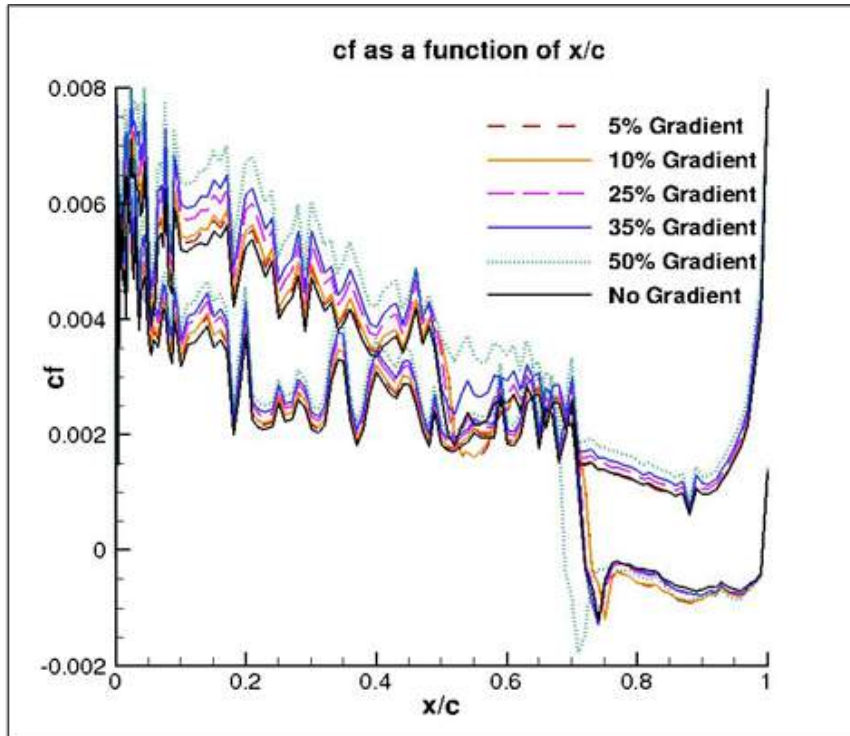


Figure 12. Coefficient of friction vs. x/c at Mach 0.83 and angle of attack of 3. -10% and -5% omitted due to similar results to 10% and 5%.

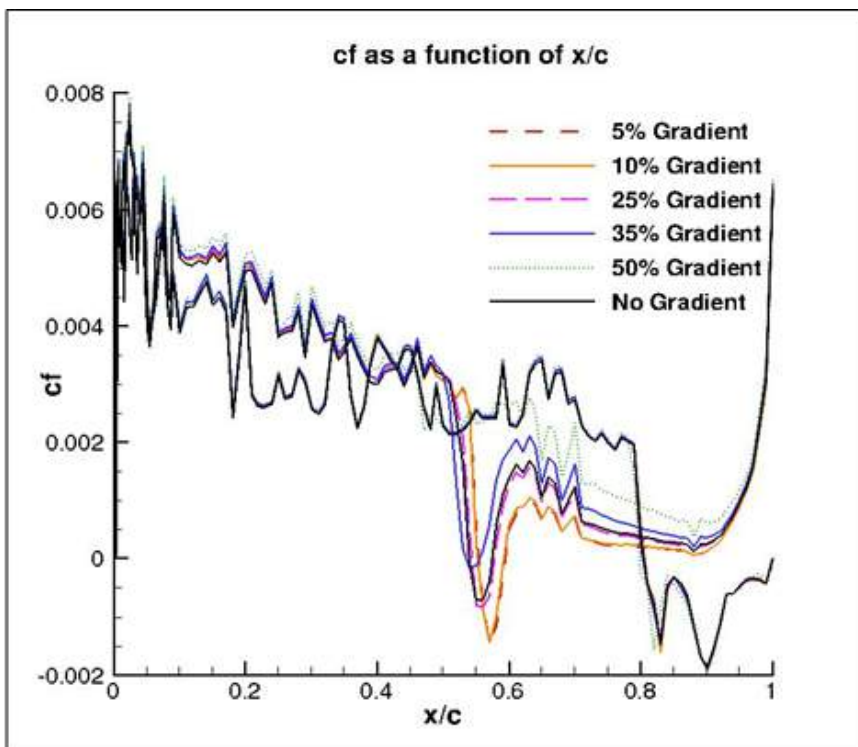


Figure 13. Coefficient of Friction vs. x/c at Mach 0.83 and angle of attack of 0. -10% and -5% omitted due to similar results to 10% and 5%.

A STUDY OF HIGH TECHNOLOGY APPLIED TO THE WOOD INDUSTRY

Matthew Spicer
Applied Physics
West Virginia Wesleyan College
Buckhannon, WV 26201

ABSTRACT

West Virginia Split Rail and West Virginia Forest Products Company are sister companies located in Buckhannon, West Virginia. This research was designed to focus on potential new products and environmental protection agency requirements for the two companies in hopes of providing solutions.

INTRODUCTION

West Virginia Split Rail and West Virginia Forest Products currently produce an assortment of products such as split rail fencing and pallets. They are, however, open to expanding their operation to create new products. They are also concerned about some environmental protection agency requirements that they must follow. A big requirement for wood industries is the Boiler MACT (maximum achievable control technology), which the EPA just released in February. This deals with air emissions from the heating of wood that many companies do. However, West Virginia Split Rail has only a small kiln that they use, and they are not concerned about their emissions from the kiln exceeding any limits. Another EPA requirement is a ban on a few wood preservatives and restrictions on the release of chemicals like formaldehyde. The main EPA requirement of concern to the company is that of their stormwater runoff because they have very little knowledge of how to manage their runoff. They are required to follow certain guidelines that are outlined in the National Pollution Discharge Elimination System permit they acquired from the EPA since they discharge their water directly into a surface water, the Buckhannon River. The EPA has created certain benchmark levels for a variety of pollutants in their runoff under which the runoff is considered to have no adverse effects on the surface water into which it flows. The benchmarks that apply to West Virginia Split Rail include a total suspended solids concentration of 100 mg/l, a chemical oxygen demand concentration of 120.0 mg/l, a biochemical oxygen demand concentration of 30 mg/l, a total recoverable zinc concentration of 0.117 mg/l, and a total iron concentration of 1.0 mg/l. West Virginia Split Rail has consistently been over each of the benchmarks in many of their outlets. As such, they are required by the EPA to continually update their Stormwater Pollution Prevention Plan to show that they are making progress towards reducing and eliminating their environmental footprint. The goal of this research is to provide West Virginia Split Rail and others like them with tangible solutions for some of their problems.

DISCUSSION

Trees take in sunlight energy, carbon dioxide from the atmosphere, and water from the soil to make their own food, glucose, through a process known as photosynthesis. Oxygen is also formed as a byproduct. Chlorophyll, a green pigment present in the leaves, is what is able to convert energy

from the sun into energy usable for the tree. Photosynthesis consists of both light-dependent and light-independent reactions (also known as the Calvin Cycle). The light-dependent reactions include chlorophyll trapping light energy to make adenosine triphosphate (ATP) and water being split into oxygen, hydrogen ions, and free electrons, which then react with nicotinamide adenine dinucleotide phosphate⁺ (NADP⁺), a carrier molecule, to form NADPH. The light-independent reactions use the NADPH and ATP to form glyceraldehyde 3-phosphate and, eventually, glucose from carbon dioxide through carbon fixation.¹

The composition of trees is important to understand in order to find creative uses for trees. Trees are composed of about 40-50 percent cellulose, 15-30 percent hemi-cellulose, 16-33 percent lignin, and 5-30 percent of other compounds, such as water, resins, and minerals. The actual structure of wood is formed by the fiber-like structure of cellulose and hemi-cellulose, while lignin acts as the binding agent.² The cells of a tree carry out the passage of food and water and the influx of nutrients in and out of the cells and are composed of a nucleus, a nuclear membrane, a cytoplasm, a cell membrane, plastids, mitochondria, ribosomes, endoplasmic reticulum (ER), Golgi apparatus, vacuoles, and vesicles. The nucleus carries the DNA for the cell and coordinates its functions. It is protected by the nuclear membrane. The cytoplasm is a jelly-like material which holds all organelles in the cell. The cell membrane and cell wall combine to give the cell a rigid shape and size, as well as monitor the transport of materials in and out of the cell. The plastids hold the pigments which absorb light and make food, such as chlorophyll, and are only present in the cells which photosynthesize. The mitochondria are responsible for breaking down complex carbohydrates to provide energy to the cell. The ER are mainly responsible for holding on to the proteins formed by the ribosomes, which are then processed by the Golgi apparatus. Vacuoles are used to store things like ions and sugars.³ The vesicles transport materials between the organelles. Lysosomes, specialized vesicles, break down the waste produced by a cell.⁴ The lignin and cellulose also have a part in the cell of a tree. Lignin is an organic substance, although it is not possible to define the exact chemical structure of a lignin molecule since a certain variation in chemical structure exists in all lignin. What all lignin have in common is that they are a dendritic network polymer of phenyl propene basic units.⁵ It is both incredibly strong and flexible. It is composed of amino compounds and is found in the cell wall and between cells. Lignin helps to support the tree and bind it together. It also helps transport liquid through the tree.⁶ Cellulose is an organic compound consisting of a linear chain of sugar molecules which forms the strong cell wall. The chemical formula is C₆H₁₀O₅.⁷

There are many unconventional ways to use the constituents of wood to make a wide variety of interesting and useful products. Lignin is currently produced as a byproduct of the pulping process. It has a variety of uses. As it helps to bind a tree together, it makes sense that lignin can be used as a binder for products like particleboard, biodegradable plastic, ceramics, fiberglass insulation, dust suppressants, and soil stabilizers. It also has uses in oil well drilling, water treatment, cement, leather tanning, clay and ceramics, and asphalt.⁸ Cellulose also comes as a byproduct from the pulping process. Among its uses are melamine dinnerware, toilet seats, cellophane, helmets, toothbrushes, electrical outlets, and rayon fabric.⁹ Nanocellulose also has a very intriguing use. When extracted, it is lightweight, flexible, stronger than steel, stiffer than Kevlar, and conducts electricity, which gives it many uses, such as lightweight armor and an alternative to glass and carbon fiber for automotive and aerospace industries. Plus, it's completely non-toxic and can even be used as a low-calorie food thickener. What is perhaps the best news of all is that it is cheap and is expected to sell for only a few dollars per kilogram. The first nanocellulose plant opened recently

and is located in Madison, Wisconsin.¹⁰ A few other uses for wood that have been discovered include 3D printing,¹¹ batteries,¹² and, potentially, solar cells.¹³

One minor EPA regulation is the restrictions placed on wood preservatives. The wood preservatives that are restricted are creosote, pentachlorophenol, and any preservative containing inorganic arsenic, such as CCA-C and ACZA. This problem has a simple fix, as there are many readily available alternatives to these preservatives, which West Virginia Split Rail already uses.

However, there is also another, more intriguing alternative to the use of such preservatives. Wood acetylation is a chemical modification to wood that helps it to better resist decay mostly by making it even dryer. The process of wood acetylation involves replacing the hydroxyl groups on lignin and cellulose with acetic anhydride. It is also much stronger than normal wood and also resists termites. However, its main downfall is that it is much more expensive than other treatment options.¹⁴

In order to reduce pollution output, the first and most important step is source reduction. In order to do that, it is first necessary to locate the sources of the pollution as much as possible. Total suspended solids pollution in the wood products industry is typically sediment, bark, grass, rock and soil, though it can also refer to other debris such as metals and organic materials. Unpaved surfaces, especially those devoid of vegetation contribute a significant amount of most total suspended solids pollution. Good housekeeping and removing waste such as bark can help reduce the solids picked up by runoff. Chemical oxygen demand pollution and biochemical oxygen demand pollution are as similar as the names would suggest. The main difference is that biochemical oxygen demand is a measure of the amount of oxygen consumed by bacteria while decomposing organic matter, while chemical oxygen demand measures the total amount of oxygen used to oxidize all organic material into carbon dioxide and water and does not distinguish between biologically available and inert organic matter.¹⁵ Organic pollutants consist of proteins, carbohydrates, fats and nucleic acids and can come from things such as residual food waste, plant matter, leaves and woody debris, and animal manure. Once again, good housekeeping is an important part of limiting BOD and COD pollution. Zinc pollution occurs mainly when water comes into contact with a zinc surface and a little bit of that zinc dissolves into the water. Major sources are tire wear and galvanized surfaces such as roofs, gutters, fencing, guard rails, and pipes. Other sources can include contact with earth, wood preservatives, motor oil, and grease. Some ways to limit zinc pollution include covering galvanized roof surfaces with green roofs, replacing galvanized surfaces with an alternative material, covering galvanized surfaces, painting galvanized surfaces with a paint that does not contain zinc, and limiting tire wear by reducing sharp turns. Iron pollution also often occurs in the dissolved form. Iron gets into stormwater mainly when the water comes into contact with things such as auto body rust, moving engine part, and earth. A way to help reduce the levels of all pollutants in the stormwater runoff is to limit the flow volume and speed. A smaller volume of runoff helps to slow the movement of the runoff and prevent flooding, both of which will help prevent erosion and reduce pollutants in the runoff. This can be done by reducing impervious surfaces, such as pavement, using porous pavement that allows some water to infiltrate, infiltration trenches or basins, green roofs, rain gardens, and other vegetated areas.

Green roofs are another method of using vegetation to reduce pollutants in stormwater runoff. A green roof is a roof that is covered with vegetation. They are frequently made using a waterproof layer, drainage layer, filter membrane, soil, and plants. They can also be created in a way that will

require very little maintenance. These green roofs require only a thin layer of soil (less than 6 inches) and often use plants such as grasses, perennials, or succulents. Green roofs are not typically used for filtration since they come in contact with the rain before it has had a chance to pick up any pollutants. However, they are a great way to prevent the rain from contacting and picking up pollutants, especially zinc since its main source is galvanized roofing. It also will greatly help to reduce the runoff volume from the roof; in general, around 50% of the water will be soaked up by the plants. A green roof can be used on a roof with up to a 40% slope and can be included in the initial construction of a building or added on to an existing building. However, it is necessary to be sure the building can handle the extra weight that a green roof will provide before making the addition. Once constructed, maintenance includes making sure the plants get enough water, particularly during a drought. The cost of a green roof is usually between 5 and 20 dollars per square foot, but they also can help reduce the energy consumption of the building and extend the life of the roof, often paying for themselves.¹⁶

Bioretention is another way to help reduce the volume of stormwater runoff. One important form of bioretention is the rain garden. Rain gardens are good for use in small areas of less than 5 acres and should be placed on or near shallow slopes of less than 5 percent to ensure that the water reaches them. A rain garden has many of the same benefits as a vegetated swale (which will be discussed shortly), as it retains some water and can also remove some pollutants from the water that does pass through. A size of between 5 and 10 percent of the size of impervious draining area is generally recommended. A sand and soil mix covered with mulch is suggested. Sometimes an underdrain is used, although the water can also simply be allowed to seep into the groundwater. Native vegetation is preferred, with a combination of shrubs, leafy plants, and trees usually used, although it may be best to avoid trees in colder climates where snow may be stored in the area during winter. The cost has been estimated at a little more than 7 dollars per square foot.¹⁷ Another option for bioretention is infiltration trenches or infiltration basins. An infiltration basin is a shallow basin with a flat bottom, and an infiltration trench is a rocky trench with no outlet. However, they each have relatively low levels of applicability since their use is greatly restricted depending on the type of soil. Soil that is not very permeable can cause it to become clogged, while soil that is too permeable heightens the risk of groundwater contamination. Each is also best when used on sites of less than 5 acres. The infiltration rate should fall between 0.5 and 3 inches per hour. Soils with less than 20 percent clay content 40 percent silt/clay content are best. It is also important to put at least two feet in between the bottom of the trench or basin and the groundwater. Costs range between 2 and 5 dollars per square foot.^{18, 19} Some other options include aerating land for better water infiltration, using as few impervious surfaces as possible, using porous pavement which allows for some infiltration, and using rain barrels to harvest the rainwater for onsite use (some states have legal restriction on this, though, so it is best to look into that before implementing this practice).

One of many ways to help remove pollution in stormwater runoff—and perhaps the way most touted by the EPA—is through the use of vegetation. There are many different ways that vegetation can be used to reduce pollution. Some, such as the filter strip and the grassed swale, are used for filtration purposes. Others, such as the rain garden, are simply used for infiltration purposes to help reduce the volume of runoff. Vegetation can even be used to help prevent pollution from getting into the rainwater in the first place, as is the case with the green roof. Vegetation alone may not always be enough to reduce pollution to below benchmark levels, however. In these cases, it is often used as pretreatment for other practices such as ion exchange and media filters. Depending

on the individual case, many different combinations of methods can be used to reduce pollution. The filter strip and the grassed swale are both quite similar. Grass is normally used for each. The main difference between the two is that swales are meant to encounter concentrated flow; while filter strips are meant to encounter sheet flow. Grassed swales are placed in ditches to concentrate the flow of water, while filter strips are simply placed on a gentle slope. They each are especially useful for removing sediment from the runoff and reducing flow velocities and volume to help prevent erosion by allowing for infiltration into the ground. Maintenance involves mowing to a height of 3 to 4 inches, reseeding bare areas, and removing sediment buildup.²⁰

The filter strip can be used to treat small drainage areas. In order to avoid concentration of flow, which would render a filter strip ineffective, a filter strip should treat one acre of impervious surface per 580-foot length. A filter strip is best if placed on a slope between 2 and 6 percent. Also, there should be at least two feet between a filter strip and the groundwater to allow the filter strip to dry in between storms. A length of at least 25 feet is necessary for a filter strip to be effective, but it is often recommended that it be closer to 100 feet long in order to provide significant pollutant removal. Placing a pea gravel diaphragm—a small ditch—at the top of the slope and a pervious berm of sand at the bottom of the slope is also useful for promoting effectiveness. Some restrictions for the use of filter strips include that filter strips should not be used on soils with a lot of clay since clay prevents infiltration, arid climates often necessitate irrigation, which can drive up the cost, and filter strips should not receive highly polluted water, such as that from a gas station, because the infiltration caused by filter strips would contaminate the groundwater.²¹ Filter strips have been shown to remove around half of the total suspended solids pollution, half the total iron pollution, and around 70% of the total zinc pollution.²² The cost of building a filter strip is difficult to pin down exactly. The cost of seed is typically around 30 cents per square foot and maintenance usually comes in around 350 dollars per year. However, in many cases, the biggest cost can be the land that it requires.²¹

Grassed swales can provide treatment for drainage areas of around 5 acres or less. They should be placed in ditches with a slope of one to two percent and a gentle side slope of less than 3:1. Also, a small forebay should be placed at the top of the channel, with a pea gravel diaphragm along the sides. It is recommended that the swale be at least 2 feet above the groundwater. There are three different types of grassed swales. One type, the grassed channel, is very similar to a conventional drainage ditch. It should be designed not based on size, but should instead be designed so that runoff takes around 10 minutes to flow from the top of the channel to the bottom. Grassed swales are the least expensive, but they also are the least effective. They have been shown to remove around two-thirds of total suspended solids and approximately 25% of metals such as zinc and iron. Dry swales incorporate a fabricated sand/soil mix in place of traditional soil, as well as an underdrain made of a perforated pipe encased by a gravel layer. Dry swales have been shown to remove an average of around 90% of total suspended solids and 80% of metals such as iron and zinc. Wet swales intersect the groundwater and incorporate a shallow pool and wetland vegetation. They have been shown to remove an average of around 75% total suspended solids and 33% of metals. One major drawback of wet swales, however, is that they may provide a breeding ground for mosquitoes. Some other drawbacks for grassed swales in general include the need for irrigation in arid and semi-arid climate (although buffalo grass can be used to help reduce that need) and a lack of applicability to pollution hot-spot runoff. The grassed channel has been estimated to cost around 25 cents per square foot, whereas swales have been estimated to cost around 50 cents per square foot.²³

Media filters can also be used to remove some pollutants from stormwater runoff. A media filter consists of a bed of a particular media through which water is directed. A layer of gravel is sometimes placed under the media. There are many different types of media that can be used, with each having different uses. Manganese greensand filters can be used for removing iron because they cause the iron to oxidize when it contacts the sand. It then easily filters out the oxidized iron particles. It is recommended for a greensand bed to be at least 30 inches deep.²⁴ Birm filters are an alternative for greensand. They, too, are mainly useful for their iron removal. In fact, birm stands for “Burgess Iron Removal Method”.²⁵ Aeration can be used to aid each of those filters in oxidizing the iron. A sand filter can be designed on the surface or underground. Underground sand filters are useful because they do not take up any surface space and they are still useful during cold months, whereas a surface sand filter would likely freeze and become unusable. The advantage of surface sand filters is that they can treat up to 10 acres, while underground sand filters are better if limited to 2 acres. Cost varies significantly depending on the design, but a typical cost can be anywhere between \$2.50 and \$7.50 per cubic foot of stormwater treated.²⁶ Typical removal rates are 70% of TSS and BOD and 45% of zinc and iron. BOD removal has been described as “modest”.²⁷ Zeolite is another option for a filtration media. Zeolite is very similar to sand and is sometimes mentioned specifically as an alternative to sand. The big advantage of zeolite is that it can remove smaller particles from the water than sand²⁸ and it has shown a better ability to remove metals and organics than sand.²⁹ Maintenance for media filters includes regular sediment removal. Backwashing can also be done, although that may be hard to do in a simple stormwater system.

Another kind of filter is the trickling filter, which typically uses a bed of rocks, slag, peat moss, sand, or plastic through which water is allowed to trickle. What separates trickling filters from media filters is a layer of microorganisms, often referred to as a slime, which consists of things such as bacteria, fungi, and protozoa, that is allowed to grow on the surface of the media. This slime layer occurs naturally. Over time, as water flows over the medium, microorganisms already in the water gradually attach themselves to the medium. It is sometimes suggested that if it will not receive constant flow, than it may be best to leave the filter submerged in water while it is not receiving flow in order to ensure the health of the slime layer. It is also necessary to ensure that the filter has a strong air source. Trickling filters are especially useful for removing organic matter via adsorption, and therefore BOD and COD, from water. A negative for trickling filters is that they can require regular attention to ensure the health and presence of a slime layer and to alleviate and prevent clogging. Also, the slime layer can sometimes come unattached from the filter and exit with the effluent water. It has been shown that a trickling filter can remove 80% of the BOD. Size and cost of trickling filters varies greatly depending on the amount of water to be treated.³⁰ A big positive for all filters is that do not consume a lot of land area.

Advanced oxidation processes are an effective way to reduce BOD and COD in water, and they can also remove some metals from water. Advanced oxidation processes use an oxidation agent to oxidize organic materials and metals, removing oxygen demand and metal pollution from the water. A commonly used agent for oxidation is hydrogen peroxide, or H_2O_2 .³¹ When oxidized, the metals will precipitate. While the precipitate is harmless and easy to filter, it would contribute to total suspended solid pollution if not removed. An alternative to this is to simply retain and aerate the water. This provides the oxygen needed for microorganisms to break down organic matter in the water. Essentially, this is satisfying the BOD and COD before releasing the water, removing their negative effects on the receiving waters.³² Aerating can also cause iron and zinc to oxidize and turn into a solid, although it may not be as effective. A downside to these methods is that they

may require temporary retention of the water to allow time for the process to do its work before the water can be safely discharged.

Activated sludge is a treatment process that combines aeration with some of the concepts of a trickling filter to provide very effective removal of organic materials, significantly reducing BOD and COD. Activated sludge mixes microorganisms, such as bacteria, fungi, and protozoa, with the water to be treated in an aeration tank to speed up the decomposition of the organic materials and reduce the oxygen demand of the treated effluent. After this, the water is sent to a settling tank, where the sludge can settle out of the water. The water is then released, while some of the sludge is returned to the aeration tank to be reused. A main problem with this is that the rest of the sludge that is not reused must be disposed of in some way.³³

Another way to remove pollution is through the use of ion exchange. Ion exchange can remove a vast array of metals and minerals, depending on what resin is used. An ion exchange resin is a collection of small beads which will exchange unwanted ions in the water for more acceptable ones. They can be selected so that they will focus on removing the specific ions desired.³⁴ Zinc is often found in water in the form of the Zn^{2+} ion,³⁵ while iron is often present as the Fe^{2+} ion.³⁶ Lenntech recommends the Lewatit TP 207 for the removal of many dissolved metals.³⁷ Ion exchange resins are often contained in a vessel designed for retention, where they can exchange ions with the water. Cation resins, which would be used with zinc and iron, can be regenerated with backwashing and hydrochloric acid.³⁸

Reverse osmosis is an extremely effective way to get heavy metals out of water. Reverse osmosis uses a semipermeable membrane separating two columns of water to remove from the water all dissolved solids whose molecules are larger than that of water from the water, such as heavy metals.³⁹ Reverse osmosis gets its name from osmosis, which is the tendency of fluid with a lower dissolved solids concentration into fluid with a higher dissolved solids concentration. This causes one water level to rise above the other, which results in an osmotic pressure. Reverse osmosis reverses this effect by applying a pressure greater than that of the osmotic pressure, causing the solid-filled water to pass through the membrane and leave the solids behind.⁴⁰ Some concerns with reverse osmosis is that the extensive demineralization can leave the water acidic.³⁹ Cost can also be a concern.

CONCLUSION

Preventing pollution from ever entering stormwater is the best method for pollution reduction. It often requires less maintenance and special skills, and can be more reliable than counting on the pollutants to be filtered out. Some good methods for this include green roofs, painting galvanized roofing, and rain gardens. However, if it is necessary, there are plenty of methods for removing pollutants from the stormwater. Out of all the filtration methods, grassed swales and/or filter strips should be tried first. They require little maintenance and can be effective. Even when they are not enough by themselves, they are still necessary as pretreatment for another method. Zeolite filter beds are the best option for further treatment. They require less maintenance than many other methods, and are also more economical than many other methods while also being effective enough to adequately remove pollutants in most cases. For those who are especially concerned with iron pollution, a manganese greensand filter could be used as an alternative. Many other methods, including some of which are discussed in this paper, may require significant maintenance and special skills and knowledge that is not likely to be found at a typical wood products plant.

Another thing to consider when implementing any of these methods is to get one of the many available devices for real-time monitoring of the stormwater quality. This will help to give the company an immediate measure of the effectiveness of newly employed methods as well as if additional steps must be taken. In the unlikely event that these methods are still not enough, or if it is simply undesirable to undertake any projects without outside help, there are plenty of companies who are more than willing to consult and who offer a variety of products that will cleanse stormwater runoff of its pollutants. Some of these companies include StormwaterRx, LennTech, WaterProfessionals, Safe Water Systems, WaterAnywhere, Pure Water Products LLC, Siemens, Beckart, and many more. Costs are hard to come by online, and it would be necessary to contact the company to receive a quote for the necessary services. After a brief investigation, StormwaterRx looks to be the best option, as it has products that are specialized for the wood industry and able to remove all pollutants of concern. On the other hand, out of all the companies, LennTech provides on their website (free of charge) one of the most useful databases of information about many different treatment methods, which should be useful if attempting to implement a method without outside help, as it will likely be necessary to do at least a little bit of additional research about a certain method before putting it into practice to ensure proper design, installation, operation, and, therefore, effectiveness. While this paper mostly provides the basics for these areas, it is important to be sure that all the details are in place before proceeding with any decisions.

FUTURE PLANS

This research is currently scheduled to continue in the fall, with the plan that some relevant experiments can be conducted on-site. Some potential experiments include designing a method of creating a biodegradable plastic from wood products, investigating a battery based upon wood products, and investigating a solar panel based upon wood products. We also plan to collect rainwater to measure the levels of pollutants that are already in the water before it gets to West Virginia Split Rail, and to develop a system for measuring the pollutants in water that would come from a wood processing plant and reduce their concentrations to below EPA limits. We are also making plans to visit some leading wood products plants to get a first-hand look at the kinds of technology and methods they employ.

ACKNOWLEDGEMENTS

The researcher would like to thank NASA and the West Virginia Space Grant Consortium for this opportunity. Also, thanks to Dr. Joseph Wiest, Dr. G. Albert Popson Jr, and Keith Barbo for their time and assistance with this research, and to James Hinkle for his support of this research program.

REFERENCES

1. "Chemistry for Biologists: Photosynthesis." *Royal Society of Chemistry | Advancing the Chemical Sciences*. Royal Society of Chemistry Publishing, n.d. Web. 29 July 2013. <<http://www.rsc.org/Education/Teachers/Resources/cfb/photosynthesis.htm>>.
2. Trappeniers, Keon. "Chemical Composition of Wood." *EzineArticles.com*. SparkNET, n.d. Web. 12 June 2013. <ezinearticles.com/?Chemical-Composition-of-Wood&id=4096045>.
3. Deo, Mrunmayi. "Plant Cell Structure and Function." *Buzzle*. Buzzle.com, n.d. Web. 29 July 2013. <www.buzzle.com/articles/plant-cell-structure-and-function.html>.

4. Port, Tami. "Photosynthetic plant cell structure - by Tami Port MS - Helium." *Helium - Where Knowledge Rules*. Helium, Inc, n.d. Web. 29 July 2013. <<http://www.helium.com/items/1977345-plant-cell-structure>>.
5. "About Lignin." *ILI*. The International Lignin Institute, n.d. Web. 30 July 2013. <<http://www.ili-lignin.com/aboutlignin.php>>.
6. Stein, Sammy. "The structure and function of lignin in plant cells - by Sammy Stein - Helium." *Helium - Where Knowledge Rules*. N.p., n.d. Web. 30 July 2013. <<http://www.helium.com/items/1633330-the-structure-and-function-of-lignin-in-plant-cells>>.
7. Brend, Tom. "The structure and function of cellulose in plant cells - by Tom Brend - Helium." *Helium - Where Knowledge Rules*. N.p., n.d. Web. 30 July 2013. <<http://www.helium.com/items/1586063-function-of-cellulose-in-plants>>.
8. "Pure Lignin Environmental Technology » Lignin." *Pure Lignin Environmental Technology*. Purelignin.com, n.d. Web. 30 July 2013. <<http://purelignin.com/lignin>>.
9. "Wood You Believe We Get So Much From Trees?." *Idaho Forest Products Commission*. Idaho Forest Products Commission, n.d. Web. 22 May 2013. <http://www.idahoforests.org/wood_you.htm>.
10. Anthony, Sebastian. "Nanocellulose: A cheap, conductive, stronger-than-Kevlar wonder material made from wood pulp | ExtremeTech." *Latest Technology News | Tech Blog | ExtremeTech*. Ziff Davis, Inc, n.d. Web. 22 May 2013. <<http://www.extremetech.com/extreme/134910-nanocellulose-a-cheap-conductive-stronger-than-kevlar-wonder-material-made-from-wood-pulp>>.
11. Perenson, Melissa. "All-natural 3D printers use salt and wood | Fox News." *Fox News - Breaking News Updates | Latest News Headlines | Photos & News Videos*. FOX News Network, LLC, n.d. Web. 31 July 2013. <<http://www.foxnews.com/tech/2013/05/23/all-natural-3d-printers-salt-and-wood-can-be-used/>>.
12. "Environmentally friendly battery made from wood." *Research & Development | Technologies & Strategies That Enable Research & Development*. Advantage Business Media, 24 July 2013. Web. 25 July 2013. <http://www.rdmag.com/news/2013/07/environmentally-friendly-battery-made-wood?et_cid=3386363&et_rid=54749314&type=cta>.
13. Bausch, Jeffrey. "Researchers develop recyclable solar cells from trees." *Electronic Product Magazine - Component and Technology News*. N.p., 4 Apr. 2013. Web. 21 May 2013. <http://www.electronicproducts.com/Optoelectronics/Image_Sensors_and_Optical_Detectors/Researchers_develop_recyclable_solar_cells_from_trees.aspx>.
14. Tullo, Alexander. "Making Wood Last Forever With Acetylation | August 6, 2012 Issue - Vol. 90 Issue 32 | Chemical & Engineering News." *Chemical & Engineering News | Serving the chemical, life sciences and laboratory worlds*. American Chemical Society, 6 Aug. 2012. Web. 30 July 2013. <<http://cen.acs.org/articles/90/i32/Making-Wood-Last-Forever-Acetylation.html>>.
15. Ellis, Timothy. "WASTEWATER QUANTITIES." *ENCYCLOPEDIA OF LIFE SUPPORT SYSTEMS (EOLSS): HOME PAGE*. Eolss Pubublishers, n.d. Web. 19 June 2013. <http://www.eolss.net/EolssSampleChapters/C06/E6-13-04-05/E6-13-04-05-TXT-05.aspx#Related_Chapters>.

16. "EPA - Stormwater Menu of BMPs." *U.S. EPA ColdFusion Server*. Environmental Protection Agency, n.d. Web. 21 June 2013.
<http://cfpub.epa.gov/npdes/stormwater/menuofbmps/index.cfm?action=factsheet_results&view=specific&bmp=114>.
17. "EPA - Stormwater Menu of BMPs." *U.S. EPA ColdFusion Server*. Environmental Protection Agency, n.d. Web. 21 June 2013.
<http://cfpub.epa.gov/npdes/stormwater/menuofbmps/index.cfm?action=factsheet_results&view=specific&bmp=72>.
18. "EPA - Stormwater Menu of BMPs." *U.S. EPA ColdFusion Server*. Environmental Protection Agency, n.d. Web. 18 July 2013.
<http://cfpub.epa.gov/npdes/stormwater/menuofbmps/index.cfm?action=factsheet_results&view=specific&bmp=69>.
19. "EPA - Stormwater Menu of BMPs." *U.S. EPA ColdFusion Server*. Environmental Protection Agency, n.d. Web. 18 July 2013.
<http://cfpub.epa.gov/npdes/stormwater/menuofbmps/index.cfm?action=factsheet_results&view=specific&bmp=70>.
20. "Stormwater." *EPA.gov*. Environmental Protection Agency, n.d. Web. 14 June 2013.
<www.epa.gov/safewater/sourcewater/pubs/fs_swpp_stormwater.pdf>.
21. "EPA - Stormwater Menu of BMPs." *U.S. EPA ColdFusion Server*. Environmental Protection Agency, n.d. Web. 11 June 2013.
<http://cfpub.epa.gov/npdes/stormwater/menuofbmps/index.cfm?action=factsheet_results&view=specific&bmp=76>.
22. "Draft Guidance Manual." *bmpdatabase.org*. Environmental Protection Agency, n.d. Web. 17 July 2013.
<bmpdatabase.org/Docs/2012%20Water%20Quality%20Analysis%20Addendum/BMP%20Database%20Categorical_SummaryAddendumReport_Final.pdf>.
23. "EPA - Stormwater Menu of BMPs." *U.S. EPA ColdFusion Server*. Environmental Protection Agency, n.d. Web. 11 June 2013.
<http://cfpub.epa.gov/npdes/stormwater/menuofbmps/index.cfm?action=factsheet_results&view=specific&bmp=75>.
24. "CEI Filtration | One company for all your filter media." *CEI Companies | Carbon Enterprises, Inc.*. Carbon Enterprises, Inc, n.d. Web. 17 July 2013.
<<http://www.ceifiltration.com/filtration.asp?p=greensand>>.
25. "Birm Filter Media for Whole House Water Filters." *premierWater*. Premier Water Technologies, Inc, n.d. Web. 26 July 2013. <www.premierwatermn.com/birm-iron-filter-whole-house-water-filter/>.
26. "EPA - Stormwater Menu of BMPs." *U.S. EPA ColdFusion Server*. Environmental Protection Agency, n.d. Web. 22 July 2013.
<<http://cfpub.epa.gov/npdes/stormwater/menuofbmps/index.cfm?action=browse&Rbutton=detail&bmp=73>>.
27. "Stormwater Technology Fact Sheet: Sand Filters." *National Service Center for Environmental Publications*. Environmental Protection Agency, n.d. Web. 22 July 2013.
<nepis.epa.gov/Exe/ZyNET.exe/200044AG.txt?ZyActionD=ZyDocument&Client=EPA&Index=2011%20Thru%202015|1995%20Thru%201999|2006%20Thru%202010|1991%20Thru%201994|2000%20Thru%202005&Docs=&Query=media%20filter&Time=&EndTime=&SearchMethod=2&TocRestrict=n&Toc=&TocEntry=&QField=&QFieldYear=>

- QFieldMonth=&QFieldDay=&UseQField=&IntQFieldOp=0&ExtQFieldOp=0&XmlQuery=&File=D%3A\ZYFILES\INDEX%20DATA\95THRU99\TXT\00000015\200044AG.txt&User=ANONYMOUS&Password=anonymous&SortMethod=h|-&MaximumDocuments=15&FuzzyDegree=0&ImageQuality=r65g4/r65g4/x150y150g16/i360&Display=p|f&DefSeekPage=x&SearchBack=ZyActionL&Back=ZyActionS&BackDesc=Results%20page&MaximumPages=1&ZyEntry=1&SeekPage=x>.
28. "ChemSorb Filter Granules." *OhioPureWaterCo.com*. Ohio Pure Water Company, n.d. Web. 23 July 2013. <www.ohiopurewater.com/shop/files/ChemSorb.pdf>.
 29. "Alternative Media Filters." *Office of Water Programs*. Sacramento State, n.d. Web. 23 July 2013. <<http://www.owp.csus.edu/research/stormwater/alternative-media-filters.php>>.
 30. "Waste Water Technology Fact Sheet: Trickling Filters." *National Service Center for Environmental Publications*. Environmental Protection Agency, n.d. Web. 19 July 2013. <nepis.epa.gov/Exe/ZyNET.exe/P10099PA.txt?ZyActionD=ZyDocument&Client=EPA&Index=2011%20Thru%202015|1995%20Thru%201999|2006%20Thru%202010|1991%20Thru%201994|2000%20Thru%202005&Docs=&Query=media%20filter&Time=&EndTime=&SearchMethod=2&TocRestrict=n&Toc=&TocEntry=&QField=&QFieldYear=&QFieldMonth=&QFieldDay=&UseQField=&IntQFieldOp=0&ExtQFieldOp=0&XmlQuery=&File=D%3A\ZYFILES\INDEX%20DATA\00THRU05\TXT\00000025\P10099PA.txt&User=ANONYMOUS&Password=anonymous&SortMethod=h|-&MaximumDocuments=15&FuzzyDegree=0&ImageQuality=r65g4/r65g4/x150y150g16/i360&Display=p|f&DefSeekPage=x&SearchBack=ZyActionL&Back=ZyActionS&BackDesc=Results%20page&MaximumPages=1&ZyEntry=1&SeekPage=x>.
 31. "Advanced Oxidation - Lenntech." *Water Treatment and Purification - Lenntech*. Lenntech, n.d. Web. 24 July 2013. <<http://www.lenntech.com/library/oxidation/oxidation.htm>>.
 32. "Aeration of waste water - Lenntech." *Water Treatment and Purification - Lenntech*. Lenntech, n.d. Web. 24 July 2013. <<http://www.lenntech.com/aeration.htm>>.
 33. "Water Treatment | Waste Water Treatment | Water Treatment Process & Plant Design» Blog ArchiveActivated Sludge Process." *Water Treatment | Waste Water Treatment | Water Treatment Process & Plant DesignWater Treatment | Waste Water Treatment | Water Treatment Process & Plant Design » A Free Educational Site and Professional Guide in Water Treatment, Sewage Treatment, Water Treatment Plant Design, Water Treatment Process, Water Analysis, Water Filter, Softener and more..* Water Treatment, n.d. Web. 25 July 2013. <<http://www.thewatertreatments.com/wastewater-sewage-treatment/activated-sludge-process/>>.
 34. "Ion Exchange." *Ohio Department of Health Home*. Ohio Department of Health, n.d. Web. 25 July 2013. <<http://www.odh.ohio.gov/odhprograms/eh/water/privatewatertreatment/ionexchange.aspx>>.
 35. "Zinc (Zn) and water." *Water Treatment and Purification - Lenntech*. Lenntech, n.d. Web. 25 July 2013. <<http://www.lenntech.com/periodic/water/zinc/zinc-and-water.htm>>.
 36. "Iron (Fe) and water." *Water Treatment and Purification - Lenntech*. Lenntech, n.d. Web. 25 July 2013. <<http://www.lenntech.com/periodic/water/iron/iron-and-water.htm>>.
 37. "Selective ion-exchange for the removal of heavy metals." *Water Treatment and Purification - Lenntech*. Lenntech, n.d. Web. 25 July 2013.

- <<http://www.lenntech.com/processes/heavy/plants/selective-ion-exchange-heavy-metals.htm>>.
38. "Ion Exchange | Deionization Resins | Anion." *Industrial Water Treatment | Water Purification | Process Water Treatment*. WaterProfessionals, n.d. Web. 25 July 2013. <http://www.waterprofessionals.com/wastewater/ion_exchange.html>.
 39. "Water Treatment Alternatives - Reverse Osmosis." *All About Water - Read, Learn, and Know about Water*. All About Water.org, n.d. Web. 24 July 2013. <<http://www.allaboutwater.org/reverse-osmosis.html>>.
 40. "The Reverse Osmosis process uses a semi." *Water Treatment and Purification - Lenntech*. Lenntech, n.d. Web. 24 July 2013. <<http://www.lenntech.com/library/reverse-osmosis/whatisro.htm>>.

SUMMER 2013 WALLOPS INFORMATION SYSTEM DATA MANAGEMENT INTERNSHIP AT WALLOPS FLIGHT FACILITY

Ashley Rachelle Webb
National Security and Intelligence, Political Science, Criminal Justice
Fairmont State University
Fairmont, West Virginia 26554

ABSTRACT

NASA Wallops Flight Facility was a wonderful place to work, between the excitement of the rockets and airplanes to the interesting and diverse group of people that I got to interact with daily, I could not imagine a better career choice. During my internship I met many new people, learned new things, and expanded my horizons both socially and educationally. I am grateful for the opportunities that this internship gave me, it was both educational and fun which is something many students do not have the chance to experience.

INTRODUCTION

During this internship there were many goals that were set for me to reach; I achieved all of those goals and accomplished many more things. The primary goal was for me to update the current ArcGIS database. Other goals included expanding my familiarity with communication electronics and their uses, and gaining experience in fiber optic infrastructure and its utilization at Wallops Flight Facility. The overall purpose of this internship was to become familiar in information technology; this includes many applications such as storage, database, transmission, and data manipulation.

BACKGROUND

I am currently a sophomore at Fairmont State University majoring in National Security and Intelligence, Political Science, and Criminal Justice with minors in Spanish and History. I graduated from Pocomoke High School in 2012 with a 5.12 GPA. During the summers of 2011 and 2012 I was also a NASA intern at Wallops Flight Facility, one summer with Information Technology (IT) and the other with Safety, making this my third experience as an intern. These internships present so many opportunities that I encourage others interested in Science, Technology, Engineering, and Mathematics (STEM) fields to apply. During high school I was actively involved with FIRST Robotics and served as team captain for two years, along with being actively involved with Pocomoke High School's MESA (Mathematics, Engineering, Science, Achievement) team.

PROJECTS

I had the opportunity to work on and complete multiple tasks in order to help with larger NASA missions. Each project was unique and taught me different aspects of the information technology field.

ArcGIS

My main project for this summer was to complete the ArcGIS/OSP InSight database that I began to update during the summer of 2011, my first summer as an intern for Code 763, the Information Technology and Communications branch, at Wallops Flight Facility (WFF). This software allows all fiber optic cables to be mapped with properties; this helps to determine where fibers are already placed in relationship to where new fiber needs to be planted to provide communication services to all employees at WFF. With this information, it allows other employees to know if a new fiber would need to be planted or if there are free terminations available for use. (See Figure 1)

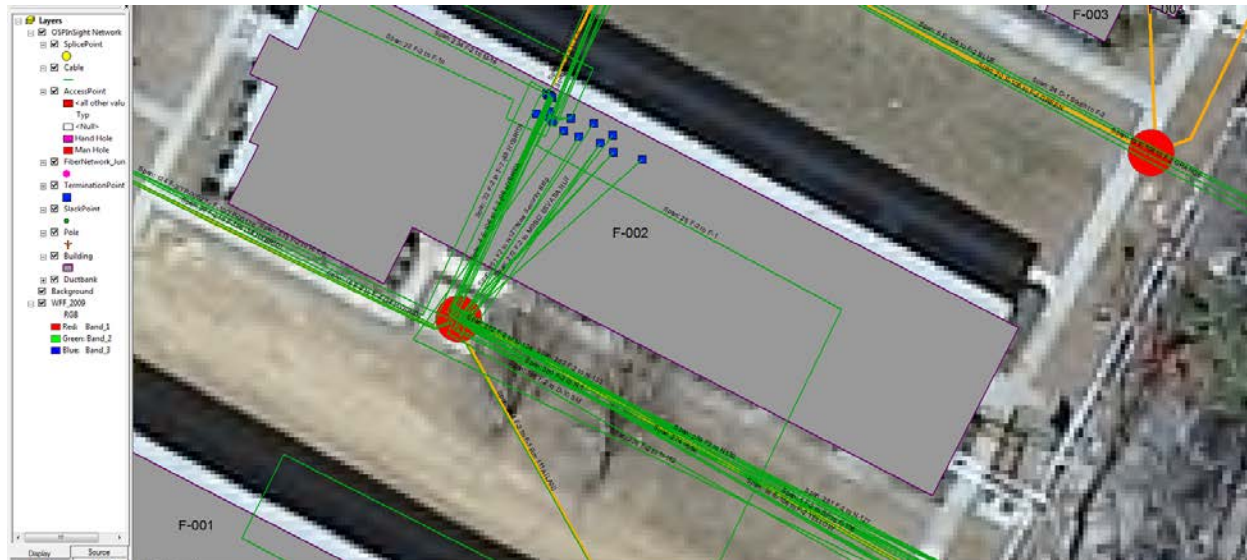


Figure 1: This is a close up of one of the buildings in ArcGIS. The green represents cables, the red represents access points, and the blue are termination points.

Wireless Internet Mapping

Another project I worked on is the wireless internet mapping. This allows people to know where new access points need to be placed in relationship to the existing access points to give the maximum amount of wireless internet coverage in each building. I mapped the D-1 hangar to ensure that the wireless internet coverage was sufficient for the upcoming Global Hawk project. To complete this project I used two types of software, Linear Projector and Swarm Analyzer to determine where the RF signal was the strongest. (See Figure 2) For the Global Hawk project, NASA will use two Global Hawk aircraft to investigate hurricane processes and changes that hurricanes undergo while over the Atlantic Ocean.

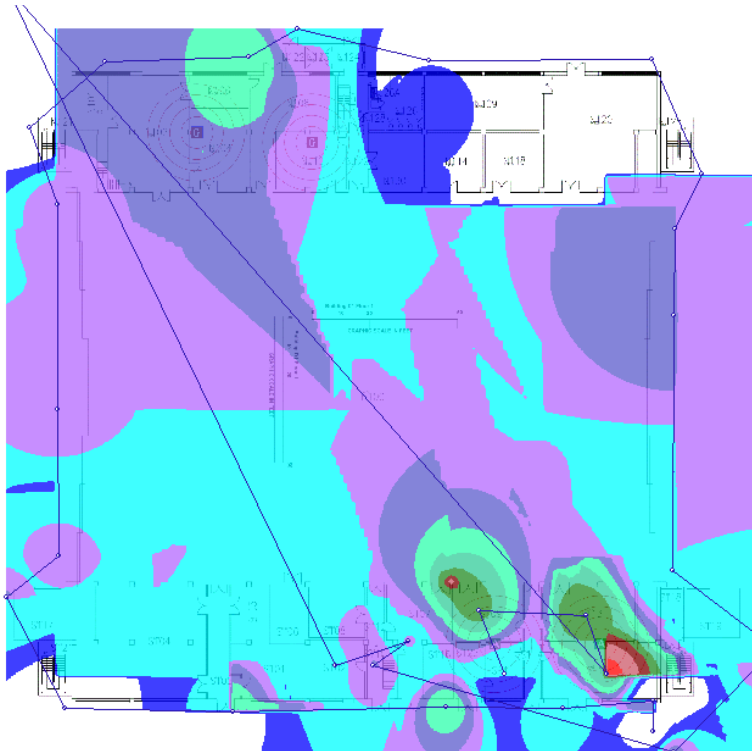


Figure 2: This is the Swarm Analyzer software which takes all the information from each data point that I mapped and creates a color coded map of where the strong wireless internet points are and where new access points need to be installed. The small amount of red shows where the wireless internet signal is strong enough to be used.

LADEE

I worked with Orbital Sciences Corporation to prepare data, time, video and telemetry for the upcoming Lunar Atmosphere and Dust Environmental Explorer (LADEE) launch between the U-40 surveillance site, the Launchpad, and the range. In preparation for the LADEE launch, we also placed new cameras near Pad 0B to give visuals of the launch site. LADEE is a 160 day robotic mission that is going to orbit the moon for approximately 100 days gathering information about the atmosphere, conditions near the surface of the moon, and environmental influences on lunar dust. (NASA) One of my favorite miscellaneous tasks was doing the technical drawings for the configuration and cable routes for the LADEE launch, these drawings will also be used for the Antares launch. (See Figure 3)

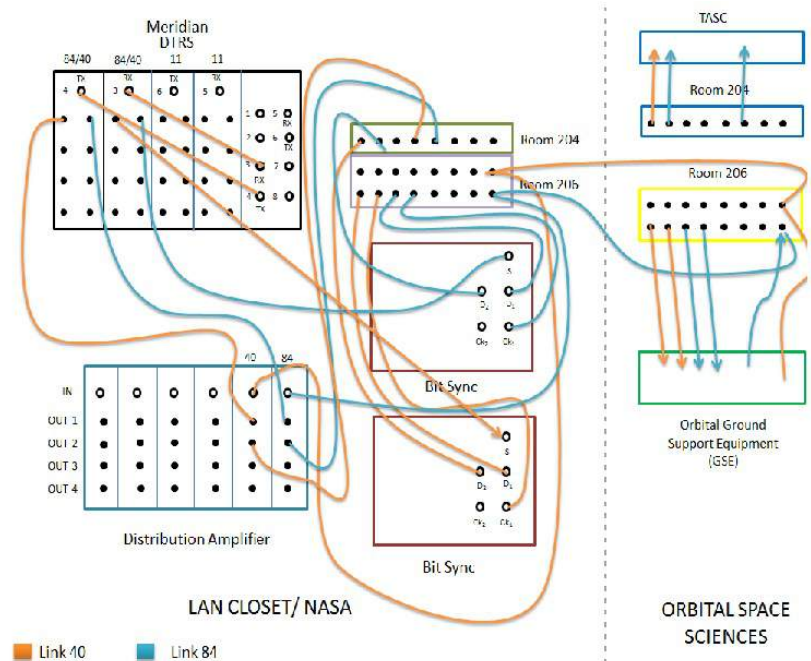


Figure 3: This is the technical communication drawing for the link 40 and 84 for the LADEE launch. This drawing shows the direction of the data flow and which parties will be receiving and transmitting information.

Closed Circuit Television

I helped to enable and configure a laptop for the closed circuit TV broadcast by connecting it to digital CCTV encoder. Another task I helped to complete was to set up a new channel on the closed circuit TV broadcast. I did this by installing a QAM TV tuner and single mode fiber media converter to route video and audio to CCTV head end. This then transmits the signal throughout the base.

Rockets

What is more patriotic than seeing the rockets' red glare on the Fourth of July? On July 4th, the Daytime Dynamo Launch occurred. This was really neat because I watched two rockets, a Black Brant V and a Terrier-Improved Orion, launch 15 seconds apart. This mission was coordinated between NASA and the Japan Aerospace Exploration Agency (JAXA).

Other Tasks

I also completed numerous other tasks that taught me many valuable skills all while having fun. I made and tested CAT-5 568-B standard version Ethernet cables, tested fiber optic cables to determine if they were ready for use in the facilities, and helped troubleshoot camera connection issues. Furthermore, I helped connected six QAM digital tuners to NTSC video switch in Global Hawk Operations Center to allow them to have access to the closed circuit television at NASA Wallops Flight Facility.

MEETINGS

Throughout my internship at Wallops Flight Facility I attended multiple meetings to further my knowledge on specific topics. These meetings allowed a combination of ideas to be heard in order

to problem solve effectively and provide good customer services. The first meetings I attended were training for the ArcGIS/OSP InSight software to refresh my memory on how to use the software. Another meeting I attended was a conversation on which software, ArcGIS or PatchManager, should be used to keep track of all fibers and equipment. During this meeting the positive and negative attributes of each program were discussed; ArcGIS is completed, however it is rarely updated and can only keep track of fiber, whereas PatchManager can track all types of equipment in more detail but has no information in it thus far. It was decided that ArcGIS will be continued to be used for fiber but PatchManager will be purchased to keep track of equipment. The goal is to eventually merge these two programs. Another meeting I attended during my internship was the Code-700 All-Hands Meeting on June 19th. This was a video conference with NASA Goddard Space Flight Center in Greenbelt to discuss the current method of customer service and how it should be improved to better meet the needs of customers and missions. At this meeting it was determined that in order to improve the current customer service we provide, it is important to emphasize, have a calm demeanor, troubleshoot issues, and have good verbal communication skills.

FUTURE PLANS

I hope to one day, after I graduate from Fairmont State University, be employed in a place where I can use the knowledge I have learned during my three internships at NASA and from my education. I hope to make a positive lasting impact on not only my community but also on my country.

CONCLUSION

The skills that I have learned throughout my internships at NASA have taught me lifelong business skills that I will be able to apply in any career and in life on a daily basis. The business etiquette, the communication skills and the professional experience are valuable life lessons. I have had three amazing experiences at NASA Wallops Flight Facility, and I am happy to say that these internships have greatly benefited me in helping me to figure out a career path. The most valuable aspects of these internships are the real-life work experience and the networking opportunities that you have while participating in the internship.

ACKNOWLEDGEMENTS

I would like to thank the people that I worked with this summer for teaching me so many new and interesting things. Paul Acuna, Brian Rhoads, Ted Schultz, Parke Atkinson, Johnny Gibbons, Rock Hilmoe and so many other people have given me a great experience this summer and I really appreciate them taking their time to teach me and train me in many different things. I appreciate their guidance at work and life lessons that they gave me throughout my internship. Most importantly, I want to thank West Virginia Space Grant Consortium and NASA Wallops Flight Facility for allowing me to participate in this wonderful internship. I learned so much this summer and it would not have been possible without the generosity and support of the West Virginia Space Grant Consortium.

REFERENCES

"NASA." *NASA Mission Overview*. NASA. Web. 06 Aug. 2013.
<http://www.nasa.gov/mission_pages/ladee/main/index.html>.

II. NASA Undergraduate Research Fellowship Program Reports

SATELLITE BASED DIAGNOSTIC APPROACH TO MONITOR HYDROCLIMATIC CONDITIONS FOR EMERGENCE OF WEST NILE VIRUS

Brandon Bowman
Civil Engineering
West Virginia University
Morgantown, West Virginia 26505

ABSTRACT

West Nile virus (WNV), mosquito-borne and water-based, is increasingly becoming a global threat to the public health. Since its appearance in the northeastern United States in 1999, WNV has since been reported in several states in the continental United States. The objective of this study is to highlight the utility of satellite sensors in capturing data on hydroclimatic processes to describe conditions favorable for emergence of vectors in historically disease free regions. We propose the hypothesis that an increase in surface temperature (as proxy of warming weather), in combination with intensification of vegetation as a result of enhanced precipitation, leads to conditions favorable for vector growth. Analysis of Land Surface Temperature (LST) pattern shows that a temperature values greater than 35⁰C, in the presence of vegetation mass (NDVI >0.89) resulting from precipitation results in abundance of the mosquito population. This hypothesis was tested in West Virginia where a sudden epidemic of WNV infection was reported in 2012. Our results emphasize the utility, of using hydroclimatic processes estimated by satellite remote sensing as well as the need for continued environmental surveillance of mosquitoes because when a vector borne infection like WNV is discovered in contiguous regions, the risk of spread of WNV mosquitoes increases at points where appropriate hydroclimatic processes intersect with the vector niche.

INTRODUCTION

West Nile virus (WNV) is a mosquito-transmitted Flavivirus belonging to the Japanese encephalitis antigenic complex of the family *Flaviviridae*. The natural transmission cycle for West Nile Virus is usually limited to birds and mosquitoes, routing to a host-which may be birds, humans, or other mammals and reptiles-all of whom become infected when bitten by mosquitoes. **Invalid source specified.** Since its appearance, in the northeastern United States in 1999, WNV has been reported throughout the entire continental US in a relatively short period of time. In fact, WNV is now a very serious vector-borne disease in the U.S because of its high morbidity rate in humans, with severe impact on avian populations as well (Chuang & Wimberly, 2012). Infected mosquitoes, in general, survive in hot, humid environments where warm temperatures prevail and the vegetation is dense (Reisen et al., 2004). The functional repertoire of a causative agent of mosquito-based disease is unusually broad, accommodating two distinctively different environments: the micro-environment of the vector and the macro-environment of the aquatic habitat. In the study reported here, the micro-environment is defined as comprising those processes within the mosquito (vector), while the macro-environment refers to hydrological, ecological, and climatic processes affecting growth and proliferation of the mosquito. The single discipline

approach, examining when the micro- or the macro-environmental factors has yielded an extensive body of information concerning mosquito-related diseases, but when and where a disease epidemic will strike cannot yet be predicted. Yet micro-environmental understanding of disease is essential if vaccines or treatment protocols are to be maximally effective. The single disciplinary approach will not be useful for prediction because *mosquitoes* adapt to their environment and new and adaptive biotypes, can emerge over time, making it unlikely that mosquitoes can be eradicated.

Remote Sensing and Geographic Information Systems (GIS) have proven to be useful tools for understanding relationships between large-scale hydroclimatic and epidemiological processes that provide assessment of the risk of human infections (Cleckner et al., 2011). Remotely sensed data in the visible and infrared spectra have been applied extensively to mapping and forecasting vector-borne disease at spatial scales ranging from landscapes to the entire globe (Henebry et al., 2012). Since mosquito abundance and survival are associated with availability of water and vegetation, the normalized density vegetation index (NDVI) (a surrogate for areas of vegetation density and availability of soil moisture/water) is a primary hydrological variable of interest (Hay et al., 1998; Patz et al., 1998; Roger and Randolph, 2002).

The U.S Centers for Disease Control reported in August 2012, that 1,118 WNV cases and 41 deaths have been confirmed nation-wide. WNV is a relatively new disease in the continental USA, hence only a handful of studies are available in the literature and these focus primarily on single outbreaks at discrete locations. Liu & Weng (2011) formulated WNV risk areas for three time periods of the year, e.g., weeks 18-26, 27-35, and 36-44 of year 2007. Similarly, Chuang & Wimberly (2012) employed hydroclimatic processes and variables, such as land surface temperature (LST), normalized difference vegetation index (NDVI) and actual evapotranspiration (ETa), all derived from the moderate resolution imaging spectroradiometer (MODIS) over the Great Plains, associating it with outbreaks of WNV. Table 1 summarizes some key information from the current literature on association of hydroclimatic variables, remote sensing, and WNV.

Table 1: Summary of available remote sensing based WNV studies in the continental US

	Author	Associated variables	Geographic Region
1	Zou et al (2006)*	Water bodies, vegetation	Wyoming, USA
2	Liu et al., (2008)	Total length of streams, size of wetlands	Indianapolis, USA
3	Liu et al (2011)	Vegetation, precipitation	Virginia, USA
4	Cleckner et al (2011)*	Vegetation, water bodies	Virginia, USA
5	Liu and Weng (2012)	Land cover, Surface temperature	Chicago, USA
6	Chuang and Wimberly (2012)	ET, vegetation, surface temperature	Great Plains, USA
7	Liu et al., (2012)	Summer temperature, deviation of temperature, vegetation, elevation, vegetation	Southern California, USA
8	Chuang et al (2012)	Air temperature, vegetation density	South Dakota, USA
9	Liu and Weng (2012)	Elevation, urban land cover	Los Angeles, USA

*primarily mapping study

Two important observations from those data are that there is no consensus on a triggering mechanism relating hydroclimatic conditions to mosquito abundance and human cases and the studies are correlative, contradicting findings from one to another. A classic example is that of Liu et al. (2011) and Liu & Weng (2012), where the authors reported absence/presence of vegetation in different regions, but failed to provide justification as to why and how hydroclimatic variables or vegetation influences WNV outbreaks. Clearly a plausible hypothesis on triggering mechanisms

for WNV is lacking, due primarily to absence of data on the disease, as well as snapshot types of analysis of individual outbreaks occurring at discrete locations.

Despite the limited amount of surveillance data available, the motivation to explore links between remote sensed data and WNV cases derive from the fact that remote sensing is the most reliable and efficient way to explore and monitor large scale terrestrial hydrological processes and associated variables. Furthermore WNV mosquito activity has distinctive seasonality, generally occurring during the early autumn season (Figure 1a), with the potential to be linked with hydroclimatic variability. Also, WNV may never be eradicated and the disease vector is naturally present in the environment. With no human vaccine yet available, a new approach of prediction and prevention of the disease is needed. Therefore the aim of this short communicate is to demonstrate the suitability of remote sensing to identify a region(s) where WNV human cases are not yet epidemic or very few and unnoticed during the past years. Within this context, differences between two key, large-scale geophysical processes, land surface temperature (LST) and normalized difference vegetation index (NDVI) correlated with abundance of WNV mosquitoes is examined. The hypothesis that an increase in temperature, in conjunction with abundant vegetation, leads to an increase in mosquito activity was tested, with the alternate hypothesis that a stable relationship between a given geophysical variable and mosquito abundance does not exist, hence satellite monitoring is not feasible for prediction of WNV disease.

DATA

West Virginia was selected as the region of interest for the study because of the relatively low number of reported WNV human cases, but a steady increase in the number of mosquitoes testing positive for WNV. A sudden increase in WNV mosquitoes during 2012 (WVDHHR, 2012) in this historically virus free region, combined with low prevalence in West Virginia, as in other states, e.g., Colorado, California, and Texas, provided an opportunity for a case study in the region. Most of the WNV positive mosquitoes collected from pools in West Virginia were reported from June through September (Fig 1a), indicating a seasonal link with geophysical changes in the environment affecting the mosquitoes (Cleckner et al., 2011). The first cases of human West Nile Virus in West Virginia occurred in 2002. Weekly data on mosquitos testing positive for arbovirus were obtained from the Centers for Disease Control and Prevention (CDC) ArboNET database, a national surveillance system for arboviral diseases in the United States. Satellite data were acquired from the moderate-resolution imaging spectroradiometer (MODIS) and reprojected using MODIS reprojection tool over the entire West Virginia (rectangular upper left corner 40⁰N and 82.67⁰W and lower right corner 37.17⁰N and 78.15⁰W). Land surface temperature (MOD11A2) data were obtained in an eight-day composite to eliminate cloud effects. Normalized density vegetation index (MOD13A1) data were available on a bi-monthly scale (16 day composite) and precipitation data from the National Oceanic and Atmospheric Administration, National Weather Service.

RESULTS

Geographically, WNV positive mosquitoes were reported in central to southern West Virginia (Fig. 1b). Interestingly, these are the regions, including Kanawha County, economically important to the state, with coal, chemical and natural gas industries. However, fewer human cases are reported for the entire state of West Virginia, mainly because of the low population density even in the urban areas. Fig 1a shows that mosquitoes have a distinct seasonality, with peak activity

during the summer season (with highest observed positive cases in the month of July), but the data are limited since sampling was not conducted during the winter, the assumption being that mosquitoes are not present in the environment in cold weather (WVDHHR, 2012). Monthly time series of WNV positive mosquitoes in the region shows that mosquito activity is steadily increasing each year (Fig 1c). Years 2012 (highest number of WNV positive mosquitoes) and 2011 (low number of WNV positive mosquitoes) were selected for analysis. 37% of the pools tested were WNV positive for *Culex restuans* and *Culex pipiens* (68% of the total mosquitoes collected during 2012), the primary WNV species in the region (WVDHHR, 2012). Two adjacent years were selected for study to quantify relative changes in large-scale hydroclimatic processes more accurately.

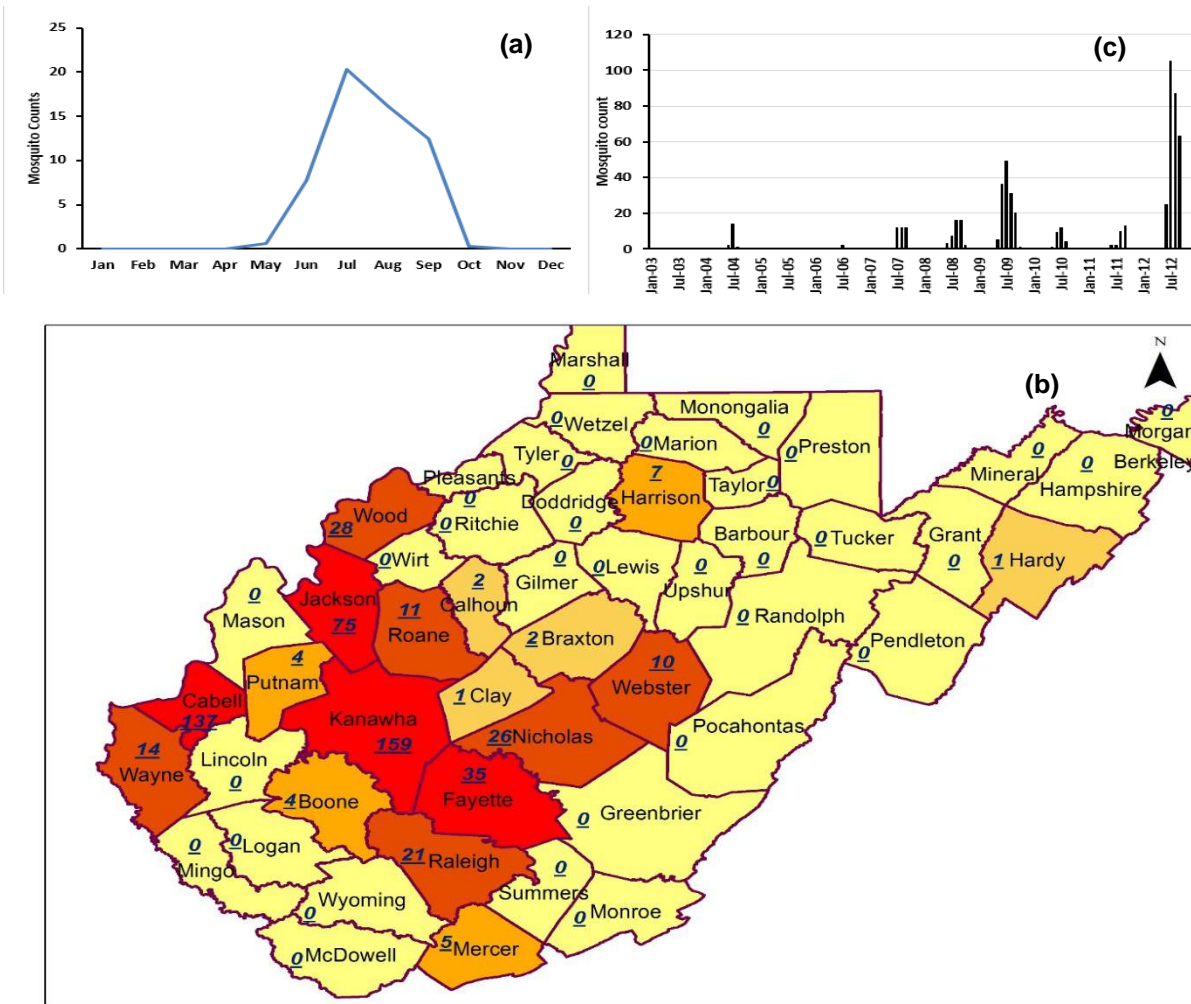


Figure 1: (a) Seasonality of West Nile Virus from 2003 to 2012; (b) cumulative spatial distribution of positive infectious mosquitoes for ten years and (c) time series for infectious mosquito counts for West Virginia in last 10 years (data from Arbonet).

The eight-day composite LST from MODIS Terra platform was used instead of daily LST data to avoid missing values due to cloud contamination. Fig 2a and 2b show eight panels for LST for June and July, respectively. In 2012, Cabell and Kanawha counties (location shown in Fig 1c)

showed highest number of WNV positive mosquitoes. Both figures are superimposed, with total number of WNV positive mosquitoes for the same year. If temperature were related to presence of mosquitoes, steady increase in temperature should be observed and regions of high temperatures should show more WNV positive mosquitoes. Fig 2a (top left panel) shows distribution of LST (average areal temperature 22.5°C). As land surface and air warm, the areal average increase over the months (to 28.5°C) at the end of the fourth week of June. The temperature peaked during the first week of July to 34.5°C, falling sharply thereafter. Two observations from Fig 2 include: (i) the highest number of WNV positive mosquitoes were found in regions where a rapid increase in LST occurred (black box in the figure) and (ii) the LST dropped within a few weeks in July, spread of WNV positive mosquitoes was limited to western counties of the region.

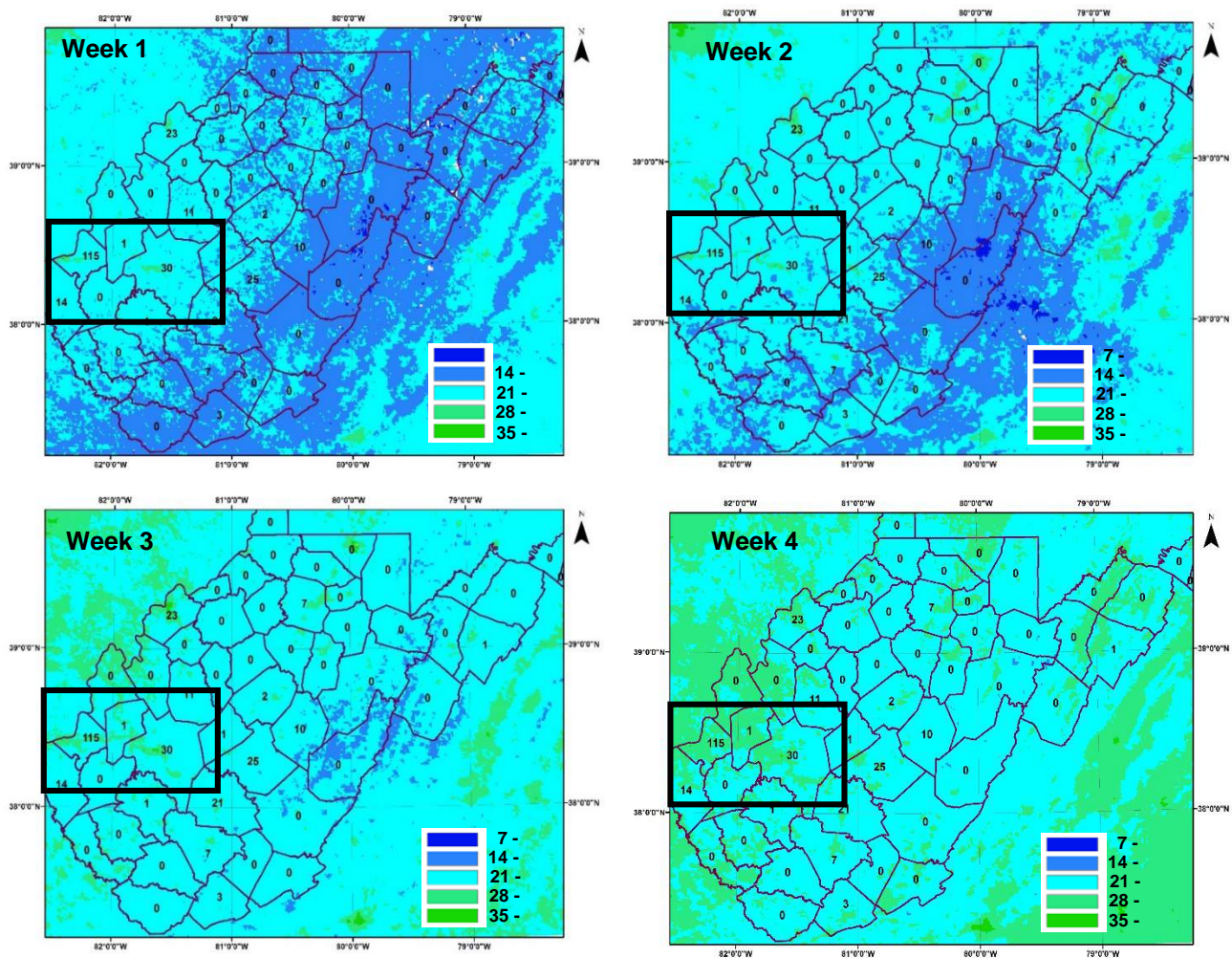


Figure 2a: Land Surface Temperature (°C) for June 2012

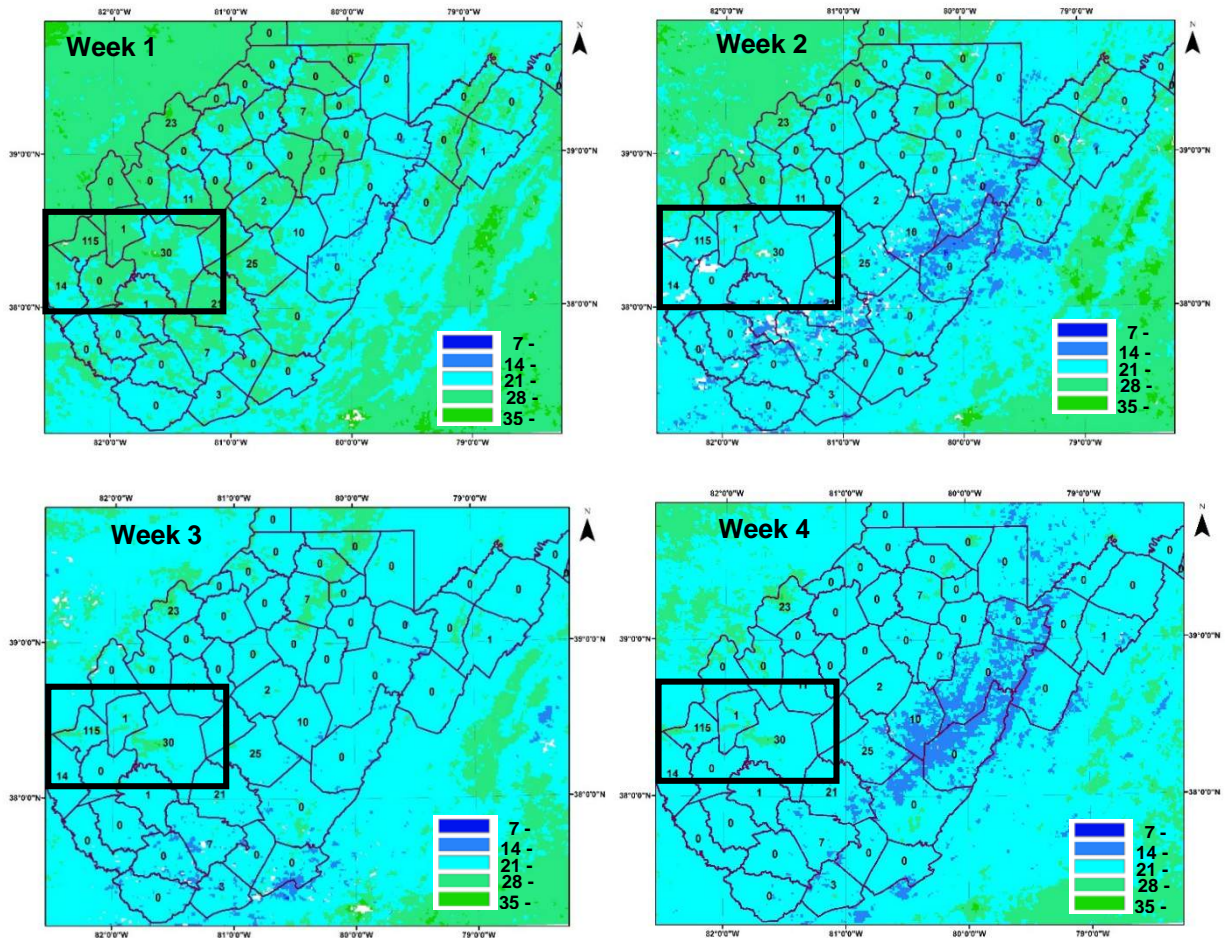


Figure 2b: Land Surface Temperature ($^{\circ}\text{C}$) for July 2012

If the relationship between LST and warm air is true, then we should observe a difference in inter-annual variability of LST also. Percent difference is shown in Fig 3, between monthly LST in July 2012 (highest number of WNV positive mosquitoes) and July 2011, (relative low number of WNV positive mosquitoes). Western counties (including Cabell and Kanawha, close to the Ohio and Elk rivers respectively) experienced 10-15% increase in LST in July of 2012, providing complementary evidence that LST is an important hydroclimatic process related to emergence and spread of WNV positive mosquitoes. One may argue that the northeastern counties experienced a similar increase in temperature during 2012. However, maximum temperature in the northeastern counties, which are also at a higher elevation than the western counties, during 2012 was 22°C , as compared to 36°C in the western counties (highlighted by the black box 38.6825°N to 37.8788°N ; 82.5844°W to 81.0955°W ; and include Cabell and Kanawha counties of West Virginia), providing a plausible explanation for the absence of mosquitoes in the region and corroborates thresholds for temperature effect on mosquito growth, documented by other investigators (*Githeko et al., 2000*; *Kilpatrick et al., 2012*).

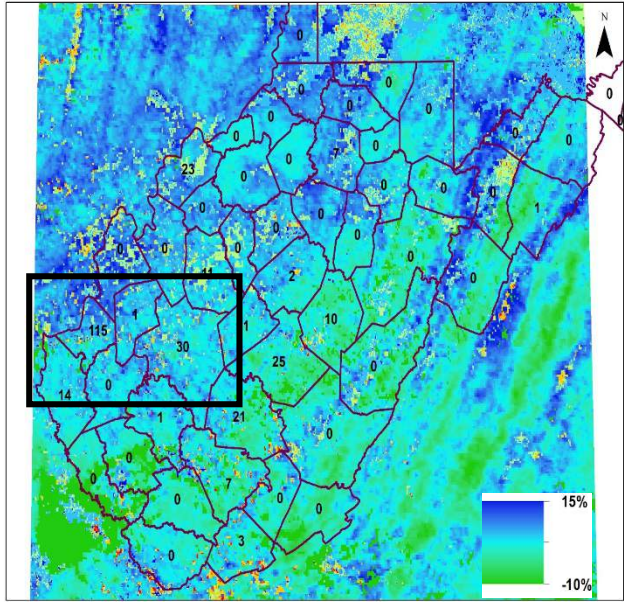


Figure 3: Percentage change in LST in July 2012 with respect to July 2011. The inset numbers on map are the WNV positive mosquitoes in year 2012 in counties of West Virginia.

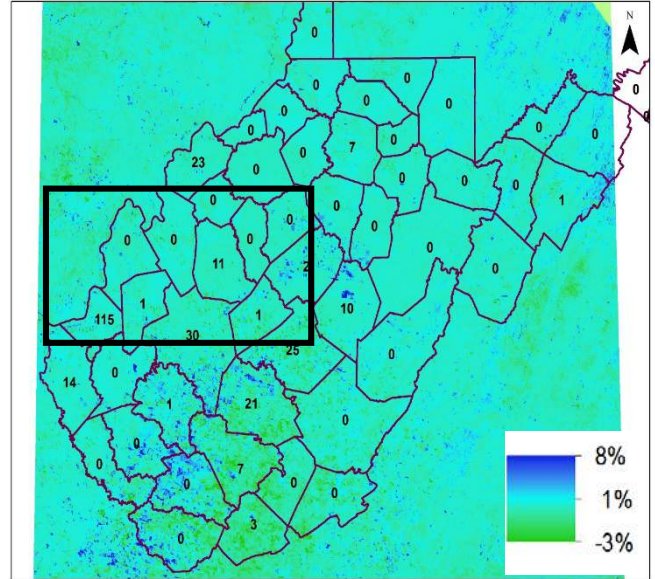


Figure 4: Percentage change in NDVI in July 2012 with respect to July 2011. The inset numbers on map are the WNV positive mosquitoes in year 2012 in counties of West Virginia.

Increase in LST may not be sufficient to explain the expansion of the mosquitoes throughout the region. Mosquitoes prefer a humid environment as often observed in areas with high vegetation, since such areas store more volumetric water in the vadoze zone easily accessible to maintain such environments. To understand effects of vegetation, we used a 16-day NDVI product from the MODIS Terra platform. Percentage difference in NDVI values between July 2012 and 2011, were computed, with the premise that NDVI values should be higher in 2012, than the preceding year. Figure 4 shows an average increase of 4.5% in NDVI, marked by the black box, where high prevalence of WNV positive mosquitoes was observed in 2012 (average NDVI 0.89). Less precipitation than average was observed for July 2012 (Fig 5a) and, 2011 (Fig 5b). Rainfall in July 2012 was 6 inches above normal (black box) compared to July 2011, with 2 inches less than normal precipitation, a contributing factor to the increase of NDVI in July 2012, substantiating the hypothesis that an increase in temperature and NDVI is correlated with the increase in the mosquito population namely *Cx. pipiens/restuans*, the primary WNV vector in the eastern United States (Turell et al. 2001; Turell et al. 2005; WVDHHR, 2012)

SUMMARY

Satellite remote sensing derived hydroclimatic processes can be useful in identifying conditions critical to the emergence of a vector-borne West Nile virus outbreak that occurred in a historically disease free region. Changes in land surface temperature, vegetation, and regional precipitation provide a favorable environment for mosquitoes. Using MODIS derived LST as surrogate for warm air temperature, an increase in temperature, in combination with increase in vegetation from

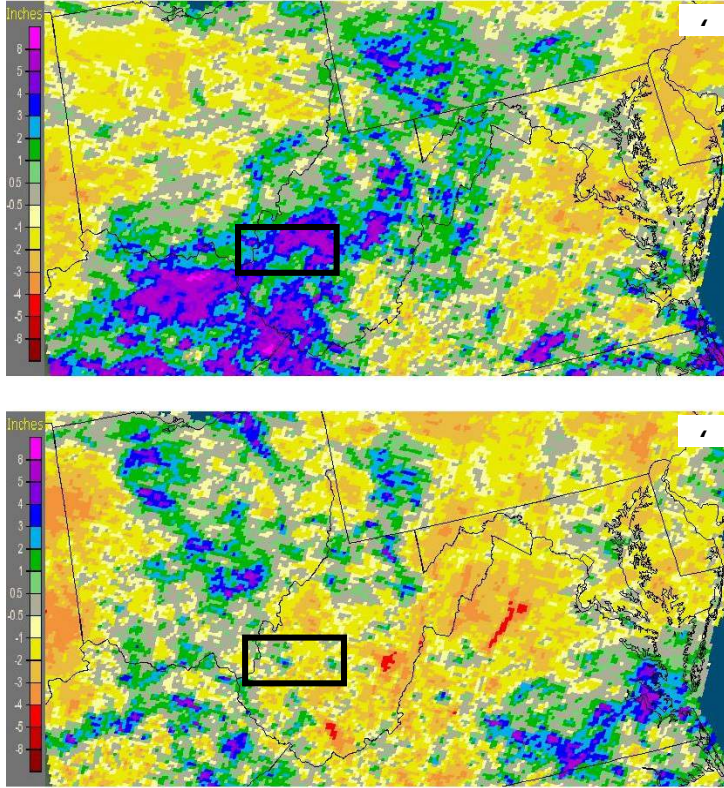


Figure 5: Departure of precipitation from historical averages during (a) July 2012 and (b) July 2011. Data and images were obtained from NOAA-National Weather Service.

heavy seasonal rainfall, is concluded to an increase in the mosquito population of southwestern West Virginia. Warm temperature has been reported to increase mosquito population (Paz et al., 2008) and subsequent human infections with the disease agent transmitted by mosquitoes. The basic mechanism relating temperature of mosquito growth is the decrease in length of the gonotrophic cycle, shortening the extrinsic incubation period of virus in the vectors, thereby enhancing the growth of the virus (Ruiz et al., 2010, Kunkel et al. 2006). The impact of vegetation, relative to prior heavy precipitation, is consistent with results of several studies associating vector borne mosquito infections with NDVI (Anyamba et al., 2002; Bisanzio et al., 2011; Chuang and Wimberly et al., 2012), but contradicting those of Lui & Weng (2012), most likely because of the spatial resolution (30-90m) of the satellite data used in their study to calculate NDVI. MODIS derived

NDVI at 1km resolution was employed in this study, with assumption that large-scale hydroclimatic processes may impact regional variability of mosquitoes when the air temperature is elevated.

Monitoring mosquito populations by satellite has been suggested by other investigators, but the integration of scale-dependent hydroclimatic processes with remote sensing data to develop areal-time surveillance and prediction of mosquito abundance is both unique and distinct. Both abundance of mosquito-borne arboviruses and data on related human infections are required to determine space-time evolution of the disease. Surveillance data cannot be gathered at large geographical scales; hence scale mismatch arises between data on geophysical processes and disease. Premature utilization of unproven intervention strategies, such as excessive use of chemicals to reduce mosquito populations has had a contrary effect, i.e., development of virulent and adaptive insect populations. Monitoring environmental processes linked to mosquito abundance offers a useful means for developing intervention and mitigation strategies.

ACKNOWLEDGEMENTS

This work was performed at West Virginia University and funded by NASA through the WV Space Grant Consortium. A special thanks to my research mentor Dr. Antarpreet Jutla.

REFERENCES

- Anyamba, A., Linthicum, K. J., Mahoney, R., Tucker, C. J., & Kelley, P. W. (2002). Mapping potential risk (Liu, Weng, & Gaines, Geographic incidence of human West Nile virus in northern Virginia, USA, in relation to incidence in birds and variations in urban environment , 2011)k of rift valley fever outbreaks in African savannas using vegetation index time series data. *Photogrammetric Engineering and Remote Sensing*, 68(2), 137-145.
- Bisanzio, D., Giacobini, M., Bertolotti, L., Mosca, A., Balbo, L., Kitron, U., & Vazquez-Prokopec, G. M. (2011). Spatio-temporal patterns of distribution of west nile virus vectors in eastern piedmont region, italy. *Parasites and Vectors*, 4(1)
- Chuang, T.-W., & Wimberly, M. C. (2012, October 5). Remote Sensing of Climatic Anomalies and West Nile Virus Incidence in the Northern Great Plains of the United States. (C. f. Yury E. Khudyakov, Ed.) *PLoS ONE*.
- Chuang, T.-W., Henebry, G., Kimball, J., VanRoekel-Patton, D., Hildreth, M., & Wimberly, M. (2012). Satellite microwave remote sensing for environmental modeling of mosquito population dynamics . *Remote Sensing Environment*.
- Cleckner, H. L., Allen, T. R., & Bellows, S. A. (2011, December 12). Remote Sensing and Modeling of Mosquito Abundance and Habitats in Coastal Virginia, USA. *Remote Sensing*.
- Hay, S. I., Snow, R. W., & Rogers, D. J. (1998). Predicting malaria seasons in Kenya using multitemporal meteorological satellite sensor data. *Transactions of the Royal Society of Tropical Medicine and Hygiene*, 92(1), 12-20.
- Henebry, G. M., Kimball, J. S., VanRoekel-Patton, D. L., Hildreth, M. B., Wimberly, M. C., & Chuang, T.-W. (2012, August 2012). Satellite microwave remote sensing for environmental modeling of mosquito population dynamics. *Remote Sensing of Environment*.
- Liu, H., & Weng, Q. (2007). Enhancing temporal resolution of satellite imagery for public health studies: A case study of West Nile Virus outbreak in Los Angeles in 2007 . *Remote Sensing of Environment*.
- Liu, H., & Weng, Q. (2008). An Examination of the effect of landscape pattern land surface temperature and socioeconomic conditions on WNV dissemination in chicago. *Environmental Monitor Assess*.
- Liu, H., & Weng, Q. (2011, December 29). Environmental Factors and Risk Areas of West Nile Virus in Southern California, 2007-2009. *Environmental Modeling and Assessment*.
- Liu, H., Weng, Q., & Gaines, D. (2008). Spatio-temporal analysis of the relationship between WNV dissemination and environmental variables in Indianapolis, USA. *International Journal of Health Geographics*.
- Liu, H., Weng, Q., & Gaines, D. (2011). Geographic incidence of human West Nile virus in northern Virginia, USA, in relation to incidence in birds and variations in urban environment . *Science of the Total Environment*.
- Reisen, W. K., Lothrop, H. D., Chiles, R. E., Madon, M. B., Cossen, C., Woods, L., . . . Edman, J. D. (2004). West Nile Virus in California. *Emerging Infectious Disease*, 10(8), 1369-1378.

- Rogers, D., & Randolph, S. (2002). Studying the global distribution of infectious disease using GIS and RS. *Nature Reviews Microbiology* .
- Turell, M., Dohm, D., Sardelis, M., O'Guinn, M., Andreadis , T., & Blow, J. (2005). An update on the potential of north american mosquitoes (Diptera; Culicidae) to transmit West Nile Virus. *Journal of medical Entomology*, 42(1), 57-62.
- Turell, M., O'Guinn, M., Dohm, D., & Jones, J. (2001). Vector competence of North American mosquitoes (Diptera: Culicidae) for West Nile virus. *Journal of Medical Entomology*, 38(2), 130-134.
- Zou, L., Miller, S., & Schmidtman, E. (2006). Mosquito Larval Habitat Mapping using remote sensing and GIS: Implications of coalbed methane development and west nile virus. *Journal of Medical Entomology*.

PIEZOELECTRIC, PDMS-BASED DEVICES

Dillon Carden
Mechanical Engineering
West Virginia University
Morgantown, WV, 26505

ABSTRACT

The following report is a summary of several experiments designed to test the durability, flexibility, and voltage output of polydimethylsiloxane-based (PDMS-based), piezoelectric devices intended for use as a haptic interface.

INTRODUCTION

This research project seeks to provide analytical support to the determination of the benefits of a device constructed using PDMS, poly(methyl methacrylate) (PMMA), and zinc oxide (ZnO) nanorods as a flexible, piezoelectric device. Specifically, this report ventures to build upon previous research through which similar devices made with polyethylene naphthalate (PEN) were used. This is intended as a provision for a cheaper and equal alternative to the PEN device that has increased flexibility, as the PEN devices have occasional problems with cracking due to fatigue or overflexing.

BACKGROUND

Within the past few centuries, technology has stood in stark contrast to the age-old idiom “the bigger the better”. In fact, in many fields, researchers and engineers are reaching the limits of theoretical size restraints. This has begun a steady and forceful push towards the promise found in the field of nanotechnology, where methods are being applied that allow for the tiniest examples of technology yet.

Within the larger field of nanotechnology, nanomaterials are becoming increasingly important towards production in several key areas, including reliable, miniature electronics. By combining nanoconductors, polymers, and nanoinsulators, the resulting devices can perform in astounding ways. As these become streamlined, consistent products, current integration of technology will reach astounding new heights.

Prior to this research, the members of the Flexible Electronics for Sustainable Technologies (FEST) research group won third place for a poster on “Flexible Contact-Based Devices for Haptics” at a poster event for Flex Conference 2013. The research behind this poster was based on a haptic device made from chromium-sputtered PEN, ZnO nanorods, and PMMA. The final design, which consisted of multiple layers, is shown in Figure 1 below in an indentation test environment.

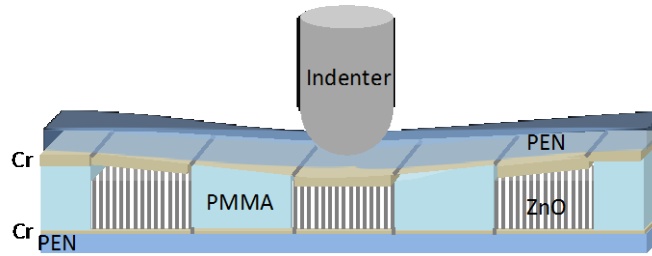


Figure 1: Flexible, Piezoelectric Device

While this introduced the concept of flexible, piezoelectric devices to FEST, there was a desire to make an improved, flexible device that could provide more favorable properties. For instance, while PEN is flexible, it may still crack under certain conditions such as over-bending or over-stressing the sample.

The aim of this project was to be able to construct and apply flexible, durable, multilayered devices to surfaces of any shape in order to make the surface a usable source of energy, or alternatively, a sophisticated haptic interface. The proposed device was designed to be:

- Flexible and mechanically durable
- Lightweight
- Replaceable
- Lower cost (compared to PEN device)
- Easily manufactured

In order to meet these criteria, PDMS will be used. This material was chosen because of its increased flexibility attributed to its low elastic modulus. PMMA will continue to be used as an insulator and buffer between the ZnO rods, while gold will be used over chromium for its improved conductive properties. This should allow for an improved electrical response. The proposed design is shown below in Figure 2.

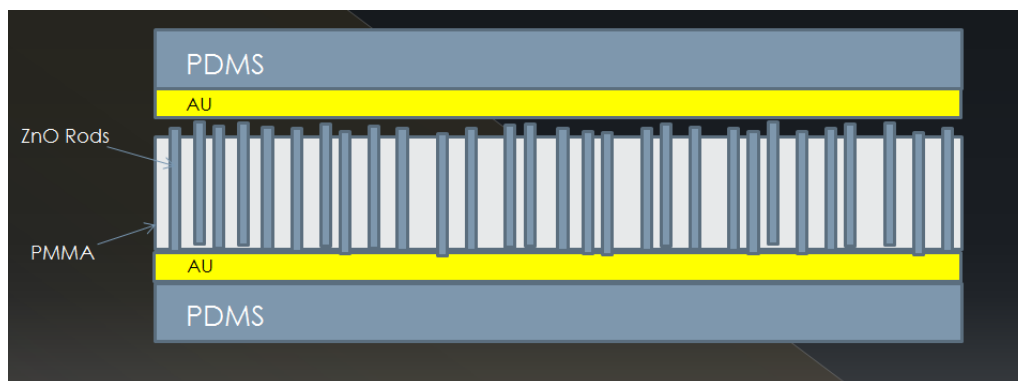


Figure 2: PDMS Device Construction

DESIGN OF EXPERIMENTS

Device Design and Construction Methodology

PDMS samples were fabricated by first mixing a pre-polymer and a cross-linker with various weight ratios of 5:1, 10:1, 15:1, and 20:1, respectively. The mixture was then deposited onto glass substrates by spin coating at 100 to 500 RPMs for 120 seconds depending on the sample. The samples were then cured at various temperatures (25°C, 75°C, 100°C, 150°C) and times (10 minutes to 48 hours) to evaluate differences in the films. From the testing a range of samples will be chosen for fabricating the piezoelectric device. After the PDMS samples are fabricated a Gold (Au) electrode will be deposited on to the top surface of the PDMS. Then zinc oxide (ZnO) nanostructures will be grown on top of the Au surface by aqueous solution. PMMA was then deposited between the rods in order to provide cushioning and increase durability. Finally, another gold-coated PDMS layer will be positioned on top of the previous stack to form the device.

Test Selection and Methodology

In order to ensure that the PDMS device would meet the desired criteria, each design specification would have to be considered and verified.

In order to test the devices' flexibility and mechanical durability, experiments using an in-house nanoindenter and a tensile tester were conducted. Conventional nanoindentation techniques using both a Berkovich diamond tip and a 10 µm diameter spherical tip were used to investigate the stiffness of the PDMS samples. Tensile testing was conducted with an in-house tester to measure fatigue. For this test, voltage measurements were taken *in situ* for each fabricated device. Microscopy analysis was also conducted using an optical microscope and scanning electron microscope (SEM).

Lightweight considerations would be compared the weight relative to other devices that perform similar tasks. In this design of experiments, it was not considered a high-level concern because solid haptic devices generally have a much higher weight than their flexible counterparts. Finally, lower cost can be accounted for through a simple comparison of component pricing.

RESULTS AND DISCUSSION

Table 1: Mechanical Properties from Nanoindenter

Concentration	5:1	10:1	15:1	20:1
Hardness (MPa)	0.614	0.567	0.546	0.511
Std. Dev.	0.008	0.002	0.003	0.004
Elastic Modulus (MPa)	2.693	2.497	2.363	2.127
Std. Dev.	0.01	0.005	0.009	0.012

***All samples spin-coated at 500 rpm and cured at 150° for 20 minutes.**

As shown above in Table 1, there are several important observations to make about the PDMS as concentration is varied while curing temperature, curing time, and the rotations per minute of the spin-coating machine. First, as the concentration of the PDMS mixture decreases (that is, less pre-

polymer per unit of the cross-linker) so does the hardness of the resulting film. At 5:1 concentration, the value of hardness was 0.614 MPa, which is a higher value than 0.511 MPa that was found for the 20:1 mixture. The elastic modulus followed the same pattern, as the values decreased from 2.693 MPa (5:1) to 2.127 MPa (20:1). The values of standard deviation for each value were at low levels, as the highest standard deviation was .008 for the hardness values and 0.012 for the elastic modulus. Each of these compositions' curve on the nanoindenter can be shown below in Figure 3. These tests were conducted using a Berkovich tip.

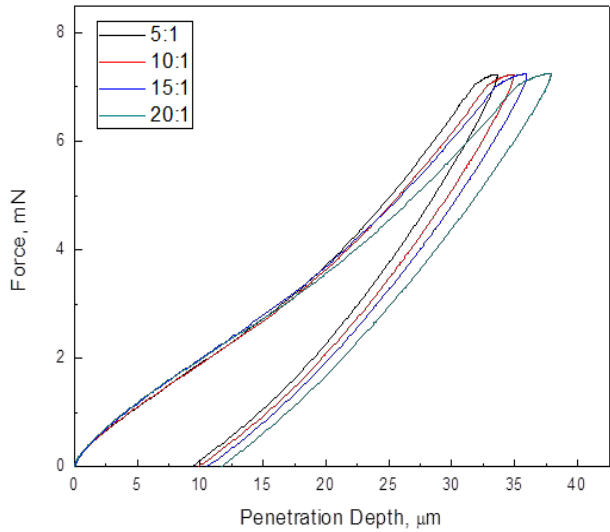


Figure 1: Force (mN) vs. Penetration Depth (µm)

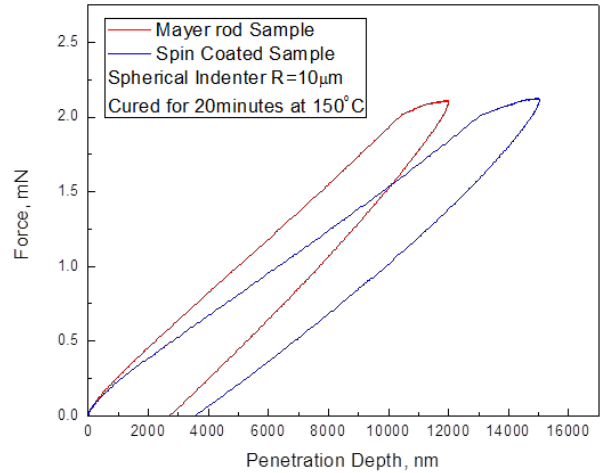


Figure 4: Penetration Depth (Mayer Rod vs. Spin Coating)

As shown in Figure 4 above, the nanoindenter was used to deform the sample using a tip of known area along with a predetermined, maximum force. In this case, a spherical indenter tip with a radius of 10 µm. Two different methods of creating PDMS film were used—Mayer rod and spin-coating. Compared to the Mayer rod sample, the spin-coated sample had a lower elastic modulus and hardness. This was desirable, as a lower elastic modulus and decreased hardness can lead to samples that will be more flexible, durable, and resistant to breaking under fatigue.

Experiments were also performed on ZnO nanorods in order to determine their effectiveness in generating voltage, following desired alignment, and resisting well against fatigue. The experimental setup (Figures 5 and 6) involved the use of a cyclic loading testing rig outfitted with electrodes in order to measure voltage output over the repeated loading of PDMS/gold film devices. These were “unfinished devices” in the sense that they did not have their top layers, but simply had the ZnO rods exposed.

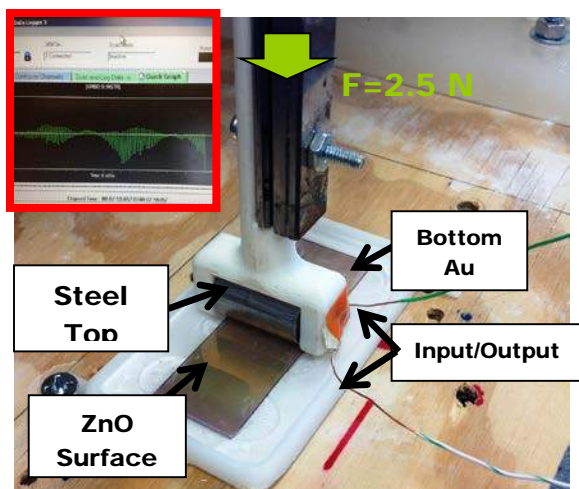


Figure 5: Fatigue Setup

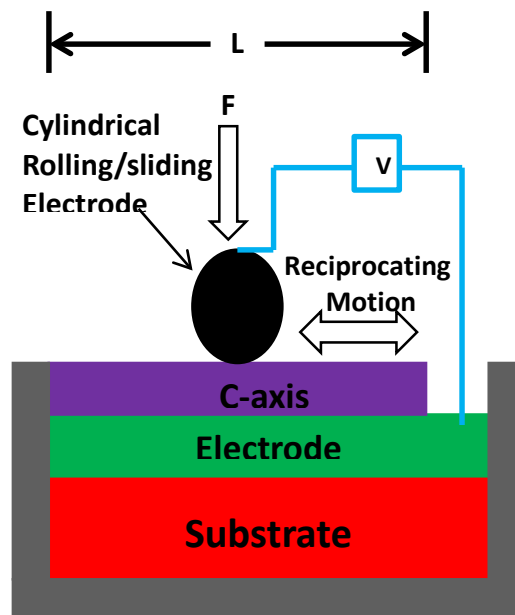


Figure 6: Experimental Setup

Data concerning the approximate maximum voltage output for 1 μm thick ZnO with an applied load of 2.5 N is shown below in Table 2.

Table 2: Approx. Maximum Voltage Output

Rolling Frequency (Hz)	Alternating Voltage (mV)	Direct Voltage (mV)
0.25	16.1	7.1
0.5	23.5	20
0.75		9.5

Although the fatigue test was designed to provide valuable voltage data, it also aided in determining the relative durability of the sample after numerous cycles. By weighing the sample frequently (after set cycle numbers), the weight loss of the sample could be determined based on the initial weight. Normal samples were found to lose approximately 1.7 mg of weight after 25,000 cycles, while samples exposed to UV for 60 minutes (in order to represent wear due to sunlight) lost a higher amount at approximately 3.1 mg. This provided a numerical representation of the visible damage to the samples as well. As the numbers of cycles increased, the sample wore down. Pictures of the sample at 200 cycles, 5000 cycles, and 25000 cycles is shown in Figure 7 below.

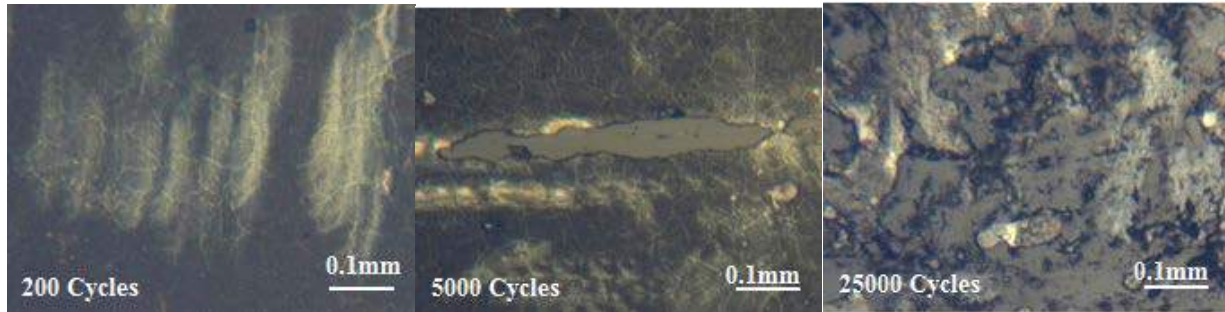


Figure 7: Fatigue Test Wear Results

When growing ZnO nanorods, constant attention was given to the alignment. The most desirable direction for the rods to grow was perpendicular to the substrate; however, they frequently aligned themselves at varying angles. This concern was never fully addressed; however, it would be necessary in the quality control of these devices if they were manufactured on a large-scale. During these experiments, rod direction was largely ignored and determined to be of little consequence when directly comparing multiple samples under the same manufacturing process.

CONCLUSION

Overall, PDMS-based devices appear to meet all of the specified design requirements, including:

- Flexible and mechanically durable
- Lightweight
- Replaceable
- Lower cost (compared to PEN device)
- Easily manufactured

This conclusion is based on the experimental evidence obtained from the aforementioned experiments. First, the devices are flexible (due to their polymer design infused with conductive, piezoelectric nanostructures) and mechanically durable, as they have shown to withstand cyclic loading well. Additionally, due to their low cost, replaceable, and easily manufacturable design, these devices could be efficiently replaced when previous devices reach their maximum useful life. These samples are also lightweight compared to mainstream, inflexible haptic interfaces. The material cost of PDMS is lower than that of PEN while performing at a similar level. This indicates that the PDMS device model is, under the stated parameters of this design of experiments, a more logical choice.

In the future, it would be beneficial to continue to improve the PDMS-based device by attempting to integrate the technology in a real-world situation to see how it performs compared to alternative technology on the market.

ACKNOWLEDGEMENTS

I would like to acknowledge several people for their helpfulness over the time of my research. First, Dr. Sierros has been encouraging as he has pushed me to become a better researcher and person. He has always made time to meet with me and help me accomplish my goals. Next, Nick and Sean have been important role models, as I have been clearly shown how one is supposed to do solid, beneficial research efficiently. Their example served to motivate me during times when

I would have rather not been in the lab. I would also like to thank the WVU NANO program for spurring my interest in nanotechnology and pursuing research. Although I have decided to leave research in favor of the pursuit of a Master's in Business Administration and industry, I will continue to remember the research skills I have learned here, as they truly help me to continue learning and applying my engineering knowledge to everyday problems. Finally, I would like to thank the NASA WV Undergraduate Space Grant Consortium for their generous financial support through the duration of this project.

REFERENCES

N. Morris, S. Cronin, G. Cordonier, D. Carden, K. Sierros. "Flexible Contact-Based Devices for Haptics," Flex Conference 2013. (Awarded third best poster).

COMPUTATIONAL ANALYSIS OF CK2 TARGETS IN *DROSOPHILA* GENETIC STUDIES

Adam Carte
Biochemistry (B.S.)
West Virginia University
Morgantown, WV 26505

ABSTRACT

CK2 is a highly conserved and ubiquitous Ser/Thr protein kinase. This enzyme is essential for cell cycle progression, cell viability, and animal development; its overexpression appears to favor oncogenic transformation. Among the ~500+ protein kinases that are encoded in eukaryotes, CK2 appears to be unique in that it is 'acidophilic', i.e., it preferentially targets Ser/Thr that are flanked by acidic amino acids (Asp/Glu). As acidic microdomains are generally solvent accessible and difficult to bury within the hydrophobic cores of proteins, the presence of CK2 sites has been widely found to be a strong predictor for phosphorylation both in vitro and in vivo. The availability of sequenced genomes favors computational screens followed by biochemical studies. *Drosophila* is an ideal model organism; the genome has been sequenced from 12 species, its genes exhibit significant similarity to human genes, mutations in many (if not most) genes have been isolated, and cloned genes/mutants are available through the *Drosophila* Genome Resource Center. I describe a computational strategy to search for putative CK2 targets in the genome of *D. melanogaster* and to determine if these are conserved in 12 *Drosophila* species. Following these 'in silico' approaches, I selected and tested the effectiveness of several maternal Gal4 drivers that will be useful in generating mutant flies via the Maternal-Gal4-shRNA system. This method of RNA interference will provide an easy way to conduct genetic confirmation of CK2-putative partner interaction. In short, I have identified and analyzed many putative CK2 targets using computational techniques and have selected and evaluated a tool for confirming those interactions. It is expected that these bioinformatics and genetic methods should provide a roadmap for long-term studies in my host laboratory to understand the roles of CK2 in development.

INTRODUCTION

In recent years, advances in genomics and sequencing technologies have allowed the genomes of many different species to be fully sequenced. Along with the genome sequences, the encoded proteomes (the complement of proteins expressed by a genome) of many organisms have also begun to be compiled into databases. Importantly, freely available web-based tools allow the genomes/proteomes to be searched for homologous proteins, and users can subsequently determine if these proteins harbor amino acid sequence motifs in a conserved manner. This approach is being widely used to identify common structure, function, cellular locale, and post-translational modifications such as phosphorylation, glycosylation, acetylation, etc.

The work in my host lab is focused on protein kinase CK2, a highly conserved serine/threonine kinase necessary for cell viability and throughout development. Among the ≥ 500 protein kinases encoded in eukaryotic genomes, CK2 appears to be unique in that it preferentially phosphorylates Ser/Thr residues in acidic microdomains, making computational prediction of its target proteins

easier and more effective than for protein kinases that favor basophilic or hydrophobic regions (Robinson et al., 1994). Discovering new partners of CK2 is especially important, because CK2 is associated with the development and progression of many types of cancers, in addition to having numerous roles in animal development (Issinger, 1993). The identification of novel targets of CK2 could provide key insights into the roles of this enzyme in signaling pathways, whose abnormalities invariably lead to developmental disorders and cancer. Such information could potentially be used in the formulation of drugs and therapies to counter the effects and onset of cancer and birth defects.

The purpose of this research was first to computationally identify partners of CK2 in *Drosophila* and to identify if these are also conserved in humans and linked to disease states. After identifying candidate genes, we hoped to analyze them through either biochemical or genetic assays to confirm the putative partner's interaction with CK2 and possibly illustrate the function of the substrate. I identified that Maternal-Gal4-shRNA could be an effective means to conduct genetic assays and proved the effectiveness of several maternal Gal4 drivers.

BACKGROUND

CK2 is a highly conserved Ser/Thr protein kinase, showing potential for oncogene activity (Trott et al., 2001). In cells/tissues, CK2 is present in the holoenzyme form, which is composed of two α (catalytic) and two β (regulatory) subunits. Although CK2 activity is messenger-independent and appears to be constitutively active, it does not phosphorylate its targets in a constitutive manner. A notable example is CDC37, whose phosphorylation by CK2 occurs only at the G1/S and G2/M transitions—a control mechanism that still remains unresolved. In recent years, it has been shown that CK2 is vital to cell survival and for cell cycle progression. Furthermore, CK2 is also involved in processes such as gene expression, growth and differentiation, embryogenesis, circadian rhythms, and apoptosis (Ruzzene and Pinna, 2010). CK2 activity has been shown to be heightened in both normal cells showing accelerated dividing and in solid-state tumors (Issinger, 1993).

CK2 is a unique protein kinase. It shows a stark preference for hyper-acidic domains in substrates; the only other kinase also showing some acidophilic tendencies is CK1 (Robinson et al., 1994). Moreover, CK2 can utilize both ATP and GTP as a phosphoryl group donor (Pinna, 1994). The CK2 consensus binding site is best described as (S/T)-D/E-X-D/E (Kuenzel et al., 1987). In fact, many proteins involved in transcription, cell-cycle progression, and signal transduction contain one or more of the aforementioned sites, where they are known to be phosphorylated by CK2 both *in vitro* and *in vivo* (Glover, 1998). As previously stated, CK2 is attracted to hyper-acidic domains—along with glutamic acid and aspartic acid, both phosphothreonine and phosphoserine can be acidic determinants. Being acidophilic, CK2 activity is inhibited by the presence of basic residues (lysine, arginine, and histidine) (Bidwai, 2000).

The unique properties of CK2 make it an especially well-fit candidate for computer-based prediction of substrates (Bidwai, 2000). Because few other kinases are attracted to acidic domains, CK2's consensus sequence is largely unique. Furthermore, hyper-acidic domains are nearly always solvent exposed, so regions containing the CK2 consensus sequence are most often available for phosphorylation by CK2 (Bidwai, 2000). In predicting substrates, *Drosophila* serves as the perfect model organism for use. With its genome being completely sequenced and its known proteome being extensive, a vast number of putative CK2 substrates can be found. With the use of

Drosophila, genetic assays can quickly and easily be conducted to determine if CK2 interacts with putative partners *in vivo*. Importantly, CK2 subunits are highly similar between mammals and *Drosophila*, so discoveries made in fly labs could have immediate ramifications on the development of human medicine (Dahmus et al., 1984). However, because CK2 is deposited maternally and functional into the embryo, it is often difficult to study in early development (Dominguez et al., 2004).

Moreover, CK2 is an essential gene, so its dual maternal and zygotic expression makes it challenging to examine a null embryonic phenotype. The maternal effect caused by deposition by heterozygotic mothers is often enough to counteract null expression in the early embryo, while lethality is caused by a homozygous mutant (Dominguez et al., 2004)(Staller et al., 2013). One way around this conundrum is to produce female flies with heterozygotic somatic tissues and homozygotic mutant germ cells. Traditionally, this could be accomplished through use of the challenging and sometimes convoluted FLP-FRT ovoD germline clone technique (Chou and Perrimon, 1996). A newly developed alternative approach that takes advantage of RNAi in generating these germline clones is called the Maternal-Gal4-shRNA system. By expressing specific short hairpin RNAs (shRNAs) during oogenesis via an upstream activating sequence (UAS) and a maternal germline-specific gal4 driver, null phenotypes can be reproduced in the early embryo (Ni et al., 2011). Using this RNAi strategy to generate null germline clones allows genetic screening to be conducted much more quickly, as it involves considerably fewer and simpler crosses than the FLP-FRT ovoD method (Staller et al., 2013).

Furthermore, different maternal Gal4 drivers can be utilized to elicit slightly different effects in the embryo (Staller et al., 2013). Flies with the gal4 maternal triple driver (MTD-Gal4) are homozygous for the following transgenes that drive expression throughout oogenesis: P(out-Gal4::VP16.R), which contains the ovarian tumor (out) promoter and fs(1)K10 3'-untranslated region (UTR) and leads to expression in stage 1 development, P(Gal4-nos-NGT), which contains the nanos (nos) promoter and 3'-UTR and leads to expression in the germarium, and P(Gal4::VP16-nos.UTR), which contains the nos promoter and α Tubulin84E 3'-UTR and leads to expression throughout oogenesis. Contrastingly, the maternal-tubulin-Gal4 (mat-tub-Gal4) driver line is homozygous for two constructs containing the maternal tubulin promoter from α Tub67C and the 3'-UTR from α Tub84B. Due to the difference in amount and variety of gal4 drivers, MTD-Gal4 lines lead to expression in early oogenesis in the germarium while mat-tub-Gal4 lines have a delayed effect (Staller et al., 2013).

In studying CK2, the difference between these two gal4 drivers could be highly useful. Because of its role in embryonic development, a CK2 null mutant could lead to lack of egg formation. This problem could potentially be experienced when using the MTD-Gal4 driver to generate a CK2 mutant but could be alleviated, however, by utilizing the delayed effect of the mat-tub-Gal4 driver. This delay could give time for egg formation to arise, providing a sample that could be investigated for early developmental effects. Further, this system can be used for conduction of genetic assays to confirm the aforementioned CK2-putative partner interactions. By coupling shRNAs for both CK2 and putative substrates with the Maternal-Gal4-shRNA system, mutants could quickly be generated such that experimental follow up to the computational studies could be carried out. By both allowing for the generation of mutants quickly and permitting early embryonic studies, the Maternal-Gal4-shRNA represents an excellent way to confirm discoveries of newly identified CK2 substrates in this study. With extensive implications in cancer cell pathways, any of these new

discoveries in CK2 substrates each have the possibility of providing new mechanisms by which oncogenic activity can be impaired (Issinger, 1993).

MATERIALS AND METHODS

Computational Analyses

First, the web-based tool, Scan-Prosit, was used to analyze the *Drosophila melanogaster* genome/proteome for members containing the amino acid sequence [ST]-[DE]-{KRH}-[DE], where [-] implies amino acids that are permitted and {-} implies amino acids that are dis-favored. After this search was completed, orthologs of specific identified putative substrates were found using the program OrthoDB, an orthology group search engine, encompassing 12 sequenced *Drosophila* species using the databases housed at flybase.org. Subsequently, the amino acid sequence of each homolog/ortholog was gathered using information stored in flybase.org's databases. Using the amino acid sequences, a multiple sequence alignment (MSA) was then performed to determine if the consensus sequence was conserved in the 12 *Drosophila* species. From the information gathered from ScanProsit and generated via the MSA, a Microsoft Excel spreadsheet was generated, which lists all of the analyzed putative targets and their accession numbers, their isoform analyzed (if any), their number and strength of specific CK2 sites, their conservation in 12 *Drosophila* species, and their locale.

Genetic Studies

Three different maternal Gal4 driver lines were utilized in this study: mat-tub-Gal4, MTD-Gal4, and 6CAD1AA mat-tub-Gal4-VP16(chromosomes II+III). They were crossed with either the UAS-shRNA-bcd-Valium22 line (positive control) or the W11B line (wild-type negative control). To determine F1 phenotypes, about 5 maternal-Gal4 virgin females were crossed with about 5 UAS-shRNA-bcd-Valium22 or W11B males and embryos were collected at 24°C. The analysis of F2 phenotypes was conducted by caging the F1 maternal-Gal4>>UAS-shRNA/W11B females and allowing them to mate with their siblings. F2 embryos were then collected on an apple juice agar plate at the bottom of the cage. The percentage of hatched embryos was determined by analyzing each embryo visible on the plate and counting dead and hatched eggs between 24 and 48 hours after they had been laid. When high lethality was observed, embryo cuticles were prepared to search for patterning or developmental defects. Unhatched eggs were collected at age 20-24 hours subsequently bleached. After dechlorination, the vitelline membranes were removed by placing the embryos in a scintillation vial with 50% heptane and 50% methanol and shaking vigorously for 1 minute. Embryos were then stored in 99.9% spectrophotometric grade methanol before being mounted in lactic acid. For images in Figure 2, images were acquired using a 40X light microscope and attached camera.

RESULTS

Computational Analyses

In total, 240 putative substrates were analyzed. Depending on the gene being analyzed, conservation of the CK2 sites ranged from being found only in *Drosophila melanogaster* to being present in all 12 species. Those putative substrates with the most well conserved CK2 sites are shown in Table 1. The number of CK2 sites present in each putative substrate also varied significantly from sample to sample, being as high as 20 sites and as low as 1. Furthermore, the strength of each site varied case by case. The majority of sites, however, exhibited a strength of 1.

The location of CK2 sites also had a wide distribution depending on the sample being analyzed and were observed near the N- and C-terminals and everywhere in between.

Table 1. Genome-wide analysis for CKII substrates in Drosophila. Potential CK2 phosphorylation sites are shown in bold print and are followed by their residue position number within the protein.

Protein	CKII Site(s)	Function
Upstream of RpIII128	S 198ELDTD	GTP1/OBG family
Parcas	T 292EDE EDACDYDEGAG	SH3BP5 family.
5-hydroxytryptamine (serotonin) receptor 1B	T 294ETDCDS; SS 408DADDYRTS	GPCR-1 family for serotonin
A6	S 79DDD; T 133 SD DE; S 316DEDD	Embryonic development via the syncytial blastoderm
Mitochondrial acyl carrier protein 1	DS 129DAE	Carrier of the growing fatty acid chain in fatty acid biosynthesis
Actin-related protein 1	S 286DMD	Axon cargo transport; cytoskeleton organization; mitosis
Ajuba LIM protein	S 16D SD YET	Regulation of organ size via inhibiting apoptosis and promoting cell proliferation
Aristaless	S 72DCEADE	Morphogenesis of proximal and distal pattern elements; early imaginal disk development
Antennapedia	T 35DLD	Segmental identity in the mesothorax; a-p axis cell identities
Adaptor Protein complex 2, α subunit	S 320DSE	Subunit of the plasma membrane adapter complex; interacts with clathrin
Alkaline phosphatase 4	T 403DPDET	Neural and renal epithelial function
Araucan	T 327DDDDDALV SD DEKDKED	Controls proneural and vein forming genes
Ariadne	S 3DNDNDFCDNVDS	Might act as an E3 ubiquitin-protein ligase, or as part of E3 complex
Tango	T 84DQE	Control of breathless expression; role in the cellular or tissue response to oxygen deprivation
Arrestin 1	DS 152DCDRSHRRST	Regulation of photoreceptor cell deactivation via rhodopsin inactivation
IplI-aurora-like kinase	S 134EGE	Serine/threonine-protein kinase
BarH1	SVDS CSQ S 536DDED	Fate determination of external sensory organs, formation of notal microchaetae, formation of presutural macrochaetae, antennal development and for distal leg morphogenesis
Bottleneck	SSSS CS 35ELEM D IED	Regulator of the microfilament network governing cellularization of the embryo
Boule	TT45EADLTRVFSAYGTVKSTK IIVDRAGVSKGYGFVTFETE QE	RNA-binding protein that plays a central role in spermatogenesis
Brahma	S 1295EEEEIE; EES 1407 DDD ; S 1557DN SD NDDDD; DD GS 1569 DDE ; S 1630DDDDDD M D	Transcriptional activator of ANTC and BXC homeotic gene clusters.

Protein	CKII Site(s)	Function
Bx42	T54DAD	May play a role in chromatin structure and function
By S6	T428DADVEYEG	Required for processing of 20S pre-rRNA precursor and biogenesis of 40S ribosomal subunits
Calbindin 53E	T58ELD	Calcium binding – member of the calbindin family and expressed in a large number of neuron of the brain and the thoracic ganglion as well as in two small muscles of the thorax.
Cactus	S463DYDSSDIEDLDDT	Formation of the dorsoventral pattern; negative regulator of the NF-kappa-B (rel) signaling pathway
Chromatin assembly factor 1 subunit	S423ELETNTA	Core histone-binding subunit that may target chromatin assembly factors, chromatin remodeling factors and histone deacetylases to their histone substrates in a manner that is regulated by nucleosomal DNA
Androcam	T44EAE; ET79DTEEE; T117DEEIDE	May be involved in calcium-mediated signal transduction
Calmodulin	T45EAE; DT80DSEEE; T118DEEVDE	Mediates the control of a large number of enzymes, ion channels and other proteins by Ca ²⁺
Calpain A	T287EAET	Calcium-regulated non-lysosomal thiol-protease; involved in the organization of the actin-related cytoskeleton during embryogenesis
Calpain B	S769DEEVD	Calcium-regulated non-lysosomal thiol-protease
Silver	T603EPE	Required for the proper melanization and sclerotization of the cuticle
CHORD	EES324DEEFFDLDD	Regulates centrosome duplication

Genetic Studies

In the five crosses that were conducted, no abnormal F1 phenotypes were observed (Table 1). When crossed with the W11B line, the mat-tub-Gal4 driver yielded high F2 viabilities and no abnormalities in cuticles were observed (Table 2 and Fig. 1B). However, the mat-tub-Gal4 driver produced total F2 embryonic lethality when crossed with the UAS-shRNA-bcd-Valium22 line (Table 2). Further, mat-tub-Gal4>> UAS-shRNA-bcd-Valium22 F2 embryos showed a distinct mutant cuticle phenotype (Fig. 1C). The majority of these mutant offspring contained only 6 denticle bands, compared to the wild-type's 11 (Fig. 1C and 2). Similar to the mat-tub-Gal4 driver, the MTD-Gal4 driver produced high F2 viability when crossed with the W11B line and absolute lethality when crossed with the UAS-shRNA-bcd-Valium22 line (Table 2). In this instance, however, most of the eggs appeared to be unfertilized. When the cuticles were analyzed, the MTD-Gal4>>W11B cross unsurprisingly yielded wild-type cuticles; however, the MTD-Gal4>>UAS-shRNA-bcd-Valium22 F2 cuticles showed two distinct phenotypes: one that appeared to be wild-type and one that suggested the eggs had not been fertilized (Fig. 1D, 1E, and 1F). Finally, the 6CAD1AA mat-tub-Gal4-VP16(II+III)>>W11B cross yielded some unexpected F2 viability and phenotypic results. As shown in Table 1, abnormally low viabilities were observed

in both viability plate analyses. Furthermore, inspection of cuticles displayed a variable number of missing denticle bands, counterintuitive to the expected wild-type phenotype (Fig. 1G and Fig.2).

Table 2. Phenotypic analysis of Gal4 drivers and shRNA lines.

Gal4 Line	shRNA Line	F ₁ Phenotype	F ₂ Phenotype	F ₂ Viability Plate 1	F ₂ Viability Plate 2
mat-tub-Gal4	n/a (W11B)	n/a	n/a	78.6%	83.6%
mat-tub-Gal4	UAS-shRNA-bcd-Valium22	n/a	80% missing 5 denticle bands	0%	0%
MTD-Gal4	n/a (W11B)	n/a	n/a	76.5%	89.7%
MTD-Gal4	UAS-shRNA-bcd-Valium22	n/a	~100% possibly unfertilized eggs	0%	0%
6CAD1AA mat-tub-Gal4-VP16(II+III)	n/a (W11B)	n/a	Variable number of missing denticle bands	55%	20.1%

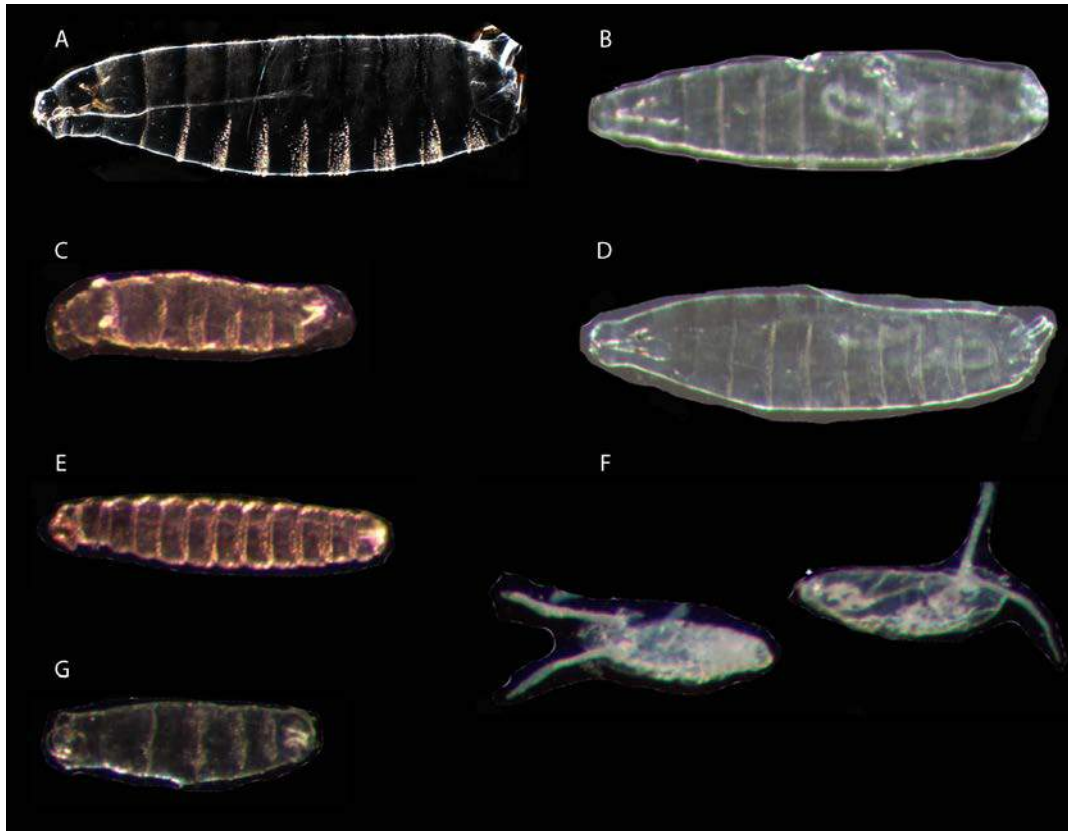


Figure 1. Cuticle phenotypes associated with the F₂ generation of each cross. (A) Wild-type (B) mat-tub-Gal4>>W11B (C) mat-tub-Gal4>>UAS-shRNA-bcd-Valium22 (D) MTD-Gal4>>W11B (E) MTD-Gal4>>UAS-shRNA-bcd-Valium22 [WT-like] (F) MTD-Gal4>>UAS-shRNA-bcd-Valium22 [mutant] (G) 6CAD1AA mat-tub-Gal4-VP16(II+III)

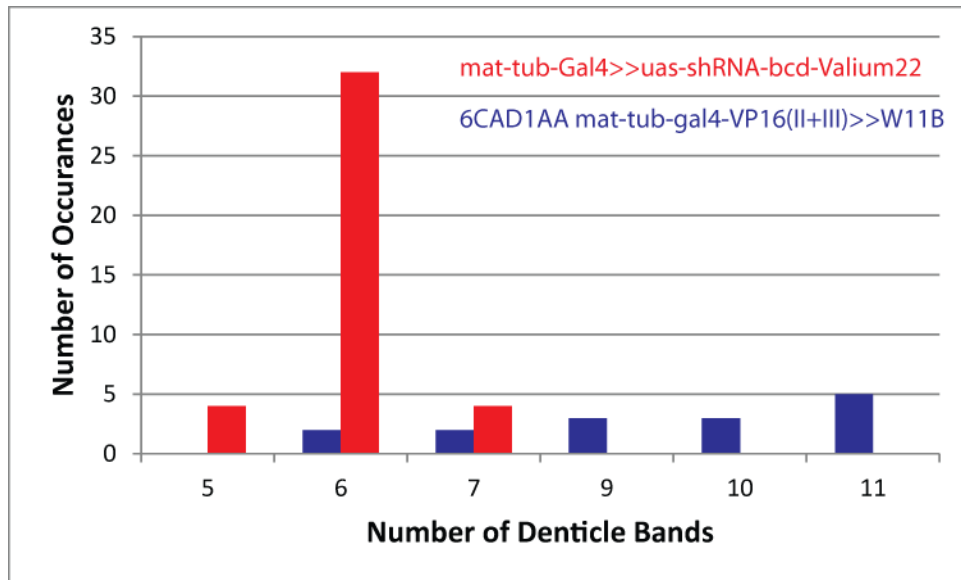


Figure 2. Dentine band distribution in mat-tub-Gal4>>UAS-shRNA-bcd-Valium22 and 6CAD1AA-mat-tub-Gal4-VP16(II+III)>>W11B F₂ cuticles.

By conducting the computational analysis, many strong CK2 target candidates were identified. However, only a portion of the over 1000 putative CK2 substrates were analyzed. Because the amount of time necessary to perform such a high volume computational tasks is extensive, it would be wise to seek the assistance of individuals proficient in coding such that scripts could be written to automate the data mining, sequence alignment, and spreadsheet input processes. Development of such software would allow for the quick identification and analysis of CK2 putative substrates, as well as the substrates of other kinases and phosphatases with known consensus sequences. For the especially strong putative substrates identified in this computational screen, experimental confirmation of CK2 interaction will be necessary. Although many approaches are available, it has been demonstrated that the Maternal-Gal4-shRNA system represents a new, quick, and possibly effective method by which the mutants necessary to test for genetic interactions can be generated.

In evaluating the possible efficacy of the Maternal-Gal4-shRNA system, the mat-tub-Gal4>>W11B and MTD-Gal4>>W11B crosses unsurprisingly led to fairly wild-type viabilities and cuticle morphologies in the F₂ generation. This is because, although Gal4 protein is expressed in the germline, there is no RNAi hairpin being expressed. What was surprising, however, were the low viability rates and presence of mutant embryos in the 6CAD1AA mat-tub-Gal4-VP16(II+III)>>W11B F₂ specimens. This is a rather perplexing occurrence, as no RNAi hairpin should be present to be expressed. Thus, either some other mechanism must be causing the abnormalities or the line of flies had been contaminated. Either way, a follow-up experiment should be done to confirm the results before the 6CAD1AA mat-tub-Gal4-VP16(II+III) driver can be deemed unfit for use.

Further, an interesting difference was observed between the mat-tub-Gal4>>UAS-shRNA-bcd-Valium22 and MTD-Gal4>>UAS-shRNA-bcd-Valium22 F₂ generations. Although both mutants led to 100% lethality in the viability assay, only the Gal4>>UAS-shRNA-bcd-Valium22 produced F₂ embryos very similar to the canonical bicoid mutant which typically contains 6 denticle bands (Staller et al., 2013). The MTD-Gal4>>UAS-shRNA-bcd-Valium22 F₂ eggs, however, appeared

to either fail to become fertilized or hatch into wild-type embryos. The small occurrence of wild-type cuticles may be explained by the sometimes variable efficacy of RNAi, while the failure of egg fertilization could be attributed to the fact that MTD-Gal4 drives expression in very early oogenesis. As previously mentioned, mat-tub-Gal4 has a delay before driving expression, which could account for its higher efficiency in generating bicoid mutants.

Based on my positive and negative control experiments, I would suggest first using the mat-tub-Gal4 and MTD-Gal4 drivers to study genetic interactions between CK2 and the identified putative targets. Furthermore, this Maternal-Gal4-shRNA system can be used to study CK2's role in early embryonic development, something that had previously been quite the challenging task due to the effect of maternal loading of CK2. The next step of this project is to order RNAi hairpin lines for CK2 and some of the promising substrates identified in this study. After using this system to study genetic interactions, biochemical techniques like GST-pulldowns, yeast-2-hybrid assays, and in vitro phosphorylation assays could be used to further confirm our findings. In conclusion, I have developed a system for finding and evaluating putative CK2 substrates and have identified and assessed a quick, easy method for both studying CK2 in early development and confirming its interaction with putative partners.

ACKNOWLEDGEMENTS

All of the utilized flies in this study, except the W11B line, were generously provided by the Angela DePace of the Systems Biology Department at Harvard Medical School. Figure 1A is a photograph provided by Max Staller, a graduate student in the DePace lab. All fly work was done in the lab of Dr. Ashok Bidwai at West Virginia University. This work was supported in part by the NASA West Virginia Space Grant Consortium.

REFLECTION

In participating in this research project, I learned a great deal about what to expect in graduate school this fall. The project required me to complete independent work and think of creative solutions for problems that arose. The financial support was essential in allowing me to work independently to a high degree, and I believe that the prestige of winning a NASA WV Space Grant assisted me in gaining admission into many graduate schools. This fall, I will be moving on to Harvard University's Systems Biology Ph.D. Program, and the training and experience that I ascertained by completing this project will undoubtedly help me succeed there.

REFERENCES

- Bidwai, A. P. (2000) 'Structure and function of casein kinase II', *Recent Res Devel Mol Cell Biol* 1: 51-82.
- Chou, T.B. and Perrimon, N. (1996) 'The autosomal FLP-DFS technique for generating germline mosaics in *Drosophila melanogaster*.' *Genetics* 144(4): 1673-1679.
- Dahmus, G. K., Glover, C. V. C., Brutlag, D. and Dahmus, M. E. (1984) 'Similarities in structure and function of calf thymus and *Drosophila* casein kinase II.', *J Biol Chem* 259: 9001-9006.
- Dominguez, I., Mizuno, J., Wu, H., Song, D.H., Symes, K., and Selden, D.C. (2004) 'Protein kinase CK2 is required for dorsal axis formation in *Xenopus* embryos.' *Dev Biol* 274(1): 110-124.

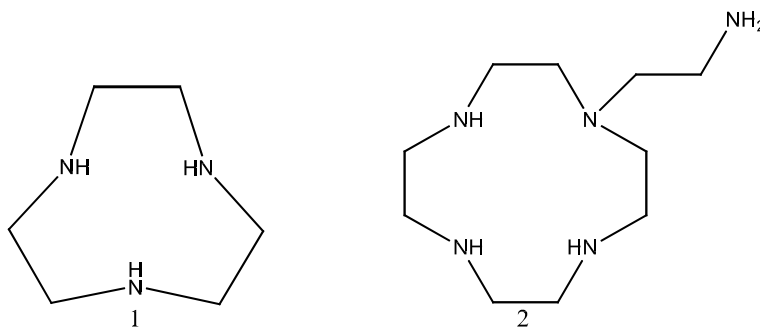
- Glover, C. V. C. (1998) 'On the physiological role of casein kinase II in *Saccharomyces cerevisiae*.', *Prog Nuc Acid Res & Mol Biol* 59: 95-133.
- Issinger, O. G. (1993) 'Casein kinases: Pleiotropic mediators of cellular regulation.', *Pharmacol Ther* 59: 1-30.
- Kuenzel, E. A., Mulligan, J. A., Sommercorn, J. and Krebs, E. G. (1987) 'Substrate specificity determinants for casein kinase II as deduced from studies with synthetic peptides', *J Biol Chem* 262: 9136-9140.
- Ni, J.Q., Zhou, R., Czech, B., Liu, H.P., Holderbaum, L., Yang-Zhou, D., Shim, H.S., Tao, R., Handler, D., Karpowicz, P. et al (2011) 'A genome-scale shRNA resource for transgenic RNAi in *Drosophila*.' *Nat Methods* 8(5): 405-407.
- Pinna, L. A. (1994) 'A historical view of protein kinase CK2.', *Cell Mol Biol Res* 40(5/6): 383-390.
- Robinson, L. C., Hubbard, E. J. A., Graves, P. R., DePaoli-Roach, A., Roach, P. J., Kung, C., Haas, D. W., Hagedorn, C. H., Goebel, M., Culbertson, M. R. et al. (1994) 'Yeast casein kinase I homologues: An essential gene pair.', *Proc Natl Acad Sci U S A* 89: 28-32.
- Ruzzene, M. and Pinna, L. A. (2010) 'Addiction to protein kinase CK2: a common denominator of diverse cancer cells?', *Biochim Biophys Acta* 1804(3): 499-504.
- Trott, R. L., Kalive, M., Karandikar, U., Rummer, R., Bishop, C. P. and Bidwai, A. P. (2001) 'Identification and characterization of proteins that interact with *Drosophila melanogaster* protein kinase CK2', *Mol Cell Biochem* 227: 91-98.
- Staller, M.V., Yan, D., Randklev, S., Bragdon, M.D., Wunderlich, Z.B., Tao, R., Perkins, L.A., DePace, A.H., and Perrimon, N. (2013) 'Depleting gene activities in early *Drosophila* embryos with the "maternal-Gal4-shRNA" system.' *Genetics* 193(1): 51-61.

COMPLEXATION OF ALUMINUM BY NITROGEN-CONTAINING LIGANDS

Hannah Cavender
Advisor: Dr. Genia Sklute

ABSTRACT

Nitrogen-containing ligands are important ligands in the coordination chemistry of aluminum (Al) and other metals. We chose to investigate nitrogen-containing macrocyclic ligands due to the high kinetic and thermodynamic stability that they show relative to their non-cyclic counterparts. To better predict the affinity of aluminum towards the ligand, *Molecular Mechanics* Merck Molecular Force Field (MMFF)* calculations were used. 1,4,7-triazonane **1** and 2-(1,4,7,10-tetraazacyclododecan-1-yl)ethanamine **2** were identified as the best two candidates using MMFF calculations.

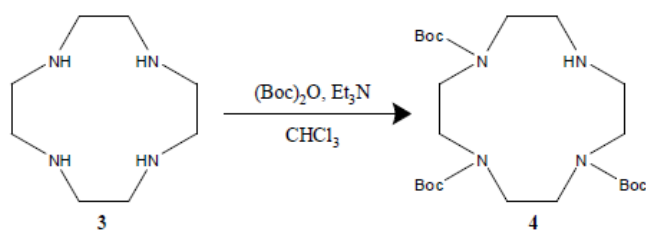


INTRODUCTION

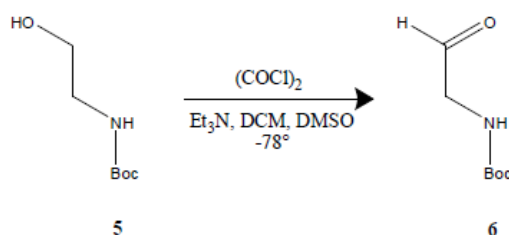
Aluminum toxicity is a major problem in large areas of the US east of the Mississippi River including WV. In acidic soil (pH < 5.0), the increased solubility of aluminum in water damages DNA and inhibits plant root growth.¹ The common practice to elevate the pH is nonselective, and lowers not only the levels of aluminum but also other important nutrients. One of the methods for the inactivation of toxic aluminum in soil is addition of organic compounds that has the ability to complex/chelate to aluminum.² The goal of the proposed research is to develop a rational design of organic compounds that can selectively chelate the aluminum and can also serve as a model for other cations as a potential solution. Nitrogen-containing ligands are important ligands in the coordination chemistry of aluminum (Al) and other main group metals.³ Macrocyclic-ligands with nitrogen donor atoms were investigated due to their higher kinetic and thermodynamic stability over their non-cyclic counterparts. This study utilized *Molecular Mechanics*

Merck Molecular Force Field (MMFF) calculations to examine ideal macrocyclic cavity size dimensions, shape and topology of Al³⁺ ion, substituent effects with addition of pendant arms, number and arrangement of nitrogen atoms, and the affect of conformational flexibility/rigidity on stability of nitrogen ligand-Al complex.

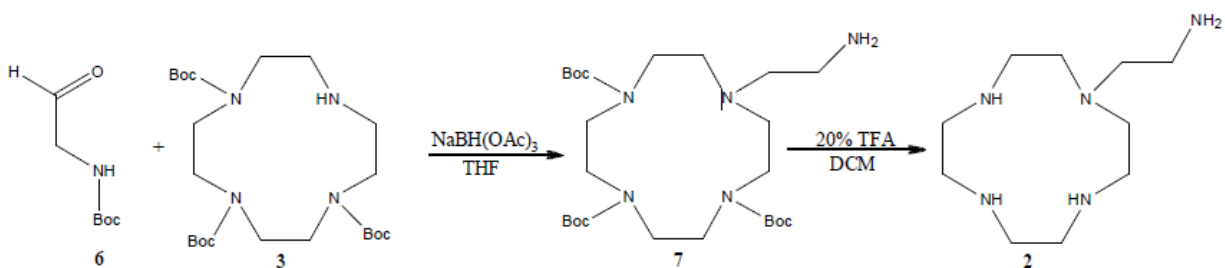
Comparisons of ideal macrocycle cavity dimensions were determined by observing the theoretical change in bond lengths and angles with the addition of the Al^{3+} ion. 1,4,7-triazonane **1** and 2-(1,4,7,10-tetraazacyclododecan-1-yl)ethanamine **2** were identified as the best two candidates using MMFF calculations. **1** is available commercially, and a synthetic route was designed for **2**. The synthesis involved four steps (Schemes 1-3): 1) protection of 1,4,7,10-tetraazacyclododecane (cyclen) **3** with three equivalents of boc- anhydride $(\text{Boc})_2\text{O}$ to give tri-boc cyclen **4**, 2) swern oxidation of *tert*-butyl (2- hydroxyethyl) carbamate **5** to yield *tert*-butyl (2-oxoethyl) carbamate **6**, 3) reductive amination of **6** and **3** will yield tri-*tert*-butyl 10-(2-((*tert* butoxy carbonyl amino) ethyl)- 1,4,7,10-tetraazacyclododecane-1,4,7-tricarboxylate **7**, and 4) removal of the protecting groups using 20% TFA will result with the desired ligand **2**.



Scheme 1: Protection of Cyclen



Scheme 2: Swern Oxidation of *tert*-butyl(2-hydroxyethyl)carbamate



Scheme 3: Reductive Amination and deprotection

RESULTS AND DISCUSSION

Both of the procedures for the synthesis of **4**^{4,6} report high percent yields (70 and 66% respectively); however, the desired product was not observed. Also, a more efficient route for the synthesis of **2** was developed. The new route is more step and atom- economic. Therefore suggesting a greener approach for the synthesis of the desired ligand. The techniques that were utilized and studied thus far include simple distillation,

TLC, various staining techniques including p-anisaldehyde and iodine, silica column chromatography, and H¹ NMR. The N-monoalkylation of cyclen will be attempted using the new protocol extrapolated from a convenient one-step synthesis involving a Michael acceptor.⁷

EXPERIMENTAL

Protection of Cyclen

A solution of di-tert-butyl dicarbonate ((Boc)₂O) (7.9 g, 36 mmol) in CHCl₃ (100 mL) was added slowly (4 hrs) via an addition funnel to a solution of **2** (2.2 g, 13 mmol) and triethylamine (5.5 mL, 39 mmol) in CHCl₃ (120 mL) at room temperature. The reaction mixture was stirred for 24 hours at room temperature and followed with TLC.⁴ The organic solvent was then removed from the product under reduced pressure. ¹H-NMR was utilized to verify the presence **4** according to peaks provided in the literature.⁵ This residue was then purified by silica gel column chromatography (PE/AcOEt 8:1). Based on ¹H-NMR no product was observed.

Alternative procedure: a solution of **3** (1.0 g, 5.8 mmol) and triethylamine (2.5 mL) in 40 mL of dry CHCl₃ was stirred for 30 minutes at room temperature, (Boc)₂O (3.8 g, 17.6 mmol) was then added drip wise via addition funnel. This solution was stirred for 72 hours and followed using TLC. H¹ NMR was used to check for the presence of the product **4** and then purified using silica gel column chromatography (ethyl acetate:petroleum ether 5:1). Based on ¹H-NMR no product was observed.

REFERENCES

*Spartan '10 Software, Wavefunction, Inc.

1. (a) Rounds, M.A., Larsen, P. B. *Current Biology*. **2008**, *18*, 1495. (b) Source: Ontario Ministry of Agriculture Food and Rural Affairs.
2. Kinraide, T.B.; Parker, D.R. *Plant Physiol*. **1987**, *83*, 546.
3. Henderson, W. *Main Group Chemistry* Wiley-VCH, Berlin **2002**
4. Kimura, E., Aoki, S., Koike, T., Shiro, M. *J. Am. Chem. Soc.* **1997**, *119*, 3076.
5. Liu, K., Meyerhoff, M.E. *J. Mater. Chem.* **2012**, *22*, 18787
6. Xia, C.Q., Zhu, L.B., Tan, X.Y., Yue, Y., Yu, X.Q. *ARKIVOC* **2005** (xv) 87
7. Fensterbank, H., Zhu, J., Riou, D., Larpent, C. *J. Chem. Soc., Perkin Trans. 1*, **1999**, 815.

BIODEGRADABLE P-N JUNCTION

Guy Cordonier
Mechanical Engineering
West Virginia University
Department of Mechanical and Aerospace Engineering
Morgantown, West Virginia, 26506

ABSTRACT

Indigo films were fabricated and characterized for use as functional layers in biodegradable optoelectronic device applications. The films were deposited onto flexible polyethylene naphthalate (PEN) and rigid glass substrates using a thermal evaporator. The films were characterized for optical transmission, surface roughness, topography, morphology, and tensile strength with respect to thickness. It was found that the films were not electrically conductive on either substrate tested.

INTRODUCTION

Indigo has shown potential as a functional layer in organic field-effect transistors and ozone filters [1,2]. Indigo powder was deposited onto glass and PEN substrates using a thermal evaporator in thicknesses ranging from 25 to 100 nm. The indigo powder was handled inside a glove box to reduce risk of inhalation. The films were maintained inside a vacuum chamber between characterization tests to prevent degradation due to ambient atmospheric contaminants. Optical transmission was taken using a spectrometer. Topography and surface roughness were taken using atomic force microscopy (AFM). Morphology was investigated using x-ray diffraction (XRD). Tensile strength was measured using a tensile tester. Crack propagation was observed using an optical microscope. Electrically conductivity was tested for using a two-point probe system.

BACKGROUND

The ever-shrinking lifespan of modern optoelectronic devices accentuates the issue of electronic waste. Currently, most devices are manufactured using a diverse range of materials, with the majority of them not being able to biodegrade within a reasonable amount of time. It is anticipated that the problem of electronic waste will become highly visible in the next few years with the advent of plastic-based, low-cost and short-lifetime optoelectronics [3]. Recently, an effort to address such a growing ecological issue has been initiated with the exploration of ‘exotic’ biodegradable materials, as the device building blocks. Such materials are usually found in nature and can be used in all different parts of a field-effect transistor, for example, thus leading to an ‘all natural’ device (Figure 1).

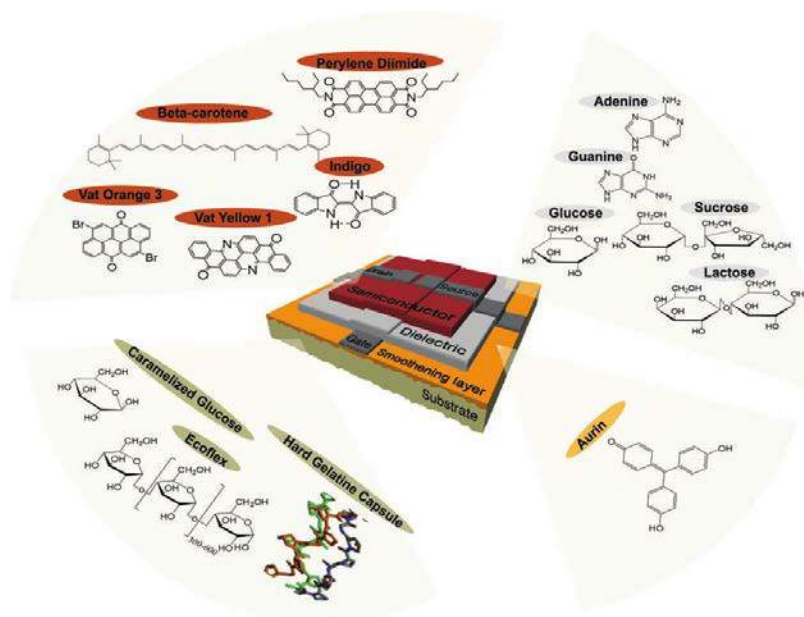


Figure 1. Organic field-effect transistor (OFET) device architecture fabricated by natural or nature-inspired materials [4].

As NASA seeks to send people on missions that take them further and further from the Earth, it is imperative that future spacecraft are designed to be as resourceful and efficient as possible by containing all-natural optoelectronic devices. For example, after experiments are performed on a voyage and the optoelectronic device/component has outlived its intended function, an astronaut should be able to safely dispose it without creating e-waste in space. This would allow missions to be more efficiently prepared in terms of resource allocation, and thus result in more scientifically productive space expeditions.

METHODOLOGY

Indigo was deposited onto glass and PEN substrates using a thermal evaporator at a pressure of 6.0×10^{-7} bar. Figure 2 illustrates the interior of the thermal evaporator chamber. Indigo is inserted in the crucible, which is then heated using an electrical resistor. The indigo evaporates up towards the substrate in a conical pattern. A mask is used to pattern the films. Quartz crystal monitors are used to measure the deposition rate and determine the thickness of the deposited films.

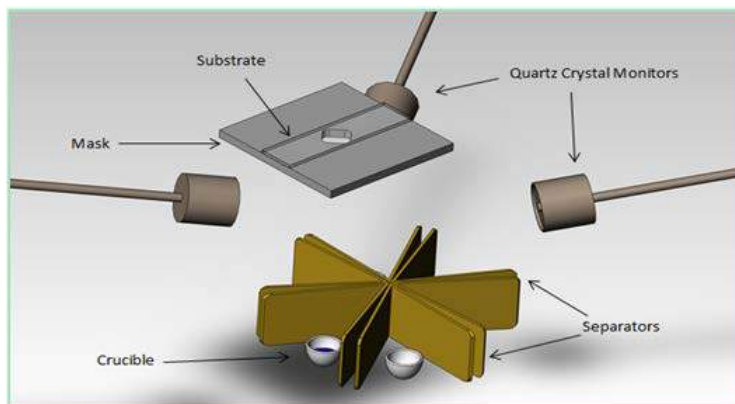


Figure 2. Perspective of the thermal evaporator chamber.

Optical transmission was taken using an Ocean Optics JAZ spectrometer. Wavelengths between 475 and 875 nm were studied. Topography and surface roughness measurements were taken using a Molecular Imaging PicoScan 3000 microscope. Sample areas of $16 \mu\text{m}^2$ were scanned using a single-pass scan type. Morphology was investigated using a Bruker D8 Discovery XRD, scanning from 20 to 60 degrees. An ADMET tensile tester was used in conjunction with a Leica optical microscope equipped with an Allied Visions Technology Guppy frame grabber to examine crack formation and propagation on the flexible PEN substrates. Figure 3 shows the experimental set-up of the ADMET and microscope.

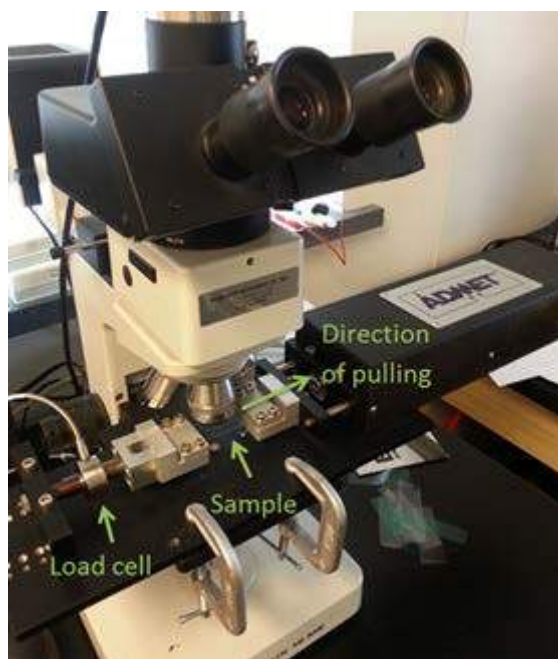


Figure 3. ADMET tensile tester mounted on optical microscope stage.

RESULTS & DISCUSSION

Optical transmission of the indigo films on the PEN and glass substrates revealed that the transmission percent decreased as film thickness increased (Figure 4). This relationship suggests that film thickness would be an important factor in the design of optoelectronic devices in which indigo forms an active layer.

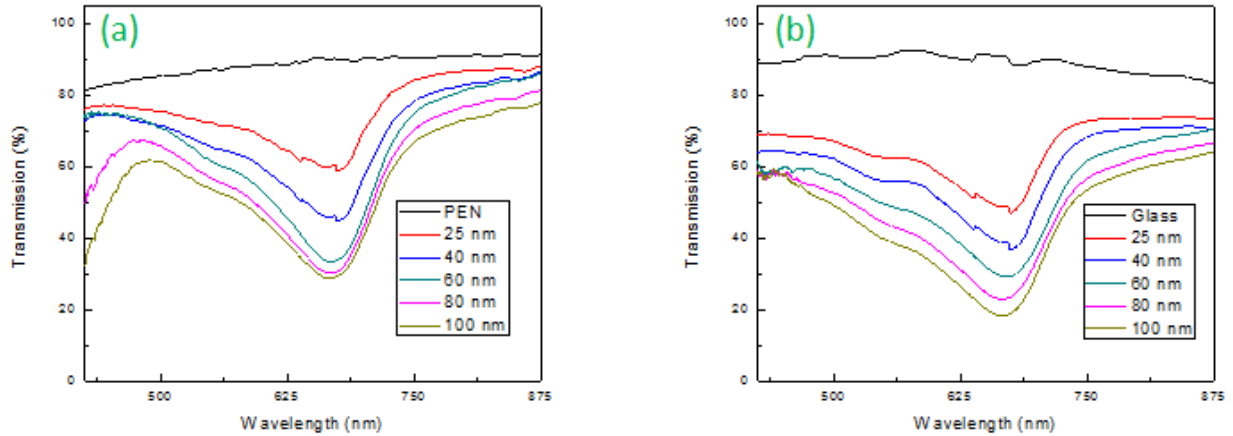


Figure 4. Optical transmission of indigo films on (a) PEN and (b) glass substrates.

Topography was taken using AFM (Figure 5). The grain size and shape was approximately equal for films of the same thickness on both substrates. This suggests that the indigo structures were likely similar. Surface roughness was also taken with AFM. The average surface roughness increased with increasing film thickness (Figure 6). This suggests film thickness must be considered in the design of optoelectronic devices, as adherence decreases as roughness increases.

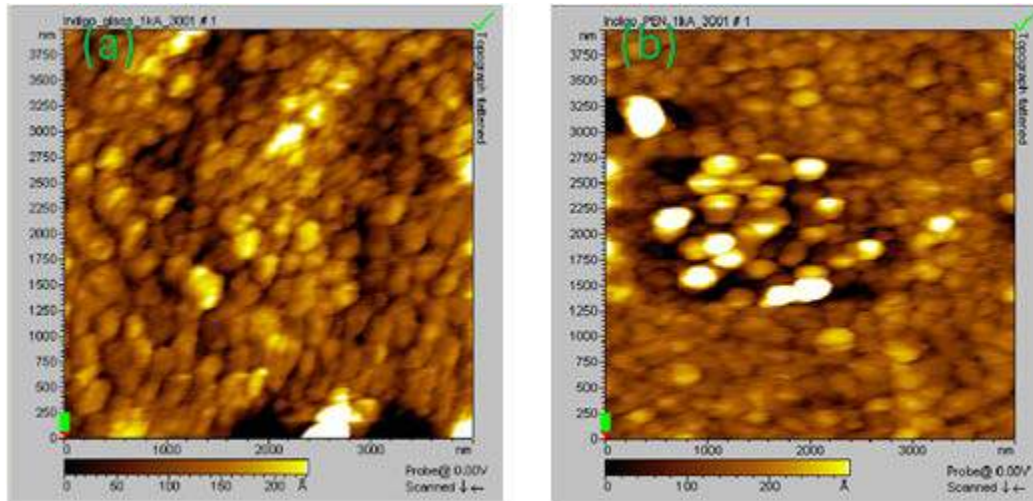


Figure 5. Topography of 100 nm indigo films on (a) glass and (b) PEN substrates.

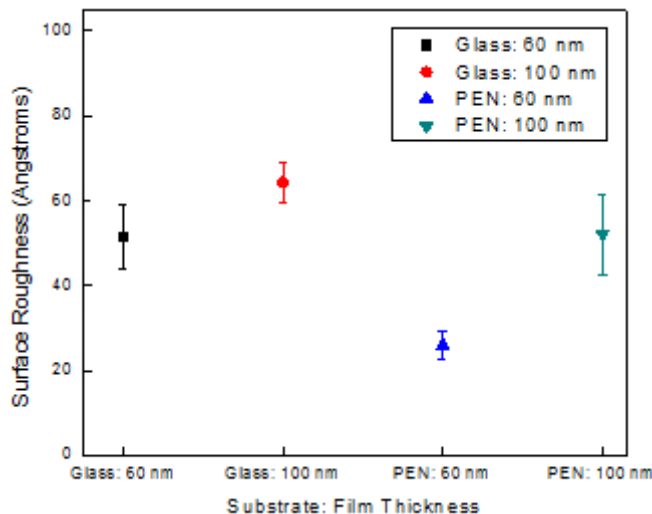


Figure 6. Surface Roughness as a function of film thickness.

A tensile tester was used to strain the films (up to 5% strain) on the flexible PEN substrates. Figure 7 shows the location of the cracks. Cracks did not form on the indigo film, but on the substrate itself. This was confirmed by changing the focus of the optical microscope to focus on the indigo layer and the PEN separately. The cracks formed straight lines that were perpendicular to the direction of loading. Additionally, XRD of the indigo films yielded no peaks, suggesting that the structure of the indigo was amorphous. A two-point probe test for electrical conductance showed that the films were insulating. This is likely a result of the amorphous nature of the indigo; the electrons were “localized” to individual areas of the films and could not travel freely.

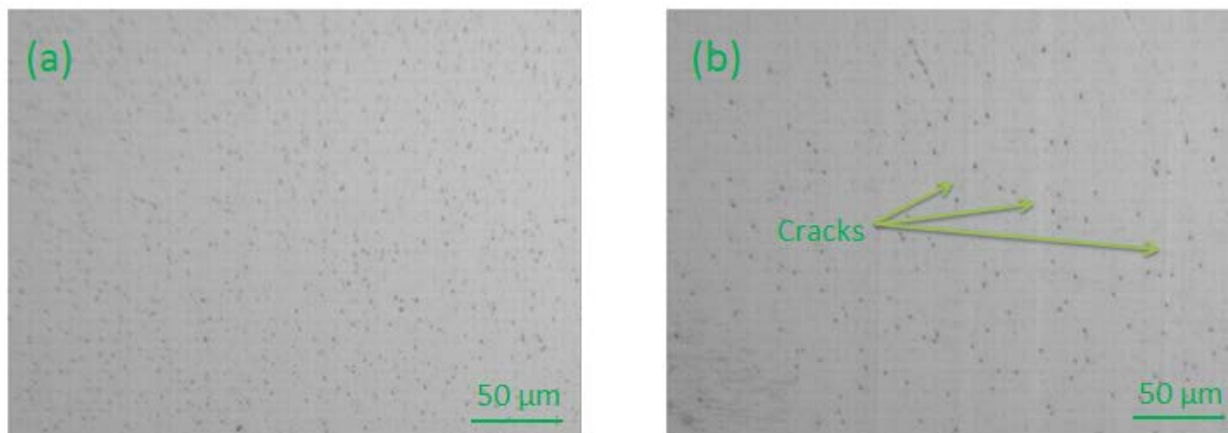


Figure 7. Indigo film (60 nm) on PEN (a) unstrained and (b) strained to 5%.

CONCLUSIONS & RECOMMENDATIONS

Indigo powder was successfully deposited on PEN and glass substrates. Optical transmission was observed to decrease with increasing film thickness on both substrates. AFM revealed the grain size to be approximately equal for both substrates. Surface roughness increased with increasing film thickness. Both substrates yielded electrically insulating films. This is likely due to the amorphous structure of the indigo. It is recommended to investigate indigo films deposited on

highly-aliphatic substrates for future work. It has been suggested that hydrogen bonding between aliphatic substrate surfaces and indigo molecules would elicit a crystalline structure that is conducive to the flow of electrons, thus enabling the potential of indigo as a functional layer in optoelectronic devices.

ACKNOWLEDGEMENTS

The author would like to acknowledge the NASA WV Space Grant Consortium for its financial support of this work and the author's research mentor, Dr. Kostas Sierros, for his continued support during this project.

PERSONAL OUTCOMES

The NASA WV Space Grant Consortium has granted me the opportunity to develop myself as a researcher in the field of nanotechnology. Through the financial support I received for my project, I was able to obtain real-life experience working in a professional laboratory environment. I gained insight on the research process, from idea conception to experimental implementation to result publishing. My findings were presented at the Summer Undergraduate Research Symposium at West Virginia University on July 25, 2013. Additionally, with the funding I had available, I was able to complete more research with my mentor. I worked throughout the year on 3D nozzle-based printing, studying the relationships between fluid deposition properties and the resulting printed structures' mechanical properties. I also was the recipient of a 2014 National Science Foundation Fellowship. I directly attribute winning this award to my time in the lab made possible by the NASA WV Space Grant Consortium.

REFERENCES

1. M. Irimia-Vladu, et al. "Green and biodegradable electronics" *Mater. Today* **15** (2012) 340-346
2. M. Irimia-Vladu, et al. "Indigo - A Natural Pigment for High Performance Ambipolar Organic Field Effect Transistors and Circuits" *Adv. Mater.* **24** (2012) 375-380
3. J. Brunet, et al. "Physical and chemical characterizations of nanometric indigo layers as efficient ozone filter for gas sensor devices" *Thin Solid Films* **520** (2011) 971-977
4. M. Irimia-Vladu et al. (2010) *Adv. Funct. Materials* **20** 4069

USING AQUATIC ORGANISMS TO ASSESS THE EFFECTIVENESS OF ACID MINE DRAINAGE REMEDIATION IN THE THREE FORK CREEK WATERSHED

Zane Dennison
Biology
Fairmont State University
Fairmont, WV 26554

ABSTRACT

Due to recent waning of the West Virginia Coal Industry several abandoned mines in the state, particularly in North-Central West Virginia have negatively impacted local streams and rivers due to the toxic effects of acid mine drainage (AMD). The projects main objective was to assess if the recent installation of limestone dosers were positively impacting stream health. Data collected during the summer of 2013 was compared to previously collected samples before and after the dosers were installed. Data indicated that the limestone dosers were producing a positive impact on overall water quality.

INTRODUCTION

Abandoned mines have been left to wreak havoc on the local environment. As rainwater and groundwater flow through these mines, acid mine drainage is formed, producing sulfuric acid. The addition of sulfuric acid to water sources lowers the pH of the water, affecting those native species that rely upon the water for a habitat, for reproduction, and for sustenance (2). As a result, the aquatic life in the bodies of water, including Three Fork Creek and its tributaries, disappear, unable to survive in the altered environment. In particular, *Daphnia magna* also known as the water flea is a model organism that is affected by AMD. A water flea is a small, aquatic arthropod that serves as a food source for larger aquatic animals, namely fish (1). When acid mine drainage is present and the pH of the water lowers, the aquatic macro-invertebrates begin to disappear, which leads to death or migration of larger species in the water source (3). In an attempt to rectify the negative chemical effects of acid mine drainage in the Three Fork Creek the current active remediation by using 3 limestone dosers should result in the eventual repopulation of the Three Fork Creek and its tributaries with abundant aquatic life.

METHODS

Water chemistry data was collected for 6 different sites in the Three Fork Creek watershed. A series of data collection occurred for both above and below the point source of remediation for the three creeks. The series of data collection included several parameters. A few of these parameters included the pH, %DO (dissolved oxygen), %TDS (total dissolved solids), and water temperature for each creek. With this data we will have the ability to compare the results of above point source of remediation to those of below point source of remediation and make conclusions as to whether the effects of acid mine drainage remediation are valid in effort to increase native aquatic organism abundance and diversity within the Three Fork Creek Watershed. Native aquatic macro-invertebrate organisms were also collected and identified from each site and their abundance and

diversity was calculated. Native aquatic organisms were used to assess the effectiveness of acid mine drainage remediation in the Three Fork Creek Watershed. The tributaries of primary focus within the Three Fork Creek Watershed were Raccoon Creek, Bird's Creek, and Squires Creek. Native macro-invertebrate collection was conducted for both above and below the point source of remediation (limestone doser) within all three creeks. Therefore, it was found that within Raccoon Creek there were no macro-invertebrates present above or below the point source of remediation. Above the point source of remediation for Bird's Creek there were a total of three distinct species of macro-invertebrates. However, below the point source of remediation for Bird's Creek there was only one species of macro-invertebrate collected. In addition, macro-invertebrate collection above the point source of remediation for Squires Creek revealed four distinct species. During collection of macro-invertebrates below the point source of remediation for Squires Creek, only one species was identified. Specifically, two standard ecological measurements that take into account the abundance and diversity of aquatic macro-invertebrates (termed the FBI index and EPT index) were used to classify the pollution level of the streams especially above and below the 3 limestone dosers that are in place in the watershed. Utilized as a model organism, *Daphnia magna* (water fleas) are small aquatic arthropods that are affected by acid mine drainage. *Daphnia magna* serves as a food source for many large aquatic organisms such as fish. A three week analysis was conducted in order to monitor the survivorship of *Daphnia magna* (10 individuals per sample) after exposure to water samples collected from both above and below the point source of remediation for all three creeks. It was clear that within a twelve hour period, all individuals were found unable to survive within the above point source of remediation samples for all three creeks. However, after the three week analysis it was observed that all 10 individuals for each sample below the point source of remediation for each creek were able to survive. Through the collection of all of the information above, we were able to determine whether the actual changes that will happen to the water quality after limestone treatment (such as pH, conductivity, and soluble metals) translates to the increase in abundance and diversity of native species and/or allows for greater survival of our model organism the water flea.

RESULTS

Collected data was analyzed and compiled in the graphs below. There was an increase in pH after doser installation (Figure. 1). In (Figure. 2) there was an increase in the FBI value for organisms collected below doser remediation sites. The longevity of *Daphnia magna* exposed water from below doser remediation sites for duration of 3 weeks is shown in Figure 3. Water fleas that were exposed to water from above doser sites all died within 24 hours (data not shown).

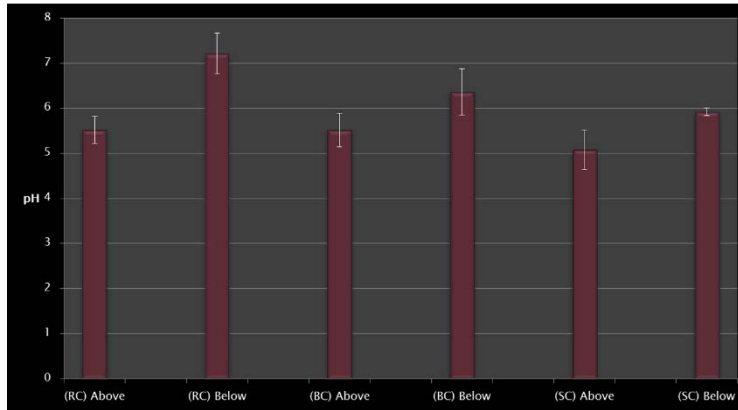


Figure. 1: pH data from sampling sites Summer of 2013

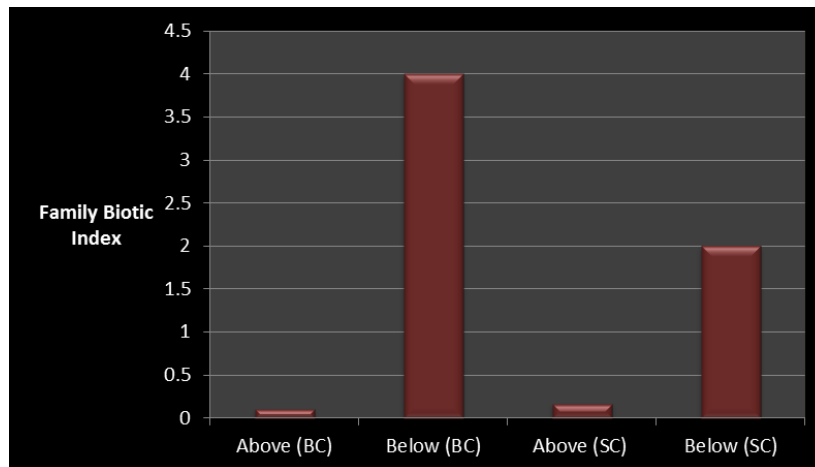


Figure. 2: FBI data from sampling sites Summer of 2013

THE HILSENHOFF INDEX		
Hilsenhoff Index Water quality Degree of Organic Pollution		
Family Biotic Index	Water Quality	Degree of Organic Pollution
0.00–3.75	excellent	organic pollution unlikely
3.76–4.25	very good	possible slight organic pollution
4.26–5.00	good	some organic pollution probable
5.01–5.75	fair	fairly substantial pollution likely
5.76–6.50	fairly poor	substantial pollution likely
6.51–7.25	poor	very substantial pollution likely
7.26–10.00	very poor	severe organic pollution likely

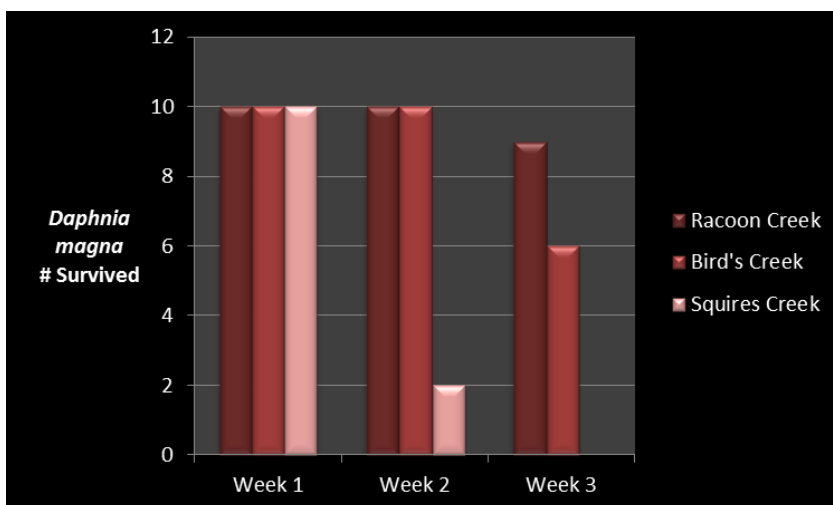


Figure. 3: *Daphnia magna* survivability over 3 week period from below doser sites

DISCUSSION

Through analysis of collected data, a substantial increase in pH was observed. A greater survivability of the water fleas was also shown below the doser remediation sites, although the native aquatic macro-invertebrate data did not correlate with an improved stream quality. The continued active remediation of acid mine drainage through 3 limestone dosers should result in the repopulation of the Three Fork Creek and its tributaries with abundant aquatic life. Stream monitoring will continue in order to assure that the quality of these AMD impacted streams does improve in the future.



Picture of limestone doser within the Three Fork Creek Watershed



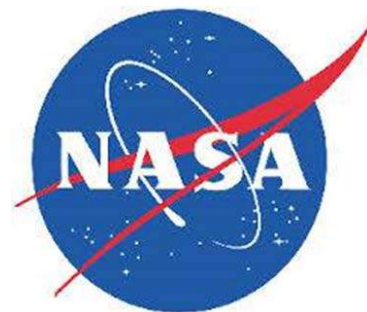
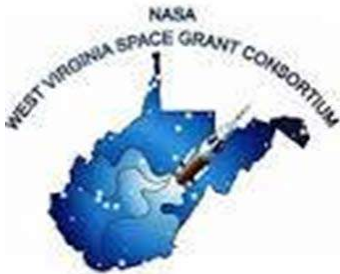
Picture of our model organism *Daphnia magna* (water flea)

CONCLUSION

Although some data has been collected, not enough information has been obtained in order to have complete assurance that the limestone dosers are properly remediating the Three Fork Creek and its tributaries. In the very near future it will be important to continue data collection within this area to insure the AMD and aquatic pollution is properly managed. In addition, since the Three Fork Creek watershed flows into the Tygart River there will hopefully be a positive impact on the drinking water quality here in Fairmont. The research project entitled USING AQUATIC ORGANISMS TO ASSESS THE EFFECTIVENESS OF ACID MINE DRAINAGE REMEDIATION IN THE THREE FORK CREEK WATERSHED was funded by the NASA West Virginia Space Grant Consortium. The program provided the opportunity to analyze, explore, and become acquainted with an issue of great importance, water conservation. Some important aspects that were involved with the project include a newly acquired knowledge of the relationship between stream ecology and water quality. In addition, the research project allowed for the education of essential skills in a research setting and created the necessary learning environment for a real life research experience.

ACKNOWLEDGMENTS

This project was supported and made possible by the NASA West Virginia Space Grant Consortium and our research mentor Dr. Mark Flood. Thank You for this research opportunity.



REFERENCES

1. Biesinger, K.E., and Christenson, G.M. 2011. Effects of Various Metals on Survival, Growth, Reproduction, and Metabolism of *Daphnia magna*. *Journal of the Fisheries Research Board of Canada*. 29(12): 1691-1700.
2. Cairns, J. and Pratt, J.R. 1993. A History of Biological Monitoring Using Benthic Macroinvertebrates. *Journal of Upper Gunnison Waters*. 2(1): 10-13.
3. Akcil, A. and Koldas, S. 2006. Acid Mine Drainage (AMD). *Journal of Cleaner Production*. 14(13): 1139-1145.

VIBRATIONS IN AIRCRAFT AT SUPERSONIC SPEEDS

Lucas Greza
Applied Physics
West Virginia Wesleyan College
Buckhannon, West Virginia, 26201

ABSTRACT

During the transition from subsonic to supersonic flight, an aircraft vibrates and creates a sonic boom that we hear. The main objective was to measure these vibrations, and then modify a model aircraft to reduce the vibrations produced.

INTRODUCTION

The purpose of this research was to first construct a supersonic wind tunnel using mainly PVC pipe, an air compressor, and a vacuum pump. Once the required materials were obtained, I would then build the wind tunnel by connecting the air compressor to a tank, the tank to the series of pipes, the pipes to a dump tank, and finally the dump tank to a vacuum pump. The vacuum pump would be turned on, evacuating the air from the entire system. The air compressor would then be turned on and the tank filled with compressed air. Once enough air was compressed in the tank, a quick release valve would be turned to release the compressed air in a burst, and would be passed through the sonic throat thus putting the air speed above Mach 1. The air would then proceed into the dump tank, and the experiment would be done at that time. Instrumentation used would be a manometer, a pressure gage, and a vacuum gage.

Trials were to be repeated, and results taken down for as many trials as were deemed necessary. Once all data was collected, graphs were expected to be compiled and show the vibrations broken down into X, Y, and Z directions. Once this data was compiled, the results would be concluded, and ideas on how to reduce these vibrations would be attached to the models based on the data received. Once modifications were made to the models, the experiment would be conducted again and results compared to see if the modifications were successful or unsuccessful at the desired function.

The main precautionary action that was expected to be taken was ruptures due to the high air speeds and pressures produced by the air compressor and the sonic throat accelerating the air through the test section. These would be taken care of by using strong glues to put the sections that would not need to be taken apart together, and by using deep threads and clamps to keep the sections that could not be glued together.

BACKGROUND

In 1947, Chuck Yeager broke the sound barrier in a Bell X-1 aircraft, ushering in a new age of aviation. Ever since, man has had the ability to travel at supersonic speeds and above, but problems still occur during the transition from subsonic to supersonic speeds. One of the biggest problems is that the aircraft vibrates at the sonic threshold. There has been research on sonic boom reduction, but not much research, if any, has been conducted on the reduction of the vibrations on the aircraft.

These vibrations effect the flight dynamics of the aircraft, and if they could be reduced by modification to the body of the aircraft, would mean a smoother transition from subsonic to supersonic flight, thus making it a smoother flight and possibly leading to a return of supersonic flight as a commercial option, when paired with other research in sonic boom reduction.

EXPERIMENT

To achieve the results I was expecting, I first needed to build a blow-down wind tunnel. I had found a design for a small blow-down wind tunnel capable of achieving speeds approaching Mach 3, which was first built at Bethel University in St. Paul, Minnesota. Using aspects from their design, and implementing my own modifications, I intended to build a blow-down wind tunnel capable of producing the conditions needed to research the problems stated above.

The design consists of two tanks, one of which would hold the high-pressure air and the other would hold the low-pressure air. The high-pressure tank was to be connected to an air compressor and be brought up to an appropriate PSI to achieve the Mach number desired. The low-pressure tank would be connected to a vacuum pump to evacuate as much air out of the tank as possible. Directly after the high-pressure tank, a ball valve will be attached to the tube that will connect the high-pressure tank, to the clear circular PVC test chamber where the test subject will be positioned and subjected to the supersonic flow, and finally to the low-pressure tank. After the ball valve, the test area will be positioned along with the supersonic nozzle to achieve supersonic flow. The test subject would be positioned just after the supersonic nozzle and would be subjected to the supersonic flow. Finally, after the test subject area, the low-pressure tank would be situated to help achieve the supersonic flow.

METHODS

When building the wind tunnel, I intended to connect the components detailed above using strong glues and threaded components to produce tight seals on the wind tunnel. Due to the high pressures, it was a very important factor when ordering prospective parts to take into account their expected operating pressures and expect to use a slightly higher pressure to account for variables in construction and weaknesses in design at critical points in the design, such as the joints and connections between components.

As for testing the vibrations in the aircraft, I intended to use an accelerometer implanted into the test subject. This would allow for accurate measurements without sacrificing aerodynamics. I intended to get a scale model of an F18 Super Hornet to act as one test subject, which has a top speed of around Mach 1.8, and the SR-71 Blackbird as the other test subject which has a top speed of Mach 3.3. The F18 Super Hornet is a great aircraft to test because it is the currently used aircraft in the US Navy and Air Force for its strong maneuverability and ability to carry a relatively large amount of armaments. The Sr-71 Blackbird made by Lockheed and Martin as surveillance aircraft. The model would be made from metal, and the accelerometer will be placed inside the models and then resealed to its original specifications. The models would have been situated inside the test chamber, and would have been subjected to the supersonic flow.

The data collected from the accelerometer would be used to calculate the forces applied to the model aircraft. After taking enough measurements, the forces would be compiled into graphs of the forces in different sections of the aircraft versus the speed of airflow. Using these graphs and

the data collected, I would draw a set of conclusions that would be used to improve on the design and fabrication of aircraft and reduce vibrations in these aircraft. Once these modifications were completed, the model would be retested in the wind tunnel and data taken again. Once this second set of data was collected and graphed, the two would be compared to see which design is better.

RESULTS

Unfortunately, the wind tunnel never actually got constructed. I ran into initial problems in June-July finding the correct materials needed. The air compressor was easily acquired, but the tanks were more elusive. I wanted to get a 5-gallon or larger tank to hold enough compressed air to run the wind tunnel for more than a fraction of a second. Once I could not find a tank compatible with my air compressor commercially, I took to junkyards around the city of Buckhannon, looking at a few different ones. After not finding any, I settled for the 1-gallon tank attached to the air compressor and a 2-gallon auxiliary tank to make a total of 3 gallons.

After resolving the tank issue, my Faculty Advisor Dr. J. Wiest and I found a vacuum pump in one of our labs that was sufficient enough to pump the desired amount of air out of the test chamber. Once those two components were acquired, I thought that the rest would be easily found. However, this was not the case.

The hardware stores in my area do not carry the clear PVC in the diameter needed to fit the model aircraft in them. I took to the Internet, and found that even the largest retailers did not carry the clear PVC needed. After looking at the local plumbing supplier and finding nothing of use there, I looked at smaller companies on the Internet. I found a suitable website to order from, found the desired diameter and took it to the head of our Physics Department for approval. After receiving approval for the purchase order, I submitted it to our financial department of our college, and was eager to receive my parts to construct the wind tunnel.

After waiting a few weeks, long enough to receive, process and send a few pieces of PVC, I had received nothing from the company. Around mid July, I called the company and after speaking with a rather inexperienced phone operator, it was concluded that they had received the purchase order and it was still being processed and would be sent out shortly. Having been assured that I would receive the parts in an appropriate amount of time, I waited longer while figuring out exactly how to connect, expand, and use the air compressor in series with the auxiliary tank. The vacuum pump was easily figured out, and the only part that was missing was the PVC.

After waiting another few weeks, I called the company back and asked why I had not received the order having been told that I would receive it in the next week. The person I talked to this time had no record of the purchase order, and suggested it was never received. By this point in the year, it was almost too late to reorder the supplies, build the wind tunnel and get the required 3.5 GPA specified in the award letter. Once I did not meet the required GPA for the fall semester, my research concluded.

DISCUSSION

Having suffered a few set backs throughout the research period, I did still learn and find out a great deal about the mechanics of supersonic flight. The subject is very interesting, having more in-depth topics than I would have ever imagined. I learned about some interesting research in the reduction of sonic booms being conducted by NASA and other private companies. This research

is ground breaking in the study of supersonic flight because, once successful, would allow the return of supersonic commercial flight and an increase in time efficiency for business around the world.

OUTCOMES

Not only did I learn a lot about the new research being conducted, but I also learned a lot about the classical mechanics of fluid dynamics. A lot of the Bernoulli's Principle came into play with my research conducted on background and I read a lot of the Fundamentals of Fluid Mechanics book written by Munson, Young, Okiishi, and Huebsch, which gave a great background and insight into how basic fluid mechanics work.

This research, along with a passion for flight mechanics and aviation in general, has prompted me to modify my research goals for my Senior Research Project. I have taken three designs and will be comparing them to see which is the best design based on life generated and drag generated. The two designs are the Flying wing modeled after the Northrop Grumman B2 Spirit and a Closed Wing design with design details taken from a Boeing 747 and modifications made through my design.

In addition to the above mentioned, I also submitted a paper and presentation to the Mid Atlantic Undergraduate Research Conference this spring, detailing my Senior Research Project. I do not think that I would have been nearly as prepared and knowledgeable with the subject matter that was presented without this NASA Fellowship.

I have always had a passion for flight and aerospace engineering, but my understanding of the inner workings and problems faced with the every day applications of fluid mechanics and design of instruments and testing of models would not be nearly as diverse without this NASA Fellowship. I have found a new respect for aerospace engineers, and now know the challenges and difficulties they go through in solving the complex problems presented in every day work.

FUTURE PLANS

As far as future plans for my research, I would love to extend this research using an already constructed wind tunnel at possibly WVU or another institution or professional location, and test the vibrations during the transition from subsonic to supersonic flight. In addition to testing these pervious implications, I would like to test the shock waves produced by the supersonic flow. These combined results would be used to improve on models of aircraft known to go above mach 1 and possibly create a whole new design that would be more efficient at these high speeds and especially more efficient at the transition point.

In addition to the above mentioned research goals, I think I would be interested in constructing a supersonic wind tunnel as I intended to. Knowing the struggles I went through in my attempt at constructing this wind tunnel, I would like a second try at building this wind tunnel with the intent of not testing a model aircraft and just testing a point and looking at the shock waves.

I find this research very interesting, and am still interested in this as a possible future job in the research and development of supersonic aircraft. I intend to go back to school for a degree in Aerospace Engineering and this research is an integral part in my future studies.

IMPORTANT DETAILS

Throughout this research experience, I have learned a great deal not having anything to deal with physics or aerospace engineering. Without the financial support of WV NASA Space Grant Consortium, my vision would not have had a chance of coming true. I also learned that it is not as easy as typing in a credit card number and getting materials like it is ordering books off of Amazon, and there are more challenges dealing with purchase orders to smaller companies.

Another important skill I learned was research skills. The ability to research a topic thoroughly and make a hypothesis based on your initial findings and intuitive reasoning is a great and necessary skill to be competitive in any field, but especially in any engineering field. Along with the ability to research, the ability to convey your research in a manner that your audience can understand it is a very important skill to have. With the various reports throughout the timeframe, I have further developed this ability and am very confident that, had everything gone perfectly, I would have been able to accurately and efficiently convey my results to either an experienced professional, or to anyone attending a general talk on the subject. This skill, more than any other, I feel is the single most important skill learned during my research.

A very close second to the previously mentioned skill learned is the real-life research experience gained during this experience. This skill is invaluable in building skills that will last a lifetime, and also helping to find a future job in the field. Despite not being able to build the wind tunnel, I have learned a lot about the research process and about the hardships encountered during this process, possibly more than others. The fact that I did run into so many problems was, in a weird way, a good thing because it made me think out of the box and explore every option I had as a solution to the problem. This skill, which I will use for the rest of my life, is a great skill to learn before getting a job because I will know what to expect when these issues arise.

CONCLUSION

Throughout this process, I have experienced a lot of setbacks, but I have also learned a great deal about the physics and engineering involved, as well as the real life skills such as problem solving, exploring every option, and dealing with setbacks along the way. Even though I did not get the ultimate goal accomplished, I still feel that the research conducted was not a failure due to the amount learned from the preliminary research conducted. I had a wonderful time researching throughout the year, and, if presented with another opportunity to finish and/or expand my research, I would take it in a heartbeat.

ACKNOWLEDGMENTS

First for foremost, I would like to express my most gracious thanks to WV NASA Space Grant Consortium for the opportunity to conduct research and for a chance to explore my interests in the field of aerospace engineering and especially in the supersonic flight dynamics.

I would also like to thank Dr. J. Wiest, my faculty mentor, as he has helped me throughout the entire process. Without his guidance and support, I would not have gotten nearly as far as I did in my research.

In addition to Dr. J. Wiest, I would also like to thank Dr. G. Albert Popson, the Department Chair of WVWC Physics for his input and help throughout.

REFERENCES

- Munson, Young, Okiishi, Huebsch, Fundamentals of Fluid Mechanics (John Wiley, 2009).
- G. B. Whitham, Linear and Nonlinear Waves (John Wiley, 1974).
- Louis V. Schmidt, Introduction to Aircraft Flight Dynamics (American Institute of Aeronautics and Astronautics, 1998).
- Russell C. Hibbeler, Mechanics of Materials (Prentice Hall, 2011).
- Mass Flow Rate: Choaking (Tom Benson, Editor)
<http://exploration.grc.nasa.gov/education/rocket/mflchk.html>
- Wing Tunnel Design (Tom Benson, Editor)
<http://www.grc.nasa.gov/WWW/k-12/airplane/tunnozdz.html>

IDENTIFICATION OF ANTIBODY FRAGMENTS SPECIFIC FOR HIGH-GRADE PROSTATIC INTRAEPITHELIAL NEOPLASIA CELLS VIA SELEX

Cyrus Hajiran
Bachelor of Arts in Biology
West Virginia University
Morgantown, WV 26506

ABSTRACT

The purpose of this study is to develop a minimally invasive molecular tool for the early detection and specific treatment of prostate cancer. An isolated molecular recognition element (MRE) can be conjugated to a fluorescent or chemotherapeutic agent. Drug-antibody conjugates can be used for targeted drug-delivery or non-invasive imaging. A prostate cell-specific MRE for the pre-cancerous cell line high-grade prostatic intraepithelial neoplasia (HGPIN) is being developed. Five rounds of *in vitro* selection have been completed. Sequencing has been performed for the initial rounds of selection in order to monitor the enrichment of the antibody fragment library.

INTRODUCTION

Molecular targeting can be used to diagnose and deliver therapeutics to prostate cells in the initial stages of cancer. A single-chain Fragment variable (scFv) Molecular Recognition Element (MRE) specific for the high-grade prostatic intraepithelial neoplasia (HGPIN) cell line is being isolated through the Systematic Evolution of Ligands by Exponential Enrichment (SELEX). A human non-immune scFv library with 10^9 diversity has been displayed on a yeast host surface with the ability to bind to whole cell targets (Figure 1).

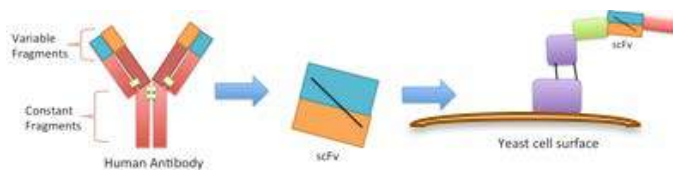


Figure 1 - Yeast displayed single-chain variable fragment (scFv) as a Molecular Recognition Element

This scFv library was cloned into plasmids and transformed into the yeast strain *Saccharomyces cerevisiae*. Surface expression of the protein library was under control of a galactose promoter preceding incubation with the target cell line.

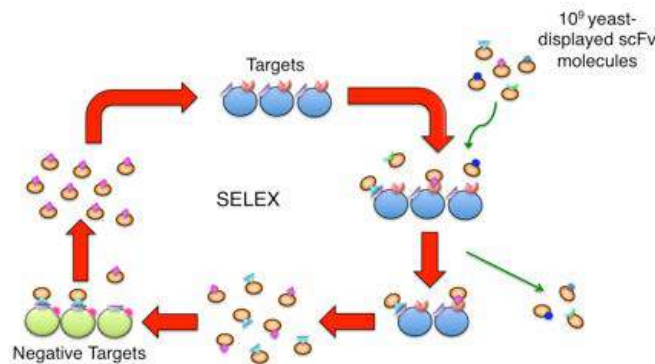


Figure 2 - Using *in vitro* selection to amplify yeast displayed antibody fragments

Also known as *in vitro* selection, the methodology involves screening a library of random biomolecules for their ability to bind to a target. Non-binding molecules are removed and binding molecules are amplified. Amplified molecules are subjected to negative targets, and molecules that don't bind to these are amplified, thus completing a round of selection (Figure 2). Stringency is increased through each successive round. After multiple rounds, one or a few strong binding, highly specific molecules are selected for.

BACKGROUND

Prostate cancer is the most diagnosed non-skin cancer and the second leading cause of cancer related deaths among men in the United States. One in six men will be diagnosed with prostate cancer in his lifetime, and one out of thirty will die. Because there is no obvious carcinogen to which less exposure leads to a direct correlation in a decline in disease-specific mortality, developing new, early methods of detection is the most effective approach to combating the disease (Vickers et al. 2012).

Standard prostate cancer diagnostics involved analyzing levels of a serine protease, prostate specific antigen (PSA), in the blood. In theory, serum PSA levels will be higher in men with prostate cancer than those with normal prostates. However, because serum PSA levels are raised by benign conditions in addition to cancerous conditions, blood work analysis often gives false positive test results. According to one published study, a biopsy for one in three men with elevated PSA levels will confirm prostate cancer. The remaining two men will therefore have false positive results from the PSA test (Woolf 1995). In May 2012, The United States Preventative Services Task Force (USPSTF) no longer recommended PSA-based screening. Referring to the PSA test, the USPSTF's claim stated: "for men of any age, the USPSTF recommends that doctors and patients do not screen for prostate cancer because the potential benefits do not outweigh the harms" (Moyer 2012). A digital rectal exam (DRE) is the recommend method of detection.

Many current treatments are non-specific. Besides watchful waiting and active surveillance, common treatment options for early stage, localized prostate cancer include prostatectomy, radiation therapy, androgen deprivation therapy, cryoablation, and high-intensity focused ultrasonography (Chou et. al 2011).

Prostate cancer is staged by the guidelines of the American Joint Committee on Cancer's tumor, node, and metastasis (TNM) system. The tumor stage is based on invasion, and the likelihood of metastasis is associated with the identification of specific cell differentiation patterns and other

histopathology (Chou et. al 2011). High-grade prostatic intraepithelial neoplasia (HGPIN) is a proliferative lesion of prostate secretory cells. HGPIN is characterized as a pre-malignancy as the benign growth does not disrupt the basal membranes of prostate epithelium acinar glands. Evidence supports HGPIN as being “the most likely morphologically distinctive pre-invasive lesion associated with the development of prostatic adenocarcinoma” (Merrimen et. al 2013).

The purpose of this study is to design effective screening and treatment methods that maximize the benefit of reducing prostate cancer mortality while minimizing overtreatment of other prostatic conditions.

METHODS

For the HGPIN MRE specific selection, five rounds of SELEX were performed in order to obtain an scFv MRE specific for the HGPIN prostate cancer cell line. For each selection scheme, the first three rounds of *in vitro* selection were performed by panning. The fourth round of *in vitro* selection was completed by fluorescence-activated cell sorting (FACS).

Normal, benign, and cancerous prostate cell lines are being used in order to obtain prostate cancer cell-specific MREs. Each cell line had its media changed every 2-3 days and was split every 5-7 days in a T75 cell culture flask for general cell culture maintenance. The prostate cells were grown in a 37°C incubator with 5% carbon dioxide and humidity.

Biosafety Level 2 protocols were used at all times when carrying out cell culture protocols. All cell culture protocols were conducted with proper Personal Protective Equipment including a laboratory coat, safety goggles, and extended cuff nitrile gloves. All cell culture procedures were conducted in the biosafety cell culture hood in EBRF 259. The following procedures were used for general cell line maintenance: frozen cell line initiation, media changing, passaging, and cell line freezing.

The androgen-dependent prostate cancer cell line LNCaP was acquired through the American Type Culture Collection (ATCC) (Manassas, VA) and cultured in RPMI 1640 growth media with L-Glutamine and 25 mM HEPES (Cellgro; Manassas, VA) and contained 10% Fetal Bovine Serum (FBS) (Fisher Scientific; Pittsburgh, PA) and 1X antibiotic/antimycotic mixture (ab/am) (Cellgro) (Horoszewicz et al. 1983) added to the media. The HPV-18-immortalized High Grade Prostatic Intraepithelial Neoplasia (HGPIN) cell line was a gift from Dr. Mark Stearns (Drexel University; Philadelphia, PA) and was cultured in Defined KFSM growth media (Gibco; Grand Island, NY) and contained 5% FBS and 1X ab/am (Wang et al. 1999) added to the media. The SV40T-immortalized Benign Prostate Hyperplasia (BPH-1) cell line was a gift from Dr. Simon Hayward (Vanderbilt University; Nashville, TN) and was cultured in RPMI-1640 growth media with L-Glutamine and 25 mM HEPES and contained 10% FBS and 1X ab/am (Hayward et al. 1995) added to the growth media. The androgen-independent DU-145 prostate cancer cell line was obtained from ATCC and cultured in EMEM growth media (Cellgro) and contained 10% FBS and 1X ab/am (Stone et al. 1978) added to the growth media. The HPV-18-immortalized normal prostatic epithelium cell line RWPE-1 was obtained from ATCC and cultured in Defined KFSM growth media (Gibco) and contained 1X ab/am (Bello et al. 1997) added to the growth media.

The full human non-immune scFv library was cloned into the pPNL6 plasmid in the EBY100 *Saccharomyces cerevisiae* yeast strain. After being originally amplified in standard dextrose media

with casamino acids (SD+CAA), containing 0.5% casamino acids, 2% dextrose, 0.17% yeast nitrogen base without ammonium sulfate amino acids, 0.53% ammonium sulfate, 1.019% sodium di-hydrogen phosphate, 0.856% sodium monophosphate, and supplemented with 10 U/mL penicillin, 10 µg/mL streptomycin, and 80 µg/mL vacuum-filtered ampicillin, surface expression of the library was induced by expressing the scFv under control of a galactose promoter in standard galactose plus casamino acids media (SG+CAA), which substituted 2% galactose, 2% raffinose, and 0.1% dextrose for the dextrose in SD+CAA. Following each induction period of scFv display, surface expression of the scFv library was confirmed by flow cytometry analysis. The monoclonal anti-HA tag antibody clone 16B12 conjugated to either DyLight 488 (Columbia Biosciences; Columbia, MD) or AlexaFluor 488 (Invitrogen; Grand Island, NY) was used to stain scFv-expressing yeast in yeast wash buffer (YWB) consisting of phosphate-buffered saline (PBS), 0.5% bovine serum albumin, and 2 mM EDTA. Amplified yeast samples were run on either a Cell Lab Quanta SC (Beckman Coulter; Brea, CA) or a FACSCalibur (BD Biosciences; San Jose, CA) flow cytometer equipped with a 488 nm argon laser and 525 nm emission filter. A minimum of 5% partial induction of the scFv library was confirmed before proceeding. This was sufficient in order to continue with selection incubations with target prostate cell lines.

For Round 1(+) selection, HGPIN cells were grown to 80-90% confluency and the cell-growth media was aspirated from the T75 flask. The HGPIN target cells were gently washed with calcium- and magnesium-free phosphate-buffered saline (PBS). The target cells were then incubated with 10^{10} yeast in order to ensure total representation of the library diversity. The naïve yeast library was amplified as discussed previously in SD + CAA and scFv surface expression was induced in SG + CAA media. After surface expression was confirmed by flow cytometry analysis, yeast were suspended in 15 mL YWB. For each selection scheme, the yeast-displayed scFv library was placed into the flask containing the target cell line and placed on a 37°C shaker at 25 RPM for four hours. Following the yeast + target cell incubation period, yeast not bound to target cells were removed from the selection scheme, and the target cells were gently washed three times with 15 mL YWB. 100 mL SD+CAA was added to the flask to promote amplification of yeast bound to the target cell line. This was allowed to grow overnight, and this enriched yeast library was prepared for negative selection.

For the HGPIN Round 1(-) selection, scFv-displaying yeast were suspended in yeast selection buffer (YSB) and incubated with rinsed LNCaP cells at 80-90% confluence for 30 minutes at 37°C with shaking at 25 RPM. The supernatant containing yeast-displayed scFvs that were not specific for LNCaP cells was removed. The supernatant was centrifuged to obtain unbound yeast, which were suspended in SD+CAA for amplification. Two more rounds of selection were performed by panning. The stringency of the selection scheme was increased in each round by decreasing incubation times and target cell numbers for positive rounds and increasing incubation times and target cell numbers for negative rounds.

The fourth round of selection was performed using FACS-based sorting. For HGPIN Round 4(+) selection, cells grown to 80-90% confluence were fluorescently dyed with CFSE (Invitrogen) according to manufacturer's protocol. HGPIN cells were then stripped from the flask using CellStriper reagent (Cellgro). Cellstriper was used to prevent the digestion of cell surface proteins. HGPIN cells were then suspended in YSB and counted with a Scepter equipped with 60 µm sensors (Millipore; Billerica, MA). In Round 4, all yeast were fluorescently dyed with Syto61 (Invitrogen) according to the manufacturer's instructions. A total of 10^7 yeast were suspended in YSB and

mixed with 10^6 HGPIN in a volume of approximately 2.5 mL. Yeast + HGPIN cells were mixed by inversion for 30 minutes at 37°C and placed on ice before FACS sorting. The sample was then sorted with a FACSAria (BD Biosciences), with excitation at 488 nm from a sapphire solid state laser and 633 nm from a HeNe laser and 525 nm and 650 nm emission filters. Events identified as bound yeast and HGPIN cells were collected. The yeast collected from this round were amplified and subjected to a round of negative selection.

In HGPIN Round 4(-)a, yeast were prepared for selection in the same manner and incubated with 10^6 LNCaP cells dyed the same with inversion for 30 minutes at 37°C in YSB. The sample was subjected to FACS and events that indicated yeast that were not bound to LNCaP cells were collected and amplified. These yeast were then prepared for selection and incubated with 10^6 dyed RWPE-1 cells for Round 4(-)b and subjected to FACS. Unbound yeast were collected and amplified. After HGPIN post-Round 4(-) amplification, yeast were prepared for Round 5(+) selection. This yeast population was subjected to the same process as before, however they were fluorescently labeled with anti-HA monoclonal antibody 16B12 conjugated to AlexaFluor 647 (Invitrogen). For HGPIN Round 5(+) selection, 10^7 yeast were incubated with 10^6 HGPIN cells. The yeast bound to HGPIN cells were collected, amplified, and prepared for Rounds 5(-) selection which are currently in progress.

In order to determine the diversity of the library, a sample of scFv-genes from the naïve library (Round 0) was sequenced. This was completed for the enriched post-Round 2(-), post-Round 3(-), and post Round 4(-) libraries for the HGPIN selection. To do this, yeast amplified from the previous round of selection were plated onto 2% agar plates containing 1% yeast extract, 2% peptone, and 2% dextrose (YPD). Yeast were grown for 36-48 hours at 30°C, and individual colonies were selected from the agar plates and subjected to polymerase chain reaction (PCR) amplification.

Individual yeast colonies were picked and placed into double distilled water and boiled. Upon boiling, the scFv-encoding DNA released from the yeast served as a template for the PCR reaction. The reaction ingredients were as follows: 400 nM forward (5'-GTACGAGCTAAAAGTACAGTG-3') and reverse (5'-TAGATACCCATACGACGTTC-3') pPNL6 primers (Eurofins MWG Operon), 250 µM deoxynucleotide triphosphates, 5% dimethyl sulfoxide, 1X Phusion Reaction Buffer (New England Biolabs, Ipswich, MA), 2 units Phusion High-Fidelity DNA polymerase (New England Biolabs), and double distilled water for a PCR reaction mixture total of 50 µL. Reaction conditions were: initial denaturation at 98°C for 30 seconds; 35 cycles of 98°C for 10 seconds, 50°C for 30 seconds, and 72°C for 30 seconds; and final extension at 72°C for 10 minutes. Results were analyzed using agarose gel electrophoresis. PCR reactions that contained bands corresponding to the 1kb scFv gene were purified for DNA sequencing. PCRs were purified using a PCR purification kit (IBI Scientific; Peosta, IA) and sent for DNA sequencing (Eurofins MWG Operon; Huntsville, AL) using both the forward and reverse pPNL6 primers. At least 30 sequences were obtained for the enriched library for each respective round of selection. The ExpASy translate tool (Swiss Institute of Bioinformatics; <http://web.expasy.org/translate/>) was used to translate the DNA sequences to amino acid protein sequences. Protein sequences were analyzed and compared for similarities between sequences. Hemagglutinin, c-Myc, and linker protein tag sequences, engineered landmarks of the scFv expression protein scaffold, were identified to ensure quality of the sequence (Boder and Wittrup 1997).

OUTCOMES

For the HGPIN selection, a representative sample of scFv-genes from the enriched post-Round 2(-), post-Round 3(-), and post Round 4(-) libraries were sequenced in order to determine the diversity of the libraries. The diversity of each library was determined by comparing scFv sequences for similarities and duplicates within the enriched libraries

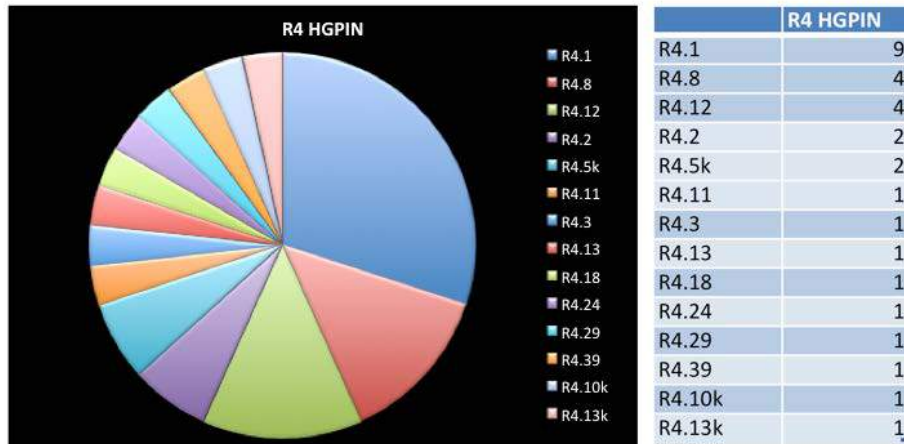


Figure 3 - MRE sequence evolution out of >30 colonies for post R4 of *in vitro* selection for the pre-cancerous cell line HGPIN. The names of scFv sequences represented by each color are shown to the right of the pie chart.

Post R4(-) HGPIN selection sequencing of scFv-encoding genes showed an enrichment of the scFv library, revealing similarities and duplicates among sequences. The post Rd4(-) population was comprised of 30% R4.1 scFv, 13% R4.8, 13% R4.12, and 3% of 13 other scFv molecules (Figure 3). This suggests that R4.1 was enriched for in the selection scheme and may be chosen as the most likely pre-cancerous prostate cell-specific MRE. Further enrichment of the library through additional rounds of SELEX will reveal the most selective MRE.

For the HGPIN Selection, four rounds of SELEX have been completed, enriching the scFv library for those which bound to the benign, high-grade prostatic intraepithelial neoplasia cell line and subtracting those that bound to other normal, benign, and cancerous cell lines RWPE-1, BPH-1 and LNCaP. Round five of SELEX is currently in progress.

For the HGPIN Selection, Round 5-(a) was most recently completed. After an scFv display induction period by amplification of post Rd 5+ yeast in SG+CAA, surface expression of the scFv library was confirmed by flow cytometry analysis. The monoclonal anti-HA tag antibody clone 16B12 conjugated to DyLight 488 and used to stain post Rd 5+ induced yeast (Figure 4).

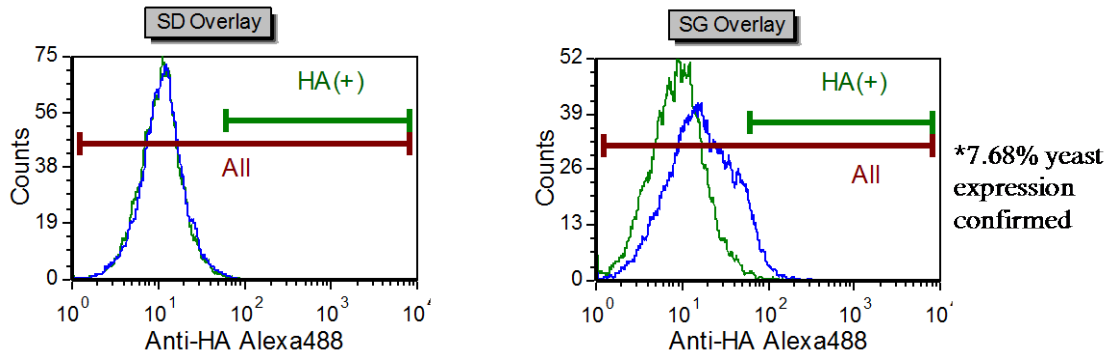




Figure 4 - SD Overlay represents scFv surface expression of Rd5 non-induced yeast. SG Overlay represents surface expression of Rd5 induced yeast.

These histograms show four, post Rd5+ yeast populations analyzed using a FACSCalibur (BD Biosciences; San Jose, CA) flow cytometer. Counts represent cell number on a log scale based on the total number of events counted. Anti-HA Alexa 488 was used to tag the HA marker of the scFv protein scaffold. The HA+ marker was set at >% 1 and served as a control; any events gated under the HA+ marker are recognized as being fluorescently tagged. The SD overlays compare non-induced yeast populations amplified in standard dextrose media. One population of yeast was untagged, and the other was tagged with the monoclonal anti-HA tag antibody. The SD- histogram represents the auto-fluorescence of the cell. There is no scFv induction or tagging here. The SD+ histogram represents a population of yeast that has had the anti-HA antibody added. There is no noticeable shift in events gated under the HA+ marker because there is no scFv scaffold being tagged.

The SG overlay shows two yeast populations amplified in standard galactose media. Under induction of the galactose promoter, yeast were induced to display the scFv marker. The SG- shows a population of induced yeast without having the anti-HA tag added. The SG+ histogram shows 7.68% of events gated under the HA+ marker; these gated events are representative of yeast confirmed as displaying the scFv protein scaffold.

Following confirmation of surface expression, Round 5(-)a of selection was performed by using fluorescence activated cell sorting (Figure 5).

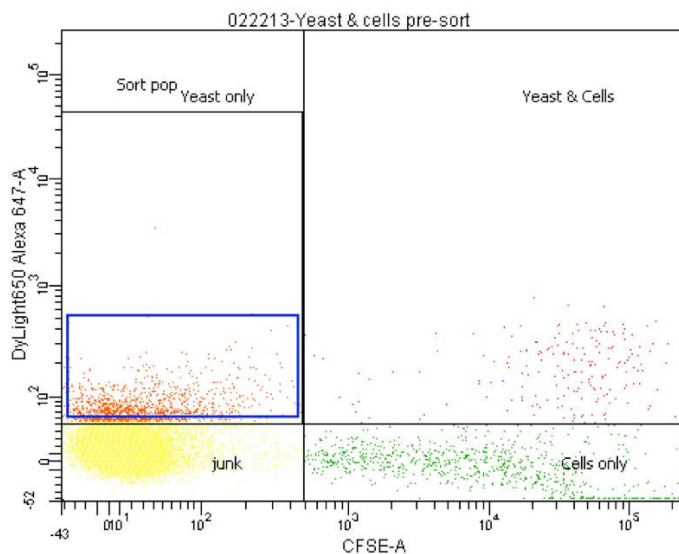


Figure 5 - Round 5(-)a fluorescent activated cell sorting of LNCaP cells incubated with Anti-HA tagged scFv displayed yeast. 6.7% of the total post-sort population was collected (Yeast only).

The sample was sorted with a FACSAria (BD Biosciences). For Round 5(-)a selection, LNCaP cells were grown to 80-90% confluence and were fluorescently dyed with CFSE (Invitrogen). In Round 5(-)a, all yeast were fluorescently dyed with AlexaFluor 647 (Invitrogen). Events identified as unbound yeast which showed single fluorescence corresponding to AlexaFluor 647 were collected and amplified. This population of yeast will be subjected to round 5(-)b of selection.

FUTURE PLANS

Further rounds of selection be performed in order to identify the most selective HGPIN cell-specific MRE. The scFv-encoding gene will be cloned into a secretion vector and be expressed. The scFv will be purified in order to conduct binding affinity assays of scFvs to cells and ex-vivo tumor tissue. Future work will focus on constructing scFv antibody-drug conjugates with fluorescent and chemotherapeutic agents. The selected scFv will be useful in future prostate cancer diagnostics and therapeutics.

ACKNOWLEDGEMENTS

I would like to thank past and present members of the Sooter Lab for their help and guidance. I would like to give special thanks to Dr. Letha Sooter and the grant provided by the NASA WV Space Grant Consortium.

REFERENCES

- Chou, R. T. Dana, C. Bougatsos, R. Fu, I., Blazina, K. Gleitsmann, and J. Ruge. "Treatments for Localized Prostate Cancer." U.S. Preventive Services Task Force Evidence Synthesis 91.1 (2011): 1-124.
- Merrimen, J., A. Evans, and J. Srigley. "Preneoplasia in the prostate gland with emphasis on high grade prostatic intraepithelial neoplasia." Pathology 45.3 (2013): 251-63.
- Moyer, V. "Screening for Prostate Cancer: U.S. Preventive Services Task Force Recommendation Statement." Annals of Internal Medicine 157.1 (2012): 120-134.
- Vickers, A., M. Roobol, and H. Lilja. "Screening for Prostate Cancer: Early Detection or Overdetection?." Annual Review of Medicine 63.1 (2012): 161-170.
- Wolf, S. "Screening for Prostate Cancer with Prostate-Specific Antigen — An Examination of the Evidence." The New England Journal of Medicine 333.1 (1995): 1401-5.

PROBE DENSITY AND CAPTURE EFFICIENCY DEPENDENCE ON DENDRIMER SIZE

Zachary Hunter*
Marshall University, Huntington, West Virginia
E-mail: hunter91@live.marshall.edu

*To whom correspondence should be addressed

ABSTRACT

Self-assembling monolayers have been a major focus for designing protein biochips and other sensors over the past few years. In this study, DNA immobilization on a gold surface using a dendrimer headgroup is analyzed, as well as how dendrimers effect the packing density of the molecules during self-assembly. Surface plasmon resonance is used to determine packing density and to analyze the monolayer's efficiency in capturing target DNA strands out of solution. The molecules used for self-assembly are synthesized using dendrimers of generation size 2-5. The robustness of the surfaces was also studied by subjecting the monolayer to 50 cycles of hybridization and dehybridization of target DNA strands.

INTRODUCTION

In recent years, there has been a major progression in the construction of protein biochips for proteomics and other biological protein analysis. Immobilization of proteins to solid supports however provides many obstacles because of the specialization of how protein binding sites interact with their environment. Recent work has suggested that DNA aptamer directed binding of proteins can overcome many of these difficulties.¹ The DNA aptamers need to be bound in a way that controls molecule density and improves durability of the surface. Moreover, because of the specificity of protein orientation, packing density must be optimized.

Previous studies have shown that DNA can be bound using a single free thiol group attachment site to gold (Figure 1(a)), however, a monolayer that is constructed using this strategy is vulnerable to desorption from the surface because there is only a single attachment site.^{2,3} During self-assembly, using DNA with a single thiol group, homogeneity of the surface cannot be guaranteed nor predicted, therefore having a reproducible surface is not likely. Previous studies have shown that DNA probe stand densities are an important factor for DNA hybridization (probe

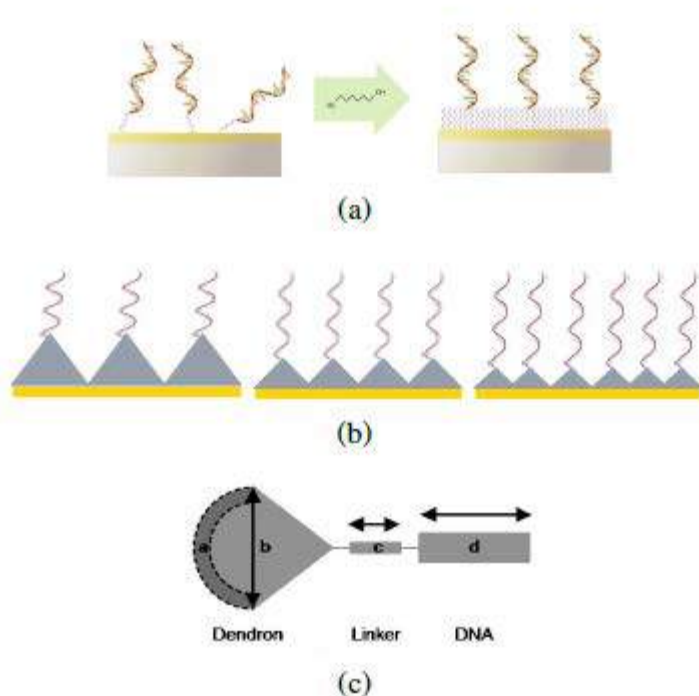


Figure 1: (a) schematic of single thiol DNA backfilled with mercaptohexanol, (b) diagram of how conjugate molecules creates a defined structure and homogeneous surface, and (c) basic schematic of proposed conjugate molecules

stands capturing target DNA strands out of solution), and unpredictable homogeneity is not conducive to density control of probe strands in the monolayer.⁴ Therefore, using DNA with a single thiol modification gives less control over the surface, which would not be beneficial when trying to use these types of surfaces as sensors. The use of dendrimers as a head group should improve the degradation problems by providing multiple attachment points (multiple thiols per dendrimer) and a structured base to control the molecular density on the surface (Figure 1(b)). Also, since dendrimers have a very defined structure, using them as a headgroup provides control of the lateral spacing between the molecules of the monolayer, therefore controlling packing density. Previous work has also shown that generation 4 (G4) dendrimers improve ligand immobilization efficiency on a gold substrate,⁵ but in this study, molecules will be synthesized using dendrimers ranging from G2 to G5, which will vary the number of thiols, and the headgroup size, which appear as (a) and (b), respectively, in Figure 1(c). By controlling the number of thiols and headgroup size, the packing density can be controlled to optimize capture efficiency.

EXPERIMENTAL

Materials

Table 1: List of materials and the company from which they came

Materials	Source
Probe DNA 5'-TAA CCA ATA GGC CGA AAT CG-3'	Integrated DNA Technologies
Complementary DNA strands 5'-TTT GGC GAT TTC GGC CTA TTG GTT A-3'	Integrated DNA Technologies
Noncomplementary DNA strands 5'-TTC AGC ATC TTG TAC TTT CAC CAG C-3'	Integrated DNA Technologies
Dendrimers (G2,G3,G4,G5)	Sigma-Aldrich Inc.
SATP (<i>N</i> -Succinimidyl- <i>S</i> -acetylthiopropionate)	ThermoScientific
SSMCC (Sulfosuccinimidyl 4- (<i>N</i> -maleimidomethyl)-cyclohexane-1 Carboxylate)	ThermoScientific
BI-200 SPR System	Biosensing Instrument Inc.
BupH phosphate buffered saline packs	ThermoScientific
Plasma Cleaner PDC-32G	Harrick Plasma

Synthesis and Functionalization

The first step in the synthesis procedure involves protecting the periphery groups of the dendrimers as these will become the binding sites for the conjugate to the gold. This can be done by reacting the dendrimer with *N*-Succinimidyl-*S*-acetylthiopropionate (SATP) to create acetate groups on the periphery (Figure 2).

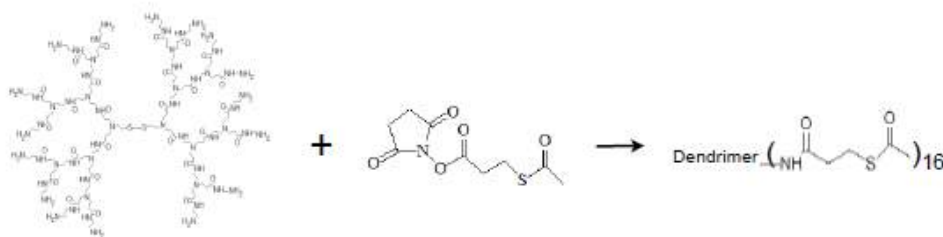


Figure 2: The amines on the periphery of the dendrimer are reacted with SATP to yield acetate groups in order to protect the periphery groups until later in the synthesis process

The dendrimer is then cleaved at the cystamine-diamine core using tris-(2-carboxyethyl) phosphine (TCEP) to create two identical dendrons (Figure 3).

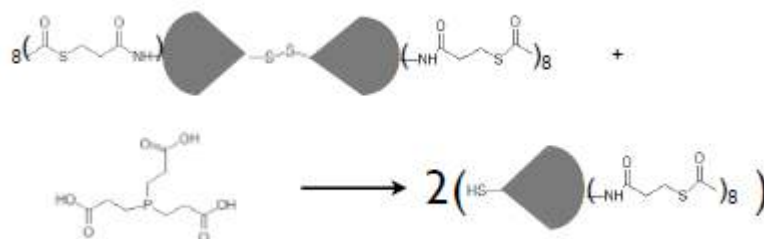


Figure 3: The dendrimer is cleaved at the disulfide core using TCEP to yield two identical dendrons

Separate from the solution of dendrons, the linker molecule, sulfosuccinimidyl 4- (*N*-maleimidomethyl)- cyclohexane-1-Carboxylate (SSMCC) is reacted with a 25 base single DNA molecule with an amine modification on the 5' end(Figure 4).

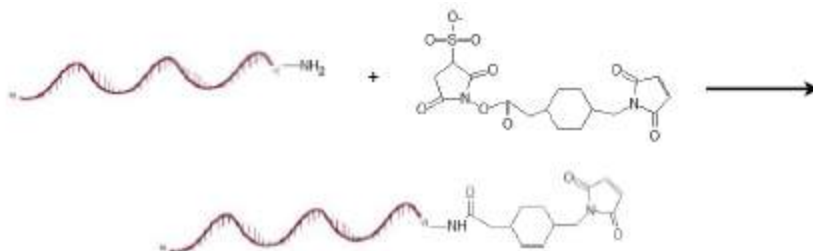


Figure 4: The linker, SSMCC, is attached to an amine terminated ssDNA

Finally, the DNA-linker complex is reacted with the dendrons to yield the proposed conjugate (Figure 5).

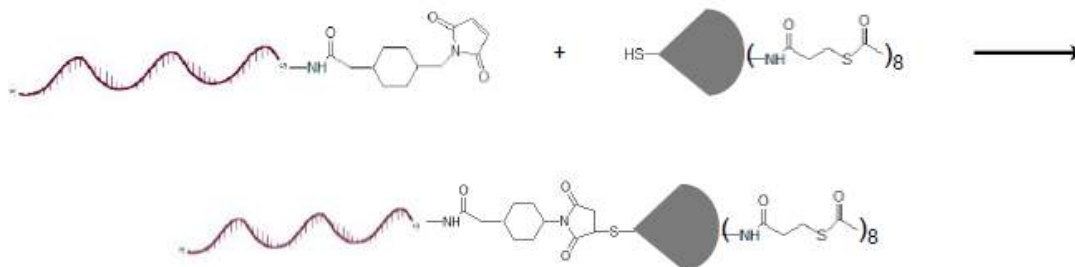


Figure 5: The dendrons and the ssDNA-linker molecules are then combined yielding the desired conjugate

The synthesis process is the same for every generation of dendrimer. Gel electrophoresis was used to separate conjugates from ssDNA by mass. The electrophoresis was conducted with 4% agarose gel, and was ran at 275 V for 15 minutes, and 20 minutes for G2. The DNA is stained with ethidium bromide so that it can be seen when exposed to UV light. Notice that in Figure 6, there are distinct bands located along the length of the gel. Since the backbone of the DNA is negatively charged, its attraction to the cathode is the driving force for the band separation. The DNA bands will travel further down the electric field due to the absence of a dendrimer, therefore a distinct band up the electric field from the DNA alone indicates a significant mass difference. These bands that contained the heavier molecules were excised from the gel and the molecules extracted. After depositing the conjugates onto a gold slide, their structure was confirmed with X-ray photoelectron spectroscopy and Grazing Angle infrared spectroscopy to confirm a successful synthesis.

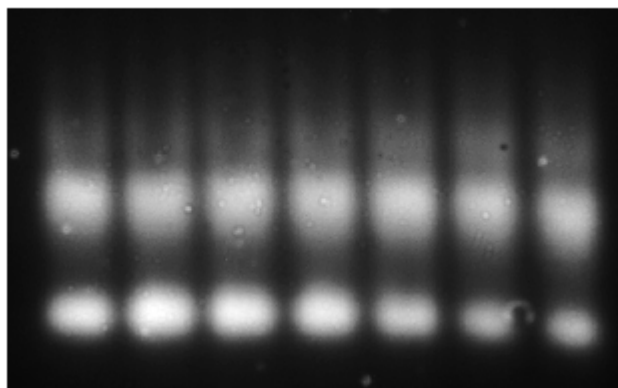


Figure 6: Image of an electrophoresis gel. Bands towards the top are successfully synthesized DNA/Dendrimer conjugates. Bands towards the bottom are just DNA strands from an unsuccessful synthesis.

After the gel bands are excised, they are allowed to soak in 10x TBE to extract the conjugates out of the gel. Before the conjugates were deposited onto a gold surface, hydroxyl amine was allowed to react with the conjugates to produce thiol groups by removing the acetate groups from the thioacetates.

FUNCTIONAL ANALYSIS

Surface Plasmon Resonance

The primary technique used to analyze the equilibrium saturation conditions of the conjugate-target strand hybridization was surface plasmon resonance (SPR). This technique utilizes the excitation of surface plasmons, and how they absorb light at different angles. A laser is focused through a prism onto the gold slide at a fixed angle. This light excites surface plasmons on the gold which absorb the incident light at a specific angle creating a band of no light in the reflected beam at the same angle at which it was absorbed (Figure 7).

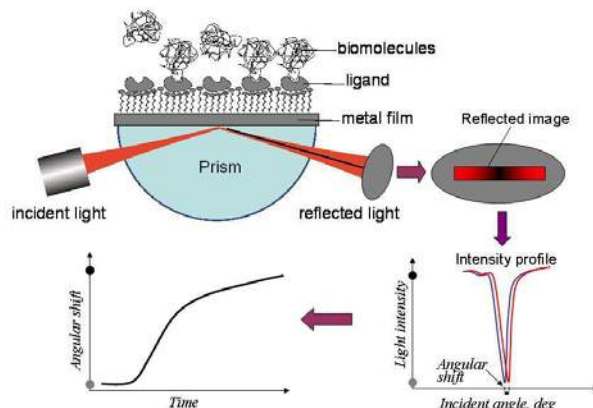


Figure 7: Graphic representation of how SPR analyzes kinetic profiles.
**Image obtained from Biosensing Instrument web page*

As the environment on and above the surface changes, the angle that is absorbed changes. Environmental change can include adsorbing the conjugate to the gold substrate, DNA probe strand hybridization with a target strand, and even changing the solution flowing above the surface. For this technique, the refractive index of any materials above the surface effect the angle at which the light is absorbed. The evanescent wave from the light penetrates through the surface and any monolayer that may be adsorbed to it, so a change in the refractive index of the solution above the surface can cause a change in absorption angle. The shift in the absorbed angle is then plotted as a function of time.

Density Calculations

The conjugate headgroup has a defined shape, therefore the packing density of the monolayer should be well defined. As the dendrimers grow in generation size, the headgroup gets larger, so the density decreases. When DNA is tethered to the gold surface using a single thiol functional group,² the density may not always be uniform, and not reproducible. The structure of a dendrimer is well defined, therefore, a uniform packing density is expected, as well as density control of the monolayer. Figure 8 confirms that packing density behaved inversely proportional to generation size. G2 conjugates produced the highest surface density of probe strands while G5 conjugates produced the lowest surface density. A conversion factor specific to the SPR changed units of mDeg to a density unit. The G5, G4, G3, and G2 dendrimers gave packing densities of $5.4 \times 10^{12} \text{Molecules} \cdot \text{cm}^{-2}$, $8.4 \times 10^{12} \text{Molecules} \cdot \text{cm}^{-2}$, $1.25 \times 10^{13} \text{Molecules} \cdot \text{cm}^{-2}$, and $1.52 \times 10^{13} \text{Molecules} \cdot \text{cm}^{-2}$, respectively. Packing density is vital to protein sensors because proteins can be very large in size, so there could be no binding if DNA probe strands are too close together. The protein may be oriented correctly, but if the probe density is too high, the active site may never be reached by the target, therefore there would be no binding.

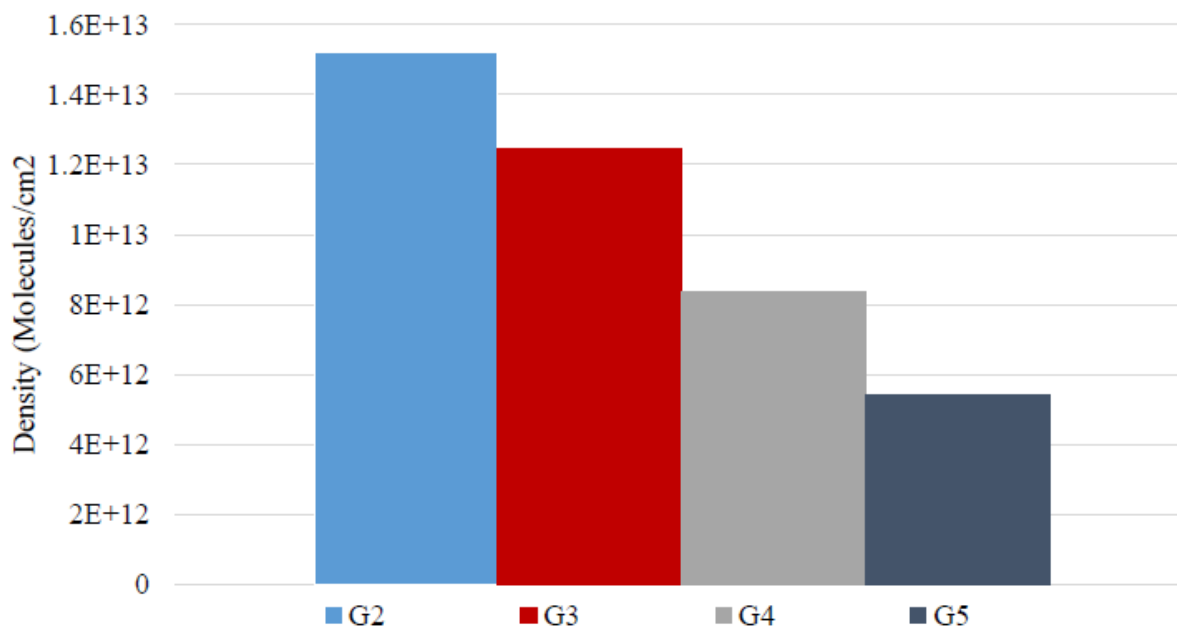


Figure 8: Probe density calculations based on SPR signal. Density is inversely proportional to generation size of dendrimer. Density values were calculated using a conversion factor specific to the BioSensing SPR ()

Measured vs. Expected Density Values

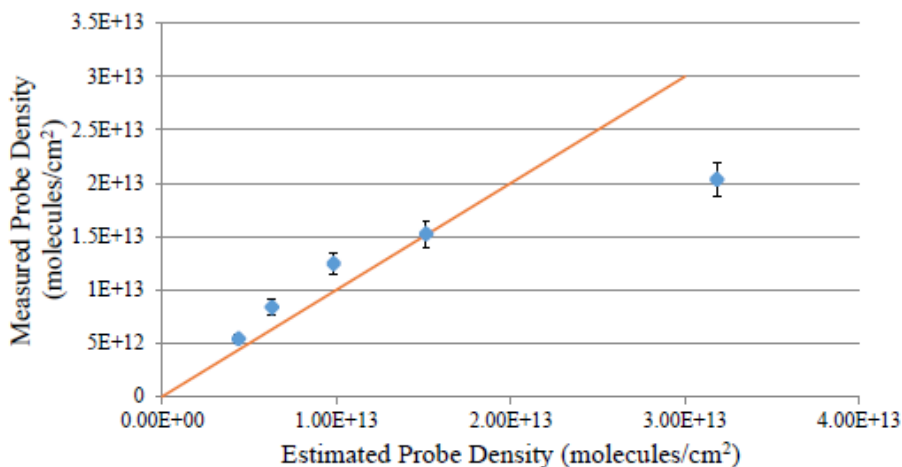


Figure 9: Plot of estimated vs. measured probe densities. Estimated densities were calculated using the hydrostatic radii of the dendrimers. The double stranded DNA estimated was made by assuming a double stranded DNA diameter of 2 nm

The dendrimers show that they can be used to control the packing density of probe DNA strands on a surface, however, the effect of the electrostatic repulsion between the DNA backbones cannot be found with density data alone. The measured probe densities are plotted against estimated probe densities to show this effect in Figure 9. The estimated values were calculated using the hydrodynamic radii of the dendrimers. Assuming the footprint of the dendrimer is the area occupied

on the surface from this radius, a theoretical density was calculated. For the single thiol DNA, a value of 2 nm was used as the diameter of double-stranded DNA. The orange line indicates a perfect correlation between measured and estimated values, meaning a measured value equal to the theoretical value calculated from the radius of the dendrimer would yield a point on the orange line. Considering the inherent error in the assumptions for the radii, and experimental error, the densities for the dendrimers correlate fairly well with theoretical values. The single thiol DNA density, however, lies well below the line. This indicates that electrostatic repulsion between the DNA backbones plays a large role in the interactions that take place during self-assembly. The use of dendrimers, however, greatly reduces the contribution of this repulsion during self-assembly because they play a dominant role in the self-assembly process, as indicated by the fact that the data point for the conjugates lie in close proximity to the orange line.

HYBRIDIZATION

The dendron headgroup of the conjugates control the packing density of the probe strand, and hybridization analysis will show if the monolayers are functioning sensors or not. Hybridization refers to the probe strand (single stranded DNA) binding its complementary strand from solution. The probe strand hybridizes the target strand out of solution. The data obtained through SPR reveal the kinetics of the adsorption of the conjugates to the gold surface, and the hybridization of the target DNA strands to the probe DNA of the monolayer. A typical hybridization cycle is represented in Figure 10.

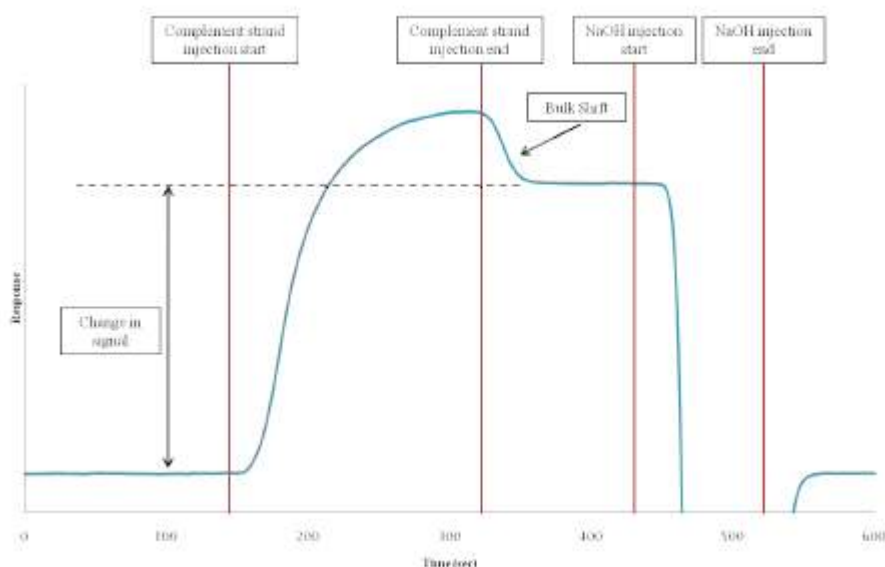


Figure 10: A representation of a typical hybridization cycle. There are five sections (from left to right) that are the various stages of the hybridization cycle. The first section is an established baseline. The next section includes the hybridization of the target stands to the probe strands, followed by a bulk shift. Sodium hydroxide is then injected into the system to disrupt the bond between the base pairs of the DNA, and the original baseline is established.

The bulk shift arises from the fact that the light penetrates through the monolayer into the solution flowing above it, so differences in the above solution changes the refractive index of the system. As hybridization reaches an equilibrium, the solution above the layer still has a concentration of ssDNA that is affecting the signal. After the injection valve is shut, the solution above the monolayer is the original buffer, so there is another small downward change in signal called the bulk shift. The difference between the baselines at about 100 s and about 400 s is the measured signal change for hybridization. Sodium hydroxide is then injected into the system to dehybridize the target strands returning the monolayer to just single stranded probe strands. Figure 11 shows hybridization curves for target strand concentrations 10 nM, 100 nM, 1 μ M, and 10 μ M.

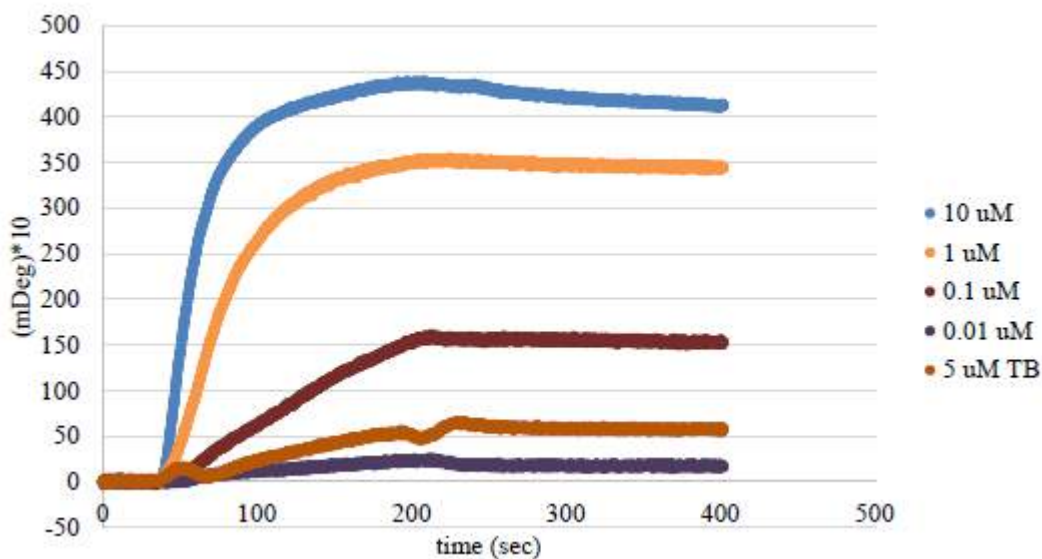


Figure 11: Hybridization profiles for G3 conjugates. Each line represents hybridization for a different concentration of target DNA. The bottom profile, 5 μ M TB is an injection of a non complementary target strand of DNA. This was used to test for non specific binding

As predicted, higher concentrations of target strands yielded a higher signal for target strand capture. Complementary strand injections of 10 μ M, 1 μ M, 100 nM, and 10 nM yielded values around 40 mDeg, 25 mDeg, 15 mDeg, and 8 mDeg respectively. This direct relationship between concentration of target strand and signal can be attributed to the probability that target strands will hybridize to the probe strands. To obtain a hybridization that is durable enough to remain until the addition of sodium hydroxide, the probe and target strand must be oriented correctly in relation to each other, and the electrostatic forces between the backbones of the DNA strands cannot be so much that they repel and are not able to penetrate the monolayer deep enough to hybridize. The electrostatic repulsion can potentially become a problem when the probe strands themselves are too close to each other. Concentrations below 10 μ M, however, appear not to reach equilibrium before the injection time over, but this is consistent through all generation sizes of conjugates. A solution of 5 μ M noncomplementary target strands were also flowed across the monolayer to test for any non-specific binding. This could include bases of the DNA strands lining up randomly or not completely, or target strands sticking to bare spots on the gold where there may have been an impurity in the monolayer. Experimentally, non-complementary yielding

response > 4 *mDeg*, which is less than 10% of the signal obtained from $10 \mu M$ complementary DNA.

Hybridization Efficiency

Packing density was found to be correlated to the generation size of the dendrimer, therefore monolayers with varying densities can be constructed. Those with a lower density of probe strands would capture less target strands out of solution than a monolayer with a higher probe strand density, assuming identical surface area. However, density calculations do not reveal any correlation to the efficiency of the surface to capture target strands out of solution. Figure 12 indicates that there is a correlation between the generation size of the dendrimer and the hybridization efficiency.

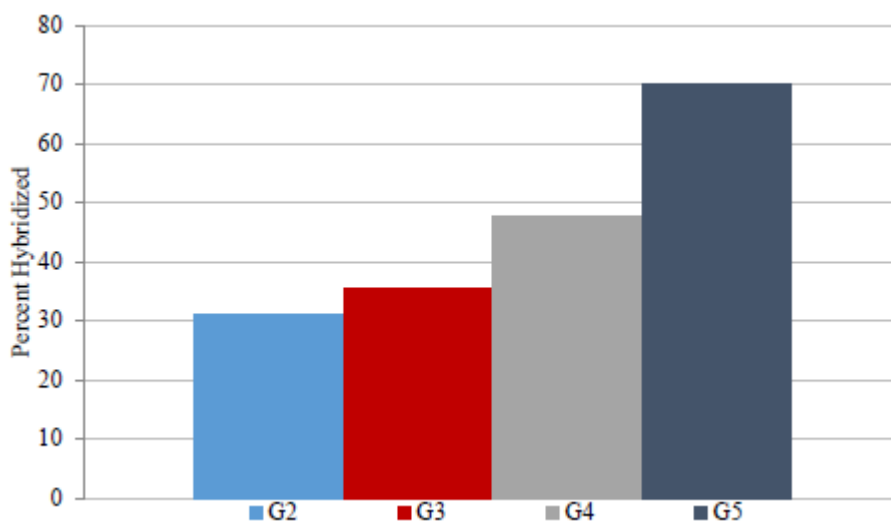


Figure 12: Target strand density and hybridization efficiency of all monolayers. Target strands decrease in density as generation size increase, as do the probe strand densities, but the hybridization efficiency increases with generation size.

These values were calculated using the technique from the density calculations since the density correlates to the number of target strands captured out of solution. Because the hybridization efficiency of the monolayer increases with generation size, there is an indication that as the probe strands become less dense, the electrostatic repulsion between the backbones of the DNA strands become less pronounced. For the single thiol monolayer, the probe strands are already tethered to the surface so close together, that trying to squeeze another negatively charged species between the probe strands to hybridize becomes very difficult. Since the probe strand density decreased with increasing generation size, target strand density should and does follow a similar trend. The hybridization efficiency, however increases with increasing generation size, so a larger percentage of the available probe strands are actually hybridizing.

Durability

Durability tests were conducted by subjecting a single surface to 50 hybridization cycles in row. Dendrimers should bind more strongly to the gold surface than singly thiolated DNA strands because dendrimers have more attachment sites. The results are plotted in Figure 13 where the percent of hybridization relative to the first hybridization cycle is plotted as a function of cycle

number. The signal was normalized to the first hybridization cycle for each surface. While there does not seem to be a solid correlation between the conjugates themselves, the plot does indicate that using larger dendrimers for tethering DNA provides more robust monolayers.

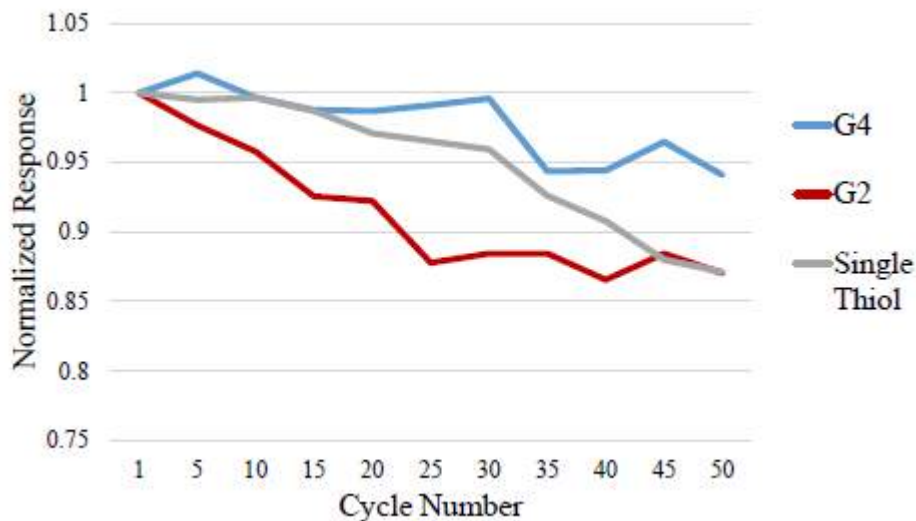


Figure 13: Durability tests conducted by subjecting the surface to 50 hybridization cycles. Single thiol and G2 conjugates were indistinguishable, however G4 dendrimers seemed to provide a more robust surface.

CONCLUSION

The development of protein biochips and other like sensors has inherently created a need to attach proteins to a surface in very specific ways. DNA can be attached to proteins which can then be adhered to a gold surface to create sensors, and biochips. The proposed conjugates provided a way to create monolayers that are more robust and allow control of lateral spacing between probe stands to control surface density. Dendrimers seemed not only to control the packing density of probe strands, but also greatly reduce the repulsive interactions between the DNA backbones during self-assembly. These systems were found to reach equilibrium in under three minutes, which would help to create sensors that can produce results very quickly. Based on the hybridization efficiency of the synthesized conjugates, G5 conjugates appear to show the most promise for binding target strands in solution most efficiently. A higher hybridization efficiency would correlate to a more sensitive surface. During hybridization cycles, the system seemed to return to its previous state after sodium hydroxide removed the target strands from the surface, indicating that the monolayers were reusable. Because of the number of binding sites on the periphery of the dendrimers, the robustness of the surfaces would be expected to increase with each successive increase in generation size. However, the single thiol DNA is indistinguishable from the G2 conjugates in that regard, and there is only about a 5%-10% increase from G2 to G4 conjugates, therefore not much can be concluded about the effects dendrimer generation size has on monolayer robustness.

ACKNOWLEDGEMENTS

I would like to acknowledge Dr. Day for allowing me to work with him on this project as well as being my advisor through my undergraduate studies. I would like to thank the NASA West Virginia

Space Consortium for funding this project. I would also like to acknowledge my peer Chris Warner who worked closely with me on this project, especially the synthesis of the conjugates. Finally, I would like to thank everyone in the Marshall University chemistry department for being supportive and helpful during my undergraduate research.

REFERENCES

- Cho, E. J.; Lee, J.-W.; Ellington, A. D. Applications of Aptamers as Sensors. *Annual Review of Analytical Chemistry* **2009**, *2*, 241–264.
- Peterlinz, K. A.; Georgiadis, R. M.; Herne, T. M.; Tarlov, M. J. Observation of Hybridization and Dehybridization of Thiol-Tethered DNA Using Two-Color Surface Plasmon Resonance Spectroscopy. *Journ. Am. Chem. Soc.* **1997**, *119*, 3401–3402.
- Franzen, S.; Brewer, S.; Anthireya, S.; Lappi, S.; Drapcho, D. The Effect of Surface Probe Density Hybridization on Gold Surfaces by Polarization Modulation Infrared Reflection Absorption Spectroscopy. *Langmuir* **2002**, *18*, 4460–4464.
- Peterson, A. W.; Heaton, R. J.; Georgiadis, R. M. The effect of surface probe density on DNA hybridization. *Nucl. Acids. Res.* **2001**, *29*, 5163–5168.
- Mark, S. S.; Sandhyarani, N.; Zhu, C.; Campagnolo, C.; Batt, C. A. Dendrimer-Functionalized Self-Assembled Monolayers as a Surface Plasmon Resonance Sensor Surface. *Langmuir* **2004**, *20*, 6808–6817.

EFFECT OF OMEGA 3 FAT DIET ON OBESITY IN ANTIOXIDANT MICE

Melissa Massie
BS Nursing
Marshall University
Huntington, WV, 25755

ABSTRACT

Oxidative stress plays an important role in obesity. My mentor's laboratory was interested in studying the mechanisms that relates oxidative stress to obesity. For this they use the animal that has higher antioxidant enzyme, catalase. Higher antioxidant levels might inhibit obesity risk. I used the catalase transgenic mice and its parent strain in my studies. These mice were divided into three groups and fed either normal diet or high fat diet or diet containing high omega 3 fat. At the end of 6 weeks I sacrificed the mice and collected blood and fat tissue. I measured the levels of factors that are secreted from the fat tissue into the blood (adipokines) using a commercial protein array. I also isolated mRNA from the fat tissue obtained from these mice and measured the expression levels of genes that play a role in obesity such as leptin, adiponectin and Peroxisome proliferator activated receptor gamma (PPARg). My results found that both adiponectin and PPARg levels were higher in catalase mice compared to parent mice and this level was further increased with diets. However, leptin level was already much higher in catalase mice on normal chow which was lowered by omega 3 diet. My data shows that there are differences in the fat derived factors between catalase and normal mice which can be influenced by diet. More studies are needed to understand this in relation to obesity.

INTRODUCTION

Statement of Problem:

Oxidative stress is an increase in oxygen and nitrogen derived free radicals (eg. superoxide radical, hydrogen peroxide, nitric oxide) that react with lipids, carbohydrates, proteins and nucleic acids to form oxidized compounds. The body protects itself from oxidative stress through its antioxidant defense mechanisms. Some of the well known antioxidant defense mechanisms are the endogenous antioxidant enzymes such as superoxide dismutase (the enzyme that scavenges/removes superoxide radicals), glutathione peroxidase and catalase (the enzyme that scavenges/removes hydrogen peroxide). An imbalance between oxidative stress and antioxidant defense results in disease. Oxidative Stress is responsible for several chronic diseases including cardiovascular disease and obesity.

Our laboratory is interested in studying the role of oxidative stress and diet in obesity. Obesity is a condition where there is an increase in body fat which leads to changes in lipid and glucose metabolism. Eating high fat diet can increase risk to obesity. Studies from our laboratory has shown that hydrogen peroxide (one of the major oxidants generated in the body) alters the function of fat cells (adipocytes). We hypothesized that if we increase the levels of *Catalase* an antioxidant enzyme that degrades hydrogen peroxide, it should prevent the damage to fat cells due to hydrogen

peroxide. In our laboratory we have access to a transgenic mouse model that expresses high levels of human catalase enzyme [Tg(CAT)⁺⁰] which is a good model to study our hypothesis.

METHODS

Male Catalase transgenic mice are available in our laboratory. Our laboratory has a Marshall University IACUC protocol approved for both the breeding of the mice and the use of these mice in experimental study. I helped breed the catalase transgenic mice (these mice have 2-4 fold higher catalase in various tissues compared to the normal mice). After adequate numbers of male catalase transgenic mice (total n=12) at the age of 16 weeks were available, I randomly assigned them into three groups. In addition to the mice that were generated in our animal facility, I also purchased age-matched male C57Bl mice (16 weeks n=4-6) from Jackson Laboratory. These mice are the parent strain of the catalase transgenic mice and will represent the control group with normal levels of catalase.

After the mice were available in our animal facility, I randomly assigned these mice to three groups of diet: (i) normal mouse chow (NC) diet (ii) High fat (36% fat from lard) diet and (iii) high omega-3 rich (36% menhaden oil) diet. The normal mouse diet is available in our animal facility. The high fat (HF) diet and the high omega-3 (OM3) diet were purchased commercially from Research Diets Inc (New Brunswick, NJ). We had four mice in each cage. Each cage was provided approximately 100 gm of diet for each week. I weighed 100 gm of diet and put them in the cage at the beginning of each week (Monday). At the end of each week, I measured the amount of diet left in each cage, to determine how much diet was consumed by the four mice in each cage that week. This will determine the weekly food consumed. I then provided them fresh 100 gm of diet. I did this for the 6 weeks of study.

In addition to weighing the diet, I also weighed each mouse at the beginning of the study and after that each week for the 6 week study period. This will determine the weekly weight gain of the mice.

At the end of 6 weeks, with the help of my mentor and other laboratory assistants, all mice were sacrificed and blood and fat tissue were collected from each mouse. The blood was collected in heparin. I spun it immediately to separate the plasma, which was aliquoted and stored separately. The total fat removed from the animal was weighed. I aliquoted 100 mg of fat tissue in a test tube containing TRI reagent that was used later for isolating RNA.

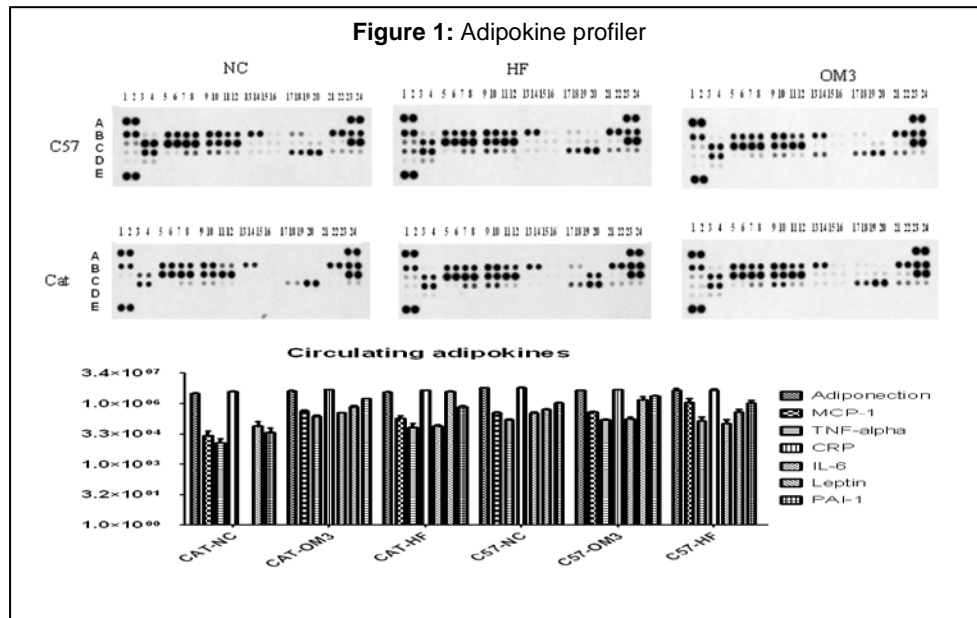
EXPERIMENT

Two specific aims were tested:

Aim 1. Effect of diet on circulating adipose derived factors in catalase transgenic mice:

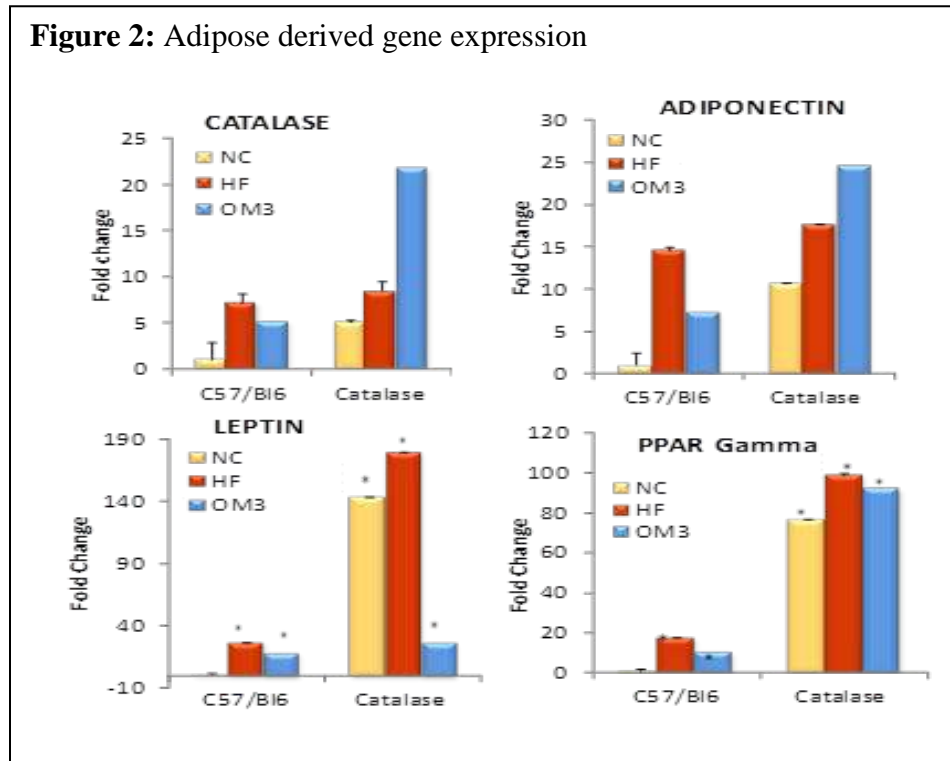
Oxidative stress plays a role in obesity. Our hypothesis was that the catalase transgenic mice because of its high levels of catalase will have lower obesity markers compared to control mice. It is also well known that high fat (HF) diet increases risk to obesity and omega 3 (OM3) rich diets is heart healthy. We determined the effect of both these diets on normal and catalase transgenic mice. In the first aim, I used the plasma that I obtained from the six groups of mice at the end of the 6 weeks study. I used commercially available Proteome profiler mouse adipokine array kit (R&D systems), that measures 38 different obesity related adipokines in the plasma obtained from various groups of mice. 25-50 µl of plasma from each mouse (n=4) was run on this array. The

density of each protein band was quantitated after densitometry scanning. Prism program was used to calculate statistical differences between the various groups. As seen in **Figure 1**: there was presence of several adipokines in both the groups. The Catalase transgenic mice on normal chow (NC) had the lowest levels of the pro-inflammatory cytokines compared to Cat- mice fed OM3 of HF.



Aim 2. Effect of diet on adipose tissue gene expression in catalase transgenic mice: During obesity there are changes in gene expression in adipose tissue. I was interested in studying differences in gene expression in fat obtained from C57BL and catalase transgenic mice fed NC, HF or OM3 diet for six weeks. For this aim, I used the 100 mg of adipose tissue that was stored in TRI reagent (Sigma) at the end of the study. I followed the manufacturer's instructions on how to isolate RNA from tissues using TRI reagent (Sigma). After isolating RNA from all the mice (n=24), I measured the total RNA amount using nanodrop. I then measured 1 micrograms of total RNA to perform the reverse transcription reaction to convert the RNA to cDNA. For this I used the Bio-Rad cDNA synthesis kit. After converting RNA to cDNA I performed real time PCR using the BioRad Sybr green kit to measure the levels of (i) catalase (ii) adiponectin (iii) leptin and (iv) PPARg in the adipose tissue in all animals. I used beta-actin as the house keeping gene. For real time PCR analysis I used primers for each of these genes and Sybr green kit and measured levels in MyIQ Biorad system. The C57bl mice fed normal chow was used as control for all calculations. The change in gene expression was calculated using the Pfaffl equation. Prism program was used to calculate statistical differences between the groups.

Figure 2: Adipose derived gene expression



In **figure 2**, I showed the changes in four genes that I measured in the adipose tissue obtained from the C57Bl and catalase mice. Catalase is the antioxidant gene that helps detoxify hydrogen peroxide (an oxidant). I measured catalase to show the differences in the levels of this gene in the control and catalase transgenic mice. As seen in the figure 2, the Catalase mice had at least 4 fold higher level of catalase in adipose tissue compared to C57 mice. Upon feeding HF diet the levels increased in both C57 and catalase mice, however, when fed with OM3 diet, the levels decreased in C57 mice but increased nearly 20 fold in catalase mice.

When adiponectin and leptin the two genes that are produced by adipose tissue was measured, there was differences in their levels in the two groups of mice. Both adiponectin and leptin were higher in catalase mice. Leptin was several fold higher in catalase mice. HF diet increased the levels of both adiponectin and leptin in C57 mice but the increase was not that dramatic in catalase mice. However, OM3 diet increased adiponectin in catalase mice but lowered in C57 mice. In contrast the leptin gene was lowered significantly in catalase mice.

Participating in this project gave me an opportunity to understand what biomedical research is and actually get to participate in it. I was able to learn several techniques that are used in biomedical research. The topic of the project on obesity was very interesting to me and was very apt to the West Virginia population. I will certainly be able to use this experience in my future career as a nurse practitioner.

DISCUSSION

My studies thus far showed that the catalase gene was higher in catalase transgenic mice and its levels increased further with diet, especially with OM3 diet. In contrast the beneficial adipokine

adiponectin levels increased significantly and leptin (the adipokine that regulates food intake) decreased significantly when catalase mice were on OM3 diet. My studies suggest that increased catalase levels certainly alter obesity markers and this can be manipulated by diet.

FUTURE PLANS

Further studies to understand the mechanisms involved in the changes in adipokine genes will be pursued. Also, since food intake and expenditure is regulated by hormones produced by adipose tissue which acts on brain satiety center, the future studies in my mentor's laboratory will try to focus on changes in satiety genes in the brains of these animals.

ACKNOWLEDGEMENTS

This project was partially supported by NIH Grant 5P20RR016477 to the West Virginia IDeA Network for Biomedical Research Excellence and NIH R01 HL074239. I thank and acknowledge the undergraduate grant that was funded to me by the NASA West Virginia Space Grant Consortium without which I would not have been able to participate in the biomedical research in my mentor's laboratory. I thank profusely the guidance and support of my mentor Dr. Nalini Santanam not only for giving me this opportunity to do research in her laboratory but also for constantly guiding me through research and academics. I thank Ms. Carla Cook, the research assistant in Dr. Santanam's laboratory for teaching me the basics of bench research and for helping me with all the techniques used in this study. I thank the other undergraduate students Akhil Gudivada and Noah Mitchell for their input and assistance.

CELL CULTURE BIOASSAY DEVELOPMENT FOR *PRYMNESIUM PARVUM* TOXINS

Brianna Mayfield
Biotechnology Major
Marshall University
Huntington, WV 25755

ABSTRACT

Prymnesium parvum, or golden algae, has made a significant impact on waters across the United States since the first documented outbreak in 1985. This 10µm diflagellated alga excretes toxins able to prevent gilled organisms' ability to absorb oxygen into the body and, ultimately, cause organismal death. This invasive type of algae is found in high salinity waters (approximately 3,000mS/cm) but have been seen migrating into rivers and streams with a lower salinity (2,500-1,500 mS/cm). *P. parvum* may excrete toxins when under stressful environmental conditions or lay dormant until such an environmental influence arises. In order to understand the genetic components and environmental triggers of such a harmful aquatic species, *P. parvum* must be thoroughly studied through a broad range of techniques. *P. parvum*, received from University of Texas at Austin Culture Collection of Algae (strain UTEX LB 2797), was examined using controlled toxins to understand the excreted toxicity factors. Alga was maintained in a room with limited access and a strict containment protocol that was carried out in order to not contaminate surrounding waters. A cell lysis assay using the RTgill W-1 cell line (ATCC® CRL-2523™) tested the cytotoxicity of algae secretions that eludes to the process of which in-vivo cells undergo in the toxic environment. Additionally, a larval fish assay was administered to determine ichthyotoxicity. This experiment assessed algal toxicity and the factors that are associated with harmful algal blooms in order to better understand the nature of this aquatic invasive species.

INTRODUCTION

Prymnesium parvum, golden algae, is an invasive species of algae that has been found in numerous lakes and inland waters around the United States. This specific species of algae is known for its ability to secrete toxins that account for massive fish kills—the most recent being Dunkard Creek, West Virginia. *P. parvum* is known to secrete multiple types of toxins, including prymnesins, hemolysins, and stearadonic acids. A specific type of toxin, called ichthyotoxin, kills aquatic life when administered into the water by making the gills impermeable to oxygen and ultimately susceptible to secondary illnesses that may cause death (Sellenave, 2). These toxins are able to eradicate an entire body of water of its aquatic life using one or a combination of these toxins. *P. parvum* toxicity triggers are unspecified but can be assumed to be associated with the manipulation of factors such as nutrient availability, salinity, light, temperature, pH, biotic factors, or a combination of such (Manning and La Claire II, 681-683). This experiment analyzes the complex interactions between toxicity and water conditions in laboratory conditions as a three part model. The effects of temperature, ion concentration, and pH are monitored in relation to varying levels of salinity in order to analyze the most common threats to *P. parvum* infested waters.

P. parvum's first domestic find occurred in the Texas Pecos River in 1985 and was the cause of millions of fish deaths along 926 miles of water (James and De La Cruz, 429). Since this outbreak, *P. parvum* has spread throughout the United States inland waters moving northward to lower salinity waters. The most recent contaminated states are Pennsylvania and West Virginia (Cosco, K.). The most prevalent outbreak of *P. parvum* in West Virginia was seen at Dunkard Creek in 2009, killing thousands of aquatic organisms and significantly depleting the fish count for many years after infestation. Because of this harmful algal outbreak at Dunkard Creek, an excess of \$6 million was spent to combat the negative effects such as water contamination, minimal fish counts, and afflicted surrounding wildlife (Cosco). In Texas, *P. parvum* accounted for 17.8 million fish deaths that have ultimately cost fish hatcheries and parks around the state an average of \$150 million annually (Ralph, et al). *P. parvum* is the culprit for extreme economic and ecological impacts throughout the United States from 1985 and are estimated to only continue this detrimental degradation of our waters.

P. parvum poses an extreme challenge to not only commercial fish hatcheries, but to the ecosystem in its entirety. With lack of knowledge on the *P. parvum* toxin triggers, a harmful bloom may arise and there will be minimal understanding how such a bloom was produced. This research aimed to assess environmental triggers so individuals can accurately prepare for algal blooms and understand the damaging capabilities of this algal species. The use of a larval fish assay analyzed the *P. parvum* ichthyotoxins and shed light on the environmental triggers that allow for production of such toxins (Bertin, Zimba, et al). Once the toxin data is thoroughly analyzed, a bioassay will be produced in the preparation to assess the cellular effects a harmful algal bloom in surrounding areas such as Dunkard Creek, WV. Such research will not only aid in the understanding of this harmful alga, but will be able to allow for prediction of harmful algal blooms and; thus, ecologically and economically saving millions.

PROJECT

Objective 1: Obtain *P. parvum* from the University of Texas at Austin Culture Collection of Algae (strain UTEX LB 2797) and optimize conditions for reproduction.

- Assist in growing *P. parvum* to grow and thrive in laboratory conditions.
- Once conditions are optimized, a larval fathead minnow assay, sheep red blood cell assay, and a rainbow trout fish gill cell assay will be used to determine toxicity.

Objective 2: Obtain RTgill-W1 cell line (ATCC[®] CRL-2523[™]) and optimize culture and bioassay conditions for these cells in the Murray lab.

- In-vitro fish gill assay will aim to support the presence of cytolytic capabilities of *P. parvum* toxins.

Objective 3: Perform bioassays to determine toxicity of *P. parvum* media once induced by three common environmental triggers.

METHODS

Algal Culture

P. parvum was purchased through the University of Texas at Austin Culture Collection of Algae (strain UTEX LB 2797). Cultures were kept in a non-vented HEPA filtered biosafety hood throughout culturing. Stock cultures were grown in artificial sea water media with f/2 nutrients (UTEX) and loosely covered with plastic wrap to deter media evaporation while allowing gas exchange. Cultures were continuously kept on a shaker at 70 rpm and a light cycle of 12h light/12h darkness at an irradiance of $50\mu\text{mol}\cdot\text{m}^{-2}\cdot\text{s}^{-1}$. Media was changed every week by pouring off media from top of beakers and replacing with fresh f/2 saltwater media. Established stock conditions consisted of a pH of 7.2, salinity of 3,000 mS/cm, and a temperature of 22°C.

RTgill W-1 culture

The rainbow trout gill (RTgill W-1) cell line was purchased from ATCC® (CRL-2523™) to examine the cytotoxic effects of *P. parvum* toxins in varying abiotic conditions. Once the cells arrived, they were immediately thawed and administered to a NUNC® 25cm³ non-vented flasks containing Leibovitz's L-15 medium (ATCC® catalog no. 20-2008) with a 10% fetal bovine serum and 1% penicillin-streptomycin antibiotic treatment. A ReptiPro 5000 incubator was used to culture cells at 19°C with 100% air intake. Humidity controls were added to the incubator to prevent media evaporation. Non-vented flask caps were loosened slightly to allow gas exchange. Cells were cultured in NUNC® 75cm³ vented flasks in 15mL of prepared media. During the first week of culture, the media was changed twice by aspirating the fluid from the flask and adding a fresh 15mL of prepared L-15 media to replenish nutrients. After the first week, the media was changed once a week when passaging cells. Flasks were passaged by trypsinization at 80% confluency and split at a 1:3 ratio to promote further growth. When mycelial contamination occurred, the flask was taken to a separate room and the contents were bleached to prevent additional contamination.

Toxicity Induction

P. parvum cultures at a conductivity of approximately 3,000 mS/cm were induced once cell counts reached approximately 2×10^5 cells/mL. Toxicity was induced by three different abiotic factors: pH, temperature, and ion concentration. Each abiotic factor test contained an examination of six experimental beakers and one control beaker. Before induction, water chemistries including temperature, conductivity, pH, and dissolved oxygen were performed to analyze the pre-induction conditions of each sample. Toxicity by increased ion concentrations was induced by adding 1mL of 1M MgSO₄ and 1 mL 1M CaCl₂ to experimental beakers and covering from light for 1 hour. Toxicity by pH was induced by increasing the pH of experimental beakers by one exponential pH degree and covering from light for 1 hour. Toxicity by temperature was induced by covering experimental beakers completely with ice and covering from light for 1 hour. After one hour, the algae media was poured into centrifuge tubes and centrifuged at 2,000 rpm for 10 minutes to produce a pellet of debris. Media was decanted for bioassays and pellet was obtained for future analysis via Next Generation Sequencing. Media was stored for future assay testing.

Hemolytic assay

Sheep erythrocytes (Sigma E9383) were reduced to 1×10^7 using a homogenized buffer media (HBM media). HBM media was prepared by diluting RPMI 1640 culture medium (Sigma R8758) by 10% with distilled water and adding 0.005 mg/mL sodium heparin (Sigma 84020) to use as an

anticoagulant. Media from each induction level was obtained as experimental samples, Triton-X100 was used as a positive control, and HBM media was used as a negative control. 330 μL of erythrocytes were added to 1.5 mL Eppendorf microcentrifuge tubes and serial dilutions of each sample were added as follows: 25%, 12.5%, 6.25%, 3.125%, 1.56%, and 0.78%. Microtubes were covered from light and kept at ambient temperature for 1 hour. All tubes were then centrifuged at 1,500 rpm for 10 minutes at 23°C. After centrifugation, the top 200 μL of media was added to a sterile 96 well plate and read at 450nm in a BioTek plate reader to analyze % hemolysis.

Larval fathead minnow assay

Larval fathead minnows (<48h) were obtained from Aquatic Research Organisms Inc. one day before estimated toxicity induction. Seven 6-well plates were used for the assay: 6 experimental media samples and one control were labeled for each plate. Serial dilutions of 25% used in the hemolytic assay were prepared using EPA water to dilute each sample of media. Each well of the 6-well plate held 10 mL of the respective serial dilution and media replicate. Once all media dilutions were added to the plates, 4 larval fish were added to each well. Fish were analyzed every 24 and 48 hours for death.

RESULTS

Analysis of algal culture

After optimizing culture conditions, different algal temperaments were detected when conductivity levels were adjusted. At a salinity of 3,000 mS/cm, algae displayed erratic temperament by moving through water and bumping into other moving algae cells. The cells were visually oval-shaped (Figure 1) and both flagella were interactive with surroundings. This conductivity level displayed no signs of distress for the algae and functions were environmentally advantageous. An increase in nutrient consumption was seen as well as an increased ability to combat other microbial colonies such as rotifers. When the conductivity was decreased to 1,400 mS/cm, algae displayed less erratic and seemingly lethargic movements with a decreased interaction with surroundings. The cells adapted to the conductivity change by curving the cell membrane inwards to form an S or figure-8 shape (Figure 2). This salinity level showed an increase in cysted cells as well as lysed cells. Cannibalism was documented in many cases as a proposed form of survival. This suggests that *P. parvum* benefits more at a conductivity of 3,000 mS/cm opposed to lower salinities.



Fig. 1 - Photo of *P. parvum* cell at 3,000 mS/cm salinity displaying an oval-shaped membrane.



Fig. 2 - Photo of *P. parvum* cell at 1,400 mS/cm displaying a figure-8 shape membrane.

RTgill W-1 Culture Analysis

RTgill W-1 cells showed an increased risk of mycelial contamination throughout the culturing process. Cells were maintained in vented flasks and antibiotics were administered to each media change. However, contamination continued to grow throughout the cultures. Interestingly, the contaminated areas seemed to attract cells rather than repel them (Fig. 3). It was proposed that the reagent Phosphate Buffered Saline (PBS) used when passaging cells was the cause of contamination. In order to combat this fungal growth, all cell culture reagents were filter sterilized for any contaminants. In addition to the penicillin/streptomycin included in the prepared L-15 media, Amphotericin B was administered at a quantity of 1mL per liter of media. Shortly after administration, there was a steep decrease in contamination colonies. Cells were cultured for two weeks and thoroughly analyzed for contamination before performing cytolytic bioassays. When performing a routine check for contamination on a Zeiss Axio Observer.Z1 microscope using high magnification, it was observed that the proposed contamination colonies were masses of overgrown cells. To combat this issue, cells were trypsinized for an additional 3 minutes and pipetted up and down to disperse clumped cells. A photo of adhered, non-contaminated cells 1 day after passaging can be seen in Figure 4. After two weeks of no apparent contamination, preliminary cytolytic bioassays commenced.

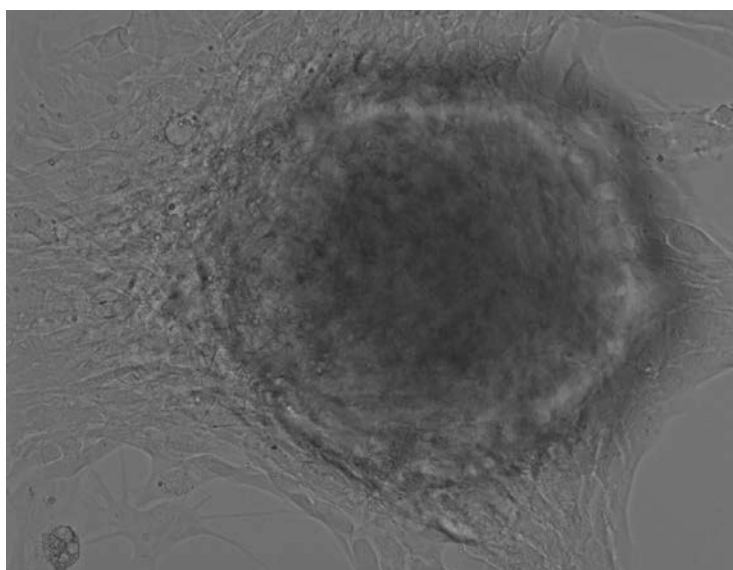


Fig. 3- Proposed mycelial contamination of RTgill W-1 cell culture.

Hemolytic activity

Data from the bioassay were read at a number of wavelengths and examined. A wavelength of 450nm was found to be most productive because hemolytic samples generally have greater than normal spectrophotometric absorbance. All media from each exposure factors were seen to lyse the sheep erythrocytes in relation to the control sample (two-way ANOVA, $p\text{-value}=3.1\text{E-}23$). The

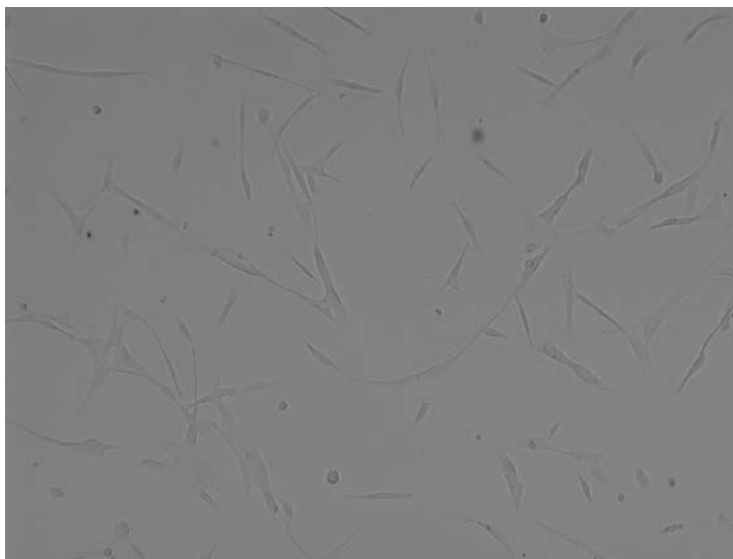


Fig. 4- RTgill W-1 cell culture 1 day after passaging.

P. parvum media generated a uniform and dose-dependent trend at this wavelength (Fig. 5). However, the % lysis to media exposure relationship showed that there was an increase in lysing capabilities as the dosage decreased. Additionally, there was a significant decrease in the lysis potency of the pH media exposure (two-way ANOVA, p -value= $8.62E-07$) in relation to the temperature and ion concentration exposures. Data obtained suggests that all three media exposures contain hemolysis attributes but increased ion concentrations and decreased temperatures can cause a more detrimental effect on aquatic life in the area.

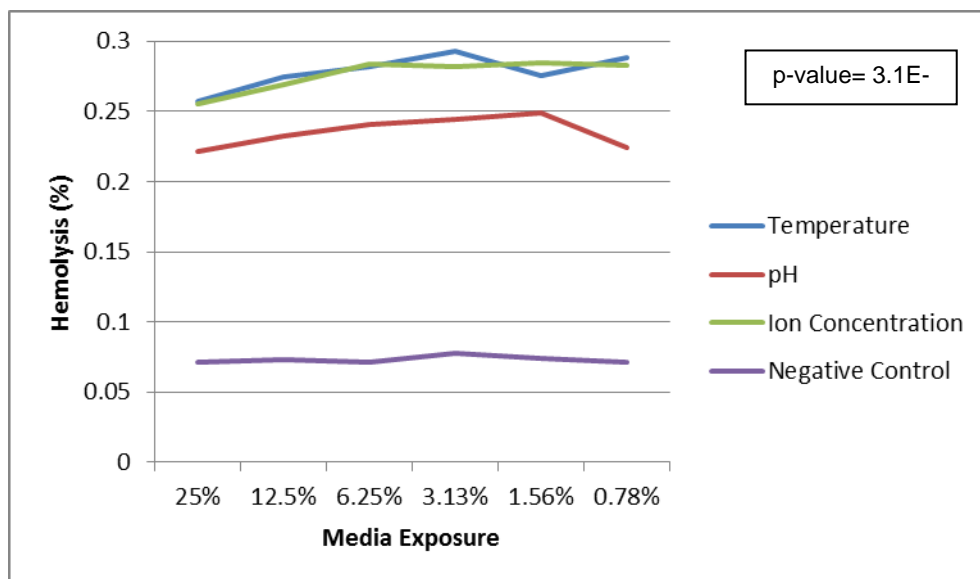


Fig 5- Sheep erythrocyte hemolysis effects from three *Prynnesium parvum* toxic media exposures. Hemolysis increased with all exposure factors but temperature and ion concentration factors yielded more hemolytic activity.

Larval Fish Viability

The larval fathead minnow bioassay, regardless of media exposure type, showed a distinct increase of death when compared to the control media. Fish survivorship data was attained by averaging all 6 experimental data sets and the second day data is presented in Figure 6. As seen by the data, fish survivorship substantially decreases at higher media concentrations (one-way ANOVA, p -value=

1.72E-12). However, lower media concentrations showed sustained survivorship at the end of day 2. Ion concentration and pH exposures yielded substantially significant survivorship curves where both follow the trend that ion concentration expresses in the graph. There was a significant decrease in fish survival in relation to control samples (one-way ANOVA, p-value= 1.29E-30). The data attained suggests that each media exposure factor linearly decreases fish survivorship with an increase in toxic media.

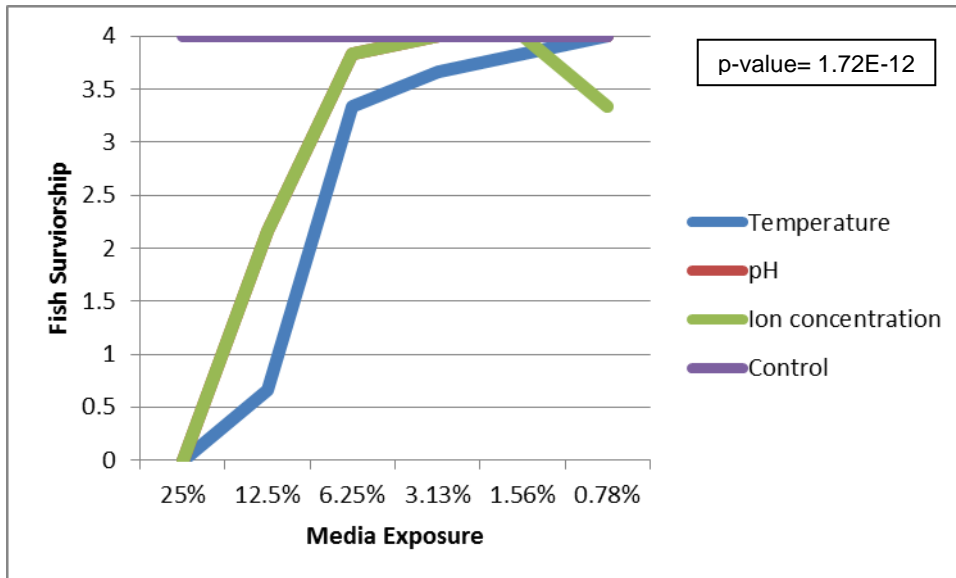


Fig 6– Fish survivorship when media was applied from three *Prymnesium parvum* toxic media exposures. Fish mortality was observed with all exposure factors. The dose-dependent relationship suggested that as media concentrations increase, fish survivorship decreases.

DISCUSSION

Attained data has shown *P. parvum* toxins produce hemolytic and ichthyotoxic effects when induced by either an increase in pH, an increase in ion concentration, or a decrease in temperature. Hemolytic capability was seen to increase with decreasing concentrations. Ichthyotoxicity increased with an increasing concentration of media. It was found that all toxicity exposure factors attributed to toxicity in at least one form. These toxins can potentially be seen during a harmful algal bloom (HAB) that consist of highly increased numbers of deceased aquatic life. However; the data cannot conclude that all harmful algal blooms HABs will produce the same results. There are many environmental factors that have not been examined in this study that may result in toxicity. There are still unknown toxins that may also contribute to aquatic deaths at the time of a HAB. Further analysis of toxins and constituents of such should be researched.

CONCLUSION

Toxicity induction by a change in ion concentration, temperature, and pH increase the probability of *P. parvum* excreting toxins into the water. Presence of a hemolytic toxin may produce an increase in fish mortality by internal bleeding. An ichthyotoxin may also be produced environmental factors chance that can directly attack the gills of aquatic life. This specific toxin also increases in potency as the concentration increases. It can be concluded that a combination of such induction factors will be unfavorable in the environment for fear of an on-site algal bloom. This bloom could cause the majority of aquatic life to then die due to multiple toxins present. Further research of environmental factors is needed to verify data attained from this study. Future research will analyze the toxic effects of water chemistry when *P. parvum* is cultured constantly

in media altered by pH, temperature, and conductivity levels. Cytotoxicity will also be researched as a possible constituent in fish mortality by gill collapse.

OUTCOMES

Through the gracious funding of the West Virginia NASA Space Grant Consortium, I have been able to learn and understand multiple bioassays that I would have otherwise been unable to perform. This funding has allowed me to work directly with an invasive species and analyze many different characteristics in a short amount of time. With the help of my mentor and my partner graduate student, I have learned many necessary techniques in the laboratory such as proper safety protocols, proper containment of an invasive species, and useful procedures when performing bioassays. The knowledge gained from this experience will most definitely translate to aid my professional career in microbiology and toxicology. With the tremendous support of Marshall University and the NASA Space Grant Consortium, I am pleased to submit this final paper with the hopes of continuing even more research later.

FUTURE PLANS

Research on algal toxin constituents will continue using a number of mechanisms. SDS-PAGE and HPLC will be run on all frozen toxins in this project. Next Generation Sequencing will also be run on algal cultures before and after induction to different salinities and different environmental factors to assess any genetic changes between factors. A three part bioassay containing CFDA-AM, alamar blue, and neutral red analyses will be completed to further identify *in vitro* significance of *P. parvum* toxins opposed to *in vivo* fish models. Comet bioassays using the RTgill W-1 cell line will be fully analyzed and applied to the further understanding of *in vitro* toxicity.

ACKNOWLEDGEMENTS

I sincerely thank the West Virginia NASA Space Grant Consortium Undergraduate Fellowship for their support during this project. I thank Amy Parsons-White for assistance with culturing and bioassay development and her mentor Dr. Mindy Yeager-Armstead for additional funding and support. Throughout this research, my mentor, Dr. Elizabeth Murray, has been a constant help with any questions or concerns. I also thank the Marshall University Summer Undergraduate Research Experience for startup funding and initial support. Without the aid of the above individuals, I would not have been able to complete this research and learn the many techniques that I now know today.

REFERENCES

- Bertin, Matthew, Paul Zimba, et al. "Identification of toxic fatty acid amides isolated from the harmful alga *Prymnesium parvum* carter." *Harmful algae*. 20. (2012): 111-116. Print.
- Cosco, K. Kathy. "Pa., WV. DEP alert residents of golden algae in private pond." *www.dep.wv.gov*. West Virginia Department of Environmental Protection, 17 May 2011. Web. 17 Feb 2013.
www.dep.wv.gov/news/Pages/Pa,WVDEPalertresidentsofgoldenalgaeinprivatepond.aspx
- Cosco, K. Kathy. "WVDEP, WVDNR and CONSOL Enter into Consent Decree." *www.dep.wv.gov*. West Virginia Department of Environmental Protection, 14 Mar 2011. Web. 17 Feb 2013.

www.dep.wv.gov/news/Pages/WVDEP,WVDNRandCONSOLenterintoconsentdecree.aspx.

Manning, Schonna, and John La Claire II. "Prymnesins: Toxic Metabolites of the Golden Alga, *Prymnesium parvum* Carter (Haptophyta)." *Mar Drugs*. 8.3 (2010): 678-704. Web. 17 Feb. 2013.

James, T.L., and A. De La Cruz. "Prymnesium parvum Carter (Chrysophyceae) as a Suspect of Mass Mortalities of Fish and Shellfish Communities in Western Texas" *The Texas Journal of Science* (1989). 429-430. Print

Ralph, Jack, and et al. "Golden Algae Frequently Asked Questions." <http://www.tpwd.state.tx.us/>. Texas Parks and Wildlife. Web. 17 Feb 2013. www.tpwd.state.tx.us/landwater/water/environconcerns/hab/ga/faq.phtml.

Sallenave, Rossana. "Toxic Golden Algae (*Prymnesium parvum*)" College of Agricultural, Consumer, and Environmental Sciences at New Mexico State University. (2010): 1-6. Print.

DOES LOCAL MARCELLUS WELL DRILLING IMPACT WATER QUALITY OF NEARBY STREAMS?

Dustin Spencer
Biology
Fairmont State University
Fairmont, West Virginia 26554

ABSTRACT

Introduction The purpose of this research was to determine if Marcellus well drilling was affecting local stream ecology. We hypothesized that stream health would be decreased below all drilling sites.

Methods and Materials Abiotic properties were tested using an YSI Multi-Parameter Data Collection System and a DREL 2400 portable quality laboratory. Biotic properties were tested by collecting macro invertebrate samples from each stream.

Results FBI and abiotic tests showed that overall the streams were healthy below and above the drill sites.

Discussion Properties tested were inconclusive in determining the effect active drilling had on the stream ecology however, the FBI showed substantial organic pollution likely below the inactive site of Cherry Camp Road and the active site of Jarvisville Road.

Conclusion Data collections of surrounding streams have not provided enough information to complete assurance that Marcellus Shale drilling is affecting local stream ecology.

INTRODUCTION

In this research, we examined the effects Marcellus well drilling had on local stream ecology. Stream health is determined by the abiotic properties and biological life of those streams. The Marcellus Shale is the largest supplier of natural gas in the United States with approximately 141 trillion cubic feet of recoverable gas. Hydraulic fracturing is the process typically used by companies to obtain natural gas from the Marcellus Shale. Natural gas drilling has grown exponentially over the last few years, both in monetary gains and popularity.

Stream health is measured by the amount of toxins, aquatic life, and dissolved organics present. Toxins are found in streams due to runoff from farms, industries dumping chemicals into streams via pipes, and home sewage waste. Aquatic life will vary according to the amount of toxins within a stream; many macroinvertebrates are sensitive to pH, salinity, and DO changes. Dissolved organics are introduced into streams through farm and home runoff; this increase in organics leads to an increase in decomposers. Decomposers require an abundance of oxygen to grow and deplete the stream of oxygen required by aquatic organisms.

The Marcellus Shale runs along the east coast from Marcellus, New York down through southern West Virginia and as far west as Ohio. The shale is derived from the Devonian Era and is formed from the fossils from multiple faunal turnovers. Black is the dominant color of the Marcellus shale which may also contain limestone, iron pyrite, and siderite.

Hydraulic fracturing is the process in which water and chemicals are introduced into the shale at high pressures to cause cracks within the shale and enable the extraction of gas. The fractured shale is then held open by various chemicals which have an array of properties from acids to surfactants. This process was first conducted in 1947 without success; it wasn't until 1952 when Soviet Russian was able to carry out the first successful hydraulic fracturing (Wikipedia).

The purpose of this research was to determine if Marcellus well drilling was affecting local stream ecology. We hypothesized that the water quality would be impacted below all sites where drilling occurred.

METHODS AND MATERIALS

Abiotic properties tested were temperature, TDS, TDS%, salinity, pH, ORP, turbidity, DO%, DO in mg/L, nitrate, and phosphate for above and below the drilling sites for all the creeks. We tested these properties using an YSI Multi-Parameter (9) Data Collection System (650 MDS) and a DREL 2400 portable quality laboratory. The sites were tested three times to get an accurate measurement of water quality.

Macro invertebrates were collected using a kick net and washing the bottoms of rocks off in the streams. The macro invertebrates were collected, using tweezers, in sample containers containing 70% EtOH and marked with the corresponding streams. Macro invertebrates were poured into a glass petri dish to be keyed out. An Olympus microscope and B&B microscope light were used to view the micro invertebrates for better observation. Data collected was placed in a Microsoft Excel spreadsheet to calculate averages and standard deviations. Graphs were created based on the averages and standard deviations.

RESULTS

Cherry Camp Road temperature above the drill site was 18.2 ± 0.01 (average \pm standard deviation), TDS was 100 ± 0 , TDS % was 0.065 ± 0 , salinity was $0.05 \pm 8.5E-18$, pH was 8.32 ± 0.18 , ORP was 109.4 ± 2.53 , turbidity was 31.1 ± 10.8 , DO% was 87.5 ± 0.15 , DO in mg/L was 8.24 ± 0.01 , nitrate was 0.73 ± 0.15 , and phosphate was 0.27 ± 0.03 . Cherry Camp Road temperature below the drill site was 18.63 ± 0.005 , TDS was 101 ± 0 , TDS % was 0.066 ± 0 , salinity was $0.05 \pm 8.5E-18$, pH was 7.96 ± 0.02 , ORP was 99.6 ± 2.22 , turbidity was 34.8 ± 2.16 , DO % was 90.3 ± 0.06 , DO in mg/L was 8.44 ± 0.005 , nitrate was 1.1 ± 0.26 , and phosphate was 0.42 ± 0.31 .

Indian Run Road temperature above the drill site was 18.7 ± 0.02 , TDS was 85.7 ± 0.58 , TDS % was 0.05 ± 0.0006 , salinity was 0.04 ± 0 , pH was 7.95 ± 0.09 , ORP was 63.5 ± 5.5 , turbidity was 16.2 ± 1.9 , DO% was 91 ± 0 , DO in mg/L was 8.49 ± 0.006 , nitrate was 0.37 ± 0.21 , and phosphate was 0.12 ± 0.12 . Indian Run Road temperature below the drill site was 18.94 ± 0.1 , TDS was 110.3 ± 0.58 , TDS % was 0.072 ± 0 , salinity was $0.05 \pm 8.5E-18$, pH was 8.12 ± 0.08 , ORP was 87.8 ± 8.64 , turbidity was 22.63 ± 5.05 , DO % was 89.6 ± 0.1 , DO in mg/L was 8.32 ± 0.006 , nitrate was 0 ± 0 , and phosphate was 0.2 ± 0.22 .

Pike Fork Road temperature above the drill site was 18.67 ± 0.01 , TDS was 85.67 ± 0.58 , TDS % was 0.06 ± 0.0006 , salinity was 0.04 ± 0 , pH was 7.95 ± 0.09 , ORP was 63.5 ± 5.49 , turbidity was 16.2 ± 1.93 , DO% was 91 ± 0 , DO in mg/L was 8.5 ± 0.006 , nitrate was 0.37 ± 0.2 , and phosphate was 0.12 ± 0.12 . Pike Fork Road temperature below the drill site was 18.94 ± 0.01 , TDS was 110.3 ± 0.58 , TDS % was 0.072 ± 0 , salinity was $0.05 \pm 8.5E-18$, pH was 8.12 ± 0.08 , ORP was 87.8 ± 8.64 , turbidity was 22.63 ± 5.06 , DO % was 89.6 ± 0.1 , DO in mg/L was 8.32 ± 0.006 , nitrate was 0 ± 0 , and phosphate was 0.21 ± 0.22 .

Jarvisville Road temperature above the drill site was 15.3 ± 0.006 , TDS was 395 ± 0 , TDS % was 0.257 ± 0 , salinity was $0.19 \pm 3.4E-17$, pH was 7.31 ± 0.035 , ORP was 145.9 ± 5.11 , turbidity was 55.1 ± 3.15 , DO% was 56.7 ± 1.61 , DO in mg/L was 5.65 ± 0.15 , nitrate was 0.33 ± 0.21 , and phosphate was 0.21 ± 0.03 . Jarvisville Road temperature below the drill site was 15.24 ± 0.035 , TDS was 476 ± 6.24 , TDS % was 0.31 ± 0.003 , salinity was 0.23 ± 0 , pH was 7.21 ± 0.14 , ORP was 158.5 ± 2.17 , turbidity was 43.4 ± 15.76 , DO % was 67.4 ± 1 , DO in mg/L was 6.74 ± 0.09 , nitrate was 0.6 ± 0.26 , and phosphate was 3.65 ± 2.93 .

Smithton Road temperature above the drill site was 15.55 ± 0.02 , TDS was 326.3 ± 0.58 , TDS % was 0.212 ± 0 , salinity was 0.16 ± 0 , pH was 7.53 ± 0.07 , ORP was 144.1 ± 1.61 , turbidity was 35.87 ± 10.52 , DO% was 86.13 ± 0.12 , DO in mg/L was 8.57 ± 0.01 , nitrate was 0.4 ± 0.1 , and phosphate was 0.09 ± 0.006 . Smithton Road temperature below the drill site was 16.21 ± 0.006 , TDS was 360 ± 0 , TDS % was 0.234 ± 0 , salinity was 0.17 ± 0 , pH was 7.43 ± 0.07 , ORP was 126 ± 2.71 , turbidity was 41.8 ± 5.54 , DO % was 77.3 ± 0.12 , DO in mg/L was 7.58 ± 0.01 , nitrate was 0.13 ± 0.15 , and phosphate was 0.12 ± 0.04 .

The Family Biotic Index (FBI) showed that Cherry Camp Road water quality above was in good condition while below was in fairly poor condition. Indian Run Road and Pike Fork Road water quality was very good above and below drill sites. Water quality was good above Skelton Run Road while it was very good below the drill site. Water quality was good above Jarvisville Road while it was fair below the drill site. Smithton Road water quality was good both above and below the drill site.

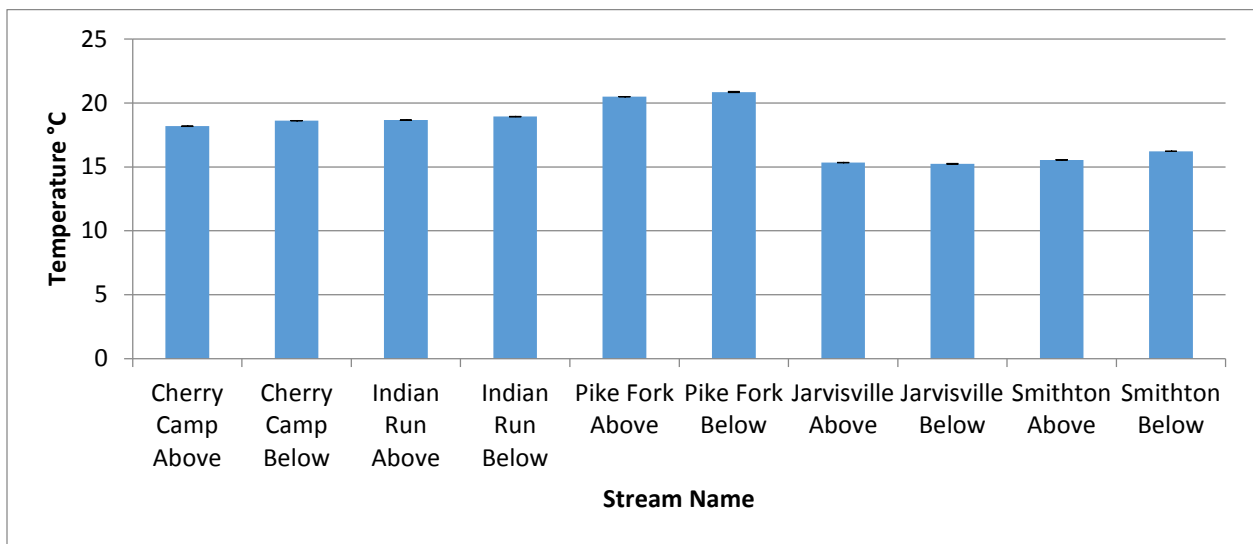


Figure 1. Average temperature \pm STD above and below drill sites for all streams.

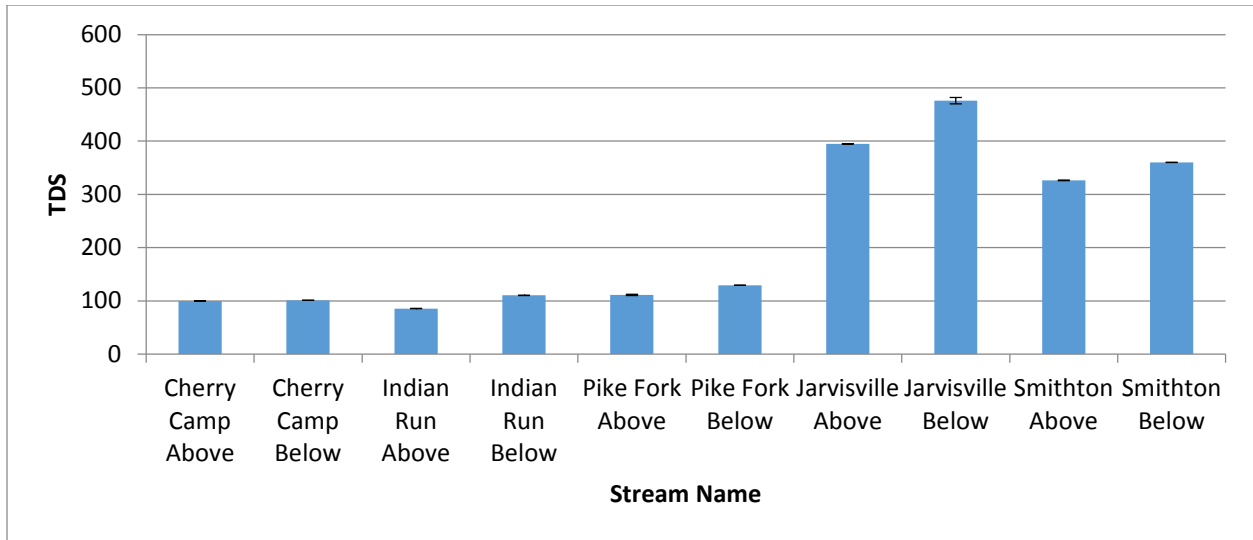


Figure 2. Average TDS ± STD above and below drill sites for all streams.

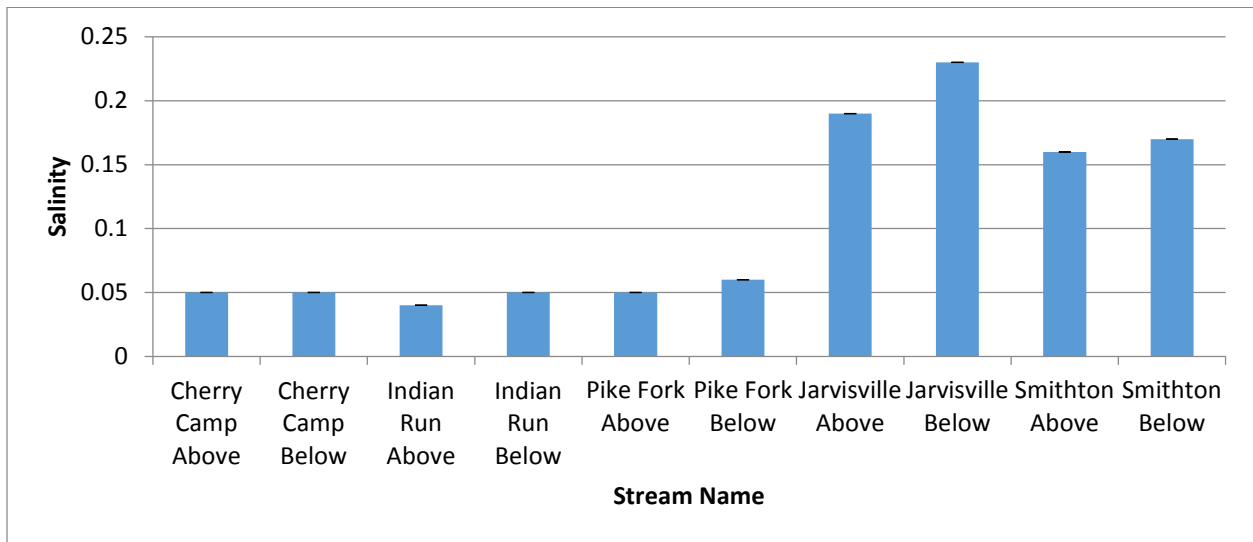


Figure 32. Average salinity ± STD above and below drill sites for all streams

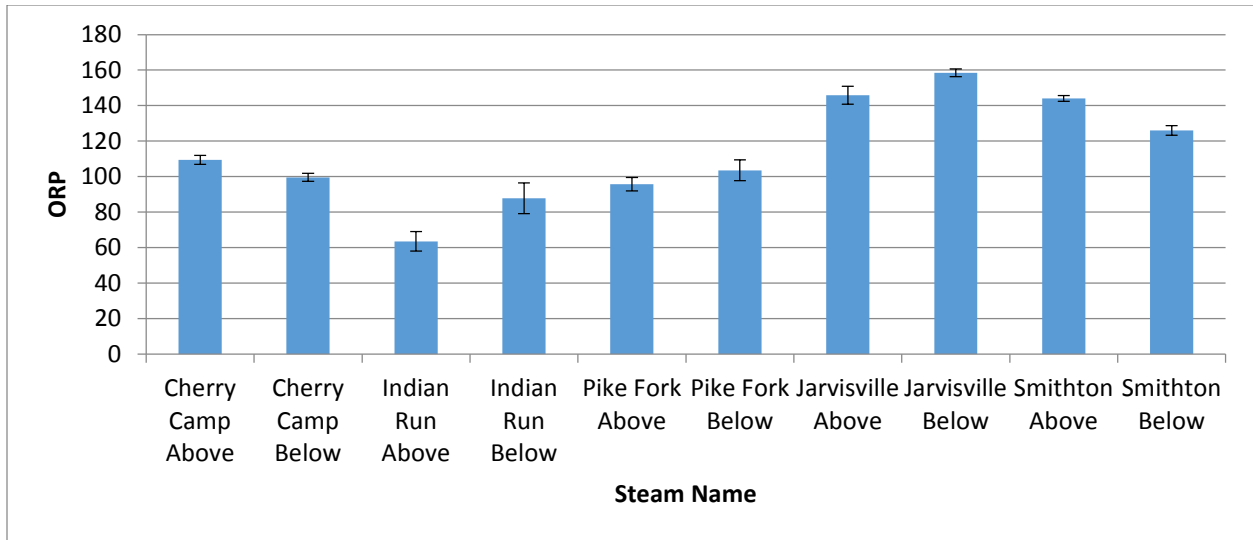


Figure 43. Average ORP ± STD above and below drill sites for all streams.

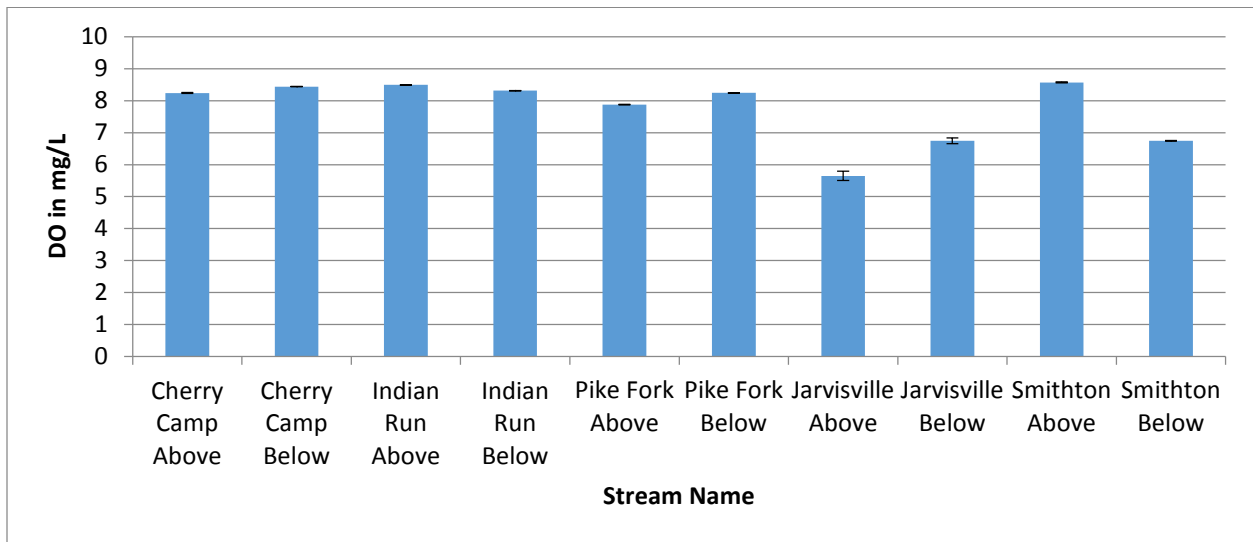


Figure 5. Average DO ± STD above and below drill sites for all streams.

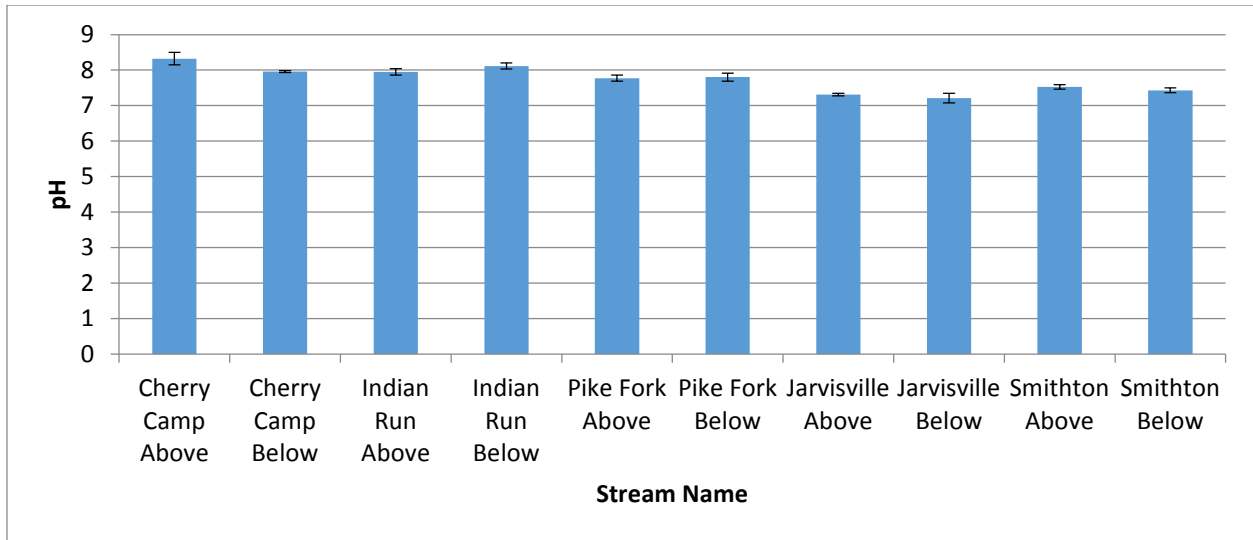


Figure 6. Average pH \pm STD above and below drill sites for all streams.

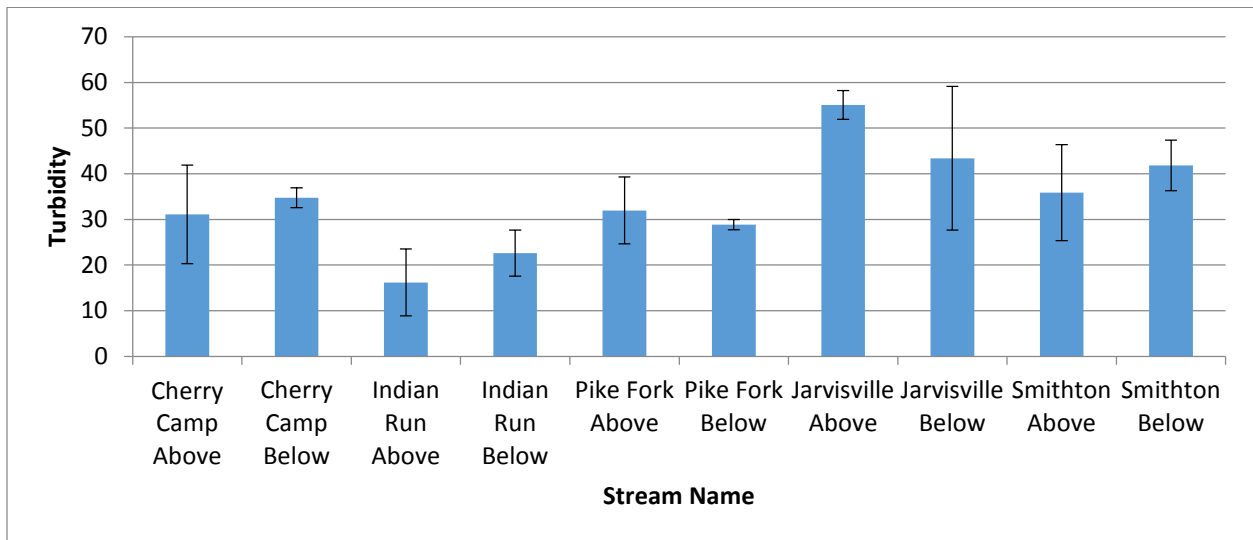


Figure 7. Average turbidity \pm STD above and below drill sites for all streams.

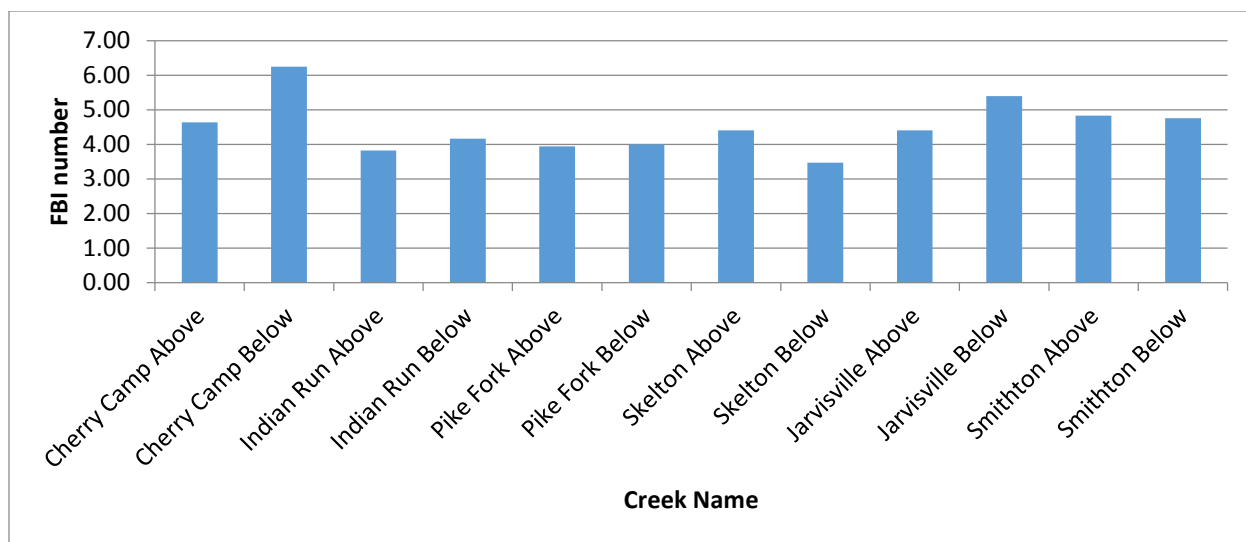


Figure 8. FBI above and below drill sites for all streams.

DISCUSSION

The overall objective of this study was to correlate active and inactive Marcellus Shale drilling sites with the impact on local stream ecology. Studies are ongoing to examine organic solvents being introduced into streams surrounding active drill sites. Properties tested were inconclusive in determining the effect active drilling had on the stream ecology however, the FBI showed substantial organic pollution likely below the inactive site of Cherry Camp Road and the active site of Jarvisville Road. We choose Cherry Camp Road as our control due to inactivity for two years.

The temperature varied between each stream due to time of day in which the measurements were taken and time of season (Figure 1). Jarvisville Road and Smithton Road reading were taken in the fall due to a high rain season in the summer of 2013. Total Dissolved Solids (TDS) (Figure 2), TDS %, and salinity (Figures 3) were higher below all streams except Cherry Camp Road. These results show that some types of cations or anions are being introduced into the streams below the drilling sites which were to be expected in all streams but Cherry Camp Road. Cations and anions within the stream lead to the formation of salts thus increasing the salinity of the stream. TDS buildup has been shown to cause gill and internal dehydration, salt accumulation, and compromised osmoregulatory functions of aquatic organisms (Bodkin, R. et al).

Oxidation reduction potential (ORP) was greater below in all streams except Cherry Camp Road and Smithton Road (Figure 4). Those streams with a higher ORP below have a tendency to gain electrons to new species (oxidize the species) while those with a lower ORP will lose electrons (reduce the species). Dissolved oxygen (DO) and DO% relate to the amount of oxygen available in the streams to be used by aquatic organisms. DO levels of less than 3 mg/L are stressful to most aquatic organisms with fish dying around 1-2 mg/L (Internet source). All DO levels were above the minimum requirements to sustain aquatic life (Figure 5).

The pH for all streams, except Indian Run Road and Pike Fork Road, were more acidic below the drill sites than above (Figure 6). This was to be expected due to the increase of hydrogen ions

being introduced into the stream from acids in the chemical makeup of fracturing solutions. Research has shown that a decrease in the pH can lead to accumulation of harmful elements due to the low content of calcium in the water; pH also plays a role in physiological effects such as osmotic regulation and even NaCl loss (Moiseenko, T.).

Turbidity was used to determine the visual clarity of the stream which can vary according to the amount of TDS present. Turbidity levels were higher below the drill sites in all streams except Pike Fork Road and Jarvisville Road but there was no significant difference noted between above and below the sites (Figure 7). These findings were unexpected because the TDS levels were higher in all streams below the drill sites thus all turbidity levels should have correlated with TDS.

The FBI showed that overall the streams were in good condition with the exception of Cherry Camp Road below. This result is based off the Hilsenhoff Index Water quality Degree of Organic Pollution which may have impacted our results due to not testing organic pollutants.

CONCLUSION

Data collections of surrounding streams have not provided enough information to complete assurance that Marcellus Shale drilling is affecting local stream ecology. We are unable to fully support our hypothesis that the water quality would be impacted below all sites where drilling occurred. Future research should be conducted to test for organic material in stream sediment, terrestrial ecology surrounding drill sites, wells from surrounding houses, and ongoing monitoring of stream health. The use of a different FBI table for testing more than organic pollution would possibly change the water quality reports of these streams.

ACKNOWLEDGEMENTS

Special thanks to the NASA West Virginia Space Grant Consortium for supporting this research and Dr. Mark Flood, student mentor.

REFERENCES

1. Hydraulic fracturing. Admin, accessed on 04/01/2014.
http://en.wikipedia.org/wiki/Hydraulic_fracturing. Searched hydraulic fracturing.
2. Moiseenko, T. I. 2005. Effects of Acidification on Aquatic Ecosystems. *Russian Journal of Ecology*. 36(2): 110-119.
3. Bodkin, R., Kern, J., McClellan, P., Butt, A., Arthur, J., & Martin, C. 2007. Limiting total dissolved solids to protect aquatic life. *Journal of Soil and Water Conservation*. 62(3): 57A-61A.
4. Water Quality Parameters. Admin, accessed on 04/01/2014.
<http://www.dnr.mo.gov/env/esp/waterquality-parameters.htm>. Searched healthy do levels in streams.

UNILATERAL HEATING: A NOVEL MODEL TO INDUCE DIFFERENTIAL EXTREMITY GROWTH IN MICE

Jenna Vance
Exercise Physiology
Marshall University
Huntington, WV 25755

ABSTRACT

Limb length inequality is a condition that sometimes occurs when the arms and legs grow to uneven lengths after a bone injury or infection in children. Studies show that differences as small as 3-4% can affect walking¹. Without proper correction, limb length inequality can cause disabling health conditions such as scoliosis, chronic back pain, and osteoarthritis². Length differences can be treated surgically, but this is typically painful and sometimes requires the patient to wear external braces that are drilled into the shorter limb. Other treatment options include drug therapies, which are not always successful because they affect the whole body and not just the stunted limb.

I joined the lab as a research assistant to aid in a new project addressing bone growth in the extremities. The goal of our study is to evaluate whether applying heat locally could be used as an alternative to surgery in order to increase bone length. Using an experimental model with mice, my mentor's previous work showed that housing animals continuously at warm temperature increased bone length by 5%³. Based on those findings, we developed a unilateral heating model in which we apply mild heat once per day to only one side of growing mice. We hypothesize that localized unilateral heat increases bone elongation rate on the heat-treated side.

Working as part of a team, I have been highly involved in the analytical aspects of the project to validate this model. I have created quantitative data templates, collected bone mass data, and helped prepare histology slides to analyze bones microscopically. I am currently analyzing vascular densities in the extremities to determine the impact that heat has on the nutrients available to aid in bone growth.

Here we present data that support our hypothesis and validate the unilateral heating model. We were able to develop consistent parameters for applying heat treatments with no adverse affects on mouse welfare. We show that localized heat increased bone length by almost 2% on the heat-treated side. Having established this result, we can move forward to test additional hypotheses in future studies to determine how heat increases bone growth rate. These results are important to society because therapeutic application of heat could be a cost-effective strategy to increase bone length using simple, noninvasive techniques.

INTRODUCTION

The effect of heat on bone and cartilage growth is an interesting concept. By studying heat's capacity to elongate long bones, its effect can be tailored to produce a desirable outcome. One such

potential outcome would be to use heat as an inexpensive, non-invasive mechanism to correct for limb length inequality. Using an experimental model with mice, my mentor’s previous work showed that housing animals continuously at warm temperature increased bone length by 5%, and that cold housing temperature stunted bone growth³. Literature dating back over 100 years to 1909 also suggests that warm ambient temperatures increase limb length⁴. In this literature, Sumner first published that warm temperature can increase the limb length of mice⁴.

From these established findings, we are now studying the effects of applying heat locally using a unilateral limb heating model. The reason for using localized heat is to reduce exposure of the entire animal to temperature variation so it would translate better to a clinical treatment. The purpose of this study is to 1) determine whether unilaterally applied heat can elicit differential extremity growth in a mouse model, and 2) established parameters for consistent heat therapy. We hypothesized that **controlled heat applied unilaterally in set regimens will increase limb length on the heat-treated side.** We tested the hypothesis using a unilateral heating model that our lab developed over the past year. Variables assessed include: long bone length, bone mass, ear area, and ear vasculature density. This model is important because it allows us to look at isolated temperature as a feasible way to increase stature in children with growth disorders.

METHODS

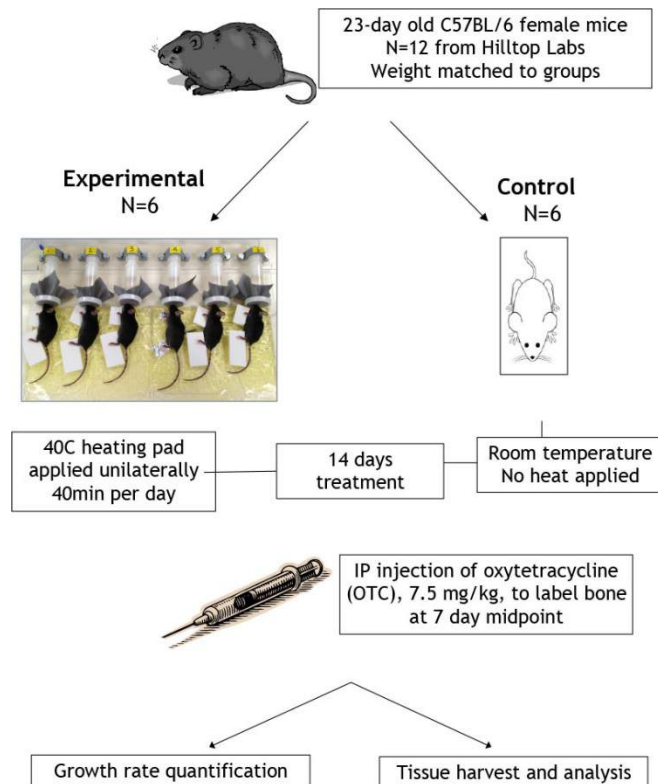


Figure 1. Experimental schematic illustrating the methods procedure.

temperatures were taken using a noncontact infrared thermometer. The respiratory rate was recorded as well to monitor physiological status.

A total of four trials have been completed for this project. For each trial, a sample of 12 mice was chosen specifically at three weeks of age. We chose to use three-week old mice because this is the period of the most rapid growth in weanling mice. The mice were then separated into 2 groups (N=6 per group). One group was administered heat unilaterally using a heating pad at 40C while under anesthesia. The second group was weight matched to the first and served as a general growth control. This control group did not receive heat or anesthesia.

The application of heat was carried out for 14 consecutive days at 40 minutes a day. Light sedation using isoflurane anesthesia via a commercial vaporizer was necessary in order to keep the mice stationary for the 40 minute time period. During each heating treatment, core body temperature, as well as the temperatures of each limb, the ears, the tail, and the heating pad were all monitored closely and recorded. The extremity

In two of the four trials, mice were given an injection of oxytetracycline (OTC) at the seven-day study midpoint. This was done in order to label bone so that we could track growth rate. OTC is a calcium chelator that binds to newly mineralizing bone and serves as a “time stamp” to quantitatively measure bone elongation rate. In most trials a tissue harvest directly followed the 14-day experimental period, in which tissues are collected for numerous subsequent analyses. In one of the trials, tissues were harvested for analysis 8 weeks after the treatment ended when they were skeletally mature adults. This was important to determine whether the heat effects persisted after the treatments had ended. For all trials the analyses include comparisons of heat-treated and non-treated sides for each of the following: femoral length, tibial length, hind foot length, and tibial elongation rate. We followed established lab protocols for collecting these measurements.

In addition to quantitative bone measurements, ear area and vascularity were assessed. This was done because others have shown that cartilaginous ears are temperature sensitive⁵. Ears were carefully removed from the animal by cutting them with quality dissection scissors. The removed ears were placed between two glass slides and scanned on an Epson Perfection V30 flat bed scanner at 1200 dpi resolution. Ear area was measured from calibrated images by tracing the outline of each ear using ImageJ software. Ear vascularity was defined by manually tracing visible blood vessels in defined regions of interest in ImageJ. Vessels were quantified as the additive length of the individual lines within the designated area. Vascularity was compared between heat-treated and non-treated sides.

One important aspect of the study design is that the designated heat-treated side was varied between trials to account for potential dominant-side effects. In other words, the left side was heat-treated for trials one, two, and three. The right side was heat-treated in the fourth trial. This enabled us to show that there was a heat effect independent of side.

RESULTS

Femur mass was measured after two weeks of unilateral heat treatment. Each bone was measured on three separate dates to correct for temperature and humidity differences as well as human error. The average mass for each individual bone is plotted in Figure 2. For nearly all mice, the mass of the heat-treated side was consistently higher (Fig. 2).

Tibial elongation rates ($\mu\text{m}/\text{day}$) were measured for the heat-treated and non-treated sides of 5-week old mice. The oxytetracycline (OTC) bone marker was analyzed using left-right tibial slab sections from the same mouse.

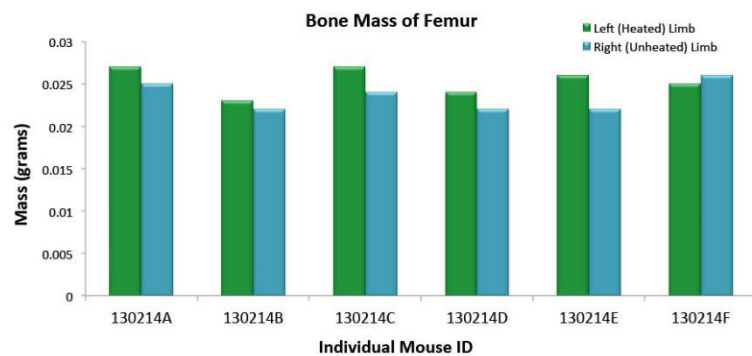


Figure 2. Comparison of femur mass measured after two weeks of unilateral heat treatment. Each bone was measured on three separate dates, and the average mass for each individual bone is plotted. The mass of the heat treated side was consistently higher.

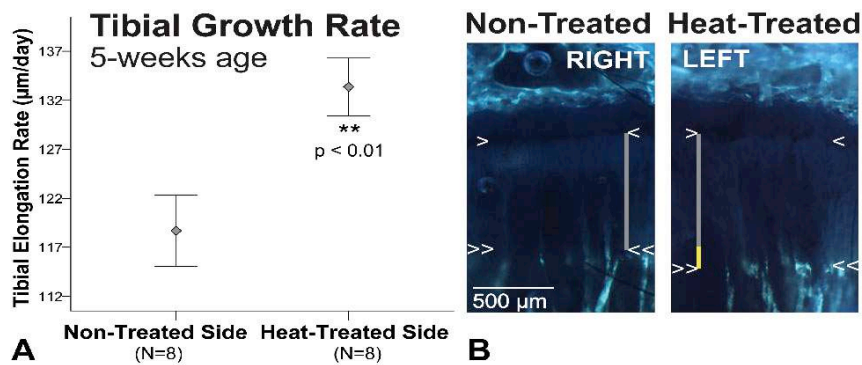


Figure 3. Extremities are lengthened on the heat-treated side.

(A) Error bar plots show > 12% increase in tibial elongation rate on the heat-treated side of 5-week old mice. (B) Left-right tibial slab sections from the same mouse labeled with OTC. The metaphyseal chondro-osseous junction (COJ) is indicated by single arrowheads. Double arrowheads show OTC band in metaphyseal bone. Growth rate was estimated by measuring vertical distance between arrowheads (gray lines). Yellow segment of the vertical line on the heat-treated side shows total difference in length measured over 7-days. Mean +/- 1 standard error.

Growth rate was estimated by measuring vertical distance between the chondroosseous junction (bone-cartilage interface) at the end of the bone, and the OTC band in the shaft. The comparison error bar plots (Figure 3-A) show > 12% increase in tibial elongation rate on the heat-treated side.

For all of the morphological parameters collected, there was a significant increase in ear area, femoral length, tibial length, hind foot length, and tibial elongation rate on the heat-treated side (Table 1). The percentage

of increase when comparing heat-treated to non-treated sides are as follows: 8.8%, 1.3%, 1.5%, 3.5%, and 12.4%, respectively.

There was no difference in total body mass or average daily gain in mass between the experimental animals and the non-treated mice that served as growth controls. Core body temperature was kept stable at 36C during the treatments. Respiration was 60 breaths per minute. The heat-treated side temperature was 40C during treatments and the non-treated side was 30C.

Table 1. Comparison of non-treated vs. heat-treated sides of 5-week old female mice.

Parameter	Non-Treated (30C)	Heat-Treated (40C)	Percent Increase	N
Ear Area (mm ²)	101.7 (6.9)	110.6 (7.2) ^c	8.8	14
Femoral Length (mm)	12.33 (0.43)	12.49 (0.45) ^c	1.3	12
Tibial Length (mm)	14.96 (0.29)	15.18 (0.27) ^a	1.5	5
Hindfoot Length (mm)	17.54 (0.63)	18.15 (0.42) ^c	3.5	14
Tibial Elongation Rate (µm/day)	118.7 (10.3)	133.4 (8.4) ^b	12.4	8

Values are mean (SD). Sample size (N) is listed as number of right-left pairs. Significantly larger on heat-treated side (paired t-test): ^a p < 0.05; ^b p < 0.01; ^c p < 0.001

Ear vasculature density quantification is still in progress. The goal of the analysis is to create a parameter by which the heat-treated and non-treated sides can be compared and analyzed. This

ongoing research is important for determining vasculature changes that could potentially underlie the differences in elongation rate of the heat-treated cartilage.

DISCUSSION

In this study we were able to determine consistent parameters for applying heat treatments with no adverse affects on mouse welfare. Our result show that localized heat increased bone length, elongation rate, and bone mass on the heat-treated side. These differences were consistent across trials regardless of which side was heat-treated. We concluded that the effect was independent of anatomical side. The heat effect persisted in adult mice that had only been heat-treated for two weeks during a period of rapid juvenile growth. Area of the cartilaginous ear, a temperature sensitive control tissue, was also increased on the heat-treated side. Collectively, these results support our hypothesis that controlled heat applied unilaterally in set regimens will increase limb length on the heated side. This model will be used in future studies to test hypotheses about the mechanisms underlying heat-enhanced limb growth.

Work in progress involving ear vascular measurements is being conducted to quantify heat effects on tissue vascularity. The ultimate goal of this ongoing investigation is to determine whether or not the heat treatment has a direct effect on the vascularity of growing tissue. If it is determined that heat has quantifiable effect on tissue vascular density, the follow-up objective would be to test whether heat is inducing increased vascularity in relation to receiving nutrients for the growing tissue, or whether the heat is creating a contrary effect in which the non-treated side increases in vascularity to physiologically overcome the nutrient deficient in comparison to the complementary side.

In the bone mass comparison analysis, the first five mice showed an increase in mass for the heat-treated side. However, the data show that the mass of the sixth mouse's non-treated side was greater than that of the treated side. Reasons for this slight discrepancy could include any of the following or a combination of one or more explanations: human error in weighing the dry bones accurately, or human error while harvesting the tissue such as cutting too much of the bone on the heat-treated side, thereby, rendering it less massive. Another possibility is that this particular mouse simply did not respond to treatment due to normal experimental variation.

This work is important because heat offers a non-invasive alternative that could possibly be used for augmenting limb growth without painful and expensive surgery. Our results suggest that therapeutic application of heat could be a cost-effective strategy to increase limb length using simple, noninvasive techniques. Although this research is targeted toward growing and developing tissue, one potential of heat therapy would be to decrease recovery time for fractured bones. This method could be used to help astronauts recover from the fractures that they are prone to encounter once returning from low gravity conditions since these conditions are known to produce a progressive loss of bone mass⁶.

Future Plans

I plan to continue to work with the lab on this research project throughout the summer until I begin medical school in the fall. We have two trials scheduled during this time period. The first trial scheduled for May 2014 will use dwarf mice that our lab will obtain from Ohio University. The methodology will be essentially the same, other than the difference in test subjects. We have

recently completely a practice trial involving younger mice so that we can harness our technique even with smaller mice. We hypothesize that the heating treatment will serve to at least partially rescue the growing mice from dwarfism. The second of the planned trials will be used to generate information on the effects of heat when combined with a drug regimen. We postulate that the use of known hormones such as (IGF1) will work to enhance the heat-treatment outcomes. Two other students in the lab, Miles Gray and Holly Tamski, plan to continue this work for the next school term once I leave this fall. Each has applied for a WV-NASA fellowship as well, and so, if they are granted this wonderful opportunity, the program will continue to fund our future plans for this ongoing project.

Valuable Aspects of the Program

The financial support has been the biggest assistance in my research experience. As a full-time student, I have used the stipend to fund my salary throughout the duration of the experiments. Without this opportunity, it is very likely that I might never have received any type of research training. I feel that a lack of research training would have been a hindrance to my overall undergraduate educational experience because I would have never grown to appreciate the processes and effort required to make research possible. I can now value scientific research on a more personal level and take what I have been privileged to learn with me as I continue my educational journey. The most significant experience that I have encountered thus far was presenting at Undergraduate Research Day at the Capitol. It was encouraging to see so many of my fellow peers working on a vast array of projects. Speaking with many of them, it was evident that they were not only knowledgeable in their particular fields of study, but also enthusiastic about their research.

CONCLUSION

We have successfully established consistent parameters for applying heat treatments with no adverse effects on mouse welfare. Our data support the hypothesis that localized heat increased bone length and bone mass on the heat-treated side. This model will be useful for testing future hypotheses about the mechanisms underlying heat-enhanced growth in the limbs. Work in progress to finish the ear vascular measurements will assess the impact of heat on tissue vascularity. These results are important because therapeutic application of heat could be a cost-effective strategy to increase limb length using simple, noninvasive techniques.

ACKNOWLEDGEMENTS

We thank C. Farnum, R. Williams, A. Williams, G. Ion and the VA Medical Center and CEB staff for support. H. Tamski, M. Efaw, T. Schlierf, J. Godby, and L. Stanko performed experiments and helped collect data. We are grateful to Dr. Howard and the Marshall Animal Resource Facility for animal husbandry, assistance with equipment set up, and room temperature monitoring. Marcos Serrat helped design and assemble the anesthesia manifold. D. Neff provided valuable imaging aid. M. Crutchfield and T. Pickens, MUSOM Graphic Designers, created artwork. This research was supported, in part, by funding from MU-ADVANCE, the Department of Anatomy and Pathology, NASA WV Space Grant Consortium, and University of Kentucky CCTS Pilot Program (NIH UL1TR000117). This work was aided by the use of facilities at the Huntington VA Medical Center.

REFERENCES

- ¹ <http://orthoinfo.aaos.org/topic.cfm?topic=a00259>
- ² Brady et al., 2003. *Journal of Orthopedic & Sports Physical Therapy*. 33: 221-234.!
- ³ Serrat et al., 2008. *Proceedings of the National Academy of Sciences*. 105: 19347-52.
- ⁴ Sumner FB., 1909. Some effects of external conditions upon the white mouse. *J Exp Zool* 7:97-155.
- ⁵ Serrat, M., 2014. Environmental temperature impact on bone and cartilage growth. *Comprehensive Physiology*. 4:621-655.
- ⁶ NASA Science News. Space Bones. Available at: http://science.nasa.gov/science-news/science-at-nasa/2001/ast01oct_1/ Accessed on: April, 11, 2014.

III. NASA Graduate Research Fellowship Program Reports

A COMPARATIVE ANALYSIS OF DAYSIDE MAGNETIC RECONNECTION MODELS

Colin Michael Komar
PhD Candidate, Physics
West Virginia University
Morgantown, WV 26506
Mentor: Dr. Paul Cassak

ABSTRACT

Magnetic reconnection occurs when oppositely directed magnetic fields in plasmas break and cross-connect, allowing energy stored in magnetic fields to convert into plasma motion and heat. Predicting where magnetic reconnection occurs at Earth's dayside magnetopause has been the subject of studies for nearly fifty years and remains an unsolved problem. The location of dayside magnetic reconnection was originally discussed in terms of anti-parallel vs. component (guide field) reconnection, but it is now known that these descriptions are too basic to fully describe the observations. Recent models suggested that reconnection orients itself such that the local plasma properties maximize some measure of reconnection efficiency. Alternatively, it was suggested that reconnection occurs along the curve where the shear angle between the magnetospheric and magnetosheath magnetic fields is a maximum. Each of these models is independent of the reconnection dissipation mechanism, so they should hold for any self-consistent magnetospheric model. We use global magnetospheric resistive magnetohydrodynamic simulations to identify the locus of possible magnetic reconnection sites by finding the magnetic separator where different magnetic topologies meet at the dayside magnetopause. Employing image processing techniques, we compare the separator locations with the predictions of these models to determine which, if any, accurately predict the location of reconnection.

INTRODUCTION

Interplanetary space is commonly thought of as an empty vacuum, but in reality it is filled with a hot ionized gas, constituted of ions and electrons. How did these ions and electrons, or plasma, get there? The source of this interplanetary plasma is our very own Sun. The Sun heats the plasma located in the solar corona to such high temperatures that ions and electrons escape the Sun's gravitational pull. This released solar plasma, called the solar wind, carries the Sun's magnetic field into interplanetary space, where it can interact with planetary magnetic fields like those of Earth. Earth is constantly barraged by this ejected solar plasma, also known as the solar wind, which contains particles with enough energy that they can damage satellites and ground-based electrical systems, and could ultimately disrupt daily life on Earth. Earth's magnetic field serves as a protective shield, where the solar wind plasma is diverted away from Earth, largely preventing plasma from entering near-Earth space; the outer edge of this magnetic shield is called the magnetopause. However, the magnetopause is not entirely impenetrable as the solar wind can gain entry through the magnetopause; one process that allows this to happen is a process known as "magnetic reconnection."

Magnetic reconnection occurs in plasmas when oppositely directed magnetic fields merge and nullify. The magnetic field lines effectively break like rubber bands, releasing their energy and heating the plasma in the process. Figure 1 is an illustration of magnetic reconnection at Earth. In this figure, the solar wind approaches Earth's magnetopause from the left, bringing a southward interplanetary magnetic field that points down. The dayside magnetopause encapsulates Earth's northward curved magnetic fields, displayed as the dark green region's boundary. The interplanetary and terrestrial magnetic fields merge and reconnect in the red box where magnetic energy and solar wind plasma are transferred into Earth's plasma environment.

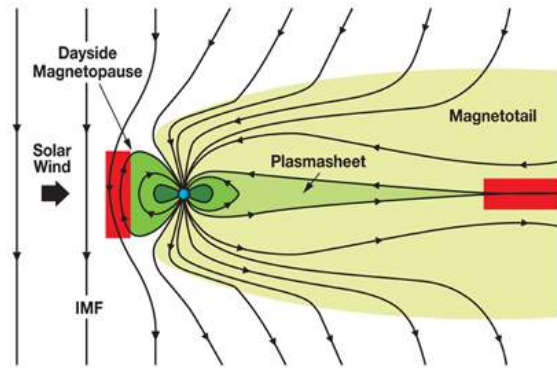


Figure 1. Reconnection locations (red) at Earth for southward interplanetary magnetic fields. Image courtesy of MMS (NASA/SWRI).

Many important dynamic processes in the Earth's magnetosphere are known or are thought to result from magnetic reconnection, from solar wind-magnetosphere coupling [Gonzalez, 1990; Borovsky, 2008], to substorm phenomena [Angelopoulos et al. [2008], and references therein]. As reconnection allows plasma to enter into Earth's magnetosphere, it is one of the first steps in magnetospheric convection, also known as the Dungey cycle [Dungey, 1961]. Knowledge of when and where reconnection occurs at Earth's magnetopause for various solar wind conditions is crucial for space weather prediction models and would greatly support satellite missions studying magnetic reconnection, specifically NASA's upcoming Magnetospheric Multiscale (MMS) mission [Burch and Drake, 2009; Moore et al., 2013].

The classical model of Dungey [1961, 1963] has reconnection occurring at the subsolar point for due southward or near the polar cusps for due northward interplanetary magnetic field (IMF) orientations. Much less is known where reconnection will occur when the IMF makes an angle θ_{IMF} with the dipole axis. Reconnection was originally believed to align itself in the plane where the reconnection layer had a uniform out-of-plane component, or guide field [Sonnerup, 1974; Gonzalez and Mozer, 1974]. An alternative hypothesis posited reconnection orients itself such that the components undergoing reconnection are equal and opposite [Cowley, 1976]. These theories comprise what is known as component reconnection. An alternative to the component reconnection hypotheses suggested the location of dayside magnetic reconnection would occur wherever the magnetic fields were perfectly anti-parallel [Crooker, 1979]. However, it is now known that these descriptions are too basic to fully describe the observations (see Dorelli et al. [2007]; Paschmann [2008], and references therein).

Trattner et al. [2007] proposed the Maximum Magnetic Shear model, in which reconnection occurs along the curve where the shear angle between the magnetospheric and magnetosheath magnetic fields is a maximum. The reconnection location predicted by the Maximum Magnetic Shear model agrees closely with Cluster [Trattner et al., 2007; Dunlop et al., 2011] and THEMIS [Trattner et al., 2012] observations of magnetic reconnection at the dayside magnetopause. This model has been further tested to show evidence of both component and anti-parallel reconnection at the magnetopause [Fuselier et al., 2011].

Recent models have suggested that reconnection orients itself such that some measure of magnetic reconnection’s efficiency is maximized: maximization of the asymmetric reconnection outflow speed [Swisdak and Drake, 2007; Schreier et al., 2010], maximization of the asymmetric reconnection rate (Shay, private communication, 2009; [Borovsky, 2008, 2013]), or a maximization of the reconnecting field’s magnetic energy [Hesse et al., 2013].

In this work, we test dayside reconnection models by comparing the predictions to the magnetic separators. The magnetic separator is the magnetic field line that simultaneously separates magnetic fields with different topologies and additionally connects those locations where the magnetic field is zero ($|\mathbf{B}| = 0$). For example, the topology of Earth’s magnetic field is “closed” as it maps to the magnetic poles, whereas the IMF extends far off into interplanetary space. Newly reconnected field lines exhibit features of both magnetic topologies where half of the field line maps to a one of Earth’s magnetic poles, and the other lies in the solar wind. Reconnection is believed to occur at the magnetic separator since the terrestrial and the IMF are “broken” and subsequently “reconnected.” We determine the magnetic separator with the algorithm described in Komar et al. [2013], which can successfully trace separators in simulations with arbitrary clock angle θ_{IMF} .

BACKGROUND

Two schools of thought regarding the location and orientation of magnetic reconnection were anti-parallel [Crooker, 1979] and component reconnection [Sonnerup, 1974; Gonzalez and Mozer, 1974; Cowley, 1976]. The anti-parallel argument states that reconnection is much more efficient at locations where the reconnecting fields are perfectly anti-parallel, and thus the most likely location for reconnection to occur. Conversely, the component hypothesis posits reconnection is possible in situations where the magnetic fields are not perfectly anti-parallel, with some oppositely directed magnetic field component undergoing reconnection. Observational evidence supporting both anti-parallel and component reconnection has been reported [Fuselier et al., 2011; Guo et al., 2013].

Trattner et al. [2007] proposed the Maximum Magnetic Shear model, arguing that reconnection is possible at the magnetopause where the magnetic shear angle θ between the magnetospheric and magnetosheath magnetic fields is a maximum. This argument identifies the anti-parallel reconnection locations of Crooker [1979] with high fidelity, while identifying additional locations away from the anti-parallel regions. Several observational studies for a variety of solar wind conditions have shown support for this model [Dunlop et al., 2011; Fuselier et al., 2011; Trattner et al., 2012]. The magnetic shear angle θ can be calculated with the dot product of the magnetospheric and magnetosheath magnetic fields, \mathbf{B}_{MS} and \mathbf{B}_{SH} , respectively

$$\cos \theta = \frac{\mathbf{B}_{\text{MS}} \cdot \mathbf{B}_{\text{SH}}}{|\mathbf{B}_{\text{MS}}| |\mathbf{B}_{\text{SH}}|}. \quad (1)$$

Alternative models have arisen due to the understanding of asymmetric reconnection as formulated by Cassak and Shay [2007]. This study looked at magnetic fields of differing strengths reconnecting in a two-dimensional plane (without an out-of-plane “guide” magnetic field). Using conservation of mass and energy, they developed expressions for the asymmetric outflow speed

$$c_{A,out}^2 \sim \frac{|\mathbf{B}_{MS}| |\mathbf{B}_{SH}| (|\mathbf{B}_{MS}| + |\mathbf{B}_{SH}|)}{\mu_0 (\rho_{MS} |\mathbf{B}_{SH}| + \rho_{SH} |\mathbf{B}_{MS}|)} \quad (2)$$

and the asymmetric reconnection rate

$$E \sim c_{A,out} \frac{|\mathbf{B}_{MS}| |\mathbf{B}_{SH}|}{|\mathbf{B}_{MS}| + |\mathbf{B}_{SH}|} \frac{2\delta}{L} \sim \sqrt{\frac{\eta c_{A,out}}{\mu_0 L}} |\mathbf{B}_{MS}| |\mathbf{B}_{SH}|. \quad (3)$$

These equations are written in terms of the upstream magnetospheric magnetic field $|\mathbf{B}_{MS}|$ and plasma mass density ρ_{MS} , the upstream magnetosheath magnetic field $|\mathbf{B}_{SH}|$ and plasma mass density ρ_{SH} , with the half-width δ and half-length L of the diffusion region. The asymmetric Sweet-Parker reconnection rate is the right-hand portion of Eq. 3 including a resistivity η , and the permeability of free space μ_0 .

Swisdak and Drake [2007] argued that the orientation of reconnection is determined by the maximization of the asymmetric outflow speed (Eq. 2), and there is some evidence supporting this [Schreier et al., 2010]. Alternatively, it has been suggested to apply the same maximization to the asymmetric reconnection rate (Eq. 3) to determine the orientation of reconnection (Shay, private communication, 2009; [Borovsky, 2008, 2013]). The models based on local reconnection physics will be compared with the magnetic separators by finding locations where each model is a local maximum.

METHODOLOGY

Reconnection does not occur at a single location, so it is important to identify a locus of points at the magnetopause where reconnection could occur. For example, Trattner et al. [2007] identified maxima in the magnetic shear angle θ at the magnetopause as a possible locus of points where reconnection occurs. They employed the T96 model [Tsyganenko, 1995] for the magnetospheric magnetic field and used the Cooling model for the draped magnetosheath magnetic field [Cooling et al., 2001]. The magnetic shear angle θ was calculated at the magnetopause from these fields using Eq. 1. The locus of possible magnetic reconnection locations was determined by projecting the magnetopause to the $x = 0$ plane (the plane through the Earth that is perpendicular to the ecliptic plane), and determining maxima in the magnetic shear angle by taking cuts along the IMF direction (K. Trattner, private communication, 2013).

We employ a similar methodology to analyze our global magnetospheric simulations. With the exception of the asymmetric Sweet-Parker reconnection rate (Eq. 3), all of the models remain independent of the reconnection dissipation mechanism, so they should hold for any self-consistent magnetospheric model. We therefore use global magnetospheric resistive magnetohydrodynamic (MHD) simulations to identify the loci corresponding to each model's maximized quantity at the magnetopause. We then compare these loci to the magnetic separators determined with the algorithm described in Komar et al. [2013] to quantify which of these models, if any, accurately predict the location of reconnection at the dayside magnetopause.

The present study employs global simulations using the Block Adaptive Tree Solarwind Roe-type Upwind Scheme (BATS-R-US) code [Powell et al., 1999; Gombosi et al., 2000; De Zeeuw et al., 2000; Tóth et al., 2012]. Simulations are performed at NASA's Community Coordinated Modeling

Center (CCMC) and are analyzed with CCMC's Kameleon software suite. The methods detailed in this section can be adapted to other global magnetospheric codes.

Identification of the Magnetopause and Plasma Parameter Sampling

We modify the method of Němeček et al. [2011] to identify the magnetopause in our global magnetospheric simulations. We employ spherical coordinates centered at the Earth where both the azimuthal angle φ (measured from the Sun-Earth line, or $+x$ axis) and polar angle θ (measured from the $+z$ axis perpendicular normal to the ecliptic plane) are discretized in 5° increments. (Other sampling rates were tested and found to converge to the 5° sampling.) We use angular ranges $-110^\circ \leq \varphi \leq 110^\circ$ and $0^\circ \leq \theta \leq 180^\circ$ to fully map the dayside magnetopause. The current density magnitude is sampled along the radial vector \mathbf{r} from $7 \leq r < 20$ Earth radii (R_E) at our highest grid cell resolution ($0.125 R_E$). The first location of maximum current density magnitude is identified as the magnetopause and this location's coordinates are saved; the chosen sampling range should automatically exclude the ring current for our simulations, but we take additional care by ensuring each point is within $2 R_E$ of the previous point's radial distance. An example of this process can be seen in Fig. 2 for a simulation with an IMF clock angle of 120° . Additionally, visual inspection of the magnetic separators from Komar et al. [2013] confirms that they lie on the determined magnetopause.

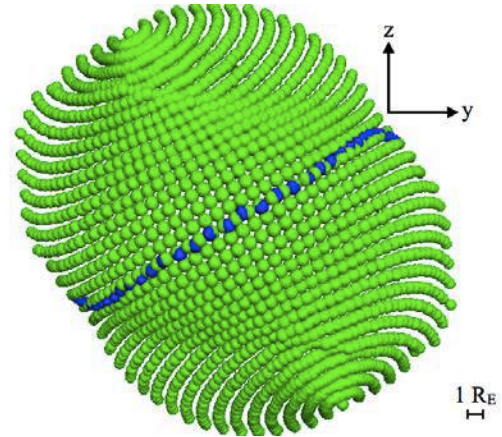


Figure 2. Magnetopause locations (green) from maxima in the current density's magnitude in a simulation with $\theta_{IMF} = 120^\circ$. The magnetic separator (blue) is shown for reference.

Once the approximate location of the magnetopause has been determined, the plasma parameters of the magnetosphere and magnetosheath need to be sampled, and thus need to be sampled along the magnetopause normal \mathbf{n} . The normal is calculated with the method described in Hoppe et al. [1992]. This technique employs a covariant analysis on the three-dimensional coordinates defining a surface to find the principal axis that minimizes the distances from a single point and its four nearest neighbors. The normal vector \mathbf{n} is the eigenvector corresponding to the minimum eigenvalue of the covariant matrix \mathbf{M} and is calculated at a point \mathbf{o} from the coordinates of its k -th nearest neighbor \mathbf{p}_k . The matrix \mathbf{M} is constructed by the equation

$$M_{ij} = \sum_k (\mathbf{o} - \mathbf{p}_k)_i \otimes (\mathbf{o} - \mathbf{p}_k)_j \quad (4)$$

Finally, this normal direction is forced to point away from Earth, i.e. $\mathbf{x} \cdot \mathbf{n} \geq 0$.

The current density is sampled along the normal vector \mathbf{n} , again at our highest resolution ($0.125 R_E$) in the region $[\mathbf{r}_{MP} - (5 R_E) \mathbf{n}, \mathbf{r}_{MP} + (5 R_E) \mathbf{n}]$, where \mathbf{r}_{MP} corresponds to the Geocentric Solar Magnetospheric (GSM) coordinates of the previously determined magnetopause location. (GSM coordinates are an orthonormal coordinate system where the Sun-Earth line is the x axis, the y axis is perpendicular to Earth's dipole axis, and the z axis completes the triplet.) The current density is

measured along \mathbf{n} to determine where it falls to $1/e$ (37%) its maximum value in the magnetosheath. The distance between the current maximum and this location determines the current sheet's half-thickness δ . The upstream plasma parameters of the magnetosphere are measured at $r_{MP} - (2\delta) \mathbf{n}$ and those of the magnetosheath at $r_{MP} + (2\delta) \mathbf{n}$. This methodology was employed to accurately measure the asymptotic plasma densities and magnetic fields undergoing magnetic reconnection in systems with asymmetries in either parameter [Cassak and Shay, 2007, 2009]

The arguments of each model are calculated from these measured quantities using Eqs. 1-3. We tacitly assumed there is no normal component of the magnetospheric and magnetosheath magnetic fields. However, we found that there are small fluctuations ($|B_n| < 1 \text{ nT}$), and these components are removed prior to each mode calculation.

Ridge Detection via Image Processing Techniques

Trattner et al. [2007] found maxima in the magnetic shear angle θ by taking cuts of the magnetic shear angle along the IMF direction (K. Trattner, private communication, 2013). This model has been employed to model reconnection for duskward and southward IMF orientations [Trattner et al., 2007; Dunlop et al., 2011; Fuselier et al., 2011; Trattner et al., 2012]. Under oblique IMF orientations, the locus of maximum magnetic shear angle goes from the southern, dawnward sector (third quadrant) and continues on to the northern, duskward sector (first quadrant). (We will show that the other model loci take similar paths across the magnetopause.) Given the general path the locus of maximum magnetic shear angle takes across the magnetopause for oblique IMF orientations, this approach will break down under northward IMF orientations since the IMF direction will be parallel to the locus. It is therefore preferable to employ a method that will work for arbitrary IMF orientations while retaining a high degree of fidelity to detect model loci.

The present study employs the image processing techniques described in Lindeberg [1993, 1998]. These techniques robustly determine the locus corresponding to each model's maximized quantity. Simply put, the loci, or ridges, are determined via finite differencing to calculate local derivatives and then local maxima are found by applying first and second derivative tests. This process is analogous to inspecting a topographic map to determine mountain ridges, with the primary advantage of computer automation.

As in Trattner et al. [2007], the magnetopause is projected to the $x = 0$ plane, resulting in a two-dimensional (2D) image, $I(y, z)$, with the model's calculated value I as a function of the magnetopause's (y, z) coordinates. At every point in the image, we construct the Hessian matrix, $\mathbf{H}(y, z) = I(y, z)$. Diagonalizing the Hessian matrix defines a (p, q) coordinate system, where the eigenvector associated with the maximum absolute eigenvalue points in the direction of the local maxima. (Without loss of generality, we assume the maximum lies along the p direction.) Local maxima are determined by finding locations where $\partial I / \partial p = 0$ (critical point test) and $\partial^2 I / \partial p^2 < 0$

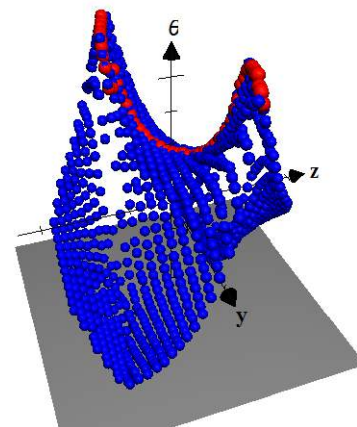


Figure 3. Surface of magnetic shear angle θ (blue spheres) and the corresponding ridge of maximum magnetic shear angle (red spheres) for a simulation with $\theta_{IMF} = 120^\circ$.

(local maximum test) using linear interpolation between nearest neighbors [Lindeberg, 1993].

Figure 3 depicts a three-dimensional surface of the magnetic shear angle θ between the magnetospheric and magnetosheath magnetic fields at the magnetopause in a simulation with $\theta_{\text{IMF}} = 120^\circ$. The magnetic shear angle surface (blue spheres) looks very similar to a saddle, and the red spheres are the result of applying the described image processing techniques. These red spheres clearly mark the ridge of the magnetic shear surface. Additional tests were made to compare with the method of Trattner et al. [2007] for comparable solar wind conditions, and the image processing techniques return qualitatively similar results (not shown). We are therefore confident that this method is fully appropriate to determine model loci at the dayside magnetopause.

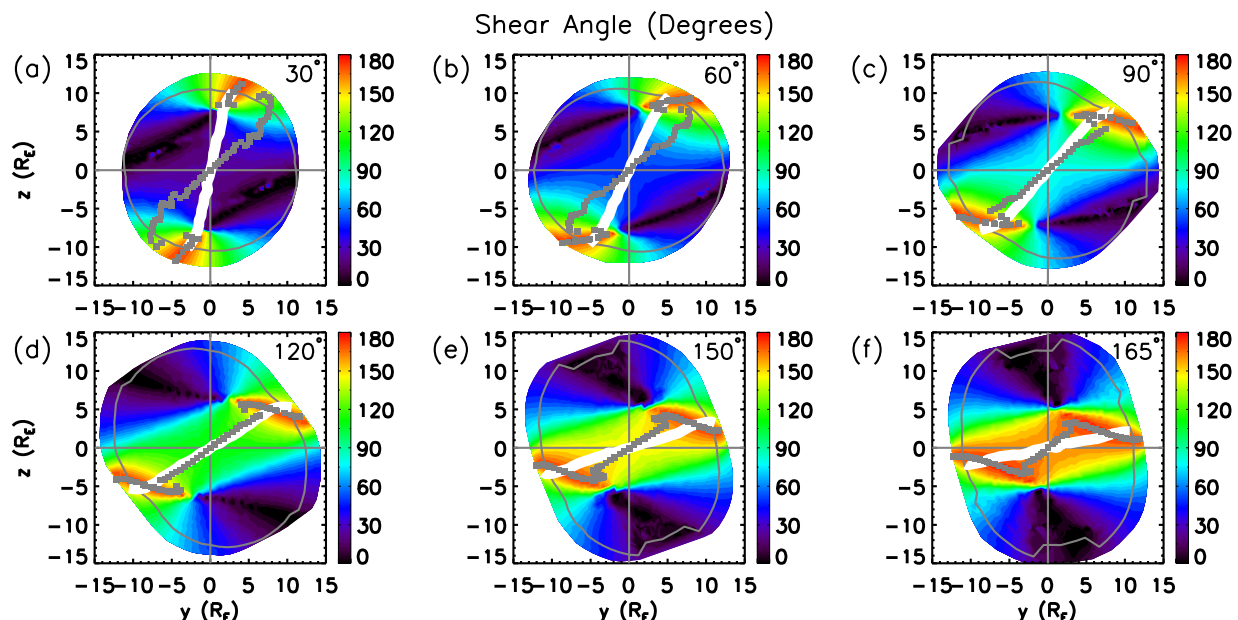


Figure 4. Image processing results for the magnetic shear angle as calculated at the dayside magnetopause in simulations with (a) $\theta_{\text{IMF}} = 30^\circ$, (b) 60° , (c) 90° , (d) 120° , (e) 150° , and (f) 165° . The calculated magnetic shear angle is the color background, the gray squares display the locus of maximum magnetic shear angle, and the magnetic separator is displayed in white. The gray oval displays the magnetopause's location in the $x = 0$ plane, and gray lines at $y, z = 0$ are provided for reference.

Magnetospheric Simulation Study

The simulations are run using BATS-R-US version 8.01 and do not use the Rice Convection Model (RCM). The simulations are evolved for two hours (02:00:00) of magnetospheric time. We look at the 02:00:00 mark of simulation data because the system has achieved a quasi-steady state by this time. BATS-R-US solves the MHD equations on a three-dimensional rectangular irregular grid. The default simulation domain is $-255 < x < 33$, $-48 < y < 48$, $-48 < z < 48 R_E$ in the GSM coordinate system. The standard high-resolution grid for CCMC simulations has 1,958,688 grid cells with a coarse resolution of $8 R_E$ in the far magnetotail, and a fine resolution of $0.25 R_E$ near the magnetopause. The present study employs a higher resolution grid of $0.125 R_E$ packed in the region $-15 < x, y, z < 15 R_E$, totaling 16,334,784 simulation grid cells.

The initial simulations do not employ a dipole tilt and use fixed solar wind inflow conditions. The solar wind has temperature $T = 232,100$ K, IMF strength 20 nT, number density $n = 20 \text{ cm}^{-3}$, and a solar wind velocity of $\mathbf{v} = -400 \text{ km/s } \mathbf{x}$. We perform distinct simulations with IMF clock angles $\theta_{\text{IMF}} = 30^\circ, 60^\circ, 90^\circ, 120^\circ, 150^\circ,$ and 165° . The IMF does not have a B_x component. Constant Pederson and Hall conductances of 5 mhos are used. The solar radio flux F10.7 index is set at a value of 150.

For the present simulations, we employ a uniform explicit resistivity η . It is known that Earth's magnetosphere is essentially collisionless, but including an explicit resistivity allows for reproducible results that are independent of the numerics. We include an explicit resistivity $\eta/\mu_0 = 6.0 \times 10^{10} \text{ m}^2/\text{s}$ in our simulations.

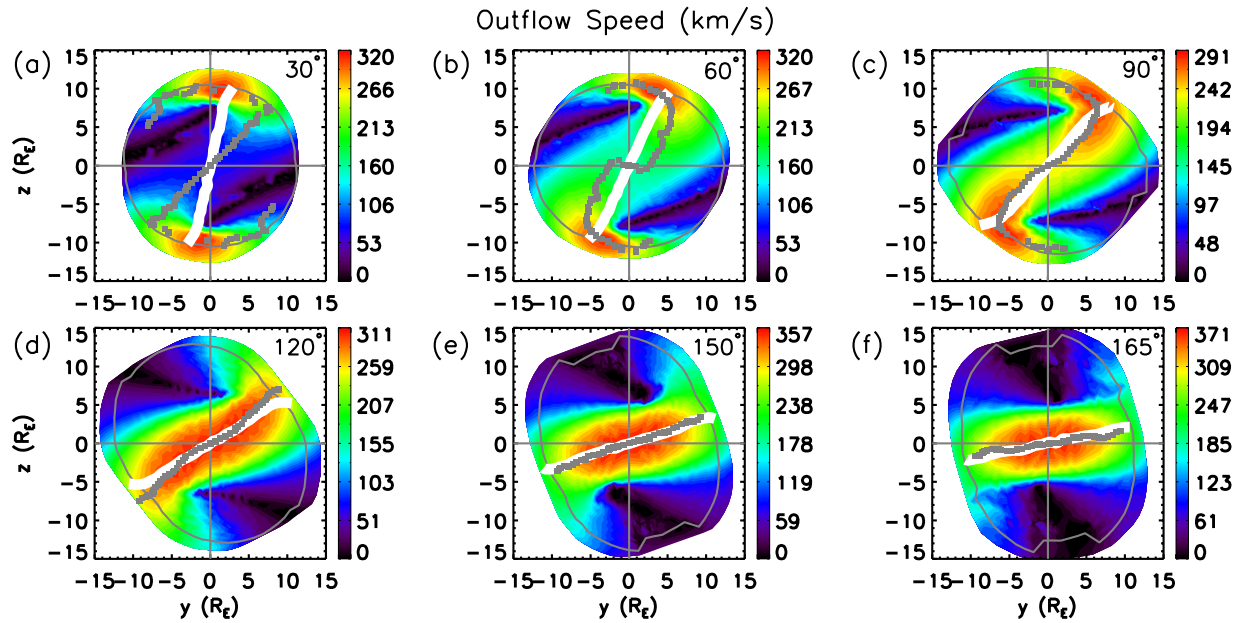


Figure 5. Image processing results for the asymmetric outflow speed as calculated at the dayside magnetopause. Figures (a) through (f) are from the same simulations as previously discussed. The calculated outflow speed, model loci, magnetic separators, reference lines and the magnetopause's location are the same as previously defined.

RESULTS

We present the image processing results for the different magnetic reconnection location models tested at the dayside magnetopause. Figures 4 through 6 display very similar information. The calculated model is displayed as the background color, the locus of each model's maximized quantity is displayed with solid gray squares, and the magnetic separators determined with the algorithm described in Komar et al. [2013] are displayed as the solid white line. The magnetopause's intersection with the $x = 0$ plane is displayed as the gray oval, and reference lines at $y, z = 0$ are provided. IMF orientations for each sub-figure correspond to IMF clock angles (a) $\theta_{\text{IMF}} = 30^\circ$, (b) 60° , (c) 90° , (d) 120° , (e) 150° , and (f) 165° . Figure 4 displays the magnetic shear angle [Trattner et al., 2007], Fig. 5 shows the asymmetric outflow speed (Equation 2; [Swisdak and Drake, 2007]), and Fig. 6 is the asymmetric Sweet-Parker reconnection rate (Equation 3; Shay, private communication, 2009; [Borovsky, 2008, 2013]).

Discussion

Figures 4-6 display the loci of possible reconnection sites for the different reconnection location models at the dayside magnetopause as a function of IMF clock angle. It is interesting that for southward orientations ($\theta_{\text{IMF}} > 90^\circ$) many of the models are within a few R_E of the magnetic separators. These differences should be within observational tolerances of satellites traversing the dayside magnetopause. These results show the differences between the models are not particularly large, and also show that all of the models do reasonably well in reproducing the separator for southward IMF.

The model loci display interesting trends for northward IMF orientations ($\theta_{\text{IMF}} \leq 90^\circ$). For these orientations, no model reproduces the separators. There are some areas that show agreement: the anti-parallel regions (located in the first and third quadrants) and at the subsolar point. The agreement at the anti-parallel regions is not entirely surprising as the location of reconnection moves to the magnetic cusps as $\theta_{\text{IMF}} \rightarrow 0^\circ$ [Dungey, 1961, 1963].

We now focus on the predictions of each model and how they compare with the separators for all IMF clock angles. Of the models tested, the maximum magnetic shear model [Trattner et al., 2007] appears to have the largest discrepancy with the magnetic separators, even for southward IMF orientations. The locus of maximum magnetic shear angle in Fig. 5 maintains a nearly constant structure as a function of IMF clock angle, where the locus through the subsolar point makes an angle of $52.2^\circ \pm 2.5^\circ$ with the $+z$ axis for all clock angles. This contrasts the general trend of the separators as they rotate around the magnetopause as the IMF clock angle increases: the separator has a vertical orientation ($|y| < 3 R_E$) for $\theta_{\text{IMF}} = 30^\circ$, whereas it nearly lies in the ecliptic plane for $\theta_{\text{IMF}} = 165^\circ$ [Komar et al., 2013].

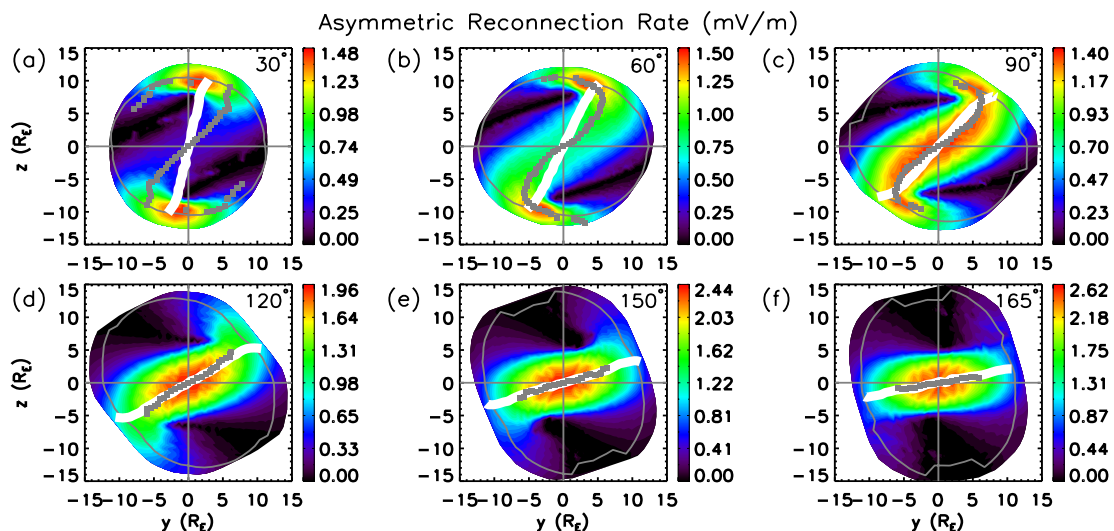


Figure 6. Image processing results for the asymmetric Sweet-Parker reconnection rate as calculated at the dayside magnetopause. Figures (a) through (f) are from the same simulations as previously discussed. The calculated reconnection rate, model loci, magnetic separators, reference lines and the magnetopause's location are the same as

The asymmetric reconnection arguments have better agreement with the magnetic separators overall. In particular, the maximization of the asymmetric outflow speed [Swisdak and Drake, 2007] and asymmetric Sweet-Parker reconnection rate (Shay, private communication, 2009, [Borovsky, 2008, 2013]) tend to agree with the separators better than the other models tested. The loci of these models rotate around the magnetopause, although there are differences in the magnitude of this tilt as compared to the separators for clock angles $\theta_{\text{IMF}} \leq 150^\circ$.

Finally, we perform additional simulations with a dipole tilt of 15° from the $+z$ axis in the x - z plane. When the IMF has a southward orientation we find that each model closely maps the magnetic separator. In fact, the locus of maximum magnetic shear angle follows the separator more closely than any other model (not shown). However, under a northward IMF orientation, no model reproduces the magnetic separator.

CONCLUSIONS

This report details a small portion of the results from an ongoing study where we calculated the prediction of several magnetic reconnection location models at the dayside magnetopause in global resistive magnetohydrodynamic simulations. We include a brief summary of our findings:

1. We find that all models are within a few Earth radii (R_E) of the magnetic separators when the IMF has a southward orientation. However, no model faithfully reproduces the magnetic separators when the IMF has a northward orientation.
2. The asymmetric outflow speed and asymmetric Sweet-Parker reconnection rate best agree with the magnetic separators under southward IMF orientations. The maximum magnetic shear model has a fixed orientation at the subsolar magnetopause and does not rotate with the magnetic separators in simulations without a dipole tilt.
3. Asymmetric magnetic reconnection orientation models should be easier to distinguish in simulations exhibiting larger magnetic field asymmetries. Separate simulations lowered the IMF strength from 20 nT to 2 nT with fixed IMF clock angle of 120° . It is found that the asymmetric orientation models tested are inconsistent with the magnetic separators at the subsolar magnetopause.
4. The reconnection location models are directly tested in separate simulations with a sunward dipole tilt of 15° for IMF clock angles of 120° and 30° . Most of the models map the magnetic separators when the IMF clock angle is 120° . However, no model faithfully reproduces the magnetic separator for a northward IMF orientation of 30° . More interestingly, the dayside portion of the magnetic separator in this simulation moves duskward by 45° in longitude (measured from the $+x$ axis). This change in the magnetic separator is consistent with other studies that have shown the location and orientation of magnetic separators depend on the magnetospheric and magnetosheath magnetic fields in simulations that included a sunward dipole tilt [Park et al., 2006; Cnossen et al., 2012], or measured magnetic separators in simulations with arbitrary IMF [Laitinen et al., 2006, 2007; Dorelli et al., 2007; Hu et al., 2009; Ouellette et al., 2010; Peng et al., 2010, Komar et al., 2013].

5. The polar cap potential difference is measured to test if reconnection is saturated for the chosen solar wind conditions. This potential difference is shown to be linear in simulations with IMF strengths of 2, 5, and 20 nT for a fixed IMF clock angle of 120°. Reconnection is not saturated for our chosen parameter regime and our results are consistent with the findings of Lopez et al. [2010].

In short, it remains unclear what controls the location of magnetic reconnection at the dayside magnetopause. At present, it remains observationally difficult to distinguish which of these models predicts the orientation of the reconnection X-line and how these models correspond to the magnetic separators. All models tested do relatively well for southward IMF orientations. NASA's upcoming Magnetospheric Multiscale (MMS) mission will provide unprecedented spatiotemporal resolution of reconnection at Earth's dayside magnetopause [Burch and Drake, 2009; Moore et al., 2013]. Testing each of these models should be accessible to MMS, providing much needed data to help determine what controls the location of magnetic reconnection at the dayside magnetopause.

ACKNOWLEDGMENTS

Support from the NASA WV Space Grant Consortium is gratefully acknowledged. I would additionally like to thank my advisor, Dr. Paul Cassak, for his unconditional support and advice as I have pursued my Ph. D. in Physics at West Virginia University. Simulations were performed at the Community Coordinated Modeling Center at Goddard Space Flight Center through their public Runs on Request system (<http://ccmc.gsfc.nasa.gov>). The CCMC is a multi-agency partnership between NASA, AFMC, AFOSR, AFRL, AFWA, NOAA, NSF and ONR. The BATS-R-US Model was developed by the Center for Space Environment Modeling at the University of Michigan. The analysis presented here was made possible via the Kameleon and Space Weather Explorer software packages provided by the CCMC. The Kameleon software has been provided by the Community Coordinated Modeling Center at NASA Goddard Space Flight Center (<http://ccmc.gsfc.nasa.gov>). Software Developers: Marlo M. Maddox, David H. Berrios, Lutz Rastaetter. Additional thanks to S. A. Fuselier, S. M. Petriner, D. G. Sibeck, V. M. Souza, and K. J. Trattner for their insight and interesting discussions.

Value of NASA Graduate Research Fellowship Program

I have found the NASA Graduate Research Fellowship Program to be extremely valuable in my Ph. D. training. The stipend provided salary support for half a year of my time as a Graduate Research Assistant in the Department of Physics and Astronomy at West Virginia University. This financial support supplemented my advisor's research funds and enabled me to succeed academically in a highly competitive funding environment.

As a direct result of this program, I have authored a paper with my advisor and collaborators at NASA's Goddard Space Flight Center and was awarded First Prize in the Magnetosphere Category of the 2013 CCMC Student Research Contest for this research. I presented a poster and gave a talk at the 2013 Geospace Environment Modeling (GEM) Summer Workshop, and received an Honorable Mention in the 2013 GEM Student Poster Contest. I gave a talk at the 2013 American Geophysical Union (AGU) Fall Meeting on the study briefly presented in this report. We are in the process of drafting a paper on these results, which we intend to submit to the *Journal of Geophysical Research* in the coming months. Finally, with support from the West Virginia Space Grant Consortium, I was able to attend the 7th Annual CCMC Workshop, where I gave a talk on my research using CCMC resources.

In closing, NASA's Graduate Research Fellowship Program through the West Virginia Space Grant Consortium has been an extremely rewarding experience. The financial support has allowed me to focus on my Ph. D. research, and enabled me to succeed academically. This generous support has presented numerous opportunities to network with colleagues and advance in my Ph. D. studies.

AWARDS, PUBLICATIONS AND PRESENTATIONS

Honors and Awards

Student Poster Award (Honorable Mention), for "Tracing Magnetic Separators in Global Magnetospheric Simulations and Their Dependence on IMF Clock Angle" at the Geospace Environment Modeling Summer Workshop, June 2013

First Prize in the Magnetosphere Category of the 2013 CCMC Student Research Contest, awarded annually by NASA's Community Coordinated Modeling Center to students performing outstanding research using CCMC resources, May 2013

Contributed Talks and Posters at Conferences

1. "On the Location of Magnetic Reconnection at the Dayside Magnetopause" □
2013 AGU Fall Meeting, Contributed Talk
San Francisco, California, December 9, 2013
2. "Tracing Magnetic Separators in Global Magnetospheric Simulations and Their Dependence on IMF Clock Angle"
2013 GEM Workshop, Contributed Poster
Snowmass, Colorado, June 18, 2013

Invited Talks

1. "A Student's Perspective on NASA's Community Coordinated Modeling Center" □
7th Annual CCMC Workshop, Annapolis, Maryland, April 2, 2014
2. "Locating Magnetic Reconnection at Earth's Dayside Magnetopause in Global Magnetospheric Simulations" (CCMC Student Research Contest Award Talk) □
2013 GEM Summer Workshop, Snowmass, Colorado, June 19, 2013
3. "Space Physics Research Using NASA's Community Coordinated Modeling Center" □
2013 GEM Student Workshop, Snowmass, Colorado, June 16, 2013

Publications

1. Komar, C. M., R. L. Fermo, P. A. Cassak (in prep), "Comparative analysis of dayside magnetic reconnection models in global magnetosphere simulations," to be submitted to *J. Geophys. Res.*
2. Komar, C. M., P. A. Cassak, J. C. Dorelli, A. Gloer, and M. M. Kuznetsova (2013), "Tracing magnetic separators and their dependence on IMF clock angle in global magnetospheric simulations," *J. Geophys. Res.*, *118*, 4998-5007.

REFERENCES

Alexeev, I. I., D. G. Sibeck, and S. Y. Bobrovnikov (1998), Concerning the location of magnetopause merging as a function of the magnetopause current strength, *J. Geophys. Res.*, *103*(A4), 6675-6684.

- Angelopoulos, V., J. P. McFadden, D. Larson, C. W. Carlson, S. B. Mende, H. Frey, T. Phan, D. G. Sibeck, K.-H. Glassmeier, U. Auster, E. Donovan, I. R. Mann, I. J. Rae, C. T. Russell, A. Runov, X.-Z. Zhou, and L. Kepko (2008), Tail reconnection triggering substorm onset, *Science*, 321, 931.
- Borovsky, J. E. (2008), The rudiments of a theory of solar wind/magnetosphere coupling derived from first principles, *J. Geophys. Res.*, 113, A08228.
- Borovsky, J. E. (2013), Physical improvements to the solar wind reconnection control function for the Earth's magnetosphere, *J. Geophys. Res.*, 118 (5), 2113.
- Burch, J. L., and J. F. Drake (2009), Reconnecting magnetic fields, *Am. Sci.*, 97, 392.
- Cassak, P. A., and M. A. Shay (2007), Scaling of asymmetric magnetic reconnection: General theory and collisional simulations, *Phys. Plasmas*, 14, 102114.
- Cassak, P. A., and M. A. Shay (2009), Structure of the dissipation region in fluid simulations of asymmetric magnetic reconnection, *Phys. Plasmas*, 16, 055704.
- Cnossen, I., M. Wiltberger, and J. E. Ouellette (2012), The effects of seasonal and diurnal variations in the Earth's magnetic dipole orientation on solar wind–magnetosphere–ionosphere coupling, *J. Geophys. Res.*, 117 (A11), A11211.
- Cooling, B. M. A., C. J. Owen, and S. J. Schwartz (2001), Role of the magnetosheath flow in determining the motion of open flux tubes, *J. Geophys. Res.*, 106 (A9), 18,763–18,775.
- Cowley, S. W. H. (1976), Comments on the merging of nonantiparallel magnetic fields, *J. Geophys. Res.*, 81 (19), 3455–3458.
- Crooker, N. U. (1979), Dayside merging and cusp geometry, *J. Geophys. Res.*, 84 (A3), 951–959.
- De Zeeuw, D., T. Gombosi, C. Groth, K. Powell, and Q. Stout (2000), An adaptive MHD method for global space weather simulations, *IEEE T. Plasma Sci.*, 28, 1956.
- Dorelli, J. C., A. Bhattacharjee, and J. Raeder (2007), Separator reconnection at Earth's dayside magnetopause under generic northward interplanetary magnetic field conditions, *J. Geophys. Res.*, 112, A02202.
- Dungey, J. W. (1961), Interplanetary magnetic field and the auroral zones, *Phys. Rev. Lett.*, 6, 47.
- Dungey, J. W. (1963), The structure of the exosphere, or adventures in velocity space, in *Geophysics: The Earth's Environment*, edited by C. De Witt, J. Hieblot, and A. Lebeau, p. 505, Gordon Breach, New York.
- Dunlop, M. W., Q.-H. Zhang, Y. V. Bogdanova, K. J. Trattner, Z. Pu, H. Hasegawa, J. Berchem, M. G. G. T. Taylor, M. Volwerk, J. P. Eastwood, B. Lavraud, C. Shen, J.-K. Shi, J. Wang, D. Constantinescu, A. N. Fazakerley, H. Frey, D. Sibeck, P. Escoubet, J. A. Wild, Z. X. Liu, and C. Carr (2011), Magnetopause reconnection across wide local time, *Ann. Geophys.*, 29 (9), 1683–1697.
- Fuselier, S. A., K. J. Trattner, and S. M. Petrinec (2011), Antiparallel and component reconnection at the dayside magnetopause, *J. Geophys. Res.*, 116 (A10), A10227.
- Gombosi, T., D. DeZeeuw, C. Groth, and K. Powell (2000), Magnetospheric configuration for Parker-spiral IMF conditions: Results of a 3D AMR MHD simulation, *Adv. Space Res.*, 26, 139.
- Gonzalez, W. (1990), A unified view of solar wind-magnetosphere coupling functions, *Planet. Space Sci.*, 38 (5), 627 – 632.

- Gonzalez, W. D., and F. S. Mozer (1974), A quantitative model for the potential resulting from reconnection with an arbitrary interplanetary magnetic field, *J. Geophys. Res.*, *79* (28), 4186–4194.
- Guo, R., Z. Pu, C. Xiao, X. Wang, S. Fu, L. Xie, Q. Zong, J. He, Z. Yao, J. Zhong, and J. Li (2013), Separator reconnection with antiparallel/component features observed in magnetotail plasmas, *J. Geophys. Res.*, *118*, pp. 6116–6126.
- Hesse, M., N. Aunai, S. Zenitani, M. Kuznetsova, and J. Birn (2013), Aspects of collisionless magnetic reconnection in asymmetric systems, *Phys. Plasmas*, *20* (6), 061210.
- Hoppe, H., T. DeRose, T. Duchamp, J. McDonald, and W. Stuetzle (1992), Surface reconstruction from unorganized points, *SIGGRAPH Comput. Graph.*, *26* (2), 71–78.
- Hu, Y. Q., Z. Peng, C. Wang, and J. R. Kan (2009), Magnetic merging line and reconnection voltage versus IMF clock angle: Results from global MHD simulations, *J. Geophys. Res.*, *114*, A08220.
- Komar, C. M., P. A. Cassak, J. C. Dorelli, A. Gloer, and M. M. Kuznetsova (2013), Tracing magnetic separators and their dependence on IMF clock angle in global magnetospheric simulations, *J. Geophys. Res.*, *118* (8), 4998–5007.
- Laitinen, T. V., P. Janhunen, T. I. Pulkkinen, M. Palmroth, and H. E. J. Koskinen (2006), On the characterization of magnetic reconnection in global MHD simulations, *Ann. Geophys.*, *24*, 3059.
- Laitinen, T. V., M. Palmroth, T. I. Pulkkinen, P. Janhunen, and H. E. J. Koskinen (2007), Continuous reconnection line and pressure-dependent energy conversion on the magnetopause in a global MHD model, *J. Geophys. Res.*, *112*, A11201.
- Lindeberg, T. (1993), Discrete derivative approximations with scale-space properties: A basis for low-level feature extraction, *J. Math. Imaging and Vis.*, *3* (4), 349–376.
- Lindeberg, T. (1998), Edge detection and ridge detection with automatic scale selection, *Int. J. Comp. Vis.*, *30* (2), 117–156.
- Lopez, R. E., R. Bruntz, E. J. Mitchell, M. Wiltberger, J. G. Lyon, and V. G. Merkin (2010), Role of magnetosheath force balance in regulating the dayside reconnection potential, *J. Geophys. Res.*, *115* (A12), A12216.
- Moore, T., J. Burch, W. Daughton, S. Fuselier, H. Hasegawa, S. Petrinec, and Z. Pu (2013), Multiscale studies of the three-dimensional dayside X-line, *J. Atmos. Sol. Terr. Phys.*, *99* (0), 32 – 40.
- Moore, T. E., M.-C. Fok, and M. O. Chandler (2002), The dayside reconnection X line, *J. Geophys. Res.*, *107* (A10), 1332.
- Němeček, Z., J. Šafránková, A. Koval, J. Merka, and L. Přech (2011), MHD analysis of propagation of an interplanetary shock across magnetospheric boundaries, *J. Atmos. Sol. Terr. Phys.*, *73* (1), 20 – 29.
- Ouellette, J. E., B. N. Rogers, M. Wiltberger, and J. G. Lyon (2010), Magnetic reconnection at the dayside magnetopause in global Lyon-Fedder-Mobarry simulations, *J. Geophys. Res.*, *115*, A08222.
- Park, K. S., T. Ogino, and R. J. Walker (2006), On the importance of antiparallel reconnection when the dipole tilt and IMF By are nonzero, *J. Geophys. Res.*, *111* (A5), A05202.
- Paschmann, G. (2008), Recent in-situ observations of magnetic reconnection in near-Earth space, *Geophys. Res. Lett.*, *35* (19), L19109.

- Peng, Z., C. Wang, and Y. Q. Hu (2010), Role of IMF B_x in the solar wind-magnetosphere-ionosphere coupling, *J. Geophys. Res.*, *115*, A08224.
- Powell, K. G., P. L. Roe, T. J. Linde, T. I. Gombosi, and D. L. D. Zeeuw (1999), A solution-adaptive upwind scheme for ideal magnetohydrodynamics, *J. Comp. Phys.*, *154*, 284.
- Schreier, R., M. Swisdak, J. F. Drake, and P. A. Cassak (2010), Three-dimensional simulations of the orientation and structure of reconnection X-lines, *Phys. Plasmas*, *17* (11), 110704.
- Sonnerup, B.U.Ö. (1974), Magnetopause reconnection rate, *J. Geophys. Res.*, *79* (10), 1546–1549.
- Swisdak, M., and J. F. Drake (2007), Orientation of the reconnection X-line, *Geophys. Res. Lett.*, *34* (11), L11106.
- Tóth, G., B. van der Holst, I. V. Sokolov, D. L. D. Zeeuw, T. I. Gombosi, F. Fang, W. B. Manchester, X. Meng, D. Najib, K. G. Powell, Q. F. Stout, A. Glocer, Y.-J. Ma, and M. Opher (2012), Adaptive numerical algorithms in space weather modeling, *J. Comp. Phys.*, *231* (3), 870 – 903.
- Trattner, K. J., J. S. Mulcock, S. M. Petrinec, and S. A. Fuselier (2007), Probing the boundary between antiparallel and component reconnection during southward interplanetary magnetic field conditions, *J. Geophys. Res.*, *112* (A8), A08210.
- Trattner, K. J., S. M. Petrinec, S. A. Fuselier, and T. D. Phan (2012), The location of reconnection at the magnetopause: Testing the maximum magnetic shear model with THEMIS observations, *J. Geophys. Res.*, *117* (A1), A01201.
- Tsyganenko, N. A. (1995), Modeling the Earth's magnetospheric magnetic field confined within a realistic magnetopause, *J. Geophys. Res.*, *100* (A4), 5599–5612.

ENHANCER ANALYSIS OF THE GENE ROUGH

Adam T. Majot
PhD Candidate, Biology
Academic Institution
Morgantown, WV 26506
Dr. Ashok P. Bidwai

ABSTRACT

Drosophila eye development remains the paradigm of cell fate specification and epithelial organization. The fly retina is comprised of ~750 repeated units, each produced in a stereotyped pattern that begins with differentiation of an R8 founder cell. Although Notch and *Egfr* signaling have each been shown to regulate the placement of R8 cells, the specific contribution of each pathway remains unclear. Herein we show that R8 cell fate requires expression of the ETS repressor Anterior open (*Aop*) to maintain R8 competency. *Aop* accomplishes such through the repression of multiple other repressors, including Rough (*Ro*). Analysis of the *Ro* locus reveals multiple conserved, putative *Aop* binding sites flanking the *ro* transcription start site, suggesting that *Aop* directly regulates *Ro*. Preliminary enhancer-reporter data recapitulates the *Ro* expression pattern.

INTRODUCTION

For all multicellular organisms, development proceeds from the fertilization of a single cell (the egg) through many cell divisions and the assumption of many specified cell-types. Despite superficial differences, all animals bodies have many commonalities, including the need to separate the environment from the inner, controlled processes within the body. As such, most animals have the need for many common systems (for example, circulation, digestion, sensory, etc.). The paradox of development arises from the fact that such complex systems are derived from a single cell that includes all of the information necessary for the many cell types that comprise sophisticated bodies. The differentiation of all the systems must then arise through the selective expression of various genes in particular cells. Thus, as cells divide, and developing bodies grow larger, subsets of cells must be directed to undertake divergent gene expression from their neighbors. This divergence of gene expression is accomplished through extracellular signaling, in which signal-sending cells secrete ligands to communicate to signal-receiving cells that have expressed cognate receptor proteins. The interaction between ligand and receptor induces a change in the intracellular environment (through the production of second-messengers or post-translational protein modifications) that is transduced to the nucleus where gene expression is affected, allowing the signal-receiving cell to diverge in function from its signal-sending neighbor.

Animal bodies are constructed almost entirely from the same six signaling pathways, including Notch and receptor tyrosine kinases such as EGFR. These pathways are conserved across hundreds of millions of years of evolution, indicating an extreme importance in the preservation of their structure and developmental function. Due to such conservation, studies in model systems have elaborated greatly upon the genetic basis for disease etiology and have suggested possible

solutions. *Drosophila*, the longest standing genetic model, is ideal for signal studies due to its comparatively small genome that includes few duplications of critical signaling components, and the variety of genetic manipulations available.

The *Drosophila* retina is unique tissue among the many available species in which developmental genetics has been extensively studied. The retina, which ultimately consists of ~750 facet, grows from an ovoid neuroepithelial monolayer in which differentiation proceeds in dorsoventral columns of cells, from posterior to anterior (Kumar 2012). The R8 neuron is the first cell to be specified within each differentiating column, and to each R8 all other cells of each facet are recruited. Thus, the specification of the R8 is of greatest importance to proper patterning of the eye (Lubensky et al. 2011). Both the Notch and EGFR signaling pathways are critical to appropriately specify each R8, but it is unclear how the pathways cooperate or antagonize each other to accomplish such (Lesokin et al. 1999, Rodrigues et al. 2005).

The specification of each R8 is dependent upon the precise restriction of expression of the proneural gene *Atonal* (*Ato*) to a single cell from a larger cluster of *Ato*-positive cells (Li and Baker 2001). We had previously determined that the gene *Aop* was responsible for maintaining *Ato* expression long enough to allow R8s to form. *Aop* has long been known as a component of the EGFR signaling pathway (Rebay and Rubin 1995), however, this early *Aop* function appeared to occur prior to known EGFR function. Previous efforts had indicated that *Aop* could perhaps operate limitedly as an effector of Notch signaling (Rohrbaugh et al. 2002), igniting speculation that further studies *Aop* might illuminate the nature of the relationship between Notch and EGFR.

RO ENHANCER ANALYSIS – IN SILICO

The genomic region of interest (the Ro enhancer, from -4.5kb through +3.7kb) was obtained from Flybase.org Gbrowse2. This sequence was analyzed using the internet-based sequence alignment tool EvoPrinter HD, which compared the sequence data from 12 species of the *Drosophila* genome (including *D. melanogaster*) to determine regions of conservation and identity. As should be expected, exonic regions are very well conserved across all species (~60 million years of evolution span the 12 species). More importantly, EvoPrinter HD is a powerful tool for the detection of conserved non-coding sequence. Such sequence conservation in noncoding regions is strongly indicative of regulatory function. Our analysis uncovered eight conserved *Aop* binding motifs within intron 1, and another two conserved sites at -66 and -1800bp. These ten sites serve as the strongest likely candidates for *Aop* binding.

MAPPING OF THE RO[D] BREAKPOINT

To sequence the roD breakpoint it was necessary to prepare DNA from flies hemizygous for only the roD allele, otherwise our assays would report information related to the wild-type locus. Thus, we crossed T(2;3)roD/+;TM6B flies to those that contained the deficiency that uncovered the Ro locus, Df(3R)ED6255/TM3 to obtain hemizygous roD flies. I had originally proposed that the breakpoint be assayed using high-throughput next-generation sequencing techniques, which elicit data production within days and require few reagents other than purified, isolated genomic DNA. However, at the behest of my adviser, who indicated mistrust of the new technology, I was rerouted into deriving the breakpoint through an older-fashioned, recursive PCR-primer walk technique. Ultimately, if the breakpoint was not located within 4.5kb upstream (-4.5kb) of the Ro transcription start site, the particular site of the translocation was of little value. Prior studies have confirmed

that a P-element-bearing genomic fragment that includes the -4.5kb through the homeobox-encoding exon is capable of rescuing ro null flies. Thus, we reasoned that if Aop was repressing Ro, it was doing so through binding to a binding motif present in this 8kb rescue construct.

The recursive PCR-primer walk worked in the following fashion: starting at the Ro transcription start site, primer sets targeted successive 1500bp regions, with each region overlapping the previous region by 300bp. The primers were designed to complement the upstream enhancer of Ro, thus a failure of PCR amplification could be interpreted as a potential interval for the 2L/3R translocation. Although we had predicted that the roD translocation likely occurred near the ro transcription start site, we were surprised to reveal that its location at an interval of 12-13kb upstream, within an intron of the gene t48.

At first, this result appeared to be paradoxical. If the breakpoint was 12-13kb upstream of the rough transcriptional start site, it would be exceedingly improbably that Aop (which is known to operate more locally than tens of thousands of bases) could have regulated the genome from such a distance. More importantly, such an effect would have provided disregulated Ro expression in the Ro-rescue constructs akin to the misregulation that has been observed in roD. We turned our attention to the exploration of alternate possibilities for Ro misexpression in the roD mutant. If not the loss of distal Aop bindings sites, then it was possible that the translocation that has previously defined roD is a red-herring in that this genomic aberration has led previous researchers to believe that the cause of Ro misexpression must be the translocation. Alternately, it is possible that 1) roD harbors other mutations that have altered repressor binding (not exclusively Aop, or 2) the translocation of roD has brought transcriptional activation sites within better proximity of the Ro transcription unit, or 3) the translocation has drastically rearranged the chromatic domain structure, altering the basal expression from the Ro locus. Options 2 and 3, in addition to having little medical significance, are both very difficult and expensive to assess for a lab of our capabilities. Thus, we are in the process of exploring option 1, that perhaps the genomic sequence from chromosome 3R of the roD chromosome has undergone a second-site mutation. We hypothesize that if this mutation is elicited by a loss of Aop binding, then one or more of the ten sites identified in through our in silico analysis are likely to be mutated.

An unfortunate drawback of this PCR primer-walk mode of analysis is the lack of definitive determination of the translocation breakpoint. Despite such, we feel confident that with our final analysis of the Ro locus from the roD genomic sequence will provide solid footing as to whether this mutant is the cause of a second-site mutation or the production of a more transcriptionally active Rough locus due to translocation.

RO ENHANCER-REPORTER STUDIES

Commonly, the role of regulatory DNA is studied using enhancer-reporters, wherein plasmids that encode an easily observed gene product such as Beta-galactosidase or green fluorescent protein (GFP). From the wild-type fly, genomic DNA was isolated. Two regions of interest were PCR-amplified: -1 through -5000bp, and +1 through +2849bp. The former was amplified with BamHI (3') and KpnI (5') flanks and the latter was amplified with HpaI sites (3' and 5'). Three enhancer-reporter constructs were made by force-cloning the aforementioned PCR products into the enhancer-reporter vector pH-Stinger, which encodes eGFP (a variant of GFP that exhibits enhanced maturation time and fluorescence) under the transcriptional control of a minimal promoter. The three constructs are as follows:

<u>Description</u>	<u>Reference Title</u>
pH-Stinger: Ro(-5000bp)-eGFP	ro-5kb-GFP
pH-Stinger: eGFP-Ro(+2849bp)	ro-GFP+2.849kb
pH-Stinger: Ro(-5000bp)-eGFP-Ro(+2849bp)	ro-5kb-GFP+2.849kb

Transgenic fly lines were established from each of the enhancer-reporter constructs shown above. Each line was mapped to their respective residential chromosomes using segregation analysis.

ro-5kb-GFP+2.849kb is, in essence, a recapitulation of the original Ro rescue constructs used by Tomlinson. As such, we expected this line to elicit expression in a pattern equivalent to that of wild-type Ro expression. Ro is expressed in a broad dorsoventral band posterior to Ato expression in the developing retina. Further posterior to this region, Ro is restricted to the first two photoreceptor pairs recruited to the nascent R8, the R2/5 and R3/4. As expected, the ro-5kb-GFP+2.849kb construct reported intermittently in cells posterior to the Ato expression domain, as well as within most R2/5 and R3/4. Specifically, the effects of enhancer-report appeared to be cumulative in that the presence of multiple copies (no more than two observed at once) provided stronger, more consistent report than was observed in heterozygous flies.

We next assessed the ability of the 2.849 intronic fragment to drive reporter expression. This point was of interest for the fact that the original rescue construct included both enhancer regions, 5' and 3' of the transcription start site although later studies suggested that only the +2.849 intron was necessary for robust Ro expression in the R2/5 and R3/4 photoreceptor pairs. Interestingly, ro-GFP-2.849kb drove GFP expression in a pattern identical to that observed with the ro-5kb-GFP+2.849kb construct. As was observed with the formerly described construct, GFP expression was present in each of the regions where Ro is traditionally observed, although its presence was more sporadic in heterozygote as compared to homozygote reporter flies. The lack of the 5' 5kb enhancer region suggests that the 5' enhancer region plays a minimal role, if any, in regulating Ro expression, in spite of the two upstream Aop binding motifs identified by the *in silico* analysis.

Lastly, we assessed the ability of the 5' 5kb enhancer to regulate Ro expression. The ro-5kb-GFP reporter construct produced two transgenic flies and both failed to report any detectable GFP within any region of the developing *Drosophila* retina. In light of the observations using the other two enhancer reporter constructs, this data is unsurprising. As shown, much, if not all, of the Ro gene's transactivational potential is achieved from the 2.849 intronic enhancer. If the 5' 5kb enhancer has any effect, it is likely so minimal that its effects lay below the detection threshold for the experiments as they were performed.

Future directions

The 2.849kb intronic enhancer has proven to be the most interesting enhancer region within the Ro locus. Within this small region we have identified eight putative Aop binding motifs, each of which are within regions of high conservation across 12 *Drosophila* species, spanning approximately 60 million years of evolutionary time. The long-held conservation of such sites within noncoding DNA strongly suggests regulatory potential. Future efforts with enhancer-reporter construction will be to construct re-engineer the 2.849kb intronic enhancer to have mutated Aop binding motifs (exchange GGAA/T motifs for CGCG motifs) to abrogate potential Aop interaction with this region of the Ro gene. If Aop is necessary to prevent early Ro expression, it is likely that mutation of these motifs will allow detection of precocious GFP from Aop binding-

mutant enhancer-reporters. However, construction of such Aop binding mutant enhancer regions is made more difficult by the relatively high number of putative Aop binding motifs and the relative proximity of the individual sites to each other. We anticipate moving forward with induction of such mutations soon, likely through use of site-directed mutagenesis, a method in which PCR is performed on a plasmid using overlapping primers that include a mutation for a small region of interest. Thus, as PCR initiates, the mutant primers are incorporated and subsequent cycles of PCR incorporate the error originally included via primer design.

MOSAIC ANALYSIS USING FLP-FRT

Background on FLP-FRT and Mitotic Recombination

The relationship between Aop and Ro was originally detected through the induction of mitotic clones using the FLP-FRT system. Many genes are required at multiple points of development. Thus, removal of a gene often results in very serious, and frequently lethal, defects during early embryogenesis, preventing the study of a gene's role during later stages development. To circumvent such problems, Drosophilists have developed a system wherein recombination between homologous chromosomes can be induced during mitosis, after a cell has copied its entire genome, but before each pair of sister chromatids are subject to segregation into separate daughter cells. To accomplish such, the FLP recombinase enzyme has been used to recognize a repetitive sequence of DNA, termed FRT, on homologous chromosomes to swap the attached chromosomal material. The cells in which recombination undergo no stress, but the rules of sister chromatid segregation can be skirted to allow a daughter cell to receive both the parent and daughter copy of a particular chromosome, allowing homozygous mutant cells to be formed at later points of development once potential embryonic 'bottlenecks' have been traversed. Thus, regulation of mitotic recombination is restricted to control of expression of the FLP recombinase, often put under regulation of the heat-shock promoter or an retina-specific enhancer fragment.

Experimental Work

As stated previously, induction of Aop mutant clones first indicated that Aop is responsible for maintaining Ato expression, a gene that is absolutely necessary for specification of R8 cells. Due to Aop's well-defined role as a transcriptional repressor, it quickly became clear that Aop must repress another repressor to positively regulate Ato. A fitting candidate target of Aop repression was Ro, which has been suggested to be a repressor of Ato and is never observed to be expressed in the same cell as Ato. Furthermore, removal of Ro elicits a mild expansion in the Ato expression domain. Staining of Aop mutant tissue with Ro antibodies confirmed our hypothesis that Ro is expressed earlier in the mutant tissue than within its wild-type counterpart. However, at the time of my original application for the NASA West Virginia Space Grant Consortium Graduate Fellowship, I had not yet confirmed that loss of both Aop and Ro could be capable of rescuing Ato expression.

I have since tested for such, and results indicate that Ato expression is NOT restored in clones of both Aop and Ro. This data is interesting in that although Ro is precociously expressed in Aop mutant tissue, such expression is not responsible (at least not solely responsible) for the loss of Ato. This outcome required us to probe the genetic landscape for other possible regulators of Ato that could be downstream of Aop. We had previously assumed that Notch signaling was aborted in Aop mutant tissue, as had previously been intimated in other reports (although not experimentally confirmed). We performed a series of tests to assess whether Notch signaling

actually occurred in Aop mutant tissue. Notch can be detected in the developing eye by observing the presence of transcription factors downstream of Notch pathway activation, E(spl) genes. Additionally, one can observe Notch effects by documenting the Hedgehog pathway activity and apical constriction (as detected by Arm accumulation) within a dorsoventral groove that travels across the developing *Drosophila* retina. Despite our preconceptions, we confirmed that Notch signaling occurs the same in Aop mutant tissue as in wild-type. E(spl) proteins accumulate as in wild-type (though aberrantly patterned) and Hh pathway activity occurs without deviation from wild-type. Apical constriction also occurs in Aop mutant cells.

Future directions

Interestingly, the determination that Notch signaling occurs within Aop mutant cells provided several possible directions for future investigations. Firstly, we had spend several months exploring Aop's potential as a direct downstream effector of Notch signaling. As such, we have provided convincing evidence that although Aop has been shown to regulate genes that cooperate with EGFR signaling, the gene is expressed throughout the developing retina in response to activation of the Notch receptor. Interestingly, our detection of E(spl) within Aop mutant tissue suggests that, in addition to Ro, Aop might delay E(spl) expression, if only mildly, to allow proper Ato expression. The nature of this delay is the subject of current speculation, whether direct or indirect, as Aop also targets the transcriptional repressor Roe. We are currently testing for a direct Aop-E(spl) connection using mosaic analysis with a repressible cell marker (MARCM). Additionally, we are looking to expand our findings on the Aop-Roe connection by probing for direct genetic interactions between Aop and Roe. If both genes compromise the same genetic pathway, it is reasonable to expect that mutation to both components will elicit eye defects that can be observed in adult flies.

FUTURE DIRECTIONS

Having only currently acquired our suite of enhancer-reporter flies, we are only currently beginning to perform complex genetic analyses with such flies. We have previously established that Aop negatively regulates Ro while Ato is expressed. We will soon analyze the GFP expression from the enhancer-reporter constructs in clones of mutant Aop tissue. Evidence for Aop regulation of GFP should further bolster any claim that Aop regulates Ro.

Even if such experiments provide the predicted data, we are still left with the confounding issue that Ro appears to not be responsible for the observed Ato phenotype. However, we have recently conducted experiments with a hypermorphic allele of EGFR, EGFR^{E1}, that implicates Ro as both a downstream effector of EGFR and Aop activity. EGFR^{E1} interacts strongly with Aop mutant alleles. However, the significance of this interaction had never been revealed or probed with modern research tools. We have shown that this interaction compromises Ato expression, resulting in diminished establishment of R8s. We have furthered this research by showing that removal of Ro is capable of reversing the effects of EGFR^{E1}-Aop interaction. This data, though at odds with our dual clonal analysis of Ro and Aop, suggests that Ro is capable of Ato repression, if not only in an EGFR gain-of-function background. We hope to use our enhancer-reporter lines to further establish any such role between Ro, EGFR and Aop.

ACKNOWLEDGEMENTS

I would like to thank NASA West Virginia Space Grant Consortium for providing the Graduate Fellowship and funding that, without which, this research absolutely could not have been possible. I am also grateful to Lucas M. Jozwick for support with EvoPrinter and to Clifton Bishop and Andrew Dacks for helpful discussion and to Ashok Bidwai for providing lab space and ancillary supplies related to the maintenance of fly stocks. I would like to thank WVU Biology (via Richard Thomas), Eberly College of Arts and Sciences, and WVU Academic Affairs for providing funding for research supplies and conference travel. I would like to thank Nick Baker, Sarah Bray, Justin Kumar, Ulrike Heberlein, Yuh Nung Jan, Hugo Bellen, Developmental Hybridoma Studies Bank, Drosophila Genomics Resource Center, and the Bloomington Drosophila Stock Center for fly stocks and reagents.

REFERENCES

- Kumar JP. 2012. Building an ommatidium one cell at a time. *Developmental Dynamics* 241:136-149.
- Lesokin AM, Yu SY, Katz J, Baker NE. 1999. Several levels of EGF receptor signaling during photoreceptor specification in wild-type, *Ellipse*, and null mutant *Drosophila*. *Developmental Biology* 205(1):129-144.
- Li Y, Baker NE. 2001. Proneural enhancement by Notch overcomes Suppressor-of-Hairless repressor function in developing *Drosophila* eye. *Current Biology* 11(5):330-338.
- Lubensky DK, Pennington MW, Shraiman BI, Baker NE. 2011. A dynamical model of ommatidial crystal formation. *Proceedings of the National Academy of Sciences of the United States of America* 108(27):11145-11150.
- Lesokin AM, Yu SY, Katz J, Baker NE. 1999. Several levels of EGF receptor signaling during photoreceptor specification in wild-type, *Ellipse*, and null mutant *Drosophila*. *Developmental Biology* 205(1):129-144.
- Rebay I, Rubin GM. 1995. Yan function as a general inhibitor of differentiation and is negatively regulated by activation of the Ras1/MAPK pathway. *Cell* 81(6):857-866.
- Rodrigues AB, Werner E, Moses K. 2005. Genetic and biochemical analysis of the role of *Egfr* in the morphogenetic furrow of the developing *Drosophila* eye. *Development* 132(21):4697-4707.
- Rohrbaugh M, Ramos E, Nguyen D, Price M, Wen Y, Lai ZC. 2002. Notch activation of yan expression is antagonized by RTK/pointed signaling in the *Drosophila* eye. *Current Biology* 12(7):576-581.

PRESENTATIONS/PUBLICATIONS (AS RESULT OF THIS FUNDING)

Poster

Majot AM, Bidwai AP. E(spl)D-mediated repression of R8 cell-fate occurs independently of *Nspl*. 55th Annual *Drosophila* Genetics Conference, March 26-30. San Diego, CA.

Manuscripts

Majot AM, Bidwai AP. *Aop* promotes proneural maintenance through a delay of restrictive Notch signaling. Manuscript in preparation.

Majot AM, Bidwai AP. E(spl)D-mediated repression of R8 cell-fate occurs independently of *Nspl*. Manuscript in preparation.

ULTRASOUND MEDIATED GENE DELIVERY IN IMMUNE-COMPETENT MICE

Rounak P. Nande
PhD Student, M.Sc., Biomedical Sciences
Marshall University
Huntington, WV, 25701
Research Mentor: Dr. Pier Paolo Claudio

ABSTRACT

The goal of our study is to develop a safe and efficient adenoviral gene delivery method for prostate cancer (PC) mediated by ultrasound targeted microbubble destruction (UTMD). Our group has extensively studied gene delivery of reporter and therapeutic genes into PC grown in nude mice. A major challenge for effective gene therapy is systemic delivery of nucleic acids into affected tissue. We have previously demonstrated that UTMD can significantly enhance adenoviral gene transfer in the presence of microbubbles (MBs) to specifically target mice PC xenografts. The advantage of using MBs for gene transfer is to protect the viral payload from rapid degradation by the immune system thus allowing for intravenous injection rather than direct target organ injection. However, the effect of microbubbles on the immune system has never been studied nor the effect on the viruses that hidden inside the bubble that act as the delivery vehicle. Thus we proposed an immune-competent mice model to study the effects of the therapeutic mda-7 gene therapy mediated by UTMD. Due to procedural limitations in breeding large colonies the study is still in its infancy. The purified adenoviral vectors harboring mda7 genes are ready for the animal study as well as all the protocols and procedures required for performing the experiment. We purchased TRAMP C2 cell line and explored the possibility of completing this study with a syngeneic immune-competent TRAMP prostate cancer mice model because adenoviruses can successfully transduce the TRAMP-C2 cells.

INTRODUCTION

The primary objective of this grant was to develop a safe and effective means of gene delivery in vivo and in the past we have studied gene delivery using ultrasound (US) contrast agent and US in an immune-incompetent nude mice model. But, we have yet to realize the therapeutic potential of mda-7/IL-24 induction combined with ionizing radiation using US mediated delivery to combat human malignancies, specifically advanced PC because the progress has been hampered by the lack of immune-competent prostate cancer mice models. As such, we decided to use a novel mice model (p53PE -/-; RbPE -/- mice) deficient in both p53 and pRb that results in the growth of primary prostate lesion as well as a metastatic disease. For this purpose, we wanted to target the primary prostate lesion with an image guided gene therapy system assisted by ultrasound (US) and US contrast agents.

To combat the metastatic disease, we will take advantage of the peculiar characteristics of mda-7/IL-24, which is a secreted protein that has been shown to elicit profound regression of metastatic disease through an autocrine/paracrine mechanism of induction of this cytokine [1, 2]. Expression of mda-7/IL-24 in the targeted primary tumor can facilitate its expression and secretion from naïve

normal and cancer cells that are exposed to the extracellular protein, thereby significantly enhancing the percentage of tumor cells expressing MDA-7/IL-24 and the metastatic anti-tumor activity. In these contexts, our vectors and our approach should provide both tumor selectivity and adequate induction of newly synthesized MDA-7/IL-24 by “autocrine” induction in the distant tumor to result in tumor elimination at both treated and distant sites in vivo.

IBC and IACUC protocols were established before the use of any recombinant infectious agent and in vivo study. These protocols were met and the training required to implement the safety measures were completed. Ad.mda7 and conditionally replication competent adenovirus (CRCAs) also known as cancer terminator virus (CTV (Ad.PEG-E1A-mda-7)) were amplified and purified as described. Every adenoviral amplification was tittered before performing transduction studies. My mentor also trained me in handling mice and maintaining the mice colony. I was also trained in different surgical procedures and injections that would be necessary for me to complete this study. I was also trained in using the X-rad irradiator and the ultrasound system by my mentor.

The in vivo study will take several more months before we get results as it will take sufficient time to cultivate a large colony from the breeder mice. Thus we looked for an alternative prostate cancer mice model while we wait on the mice colony. TRAMP mice model has been used in some other studies to look at viral gene therapy in an immune-competent model [3, 4]. We performed viral transduction studies and western blot analysis on the transduced TRAMP-C2 cells. We were able to transduce these cells successfully. As TRAMP-C2 mouse cell line can be allografted in TRAMP mice for syngeneic model should allow us to complete the experiment.

BACKGROUND

Prostate cancer is the most commonly diagnosed malignancy and the second leading cause of cancer mortality in American males. Prostatic adenocarcinoma is a rare disease before age 40, however its incidence increases by the age of 70. Prostate cancer is not only significant for its lethality but also for the extremely high morbidity associated with it. Therapeutic options vary according to the stage of the disease at the time of presentation and diagnosis. Patients with localized disease may be treated with surgery or radiation, whereas the treatment for patients with metastatic disease is purely palliative. Hormonal treatment with anti-androgens is the standard therapy for stage IV prostate cancer, but patients ultimately become non-responsive to androgen ablation. Current therapy options for patients with hormone-refractory prostate cancer include radiotherapy and cytotoxic chemotherapeutic agents, such as mitoxantrone, estramustine and taxanes. Despite a palliative benefit, none of these approaches engender a beneficial impact on the overall survival of patients. Consequently, no consistently effective therapy exists for these patients mandating the development of novel, more efficacious and innovative treatment approaches, especially those targeting metastasis.

Different approaches have been tested, so far, to enhance the response of prostate adenocarcinoma to different therapies with variable results. For example, gene therapy offers a magnitude of potential for combating and curing a wide range of pathology. The melanoma differentiation associated gene-7/interleukin-24 (mda-7/IL-24) was originally identified as a gene associated with terminal differentiation and irreversible growth suppression of metastatic human melanoma cells. Mda-7 belongs to the IL-10 family of cytokines that include IL-19, IL-20, IL-22, mda-7 and IL-26 [5]. A unique property of mda-7/IL-24 when delivered by an adenoviral expression system (Ad.mda-7) is selective induction of growth suppression and apoptosis in a broad spectrum of

human cancers, including pancreatic carcinoma, without exerting any deleterious effects to their normal counterparts. In addition to its direct apoptosis-inducing properties, Ad.mda-7 also demonstrates anti-angiogenic, radiosensitizing, immunostimulatory and potent 'bystander' anti-tumor activity [6, 7]. A phase I clinical trial evaluating Ad.mda-7 (INGN 241) activity by intratumoral injection in patients with advanced solid tumors was performed and the results indicate that mda-7/IL-24 is safe and could induce as much as 70% apoptosis in tumors following a single injection of recombinant virus and multiple injections promotes an objective clinical responses [1]. These exciting results provide direct support for using mda-7/IL-24 in potentially developing an effective gene-based therapy for cancer. In multiple cancer subtypes, Ad.mda-7 infection reduces the levels of anti-apoptotic proteins, including Bcl-2 and/or Bcl-xL, and enhances expression of pro-apoptotic proteins, including Bax and/or Bak, thus shifting the balance towards an apoptotic phenotype and tumor cell death [1].

The major limiting factor has been the development of effective delivery systems. Metabolism of genetic materials by serum esterases prohibits intravenous administration. Additionally, genes are macromolecules and their size greatly hinders passage across the capillary fenestrations of blood vessels without assistance. We and others have demonstrated viral vectors to be efficient delivery systems resulting in high levels of transgene expression. However, the antigenic nature of viruses leads to their rapid inactivation by the immune system. Additionally, the viruses are non-specific. This requires direct target organ injection with or without image guidance or operative bed injection.

Our group [8, 9] has extensively studied gene delivery of reporter and therapeutic genes mediated by adenoviruses into xenografted human tumors grown in nude mice. A major challenge for effective gene therapy is systemic delivery of nucleic acids into affected tissue. We have demonstrated that UTMD can significantly enhance adenoviral gene transfer in the presence of microbubbles (MBs) to specifically target mice tumor xenografts. The advantage of using MBs for gene transfer is to protect the viral payload from rapid degradation by the immune system thus allowing for intravenous injection rather than direct target organ injection. The microbubbles can be designed to entrap various drugs or genetic material. The gas filled microspheres effectively lower the energy threshold for cavitation. This allows diagnostic transducers operating within the energy levels mandated by the FDA to be used for drug/gene delivery. In the sonification zone the microbubbles undergo cavitation, destroying the bubbles and releasing their contents. Cavitation also creates small shockwaves that increase cell permeability [9]. This has been shown to increase transcapillary passage of macromolecules or nanospheres co-delivered by the microbubbles in experimental animals. In this grant application, we propose to develop a novel and unique UTMD system into a clinically translatable technology for the effective delivery of therapeutic genes to treat prostate cancer.

PROTOCOLS

To conduct the study outlined in the grant several protocol approvals were required. An approval from the IACUC (Institutional Animal Care and Use Committee) was required to perform the required animal study. Our goal was to develop a safe and effective means of gene delivery in vivo (immune-competent mice) that realizes the therapeutic potential of mda-7/IL-24 induction to combat human advanced Prostate Cancer malignancy. The protocol aims at targeting the primary prostate lesion in immune-competent mouse model mice (p53PE -/-; RbPE -/- mice) with advanced prostate cancer along with the presence of a metastatic disease. The adenoviral vectors carrying

the therapeutic gene are known to elicit an immunological response, which can only be studied in immune competent animals. To protect these viruses from the immune system the delivery of the adenoviral vector carrying mda7 gene needed to be delivered by ultrasound (US) and US contrast agents/microbubbles. US would break open these microbubbles at the tumor site, which would allow us to transfect only the tumor region. This protocol has now been approved.

As the project involves the uses of recombinant DNA and an infectious agent, an IBC (Institutional Biosafety Committee) approval was established before the study was started. This details the use of all conditionally replication competent adenovirus (CRCAs) also known as cancer terminator virus (CTV (Ad.PEG-E1A-mda-7)) and non-replicating E1A deleted adenovirus carrying the mda-7 gene (Ad.mda-7) in HEK-293 (Human embryonic kidney cells) cells and immune-competent mice (p53PE ^{-/-}; RbPE ^{-/-} mice) for amplification, purification, titration, and infection. The protocol also details the disposal, housekeeping, storage procedures and biosafety standards for all viral vectors and contaminated instruments. The protocol has been approved and as per IBC we have complied with all BL2 and BL2-N regulations.

Additionally, mice outlined in the grant are not for sale, and are established from breeder animals that have conditional inactivation of p53 and Rb tumor suppressor genes in the prostate epithelium. Breeding was carried out with B6.D2-Tg(Pbsn-Cre)4Prb (PB-Cre4) mice which express Cre recombinase under the control of a composite prostate epithelium-specific ARR2PB promoter in all prostatic lobes. A breeder protocol was established where these mice have inactivated p53 and Rb that develop prostate carcinomas which are highly metastatic, resistant to androgen depletion from early onset, and marked with multiple gene expression signatures commonly found in human prostate carcinomas. Metastases are also detected in p53PE ^{-/-}; RbPE ^{-/-} mice. This protocol details the procedure and number of mice required for the breeding process to establish a workable animal study.

Thus, all protocols required to conduct the study were established and all safety measures detailed by the IBC and IACUC have been met.

METHODS

Cell Culture

TRAMP C2 cell line is isolated from a heterogeneous 32 week male transgenic PB-Tag C57BL/6 (TRAMP) mouse with prostate tumor was purchased from American Type Culture Collection (ATCC, CRL-2731) and cultured in D-MEM supplemented with 5% FBS and 100 µg/mL penicillin, and 100 µg/mL streptomycin (both from Hyclone, Waltham, MA) at 37°C in a water-saturated atmosphere of 95% air and 5% CO₂ [3]. TRAMP is a transgenic line that expresses SV40 early genes (T and t antigens) under the transcriptional control of the minimal -426/+28 rat probasin promoter. Cells were detached from the culturing dishes with 0.25% trypsin under aseptic conditions. The DU-145 (human prostate adenocarcinoma), cell line was obtained from ATCC, Rockville, MD. DU-145 cells were grown in RPMI 1640 (Hyclone, Waltham, MA) supplemented with 10% FBS (Hyclone, Waltham, MA), and 100 µg/mL penicillin, and 100 µg/mL streptomycin (both from Hyclone, Waltham, MA) at 37°C in a water-saturated atmosphere of 95% air and 5% CO₂ [8]. The human embryonic kidney cell line HEK-293 was purchased from ATCC (CRL-1573) and cultured in DMEM supplemented with 10% FBS, 1% Penicillin and Streptomycin all from Hyclone, Waltham, MA, in 95% air and 5% carbon dioxide (CO₂) at 37°C. HEK-293 cells were used to titer, amplify and purify adenoviruses [9].

Breeding

To establish a potentially more germane link with human prostate carcinoma, we will use an immune-competent mouse model of prostate carcinogenesis that has been generated by Dr. Alexander Yu Nikitin (Cornell University, New York). ARR2PB-Cre transgenic line expressing Cre recombinase in urothelium-specific manner, PB-Cre4 male mice on C57BL/6xDBA2 background need to be crossed with “floxed” p53 female mice where exons 5 and 6 were flanked by two loxP sites or “floxed” Rb1 female mice where exon 19 was flanked with two loxP sites on FVB/N 129 background. The resulting F1 generation male offsprings have PB-Cre4, partially “floxed” p53(loxP/+) or PB-Cre4, partially “floxed” Rb(loxP/+) genotypes. These F2 males are then crossed with “floxed” p53 and “floxed” Rb females, respectively. The resulting F2 male offsprings have PB-Cre4, “floxed” p53 and PB-Cre4, “floxed” Rb genotypes. The F2 males are then crossed to “floxed” Rb and “floxed” p53 females, respectively to generate F3 generation of male offspring with PB-Cre4, “floxed” p53 “floxed” Rb genotype needed for this study. They are designated as p53PE^{-/-}, RbPE^{-/-} [10].

These mice have both p53 and Rb inactivated. The mice develop rapidly growing prostate carcinomas that are highly metastatic, resistant to androgen depletion from early onset, and marked with multiple gene expression signatures commonly found in human prostate carcinomas. Metastases are detected in p53PE^{-/-}; RbPE^{-/-} mice from 200 days of age. P53^{-/-} pRb^{-/-} mice develop tumors between 160-200 days of age.

Viruses

Ad.mda7 is a non-replicating adenovirus that is E1A deleted. Thus Ad.mda7 needs a packaging cell line such as the HEK-293 human embryonic kidney carcinoma that is E1A transformed) to produce non-replicating adenovirus type 5. The protein expression is driven by a cytomegalovirus (CMV) constitutively expressing promoter. Conditionally replication competent adenoviruses (CRCAs) are also known as cancer terminator virus (CTV). CTVs (Ad.PEG-E1A-mda-7) have a progression elevated gene (PEG) promoter with an intact E1A. These CTVs are also able to replicate in HEK-293 human embryonic carcinoma in a similar way as the non-replicating adenovirus. CRCA is an adenoviral vector in which replication is driven by a minimal active region of the promoter of progression elevated gene-3 (PEG-3), which functions selectively in diverse cancer cells with exclusive activity in cancer cells, generating a cancer terminator virus (CTV) [11, 12]. PEG-3 was cloned as an up-regulated transcript from a transformation progression rodent cancer model, and attractively, the activity of its promoter (PEG-Prom) was found to be significantly and often markedly higher not only in rodent but also in human cancer cells of diverse origin when compared with normal cells [6, 13]. The cancer cell specificity of the PEG-Prom is governed by two transcription factors (activator protein-1 and polyoma enhancing activator-3) that are expressed at elevated levels, either singly or in combination, in virtually all types of cancers [6, 12-14]. The PEG-Prom drives the expression of the E1A gene, necessary for adenovirus replication, to create cancer cell-specific CRCAs [11, 14]. The engineered CRCA simultaneously expresses mda-7/IL-24 in the E3 region (Ad.PEG-E1A-mda-7; CTV), thereby mediating robust production of this cytokine as a function of adenoviral replication [11].

Virus Purification

CTV-Mda7 (Ad.PEG-E1A-mda-7), and Ad.mda-7/IL-24 were provided by Dr. Paul Fisher (Virginia Commonwealth University, Richmond VA). Ad.GFP (Green Fluorescent Protein) virus was generated using the AdEasy system (Carlsbad, CA). Each viral stock was propagated and

purified from HEK-293 cell cultures. Cells were harvested 24-36 hours after infection. HEK-293 cells were centrifuged and pelleted. The pellet was re-suspended in heat-inactivated (HI) 2% Fetaclone-III Fetal bovine serum (FBS) media was lysed by a three-freeze/thaw cycle method. Cell debris was removed with a 0.45 μ m vacuum filter. Free DNA is degraded with the DNase enzyme at 37°C for 30min, the supernatant is then passed through 0.22 μ m filter concentrating the viruses. Viruses were then purified by chromatography followed by dialysis. Viruses are aliquoted and stored at -80°C. Viral titers were determined by a plaque assay in a 24-well plate. Each well contained 2.4 x 10⁵ HEK-293 cells. The following day HEK-293 cells were infected with serial dilution of the amplified or purified viruses.

Transduction Studies

Adenovirus transductions were performed using 50 MOI Adenoviruses (Ads), in DMEM media with 2% Fetaclone-III heat-inactivated FBS (Hyclone, Thermo Scientific, Waltham, MA) [8, 9, 15]. After 16h, the media was replaced with fresh media and cells were collected after 24- hours.

Western Blots

HEK-293 cells and TRAMP C2 cells were transduced with Ad.mda7 and Ad.GFP. The cells were lysed on ice for 1hr with lysis buffer. Bradford's reagent was used to measure the protein concentration on an Eppendorf Biophotometer. The 50 μ g of protein from cell extracts were subjected to western blot analysis [15]. SDS-PAGE was run using 8-12% bis-acrylamide gel at room temperature. 20 μ L of total proteins plus loading buffer were loaded in each well. Samples were transferred onto a nitrocellulose membrane. To detect proteins the membranes were blocked with 5% Milk-TBST overnight at 4°C and incubated with primary antibodies for 2hr at room temperature with constant motion on an orbital shaker while overnight incubation for proteins below 50kda. The membranes were washed with TBST to remove excess primary antibodies. Incubation for 45 minutes with 1/5000 anti-mouse or 1/10000 anti-rabbit secondary antibodies diluted in TBST followed. Immunodetection was performed using the enhanced chemiluminescence (ECL) system (Amersham, IL) according to the manufacturer's instructions. Western blot analyses with antibodies against the targeted proteins were performed to validate successful viral transfection of the cells. The following primary antibodies were used: mouse monoclonal antibodies against β -actin cat#A3853 (1:1,500) (Sigma Aldrich), Mda-7/IL-24 k101 (GenHunter Corporation) and rabbit polyclonal antibodies against GFP cat#632377 (1:500) (BD Bioscience) [15].

RESULTS

Transduction with viruses

Western Blot studies were carried out on HEK-293 cells and TRAMP C2 cells to confirm the transduction of Ad.mda7 and Ad.GFP. Western blot analysis was performed 24 hours after media change following transduction. Figure 1 shows that the fore mentioned adenoviruses successfully transferred and expressed the targeted transgene in both HEK-293 and TRAMP C2 cells.

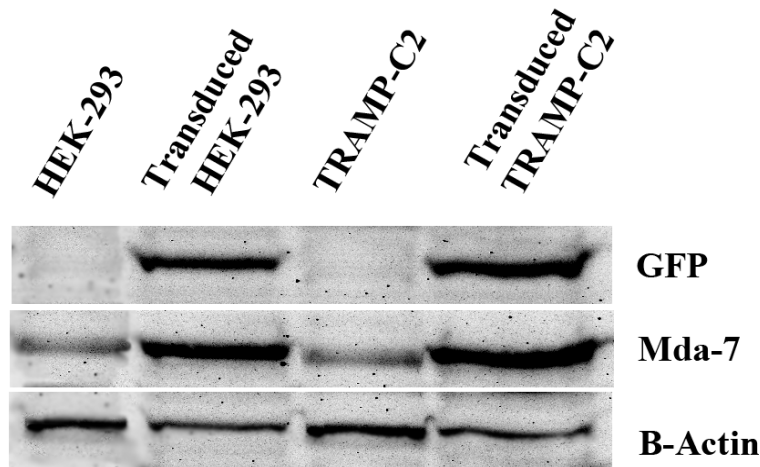


Figure 1. Western blot analysis of HEK-293 and TRAMP C2 cell lysates following adenoviral transduction. On the left lane is control HEK-293 cells. The second lane is loaded with transduced HEK-293 cells. The third lane is loaded with non-transduced control TRAMP C2 cells. On the right transduced TRAMP C2 cells. Anti-beta-actin was used as a loading control. 50µg of total lysates were run in SDS polyacrylamide gels. On the right side are indicated the different adenoviral transductions.

CONCLUSIONS

The p53PE ^{-/-}; RbPE ^{-/-} mice takes roughly 160-200 days before primary and metastatic tumor are established. Also from the breeder mice to workable mice colony would take roughly four months as the third generation mice will have the required p53 and Rb genes inactivated. As this is a long process we are currently looking at an alternative prostate cancer immune-competent mice model. TRAMP mice are an immune-competent C57Bl/6 mice model for prostate carcinogenesis. TRAMP is a transgenic line of C57Bl/6 mice that expresses SV40 early genes (T and t antigens) under the transcriptional control of the minimal -426/+28 rat probasin promoter. As a consequence, male TRAMP mice uniformly and spontaneously develop prostate tumors following the onset of puberty. We purchased TRAMP C2 cell line from ATCC (Rockville, MD) which were derived from TRAMP mice [3]. This allowed us to test our viruses in an in vitro setting quickly and efficiently. Based on Figure 1, we were able to transduce TRAMP C2 cells with Ad.mda7 and Ad.GFP. Additionally, TRAMP C2 cell line can be allografted onto C57Bl/6 mice to establish tumors on both flanks that allow us to study the effects of primary and metastatic prostatic tumors. Thus TRAMP mice allows for a syngeneic tumor model to be established without the fear of rejection for TRAMP C2 cells.

To establish whether conditionally replicative viruses can be used in the TRAMP mice model we intend to compare the viral burst activity of Ad. GFP, Ad.mda7 and CTV-Mda7 for TRAMP C2 cell line, human DU145 and LnCaP cell lines. As well as perform in vitro viability studies to test the efficacy of Ad.GFP, Ad.mda7, CTV-Mda7 in combination with radiation (RT) against TRAMP C2 cell line. Thus giving us a baseline of what the results should yield and whether the immune system in these mice play a role in hampering the delivery of viruses to the targeted tumor site.

During the course of completing this study, I received invaluable experience in handling mice, use of the ultrasound machine, microscopy, working with adenoviruses, and animal surgical procedures required for the study. I also completed the radiation certification required for the use of X-rad irradiator. I was also exposed to several procedural or protocol approval required to perform such a study. Altogether this experience has allowed me great insight into performing and designing an animal studies.

ACKNOWLEDGEMENTS

I acknowledge the grant by the NASA WV Space Grant Consortium as well as my Research Mentor, Dr. Pier Paolo Claudio.

REFERENCES

1. Lebedeva, I.V., et al., *mda-7/IL-24: exploiting cancer's Achilles' heel*. Mol Ther, 2005. 11(1): p. 4-18.
2. Lebedeva, I.V., et al., *mda-7/IL-24, novel anticancer cytokine: focus on bystander antitumor, radiosensitization and antiangiogenic properties and overview of the phase I clinical experience (Review)*. Int J Oncol, 2007. 31(5): p. 985-1007.
3. Dzojic, H., et al., *Adenovirus-mediated CD40 ligand therapy induces tumor cell apoptosis and systemic immunity in the TRAMP-C2 mouse prostate cancer model*. Prostate, 2006. 66(8): p. 831-8.
4. Freytag, S.O., K.N. Barton, and Y. Zhang, *Efficacy of oncolytic adenovirus expressing suicide genes and interleukin-12 in preclinical model of prostate cancer*. Gene Ther, 2013. 20(12): p. 1131-9.
5. Dalloul, A. and A. Sainz-Perez, *Interleukin-24: a molecule with potential anti-cancer activity and a cytokine in search of a function*. Endocr Metab Immune Disord Drug Targets, 2009. 9(4): p. 353-60.
6. Su, Z.Z., Y. Shi, and P.B. Fisher, *Subtraction hybridization identifies a transformation progression-associated gene PEG-3 with sequence homology to a growth arrest and DNA damage-inducible gene*. Proc Natl Acad Sci U S A, 1997. 94(17): p. 9125-30.
7. Chada, S., et al., *Bystander activity of Ad-mda7: human MDA-7 protein kills melanoma cells via an IL-20 receptor-dependent but STAT3-independent mechanism*. Mol Ther, 2004. 10(6): p. 1085-95.
8. Nande, R., et al., *Microbubble-assisted p53, RB, and p130 gene transfer in combination with radiation therapy in prostate cancer*. Curr Gene Ther, 2013. 13(3): p. 163-74.
9. Greco, A., et al., *Eradication of therapy-resistant human prostate tumors using an ultrasound-guided site-specific cancer terminator virus delivery approach*. Mol Ther, 2010. 18(2): p. 295-306.
10. Zhou, Z., et al., *Synergy of p53 and Rb deficiency in a conditional mouse model for metastatic prostate cancer*. Cancer Res, 2006. 66(16): p. 7889-98.
11. Sarkar, D., et al., *Dual cancer-specific targeting strategy cures primary and distant breast carcinomas in nude mice*. Proc Natl Acad Sci U S A, 2005. 102(39): p. 14034-9.
12. Sarkar, D., et al., *Targeted virus replication plus immunotherapy eradicates primary and distant pancreatic tumors in nude mice*. Cancer Res, 2005. 65(19): p. 9056-63.

13. Su, Z., Y. Shi, and P.B. Fisher, *Cooperation between AP1 and PEA3 sites within the progression elevated gene-3 (PEG-3) promoter regulate basal and differential expression of PEG-3 during progression of the oncogenic phenotype in transformed rat embryo cells*. *Oncogene*, 2000. 19(30): p. 3411-21.
14. Su, Z.Z., et al., *Targeting gene expression selectively in cancer cells by using the progression-elevated gene-3 promoter*. *Proc Natl Acad Sci U S A*, 2005. 102(4): p. 1059-64.
15. Nande, R., et al., *Targeting a newly established spontaneous feline fibrosarcoma cell line by gene transfer*. *PLoS One*, 2012. 7(5): p. e37743.

ROLE OF K_v7 CHANNELS IN CONTROLLING NEURONAL EXCITABILITY

Benjamin Owen
Ph.D., Biomedical Sciences
Marshall University
Huntington, WV, 25755
Dr. Lawrence M. Grover

ABSTRACT

Traumatic brain injury can occur during occupational and recreational activities, such as mining and sports, and can cause excitotoxicity by stimulating excessive glutamate release. During excitotoxicity, sustained increases in intracellular calcium levels can be observed, which can alter cellular function and lead to cell death. An example of cell function altered by increased intracellular calcium levels is inhibition of voltage-gated potassium (K_v) channels in the K_v7 family. These channels regulate excitability, and are found on the axon initial segment of axons such as the Schaffer collateral axons in the hippocampus. The Schaffer collaterals originate from pyramidal neurons in area CA3 and form synapses with pyramidal neurons in area CA1. Previously, our lab has observed the Schaffer collaterals to undergo region-specific, activity-dependent changes in excitability during high-frequency and burst stimulation. Using *in vitro* hippocampal slices, I examined the role of K_v7 channels in the Schaffer collateral axon excitability changes by blocking or activating K_v7 channels. I also examined the effects on Schaffer collateral excitability of simulating excitotoxicity by applying N-methyl-D-aspartate (NMDA). Finally, I examined the effects of NMDA after pre-treatment with a K_v7 channel activator. My experiments indicate that K_v7 channels have little, if any, role in Schaffer collateral excitability changes. My experiments with NMDA showed an increase in distal Schaffer collateral excitability that was reduced by pre-treatment with the K_v7 activator.

INTRODUCTION

The purpose of this project was to examine the role of K_v7 channels in regulating Schaffer collateral excitability, with my goals being to (1) determine whether K_v7 channels are responsible for regional differences (proximal *vs* distal collateral) in excitability changes and (2) whether K_v7 channels regulated excitability changes during excitotoxicity. To achieve my goals, I performed simultaneous recordings of distal Schaffer collateral responses (fiber volleys) in area CA1 and proximal Schaffer collateral responses (population spikes) in area CA3 in *in vitro* rat hippocampal slices. Responses were evoked by 100Hz high-frequency stimulation (HFS) and 100-500ms interval burst stimulation under control conditions and after drug application. The drugs I used were XE-991, a specific K_v7.2/3 blocker, and ICA069673, a specific K_v7.2/3 activator. I quantified excitability changes by measuring peak-to-peak amplitudes and conduction latencies. I also examined the effects of applying N-methyl-D-aspartate (NMDA) on Schaffer collateral axon function during high-frequency and burst stimulation with and without ICA069673 pre-treatment, using the same methods and measurements mentioned above.

For the statistical analyses, I compared the effects of XE-991, ICA069673, NMDA alone, and NMDA with ICA069673 pretreatment, on the amplitudes and latency changes of the first and last 20 responses during high-frequency and burst stimulation. I used either paired t-tests or two-way (treatment, burst position) repeated measures analysis of variance (ANOVA). Post-hoc comparisons for repeated measures ANOVAs were made using paired t-tests with a Bonferroni correction.

BACKGROUND

Each year in the U.S., there are an estimated 1.7 million cases of traumatic brain injury (TBI) (Centers for Disease Control and Prevention, 2013). Risk of TBI is increased during some recreational activities (ex. sports, ATV wrecks) and in several occupations (ex. mining, military service), and head injuries are common in aviation accidents (Baker et al 2009). TBI has been

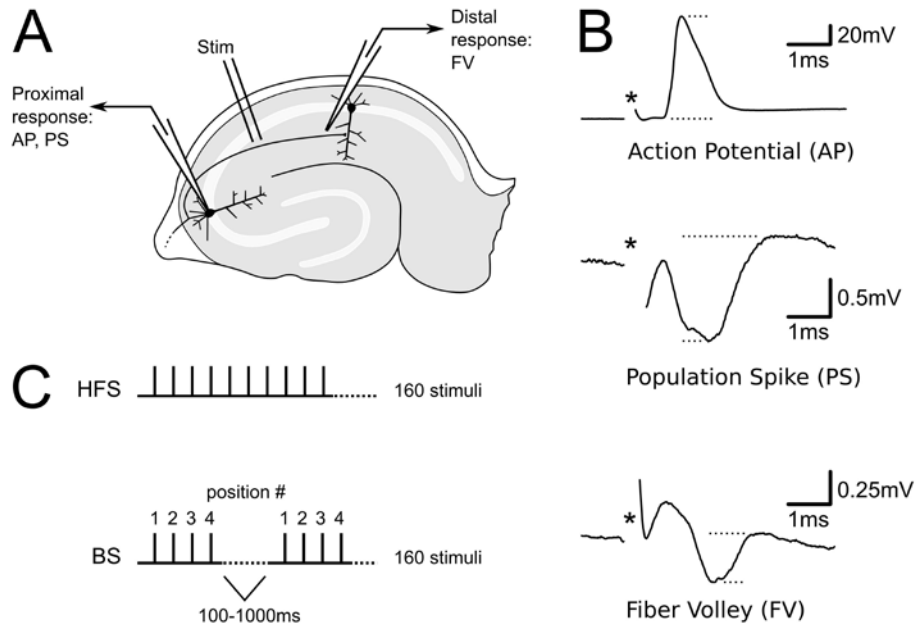


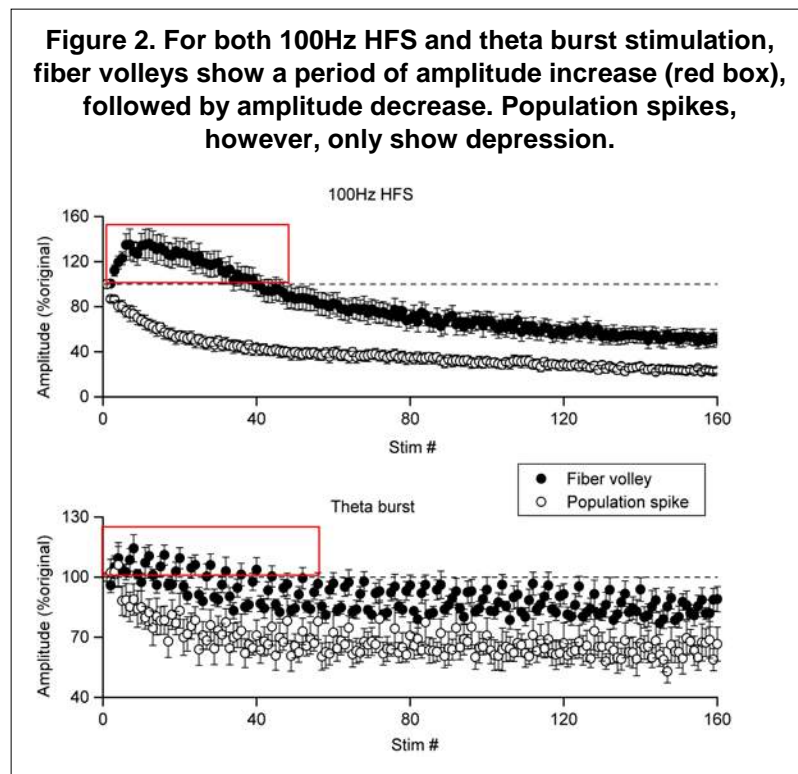
Figure 1. Illustration of stimulation and recording methods. A. The stimulating electrode was placed in stratum radiatum near the border of areas CA3 and CA1. In some experiments, whole cell current clamp recordings of antidromic action potentials were made from CA3 pyramidal neurons, in other experiments, simultaneous extracellular recordings were made from stratum pyramidale in area CA3 (population spike) and stratum radiatum in area CA1 (fiber volley). **B.** Typical whole cell and field potential responses. Stimulus artifacts (*) have been partially removed. Top: antidromic action potential recorded from CA3 pyramidal neuron; action potential amplitude was determined as illustrated as the difference in membrane potential immediately prior to and at the peak of the action potential. Middle: population spike recorded from CA3 stratum pyramidale; amplitude was determined as illustrated as the difference between the negative peak and following positive deflection. Bottom: fiber volley recorded from CA1 stratum radiatum; amplitude was determined by the difference between negative peak and following positivity. **C.** 160 stimuli were given either as continuous HFS (top) or as burst stimulation with inter-burst intervals of 100-500ms.

linked to posttraumatic seizures and epilepsy, where the chances of developing posttraumatic seizures and epilepsy increase with the severity of TBI (reviewed in Christensen, 2012). Proposed definitions of posttraumatic seizures include late (occurring >1 week post-injury), early (occurring <1 week post-injury), and immediate seizures (occurring <24 hours post-injury) (Christensen, 2012). Early and immediate seizures have been identified as risk factors for the later development of epilepsy (Christensen 2012). TBI stimulates the excessive release of glutamate, an excitatory neurotransmitter, leading to glutamate-mediated excitotoxicity, a process that contributes to further brain injury (Greve and Zink, 2009).

The K_v7 potassium channel family consists of voltage-gated ion channels whose purpose is to control neuronal excitability (reviewed in Brown and Passmore, 2009). These channels are concentrated in the proximal axon/initial segment of hippocampal neurons (Klinger et al. 2011). Defective K_v7 channels can result in hyper-excitable cells, and disorders such as familial benign epilepsy; defective $K_v7.2/3$ channels have also been linked to idiopathic epilepsies (reviewed in Maljevic et al. 2008). Calcium entry through voltage-gated calcium channels has been shown to inhibit K_v7 channels temporarily after the initial action potential during a burst of firing in CA1 pyramidal cells (for review, see Brown and Passmore, 2009). Excitotoxicity leads to a sustained increase in intracellular calcium (Greve and Zink, 2009), leading me to propose that **TBI may cause neuronal hyper-excitability through excitotoxic down-regulation of the K_v7 channel function.**

Previously, we reported that distal Schaffer collateral axons from CA3 pyramidal cells show a biphasic response to 100Hz high-frequency stimulation (HFS) in area CA1: a period of amplitude increase (hyper-excitability) followed by amplitude depression (Kim et al. 2012). This differed from whole-cell recordings of antidromic action potentials conducted by proximal axons, which

only depressed during HFS (no hyper-excitable period) (Kim et al. 2012). When I simultaneously recorded distal and proximal axon responses (fiber volleys and population spikes, respectively) during HFS (see Fig. 1 for experimental setup), I found that the population spikes follow the same pattern seen during the whole-cell recordings: amplitude depression with no hyper-excitable period (Fig. 2). I observed the same difference between fiber volley and population spike amplitudes during theta frequency (5 Hz or 200ms interval) burst stimulation, which mimics the natural firing pattern of these neurons (Fig. 2). **I hypothesized that K_v7 channels present on the proximal axon**



normally prevent hyper-excitability during periods of high activity, and activating Kv7 channels would reduce changes caused by excitotoxicity.

METHODS

Tissue Preparation

Hippocampal slices were prepared as previously described (Kim et al. 2012). Male and female Sprague-Dawley rats (30-150 days old, Hilltop Lab Animals, Scottdale, PA) were sedated by CO₂/air inhalation, and decapitated. The brain was removed and placed into chilled artificial cerebrospinal fluid (ACSF) composed of (in mM): 124 NaCl, 26 NaHCO₃, 3.4 KCl, 1.2 NaH₂PO₄, 2 CaCl₂, 2 MgSO₄, 10 glucose (pH 7.35, equilibrated with 95% O₂/5% CO₂). The brain was sectioned, and a block containing both hippocampi was glued to the stage of a vibratome (Campden Instruments, Lafayette, IN), immersed in chilled ACSF, and sectioned into 400-500µm thick slices. Slices containing the hippocampus in coronal or horizontal orientation were dissected to remove the hippocampus from the surrounding structures. Hippocampal slices were stored at room temperature (20-22° C) in an interface holding chamber. For recordings, individual slices were transferred to a small volume (approximately 200µL) interface recording chamber heated to 34.5-35.5°C. Slices were perfused with oxygenated ACSF at a rate of 1-1.5mL/min. All procedures were approved by the Institutional Animal Care and Use Committee at Marshall University.

Field Potential Recordings

Extracellular field potentials were recorded through glass micropipettes filled with ACSF (3-5MΩ); in some recordings the tip was broken, prior to placement in the slice, to lower resistance and reduce noise. To record Schaffer collateral fiber volleys, the micropipette was placed in stratum radiatum of CA1. In some recordings, fiber volleys and antidromic population spikes were measured simultaneously by placing two electrodes in the slice: one in CA1 stratum radiatum and one in CA3 stratum pyramidale (Fig. 1A). Signals were amplified (gain 100-1000), filtered (high pass filter at 0.05-0.1 Hz, low pass filter at 310kHz), digitized (10-100kHz; National Instruments), and stored on a personal computer using WinWCP and WinEDR software (Strathclyde Electrophysiology Software, John Dempster, University of Strathclyde). Fiber volley and population spike amplitude were measured as the difference between the maximum negativity and following positivity (Fig. 1B). Latencies were measured as the time difference between the beginning of the stimulus artifact and the response at 10% of its peak amplitude.

Stimulation

Figure 1 shows the electrode arrangements for simultaneous recording of extracellular responses in area CA3 stratum pyramidale and area CA1 stratum radiatum. A bipolar Teflon® insulated, stainless steel stimulating electrode was placed in stratum radiatum near the border between area CA1 and CA3. Constant voltage, biphasic stimuli (duration 0.1ms) were delivered using an A-M Systems model 2100 stimulator. The stimulus intensity was adjusted to produce the largest response which could be obtained without contamination of the response by the stimulus artifact. Two types of stimulus protocols were used: continuous high-frequency stimulation (HFS) and burst stimulation (Fig. 1C). For HFS, trains of 160 pulses at 10-100Hz were delivered. For burst stimulation, bursts of 4 stimuli at 100Hz were repeated at inter-burst intervals of 100, 200, and 500ms for a total of 40 bursts (160 stimuli). Fiber volleys were isolated by blocking excitatory postsynaptic potentials (EPSPs) using an AMPA receptor blocker (30µM DNQX).

Drug Application

To examine the roles of K_v7 channels during high-frequency and burst stimulation, I recorded fiber volley and population spike responses before and after bath application of either XE-991 (10 μ M), a specific K_v7 channel blocker, or ICA069673 (10 μ M), a specific K_v7 channel activator, for at least 20 min.

To examine the effects of NMDA-mediated excitotoxicity, I recorded fiber volleys and population spikes during high-frequency and burst stimulation in normal ACSF as control. Then I applied NMDA (50 μ M) for 5-15 min, followed by washout. Fiber volleys and population spikes were recorded during high-frequency and burst stimulation after 5, 30, and 60 min of washout. To determine if activating K_v7 channels would reduce effects of NMDA, I pre-treated slices with ICA069673 for 10 min before applying a cocktail of NMDA and ICA069673 (5-15 min). Washout of NMDA followed, with fiber volleys and population spikes recorded during high-frequency and burst stimulation at the intervals above.

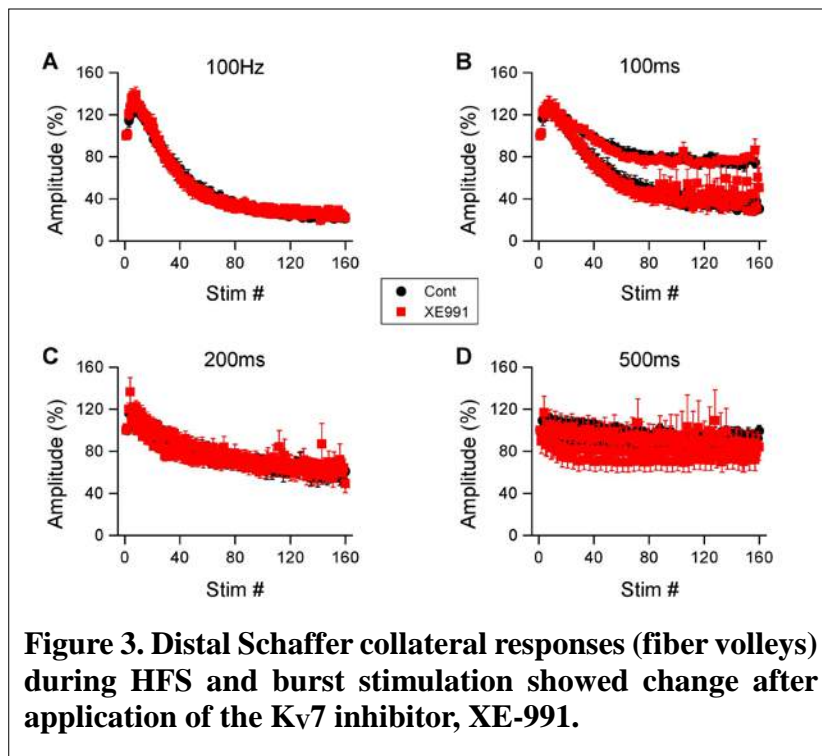
Reagents

Drugs were prepared as concentrated stock solutions. 6,7-dinitroquinoxaline-2,3-dione (DNQX 30mM; Tocris), XE-991 (10mM; Abcam), and ICA069673 (10mM; Santa Cruz) were dissolved in DMSO. N-methyl-D-aspartate (50mM, Abcam or Research Biochemicals International) was dissolved in distilled water. Stock solutions were diluted to final concentrations by addition to ACSF perfusing the tissue. Salts and all other reagents were from Sigma or Fisher.

Statistical Analysis

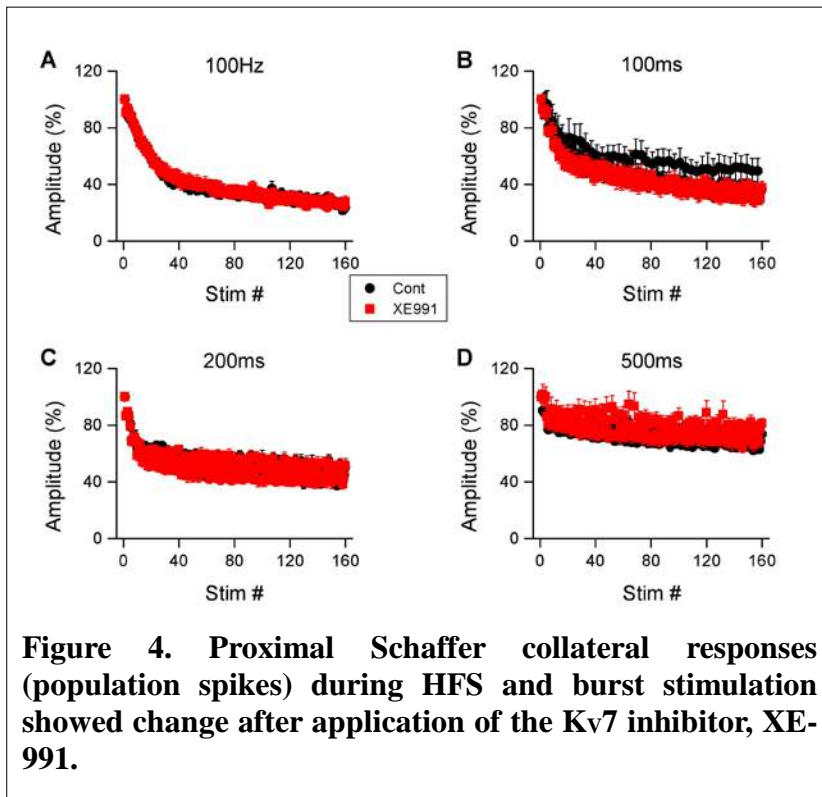
For the statistical analyses of HFS data, I averaged amplitudes and latency changes of the first 20 responses and performed paired t-test comparisons between control and drug treatment. The same was done for amplitudes and latency changes of the last 20 responses. For the burst stimulation data, I used 2-way (treatment, burst position) repeated measures ANOVA with post-hoc comparisons using paired t-tests with Bonferoni correction. Distal and proximal axon responses were analyzed separately.

RESULTS

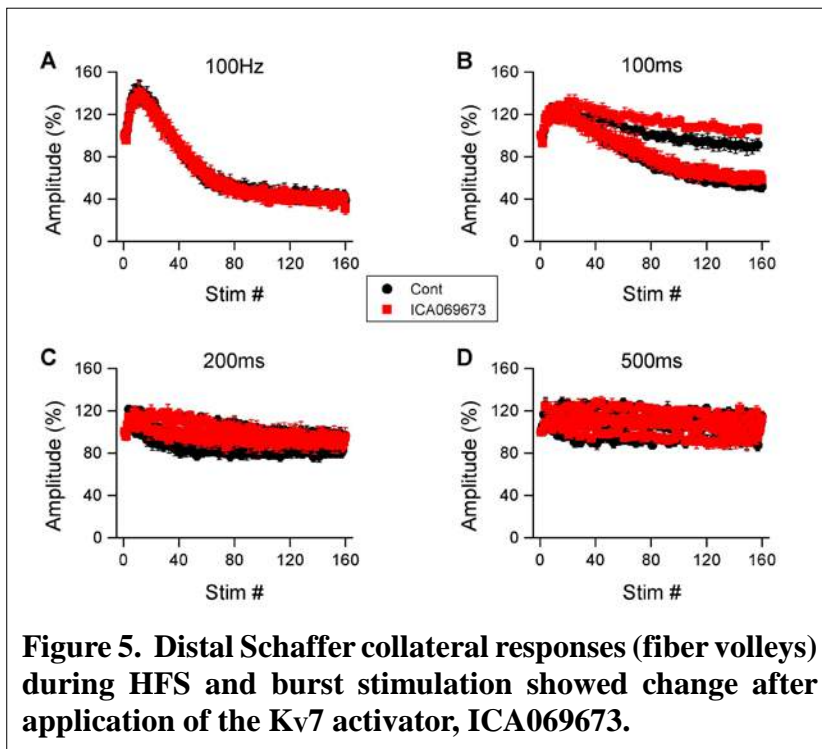


Effects of XE-991 on Schaffer collateral excitability during high-frequency and burst stimulation. I examined effects of the Kv7 channel blocker XE-991 (10 μ M) in a total of 8 slices. Visual inspection of the mean fiber volley amplitudes (Fig 3) and latency changes (not shown) and mean population spike amplitudes (Fig. 4) and latency changes (not shown) during HFS and burst stimulation did not suggest any effects of XE-991 application. Analysis of the mean amplitudes and latency changes during the first and last 20 responses during HFS did not reveal any significant effects of XE-991.

For the first 20 responses during burst stimulation, a significant interaction between XE-991 and burst position was detected for the fiber volley amplitudes during 200ms interval burst stimulation ($p < 0.05$), but post-hoc comparisons did not detect any significant effects of XE-991. For the last 20 responses during burst stimulation, a significant interaction between XE-991 and burst position was detected for the fiber volley latency changes during 200ms interval stimulation ($p < 0.05$), and a significant interaction between XE-991 and burst position was detected for the population spike amplitudes during 100ms interval burst stimulation ($p < 0.05$); post-hoc analysis did not detect any significant effects of XE-991 in either the fiber volley latency changes or the population spike amplitudes. No other interactions or significant main effects of XE-991 were detected for either the first or last 20 responses for either the fiber volleys or population spikes.



burst stimulation protocols used above. Visual inspection of amplitudes (Figs. 5, 6) and latency

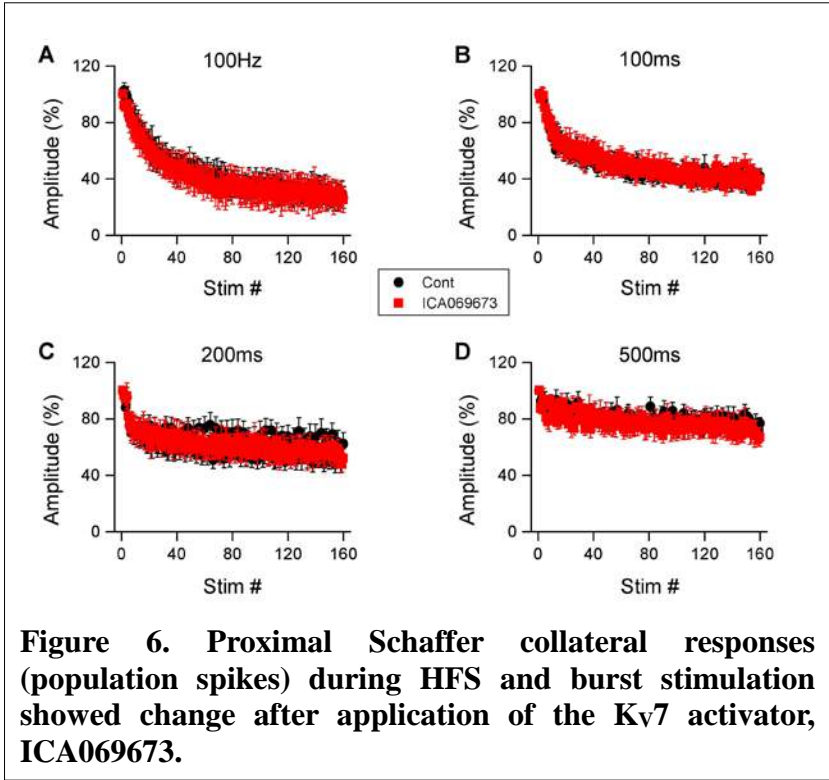


In summary, while statistical analyses detected some significant effects of XE-991 application, these effects were not consistently obtained across all stimulation conditions. In the next section, I examine the effects of the Kv7 activator, ICA069673, on proximal and distal Schaffer collaterals. If the effects I obtained with XE-911 represent involvement of Kv7 channels, then the activator should produce results opposite to those reported here.

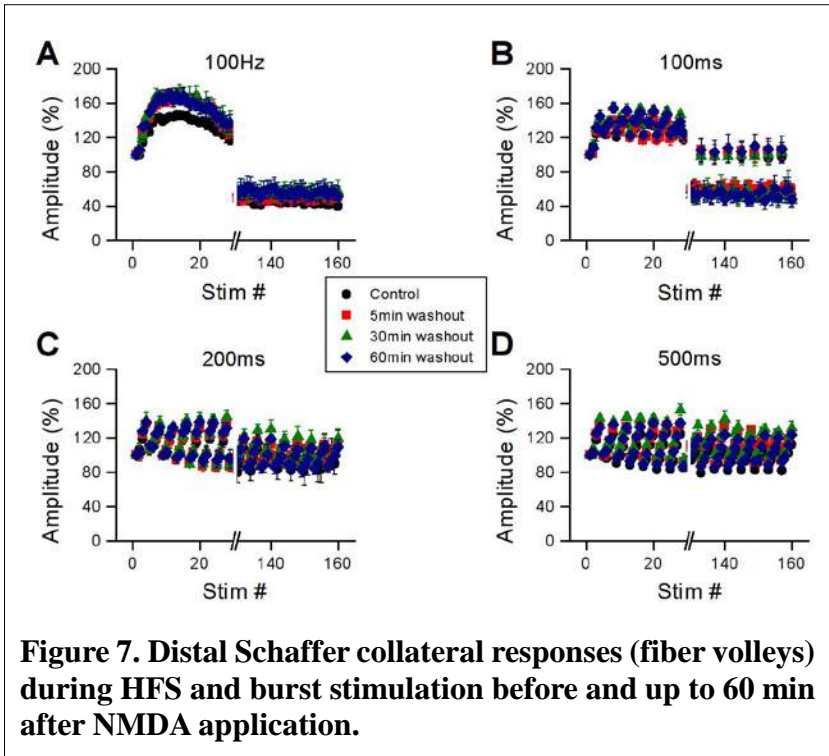
Effects of ICA069673 on Schaffer collateral excitability during high-frequency and burst stimulation.

I applied the Kv7 activator ICA069673 (10 μ M, n=6 slices) and repeated the same HFS and burst stimulation protocols used above. Visual inspection of amplitudes (Figs. 5, 6) and latency changes (not shown) during stimulation suggested possible effects of ICA069673 during burst stimulation. However, statistical analysis failed to detect any significant effects of ICA069673, or any significant interactions between ICA069673 and burst position, for the distal (fiber volleys) or proximal (population spikes) responses.

In summary, treating slices with the Kv7 channel activator, ICA069673, consistently failed to alter excitability of distal or proximal Schaffer collaterals during either HFS or burst stimulation. The absence of any effects of ICA069673 combined with the minimal



enhanced during 100Hz HFS even after 60 min of washout (Fig. 7A). However, there were no obvious effects on fiber volley amplitudes during any interval of burst stimulation (Fig. 7B-D). Latencies changes showed smaller and less consistent changes during the washout period (not shown).



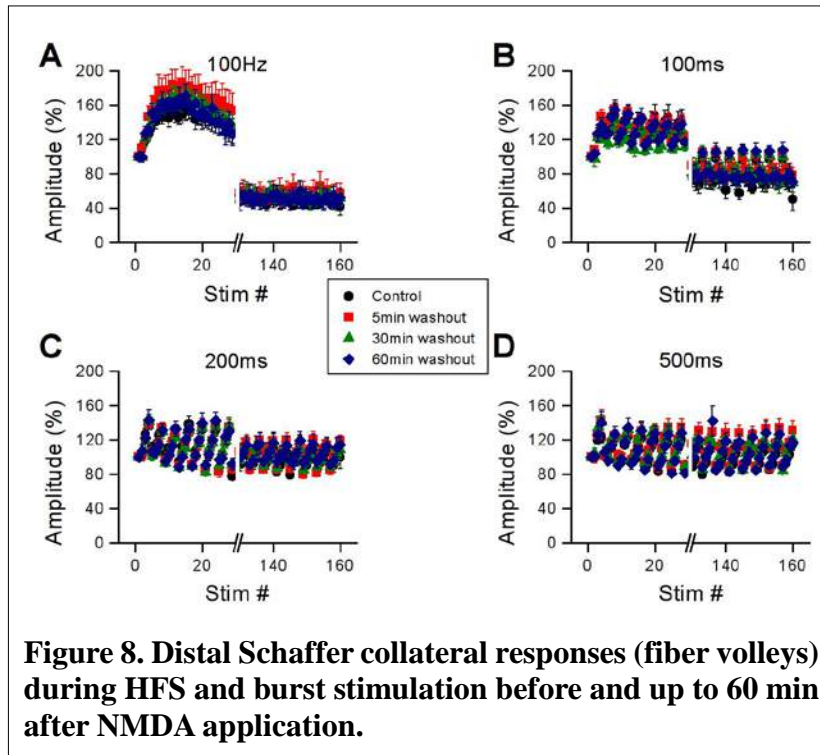
effects of the inhibitor, XE-911 (above), indicates that Kv7 channels have little role in excitability changes under normal conditions. In the next section, I examined the effects of applying NMDA with or without pretreatment with ICA069673.

Effects of NMDA on Schaffer collateral excitability during high-frequency and burst stimulation.

In a separate set of slices (n= 6), I applied NMDA (50μM) for 5-15 min. NMDA was then washed out and responses recorded 5, 30, and 60 min after washout began. As seen in Figure 7, amplitudes of the first 20 fiber volley responses were enhanced during 100Hz HFS even after 60 min of washout (Fig. 7A). However, there were no obvious effects on fiber volley amplitudes during any interval of burst stimulation (Fig. 7B-D). Latencies changes showed smaller and less consistent changes during the washout period (not shown). Amplitudes and latency changes of proximal Schaffer collateral responses (population spikes) were not consistently affected by NMDA (not shown).

In summary, NMDA enhanced distal Schaffer collateral excitability, but this was only observed as an amplitude increase during the first 20 stimuli of 100Hz HFS. Meanwhile, NMDA did not appear to have any effect on proximal Schaffer collateral excitability, as no effects were observed on population spike amplitudes or latency changes. These conclusions are preliminary and are based on

visual inspection of the data. Completion of statistical analysis may reveal subtle effects of NMDA that were not apparent by visual comparisons. In the next section, I examine whether activating Kv7 channels will mitigate the increase in excitability from NMDA application.



Effects of ICA069673 pretreatment on NMDA-mediated excitability changes during high-frequency and burst stimulation.

In another set of slices (n=7), I repeated the NMDA experiment above, but pretreated slices with 10 μ M ICA069673 before applying NMDA (50 μ M). Pretreatment with the Kv7 activator did not appear to alter the initial (5 min) effect of NMDA application, but did prevent the sustained increase in fiber volley (distal Schaffer collateral) amplitude during the first 20 stimuli of HFS (Fig. 8A, compare with Fig. 7A). Pretreatment with ICA069673 did not appear to affect distal

Schaffer collateral latency changes or proximal Schaffer collateral amplitudes or latency changes.

In summary, pre-treatment with ICA069673 appeared to counteract the NMDA-induced sustained enhancement of distal Schaffer collateral hyper-excitability during HFS. These conclusions are also preliminary and are based on visual inspection. Completion of statistical analysis may reveal subtle effects of NMDA that were not apparent by visual comparisons.

DISCUSSION

In conclusion, my hypothesis was partially supported: NMDA application enhanced distal Schaffer collateral hyper-excitability and this effect of NMDA was counteracted by activating Kv7 channels prior to applying NMDA. This demonstrates that Kv7 channels can mitigate abnormal excitability during excitotoxicity. This is interesting because my experiments showed that Kv7 channels play a small role, if any, in normal activity-dependent excitability changes in Schaffer collateral axons.

The minimal effects of Kv7 modulating drugs (XE-991 and ICA069673) may be due to functional redundancy in Kv channel function: other, unaffected channels may compensate for the altered function of Kv7 channels. This idea is supported by other data I have collected as part of my doctoral research where I examined the effects of specific Kv1 blockers. In those experiments, the specific Kv1 blockers had little, if any, effects on Schaffer collateral excitability, whereas non-specific Kv blockers dramatically altered Schaffer collateral responses during both HFS and burst stimulation. This inability of selective Kv1 or Kv7 blockers to alter Schaffer collateral responses,

but the profound effect of non-selective K_v block could be explained by functional redundancy amongst K_v channels.

My experiments also showed that the distal Schaffer collaterals were more sensitive to NMDA than the proximal Schaffer collaterals. However, the effects of NMDA appeared to be restricted to a particular range of stimulation, as the effects were only apparent early during 100Hz HFS. The ability of ICA069673 pretreatment to counteract effects of NMDA is interesting because localization studies show that K_v7 channels are concentrated in proximal axons at the axon initial segment (Klinger et al. 2011; for review, see Vacher et al. 2008). Because of this, I expected ICA069673 pretreatment to be ineffective in distal Schaffer collaterals. Although not as abundant in distal Schaffer collaterals, my data indicate that K_v7 channels can nonetheless have a functionally important role in limited the effects on axon excitability of the excitotoxin, NMDA. To compliment my experiments with ICA069673, I had planned to pretreat slices with XE-991 before applying NMDA. Since XE-991 and ICA069673 have opposite effects on K_v7 channels, I predicted that XE-991 will exacerbate NMDA's effects. Completion of this additional experiment should provide a clearer picture of the role of K_v7 channels during excitotoxicity.

ACKNOWLEDGEMENTS

I would like to acknowledge the NASA West Virginia Space Grant Consortium for funding my research, my mentor Dr. Grover for his support and guidance during my project, and Rishi Reddy whose help was extremely valuable on this project.

MOST VALUABLE ASPECTS OF THE PROGRAM

Three aspects of my participation in this program stand out to me: the financial support provided by the grant, the ability to help mentor an undergraduate student (Rishi Reddy) and develop a new friendship, and the chance to pursue a topic of research I had been interested in for some time.

PRESENTATIONS AND PUBLICATIONS

Posters

B. Owen, R. Reddy, L. M. Grover. "Role of K_v Channels in Activity-dependent Biphasic Changes of Schaffer Collateral Fiber Volleys." 16th International Winter Neuroscience Conference. Sölden, Austria. April 8th-12th, 2014

Rishi Reddy, Benjamin Owen, Lawrence Grover. "Are K_v7 channels responsible for difference in function between proximal and distal Schaffer collateral axons in rat hippocampus." WV INBRE Symposium. Marshall University, Huntington WV. July 29th, 2013

Publications

A portion of this work is being published as part of Benjamin Owen's dissertation entitled *Short-term Activity-dependent Changes in Schaffer Collateral Axon Function*. Successfully defended March 31st, 2014

REFERENCES

- Baker, S.P., Brady, J.E., Shanahan, D.F., and Guohua, L. 2009. Aviation-related morbidity and mortality Data from U.S. Health Information Systems. *Aviat Space Environ Med* 80:1001-1005.
- Brown, D.A. and Passmore, G.M. 2009. Neural *KCNQ* (K_v7) channels. *British Journal of Pharmacology* 156:1185-1195

- Centers for Disease Control and Prevention. 2013. Traumatic Brain Injury in the United States: Emergency Department Visits, Hospitalizations and Deaths, 2002-2006
- Christensen, J. 2012. Traumatic brain injury: Risks of epilepsy and implications for medicolegal assessment. *Epilepsia* 53(Suppl. 4):43-47
- Greve, M.W. and Zink, B.J. 2009. Pathophysiology of Traumatic Brain Injury. *Mount Sinai Journal of Medicine* 76: 97-104
- Kim, E., **Owen, B.**, Holmes, W.R., and Grover, L.M. 2012. Decreased afferent excitability contributes to synaptic depression during high-frequency stimulation in hippocampal CA1. *Journal of Neurophysiology* 108: 1965-1976
- Klinger, F., Gould, G., Boehm, S., and Shapiro, M.S. 2011. Distribution of M-channel subunits KCNQ2 and KCNQ3 in rat hippocampus. *Neuroimage* 58:761-769
- Maljevic, S., Wuttke, T.V., and Lerche, H. 2008. Nervous system Kv7 disorders: breakdown of a subthreshold brake. *Journal of Physiology* 568: 1792-1801
- Vacher H, Mohapatra DP, Trimmer JS. Localization and targeting of voltage-dependent ion channels in mammalian central neurons. *Physiol. Rev.* 88: 1407–1447, 2008.

MEASURING FOREST QUALITY IN GRAZED TROPICAL DRY FORESTS OF SOUTHERN MADAGASCAR

Lyndsay Rankin
MS, Biological Sciences
Marshall University
Huntington, WV 25755

ABSTRACT

Tropical dry forests (TDFs) possess high biodiversity yet few intact areas remain. The ability to accurately measure the condition of these forests is important to their conservation and management. Traditionally these efforts have focused on large areas minimally impacted by humans. However, human dominated landscapes far outnumber pristine areas, provide critical habitat for species worldwide. In Madagascar, as in other parts of the world, the TDF consists of multiple classes that vary by structure and species composition, each responding differently to disturbances. This system is heavily impacted by livestock grazing, affecting the understory and the canopy as herders will lop large branches to provide fodder for livestock in the dry season. The effects of grazing were measured via habitat, lemur occupancy, soundscape, and satellite image sampling within the Beza Mahafaly Special Reserve. Twenty-four sampling sites were divided between two dry forest classes (gallery and dry deciduous) and three levels of grazing intensity (ungrazed, moderate, and heavily grazed). Grazing presence resulted in decreased ring-tailed lemur occupancy with no affect on Verreaux's sifaka occupancy. Biological sound activity was not significantly different among grazing categories within the gallery forest but higher in ungrazed dry deciduous forests. To remotely detect differences in forest class and quality, ground habitat measurements were combined with vegetation and textural indices from Landsat-8 images to build a decision tree model (Random Forest). This classification was reliable in determining forest class and disturbance presence but not intensity in the TDF, a landscape traditionally difficult to classify. This method of remotely classifying disturbances combined with ground measurements is useful in management decisions and could be applied to other disturbed habitats worldwide.

INTRODUCTION

The purpose of this study was to measure how human activities can affect the tropical dry forest system. The TDF of Madagascar was chosen due to its extremely high biodiversity and conservation needs. Humans utilize this forest throughout its range, compelling land managers to find a balance between conservation and human use. In the south-western portion of the Malagasy TDF, livestock grazing is the largest human impact. Located in this region, the Beza Mahafaly Special Reserve maintains areas protected from and open to grazing. Since human disturbances, such as livestock grazing, can affect the flora and fauna of a system in various ways, I used both direct and indirect sampling methods to detect these impacts.

I conducted visual detection surveys of two diurnal lemur species that share the same food resources as the livestock, the ring-tailed lemur (*Lemur catta*) and Verreaux's sifaka (*Propithecus verreauxi*). Using single-season, single species occupancy estimates (MacKenzie et al. 2002), I

was able to determine if and how grazing presence affected the occupancy of these two flagship conservation species. To indirectly measure grazing impacts on wildlife, I collected three months of acoustic samples from automated recording sensors. The resulting spectrograms were analyzed using the Normalized Difference Sound Index (NDSI), a ratio of human to biologically related sounds (Qi et al. 2008). Grazing impact on the vegetation was measured through detailed habitat sampling including tree and seedling richness and diversity, canopy characteristics, and soil conditions. Since grazing in this particular area also affected the canopy structure, multiple vegetation and textural indices were applied to dry and wet season Landsat 8 images to remotely detect the differences in forest quality. A Random Forests model was built with these satellite and ground habitat variables to classify the study area by forest class alone, forest plus grazing presence, and forest plus grazing intensity. The resulting classifications were evaluated by error rate, variables of importance, and significance between classified groups. By combining habitat, lemur occupancy, soundscape, and satellite sampling, I attempted to determine how grazing affects multiple aspects of the TDF system, information that could be useful for grazing management in the region.

BACKGROUND

The tropical dry forest (TDF) system is defined by warm climates year-round, high rainfall, and long dry seasons (Murphy and Lugo 1986, Mooney et al. 1995). As of 2000, the TDF spanned 1,048,700 km² within the Americas, Africa, Eurasia, and Australasia (Miles et al. 2006). The hospitable climate and vegetation structure provides favorable conditions for human use including agriculture, forest product extraction, and livestock grazing (Murphy and Lugo 1986). Additional threats to TDFs include climate change, fire, forest fragmentation, and human population growth (Miles et al. 2006). The TDF was estimated to cover 20% of global forest area in 2000 with a loss of 2.9% by 2005 (Hansen et al. 2010). In Africa, a net annual loss of 0.34% occurred between 1990 and 2000 (Bodart et al. 2013) where 70-80% of all forest cover is defined as TDF (Murphy and Lugo 1986) and approximately half of the continent's population resides and relies on its resources (Chidumayo and Gumbo 2010).

As a biodiversity hotspot (Myers et al. 2000) the forests of Madagascar are home to more than 90% of the endemic animal species of the island (Dufils 2003) yet have experienced a 40% loss in forest cover from 1950-2000 (Harper et al. 2007). The tropical dry forest of Madagascar is of particular interest as it contains the country's highest plant endemism at 95% (Koechlin 1972) and is experiencing a higher rate of deforestation than that of Malagasy rainforests (Sussman and Rakotozafy 1994). The majority of the remaining TDF is disturbed to some degree yet supports some of Madagascar's flagship species. Small forest patches of southern Madagascar may still be capable of sustaining wildlife (Bodin et al. 2006) since the collective area of suitable habitat in close proximity to one another may remain functional to certain species (Andr n 1994).

Livestock grazing is one of the main disturbances in the southern TDF of Madagascar as the local population's primary supply of income (Sussman et al. 1994). Overgrazing in similar semi-arid systems has shown changes in system dynamics and structure towards more shrubby vegetation (Ad mole et al. 1990, Boardman et al. 2010), known as 'desertification' (Ibrahim 1978). Species reactions to disturbances in Malagasy forests have been generally negative resulting in reduced species diversity yet vary in factor importance, between ecoregions, and even among related species (Irwin et al. 2010). However, in a study of grazed and ungrazed dry forests, sifaka abundance was higher in grazed gallery forest than in its ungrazed counterpart (Axel and Maurer

2011). The high variability of vegetation composition, structure, and climate within the TDF in particular (Murphy and Lugo 1986) could result in variable responses to disturbances.

Remote sensing has long been used to measure large scale changes in land cover (Lambin and Strahler 1994, Mas 1999, Van Asselen and Verberg 2013) including changes in the tropical dry forest (Hansen et al. 2010, Bodart et al. 2013). Changes due to large-scale disturbances have been regularly measured using remote satellite imagery yet there is little research on identifying forest condition with respect to more subtle disturbances, such as the changes that occur in Madagascar's tropical dry forest. There is a need for a remote monitoring method that could accurately identify forest quality in respect to disturbances.

METHODS

Study Area

Research was conducted at the Beza Mahafaly Special Reserve located in the south-western region of Madagascar. The Reserve consists of two main parcels and an extension surrounding these areas (Figure 1). Parcel 1 is a 1 km² area consisting of gallery and dry deciduous forest surrounded by a fence that has prevented livestock grazing within the parcel since it was installed in 1979 (Richard et al. 1988). Grazing is unrestricted within parcel 2 and the extension, creating a mixture of moderately to heavily grazed areas outside of parcel 1.

Twenty four sampling sites were established within two dry forest classes (gallery and dry deciduous) and three levels of grazing intensity (ungrazed, moderately, and heavily grazed). Forest class was established from a 2007 land cover analysis and grazing intensity determined from multi-year GPS tracking data of the two largest livestock herds within the reserve as well as knowledge of local grazing history.

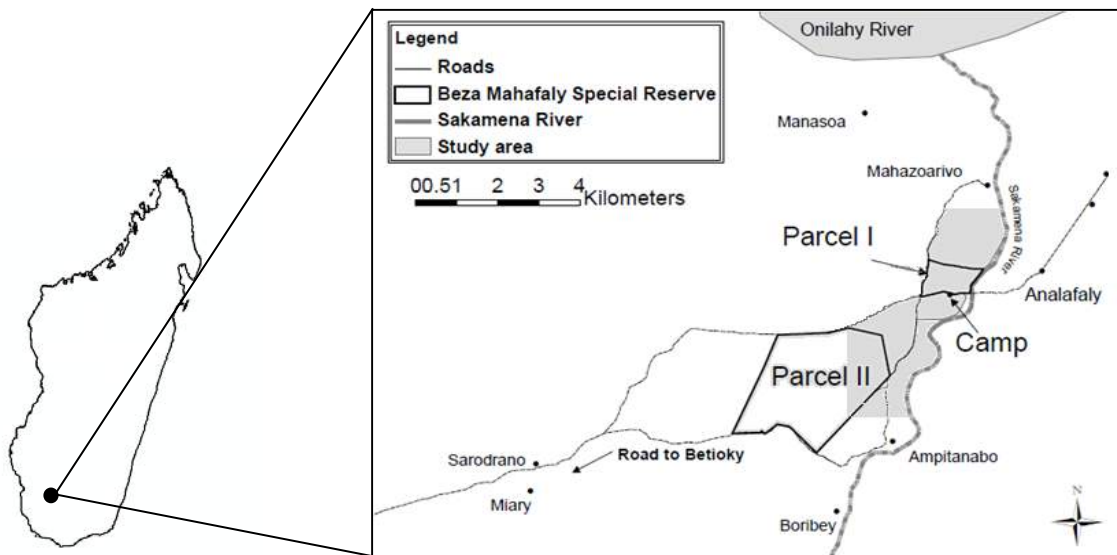


Figure 1. Map of the Beza Mahafaly Special Reserve with study area in gray and reference to location in Madagascar.

Lemur Occupancy

Visual detection surveys of two diurnal lemur species, the ring-tailed lemur (*Lemur catta*) and Verreaux's sifaka (*Propithecus verreauxi*), were conducted to determine presence/absence at each of the twenty-four sampling sites on ten occasions between June and July 2014. Both lemur species

share the same food resources as the livestock which should illustrate direct impacts from livestock grazing. Occupancy modeling developed by MacKenzie et al. (2002) accounts for imperfect detection by combining detection/non-detection data to estimate detection probability. Site specific covariates measured in this study included: grazing intensity (ungrazed, moderately grazed, or heavily grazed), forest class (gallery or dry deciduous), and percent canopy cover. Sampling specific covariates included: time of sampling and presence of wind. Single-season occupancy estimates were calculated by modeling the highest probability of occupancy and detection based on listed covariates using Bayesian analysis. Multiple candidate models with different covariate combinations were tested for importance and significance. Top performing models were indicated by low deviance information criterion (DIC) values (Spiegelhalter et al. 2002), with the best models defined by $\Delta DIC < 4$. Model selection was first analyzed using vague non-informative prior distributions for each covariate followed by selection with informative prior distributions for forest class and grazing presence from a 2010 detection study at the study site. Significant covariates (95% beta confidence intervals did not overlap with zero) were then used to estimate occupancy and detection probability.

Soundscape Sampling

Twelve Wildlife Acoustics automated recorders were installed across both forest classes and three grazing categories. One minute acoustic samples were recorded every fifteen minutes for three months, accounting for daily variations in the soundscape. Resulting spectrograms were analyzed using the normalized difference soundscape index (NDSI), an indicator of biological activity to human disturbance (Qi et al. 2008):

$$NDSI = \frac{\beta - \alpha}{\beta + \alpha}$$

where α is the anthrophony, or the amount of acoustic energy from human-generated sound, and β is the biophony, or acoustic energy from biological sounds. NDSI values range from -1 to 1, with -1 indicating a soundscape consistent of only human sounds and +1 indicating a completely biological soundscape. NDSI values were averaged across grazing and forest classes to determine patterns in biological to human related sounds.

Habitat Sampling

A grid of 9 circular plots with a radius of 10 m spaced 30 m apart was located at each sampling site. Habitat variables sampled within each plot included: tree species richness, tree species diversity, number of kily (*Tamarindus indica*), kily dbh (diameter at breast height), basal area (m^2/ha), canopy height (m), and percent canopy cover. The kily is a deciduous tamarind tree and defining species of gallery forest (Jolly 1966, Sussman and Rakotozafy 1994). Basal area is the area of land occupied by the cross-section of tree trunks measured at the diameter at breast height (1.3 m). A wedge prism is used to calculate basal area by measuring the number of trees larger than a set diameter (Hush et al. 1972). The diameter threshold is determined by the prism factor or basal area factor (BAF) in m^2/ha , describing the angle of the prism. The number of trees that fell within the measurement were multiplied by the basal area factor (BAF 10) to determine basal area in m^2/ha . To determine percent canopy cover, hemispherical photos were taken 1 m above ground at the center of each plot and converted to black and white pixels using the software program GLA (Gap Light Analyzer) (Fraze et al. 2000) resulting in a sine-weighted measure of canopy openness. The inverse of this measurement was assigned as canopy cover.

Three 1 m² sub-plots were randomly placed within each circular plot to measure understory characteristics including: seedling richness, seedling diversity, seedling cover, soil hardness (pound force, lbf), leaf litter thickness (cm), and herbaceous cover. Soil hardness is determined by pressing a Lang penetrometer into the soil and recording the force in pounds required to force the probe into the soil. The Lang penetrometer has been used before to measure human-impacts on soil in Madagascar (Zavada et al 2009).

Satellite Analysis

Two Landsat 8 images were used in vegetation, texture, and elevational analysis. A January 26, 2014 image from the middle of the rainy season (November through March) and a July 2, 2014 image from the middle of the dry season (April through October) were chosen to illustrate differences in vegetation seasonality and responses to grazing pressure. Both images were pre-processed by converting to top of atmosphere reflectance followed by dark object subtraction.

A collection of vegetation indices (VI) and textural algorithms (Table) were applied to both images. The normalized difference vegetation index (NDVI) is one of the most used indices in land cover classifications (Ali et al. 2013, Rodrigues et al. 2013). Although in arid and semiarid landscapes with bare soil patches present, the modified soil adjusted vegetation index (MSAVI2) has been shown to measure greenness more accurately (Qi et al. 1994). The Enhanced Vegetation Index (EVI) (Waring et al. 2006) has also been successful at dealing with soil background and atmospheric aerosol influences (Liu and Heute 1995) as well as displaying a more dynamic range than NDVI (Heute et al. 2002). The modified triangular vegetation index (MTVI2) was found to be a highly accurate predictor of green leaf area index (Haboudane et al. 2004). The moisture stress index (MSI) (Rock et al. 1985) can detect large scale disturbances based on moisture content. The normalized infrared index (NDII) has also been shown sensitive to moisture changes in the canopy (Hardisky et al. 1983) while the mid-infrared index (MIRI2) (Solaimani et al. 2011) has been related to percent canopy cover. Textural differences indicating disturbances in the homogeneity of the canopy were observed using a moving standard deviation index (MSDI) (Tanser and Palmer 2000) applied to the red, near infrared and shortwave infrared bands. Additional data included a digital elevation model (DEM). The previous algorithms were applied to both wet and dry season images, as well as image differencing of the vegetation indices. All algorithms used in the analysis are defined in Table 1.

Table 1. List of spectral indices used in the satellite analysis. Variables include the visible blue, green, and red bands, near infrared band (NIR), first shortwave infrared band (SWIR1), and pixel digital number (DN).

Spectral Index	Equation	Spectral Index	Equation
NDVI	$\frac{NIR - RED}{NIR + RED}$	MSAVI2	$\frac{(2 * NIR + 1 - \sqrt{(2 * NIR + 1)^2 - 8 * (NIR - RED)})}{2}$
MSI	$\frac{SWIR1}{NIR}$	EVI	$2.5 \left(\frac{NIR - RED}{NIR + (6 * RED) - (7.5 * BLUE) + 1} \right)$
NDII	$\frac{NIR - SWIR1}{NIR + SWIR1}$	MTVI2	$\frac{1.8(NIR - GREEN) - 3.75(RED - GREEN)}{\sqrt{(2 * NIR + 1)^2 - (6 * NIR - 5\sqrt{RED})} - 0.5}$

MIRI2	$\frac{SWIR1 - RED}{SWIR1 + RED}$	MSDI	$\sqrt{\frac{\sum_{i=1}^N (DN_i - \overline{DN})^2}{N}}$
-------	-----------------------------------	------	--

The resulting satellite variables were combined with the ground habitat sampling variables to build a Random Forests (RF) classification algorithm (Breiman 2001). Random Forests is a decision tree based model that classifies an image resulting from random subsets of data run through thousands of trees built from random collections of variables. It has been shown to be highly accurate while handling large datasets, missing data, and correlated variables (Cutler et al. 2007). The RF model was used to classify the study by forest class alone, forest class plus grazing presence, and forest class plus grazing intensity. The classifications were analyzed by group error rate, variables of most importance, and significance using a multiresponse permutation procedure (MRPP), a nonparametric multivariate test.

RESULTS

Lemur Occupancy

While the categorical site covariates of forest class and grazing intensity may not emerge as significant covariates when modeling lemur occupancy, canopy cover was found to be directly correlated with forest class and grazing presence (Figure 2). Canopy cover separated by four forest and grazing categories (dry deciduous grazed and ungrazed, gallery grazed and ungrazed) failed to reject the null hypothesis of significance between groups (ANOVA, $p\text{-value}=8.39e-9$, $\alpha=0.05$) with significance found between each pair-wise comparison (Tukey's HSD). Canopy cover could then used as inference of forest and grazing presence.

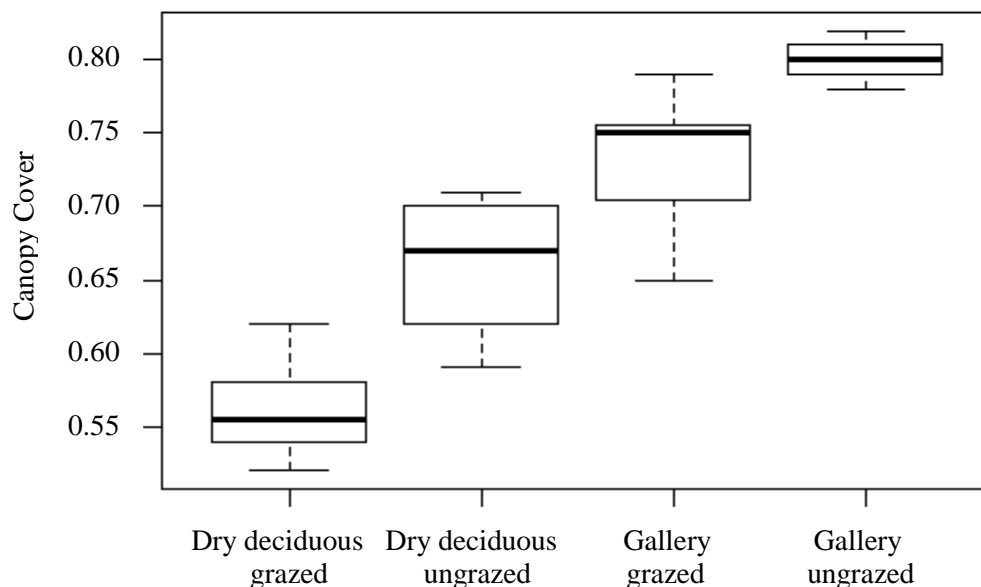


Figure 2. Boxplot of canopy cover by forest and grazing categories.

For the ring-tailed lemur, the top models of best fit ($\Delta DIC < 4$) with strongest covariates (95% CI of covariate betas do not overlap with zero) included canopy cover as a covariate of occupancy with the additive effect of forest, time, and time² as covariates of detection probability. Using informative versus non-informative prior distributions for forest and grazing had little effect upon

the resulting model significance. As canopy cover increased, occupancy estimates increased (Figure 3). Detection probability was higher in the gallery forest compared to the dry deciduous forest (Table 2). The additive effect of time and time² indicated that detection probability was highest in the morning and late afternoon with the lowest detection around 11:00am (Figure 4).

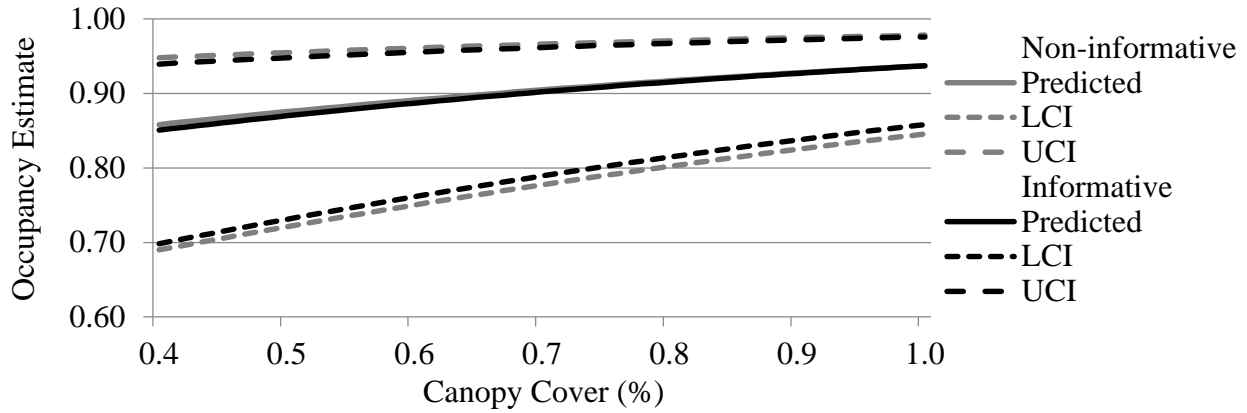
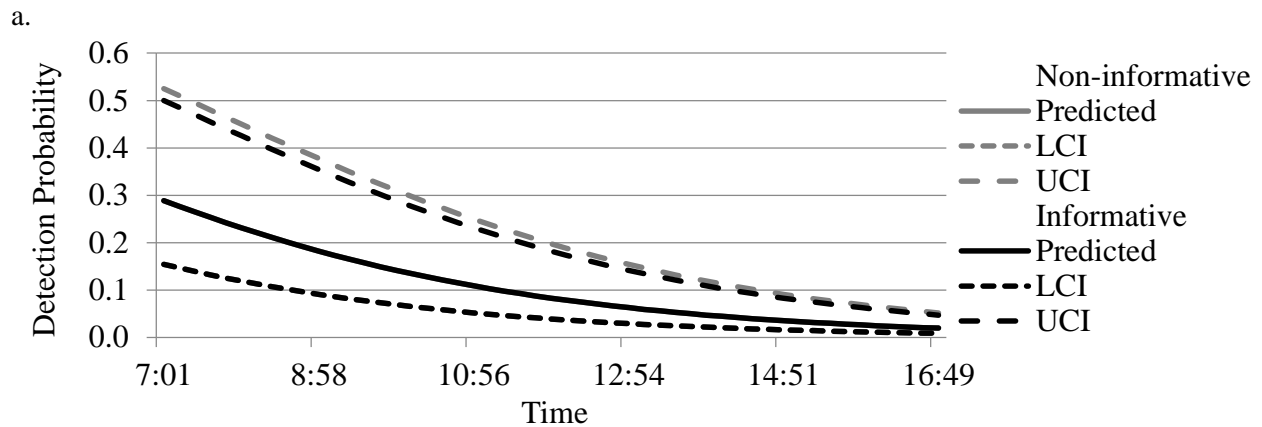


Figure 3. Occupancy estimate of ring-tailed lemur by percent canopy cover with upper (UCI) and lower confidence intervals (LCI) for non-informative (gray) and informative priors (black).

Table 2. Detection probability of ring-tailed lemur by forest class with upper (UCI) and lower confidence intervals (LCI) for non-informative and informative priors.

Detection Probability	Dry Deciduous			Gallery		
	Mean	UCI	LCI	Mean	UCI	LCI
Non-informative prior distribution	0.11	0.23	0.05	0.25	0.45	0.13
Informative prior distribution	0.11	0.23	0.05	0.25	0.45	0.13



b.

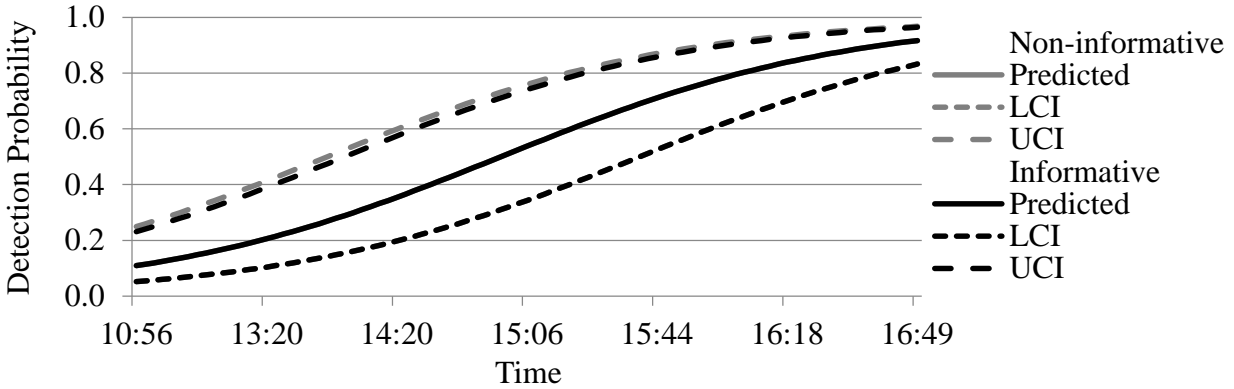


Figure 4. Detection probability of ring-tailed lemur by time (a) and time² (b) with upper (UCI) and lower confidence intervals (LCI) for non-informative priors (gray lines) and informative priors (black lines).

For the Verreaux’s sifaka, the top models of best fit ($\Delta\text{DIC} < 4$) with strongest covariates (95% CI of covariate betas do not overlap with zero) included forest as covariate of occupancy and detection probability when using informative prior distributions. Forest as a variable of occupancy was not detected when using non-informative prior distributions. Occupancy estimates were higher in the gallery forest while detection probably was higher in the dry deciduous forest compared to the dry deciduous forest (Table 3).

Table 3. Occupancy estimate and detection probability of Verreaux’s sifaka by forest class with upper (UCI) and lower confidence intervals (LCI) for non-informative and informative prior distributions.

Detection Probability	Dry Deciduous			Gallery		
	Mean	UCI	LCI	Mean	UCI	LCI
Non-informative prior distribution	0.57	0.67	0.48	0.43	0.53	0.33
Informative prior distribution	0.57	0.67	0.48	0.40	0.50	0.31
Occupancy Estimate	Dry Deciduous			Gallery		
	Mean	UCI	LCI	Mean	UCI	LCI
Informative prior distribution	0.65	0.86	0.33	0.95	0.98	0.83

Soundscape Analysis

Averaged NDSI values by forest and grazing category were separated by time of day to depict trends in the biological to human sound activity (Figure 5). In the gallery forest, there was no significant difference in sound ratios by grazing category for most of the day. The only difference is detected during the night when the biological sound activity was observed in the heavily grazed sites followed by moderately grazed and ungrazed sites.

In the dry deciduous forest, grazing categories are significantly different throughout the day. Heavily grazed sites consistently exhibited the most biological sound to human sound activity followed by ungrazed and moderately grazed sites.

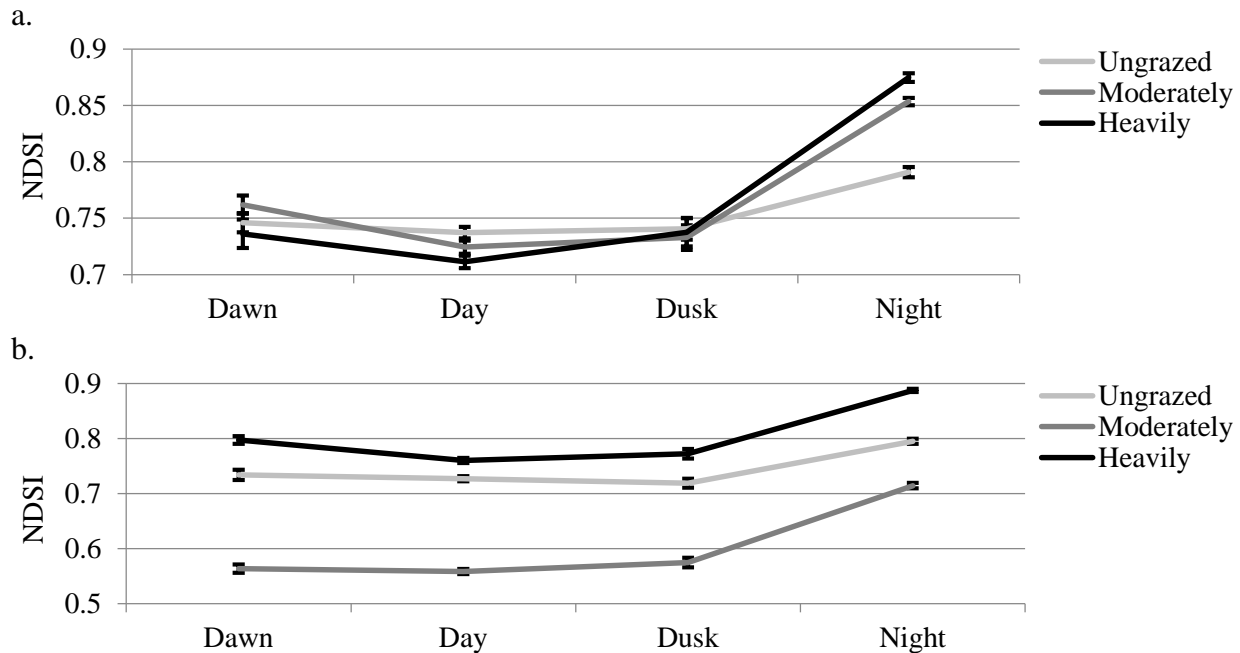


Figure 5. Averaged NDSI values for grazing categories by time of day within the gallery (a) and dry deciduous (b) forest.

Habitat and Satellite Analysis

Two separate random forest models were built, one with combined habitat and satellite variables and a second with satellite variables alone. The error rates for classifying the study site by forest alone, forest and grazing presence, and forest and grazing intensity increased from 5% to 13% to 22% (Table 4). Both models exhibited nearly the same error rates regardless of the presence of habitat variables. The top variables of importance in both models and all classification methods were satellite derived variables. The resulting land cover classifications from the satellite RF model are shown in Figure 6. Results from the multiresponse permutation procedure (MRPP) indicate significance among forest classes and forest class with grazing presence (Table 5). Differences between forest class and grazing intensity were overall significant but not all pair-wise comparisons were significant.

Table 4. Random Forest error rates by classification type (forest and grazing) and RF model.

	Habitat and Satellite Error Rate	Satellite Error Rate
Forest class	5.09%	4.63%
Forest class and grazing presence	12.50%	13.43%
Forest class and grazing intensity	21.76%	22.69%

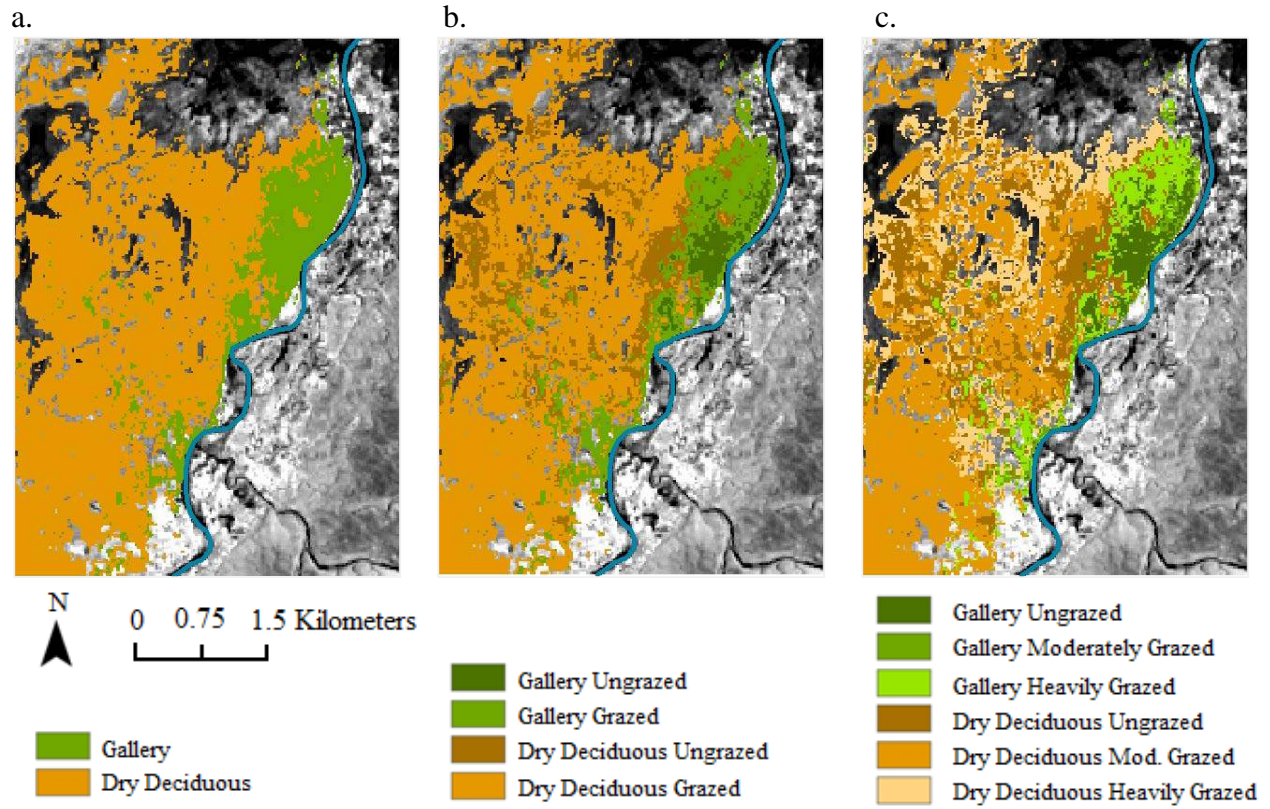


Figure 6. Land cover classifications by forest (a), forest plus grazing presence (b), and forest plus grazing intensity (c).

Table 5. Multiresponse permutation procedure (MRPP) results of significance between classified groups (* denotes significance at $\alpha=0.05$).

Forest Class	p-value
Gallery vs. Dry Deciduous	0.001 *

Forest Class and Grazing Presence	p-value
Gallery Grazed vs. Ungrazed	0.046 *
Dry Deciduous Grazed vs. Ungrazed	0.008 *

Forest Class and Grazing Intensity	p-value
Gallery All Grazing Categories	0.036 *
Gallery Ungrazed vs. Moderately Grazed	0.185
Gallery Ungrazed vs. Heavily Grazed	0.027 *
Gallery Moderately Grazed vs. Heavily Grazed	0.213
Dry Deciduous All Grazing Categories	0.002 *
Dry Deciduous Ungrazed vs. Moderately Grazed	0.003 *
Dry Deciduous Ungrazed vs. Heavily Grazed	0.016 *
Dry Deciduous Moderately Grazed vs. Heavily Grazed	0.185

DISCUSSION AND CONCLUSIONS

Grazing activities appear to have varied effects on the TDF system. Lemur occupancy and detection probabilities differed by forest class and grazing presence dependent on the species of interest. Ring tailed lemurs exhibited higher probabilities of detection during early morning or late afternoon sampling times while sifaka detection was not dependent on sampling time. Ring tailed lemurs are known to be active in the morning while individuals are thermoregulating in the sun as well as in the late afternoon as groups are settling for the evening (Jolly 1966). Higher detection during these times would be expected when they are most active. Sifaka have similar activity patterns (Erkhert and Kappeler 2004) so it is unexpected that their detection was not dependent on sampling time as well. Occupancy surveys were conducted between 8:00-11:30am and 2:00-4:00pm. The low detection probability around 11:00am could be overestimated due to the small number of surveys around during that time. Detection probability also varied by forest class with ring tailed lemurs exhibiting a lower estimate in the dry deciduous forest and sifaka exhibiting a higher estimate in the same forest class. During my surveys I noticed that ring tailed lemurs were more vocal causing observers to audibly detect their presence more often than visually detecting them. Sifaka were quieter and more frequently detected by sight rather than sound. The gallery forest has a significantly higher canopy making it difficult to visually detect sifaka compared with the lower and more open canopy of the dry deciduous forest.

Occupancy estimates also varied in covariate significance by lemur species. For ring tailed lemurs, canopy cover was a significant variable in occupancy estimation. Mean occupancy remained high

although confidence intervals narrowed as canopy cover increased. Used as inference for forest class and grazing presence, this indicates that moving from dry deciduous grazed and ungrazed to gallery grazed and ungrazed results in more reliable occupancy estimates. For sifaka, forest class was a significant covariate of occupancy estimate only when modeling with prior distributions. Higher occupancy estimates with narrow confidence intervals were observed in the gallery forest with lower estimates and wider confidence intervals in the dry deciduous forest.

Variance by forest class was also observed in soundscape analysis. The lack of significance between grazing intensities in the gallery forest indicates that this forest could be less affected by and more resilient to grazing pressures. The significance between grazing categories in the dry deciduous forest throughout all time periods could indicate possible effect from grazing. The highest sound activity in the heavily grazed dry deciduous forest could imply certain species well fit to this habitat are overpowering sound activity. As the category with the lowest biological to human sound activity, the moderately grazed dry deciduous sites exhibit the most drastic effect from the presence of grazing.

The roughly equal error rates between Random Forest models and satellite variables of most importance in all three classifications indicate that satellite analysis is just as good or better at detecting disturbance effects in this system. Although grazing intensity classifications were not significant between one another, forest class and grazing presence was. This RF model demonstrates a reliable method to remotely identify land cover differences in forest class and disturbance presence in a TDF, a system traditionally difficult to classify. Combining lemur, soundscape, habitat, and satellite analysis would allow land managers decide how to manage the effects of grazing and where to target conservation and management activities.

FUTURE WORK

Results of this study would be greatly improved by repeating occupancy surveys during different seasons when other food sources in demand that could be affected by grazing. Collected acoustic samples could be further analyzed by evaluating presence and amount of sound activity from major wildlife classes such as birds, insects, and mammals to determine how different taxa respond to grazing pressures. Lemur calls could be used as training files to determine occupancy based on acoustic data and relate occupancy results to field surveying for lemur presence. To improve classification results, different spectral indices or higher resolution imagery could be used to differentiate grazing intensities even further.

VALUABLE ASPECTS

I believe the most valuable aspects of this program are the financial support and research experiences. The funding I received from the Graduate Fellowship supported my living costs and research throughout the summer, allowing me to concentrate all of my time and energy on the data collection and analysis. The research experiences I gained through the program included multiple disciplines. Without the provided funding and time, I would not have been able to explore the different aspects associated with my research questions.

ACKNOWLEDGEMENTS

I would like to thank the NASA WV Space Grant Consortium for valuable funding in the form of a Graduate Fellowship. Funding for research and presentations was also provided by research and

travel grants from the Marshall University Graduate College. I would like to thank my assistants Efitiria and Enafa for their friendship and unbelievable knowledge in the field. Finally, I would most like to thank my advisor Anne Axel for her never ending support and encouragement.

REFERENCES

- Adamoli, J, Sennhauser, E, Acero, JM, and Rescia, A. 1990. Stress and disturbance: Vegetation dynamics in the dry Chaco region of Argentina. *Journal of Biogeography* 17: 491-500.
- Ali, A, de Bie, CAJM, Skidmore, AK, Scarrott, RG, Hamad, A, Venus, V, and Lymberakis, P. 2013. Mapping land cover gradients through analysis of hyper-temporal NDVI imagery. *International Journal of Applied Earth Observation and Geoinformation* 23: 301-312.
- Andr n, H. 1994. Effects of habitat fragmentation on birds and mammals in landscapes with different proportions of suitable habitat: a review. *Oikos* 71: 355-366.
- Axel, AC and Maurer, BA. 2011. Lemurs in a complex landscape: Mapping species density in subtropical dry forests of southwestern Madagascar using data at multiple levels. *American Journal of Primatology* 73: 38-52.
- Biardman, J, Foster, I, Rowntree, K, Mighill, T, and Gates, J. 2010. Environmental stress and landscape recovery in a semi-arid area, The Karoo, South Africa. *Scottish Geographical Journal* 126: 64-75
- Bodart, C, Brink, AB, Donnay, F, Lupi, A, Mayaux, P, and Achard, F. 2013. Continental estimates of forest cover and forest cover changes in the dry ecosystems of Africa between 1990 and 2000. *Journal of Biogeography* 40: 1036-1047.
- Bodin, O, Teng , M, Norman, A, Lundberg, T, and Elmqvist, T. 2006. The value of small size: Loss of forest patches and ecological thresholds in southern Madagascar. *Ecological Applications* 16:440-451.
- Breiman, L. 2001. Random Forests. *Machine Learning* 45: 5-32.
- Chidumayo, E.N. and Gumbo, D.J. 2010. *The dry forests and woodlands of Africa: managing for products and services*. Earthscan: London.
- Cutler, DR, Edwards, TC, Beard, KH, Cutler, A, and Hess, KT. 2007. Random forests for classification in ecology. *Ecology* 88: 2783–2792.
- Dufils, JM. 2003. Remaining forest cover. In: *The Natural History of Madagascar*, ed. S.M. Goodman & J.P. Benstead, pp. 88–96. Chicago, IL, USA: University of Chicago Press.
- Erkhert, H and Kappeler, P. 2004. Arrived in the Light: Diet and seasonal activity patterns in wild Verreaux’s sifakas (*Propithecus v. verreauxi*; Primates: Indriidae). *Behavioral Ecology and Sociobiology* 57: 174-186.
- Frazer, GW, Canham, CD, Lertzman, KP. 2000. Gap light analyzer (GLA), Version 2.0: image-processing software to analyze true-color, hemispherical canopy photographs. *Bulletin of the Ecological Society of America* 81: 191–197.
- Haboudane, D, Miller, JR, Pattey, E, Zarco-Tejada, PJ, and Strachan, IB. 2004. Hyperspectral vegetation indices and novel algorithms for predicting green LAI of crop canopies: Modeling and validation in the context of precision agriculture. *Remote sensing of environment* 90: 337-352.
- Hansen, MC, Stehman, SV, and Potapov, PV. 2010. Quantification of global gross forest cover loss. *Proceedings of the National Academy of Sciences USA* 107: 8650-8655.

- Hardisky, MA, Klemas, V, and Smart, RM. 1983. The influence of soil salinity, growth form, and leaf moisture on the spectral radiance of *Spartina alterniflora* canopies. *Photogrammetric Engineering and Remote Sensing* 49: 77–83.
- Harper, G, Steininger, MK, Tucker, CJ, Juhn, D, and Hawkins, F. 2007. Fifty years of deforestation and forest fragmentation in Madagascar. *Environmental Conservation* 34: 1–9.
- Huete, A, Didan, K, Miura, T, Rodriguez, EP, Gao, X, and Ferreira, LG. 2002. Overview of the radiometric and biophysical performance of the MODIS vegetation indices. *Remote Sensing of Environment* 83: 195-213.
- Husch, B, Miller, CI, and Beers, TW. 1972. Forest mensuration. Ronald, New York, New York, USA. Ibrahim, F. 1978. Anthropogenic causes of desertification in Western Sudan. *GeoJournal* 2.3: 243-254.
- Irwin, MT, Wright, PC, Birkinshaw, C, Fisher, BL, Gardner, CJ, Glos, J, Goodman, SM, Loiselle, P, Rabeson, P, Raharison, J-L, Raheirilalao, MJ, Rakotondravony, D, Raselimanana, A, Ratsimbazavy, J, Sparks, JS, Wilme, L, and Ganzhorn, J. U. 2010. Patterns of species change in anthropogenically disturbed forests of Madagascar. *Biological Conservation* 143: 2351-2362.
- Jolly A. 1966. Lemur behavior. Chicago: University of Chicago Press. 187p.
- Koechlin, J. 1972. Flora and vegetation of Madagascar. In *Biogeography and ecology in Madagascar*, R. Battistini, G. Richard-Vinard, Eds. (Dr. W Junk B.V. Publishers, The Hague). Lambin, EF and Strahler, AH. 1994. Change-vector analysis in multispectral space: A tool to detect and categorize land-cover change processes using high temporal-resolution satellite data. *Remote Sensing of Environment* 48: 231-244.
- Liu, HQ and Huete, AR. 1995. A feedback based modification of the NDVI to minimize canopy background and atmospheric noise. *IEEE Transactions on Geoscience Remote Sensing* 33: 457-465.
- MacKenzie, DI, Nichols, JD, Lachman, GB, Droege, S, Royle, JA, and Langtimm, CA. 2002. Estimating site occupancy rates when detection probabilities are less than one. *Ecology* 83: 2248–2255.
- MacKenzie, DI, Nichols, JD, Royle, AJ, Pollock, KH, Bailey, LL, and Hines, JE. 2006. Occupancy estimation and modeling: inferring patterns and dynamics of species occurrence. Elsevier, Amsterdam.
- Mas, J–F. 1999. Monitoring land-cover changes: A comparison of change detection techniques. *International Journal of Remote Sensing* 20: 139-152.
- Miles, L, Newton, AC, DeFries, RS, Ravilious C, May, I, Blyth, S, Kapos, V, and Gordon, JE. 2006. A global overview of the conservation status of tropical dry forests. *Journal of Biogeography* 33: 491-505.
- Murphy, PG and Lugo, AE. 1985. Ecology of tropical dry forest. *Annual Review Ecology and Systematics* 17: 67-88.
- Mooney, HA, Bullock, SH, and Medina, E. 1995. Introduction. In: *Bullock, S.H., Mooney, H.A. & Medina, E. (eds.) Seasonally dry tropical forests*, pp. 1-8. Cambridge University Press, Cambridge, UK.
- Myers, N, Mittermeier, RA, Mittermeier, CG, da Fonseca, GAB, and Kent, J. 2000. Biodiversity hotspots for conservation priorities. *Nature* 403: 853-858.

- Richard, AF, Rakotomanga, P, and Sussman, RW. 1988. Beza-Mahafaly: Recherches Fondamentales et Appliquées. pp.209-215 in Rakotovao, L., V. Barre, and J. Sayer: L'Equilibre des Ecosystèmes Forestiers à Madagascar. Actes d un séminaire international. IUCN, Gland et Cambridge, 344.
- Rock, BN, Williams, DL, and Vogelmann, JE. 1985. In *Machine Processing of Remotely Sensed Data Symposium*, Purdue University, West Lafayette, IN, pp. 71-81.
- Qi, J, Chehbouni, A, Huete, AR, Kerr, YH, and Sorooshian, S. 1994. A modified soil adjusted vegetation index. *Remote Sensing of Environment* 48:199.
- Qi, J, Gage, SH, Joo, W, Napoletano, B, and Biswas, S. 2008. Soundscape characteristics of an environment: A new ecological indicator of ecosystem health. In *Wetland and Water Resource Modeling and Assessment*, W. Ji, Ed. (CRC Press, New York), pp. 201-211.
- Rodrigues, A, Marcal, ARS, and Cunha, M. 2013. Identification of potential land cover changes on a continental scale using NDVI time-series from SPOT VEGETATION. *International Journal of Remote Sensing* 34: 8028-8050.
- Solaimani, K, Shokrian, F, Tamartash, R, and Banihashemi, M. 2011. Landsat ETM+ based assessment of vegetation indices in highland environment. *Journal of Advances in Developmental Research* 2:5-13.
- Spiegelhalter DJ, Best NG, Carlin BP, and van der Linde A. 2002. Bayesian Measures of Complexity and Fit. *Journal of the Royal Statistical Society* 64: 583–639.
- Sussman, RW and Rakotozafy, A. 1994. Plant diversity and structural analysis of a tropical dry forest in southwestern Madagascar. *Biotropica* 26: 241-54.
- Tanser, F and Palmer, AR. 2000. Vegetation mapping of the Great Fish River basin, South Africa: Integrating spatial and multi-spectral remote sensing techniques. *Applied Vegetation Science* 3:197-204.
- Van Asselen, S and Verburg, PH. 2013. Land cover change or land-use intensification: simulating land system change with a global-scale land change model. *Global Change Biology* 19: 3648-3667.
- Waring, RH, Coops, NC, Fan, W, and Nightingale, JM. 2006. MODIS enhanced vegetation index predicts tree species richness across forested ecoregions in the contiguous U.S.A. *Remote Sensing of Environment* 103: 218–226.
- Zavada, MS, Wang, Y, Rambolamanana, G, Raveloson, A, and Razanatsoa, H. 2009. The significance of human induced and natural erosion features (lavakas) on the central highlands of Madagascar. *Madagascar Conservation and Development* 4: 120-127.

PRESENTATIONS

- Rankin, L. and Axel, A. Defining forest condition in grazed tropical dry forests. Paper presented at the American Society for Photogrammetry and Remote Sensing 2014 Annual Conference, Louisville, KY, March 2014.
- Rankin, L. and Axel, A. Soundscapes as a measure of forest condition in grazed forests of Madagascar. Paper presented at the XXIV International Bioacoustic Congress, Pirenópolis, Brazil, September 2013.
- Rankin, L. and Axel, A. Soundscapes as a measure of ecological integrity. Paper presented at the 2013 International Prosimian Congress, Ranomafana, Madagascar, August 2013.

Rankin, L. and Axel, A. Assessing ecological integrity of grazed and ungrazed tropical dry forests through soundscape analysis. Poster presented at the 2013 Annual Meeting of the Association of Southeastern Biologists, Charleston, WV, April 2013.

Rankin, L. and Axel, A. Assessment of landscape degradation using Landsat images and vegetation sampling in Southern Madagascar. Paper presented at the 2013 Annual Meeting of the West Virginia Academy of Science, Davis, WV, April 2013.

INVESTIGATION OF BENZYL ISOTHIOCYANATE'S REGULATION OF METASTATIC PROCESSES IN HNSCC CELL LINES

M. Allison Wolf
Ph.D., Biomedical Sciences
Marshall University – Translational Genomic Research Institute
Huntington, WV, 25701
Pier Paolo Claudio, M.D., Ph.D.

ABSTRACT

Despite recent improvements in cancer treatment, overall survival of advanced head and neck squamous cell carcinoma (HNSCC) has not improved in the past three decades. Metastasis represents a detrimental event that greatly hinders the outcome for those suffering with HNSCC. In our *in vitro* studies, we evaluated the use of BITC as a treatment to prevent migration and invasion of HNSCC. Our study had two objectives; the first being to investigate if this compound can prevent HNSCC cell migration and invasion and the second was to identify a mechanism through which BITC was eliciting its anti-tumor response.

Our *in vitro* data suggests that BITC treatments decrease the migration and invasion of the HN12 cell line, in a dose dependent manner, at concentrations that did not affect cell viability. Additionally, the expression of the epithelial-mesenchymal transition (EMT) marker, vimentin, and putative cancer stem cell marker, ALDH1A1, was significantly reduced after a BITC treatment in the HN12 cell line. However, E-cadherin expression increased in the HN12 cell line after BITC treatment. We also observed that BITC treatments significantly increased the amount of reactive oxygen species (ROS) in HNSCC cells. Blocking BITC induced ROS with co-administration of catalase or NAC significantly inhibited BITC's ability to prevent cellular migration.

Taken together these data suggest that BITC has the capacity to inhibit processes involved in HNSCC cell migration and invasion and BITC induced ROS may regulate these processes.

INTRODUCTION

Currently, the National Cancer Institute (2014) suggests that the overall five-year survival rate for HNSCC is 40-50%, and this percentage is significantly lower if a patient develops metastasis or a secondary tumor in the head and neck region. Around 60% of patients are diagnosed with locoregionally-advanced disease, and treatment of advanced HNSCC is aggressive, with significant acute and long-term effects [1]. Even with aggressive multi-modality therapy the five-year survival rate of locally advanced disease is only 30% [2]. Consequently, safe and effective treatments that prevent metastasis could improve quality of life and survival for HNSCC patients.

The use of natural products, such as isothiocyanates (ITCs), which are known to target many cellular pathways linked to metastasis provides a unique therapy option for HNSCC. ITCs are phytochemicals produced by cruciferous vegetables [3,4]. ITCs are a product of glucosinolate hydrolysis, which is initiated by an enzyme called myrosinase [5]. This enzyme is found spatially

separated from glucosinolates in cruciferous vegetables and in our own human enteric microflora [5].

Benzyl isothiocyanate (BITC) is an ITC of particular interest in cancer therapy because of its ability to inhibit cell growth and induce apoptosis in several types of cancer cell lines, including HNSCC [5-7]. In addition to inhibiting cell growth and inducing apoptosis, BITC may play a role in inhibiting angiogenesis, epithelial-mesenchymal transition (EMT), and metastasis [8-10].

The present study builds on recent findings, which indicate that BITC inhibits migration and invasion of HNSCC cells. Current results suggest that there are changes in markers associated with EMT and cancer stem cells after BITC treatment. Additionally, our study supports that induction of reactive oxygen species (ROS) is a possible mechanism by which BITC can prevent migration.

Traditionally, the research on ROS-inducing anti-neoplastic drugs focuses on whether the treatment kills cancer cells, and little attention has gone in to understanding how ROS inducers may effect migration and invasion [11,12]. The conundrum of ROS therapy is that ROS inducing agents are strongly associated with increased migration and invasion of cells [13,14]. However, a study by Luanpitpong *et al.* (2010) showed that in HN460 lung cancer cells certain ROS ($\text{OH}\bullet$) increased cell migration while others ($\text{O}_2^{\text{--}}$ and H_2O_2) decreased cell migration. This same study indicated that catalase, which is a H_2O_2 scavenger, increased migration [15].

Results from our lab using HNSCC cells support the findings of Luanpitpong *et al.* (2010) and suggest that the type of ROS induced may be important in dictating HNSCC cell migration [15]. Here we show that BITC treatments significantly induced ROS in HNSCC cell lines and that by modulating BITC induced ROS levels with either *N*-acetyl-L-cysteine (NAC) or catalase we restored HNSCC cell migration. Additionally, we have shown that NAC inhibited BITC induced chemo-enhancement in HNSCC cell lines.

In conclusion, BITC targets many molecular pathways in the cell that alter migration, invasion, and cell death. Here, we demonstrate that ROS play an important role in the ability of BITC to alter migration and invasion and induce cell death.

METHODS

Materials

Benzyl isothiocyanate (99.5% pure) was purchased from LKT Laboratories, Inc. (St. Paul, MN). Stock solutions of BITC (100mM) were prepared in DMSO and diluted into growth medium such that the final concentration of DMSO did not exceed 0.01% (vol./vol.), a concentration that did not induce toxicity in HN12 and HN30 cells. 2',7'-dichlorodihydrofluorescein diacetate (H_2DCFDA) was purchased from Molecular Probes (Grand Island, NY). Stock solutions of H_2DCFDA (50mM) were prepared in DMSO in the dark and diluted into serum free growth medium. *N*-Acetyl-L-cysteine (NAC) and Catalase from bovine liver were both purchased from Sigma-Aldrich (St. Louis, MO). Stock solutions of NAC (100mg/mL) were prepared in sterile Milli-Q water and diluted into serum free growth medium. Catalase treatments (2,500U/mL) were prepared in serum free growth medium.

Cell Culture and Reagents

The highly metastatic HNSCC cell line, HN12, and moderately metastatic HNSCC cell line, HN30, were a kind gift from Dr. George Yoo (Karmanos Cancer Center, Wayne State University, OH) [16,17]. Monolayer cultures of HN12 and HN30 were maintained in Dulbecco's Modified Eagles Medium (DMEM) (HyClone, Thermo-Scientific) adjusted to contain 10% fetal bovine serum (FBS) (PAA Laboratories GmbH, Pasching, Austria) and supplemented with 1% (vol./vol.) penicillin-streptomycin (P/S) (Corning Cellgro, Manassas, VA). Cells were grown in a humidified incubator at 37°C and with 5% CO₂.

Wound-healing Assay

Cell migration was determined using wound healing assay. HN12 cells were cultured in DMEM (10% FBS, 1% Pen-Strep) in 6-well plates until 90% confluent, and then media was changed to DMEM with 0.05% FBS, 1% P/S overnight to synchronize the cells. A permanent line was drawn horizontally on the bottom of each well, and a plastic pipette tip was used to generate 3 vertical scratches per well. Cell debris was washed away with PBS and initial scratch sizes were determined with an inverted light microscope (Olympus IX51, Center Valley, PA) at 100X magnification. Six measurements were made per well, 1 below and 1 above the horizontal line for each scratch before treatment. Cells were treated with 2.5-5µM BITC for 1-hour at 37°C. DMSO, at the same concentration as in the BITC treated wells, was used for the vehicle control. After 1-hour plates were washed with PBS and treatment was replaced with DMEM (10% FBS, 1% P/S). Wound healing was analyzed 24 hours after treatment. Images were taken at 100X magnification, as described above, and changes in cell migration were determined by calculating the percent of wound healing. Percent wound healing = $([scratch_{t=0hr} - scratch_{t=24hr}] / scratch_{t=0hr}) * 100$. Experiments were repeated 3 times.

Invasion Assay

The effect of BITC on invasion of HN12 cells was determined using Invasion Chambers with 8µm pores (BD Biocoat, Franklin Lakes, NJ). Polycarbonate membranes on the bottom of the Boyden chamber inserts were rehydrated following manufacturer's instructions and 0.5mL of HNSCC cell suspension containing 5×10^4 cells was added to each insert. Cells were allowed to attach for 4 hours prior to treatment in complete DMEM media (10% FBS, 1% P/S). After attachment the appropriate wells were treated for 1-hour with BITC (2.5-5µM) in serum free DMEM. Epidermal growth factor (EGF) was used at (10ng/1mL in serum free DMEM (0.5% BSA, 1% P/S)) was added to the bottom well in all wells, except for the negative control, as a chemoattractant. Media in all inserts was replaced after 1-hour with DMEM (0.5% BSA, 1% P/S). Analysis of cell invasion was performed 24 hours after beginning treatment. Media and cells were removed from the top of the matrigel following manufactures' instructions and cells were fixed with 100% methanol, washed with PBS, and stained with 0.1% Crystal Violet. Cells counts were performed and images taken using an Olympus IX51 inverted light microscope (Olympus, Center Valley, PA) at 400X magnification. Twenty fields of view were counted for each sample and averaged to determine the mean number of cells/field of view. Experiments were repeated a minimum of 3 times.

Western Blot Analysis

Vimentin, E-cadherin, and ALDH1A1 expression were analyzed 24 hours after BITC treatment in HNSCC cells. Cell pellets were lysed with RIPA buffer (1% NP-40, 0.1% SDS, 50mM Tris-HCl

pH 7.4, 150mM NaCl, 0.5% Sodium Deoxycholate, 1mM EDTA) for analysis. Densitometry was calculated using α -actin (SantaCruz, Santa Cruz, CA) as a loading control for all Western blots.

Vimentin antibody (AVIVA, San Diego, CA) was used at a 1:1000 dilution in a 5% milk/TBST buffer. E-cadherin antibody (Cell Signaling Technology) was used at a 1:200 dilution in a 5% milk/TBST buffer. ALDH1A1 antibody (AVIVA, San Diego, CA) was used at a 1:1000 dilution in a 5% milk/TBST buffer. Horseradish peroxidase-conjugated goat anti-rabbit secondary antibody (Rockland, Gilbertsville, PA) was used (1:5,000) for all blots. The signal was developed with ECL Prime Western blotting detection reagent (Amersham, Piscataway, NJ).

Indirect Immunofluorescence

HN12 cells were seeded initially at a density of 4×10^4 in Nunc Lab Tek II immunofluorescence chambers (Fisher Scientifics, Pittsburgh, PA). Cells were allowed to attach overnight before treatment with BITC (5-10 μ M) for 1-hour. Treatment media was then removed and replaced with complete DMEM (10%FBS, 1%P/S). Twenty-four hours after treatment, cells were fixed with 4% paraformaldehyde and permeabilized in PBS containing 1% BSA and 0.1% Triton X-100. Cells were blocked with PBS/1% BSA prior to staining. Vimentin (AVIVA, San Diego, CA) was diluted 1:400 with PBS containing 1% BSA and appropriate wells were incubated with primary antibody in a dark humidified chamber for 1-hour. Cells were then washed and incubated with Alexa Fluor 488 (Invitrogen, Grand Island, NY) secondary antibody (1:200) in humid and dark conditions for 45 minutes. Slides were detached from immunofluorescence chambers and Vectashield mounting media with DAPI (Vector Laboratories, Burlingame, CA) was added to slides before analysis. Images taken using an Olympus IX51 inverted microscope equipped with epifluorescence (Olympus, Center Valley, PA).

Intercellular ROS Generation

Cells were seeded in 6-well plates (3×10^5 cells/well) 24 hours prior to treatment. Levels of intracellular ROS were determined using 5-(and-6-) chloromethyl-2',7'-dichlorodihydrofluorescein diacetate, acetyl ester (CM-H₂DCFDA) (Molecular Probes, Eugene, OR). Cells were washed twice with 1X Dulbecco's PBS (PBS) (GIBCO, Invitrogen) and incubated for 5 minutes in the presence or absence of 2.5 μ M H₂DCFDA in serum free DMEM. Following a 5 minute incubation, cells were washed three times with 1X PBS and treated with BITC (1.25-10 μ M), 5mM NAC, 2,500U catalase, or a combination of BITC and NAC or BITC and catalase for 1 hour. After treatment cells were washed two times with 1X PBS and then incubated with StemPro® Accutase® (Life Technologies, Grand Island, NY) for 5 minutes. H₂O₂ (10 μ M) was used as positive control. Cells were collected and transferred to 1.5mL microcentrifuge tubes and spun down at 400xg for 5 minutes. The supernatant was removed and cells were washed two times with 500 μ L PBS. Prior to reading fluorescence using an Accuri C6 Flow Cytometer (BD Accuri, San Jose, CA) cells were re-suspended in 400 μ L of PBS and kept on ice. Assays for intracellular ROS generation were performed in technical triplicates and biological triplicates.

Co-treatment Wound-Healing Assay

Cell migration was determined using a wound-healing assay. HN12 cells were cultured in DMEM containing 10% FBS, and 1% Pen-Strep in 6-well plates until 90% confluent, and then media was changed to DMEM with 0.05% FBS and 1% P/S overnight to synchronize the cells. A line was drawn horizontally on the bottom of each well with a permanent marker, and a plastic pipette tip (p200) was used to generate 3 vertical scratches per well (90 degrees to the permanent line). Cell

debris were washed away with PBS and initial scratch sizes were determined with an inverted light microscope (Olympus IX51, Center Valley, PA) at 100X magnification. Six measurements were made per well, 1 below and 1 above the horizontal line for each scratch before treatment. Cells were treated with BITC (1.25 and 2.5 μ M), 5mM NAC, 2,500U/mL catalase, and a combination of BITC and NAC or BITC and catalase for 1 hour at 37°C. DMSO, at the same concentration as in the BITC treated wells, was used for the vehicle control. After 1-hour, plates were washed with PBS and treatment was replaced with DMEM (10% FBS, 1% P/S). Wound healing was analyzed 24 hours after treatment. Images were taken at 100X magnification, as described above, and changes in cell migration were determined by calculating the percent of wound healing. Percent wound healing = $((\text{scratch}_{t=0\text{hr}} - \text{scratch}_{t=24\text{hr}}) / \text{scratch}_{t=0\text{hr}}) * 100$. Experiments were repeated 3 times.

Statistical Analysis

All experiments were performed at least three times as independent experiments. Statistical analyses were done with a multiple comparison test with appropriate post-hoc test. GraphPad Prism (La Jolla, CA) was used for all statistical analysis. A *p*-value of <0.05 was considered statistically significant.

RESULTS

BITC Inhibited Migration and Invasion of HNSCC Cells

A wound-healing assay indicated that BITC inhibits migration of the highly metastatic HN12 cells in a dose dependent manner. After 24 hours, inhibition of cellular migration was observed in the highly metastatic HN12 cell line when using a 2.5 μ M BITC treatment, however a significant decrease in wound healing required 5 μ M BITC ($p \leq 0.05$) (**Figure 1**). Similar results were observed when using the HN8 cell line, but not the HN30 cell line (data not shown). Although, it should be noted that the HN30 cell line did not undergo “wound-healing” under control conditions.

The ability of BITC to inhibit the migration of HN12 cells prompted us to investigate the effect of BITC on invasion through Matrigel. **Figure 2** (panels A and B) depict that 1-hour treatment of BITC significantly inhibited the invasion of HN12 cells ($p \leq 0.05$). Compared to the vehicle control the average number of invading cells per field of view decreased by 52.34% after a 2.5 μ M BITC treatment and 90.96% after a 5 μ M BITC treatment ($p \leq 0.05$). Viability assays confirmed that the addition of the chemo-attractant, EGF, to the cells did not change the viability and proliferation of HNSCC cells after BITC treatment (data not shown). These results substantiate the wound-healing assay data and indicate that BITC targets both migration and invasion of certain HNSCC cell lines.

Vimentin and ALDH1A1 Expression Decreased and E-cadherin Expression Increased after BITC Treatment

Immunofluorescence results suggested that vimentin expression was inhibited 24 hours after a 1-hour BITC treatment (5-10 μ M), in a dose dependent manner (**Figure 3 A**). The localization of vimentin also appeared altered after BITC treatment. Our immunofluorescence results are supported by Western blot analysis showing a significant decrease in vimentin expression occurred after a 24 hour BITC treatment of 5 and 10 μ M ($p \leq 0.05$) (**Figure 3 B and C**).

Western blot analysis also indicated E-cadherin expression increased 24 hours after a 1-hour BITC treatment (**Figure 4**). However, expression of CSC marker, ALDH1A1, decreased 24 hours after a 1-hour BITC treatment (**Figure 5**).

BITC Increases ROS in HNSCC Cell Lines and NAC or Catalase Attenuate BITC Induced ROS

A dichlorofluorescein (DCF) assay indicated that BITC dramatically increased the ROS production in the HN12 and HN30 cell lines ($p \leq 0.05$) (**Figure 6 and 7**). Interestingly, the non-metastatic HN30 cell line showed a significant increase in ROS production, the increase in ROS was over 3 folds greater in the highly metastatic HN12 cell line. However, even though the 2.5 μ M BITC induced significant elevations in ROS in HN12 and HN30, this concentration of BITC did not induce significant changes in cell viability after 24 or 48 hours (data not shown).

ROS production induced by a 1-hour BITC treatment was attenuated by the addition of N-acetyl-L-cysteine (NAC) in the HN30 and HN12 cell line ($p \leq 0.05$) (**Figure 6**). ROS production was also significantly inhibited by catalase in the HN12 and HN30 cell line ($p \leq 0.05$), but to a lesser extent than NAC (**Figure 7**). Interestingly, the addition of catalase to BITC treatments kept HN30's ROS production down near basal levels, but ROS production was markedly higher when catalase was added to BITC treatments in the HN12 cell line.

NAC and Catalase Prevent BITC from Inhibiting Migration of HNSCC Cells

A wound-healing assay indicated that BITC inhibited the migration of the highly metastatic HN12 cells in a dose dependent manner, after 24 hours ($p \leq 0.05$). However, NAC (**Figure 48**) and catalase (**Figure 9**) inhibited the ability of BITC to prevent wound healing in the HN12 cell line. Under the conditions used for this assay catalase treatment alone appeared to increase the wound healing, although this was not statistically significant.

DISCUSSION

Previous studies from our lab indicated that BITC has a dual function of targeting both cell viability and cell migration [17,18]. BITC, like other isothiocyanates, targets a variety of molecular pathways making it difficult to pinpoint how BITC elicits its therapeutic response in HNSCC cells [5,18]. Here, we show that BITC treatments inhibit HNSCC cell migration and invasion. Additionally, BITC treatments altered the expression of markers correlated with EMT. Many EMT markers are associated with poor HNSCC prognosis, but few therapies have been shown to actually regulate the expression of these markers. Additionally, EMT, directly or indirectly links HNSCC metastasis and chemoresistance.

Our findings suggest that BITC treatment decreased expression of vimentin and ALDH1A1, while increasing expression of E-cadherin. Vimentin is a mesenchymal filament protein and it increases motility of cells undergoing mesenchymal conversion in coordination with dephosphorylated microtubules to provide support to microtentacle extension of detached tumor cells [19]. ALDH1A1 is a putative cancer stem cell marker, but it is also associated with cells undergoing EMT. Vimentin and ALDH1A1 overexpression in HNSCC correlates well with accelerated tumor growth, invasion, and poor prognosis [20]. E-cadherin is important for epithelial integrity and is regarded as a tumor suppressor because of its role in maintenance of epithelial phenotype. Consequently, BITC's ability to inhibit vimentin and ALDH1A1 expression while increase E-cadherin expression could be clinically significant.

Additionally, the results of the present study demonstrate that BITC induced ROS regulates both HNSCC cell viability and migration. By attenuating BITC induced ROS with NAC and catalase we were able to inhibit BITC's ability to prevent cell migration. NAC and catalase are both antioxidants that scavenge free radicals. NAC is a GSH precursor and thereby increases cellular GSH [11,21,22]. Cellular GSH plays a central role in maintaining redox homeostasis, and reduced GSH act as a direct scavenger of ROS by reacting with singlet oxygen, hydroxyl radicals, and superoxide radicals [11]. We used NAC to investigate a mechanism of action of BITC in HNSCC cells. NAC in combination with ITCs has been used to investigate ITC's mechanism of action in other cell lines, and recently Gong *et al.* (2009) used NAC in combination with ITCs to support that ROS alters STAT3 activation in prostate cancer cells [23].

In our study BITC treatments significantly increased ROS production in HNSCC cell lines.

BITC initiated ROS production was significantly decreased when NAC and BITC were co-administered. Additionally, NAC prevented BITC induced cytotoxicity (data not shown).

Catalase is a scavenger of H₂O₂ and we used this reagent to further support the NAC studies. Catalase significantly prevented BITC induced ROS production in the HNSCC cell lines. The prevention of ROS production was not to the same extent as NAC, probably because catalase is more specific in its ROS scavenging abilities. Although, catalase highlighted the potential of H₂O₂ induction in HNSCC cell lines. Furthermore, catalase alone appeared to increase HNSCC cell migration, which is interesting because several reports suggest that increasing ROS production is usually associated with increased cellular migration [13,14]. Our results are supported by Luanpitpong *et al.* (2010) and because their study also showed that catalase stimulated cell migration while H₂O₂ inhibited cellular migration [15]. Inokuma *et al.* (2012) also suggest that increased ROS is pertinent to preventing lymph node metastasis in colorectal cancer [24]. Furthermore, Das *et al.* (2012) report that ROS generation inhibits EMT and promotes growth arrest in prostate cancer cells [25]. Taken together, our results combined with others indicate that investigating ROS has a whole may lead to confounding results. Our results support that specific types of ROS combined with the molecular pathways that are altered in certain cancer cells can have untraditional results.

More investigation on the relationship between BITC anti-oxidants will be needed, but the relationship between BITC and NAC or catalase co-administration should not be overlooked. Regardless of why NAC or catalase inhibited ROS production, it is still evident that NAC and catalase prevented the therapeutic effects of BITC when co-administered. This knowledge is critical for future clinical trials. Our results stress the importance of a monitoring a patient's antioxidant consumption, because our data supports that administering BITC with anti-oxidants would have not been beneficial for a patient.

Future *in vivo* studies will shed the greatest light on the potential and feasibility of BITC as an adjuvant to anti-cancer agent.

CONCLUSIONS

In conclusion, the present study sets the framework for future investigation into the mechanism through which BITC inhibits migration and invasion. While we did not observe a change in STAT3 activity, which was the focus of specific aim 2, our study does suggest that ROS is one

important mechanism by which BITC elicits its response. Future studies, will work to continue to unravel the role of BITC induced ROS in HNSCC by including experiments to evaluate the role of other antioxidants, like vitamin E.

OUTCOMES

I published a manuscript in Nutrition and Cancer (January of 2014) highlighting the work presented in this report and the work supported under previous WV NASA SGC grants. I also have two other manuscripts in review. I defended my thesis on April 4, 2014 and passed my defense. My thesis is entitled: “Benzyl isothiocyanate as an adjuvant chemotherapy option for head and neck squamous cell carcinoma”.

I also presented portions of the present research at the 4th World Congress of International Academy of Oral Oncology in May of 2014. Additionally, I was selected to give an oral presentation at the 2014 Marshall University School of Medicine Research Day, and I was awarded “Best Basic Science Oral Presentation”.

Publication reference:

Wolf MA, Claudio PP (2014) Benzyl Isothiocyanate Inhibits HNSCC Cell Migration and Invasion, and Sensitizes HNSCC Cells to Cisplatin. Nutr Cancer 66: 285-294.

FUTURE PLANS

I will graduate with my Ph.D. in May of 2014. I am currently looking for teaching positions or teaching intensive postdoctoral positions in Biology/Biochemistry.

ACKNOWLEDGEMENTS

I would like to thank my mentor Dr. Pier Paolo Claudio for being a constant source of encouragement and advice throughout my Ph.D. studies. I would also like to acknowledge member of the TGRI, especially, Dr. Flavia DeCarlo, Dr. Sarah Miles, Dr. Johannes Fahrman and Miranda Carper for their guidance on this project. I am also grateful to Marshall’s Biomedical Sciences graduate program for giving me numerous opportunities to present my research.

Lastly, I would like to acknowledge the NASA WV-SGC for the support I have received over the past 3 years. This funding was instrumental to my research project and allowed me obtain my Ph.D. from the Marshall University Biomedical Sciences program. Funding for research continues to diminish and without the support of the NASA WV-SGC many graduate students in the state of West Virginia would not be able to continue their projects.

FIGURES

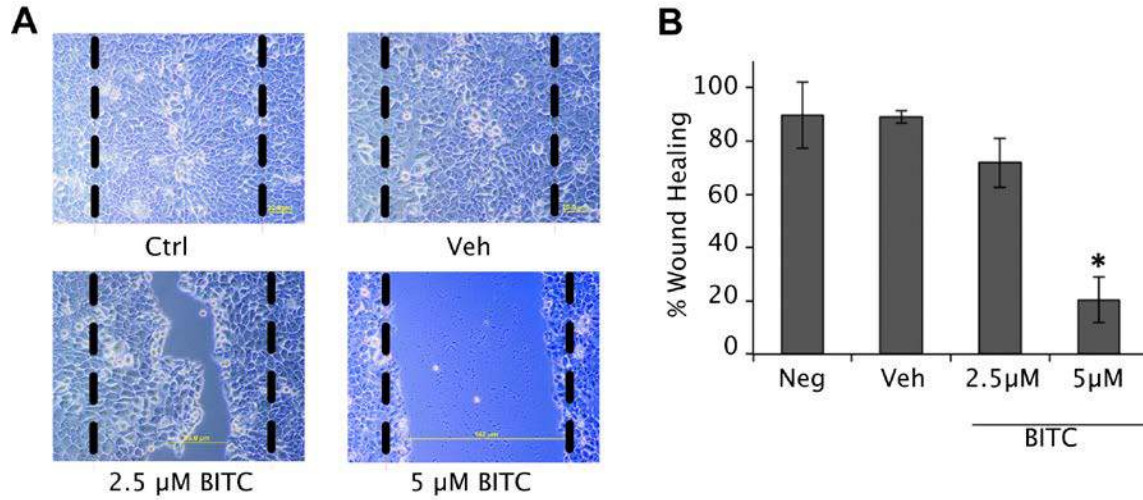


Figure 1. BITC inhibited wound-healing of HN12 cells after 24 hours. **(A)** Inverted light microscope pictures of HN12 cells before and after BITC treatment (2.5-5µM). Dashed lines represent scratch size before treatment. Vehicle control was DMSO. Magnification 100X. **(B)** Bar diagram represents the percent wound healing determined after 24 hours using wound size measurements. Error bars represent standard deviation. One-way ANOVA for multiple comparisons with Dunnet's Post-Hoc test (* $p \leq 0.05$).

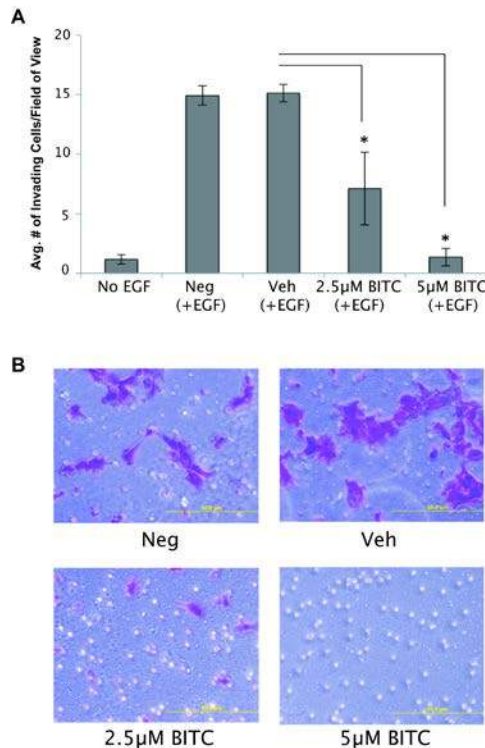


Figure 2. Invasion assay of HN12 cells following BITC treatment at 24 hours. **(A)** Bar diagram represents the average number of invading cells/field of view counted at 24 hours following a one-hour treatment of HN12 cells with BITC. EGF was used as chemoattractant. Error bars represent standard deviation. One-way ANOVA for multiple comparisons with Dunnet's Post-Hoc test (* $p \leq 0.05$). **(B)** Inverted light microscope pictures of HN12 cells stained with crystal violet following BITC treatment. NEG: negative control. VEH: vehicle control. Magnification x200.

Figure 3. Vimentin expression in HN12 cells following one-hour treatment with a range of concentrations of BITC. **(A)** Representative immunofluorescence images of a vimentin immunostaining acquired with an inverted epifluorescence microscope before and after 1-hour treatment of HN12 cells with a range of concentrations of BITC (5-10 μ M). Anti-vimentin (1:400); AbII anti-rabbit Alexa Fluor 488 (1:200); DAPI to counterstain the nuclei. Magnification 400X. Bar size is 10 μ m. **(B)** Western blot analysis of vimentin expression in HN12 cells after 1-hour treatment with a range of concentrations of BITC (1.25-10 μ M). Actin was used to normalize the blot. **(C)** Densitometric analysis of vimentin and actin protein expression. Diagram represents the fold change of vimentin after 24 hours normalized to actin control. One-way ANOVA for multiple comparisons with Dunnett's Post-Hoc test (*Charl p ≤0.05).

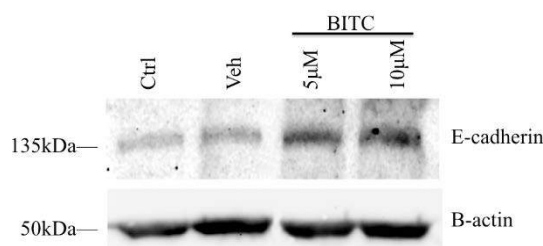


Figure 4. Western blot analysis of E-cadherin expression in HN12 cells 24 hours after a one-hour treatment with a range of concentrations of BITC (5-10 μ M). Actin was used to normalize the blot.

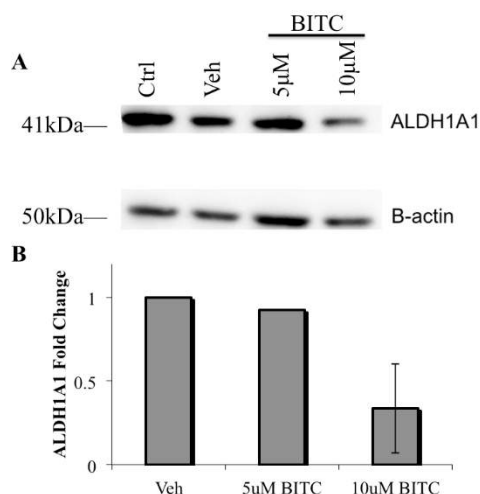


Figure 5. ALDH1A1 expression in HN12 cells following a one-hour treatment with BITC. **(A)** Western blot analysis of ALDH1A1 expression in HN12 cells 24 hours after a one-hour treatment with a range of concentrations of BITC (5-10 μ M). Actin was used to normalize the blot. **(B)** Densitometric analysis of ALDH1A1 and actin protein expression. Diagram represents the fold change of ALDH1A1 after 24 hours.

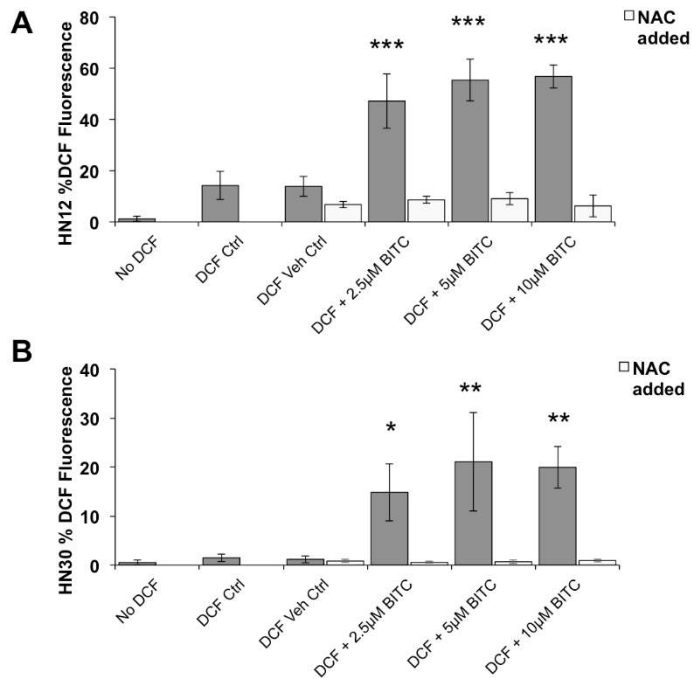


Figure 6. NAC inhibits BITC induced DCF fluorescence in the HN12 and HN30 cell lines. DCF fluorescence was determined in the **A)** HN12 and **B)** HN30 cell line 24 hours after a 1-hour treatment with BITC (2.5-10μM), a 1-hour co-administration of BITC (2.5-10μM) and 5mM NAC, or a 1-hour treatment with 5mM NAC. DCF assay was used to determine ROS production. Dark grey bars represent cells treated with BITC only. Light grey bars represent cells co-treated with BITC and NAC. Error bars represent standard deviation. One-Way ANOVA for Multiple Comparison with Dunnet's Post-Hoc test (* $p \leq 0.05$; ** $p \leq 0.001$; *** $p \leq 0.0001$).

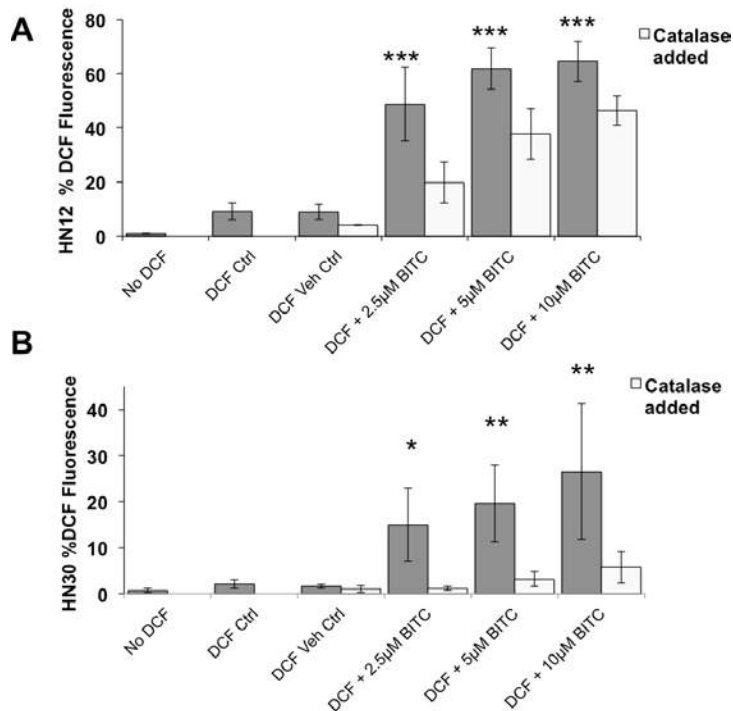


Figure 7. Catalase inhibits BITC induced DCF fluorescence in the HN12 and HN30 cell lines. DCF fluorescence in the **A)** HN12 and **B)** HN30 cell line after a 1-hour treatment with BITC (2.5-10μM), a 1-hour co-administration of BITC (2.5-10μM) and Catalase (2,500U/mL), or a 1-hour treatment with Catalase (2,500U/mL) alone. DCF assay was used to determine ROS production. Dark grey bars represent cells treated with BITC alone. Light grey bars represent cells treated with BITC and Catalase. Error bars represent standard deviation. One-Way ANOVA for Multiple Comparison with Dunnet's Post-Hoc test (* $p \leq 0.05$; ** $p \leq 0.001$; *** $p \leq 0.0001$).

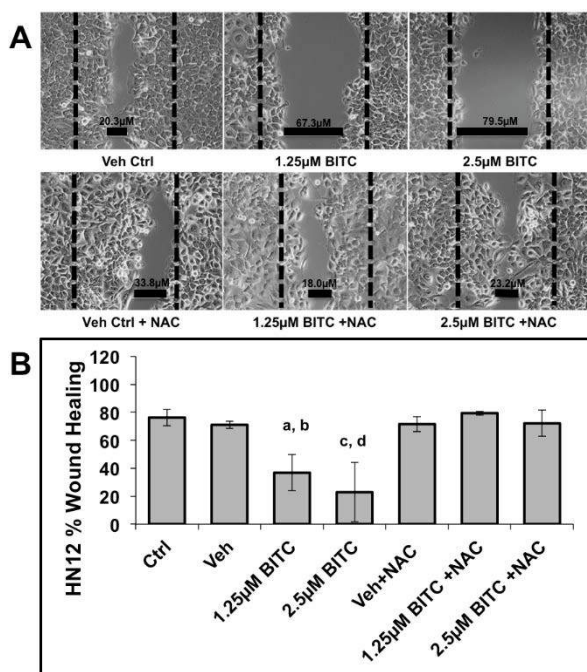


Figure 8. NAC co-administered with BITC prevents the effect of BITC treatments on wound healing in the HN12 cell line. (A) Inverted light microscope images of HN12 cells 24 hours after cells were treated with BITC (2.5-10µM) for 1-hour, a NAC and BITC (2.5-10µM) co-treatment for 1-hour, NAC alone for 1-hour, or appropriate vehicle control. Dashed lines represent scratch size before treatment. Magnification 100X. (B) Bar diagram represents the percent wound healing of the HN12 cell line 24 hours after treatment. Percent wound healing was calculated using wound size measurements. Error bars represent standard deviation. One-way ANOVA for multiple comparisons with Dunnet's Post-Hoc test. **a**= significantly different from Veh ($p \leq 0.05$); **b**= significantly different from 1.25µM BITC+NAC ($p \leq 0.05$); **c**= significantly different from Veh ($p \leq 0.0001$); **d**= significantly different from 2.5µM BITC+NAC ($p \leq 0.0001$). Ctrl: negative control. Veh: vehicle control.

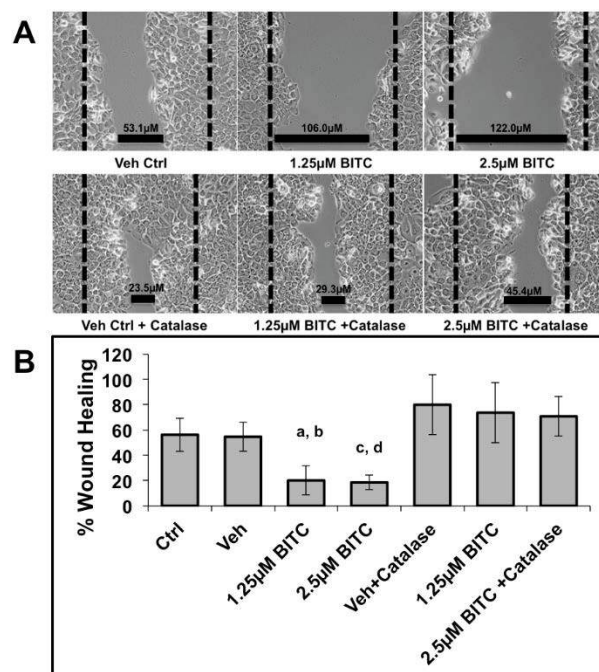


Figure 9. Catalase co-administered with BITC prevents the effect of BITC treatments on wound healing in the HN12 cell line. (A) Inverted light microscope images of HN12 cells 24 hours after cells were treated with BITC (2.5-10µM) for 1-hour, a Catalase and BITC (2.5-10µM) co-treatment for 1-hour, Catalase alone for 1-hour, or appropriate vehicle control. Dashed lines represent scratch size before treatment. Magnification 100X. (B) Bar diagram represents the percent wound healing of the HN12 cell line 24 hours after treatment. Percent wound healing was calculated using wound size measurements. Error bars represent standard deviation. One-way ANOVA for multiple comparisons with Dunnet's Post-Hoc test. **a**=significantly different from Veh ($p \leq 0.001$); **b**=significantly different from 1.25µM BITC+Catalase ($p \leq 0.0001$); **c**= significantly different from Veh ($p \leq 0.0001$); **d**=significantly different from 2.5µM BITC+Catalase ($p \leq 0.0001$). Ctrl: negative control. Veh: vehicle control.

REFERENCES

1. Siegel R, Ma J, Zou Z, Jemal A (2014) Cancer statistics, 2014. *CA Cancer J Clin* 64: 9-29.
2. Monnerat C, Faivre S, Temam S, Bourhis J, Raymond E (2002) End points for new agents in induction chemotherapy for locally advanced head and neck cancers. *Ann Oncol* 13: 995-1006.
3. Nakamura Y (2009) Chemoprevention by isothiocyanates: molecular basis of apoptosis induction. *Forum Nutr* 61: 170-181.
4. Nakamura Y, Miyoshi N (2010) Electrophiles in foods: the current status of isothiocyanates and their chemical biology. *Biosci Biotechnol Biochem* 74: 242-255.
5. Wu X, Zhou QH, Xu K (2009) Are isothiocyanates potential anti-cancer drugs? *Acta Pharmacol Sin* 30: 501-512.
6. Hutzen B, Willis W, Jones S, Cen L, Deangelis S, et al. (2009) Dietary agent, benzyl isothiocyanate inhibits signal transducer and activator of transcription 3 phosphorylation and collaborates with sulforaphane in the growth suppression of PANC-1 cancer cells. *Cancer Cell Int* 9: 24.
7. Zhang R, Loganathan S, Humphreys I, Srivastava SK (2006) Benzyl isothiocyanate-induced DNA damage causes G2/M cell cycle arrest and apoptosis in human pancreatic cancer cells. *J Nutr* 136: 2728-2734.
8. Boreddy SR, Sahu RP, Srivastava SK (2011) Benzyl isothiocyanate suppresses pancreatic tumor angiogenesis and invasion by inhibiting HIF- α /VEGF/Rho-GTPases: pivotal role of STAT-3. *PLoS One* 6: e25799.
9. Warin R, Chambers WH, Potter DM, Singh SV (2009) Prevention of mammary carcinogenesis in MMTV-neu mice by cruciferous vegetable constituent benzyl isothiocyanate. *Cancer Res* 69: 9473-9480.
10. Warin R, Xiao D, Arlotti JA, Bommareddy A, Singh SV (2010) Inhibition of human breast cancer xenograft growth by cruciferous vegetable constituent benzyl isothiocyanate. *Mol Carcinog* 49: 500-507.
11. Manda GN, M.T.; Neagu, T.M (2009) Reactive Oxygen Species, Cancer and Anti-Cancer Therapies. *Current Chemical Biology* 3: 342-366.
12. Trachootham D, Alexandre J, Huang P (2009) Targeting cancer cells by ROS-mediated mechanisms: a radical therapeutic approach? *Nat Rev Drug Discov* 8: 579-591.
13. Ma J, Zhang Q, Chen S, Fang B, Yang Q, et al. (2013) Mitochondrial dysfunction promotes breast cancer cell migration and invasion through HIF1 α accumulation via increased production of reactive oxygen species. *PLoS One* 8: e69485.
14. Tochwang L, Deng S, Pervaiz S, Yap CT (2013) Redox regulation of cancer cell migration and invasion. *Mitochondrion* 13: 246-253.
15. Luanpitpong S, Talbott SJ, Rojanasakul Y, Nimmannit U, Pongrakhananon V, et al. (2010) Regulation of lung cancer cell migration and invasion by reactive oxygen species and caveolin-1. *J Biol Chem* 285: 38832-38840.
16. Yoo GH, Piechocki MP, Ensley JF, Nguyen T, Oliver J, et al. (2002) Docetaxel induced gene expression patterns in head and neck squamous cell carcinoma using cDNA microarray and PowerBlot. *Clin Cancer Res* 8: 3910-3921.
17. Wolf MA, Claudio PP (2014) Benzyl Isothiocyanate Inhibits HNSCC Cell Migration and Invasion, and Sensitizes HNSCC Cells to Cisplatin. *Nutr Cancer* 66: 285-294.

18. Wolf MAC, P.P. (2013) Isothiocyanates Target Carcinogenesis During Tumor Initiation, Promotion and Progression In: Claudio PPaN, R., editor. Nutrition and Cancer, From Epidemiology to Biology Bentham Science Publisher.
19. Sehrawat A, Singh SV (2011) Benzyl isothiocyanate inhibits epithelial-mesenchymal transition in cultured and xenografted human breast cancer cells. *Cancer Prev Res (Phila)* 4: 1107-1117.
20. Satelli A, Li S (2011) Vimentin in cancer and its potential as a molecular target for cancer therapy. *Cellular and molecular life sciences : CMLS* 68: 3033-3046.
21. Simons AL, Parsons AD, Foster KA, Orcutt KP, Fath MA, et al. (2009) Inhibition of glutathione and thioredoxin metabolism enhances sensitivity to perifosine in head and neck cancer cells. *J Oncol* 2009: 519563.
22. Sobhakumari A, Love-Homan L, Fletcher EV, Martin SM, Parsons AD, et al. (2012) Susceptibility of human head and neck cancer cells to combined inhibition of glutathione and thioredoxin metabolism. *PLoS One* 7: e48175.
23. Gong A, He M, Krishna Vanaja D, Yin P, Karnes RJ, et al. (2009) Phenethyl isothiocyanate inhibits STAT3 activation in prostate cancer cells. *Mol Nutr Food Res* 53: 878-886.
24. Inokuma T, Haraguchi M, Fujita F, Torashima Y, Eguchi S, et al. (2012) Suppression of reactive oxygen species develops lymph node metastasis in colorectal cancer. *Hepatogastroenterology* 59: 2480-2483.
25. Das TP, Suman S, Damodaran C (2013) Reactive oxygen species generation inhibits epithelial-mesenchymal transition and promotes growth arrest in prostate cancer cells. *Mol Carcinog*.